University of Glasgow

Using simple and complex wound *in vitro* biofilm models for testing of novel therapeutics

Abdullah Abed Baz
BSc, MSc

Submitted in fulfilment of the requirements for the Degree of Doctor of Philosophy

School of Medicine, Dentistry and Nursing

College of Medical, Veterinary and Life Sciences

University of Glasgow

May 2025

Abstract

Chronic wound infections, driven by resilient polymicrobial biofilms and escalating antimicrobial resistance (AMR), present a critical therapeutic challenge that requires alternative interventions. This thesis investigates innovative strategies to combat biofilm-associated infections, primarily focusing on cold atmospheric plasma (CAP) and repurposed compounds as alternatives to conventional therapies. Using *in vitro* models mimicking chronic wound microenvironments, including mono- and triadic-species biofilms of *Staphylococcus aureus*, *Pseudomonas aeruginosa*, *Candida albicans*, the study evaluates three key themes relating to antimicrobial testing.

CAP monotherapy (chapter 3) demonstrated time- and strain-dependent antimicrobial efficacy, with ≥3-$\log_{10}$ reductions in biofilm viability linked to hydrogen peroxide (H_2O_2) and reactive species generation. *S. aureus* exhibited strain-specific tolerance, while CAP disrupted polymicrobial community dynamics and induced oxidative damage visible via scanning electron microscopy (SEM). Dual therapies (chapter 4) combining CAP with repurposed agents (e.g., KHS 101 hydrochloride) or antiseptics H_2O_2, and povidone-iodine (PVP-I) overcame biofilm tolerance, achieving synergistic eradication (>3-$\log_{10}$ CFE reductions) in recalcitrant *S. aureus*-containing models with the novel dual intervention: KHS+CAP emerged as a lead strategy, destabilising biofilm matrices and enhancing oxidative stress. H_2O_2-antibiotic combinations (chapter 5) showed that H_2O_2 potentiated flucloxacillin and gentamicin against early-stage *S. aureus* biofilms, particularly in strain Newman. Synergy depended on treatment sequence, suggesting that such an intervention, if used clinically, would require careful consideration.

Key findings from this thesis have shown that such alternative therapies could be utilised for biofilm treatment in chronic wound management. In particular, the broad-spectrum activity of CAP and synergy with a repurposed agent (KHS) offers a potential replacement for antibiotic interventions during the care of such patients, which was demonstrated here using *in vitro* model systems. Alternatively, H_2O_2-mediated antibiotic re-sensitisation offers another pathway to mitigate AMR. Ultimately, multi-modal approaches rather than single-agent treatments, particularly those that "break" antimicrobial tolerance provide the most promising alternatives.

Table of Contents

List of Tables

List of Figures

List of publications based on thesis

Bryn Short, Ahmed Bakri, **Abdullah Baz**, Craig Williams, Jason Brown & Gordon Ramage 2023. There is more to wounds than bacteria: fungal biofilms in chronic wounds. *Current Clinical Microbiology Reports*, 10, 9-16.

Abdullah Baz, Ahmed Bakri, Mark BUTCHER, Bryn SHORT, Bhagirath GHIMIRE, Nishtha GAUR, Toby JENKINS, Robert D. SHORT, Marcello RIGGIO, Craig WILLIAMS, Gordon RAMAGE & Jason L. BROWN. 2023. *Staphylococcus aureus* strains exhibit heterogenous tolerance to direct cold atmospheric plasma therapy. *Biofilm*, 5, 100123.

Jontana Allkja, Zainab Bilal, **Abdullah Baz**, Eve Hughes, Olivia Sealy, Craig Williams, Karen Faulds, Gordon Ramage, Jason L. Brown. A matter of strain: Strain dependent tolerance to antimicrobial treatment in early-stage *Staphylococcus aureus* biofilms. **Manuscript under review**.

Abdullah Baz, Jontana Allkja, Craig Williams, Gordon Ramage, Jason L. Brown. Breaking tolerance: combinational plasma therapy for treating *Staphylococcus aureus* biofilms. **Manuscript under preparation**.

Acknowledgement

All praise be to Allah, the All-Knowing, the All-Wise, for all the blessings which He has bestowed upon me—blessings too numerous to count. I am deeply grateful to my supervisors Dr Jason Brown and Professor Marcello Riggio for their invaluable guidance and support throughout my PhD journey.

Dr Brown, your support at the start of my PhD, when I had difficult time during of the lockdown, was instrumental. Your insights and knowledge made it easier to proceed in the right direction and complete this project. I am deeply grateful to you Jason, now and always, for all the opportunities and learning experiences you have given to me over the past five years. Saying “thank you” is not enough to express how grateful I am to you. Your continuous support, patience, thoughtful comments, encouragement and understanding have been invaluable to me since the first day I was honoured to work under your supervision. Thank you for being you!

I would like to thank all members of the oral science group and University of Glasgow, past and present, who have provided support and advice throughout the way. Professor Gordon Ramage, Dr Om Alkhir Alshanta, Dr Saeed Alqahtani, Dr Sumaya Abuserwil, Dr Bryn Short, Dr Jontana Allkja, Dr Mark Butcher and Mr Steven Milligan, thank you for all the technical help and training you have provided throughout my PhD course - this was really appreciated. Muhanna Alshehri, Othman Baradwan, Mohammad Tiba, Dr Hafsa Abduljalil, Suror Shaban, Dr Ahmed Bakri, Kristyna Piela, Nasser Binsaif, Zainab Bilal, Lauren Ashcroft and Laurence Rowan, thank you for always being valued friends who have made my days in the school brighter and better, thank you for always being very kind, supportive and great team members.

I would like to express my heartfelt appreciation to my mom and dad, my brothers and sisters, for their unwavering love and prayers.

Special thanks are due to my lovely wife, Maryam, and my little boy, Abed, for their patience and understanding during the long periods I spent away from them while pursuing my studies in the UK, even as they remained in Saudi Arabia. Their support and sacrifices have been fundamental to the completion of this work.

My sincere thanks also go to my friends at ‘‘101 Maxwell Street’’, whose encouragement and companionship have been a source of strength.

Finally, I gratefully acknowledge the Saudi Ministry of Higher Education, Saudi cultural bureau and King Abdulaziz University for funding my PhD study.

Author's Declaration

I declare that I have carried out the work described in this thesis unless otherwise acknowledged or cited, under the supervision of Dr Jason Brown and Professor Marcello Riggio. I further declare that this thesis has not been submitted for any other degree at the University of Glasgow, or any other institution.

Abdullah Baz

May 2025

1 Chapter 1: General introduction

1.1 Introduction

Wounds and their associated infections can greatly diminish patients' quality of life and pose a growing challenge to healthcare systems globally. In the United Kingdom (UK), for example, it was estimated that the National Health Service (NHS) treated approximately 2.2 million wounds—including diabetic foot ulcers (DFUs), burns, and venous leg ulcers (VLUs) during the 2012/2013 period (Guest et al., 2015). By 2018, this figure had risen to about 3.8 million cases (Guest, Fuller and Vowden, 2020). Data from the National Diabetes Foot Care Audit (NDFA) between 2015 and 2018 indicated that one in three individuals with severe ulcers required hospitalisation for foot-related conditions within six months of their initial specialist assessment (NHS England, 2019). Furthermore, nearly half of these patients still had unresolved foot ulcers 12 weeks after their first evaluation by a specialist (NHS England, 2019). According to the NDFA, from 2018 to 2023, more than 40% of DFUs were classified as severe, and between 2.6% and 3.2% of these severe cases resulted in amputation within six months following the initial expert assessment (NHS England, 2023).

All wounds can be classified as either acute or chronic, depending on the severity and nature by which they heal. Acute wounds typically exhibit clear signs of healing within approximately four weeks, progressing through the standard phases of wound repair, while complete closure may take up to twelve weeks. However, a notable number of wounds do not heal within this expected timeframe or sequence, and these are classified as chronic wounds (Frykberg and Banks, 2015, Morton and Phillips, 2016). Research has indicated that chronic wounds represent a considerable portion of all wounds in the UK, with around 30% remaining unhealed for extended periods, leading to significant financial implications for the NHS (Guest et al., 2015, Guest, Fuller and Vowden, 2020). The likelihood of wounds becoming chronic is heightened by underlying health issues and comorbidities such as diabetes, obesity, impaired mobility, and vascular disorders (Beyene, Derryberry and Barbul, 2020, Guo and DiPietro, 2010, Sen, 2019).

A wound is defined as a break or injury to the skin's epithelial layer, often extending to the tissues beneath. Such injuries can result from a variety of causes, including physical trauma, surgical procedures, or burns. Once a wound occurs,

the body initiates a healing process that generally progresses through four distinct stages: bleeding and haemostasis, inflammation, proliferation, and remodelling (Figure 1.1) (Yang et al., 2021a, Demidova-Rice, Hamblin and Herman, 2012). Throughout these stages, the injured skin undergoes a series of changes, and the local wound environment becomes conducive to tissue repair (Demidova-Rice, Hamblin and Herman, 2012, Shaw and Martin, 2009, Wilkinson and Hardman, 2020, Yang et al., 2021a). The initial haemostasis phase involves the formation of a blood clot to control bleeding. This is followed by the inflammatory phase, during which various immune cells are recruited to the site of injury (Shaw and Martin, 2009, Wilgus, Roy and McDaniel, 2013, Caballero-Sánchez, Alonso-Alonso and Nagy, 2024). These immune cells secrete a range of factors and signalling molecules, such as cytokines, matrix metalloproteinases, and growth factors, which facilitate the migration and proliferation of fibroblasts, angiogenesis, collagen production, and the development of new extracellular matrix (ECM). These processes also support re-epithelialisation and the eventual remodelling of the wound area (Demidova-Rice, Hamblin and Herman, 2012, Martin and Nunan, 2015, Yang et al., 2021a, Kandhwal et al., 2022). In addition, these phases overlap, they are tightly coordinated, ultimately resulting in wound closure and tissue restoration.

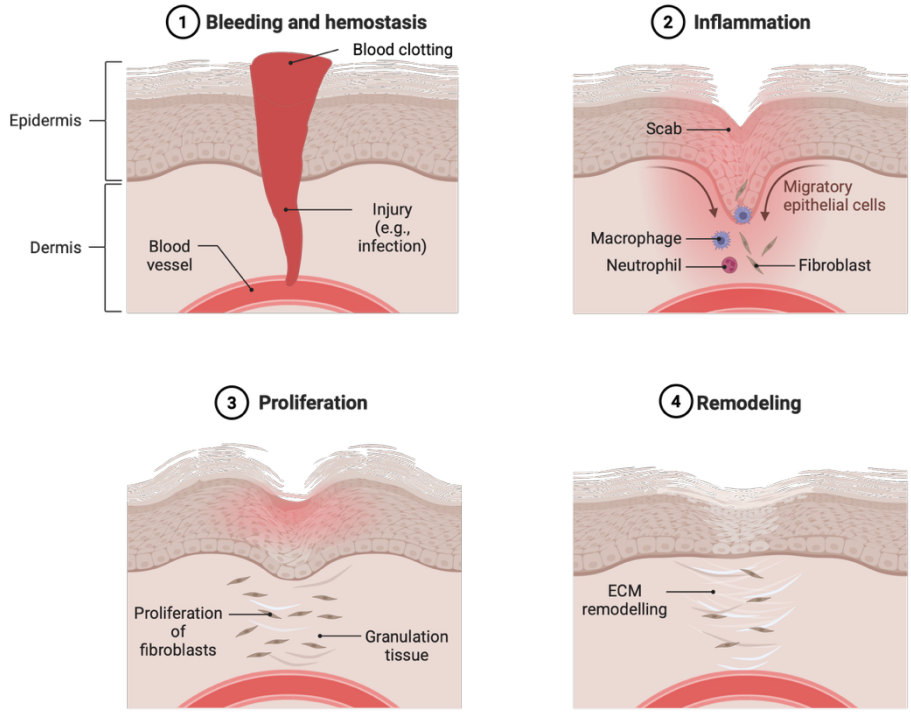

Figure 1.1: Wound healing progresses through four interconnected yet distinct phases. (1) Haemostasis, during which a blood clot forms to control bleeding; (2) Inflammation, marked by the activation of immune cells that release various factors and signalling molecules, facilitating the recruitment of fibroblasts; (3) Proliferation, where fibroblasts proliferate, collagen is produced, and new tissue is generated; and (4) Remodelling, in which the newly formed tissue undergoes maturation and strengthening, ultimately restoring tissue integrity. Diagram was created in BioRender.

The healing timeframe for wounds is affected by various external elements, including the cause of the injury, as well as its depth and size. Internal factors also play a role, including the presence of comorbidities like diabetes, kidney disease, venous insufficiency, and immune system disorders (Beyene, Derryberry and Barbul, 2020). Chronic wounds are often marked by an extended inflammatory and proliferative phase, where elevated levels of cytokines, biochemical agents, and immune cells persist, hindering the normal healing process (Barrientos et al., 2008, Guo and DiPietro, 2010, Landén, Li and Ståhle, 2016, Versey et al., 2021). For example, ongoing inflammation can increase the concentration of matrix metalloproteinases in the wound environment, which break down the ECM in the wound bed (Sabino and auf dem Keller, 2015, Caley, Martins and O'Toole, 2015, Kandhwal et al., 2022). This loss of ECM is especially evident in DFUs (Sutcliffe et al., 2017), further restricting cell movement and preventing wound closure. Additionally, the wound microenvironment becomes even more complex when

prolonged inflammation is combined with the presence of various microorganisms; arising from biofilm formation in the favourable conditions of the wound bed.

1.2 Wound infections

Both acute and chronic wounds are vulnerable to infection due to the inevitable presence of microorganisms on the skin, and through transient spread from human-to-human and environment-human. During the normal healing process, immune cells such as neutrophils are crucial for engulfing and eliminating pathogens, thereby reducing the risk of infection (Raziyeva et al., 2021, Zhu et al., 2021), but can become ineffective when overwhelmed with microbial colonisation. Wounds are typically colonised by a variety of commensal and pathogenic microbes. When healing is delayed, the risk of infection increases, as the extended timeframe allows pathogens more opportunity to multiply, making infections a frequent complication. A variety of pathogens present within the wound microbiome can be responsible for these infections as discussed above, which in turn can hinder both treatment effectiveness and the healing process. Traditionally, wounds containing more than approximately 10^5 colony forming units (CFU) per gram of tissue have been classified as infected according to earlier studies, and this threshold can differ depending on the specific pathogens involved and the criteria used in different research (Hurlow and Bowler, 2022b, Caldwell, 2020).

Clinically, infected wounds present with local signs such as purulence (pus), erythema, warmth, oedema, pain, malodour, friable or bleeding granulation tissue, and tissue breakdown, progressing in severe cases to systemic illness; diagnostically, inflammatory markers like C-reactive protein (CRP) with erythrocyte sedimentation rate, white blood cell count, and procalcitonin support assessment, while elevated wound protease activity, predominantly host matrix metalloproteinases (MMPs)/neutrophil elastase, has been linked to hard-to-heal infected wounds, whereas direct bacterial protease testing is not yet routine in clinical practice (Healy and Freedman, 2006, Durand et al., 2022, Burnet et al., 2022, Sharma et al., 2022, Senneville et al., 2024).

Pressure injuries, VLUs, DFUs, arterial ulcers, and mixed arterial–venous ulcers can be characterised by established classifications that link cause, depth,

duration, and tissue involvement to management. The National Pressure Injury Advisory Panel/National Pressure Ulcer Advisory Panel staging system defines pressure injuries from superficial epithelial damage to deep tissue involvement and unstageable lesions, aligning stage with progressive tissue loss over time (Edsberg et al., 2016). VLUs are categorised within Clinical–Etiology–Anatomy–Pathophysiology (category 6) indicating active ulceration, and duplex ultrasound is used to confirm reflux or obstruction to guide compression and venous interventions (Hess, 2020). DFUs are commonly graded by the Wagner–Meggitt scale (depth/ischemia scale from 0–5) and complemented by Wound–Ischemia–foot Infection to integrate perfusion and infection status, stratifying amputation risk and prioritizing revascularization where needed (Shah et al., 2022, Liu et al., 2024a). Arterial ulcers due to peripheral artery disease require vascular assessment with the ankle–brachial index and imaging because tissue hypoxia drives chronicity and mandates perfusion restoration for healing (Wang et al., 2023b). Mixed arterial–venous disease combines venous hypertension with arterial insufficiency, necessitating integrated work-ups and staged treatment to address both components and prevent stalled healing trajectories (Alagha et al., 2024).

In the UK, the standard approach to managing wound infections generally relies on antibiotic therapy, which may be supplemented with antimicrobial dressings or topical agents (Lipsky et al., 2016, Edwards-Jones, 2020). Chronic wounds, however, frequently experience repeated infections, often necessitating several courses of antibiotics and prolonged treatment durations (Eriksson et al., 2022, Leaper, Assadian and Edmiston, 2015). This pattern of antibiotic use can promote the emergence of multidrug-resistant bacteria within the wound microbiome. Furthermore, infections in wounds are commonly associated with the development of biofilms—structured bacterial communities that are notably resistant to antibiotic treatment (Percival, McCarty and Lipsky, 2015, Wu, Cheng and Cheng, 2019).

The National Institute for Health and Care Excellence (NICE) antimicrobial prescribing guidelines offer evidence-based advice to help health professionals and patients manage common infections and reduce antimicrobial resistance. NICE's antimicrobial prescribing guidelines specifically include recommendations for managing leg ulcer infection (NICE guideline 152), providing structured

guidance for clinicians managing chronic wound infections (Chaplin, 2020). Recent audits have revealed significant challenges in compliance with NICE guidance. A study of antibiotic prescribing in acute wound management found that only 42.8% of cases met NICE criteria for antibiotic indication, while documentation deficiencies were prevalent, with only 61.9% of prescriptions featuring complete wound assessments. This highlights the gap between established guidelines and clinical practice implementation (Al-khatib, Corn and Ozidu, 2024). The NICE guidelines for the prevention of surgical site infection emphasize the importance of appropriate antimicrobial use, recommending that clinicians only apply an antiseptic or antibiotic to the incised wound before closure as part of a clinical research trial. The guidelines also suggest considering gentamicin-collagen implants used in cardiac surgery and sutures, rather than staples to close the skin to reduce surgical site infection risk (Leaper et al., 2019).

The International Wound Infection Institute (IWII) 2022 Wound Infection in Clinical Practice consensus document provides multidisciplinary healthcare providers with effective guidance and support on terminology, paradigms related to biofilm, identification of wound infection, wound cleansing, debridement and antimicrobial stewardship. The document incorporates wound infection management strategies within the IWII's Wound Infection Continuum (IWII-WIC) and management plan (Swanson et al., 2022). The IWII consensus emphasizes that accurate and timely identification of wound infection is critical to achieving clinical and cost-effective management, and promotion of healing. The guidelines specifically address biofilm paradigms and antimicrobial stewardship, recognizing the challenges posed by biofilm-associated infections in chronic wounds (Swanson et al., 2022).

The UK has implemented comprehensive antimicrobial stewardship programs with specific focus on wound infection management. Updated good practice recommendations for outpatient parenteral antimicrobial therapy in adults and children in the UK provide guidance for managing severe wound infections requiring intravenous antibiotics (Chapman et al., 2019). Analysis of antimicrobial prescribing guidance across NHS trusts shows that most guidelines included sepsis management (98.3%) and antimicrobial stewardship (94.1%), though only 9.2% included all key general guideline sections. This variability in guideline

implementation across different healthcare settings may contribute to inconsistent wound infection management practices (Ashfield et al., 2023). For complex wound infections, particularly those involving multidrug-resistant organisms, the UK has developed specialized guidance. The updated guidelines from the UK for treatment of methicillin-resistant *Staphylococcus aureus* (MRSA) were developed following a review of the published literature (2007–2018) pertaining to the treatment of infections caused by MRSA, taking into account changes in the UK epidemiology of MRSA, ongoing national surveillance data and the efficacy of novel anti-staphylococcal agents licensed for use in the UK (Brown et al., 2021). The British Orthopaedic Association released updated guidelines in 2020 for the management of open fractures, recommending a two-phase approach with initial intravenous antibiotics followed by treatment for 24 hours after wound excision. These guidelines recognize the particular challenges posed by contaminated wounds with high infection risk (Bangash, Muddassir and Barlow, 2023).

Chronic wounds represent a significant healthcare challenge characterised by persistent infection and impaired healing processes. Recent research has established that the microbiology of chronic wounds is remarkably complex, involving diverse bacterial and fungal communities that contribute significantly to wound chronicity and treatment resistance (Diban et al., 2023). Unlike acute wounds, chronic wounds remain in a persistent inflammatory state partly due to the complex microbial ecosystem that develops within them (Hurlow and Bowler, 2022a). Studies have revolutionised our understanding of chronic wound microbiology, revealing that rather than being caused by individual pathogens, these wounds harbour intricate polymicrobial communities that work synergistically to impede healing (Ancira et al., 2025). The European Society of Clinical Microbiology and Infectious Diseases (ESCMID) has explicitly stated that "biofilms cause chronic infections" with chronic wounds being cited as a prime example of biofilm infection (Wolcott, 2017). This fundamental shift in understanding has established that chronic venous ulcers, pressure injuries, and DFUs harbour sophisticated polymicrobial communities that cooperatively impede healing through complex intercellular signalling networks and shared protective mechanisms (Hurlow and Bowler, 2022a, Wolcott, 2017). For the microbial community, the key benefits of impeding healing are sustained access to

nutrients, community-level tolerance to host defences and drugs, cooperative metabolism and spatial organization that enhance persistence, accelerated adaptation via gene exchange and phenotypic shifts, and efficient dispersal to maintain colonization across the wound landscape (Percival, Thomas and Williams, 2010, Pouget et al., 2022b, Zhao et al., 2013, Khalid et al., 2023, Omar et al., 2017).

1.2.1 Biofilm formation in chronic wounds

In the 1670s, Antonie van Leeuwenhoek recorded microscopic “animalcules” from dental plaque, widely regarded as the first description of oral biofilms and a foundational observation for oral microbiology and biofilm science (He and Shi, 2009). Contemporary reviews of oral biofilms explicitly trace their origins to Leeuwenhoek’s plaque observations, noting his descriptions of sessile consortia that disperse when perturbed, consistent with modern biofilm behaviour (Săndulescu and Săndulescu, 2023). In the 1940s, Zobell (1943) demonstrated that bacteria attach to and thrive on solid surfaces in dilute environments, showing enhanced activity associated with surfaces and distinguishing benthic (surface-associated) from planktonic lifestyles. Historical retrospectives emphasize early demonstrations of reversible and irreversible attachment, microcolony formation, and the role of conditioning films on submerged surfaces, which anticipated core stages of biofilm development recognized today (O'Toole, 2016). From the 1970s through the 1990s, the work of J. William Costerton and collaborators popularized the term “biofilm” and firmly established the importance of adherent, matrix-embedded communities as the prevailing microbial lifestyle in nature and a driver of persistent infections (McLean, Lam and Graham, 2012). This shift catalysed medical microbiology’s embrace of biofilms as central to chronic device- and tissue-associated infections, paving the way for modern *in vitro* and *in vivo* models and clinical diagnostics targeting biofilm phenotypes (Lebeaux et al., 2013). Modern ideologies portray biofilms as structured, matrix-encased communities with emergent properties (e.g., tolerance, heterogeneity), a conceptualization now commonly applied to chronic wound infections where biofilms underpin persistence and treatment failure (Watnick and Kolter, 2000). Focused reviews on wounds integrate this history with clinical evidence, detailing how polymicrobial biofilms in wound beds resist

antibiotics and immune clearance, thereby sustaining chronic inflammation and non-healing states (Omar et al., 2017).

Today, biofilms are understood to be intricate assemblies of one or more microbial species that adhere to one another and/or surfaces (Rather, Gupta and Mandal, 2021, Flemming et al., 2016), and they are now considered a universal feature in most microbial infections. These three-dimensional structures consist primarily of an extracellular polymeric substance (EPS) matrix, which encases the microbial cells and offers them protection. Biofilms are often made up of multiple microbial species, enabling nutrient sharing, horizontal gene transfer, and mutual support among the different organisms present (Gabrilska and Rumbaugh, 2015, Wolcott et al., 2013, Yao et al., 2022). Microbes within biofilms interact and cooperate to withstand environmental challenges, such as attacks from the immune system and exposure to antibiotics, and biofilms are widely implicated in the persistence of infections (Malone et al., 2017, Percival et al., 2018, Percival, McCarty and Lipsky, 2015, Wu, Cheng and Cheng, 2019, Zhao et al., 2013). This increased resistance is particularly evident when trying to control infected wounds, and a major reason why such wounds fail to heal even with antimicrobial intervention.

The biofilm matrix is composed of various elements, including polysaccharides, lipids, extracellular DNA, and a range of proteins, which together form a protective shield (known as EPS) around bacterial cells (Ragupathi et al., 2024, Karygianni et al., 2020). This matrix not only limits the penetration of antibiotics into the deeper layers of the biofilm but also serves as a physical barrier against immune system attacks, thereby helping bacteria evade immune destruction (Almatroudi, 2025, Jones and Wozniak, 2017). Within biofilms, bacteria are exposed to diverse microenvironments, resulting in variations in oxygen and nutrient levels. This leads to reduced metabolic activity in some cells (Zhang et al., 2021, Sønderholm et al., 2017), creating populations of dormant or persister cells that are highly tolerant to antibiotics (Zhang et al., 2021, Ayrapetyan, Williams and Oliver, 2018, Harms, Maisonneuve and Gerdes, 2016). Furthermore, when multiple species coexist within a biofilm, their differing resistance traits can be shared through horizontal gene transfer, while metabolic cooperation and increased production of virulence factors provide additional benefits (Michaelis and Grohmann, 2023, Sadiq et al., 2022). These combined factors make biofilms

significantly more resistant to antibiotics than free-floating (planktonic) bacteria, allowing the diverse microbial species in wounds to survive antimicrobial treatments (Almatroudi, 2025, Shree et al., 2023, Rahim et al., 2017). The biofilm lifestyle offers microbes enhanced protection from both immune clearance and antibiotic therapy, exacerbating inflammation in the wound environment (Versey et al., 2021, Lamret et al., 2020). The EPS matrix reduces microbial exposure by retarding and redistributing antimicrobial penetration, adsorbing and inactivating agents at the biofilm periphery, and physically and chemically sequestering host immune effectors—thereby lowering the effective concentrations that reach embedded cells and diminishing killing (Davenport, Call and Beyenal, 2014, Mulcahy, Charron-Mazenod and Lewenza, 2008, Pier et al., 2001). As a result, biofilms represent a major obstacle in wound care and significantly complicate the management of wound infections. Numerous studies have demonstrated that microorganisms often form biofilms within wounds (Darvishi et al., 2022, Azevedo et al., 2020, Hurlow et al., 2015, Malone et al., 2017). These biofilms typically consist of a mix of different species, including both aerobic and anaerobic bacteria, Gram-positive and Gram-negative organisms, as well as fungi (Percival et al., 2018, Wolcott et al., 2013, Gabrilska and Rumbaugh, 2015).

Research into wound-associated biofilms has accelerated through the use of various *in vitro*, *ex vivo*, and *in vivo* models (Vyas, Xia and Mai-Prochnow, 2022, Cárdenas-Calderón et al., 2022, Dhekane, Mhade and Kaushik, 2022, Jensen, Johansen and Jensen, 2017, Brackman and Coenye, 2015). These experimental systems have been invaluable in revealing how different species interact within polymicrobial biofilms, identifying important virulence factors, and illustrating the heightened antibiotic resistance seen in biofilms. Many of these models utilise two bacterial pathogens most frequently linked to wound infections, *Staphylococcus aureus* and *Pseudomonas aeruginosa* (Serra et al., 2015a, Vestweber et al., 2024). However, we now know that the wound microenvironment can harbour ten to hundreds of different microbial species. The following section will introduce the diverse nature of the chronic wound microbiome.

1.2.2 Wound microbiome

Infected chronic wounds harbour complex microbial populations, which include both opportunistic pathogens and normal skin flora. In chronic wounds, microorganisms are judged "pathogenic" when they are causing tissue damage and host response. This is evidenced by clinical infection, recovery of microorganisms from deep tissue/bone rather than surface, sufficient bioburden, tissue invasion with inflammation, expression of virulence or biofilm traits, and association with non-healing. Conversely, microorganisms detected only superficially or without host response are more likely colonizers or bystanders (Han et al., 2011, Kallstrom, 2014, Cortes-Penfield et al., 2023, Zhao et al., 2013, Senneville et al., 2024). Numerous investigations have examined the wound microbiome, revealing a wide variety of bacterial species present in different wound types (Johnson et al., 2018, Kalan et al., 2019, Liu et al., 2020, Wolcott et al., 2016). The specific makeup of these microbial communities varies depending on the wound's type, cause, and characteristics, and is further shaped by factors such as underlying health conditions, medications, lifestyle, and hygiene practices as discussed above. Despite the diversity seen among wound microbiomes, several key pathogens have been consistently identified in wound infections, such as *Staphylococcus* species particularly *S. aureus* and MRSA as well as *P. aeruginosa* (Verbanic et al., 2020, Bessa et al., 2015, Rahim et al., 2017, Tom et al., 2019, Kalan et al., 2019). *S. aureus* is frequently isolated from a range of wounds, including surgical, burn, and diabetic wounds (Mohammed et al., 2017, Tom et al., 2019, Jneid et al., 2017, Linz et al., 2023). Likewise, *P. aeruginosa* is commonly detected in wound infections of various origins (Besse et al., 2022, Phan et al., 2023, Rahim et al., 2017). Further research into wound microbiomes has revealed their polymicrobial nature, with other genera such as *Enterococcus* spp., *Escherichia coli*, *Klebsiella* spp., *Streptococcus* spp., *Acinetobacter* spp., *Corynebacterium* spp., and more also being identified (Jneid et al., 2017, Sloan et al., 2019, Uberoi, McCready-Vangi and Grice, 2024, Anju et al., 2022), with several more commonly reporting the presence of fungal pathogens such as *Candida* species as well (Verbanic et al., 2020).

The polymicrobial character of chronic wounds significantly affects healing trajectories. A structural equation model analysing chronic wounds revealed that

the microbiome composition contributes more significantly to variations in healing time than other clinical factors including patient age, wound size, and duration, explaining up to 46% of variation in healing outcomes (Ancira et al., 2025). This underscores the critical importance of understanding the collective microbial ecosystem rather than focusing on individual pathogens. The complex interactions between different species create intricate relationships including nutrient sharing, co-aggregation, and metabolic cooperation that enhance community resilience (Diban et al., 2023, Biswas, Ahmed and Mondal, 2024, Roque-Borda et al., 2025). For example, metabolic cooperation between aerobic and anaerobic species establishes oxygen gradients that protect obligate anaerobes while simultaneously strengthening overall community resistance (Verbanic et al., 2020, Lu and Imlay, 2021). Recent research also indicates that increased bacterial diversity and community stability correlate with poorer healing outcomes, challenging earlier assumptions about microbial diversity in wound environments (Verbanic et al., 2020, Kalan et al., 2016).

Chronic wound-host complex ecosystems where diverse microbial communities assemble under selection pressures from immunity, tissue perfusion, and exudate chemistry result in the generation of spatially and temporally distinct niches across the wound bed and within biofilms (Scales and Huffnagle, 2013). Resource and oxygen gradients promote spatial partitioning of taxa (e.g., aerobes at oxygenated interfaces and anaerobes in deeper layers), with biofilm architecture creating micro-niches that stabilize polymicrobial consortia and modulate function (Pouget et al., 2022b, Khalid et al., 2023). Interspecies interactions, including competition, mutualism, co-aggregation, and metabolic cross-feeding, coordinate community metabolism and virulence, enhancing resilience and tolerance that impede healing in wound environments (Durand et al., 2022, Pouget et al., 2022a). Community composition is dynamic, showing turnover and priority effects, and disturbances such as surgical or bedside debridement can reset community structure, underscoring the value of longitudinal, multifaceted profiling to link ecology with outcomes (Han et al., 2011, Misic, Gardner and Grice, 2014, Durand et al., 2022). Nonbacterial members (e.g., fungi) integrate into these communities and have been associated with delayed healing, reinforcing that chronic wound microbiota operate as a multispecies ecosystem rather than isolated pathogens (Kalan et al., 2016, Scales and Huffnagle, 2013).

1.2.3 Bacterial species in wounds

Several bacterial species have been consistently identified as key players in chronic wound infections (Ancira et al., 2025). The final structural equation model identified three species specifically associated with diminished healing: *Anaerococcus vaginalis*, *Finegoldia magna*, and *P. aeruginosa*. As discussed before, *P. aeruginosa* and *S. aureus* are particularly prevalent and frequently co-exist in chronic wounds, exhibiting synergistic relationships that enhance their survival and virulence (Serra et al., 2015b, Yung, Sircombe and Pletzer, 2021). In co-culture environments mimicking chronic wounds, *S. aureus* growth increases when cultured alongside *P. aeruginosa*, demonstrating bacterial cooperation (Pouget et al., 2022a). *In vivo*, recent research utilising RNA sequencing has demonstrated that *P. aeruginosa* actively expresses virulence genes in chronic wound environments, resulting in tissue destruction and impaired healing even at relatively low abundance (Karna et al., 2016).

Aerobic bacteria are predominant colonisers in chronic wound infections, with a reported prevalence of 82% in clinical samples (Kulayta et al., 2024). The most frequently isolated aerobic pathogens include *S. aureus*, *P. aeruginosa*, *Klebsiella* species, and *Streptococcus* species, which collectively account for the majority of chronic wound infections (Diban et al., 2023, Mengesha et al., 2014, Rahim et al., 2016). In post-surgical wound infections, *S. aureus* represents approximately 35.77% of isolates, followed by *Klebsiella* species (22.76%) and coagulase-negative *staphylococci* (14.63%), highlighting the consistent dominance of these pathogens across various wound types (Mengesha et al., 2014). Similarly, in DFUs and other chronic wounds, *P. aeruginosa* (27%), *K. pneumoniae* (16%), *Staphylococcus* species (14%), and *Streptococcus* species (13%) are the predominant isolates (Rahim et al., 2016). These findings demonstrate that while the specific distribution may vary by wound type and severity, a relatively consistent group of aerobic pathogens tends to colonize chronic wounds.

Aerobic colonisers may predominate initially. As wounds become chronic, the environment becomes predominantly hypoxic or anoxic, creating ideal conditions for anaerobic bacterial growth and persistence (Coluccio, Lopez Palomera and Spero, 2024, Kim et al., 2024). These oxygen-limited conditions drive the composition and behaviour of the wound microbiota, with obligate anaerobes

being among the most prevalent taxa colonising established chronic wounds, yet their significance is often underappreciated in clinical practice (Coluccio, Lopez Palomera and Spero, 2024). Molecular analysis of wound samples has confirmed the consistent presence of anaerobic bacteria in non-healing wounds, with multiple studies identifying diverse anaerobic communities using next-generation sequencing technologies (Hussain, Rathnayake and Huygens, 2016). The predominant anaerobic organisms in chronic wounds include members of the *Bacteroides* spp., *Peptostreptococcus* spp., *Finegoldia* spp., *Peptoniphilus* spp., *Porphyromonas* spp., and *Prevotella* genera, which frequently co-exist with the more commonly identified aerobic species (Coluccio, Lopez Palomera and Spero, 2024, Villa et al., 2024, Hussain, Rathnayake and Huygens, 2016). This polymicrobial reality highlights the importance of considering both aerobic and anaerobic components when managing chronic wound infections.

1.2.4 Fungal species in wounds

Chronic wounds represent a significant global health challenge, with fungi playing a substantial but often underestimated role in their pathogenesis and persistence. Studies have revealed that approximately 23% of 915 chronic wounds, including DFUs, pressure ulcers, non-healing surgical wounds, and VLUs, test positive for fungal species (Kalan et al., 2016, Ge and Wang, 2023). Despite this significant presence, fungi are frequently overlooked in clinical treatment strategies, leading to persistent infections and delayed healing outcomes (Short et al., 2023, Kalan and Grice, 2018).

Similar to the bacterial populations, the fungal composition in chronic wounds is diverse and complex. The most abundant fungi isolated from these wounds are yeasts from the *Candida* genus, particularly *Candida albicans*, which has been identified as one of the most important wound fungal pathogens (Kalan and Grice, 2018, Short et al., 2023, Ge and Wang, 2023). However, other non-conventional fungi found in chronic wounds include species from genera such as *Curvularia* spp., *Malessezia* spp., *Aureobasidium* spp., *Cladosporium* spp., *Ulocladium* spp., *Engodontium* spp., *Trichophyton* spp., *Aspergillus* spp., and *Fusarium* spp. (Chahal et al., 2021, Short et al., 2023). This diversity highlights the complex fungal ecology present in chronic wounds and suggests that the fungal component

of chronic wound infections is more varied than previously recognised (Kalan et al., 2016).

Fungi in chronic wounds contribute significantly to the formation of biofilms. These biofilms can be polymicrobial and interkingdom in nature, involving both bacteria and fungi in complex interactions (Cox et al., 2024, Short et al., 2023). For instance, *C. albicans* can provide a scaffold for bacterial attachment and proliferation, as demonstrated in studies of inter-kingdom interactions (Morsli et al., 2024, Kalan et al., 2016). The presence of *C. albicans* in multi-species biofilms has been shown to drive the recalcitrant nature of the biofilm, where antimicrobial treatments merely influence biofilm composition rather than reducing overall biofilm biomass (Morsli et al., 2024, Short et al., 2023). This interaction between fungi and bacteria contributes to the microbial bioburden of wounds and ulcers, further complicating treatment approaches (Short et al., 2023).

The presence of fungi in chronic wounds has significant clinical implications. Fungal communities in chronic wounds are frequent, dynamic, and linked to delayed healing. Pathogenic yeasts and moulds can form biofilms, exploit necrotic niches, and modulate host inflammation. In addition, changes in metabolic states in conditions such as diabetes that can lead to uncontrolled ketoacidosis and elevated available iron further predispose such individuals to invasive *Mucorales* spp. underscoring the need to interpret fungi within wound ecology and host context for balanced management (Ibrahim et al., 2012, Alqarihi, Kontoyiannis and Ibrahim, 2023, Kalan et al., 2016, Kalan and Grice, 2018). Uncontrolled diabetic ketoacidosis (DKA) creates a permissive niche for *Mucorales* spp.; acidosis and hyperglycaemia increase available serum iron and impair phagocyte function, which together heighten susceptibility to invasive mucormycosis (Kumar et al., 2014). Wounds that ultimately required more than 8 weeks to heal had a significantly higher abundance of *Ascomycota* fungi at the initial time point, compared to wounds that healed in less than 8 weeks (Kalan et al., 2016, Kalan and Grice, 2018).Notably, not all detected fungi are equal; pathogenic yeasts and moulds tend to associate with necrotic tissue and adverse outcomes, whereas some allergenic filamentous fungi correlate with lower systemic inflammation, potentially blunting systemic markers despite local pathology, so interpretation

must integrate clinical signs and sampling depth (Kalan et al., 2016). This finding suggests a potential link between the presence of certain fungal communities (like *Ascomycota* spp.) and delayed wound healing, and it raises the possibility that the composition of the wound microbiome could influence or predict wound healing outcomes. Pathogenic fungi like *Candida* spp. and *Fusarium* spp. are strongly associated with necrotic tissue, likely due to protease activity and biofilm formation, while allergenic filamentous fungi (e.g., *Aspergillus* spp., *Cladosporium* spp.) correlate with reduced systemic inflammation, potentially masking infection severity (Kalan et al., 2016). In diabetics with poor glycaemic control, especially DK, clinicians should consider invasive *Mucorales* spp. risk in addition to *Candida* spp. biofilm contributions, with attention to iron status and host metabolic parameters that modulate fungal virulence and invasion (Alqarihi, Kontoyiannis and Ibrahim, 2023, Ibrahim et al., 2012). Because fungal biofilms and interkingdom communities underpin persistence, management benefits from combined debridement, targeted antimicrobials/antifungals, and correction of host metabolic drivers (e.g., ketoacidosis) to shift the wound ecosystem toward healing (Gebremariam et al., 2016, Kalan et al., 2016).

Directed culturing of wounds stably colonised by pathogens has revealed that interkingdom biofilms formed between yeasts and co-isolated bacteria, further complicating the management of these infections (Kalan et al., 2016, Ge and Wang, 2023). Recent profiling of diabetic ulcers revealed fungi in 62% of cases, far exceeding culture-based detection, with *Candida* spp. and *Aspergillus* spp. frequently forming interkingdom biofilms alongside bacteria like *S. aureus* (Allkja et al., 2025). These polymicrobial consortia exhibit shared antibiotic resistance mechanisms and enhanced tolerance to therapies, exacerbating inflammation and delaying recovery. Together, these findings underscore fungi as under recognised contributors to chronicity, necessitating dual-targeting approaches for biofilm disruption and improved diagnostics.

Proper diagnosis and treatment of fungal infections in chronic wounds are essential for effective management. The high relative abundance of fungi within the polymicrobial ecology of wound infections suggests that, when fungi are present, they can be major contributors to the bioburden or biofilm of wounds (Kalan et al., 2016, Uberoi, McCready-Vangi and Grice, 2024). Furthermore, the

diversity of fungal genera and species represented in and among such wounds is higher than previously suspected or reported (Short et al., 2023). This underscores the importance of comprehensive diagnostic approaches that can identify the full spectrum of fungal pathogens present in chronic wounds (Morsli et al., 2024).

Within the context of healthcare environments, other fungal pathogens carry nosocomial threats for open, non-healing wounds. One such example, *Candida auris*, represents an emerging concern in the context of chronic wounds. This multidrug-resistant fungus poses a serious global health threat, causing severe infections with high mortality rates in hospitalised patients with significant underlying comorbidities (Sanyaolu et al., 2022, Malik et al., 2024, Tajane, Pawar and Patil, 2024). *C. auris* efficiently colonises the skin and can contaminate the patient's environment, leading to healthcare-associated outbreaks (Tajane, Pawar and Patil, 2024, Eix and Nett, 2022, Sanyaolu et al., 2022). Risk factors for *C. auris* colonisation and infection include chronic wounds, prior broad-spectrum antibiotic use, and indwelling devices (Southwick et al., 2018, Truong et al., 2023). A study from New York State found that patients who progressed from *C. auris* colonisation to bloodstream infection all had chronic wounds at the time of bloodstream infection (Southwick et al., 2018). Therefore, the emergence of *C. auris* in healthcare settings represents a significant public health concern, particularly for patients with chronic wounds who may be more susceptible to colonisation and subsequent infection with this difficult-to-treat pathogen (Sanyaolu et al., 2022, Tajane, Pawar and Patil, 2024). Careful consideration of all opportunistic fungal pathogens are required when trying to treat and control wound infections.

1.2.5 Biofilm implications on the host

The physical and chemical characteristics of the wound environment significantly influence microbial behaviour and contribute to infection persistence (Jakobsen et al., 2025, Uberoi, McCready-Vangi and Grice, 2024). Research has demonstrated that chronic wounds typically develop altered pH levels and oxygen gradients that favour certain microbial species and biofilm formation (Jakobsen et al., 2025, Jo, Price-Whelan and Dietrich, 2022). These variations create distinct microniches within the wound that support different microbial communities (Jakobsen et al., 2025, Uberoi, McCready-Vangi and Grice, 2024).

Chronic wounds are host-associated microbial ecosystems in which abiotic filters, oxygen tension, pH, temperature, moisture, micronutrients, and redox state. These elements structure heterogeneous niches that are differentially occupied by interacting microbial communities (Tomic-Canic et al., 2020, Pereira et al., 2017). Within these ecosystems, gradients and patchiness drive community assembly and spatial partitioning, with aerobes favoured at oxygenated interfaces and anaerobes persisting in hypoxic layers created by biofilm architecture and tissue depth (Pouget et al., 2022b, Khalid et al., 2023). Community interactions (competition, mutualism, co-aggregation, quorum signalling, and metabolic cross-feeding) produce emergent ecosystem properties—tolerance, resilience, and virulence expression, that sustain inflammation and impede repair (Durand et al., 2022). Wound-like physicochemical conditions, including elevated oxidative stress and altered pH/redox, act as abiotic filters that reduce diversity, accelerate biofilm assembly, and stabilize dysbiotic states adapted to the wound niche (Kim et al., 2020). Assembly dynamics and stability matter for outcomes: temporally stable, entrenched communities are associated with non-healing trajectories, whereas shifts in composition following ecological disturbance can align with improved healing (Loesche et al., 2017). Clinically, sharp debridement functions as an ecosystem-level disturbance that perturbs community structure (for example, depleting anaerobes) and, in concert with optimized host factors, can redirect succession toward states more compatible with healing (Kalan et al., 2019). Accordingly, interventions should be framed as ecological management, modulating abiotic filters and applying targeted disturbances, so that ecosystem function is steered from a persistent, dysbiotic biofilm state toward a reparative state that supports tissue regeneration (Liu et al., 2020, Pereira et al., 2017).

Laboratory studies have shown that bacteria form biofilms faster in wound-like environments compared to standard laboratory media, indicating that the wound environment actively promotes biofilm development (Verbanic et al., 2020, Kadam et al., 2021). Research using microelectrodes to measure oxygen levels within wounds has revealed steep oxygen gradients, with oxygen concentration decreasing significantly with depth from the wound surface, creating distinct aerobic and anaerobic zones that support diverse microbial communities (Jakobsen et al., 2025). Temperature variations also arise within wounds further influencing microbial metabolism and biofilm development. These

microenvironmental factors represent important considerations in understanding chronic wound microbiology and developing effective treatments (Verbanic et al., 2020, Uberoi, McCready-Vangi and Grice, 2024).

The host inflammatory response plays a crucial role in the pathophysiology of chronic wounds (Raziyeva et al., 2021). Unlike acute infections characterised by host-controlled inflammation, chronic wound infections involve microbe-controlled inflammation, which results in ongoing tissue damage rather than healing (Hurlow and Bowler, 2022a). In chronic wound environments, biofilms trigger the accumulation of neutrophils that attempt but fail to phagocytose bacterial cells within the protective biofilm matrix (Hurlow and Bowler, 2022a, Raziyeva et al., 2021). However, these neutrophils continue to release enzymes and oxygen metabolites that damage surrounding host tissue while the biofilm persists (Hajdamowicz et al., 2019). Recent research describes this as "biofilm-hijacked host inflammation," where wound biofilm manipulates the host inflammatory response by upregulating pro-inflammatory cytokines and inducing a persistent, tissue-destructive immune response (Hurlow and Bowler, 2022a). The resulting exudate production and accumulation of devitalised tissue provides continuous nutrients for the biofilm, creating a self-sustaining cycle that promotes chronicity (Rathna and Kulandhaivel, 2024). This series of events contrasts sharply with the immune response to acute infections, where planktonic bacteria actively invade tissues, and the host response effectively controls and eliminates the pathogens (Hakansson, Orihuela and Bogaert, 2018). Taken together, this highlights the complex host-pathogen nature of biofilm-infected wounds.

1.3 Biofilms: microbial protagonists in chronic wounds

The preceding sections have introduced the extensive diversity of the chronic wound microbiome. However, focus of any microbial biofilm research is often on individual organisms, and this section will highlight mechanisms utilised during biofilm formation of three common microbial pathogens found in chronic wounds *P. aeruginosa*, *S. aureus* and *C. albicans*, with consideration of *C. auris* as well due to its presence in nosocomial environments. It is of course noteworthy, that in their natural habitats, biofilms consist of a wide range of species, such as bacteria, fungi, archaea, and viruses (Flemming and Wuertz, 2019, Zhao, Sun and

Liu, 2023). In addition, from a host perspective, components such as minerals, platelets, and RBCs are also often found in these biofilms as their maturity increases (Moser et al., 2017, Pugazhendhi et al., 2022).

All biofilms develop through distinct phases, culminating in a complex three-dimensional architecture of microbial communities (Figure **1.2**) (Sauer et al., 2022). Within biofilms, microorganisms utilise quorum sensing (QS) for intercellular communication, enabling them to function as a unified entity (Wong et al., 2021). All bacteria can participate in biofilm formation, certain species such as *staphylococci*, *streptococci*, and *pseudomonas* show a particular propensity for the biofilm lifestyle (Zhao, Sun and Liu, 2023). Additionally, dimorphic *Candida* fungi are often associated with biofilm-related infections (Ponde et al., 2021).

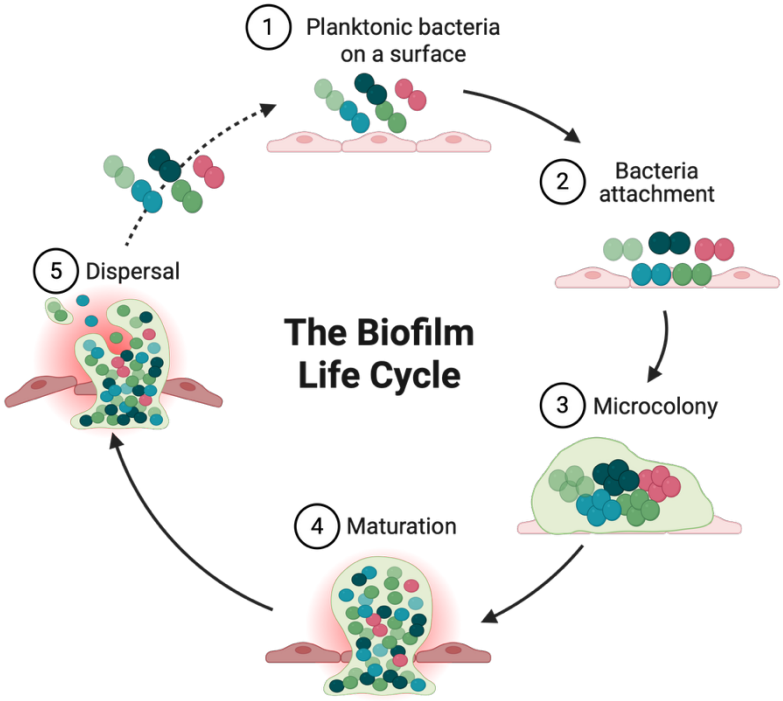

Figure 1.2**: Diagrammatic illustration depicting the biofilm development stages of a single bacterial species.** (1) Initial adhesion, planktonic bacteria reversibly attach to surfaces, influenced by environmental factors like nutrient availability, pH, and temperature; (2) Cluster formation, Bacteria aggregate and establish irreversible, permanent attachment; (3) Matrix production: microcolonies emerge as bacteria secrete EPS, forming a protective matrix. Polysaccharides released by biofilm-forming strains enhance surface adherence, aggregation, and colonisation; (4) Structural maturation: Biofilms develop complex three-dimensional architectures anchored by self-synthesized extracellular matrix components. (5) Dispersion; mature biofilms release bacterial cells, reverting them to a free-floating planktonic state to spread and colonise new sites (Sharma et al., 2023). Diagram was created in BioRender.

1.3.1 *S. aureus* biofilms

S. aureus biofilm infections represent a significant global health challenge, with approximately 20-41% of the world's population either transiently or permanently colonised by this pathogen (Bhattacharya and Horswill, 2024). These bacterial communities form structured environments that shield bacteria from antimicrobial treatments and host defences. Research indicates that biofilm-associated multi-drug resistance among healthcare-associated infections ranges from 17.9% to 100% worldwide, with 80% of nosocomial infections attributed to biofilm-association (Assefa and Amare, 2022). *S. aureus* biofilms are implicated in numerous clinical conditions including prosthetic joint infections, chronic rhinosinusitis, skin and soft tissue infections, urinary tract infections (UTI), cystic fibrosis (CF) airway infections, and infective endocarditis (Eiselt, Bereswill and Heimesaat, 2024, Magalhães et al., 2022). Regional variations are notable, with studies across 71 countries on 6 continents revealing significant differences in *S. aureus* treatment practices (Westgeest et al., 2023). In Nepal, 81.4% of *S. aureus* isolates were MRSA with most capable of forming biofilms (Manandhar et al., 2018), while Polish research found 91% of MRSA strains harboured the icaD gene responsible for biofilm formation (Grinholc, Wegrzyn and Kurlenda, 2007). Laboratory studies indicate between 47% of MRSA and 69% of methicillin-sensitive *S. aureus* (MSSA) strains produced biofilm *in vitro* (Grinholc, Wegrzyn and Kurlenda, 2007). In the United States, MRSA infections result in over 19,000 deaths annually, surpassing human immunodeficiency virus (HIV) mortality (Bhattacharya and Horswill, 2024). The clinical impact is compounded when *S. aureus* biofilms form on medical devices, creating persistent infections that are tolerant to approximately 1000 times the clinically prescribed dose of antibiotics (Bhattacharya and Horswill, 2024).

S. aureus and other *staphylococci* are frequently implicated in biofilm infections associated with medical devices (Oliveira et al., 2018, Zheng et al., 2018). A significant proportion of *S. aureus* clinical isolates, including MRSA, have demonstrated biofilm-forming capabilities, with evidence suggesting that drug-resistant strains may be more prone to biofilm formation (Craft et al., 2019, Neopane et al., 2018). The initial adhesion of *S. aureus* during biofilm formation is primarily mediated by proteins such as polysaccharide intercellular adhesin

(PIA), expressed from the icaADBC operon (Arciola et al., 2015, Peng et al., 2022). In mature biofilms, extracellular DNA (eDNA) plays a more significant structural role than PIA (Campoccia, Montanaro and Arciola, 2021, Sharma and Rajpurohit, 2024). External factors, such as the anticoagulant heparin, can stimulate *S. aureus* biofilm formation on surfaces like catheters by enhancing cell-to-cell interactions and surface adhesion (Pugazhendhi et al., 2022, Francolini et al., 2017). As biofilms mature, *S. aureus* cells undergo metabolic changes, evidenced by the increased appearance of small colony variants (SCVs) with reduced treatment susceptibility (Tuchscherr, Löffler and Proctor, 2020, Kahl, Becker and Löffler, 2016). The biofilm community is coordinated by the accessory gene regulator (agr) QS system, which responds to extracellular auto-inducing peptides (AIP, QS molecule) (Wang, Bian and Wang, 2022, Aboelnaga et al., 2024). Gene expression in biofilms differs from planktonic cells, with upregulation of genes related to the cell envelope, including synthesis of binding factors, peptidoglycan, and PIA, as well as detoxification of metabolites and reactive oxygen species (Aboelnaga et al., 2024). Conversely, planktonic cells show upregulation of virulence factors such as toxins and proteases, suggesting a more aggressive infection course with the potential to spread (Johnson, 2018). (Kamble and Pardesi, 2021, Craft et al., 2019). This resistance is partially attributed to drug diffusion barriers in the extracellular matrix, and the extent of this effect varies by drug type. For instance, ß-lactams and glycopeptides struggle to fully penetrate the biofilm, while aminoglycosides and fluoroquinolones can penetrate more effectively (Kranjec et al., 2021). This suggests that factors beyond poor antimicrobial penetration contribute to *S. aureus* recalcitrance in biofilms. These biofilms also demonstrate resistance to the human immune system. While leukocytes can bind and penetrate the biofilm, they are unable to engulf the bacteria within (Arciola, Campoccia and Montanaro, 2018, de Vor, Rooijakkers and van Strijp, 2020), further highlighting the complex nature of *S. aureus* biofilm infections and their resistance to host defences.

S. aureus plays a central role in chronic wound infections, frequently emerging as one of the most common pathogens isolated from these wounds (Serra et al., 2015b, Morguette et al., 2023). Its capacity to form robust biofilms on wound surfaces contributes to delayed healing, persistent infection, and increased resistance to antibiotics, especially in the case of MRSA strains (Morguette et al.,

2023, Simonetti et al., 2022). *S. aureus* often coexists with other bacteria, such as *P. aeruginosa*, in chronic wounds, and these polymicrobial interactions further enhance biofilm formation, virulence, and antimicrobial tolerance, making infections more difficult to treat (Keim et al., 2024, Serra et al., 2015b). The chronicity and severity of wounds infected with *S. aureus* underscore the need for effective management strategies, as these infections are associated with significant morbidity and healthcare costs worldwide.

1.3.2 *P. aeruginosa* biofilms

P. aeruginosa biofilm infections pose a substantial global health burden, with biofilm formation observed in 75.9% to 93% of clinical isolates across diverse geographical regions (Rajabi et al., 2022). Regional studies highlight variations, such as Egypt reporting biofilm production in 89.4% of isolates from hospital settings (Edward et al., 2023), while Cameroonian healthcare facilities identified the pathogen in diverse samples including pus, wounds, and blood (Tchuedji et al., 2024). These infections dominate critical clinical contexts, accounting for 49-74% of ventilator-associated pneumonia cases, 72% of catheter-associated urinary tract infections, and 52.2% of surgical site infections globally (Heidari et al., 2022, de Sousa et al., 2023). Vulnerable populations include CF patients, among whom *P. aeruginosa* biofilms cause 70-80% of chronic lung infections linked to high morbidity, and immunocompromised individuals facing 44-60% multidrug resistance rates in biofilm-associated strains (Elfadadny et al., 2024, Soltani Borchaloee et al., 2024). Carbapenem-resistant variants exhibit particularly alarming profiles, with 95% demonstrating multidrug resistance and 72% showing resistance patterns in nosocomial environments (Soltani Borchaloee et al., 2024, Heidari et al., 2022). Treatment complexities are exacerbated by persister cell phenotypes, which survive antibiotic concentrations 100-fold above minimum inhibitory levels in 8% of clinical isolates, contributing to the 20-30% failure rates observed in chronic wound management (Žiemytė et al., 2021, Cai and Webb, 2020). The convergence of extensive biofilm-mediated antibiotic tolerance and rising resistance underscores the pathogen's clinical persistence across healthcare systems worldwide (Edward et al., 2023).

P. aeruginosa has the ability to form biofilms in various medical contexts, including CF lungs (Tajdari, 2024, Juntke et al., 2021), ventilator-associated pneumonia (Ma'aitah, 2024), catheter-associated urinary tract infections (Hou et al., 2022, El Husseini, Carter and Lee, 2024), and on other medical devices such as orthopaedic implants (De Soir et al., 2024), renal catheters (Kadhim, 2024), and wound dressings (Yadav, Pawar and Patil, 2025). Recent review highlight the structural complexity and clinical persistence of these biofilms (Ma'aitah, 2024). The process of *P. aeruginosa* biofilm formation begins with surface attachment, primarily facilitated by flagella and type IV pili, with recent studies emphasising the role of Psl polysaccharides in mediating initial adhesion (Davis and Horzempa, 2024, Sánchez-Peña et al., 2024). As cell density increases, microcolonies form through twitching motility enhanced by pilin glycosylation (Davis and Horzempa, 2024), eventually developing into complex mushroom-like structures regulated by cyclic di-GMP signalling (Hu, Webb and An, 2023). The biofilm matrix is a highly organised structure composed of polysaccharides and alginate, which are strategically located to support the overall architecture (Ma'aitah, 2024, Egorova et al., 2022, Labadie et al., 2024). Within *P. aeruginosa* biofilms, the las and rhl QS systems operate as a reciprocal signalling network rather than a strict hierarchy (Thomas et al., 2023), coordinating virulence factor production (e.g., elastase, pyocyanin) through 3-oxo-C12-HSL and C4-HSL autoinducers (Cao et al., 2025, Mirpour and Zahmatkesh, 2024). Pharmacological inhibition of QS via trigonelline hydrochloride (Kar et al., 2024) or ketoprofen (Mirpour and Zahmatkesh, 2024) has been shown to reduce biofilm formation and virulence factor expression, while synergistic approaches combining QS interference with phage therapy demonstrate enhanced antimicrobial efficacy (Cao et al., 2025, Maset et al., 2023). The EPS confers multidrug resistance through physical barrier formation, efflux pump activation (Yang, Xu and Liang, 2024), and metabolic adaptations such as persister cell development (Hu, Webb and An, 2023). Matrix components like eDNA and α-polysaccharides reduce treatment efficacy by shielding cells from UV-C irradiation (Labadie et al., 2024) and antibiotic penetration (Yadav, Pawar and Patil, 2025). Different studies reveal organised dispersal mechanisms involving alginate lyase activity (Skariyachan et al., 2018) and QS-regulated biofilm differentiation (Ma'aitah, 2024), which enable pathogen dissemination to new niches.

P. aeruginosa is a major contributor to chronic wound infections worldwide, consistently ranking as the second most common pathogen isolated from such wounds across most continents and even surpassing other bacteria in certain regions like Southeast Asia (Phan et al., 2023). Its ability to form robust biofilms, especially in combination with *S. aureus*, leads to increased persistence, enhanced resistance to treatment, and greater wound chronicity (Keim et al., 2024, Bhattarai and Christopher, 2025). These biofilm communities protect *P. aeruginosa* from both antibiotics and the host immune system (Fleming et al., 2022), making infections difficult to eradicate and contributing to prolonged healing times and higher morbidity in affected patients.

1.3.3 *Candida* biofilms

Fungal infections are becoming increasingly widespread, now affecting a billion of the global population (Mancuso et al., 2022). These diseases are responsible for over 1.5 million deaths each year, underscoring their significant impact on public health (Rodrigues and Nosanchuk, 2023). In response to the growing threat, the World Health Organization (WHO) released a priority list of 19 fungal pathogens on October 2022, ranking them as critical, high, or medium threats based on their risk to human health (De Gaetano et al., 2024). Among these, species from the genus *Candida* are recognised as the most frequent culprits behind invasive fungal infections worldwide (De Gaetano et al., 2024).

C. albicans biofilms remain a dominant clinical concern, implicated in 70.6-73.9% of invasive candidiasis cases globally, with systemic infections exhibiting mortality rates up to 60% (Jabbar Al-sabti and Hussain Shabaa, 2024, Parambath et al., 2024). However, other *Candida* species post a significant healthcare risk as well. Recent surveillance reveals regional shifts, as *C. auris* now accounts for 32% of *Candida* bloodstream infections in Saudi Arabia compared to 20% for *C. albicans*, while New York City hospitals report *C. auris* comprising 17% of candidemia cases versus 29% for *C. albicans* (Singh, Malik and Lal, 2024, Ahmed et al., 2025). Biofilm-forming strains demonstrate heightened clinical persistence, with 73.9% of *C. albicans* isolates producing biofilms in South India and 95.5% of *C. auris* infections linked to biofilm-contaminated Intensive Care Unit (ICU) environments (Mohanraj, Vinodhini and Vajravelu, 2024, Alasmari et al., 2025).

Antimicrobial resistance patterns diverge sharply: *C. albicans* exhibits 35.8% fluconazole resistance, whereas *C. auris* shows near-universal resistance (97.4%) to this azole alongside 67.1% amphotericin B resistance (Sokou et al., 2024). Geographically, *C. auris* has formed four distinct clades across six continents, with the South American clade demonstrating 96% mortality in murine models, compared to 44-80% for other lineages (Forgács et al., 2020). Biofilm-mediated treatment failures affect 20-30% of chronic candidiasis cases, driven by matrix-enclosed persister cells and upregulated efflux pumps in both species (Kean and Ramage, 2019, Gao et al., 2024). Taken together, *Candida* biofilms result in an extra level of complexity when considering interkingdom infections of chronic wounds.

1.3.3.1 *C. albicans* biofilms

Fungal biofilm infections are predominantly caused by *Candida* species, as extensively reviewed in different studies of clinical isolates and polymicrobial interactions (Kean et al., 2018a, Chong et al., 2018). These organisms demonstrate a remarkable ability to form biofilms on various medical devices, including central venous catheters (McCafferty et al., 2018), urinary catheters (Larkin, Dharmaiah and Ghannoum, 2018), joint prostheses (Viehman et al., 2018), cardiovascular devices (Viehman et al., 2018, McCafferty et al., 2018), and dialysis-related equipment (McCafferty et al., 2018). Notably, *C. albicans* are associated with significant mortality in device-related infections, particularly in cases involving multidrug-resistant strains (Viehman et al., 2018, McCafferty et al., 2018).

The process of biofilm formation involves several critical stages. Initial attachment is facilitated by cell surface hydrophobicity (Chong et al., 2018) and specific adhesion proteins regulated by transcriptional networks (Chong et al., 2018, Nett, 2018). As the biofilm develops, *C. albicans* undergoes a morphological transition from yeast cells to hyphae, a process modulated by QS molecules and epigenetic factors (Chong et al., 2018, Nett, 2018). This transformation is further regulated by cyclic AMP signalling pathways and biofilm-specific gene clusters (Chong et al., 2018).

The hyphal cells within the biofilm are encased in a self-produced EPS composed of polysaccharides, eDNA, and immunomodulatory proteins (Kean et al., 2018a, Chong et al., 2018). The EPS contributes to biofilm resilience by shielding cells from antifungals and host immune responses (Kean et al., 2018a, Nett, 2018). High biofilm-forming strains exhibit enhanced hyphal production, which correlates with overexpression of virulence factors such as secreted aspartyl proteases and phospholipases (Nett, 2018, Chong et al., 2018).

Numerous studies have demonstrated that *C. albicans* biofilms exhibit reduced susceptibility to antimicrobial treatments compared to their planktonic counterparts (Ramage et al., 2012, Larkin, Dharmaiah and Ghannoum, 2018). This resistance is attributed to several factors, similar to those observed in bacterial biofilms. These include the protective effects of the EPS, the presence of efflux pumps, the formation of persister cells, stress responses, increased cell density, and the overexpression of drug targets (Ramage et al., 2012, Chong et al., 2018). Emerging research highlights the role of *Candida* biofilm heterogeneity in driving therapeutic failure, particularly in infections involving non-albicans species or polymicrobial communities (Kean et al., 2018a).

C. albicans is a significant contributor to chronic wound infections, largely due to its robust ability to form biofilms on wound surfaces (Pereira et al., 2021). These biofilms protect the fungus from antifungal treatments and the host immune response, making infections persistent and difficult to eradicate (Fan et al., 2022). *C. albicans* is also highly adaptable, capable of switching between different morphological forms and thriving in diverse host environments (Alves et al., 2020), which further enhances its pathogenicity in chronic wounds. Chronic infections involving *C. albicans* are associated with increased morbidity, prolonged healing times, and greater healthcare costs, as the organism's biofilm-related resilience often leads to treatment failures and recurrent infections (Almatroudi, 2025). Consequently, exploring new therapeutic approaches are needed to improve outcomes in patients with chronic wounds infected by *C.* albicans.

1.3.4 Inter-kingdom interactions

The clinical prevalence of mixed inter-kingdom biofilm populations, comprising aggregates of bacteria and fungi, has gained increasing recognition in recent years. This growing awareness is reflected in the gradual expansion of literature addressing this important yet under-recognised clinical entity (Deveau et al., 2018a, Eichelberger et al., 2023). However, progress in this field has been somewhat hindered by the lack of appropriate tools to fully elucidate the intricacies of the microbial interactome: the mapped network of microbe–microbe and microbe–host interactions; physical, chemical, and signalling that structure chronic wound communities and influence healing trajectories (Pereira et al., 2017, Durand et al., 2022). Historically, conventional microbiological approaches have been the primary means of unravelling the significance of specific bacterial-bacterial and fungal-bacterial interactions (Ramage et al., 2017, Arzmi et al., 2015, Marin et al., 2022). However, the advent of molecular techniques, OMICs technologies, and advanced optical methods has revolutionised our ability to study these complex microbial communities. QS has emerged as a crucial mechanism for regulating these microbial communities. Signalling molecules involved in QS can affect other species and kingdoms, facilitating a form of inter-microbial communication (Shastry and Rekha, 2021, He et al., 2023). This concept is central to sociomicrobiology: how microorganisms behave, interact, and function collectively as a community, with a focus on the social aspects of microbial life, and underpins the ability of microorganisms to function as a community within polymicrobial biofilms (Xavier, 2016, Deo et al., 2024). The importance of polymicrobial interactions is underscored by their potential to synergistically enhance the pathogenic potential of constituent microorganisms (Stacy et al., 2014, Smith et al., 2015, Eichelberger et al., 2023), or to provide mutual antimicrobial protection. These observations highlight the necessity of adopting a dual approach to microbial analysis, considering both bacterial and fungal components simultaneously (Deveau et al., 2018b, Kahl et al., 2023).

1.3.5 Fungal-staphylococcal interactions

The human body serves as a host to various microbial communities, among which *Candida* species and *S. aureus* are frequently found in close association. These microorganisms have been jointly isolated from a spectrum of infections, ranging

from superficial conditions like angular cheilitis to more severe systemic and bloodstream infections (Hernandez-Cuellar et al., 2022, Dühring and Schuster, 2024). The healthcare sector has placed significant emphasis on these pathogens due to their biofilm-forming capabilities and the increasing prevalence of antimicrobial-resistant strains (Rodrigues, Gomes and Rodrigues, 2019). Research has revealed that the relationship between *Candida* species and *S. aureus* extends beyond mere co-isolation. Studies have demonstrated their ability to interact and form co-aggregates (Khan et al., 2021, Peters et al., 2012). While the exact nature of their association remains a subject of ongoing investigation, a growing body of evidence points towards a symbiotic relationship. This partnership appears to enhance the pathogenic potential of both organisms and contribute to increased disease severity (Peters and Noverr, 2013, Schlecht et al., 2015, Eichelberger and Cassat, 2021). In contrast, recent *in vitro* study highlighted the interaction between *C. auris* and (S. *aureus*/ *S. epidermidis*) in dual species biofilm did not enhance *C. auris* tolerance to antiseptics, with no evidence of synergistic resistance (Gülmez et al., 2022). This contrasts sharply with documented *Staphylococcus-C. albicans* interactions, which mutually amplify virulence in both organisms.

The interactions between *C. albicans* and *S. aureus* that led to enhanced pathogenicity have been extensively studied and summarised in (Figure 1.3) (Nair et al., 2014, Eichelberger and Cassat, 2021). Within polymicrobial biofilms, *S. aureus* cells have been observed to adhere to the hyphal filaments of *C. albicans* (Hernandez-Cuellar et al., 2022, Lin et al., 2013). However, the spatial organisation of these species within the biofilm structure remains a subject of debate. Some studies suggest that both organisms are distributed throughout the three-dimensional biofilm structure (Lin et al., 2013), while others have observed co-aggregation primarily in the uppermost layers of cells (Baxter et al., 2024). These discrepancies may be attributed to variations in experimental conditions, such as growth media. The synergistic relationship between *C. albicans* and *S. aureus* is most pronounced when both organisms colonise simultaneously. Interestingly, pre-existing *S. aureus* biofilms have demonstrated resistance to *C. albicans* colonisation, and the underlying mechanism remains unclear (Lin et al., 2013, Kong et al., 2016).

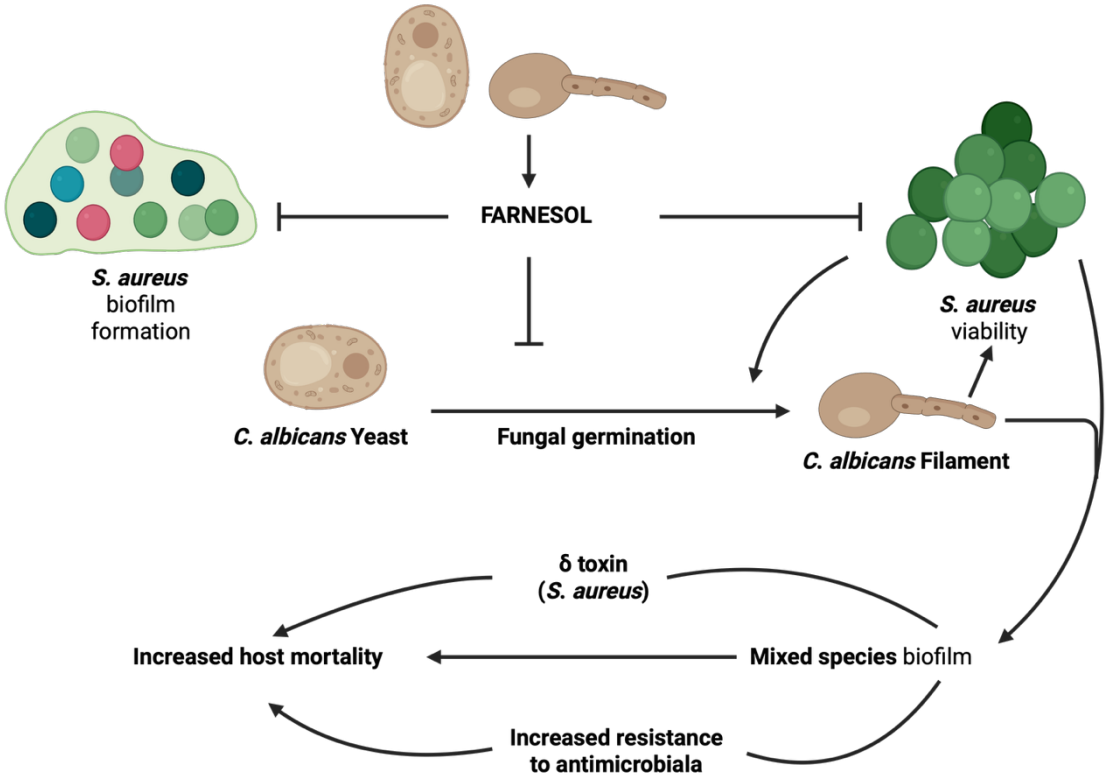

Figure 1.3: Interactions between Staphylococcus and Candida Species. *C. albicans* produces farnesol, a compound that reduces *S. aureus* biofilm development and compromises bacterial cell survival. However, *S. aureus* selectively attaches to *C. albicans'* hyphal structures, which improves its ability to persist. When these two pathogens form a mixed biofilm together, their combined interaction increases both infectious potential and resistance to treatments, largely driven by the release of the δ toxin (Lindsay and Hogan, 2014). Diagram was created in BioRender.

In addition to physical interactions, chemical signalling mechanisms, particularly QS molecules, play a significant role in facilitating communication between *C. albicans* and *S. aureus*. Farnesol, a key QS molecule produced by *C. albicans*, has been shown to influence *S. aureus* antibiotic resistance and biofilm formation capabilities (Kong et al., 2017, Gaálová-Radochová et al., 2023). Furthermore, farnesol has been observed to reduce *S. aureus* lipase activity through competitive inhibition (Kitadokoro et al., 2025). Interestingly, the relationship appears to be reciprocal. Lin et al. (2013) demonstrated that the addition of *S. aureus* conditioned media enhanced the growth rate of *C. albicans*, suggesting the presence of a QS molecule from *S. aureus* that stimulates fungal growth. However, it is important to note that these interactions have primarily been studied *in vitro*, and their relevance *in vivo* remains to be fully elucidated. Despite the limitations of *in vitro* studies, the accumulated evidence points towards a synergistic relationship between *C. albicans* and *S. aureus* (Weidt et al., 2016).

Recent studies have shed light on the complex interactions between *C. albicans* and *S. aureus* during biofilm formation and host colonisation. Fehrmann et al. (2013) demonstrated that *S. aureus* secretes an extracellular fibrinogen-binding protein (EFB) when interacting with *C. albicans* biofilms. This protein encases yeast cells, effectively shielding them from phagocytosis by granulocytes, thus enhancing their survival in the host environment.

The synergistic relationship between *C. albicans* and *S. aureus* presents significant challenges in the clinical management of co-infections. Effective treatment strategies must address both fungal and bacterial components, necessitating the use of both antifungals and antibiotics. One promising approach involves the use of broad-spectrum antimicrobial agents, Peters et al. (2013) demonstrated the efficacy of ethanol as a catheter lock solution against both mono- and polymicrobial biofilms. Interestingly, certain antifungal agents have shown unexpected efficacy against bacterial pathogens in mixed infections. For instance, miconazole, an imidazole antifungal, has been successfully used in the treatment of angular cheilitis, a condition often involving both *C. albicans* and *S. aureus*. Sud and Feingold (1982) reported this clinical success, despite the lack of a clear mechanism of action against *S. aureus*. One hypothesis to explain this phenomenon is that antifungal agents may disrupt the hyphal scaffold of *C. albicans* biofilms, which in turn could destabilise *S. aureus* colonisation.

Extracellular DNA (eDNA) plays a crucial role in supporting mixed biofilm growth. Pammi et al. (2013) observed that eDNA released through autolysis supports mixed biofilm growth with *S. epidermidis*. Similarly, eDNA contributes to the integrity of the EPS in *C. albicans* biofilms (Rajendran et al., 2014b, Sapaar et al., 2014, Campoccia, Montanaro and Arciola, 2021). Kean et al. (2017) demonstrated that *C. albicans* hyphae in a mycofilm facilitate the adhesion and colonisation of *S. aureus*, supported by eDNA within the matrix, resulting in enhanced resistance to miconazole. This synergism was also observed *in vivo*, where dual-species infections exhibited increased virulence despite miconazole treatment.

The EPS produced by both species significantly affects the efficacy of antimicrobial agents. Harriott and Noverr (2009) showed that *C. albicans* EPS impedes drug diffusion and access to cells, allowing *S. aureus* to survive

vancomycin concentrations as high as 1600 µg/mL. Kong et al. (2016) found that inhibiting *C. albicans* ß-1,3-glucan synthesis with caspofungin sensitises *S. aureus* cells to vancomycin treatment, suggesting that fungal polysaccharides provide protection to the bacterial cells. Drug resistance in polymicrobial biofilms is not solely attributed to reduced diffusion of antimicrobial agents. Adam, Baillie and Douglas (2002) observed increased resistance to both fluconazole and vancomycin in dual-species biofilms compared to mono-species biofilms. While this enhanced resistance is partially attributed to slime production by *S. epidermidis*, the presence of *Candida* also plays a significant role.

1.3.6 Fungal-pseudomonal interactions

Fungi are often found co-colonised with *P. aeruginosa* in infections of the human body, due to their joint propensity to form biofilms. The CF lung represents one of the most extensively studied biofilm infections, characterised by the predominance of *P. aeruginosa*. The relationship between *P. aeruginosa* and *C. albicans* in this context is notably antagonistic. *P. aeruginosa* has been observed to form biofilms on *C. albicans* hyphae, leading to their demise, while having no impact on the yeast form. This effect is attributed to the *P. aeruginosa* phenazine toxin (Kasetty et al., 2021). Furthermore, a *P. aeruginosa* QS molecule, 3-oxo-C12 homoserine lactone, has been shown to inhibit the morphological transition of *C. albicans* (Grainha et al., 2020). This inhibitory effect extends beyond *C. albicans*, also affecting *Aspergillus fumigatus* biofilms (Morelli, Kerkaert and Cramer, 2021). The competitive nature of this relationship has been demonstrated in a mouse model, where *C. albicans* colonisation of the lung mitigated symptoms of lung tissue injury caused by *P. aeruginosa* (Ader et al., 2011). This protective effect was attributed to *C. albicans* activating the immune system through IL-22 producing innate lymphoid cells, priming it against *P. aeruginosa* (Mear et al., 2014). Conversely, *C. albicans* can modulate *P. aeruginosa* virulence through the release of the fungal QS molecule farnesol. This compound inhibits bacterial quinolone signalling, which regulates pyocyanin production (Figure 1.4) (Grainha et al., 2020). The complex dynamics and interactions between these microorganisms play a crucial role in shaping the polymicrobial environment of the CF lung, significantly impacting disease outcomes (Reece, Bettio and Renwick, 2021). This concept has been validated in the Drosophila fruit fly infection model

of polymicrobial infection, where infection outcomes were influenced by the microbiota of the CF lung and the presence or absence of *P. aeruginosa* (Sibley et al., 2008a, Sibley et al., 2008b).

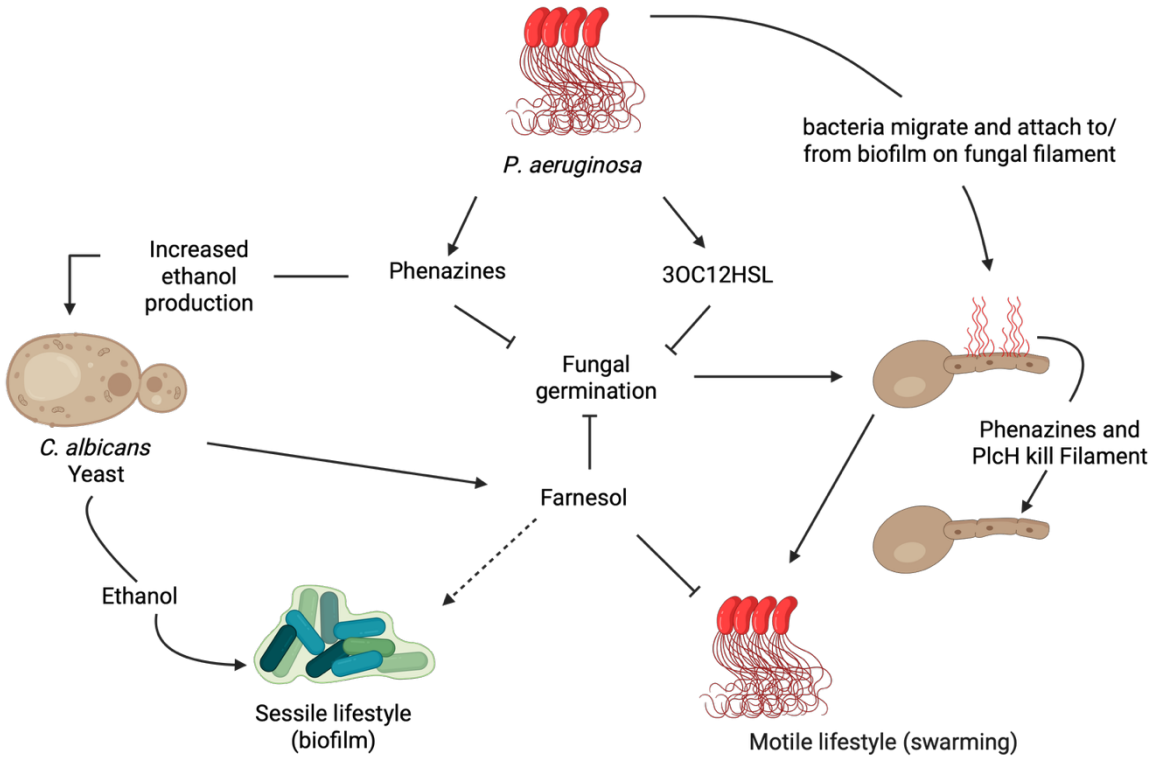

Figure 1.4: Pseudomonas and Candida interactions. *P. aeruginosa* selectively binds to *C. albicans* hyphal structures, inducing hyphal cell death via phenazine compounds. The fungal yeast form survives and thrives, supported by bacterial quorum-sensing signals like phenazines. These bacterial molecules additionally stimulate *C. albicans* to generate higher farnesol levels, which inhibits *P. aeruginosa* motility, thereby enhancing biofilm formation (Lindsay and Hogan, 2014). Diagram was created in BioRender.

The interactions between *P. aeruginosa* and *A. fumigatus* in the context of polymicrobial infections have been the subject of increasing research interest. As previously noted, *P. aeruginosa* has been shown to inhibit *A. fumigatus* filamentation through QS signalling mechanisms (Mowat et al., 2010). Nonetheless, the full extent and complexity of these interactions remain to be fully elucidated, with current understanding primarily focused on the exchange of small molecules that influence fungal growth. One key aspect of this interaction involves the secretion of phenazines by *P. aeruginosa*, which have been demonstrated to impede *A. fumigatus* biofilm formation. Interestingly, *A. fumigatus* has developed a counter-mechanism, whereby it can convert these bacterial phenazines into fungal siderophores, potentially influencing the

progression of CF disease (Moree et al., 2012). This adaptive response highlights the dynamic nature of microbial interactions in polymicrobial environments. Moreover, *P. aeruginosa* produces a metalloprotease elastase as a virulence factor that targets host tissues (Smith et al., 2015). While elastase production is constitutive in *P. aeruginosa*, its secretion was found to be significantly enhanced in dual-species biofilms with *A. fumigatus*. Given the toxicity of elastase towards host lung cells, this observation suggests that co-infections involving *A. fumigatus* and *P. aeruginosa* could potentially lead to more severe deterioration of patient health (Smith et al., 2015). The cumulative evidence from these studies implies that co-infections involving these two pathogens may have detrimental effects on patient outcomes. However, it is important to note that our understanding of these polymicrobial interactions is still incomplete, and further research is needed to fully elucidate the mechanisms and consequences of these microbial associations in the context of respiratory infections, particularly in CF patients.

1.3.7 Bacterial-bacterial interactions

The establishment of polymicrobial biofilms is heavily influenced by bacterial interactions, ranging from simple physical forces to complex chemical signalling. These interactions can be as fundamental as electrostatic and hydrogen bonding (Chen and Stewart, 2002, Achinas, Charalampogiannis and Euverink, 2019), and progress to more intricate mechanisms involving diffusible molecules (Tait and Sutherland, 2002, Al-Bakri, Gilbert and Allison, 2004, Alonso, Harada and Kabuki, 2020). In many cases, certain bacterial species can induce biofilm formation in others, facilitating the development of communities that would not otherwise form (Castonguay et al., 2006, Wollenberg et al., 2014, Giaouris et al., 2015, Beaudoin et al., 2017). Once established, these mixed-species biofilms exhibit specific organisational structures that are optimised for nutrient conditions and growth rates (Lee et al., 2014b, Luo et al., 2022). Within this architecture, oxygen gradients emerge, allowing anaerobic bacteria to thrive in predominantly aerobic environments (Dowd et al., 2008a, Dowd et al., 2008b, Rendueles and Ghigo, 2015). The community structure of polymicrobial biofilms enables bacteria to benefit from the enzymatic activities and metabolites of their neighbours. This cooperative environment can enhance resistance mechanisms and expand carbon source utilisation, allowing certain species to persist within the community where

they would not survive in isolation (Jagmann, Brachvogel and Philipp, 2010, Lee et al., 2014b, Jagmann, von Rekowski and Philipp, 2012, Orazi and O'Toole, 2019).

While cooperation is prevalent within biofilms, competition also plays a crucial role in shaping these communities. Bacteria produce species-specific antibacterial molecules, or bacteriocins, to eliminate competitors. Interestingly, bacteriocin-producing and -sensitive strains can coexist within a biofilm by forming segregated microcolonies (Tait and Sutherland, 2002, Rendueles and Ghigo, 2015). This competitive advantage is particularly evident during the colonisation of pre-existing biofilms, where bacteriocin-producing strains can successfully infiltrate sensitive biofilms and resist invasion by other species (Tait and Sutherland, 2002, Al-Bakri, Gilbert and Allison, 2004, Rendueles and Ghigo, 2015). Both pathogenic species, such as *P. aeruginosa*, and commensals, like *Lactobacillus acidophilus*, utilise this strategy (Al-Bakri, Gilbert and Allison, 2004, Sadowska et al., 2010, Orazi, Ruoff and O'Toole, 2019). Some bacteria have evolved mechanisms to prevent surface colonisation by other species. For instance, uropathogenic *Escherichia coli* secretes polysaccharides that induce physicochemical surface alterations, inhibiting bacterial adhesion and subsequent biofilm formation (Valle et al., 2006, Rendueles et al., 2011, Hotterbeekx et al., 2017).

Staphylococci and *P. aeruginosa* are among the most common biofilm-associated diseases (Wisplinghoff et al., 2004, Beaudoin et al., 2017, Sahoo and Meshram, 2024). These two bacteria commonly interact with one another at different locations inside the human body, and these pathogens have shown that they are capable of outcompeting commensal bacteria in polymicrobial biofilms (Malic et al., 2011, Yung, Sircombe and Pletzer, 2021). *S. aureus* strains have been demonstrated to be more susceptible to the production of biofilm when exposed to *P. aeruginosa* strains that have been obtained from individuals with CF. Fugère et al. (2014) found that strains that were co-isolated from the same patient had a decreased effect, which suggests that the strains co-existed in an adaptive manner. *S. aureus* and *P. aeruginosa* generate separate microcolonies in biofilm co-cultures, which is facilitated by *P. aeruginosa* type IV pili (Yang et al., 2011, Vestweber et al., 2024).

The biofilm matrix provides support for both species, with eDNA playing a vital role (Yang et al., 2011, Vestweber et al., 2024). The organisation of these dual-species biofilms relies on two polysaccharides, Pel and Psl, produced by *P. aeruginosa*. The presence of Pel polysaccharide facilitates the separation of microcolonies when *S. aureus* and *P. aeruginosa* are in close proximity, enabling interaction via a flexible matrix (Chew et al., 2014). On the other hand, Psl polysaccharide, due to its more closely connected structure, functions as a physical obstacle between the two species when *P. aeruginosa* develops a biofilm on top of *S. aureus* (Chew et al., 2014). The biofilms exhibit synergistic relationships, where *S. aureus* supplies iron to *P. aeruginosa* (Mashburn et al., 2005, Nguyen and Oglesby-Sherrouse, 2016). Observations have shown that biofilms consisting of two different species may boost the virulence of *S. aureus*. This enhancement includes an increase in the production of Panton-Valentine leukocidin and α-haemolysin. Additionally, these biofilms hinder the healing process in a model of porcine partial thickness wounds by inhibiting the development of keratinocyte growth factor 1 (Pastar et al., 2013, Vestweber et al., 2024).

Biofilms often contribute to the amplification of antimicrobial resistance. *P. aeruginosa* synthesises 4-hydroxy-2-heptylquinoline-N-oxide (HQNO), which inhibits the respiration of *S. aureus*, therefore providing protection against aminoglycoside drugs. Extended exposure of *S. aureus* to *P. aeruginosa* or HQNO leads to the selection of the SCVs phenotype, which is linked to chronic infections and resistance to therapy (Hoffman et al., 2006, Hotterbeekx et al., 2017). HQNO triggers the activation of the alternative sigma factor B in *S. aureus*, which leads to the expression of fibronectin-binding protein A and biofilm-associated sarA genes. At the same time, it suppresses the QS agr system and the α-haemolysin gene (Mitchell et al., 2010, Orazi and O'Toole, 2017, Biswas and Götz, 2022). *P. aeruginosa* also synthesises cis-2-decenoic acid, a compound that triggers the dispersal of biofilms in several species, including *S. aureus*. This process likely facilitates the spread of infection (Davies and Marques, 2009, Amari, Marques and Davies, 2013).

1.4 Treatment therapies for chronic wounds

1.4.1 Debridement-based approaches

Debridement remains the cornerstone of biofilm management in chronic wounds, serving to physically disrupt the biofilm structure and temporarily increase susceptibility to antimicrobial agents (Wolcott et al., 2010, Alves et al., 2021). Several debridement modalities have demonstrated efficacy in biofilm management with varying degrees of success and limitations. Surgical debridement, considered the "gold standard," provides rapid removal of large amounts of necrotic tissue and biofilm material, though outcomes depend heavily on clinician expertise and may result in damage to healthy tissue (Liu et al., 2024b).

Mechanical debridement using monofilament fiber pads removes 93.4% of slough/biofilm in ≤2.5 minutes per session while maintaining patient comfort (Dissemond et al., 2018). Compared to gauze, these pads achieve 100-fold greater bacterial reduction in ex vivo models (Wilkinson et al., 2016). Enzymatic methods provide targeted action against necrotic tissue but carry higher costs and longer clearance times (Liu et al., 2024b, Alves et al., 2021). For instance, Larval debridement therapy (LDT) using Lucilia sericata maggots enzymatically degrades necrotic tissue via protease secretion, achieving 96.6% debridement efficacy in recalcitrant DFUs (Lam, Beraja and Lev-Tov, 2025, Nair et al., 2021). LDT also reduces antibiotic-resistant pathogens by consuming biofilm matrices, circumventing systemic drug use (Lam, Beraja and Lev-Tov, 2025, Nair et al., 2021).

Monofilament debridement technology (MFDT) shows particular promise, reducing *P. aeruginosa* biofilms by 6-$\log_{10}$ CFU/cm² and *S. aureus* by 7-$\log_{10}$ CFU/cm² in porcine models (Wilkinson et al., 2016). Clinical studies report 77% wound size reduction after 4 weeks of MFDT combined with antimicrobial dressings (Roes, Calladine and Morris, 2019, CHOUDHURY and DOWNIE, 2022). This approach enables 90% biofilm removal versus 40% with standard gauze, while causing minimal pain (45% patients report no discomfort) (Dissemond et al., 2018).

The post-debridement "window of opportunity" lasts 24-72 hours, during which biofilms exhibit 9-fold increased antibiotic susceptibility (Wolcott et al., 2010). Gentamicin efficacy improves from 0% to 90% bacterial kill rates during this period (Wolcott et al., 2010, Schultz et al., 2018). This supports clinical protocols recommending debridement every 48-72 hours combined with topical antimicrobials (Alves et al., 2021, Attinger and Wolcott, 2012, CHOUDHURY and DOWNIE, 2022). Biofilm regrowth reaches pretreatment resistance levels by 72 hours, emphasising the need for repeated intervention (Wolcott et al., 2010). This supports the clinical practice of frequent debridement as part of a comprehensive biofilm-based wound care strategy.

1.4.2 Antimicrobial and antibiofilm therapeutic approaches

Following effective debridement, application of appropriate antimicrobial and antibiofilm agents represents a critical component of chronic wound biofilm management. A recent study demonstrated that empirical antibiotic therapy increases hospitalisation rates by 1.87-fold compared to culture-directed regimens, underscoring the importance of tissue cultures for targeted treatment (Schmidt et al., 2023). Current guidelines stratify antibiotic use by infection severity: flucloxacillin (1 g four times daily orally) remains first-line for mild infections due to its β-lactamase resistance and efficacy against MSSA (Barwell et al., 2017). Moderate infections require broader coverage, combining ciprofloxacin (500 mg twice daily) with metronidazole (400 mg three times daily) to address Gram-negative and anaerobic pathogens (Barwell et al., 2017). For severe infections, intravenous piperacillin-tazobactam (4.5 g three times daily) paired with teicoplanin or vancomycin provides anti-MRSA coverage, though treatment durations vary from 10–14 days for acute cases to ≥6 weeks for osteomyelitis. Systemic antibiotics face limitations due to poor biofilm penetration, prompting the use of localised delivery systems like gentamicin-impregnated beads, which achieve 3-$\log_{10}$ CFU reductions by disrupting ribosomal function in *P. aeruginosa* biofilms (Yi, Huang and Tang, 2025).

Fungal co-infections, particularly with *Candida* species, are identified in 84.6% of non-healing DFUs, necessitating a re-evaluation of antifungal protocols (Öztürk et al., 2019). Fluconazole (200–400 mg daily) combined with standard care accelerates wound closure by 40% compared to antibacterial therapy alone,

attributed to its inhibition of ergosterol synthesis and biofilm dispersal (Öztürk et al., 2019, Ge and Wang, 2023). Deep tissue cultures, rather than surface swabs, are critical for detecting invasive fungal infections, as poor glycemic control (HbA1c >8%) elevates fungal colonisation risks (Öztürk et al., 2019). While not universally adopted in guidelines, antifungal therapy should be considered when ulcers exhibit persistent inflammation or fail to respond to antibacterial regimens, particularly in patients with recurrent infections (Ahmadian et al., 2021, Ge and Wang, 2023).

Antiseptics like povidone iodine (PVP-I) (10%), chlorhexidine (CHX) (2%), hydrogen peroxide (H_2O_2) (3%), and polyhexamethylene biguanide (PHMB) remain cornerstone adjuncts for biofilm disruption (Zhang et al., 2023). PVP-I releases free iodine, iodinating microbial proteins and DNA, achieving 4-$\log_{10}$ CFU reductions in MRSA biofilms while maintaining low cytotoxicity (Jiang et al., 2024, Sharma et al., 2017). CHX's cationic properties disrupt bacterial membranes, though efficacy diminishes in mature biofilms due to EPS binding (Zhang et al., 2023, Barwell et al., 2017). H_2O_2 generates reactive oxygen species (ROS), effective against early-stage biofilms but neutralised by catalase in chronic wounds (Zhang et al., 2023). A meta-analysis study confirmed silver dressings reduce healing time by 9.5 days compared to iodine, leveraging Ag^+ ions to interfere with bacterial DNA replication and EPS integrity (Yi, Huang and Tang, 2025). Moreover, PHMB demonstrated 60% eradication of *S. aureus* in chronic wounds with lower cytotoxicity compared to iodine, making it suitable for shallow ulcers (Zhang et al., 2023).

Topical silver sulfadiazine (1% cream) reduced *P. aeruginosa* viability by 90% in burn wounds via Ag^+ ion interference with DNA replication (Tran et al., 2023). For fungal infections, nystatin (100,000 units/g) combined with steroids in Trimovate® improved healing rates by 77% in inflamed ulcers by suppressing *Candida*-driven inflammation (Bosanquet et al., 2013). Manuka honey (UMF 16+ is considered therapeutic grade and suitable for wound care) enhanced 4-fold tobramycin efficacy in DFUs through osmotic stress and methylglyoxal-mediated QS inhibition (Tran et al., 2023).

Several studies have explored repurposing drugs to combat biofilms in chronic wounds. For example, bronopol and bronidox—preservatives historically used in personal care products—demonstrate broad-spectrum antibiofilm activity against pathogens like *S. aureus* and *P. aeruginosa* in chronic wound models, even enhancing the efficacy of existing antibiotics when used in combination (Lee and O'Neill, 2019). Similarly, non-steroidal anti-inflammatory drugs (NSAIDs), such as acetylsalicylic acid and diclofenac, exhibit anti-biofilm activity by inhibiting QS and downregulating virulence genes (e.g., fnbA, icaA) in *S. aureus* and *P. aeruginosa* biofilms, reducing biofilm formation by up to 53% (Paes Leme and da Silva, 2021). Metformin, traditionally used for diabetes, disrupts *P. aeruginosa* biofilm formation by 67.9% via LasR/rhlR receptor binding and enhances diabetic wound healing by promoting collagen synthesis and reducing apoptosis (Tombulturk, Soydas and Kanigur-Sultuybek, 2024, Lee et al., 2014a, Abbas, Elsherbini and Shaldam, 2017). Statins like simvastatin interfere with ergosterol biosynthesis in *C. albicans* and disrupt amyloid structures in bacterial biofilms, demonstrating dual antifungal and anti-biofilm efficacy (Wang et al., 2016, Verma et al., 2025). These repurposed agents leverage established safety profiles and offer novel strategies to address biofilm-mediated antibiotic resistance in wound care.

Bacteriophage therapy has experienced renewed interest for chronic wound biofilm management, particularly in the context of antibiotic-resistant and multidrug-resistant pathogens (Haq, Figgitt and Lee, 2024). Bacteriophages, viruses that specifically infect and kill bacteria, offer targeted antimicrobial activity against biofilm-forming pathogens in chronic wounds (Pinto et al., 2020a). The efficacy of bacteriophages against antibiotic-resistant clinical isolates makes them valuable additions to the therapeutic arsenal for chronic wound biofilms (Subramanian, 2024). Recent developments in delivery systems have further enhanced bacteriophage therapy by protecting phages from harsh environmental conditions, increasing shelf life, and enabling species-targeted antibacterial control (Pinto et al., 2020a, Haq, Figgitt and Lee, 2024). The prospect of using phages in non-bacterial infections (e.g., in interkingdom wound infections) has yet to be explored and emerging evidence suggests that certain bacteriophages can also control fungal growth (Górski et al., 2019).

Nanoparticle-based strategies represent another frontier in biofilm management for chronic wounds (Jing et al., 2024). These approaches can be categorised into four main types based on their mechanisms against biofilms: metallic nanoparticles (such as silver and copper) that disrupt bacterial cell membranes and induce oxidative stress; phototherapy-based nanoparticles that generate ROS or localised heat; nanoparticles designed to disrupt EPS; and nanoparticles that induce biofilm dispersion (Sedighi et al., 2024). The versatility and targeted nature of nanoparticle-based approaches offer significant potential for overcoming the challenges of biofilm resistance in chronic wounds (Sedighi et al., 2024, Pinto et al., 2020b).

Novel biofilm-disrupting technologies have emerged that specifically target the structural integrity of biofilms (Salem and Mont, 2021). For instance, specialised wound gels containing sodium citrate and citric acid have demonstrated efficacy in inhibiting biofilm development through multiple mechanisms, including disruption of QS, suppression and degradation of EPS, and blockage of bacterial attachment sites (Edwards-Jones, 2018, Salem and Mont, 2021).

Clinical studies have evaluated the efficacy of these biofilm-disrupting agents, with promising results. In one 12-week trial involving chronic, recalcitrant wounds, patients whose wounds were treated with a biofilm-disrupting wound gel following sharp debridement demonstrated significantly greater wound size reduction and closure rates compared to those treated with conventional topical antibiotics (Edwards-Jones, 2018). Similarly, another study found that wound volume reduction and healing were significantly improved when antibiofilm wound gel was used to degrade the biofilm matrix, with the greatest success observed when combined with standard care including regular debridement (Salem and Mont, 2021). These findings highlight the potential of targeted antibiofilm agents as components of a comprehensive treatment approach for chronic wound biofilms.

1.4.3 Energy-based therapeutic approaches

Innovative physical and energy-based therapies are gaining traction for their dual antimicrobial and pro-healing effects in chronic wound biofilm management (Ciarolla et al., 2022). Blue light therapy (400–470 nm) has emerged as a non-

invasive modality that combats biofilms while promoting tissue regeneration. At 405 nm, blue light activates endogenous porphyrins in microbial cells, generating ROS that disrupt biofilm matrices and induce bacterial death without harming host tissues (Haridas and Atreya, 2022). This wavelength achieves 6.3-$\log_{10}$ reductions in *P. aeruginosa* biofilms and 3.5-$\log_{10}$ reductions in MRSA, outperforming conventional antibiotics in polymicrobial settings (Haridas and Atreya, 2022, Plattfaut et al., 2021). Beyond its bactericidal effects, blue light enhances fibroblast proliferation by 1.4-fold and accelerates angiogenesis via nitric oxide release, critical for re-epithelialisation in diabetic ulcers (Liu et al., 2024b, Zhang, Leong and McMullin, 2023). Clinical trials report 51% wound area reduction when combined with standard care, attributed to ROS-mediated resolution of chronic inflammation and biofilm dispersal (Zhang, Leong and McMullin, 2023, Conti et al., 2023).

However, wavelength optimisation is essential: while 420 nm light shows potent antibiofilm activity, it causes >40% cytotoxicity to human fibroblasts at doses >30 J/cm^2 (Plattfaut et al., 2021). In contrast, 455–480 nm wavelengths maintain efficacy against *P. aeruginosa* (≥5-$\log_{10}$ kill) with minimal cell toxicity, making them safer for clinical use (Plattfaut et al., 2021). Advanced delivery systems, such as 405 nm LED arrays, now enable targeted biofilm eradication in complex wounds, reducing *S. epidermidis* viability by 99% in preclinical models without impairing granulation tissue formation (Haridas and Atreya, 2022). These therapies are particularly advantageous for antibiotic-resistant infections, as their mechanism bypasses traditional resistance pathways. Despite promising results, large-scale randomised trials are needed to standardise protocols and validate long-term outcomes (Zhang, Leong and McMullin, 2023).

Cold atmospheric plasma (CAP), a partially ionised gas generated at room temperature using noble gases like helium or argon, has emerged as a transformative therapy for biofilm-infected chronic wounds (Bolgeo et al., 2023). CAP delivers reactive oxygen and nitrogen species (RONS), including H_2O_2, nitric oxide (NO), and ozone (O_3), which disrupt biofilm matrices via oxidative damage to microbial proteins, lipids, and eDNA (Figure 1.5) (Raissi-Dehkordi et al., 2025). These RONS achieve 5–6-$\log_{10}$ reductions in MRSA and *P. aeruginosa* biofilms while sparing human fibroblasts, making CAP uniquely selective against pathogens

(Raissi-Dehkordi et al., 2025, Bolgeo et al., 2023). Beyond its antimicrobial effects, CAP accelerates tissue regeneration by modulating inflammatory pathways: it upregulates pro-healing cytokines like IL-6 and IL-8 in dermal fibroblasts, recruiting macrophages and neutrophils to resolve chronic inflammation (Bolgeo et al., 2023). Angiogenesis is enhanced through CAP-induced expression of vascular endothelial growth factor (VEGF) and fibroblast growth factor-2 (FGF-2), restoring microcirculation in ischemic DFUs (Raissi-Dehkordi et al., 2025). Clinical trials demonstrate CAP's dual efficacy, with a multicenter randomized open-label non-inferiority trial of chronic wounds (N = 78; 39 CAP-jet, 39 best-practice), the primary endpoint (sum of granulation at day 42) and multiple secondary endpoints were assessed over 6 weeks, including wound area change, complete healing and time to healing, wound pH, infection score, exudate, and safety. CAP-jet significantly outperformed best-practice for granulation (mean difference 21.21 pp), wound area reduction (5.32% vs 43.72% of baseline), complete healing (58.97% vs 5.13%), time to healing (log-rank $p < 0.0001$), faster pH decrease ($p = 0.0123$), and faster infection resolution ($p = 0.0129$). The between-arm infection count at day 42 was not significant after adjustment ($p = 0.2598$) (Strohal et al., 2022). CAP also improves tissue remodelling by stimulating collagen-I synthesis via TGF-β/Smad pathway modulation and upregulating MMPs to degrade necrotic debris (Raissi-Dehkordi et al., 2025). Notably, CAP's safety profile is robust, with no adverse events reported in trials even after prolonged use, though standardisation of treatment parameters (e.g., exposure time, gas composition) remains critical for clinical translation (Strohal et al., 2022). These multimodal mechanisms position CAP as a versatile, non-invasive adjunct to conventional therapies, addressing both biofilm persistence and impaired healing in chronic wounds (Raissi-Dehkordi et al., 2025).

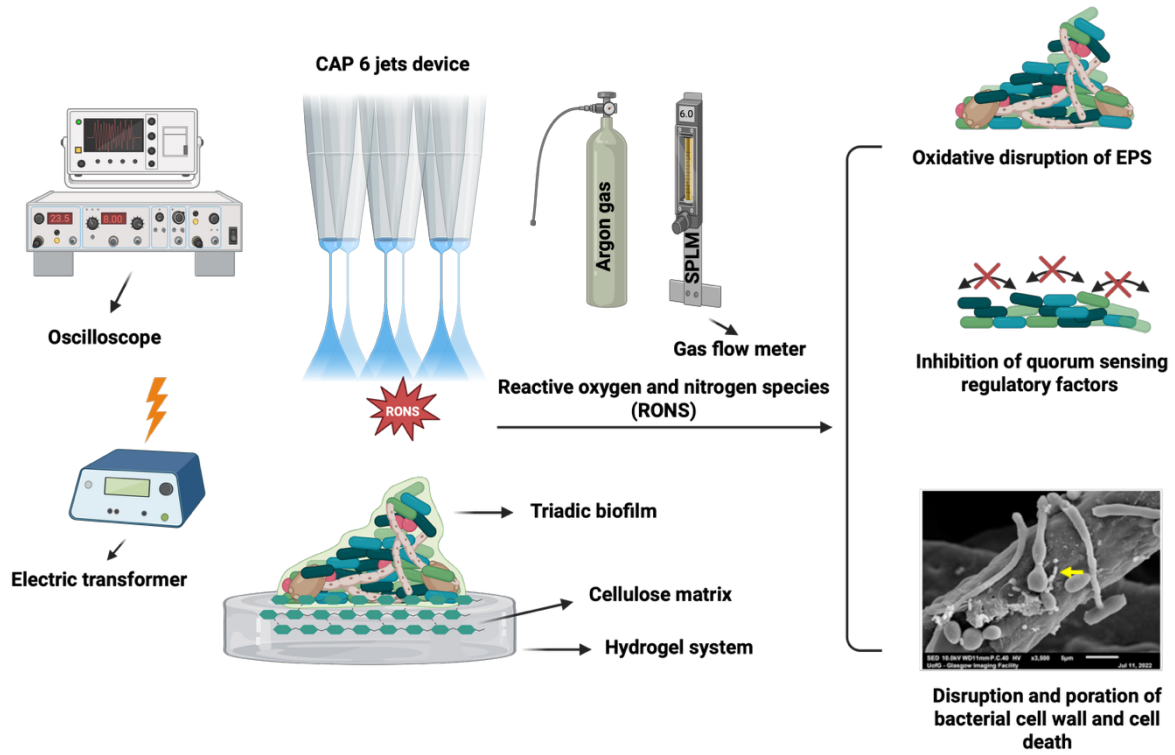

Figure 1.5: Schematic diagram illustrated the proposed CAP mode of action against the biofilm. CAP generates RONS which disrupt biofilm matrices via oxidative damage to microbial proteins, lipids, and eDNA (Raissi-Dehkordi et al., 2025). Diagram was created in BioRender.

1.5 Advances *in vitro* chronic wound research

Significant advances in research methodologies have enhanced our understanding of chronic wound microbiology (Jakobsen et al., 2025). Innovative *in vitro* models that closely mimic the chronic wound environment have been developed to study polymicrobial and inter-kingdom interactions (Jakobsen et al., 2025, Kalan et al., 2016). These models incorporate appropriate wound-like conditions including pH, oxygen levels, and inflammatory components (Jakobsen et al., 2025). Recently developed models include both bacterial species and fungal elements, allowing for investigation of complex inter-kingdom interactions in a wound-relevant environment (Jakobsen et al., 2025, Kalan et al., 2016). These models have revealed how microbial communities respond to antimicrobial treatments and how species ratios shift following interventions (Jakobsen et al., 2025). Advanced statistical approaches, such as structural equation modelling, have also provided new insights into the relative importance of various factors in wound healing, with recent models able to explain up to 60% of the variation in healing time (Ancira et al., 2025). These innovations provide platforms for testing novel antimicrobial

strategies targeting both bacterial and fungal components of biofilms, potentially leading to more effective treatments for chronic wounds (Ancira et al., 2025, Jakobsen et al., 2025, Kalan et al., 2016).

1.5.1 Biofilm and organotypic models in wound research

1.5.1.1 Biofilm models

Model systems are effective, reproducible methods by which to investigate microbe-microbe and host-microbe interactions occurring within chronic wounds. These can also be excellent testing-platforms for novel and conventional therapeutics. Early *in vitro* models focused primarily on monoculture biofilms grown in standard laboratory media, which failed to capture the polymicrobial, nutrient-rich, and host-influenced conditions of chronic wounds (Kadam et al., 2019, Bahamondez-Canas, Heersema and Smyth, 2019). Recognising these limitations, researchers began integrating wound-specific components into experimental systems. For instance, the development of chronic wound medium (CWM)—a formulation incorporating plasma, red blood cells, and adjusted pH—enabled the study of bacterial interactions under conditions mimicking the wound bed (Pouget et al., 2022a). When clinical isolates of *S. aureus* and *P. aeruginosa* were co-cultured in CWM, synergistic behaviours emerged, including enhanced biofilm biomass and the formation of SCVs of *S. aureus*, phenomena frequently observed in clinical samples (Pouget et al., 2022a, Diban et al., 2023). These findings underscored the importance of medium composition in driving pathogen behaviour reflective of *in vivo* infections.

Similarly, the Lubbock Chronic Wound Biofilm (LCWB) model incorporated Bolton broth supplemented with plasma and erythrocytes to simulate the nutrient profile of wound exudate, facilitating the growth of polymicrobial biofilms with species commonly co-isolated from diabetic foot infections (Diban et al., 2023). These advancements addressed critical gaps in earlier systems by introducing gradients of oxygen, nutrients, and host-derived factors that influence microbial metabolism and virulence (Diban et al., 2023, Bahamondez-Canas, Heersema and Smyth, 2019).

The category of three-dimensional (3D) models includes several wound-relevant systems. For example, Reddersen, Tittelbach and Wiegand (2022) created a 3D biofilm model using a combination of agar and gelatine with a nutrient-rich medium, resulting in a semi-solid, permeable surface that simulates the texture of chronic wounds and supports the formation of biofilm micro clusters (Reddersen, Tittelbach and Wiegand, 2022). By vigorously mixing the agar-gelatine medium to incorporate air bubbles, they encouraged the development of biofilm clusters throughout the model, which was then used to evaluate the effectiveness of antimicrobial wound dressings.

Another approach, described by Townsend et al. (2016), involved an *in vitro* wound model based on a single cellulose layer combined with a horse serum hydrogel. Because it lacks living tissue, this model is not strictly organotypic; it nonetheless recapitulates an ECM substratum (e.g., underlying skin tissue) supplemented with rich nutrient source or serum (e.g., the wound exudate). This model allowed the study of topical antimicrobial treatments on polymicrobial biofilms and revealed that biofilms grown in this system showed much greater resistance to PVP-I and CHX than those tested in standard *in vitro* conditions. These findings aligned with clinical observations that these agents are less effective against chronic wound biofilms (Townsend et al., 2016).

1.5.1.2 Organotypic models

To better replicate the spatial organisation of chronic wound biofilms, organotypic models were introduced. A variety of models are available to replicate skin infections for research, including engineered 3D skin constructs, human skin explants, porcine tissue samples, and *in vivo* models using mice or pigs. One such system employs a dual-layer agar structure simulating dermal and subcutaneous tissues, with *S. aureus* localised superficially and *P. aeruginosa* in deeper layers—a distribution consistent with clinical observations (Diban et al., 2023, Chen et al., 2021). This model demonstrated utility in evaluating antimicrobial penetration and efficacy, revealing that conventional treatments often fail to eradicate deeply embedded pathogens (Diban et al., 2023).

More sophisticated models have also been developed by Brown et al. (2022), by developing an advanced 11-species interkingdom biofilm model incorporating *C.*

albicans, aerobic and anaerobic bacteria to better replicate clinical wound environments. While antiseptic treatments reduced biofilm viability, residual cells persisted, with H_2O_2 and PVP-I showing superior efficacy in both microbial clearance and modulating host immune responses in adjacent 3D epidermal tissue (Brown et al., 2022). Environmental oxygen levels critically influenced microbial dominance: *C. albicans* thrived in aerobic/CO_2-rich conditions, while *Staphylococcus hominis* proliferated in anaerobic settings. These findings underscore the necessity of simulating physiologically relevant atmospheric conditions (e.g., oxygen gradients, microbial diversity) in biofilm models to improve their translational accuracy for testing antimicrobial therapies and understanding host-pathogen interactions in chronic wounds (Brown et al., 2022).

Brackman and Coenye (2015) used an artificial dermis to examine the ability of various antimicrobial gauzes to eradicate biofilms, focusing on their impact on bacterial QS. Their model, which included chemically crosslinked hyaluronic acid and a secondary layer of hyaluronic acid with collagen, partially immersed in a wound-simulating medium, demonstrated that functionalised gauzes had a stronger inhibitory effect compared to standard antimicrobial gauzes (Brackman and Coenye, 2015).

Chen et al. (2021) constructed a two-layered model featuring a deliberate breach in the skin to mimic subcutaneous wounds, incorporating pig fat to represent the subcutaneous layer and creating a void to simulate dermal damage and expose nutrient-rich fat. The breached two-layer construct recreates a realistic interface where microbes can colonize the superficial “dermis” while also accessing and exploiting the exposed, nutrient-rich fat to establish deeper, treatment-recalcitrant biofilms, mirroring clinical chronic wound niches. This architecture is useful for testing antimicrobial penetration and efficacy across depths, often revealing that standard treatments clear surface communities but leave deeply embedded pathogens largely unaffected (Chen et al., 2021).

Considering these factors, tissue-engineered human epidermis offers a promising platform for antimicrobial susceptibility testing. Companies such as Epiderm, Episkin, and Labskin have created human skin equivalents that help reduce reliance on animal testing (Lerebour, Cupferman and Bellon-Fontaine, 2004,

Kandárová et al., 2005, Roguet et al., 1994). While models like Episkin and Epiderm were initially designed for assessing skin irritation caused by topical products (Roguet et al., 1994), the Episkin system has evolved to include protocols for evaluating microbial adhesion (Roguet et al., 1994, Kandárová et al., 2005, Lerebour, Cupferman and Bellon-Fontaine, 2004). For instance, Lerebour, Cupferman and Bellon-Fontaine (2004) examined how *S. aureus* and *S. epidermidis* adhered to Episkin compared to stainless steel, finding that *S. aureus* exhibited a stronger attachment to the skin model than to the abiotic surface.

Other innovative models have also been developed, such as a dermal matrix composed of fibrin and fibroblasts with a layered epidermis, which has been used to study how skin microbiota colonise these structures (Holland et al., 2008). Additionally, Shepherd et al. (2009) used engineered 3D skin models with two types of wounds to track bacterial infection over 72 hours, observing that *P. aeruginosa* was able to move into deeper dermal layers, while *S. aureus* remained in the upper epidermis.

Despite their advantages, these engineered skin models still face challenges, particularly regarding the consistency of tissue physiology, which can affect reproducibility (Couto et al., 2021). For example, Couto et al. (2021) compared xenobiotic metabolism in the Labskin 3D model to *ex vivo* human skin and found notable variability in enzyme and protein markers between Labskin samples, with some markers absent compared to real human skin. Such inconsistencies highlight the need for further refinement of tissue-engineered skin to ensure these models can reliably simulate actual skin and wound environments.

To address these limitations, *ex vivo* models have been increasingly developed to better mimic clinical conditions for antimicrobial susceptibility testing. These models employ tissues or organs harvested from living organisms and maintained under controlled laboratory conditions (Andersson et al., 2021). A review by Parnell and Volk (2019) noted that, despite over 25 years of wound model research, only 3% of studies utilised *ex vivo* or computational (in silico) approaches. The same analysis highlighted that 74% of wound studies relied on *in vivo* animal models, which remain the benchmark for investigating wound healing processes across species (Parnell and Volk, 2019). However, *in vivo* models pose

challenges for studying infections due to variability in infection outcomes, difficulties in sample collection, and complexities in treatment administration (Andersson et al., 2021). Ethical concerns, animal welfare regulations, and high costs further complicate their use (Andersson et al., 2021).

1.6 Concluding remarks and aims for current study

Chronic wounds represent a persistent global healthcare burden, driven by their complex polymicrobial nature and the recalcitrance of biofilm-associated infections. The wound microbiome, comprising diverse bacterial and fungal communities, plays a pivotal role in delaying healing, with biofilm formation conferring up to 1,000 times increased antibiotic tolerance compared to planktonic cells. Key pathogens such as *S. aureus*, *P. aeruginosa*, and *C. albicans* dominate chronic wound infections, often coexisting in synergistic relationships that enhance virulence and resistance.

Current treatment paradigms, including debridement, antiseptics, and systemic antibiotics, face limitations due to biofilm heterogeneity, metabolic adaptations, and interspecies protective mechanisms. While advanced therapies like CAP therapy show promise, their efficacy against polymicrobial biofilms requires rigorous evaluation. A critical gap persists in understanding how interkingdom biofilm interactions influence the efficacy of novel therapeutics for controlling wound infections.

The aims of this study were therefore to:

1. Evaluate the antimicrobial efficacy of CAP treatment on simple and triadic *in vitro* biofilm models.

2. Evaluate the antimicrobial efficacy of repurposing drugs on these models alone and in combination with CAP.

3. Investigate mode of action of CAP using H_2O_2 when combined with conventional antibiotics (flucloxacillin and gentamicin) against tolerant biofilm models.

2 Chapter 2: Materials and methods

2.1 Microbial growth conditions and standardisation

For long-term storage, all microbial isolates were preserved on Microbank™ beads (Pro-lab Diagnostics, UK) at -80°C before revival. This study utilised the following strains: *Candida albicans* (SC5314) originally isolated from patient with systemic candidiasis (Fonzi and Irwin, 1993), *Staphylococcus aureus* (ATCC 25904) referred to as Newman originally isolated from human infection (Duthie and Lorenz, 1952), *S. aureus* (NCTC 6571) laboratory reference strain (Wilcox et al., 1996), *S. aureus* SH1000 laboratory reference strain that derived from *S. aureus* (NCTC 8325) (O'Neill, 2010), *S. aureus* (S 235) clinical isolate (kindly provided by the Sheffield School of Clinical Dentistry), *S. aureus* (ATCC 25923) widely recognised laboratory standard strain, *Pseudomonas aeruginosa* PA14 originally isolated from a human patient with a burn wound (Rahme et al., 1995), *Candida auris* (NCPF 8973), and *C. auris* (NCPF 8978) both are well characterised clinical isolates, part of the United Kingdom National Collection of Pathogenic Fungi. The two *C. auris* strains were chosen to represent the non-aggregating and aggregating phenotypes, respectively, as described by Borman, Szekely and Johnson (2016). For revival and cultivation, bacterial strains were first grown on Luria Bertani (LB) agar (Sigma-Aldrich, Dorset, UK) for 24 hours (h) at 37°C aerobically. Overnight broths were prepared in a sterile universal tube (Sterilin® Limited, Cambridge UK) in 10 mL of LB broth (Sigma-Aldrich, Dorset, UK) for 16-18 h at 37°C with shaking at 200 revolutions per minute (rpm) in an orbital shaker (MAXQ 600, Thermo Scientific, Loughborough, UK). Fungal strains were subcultured on Sabouraud's dextrose agar (SAB) (Sigma-Aldrich, Dorset, UK) and incubated aerobically at 30°C for 24-48 h until colonies of about 1 mm in diameter were formed.

Following incubation, the plates were stored at 4°C for a maximum of two weeks. To prepare overnight broths, a loopful of yeast colonies was inoculated into 10 mL of yeast peptone dextrose (YPD) medium (1% w/v yeast extract, 2% w/v peptone, 2% w/v dextrose, 1.5% agar) (Sigma-Aldrich, Dorset, UK) in a sterile universal tube. The cultures were then incubated aerobically at 30°C with shaking at 200 rpm in an orbital shaker (IKA KS 4000 i control, Berlin, Germany). After 16-18 h of incubation, the cells were pelleted by centrifugation at 3,500 rpm for 5 minutes. The supernatant was discarded, and the cell pellet was washed twice with 10 mL sterile phosphate-buffered saline (PBS) [10 mM phosphate buffer, 2.7 mM

potassium chloride, 137 mM sodium chloride, pH 7.4] (Sigma-Aldrich, UK). The washed pellet was then resuspended in 10 mL of PBS. To prepare yeast cells concentrations, a 1:100 dilution was made by adding 10 µL of the cell suspension to 990 µL of PBS in a sterile Eppendorf. The cell count was determined using a Neubauer haemocytometer (cell count × dilution factor × volume of square = colony forming unit [CFU/mL]). Bacterial suspensions were standardised to 1×10^8 colony-forming units (CFUs) per mL using spectrophotometric measurements at 600 nm (OD600), with an optical density of 0.6. The standardised cell cultures can subsequently be used for growing planktonic or biofilm forms in suitable media, either in microtiter plates or on appropriate substrates. These steps are schematically represented in (Figure 2.1).

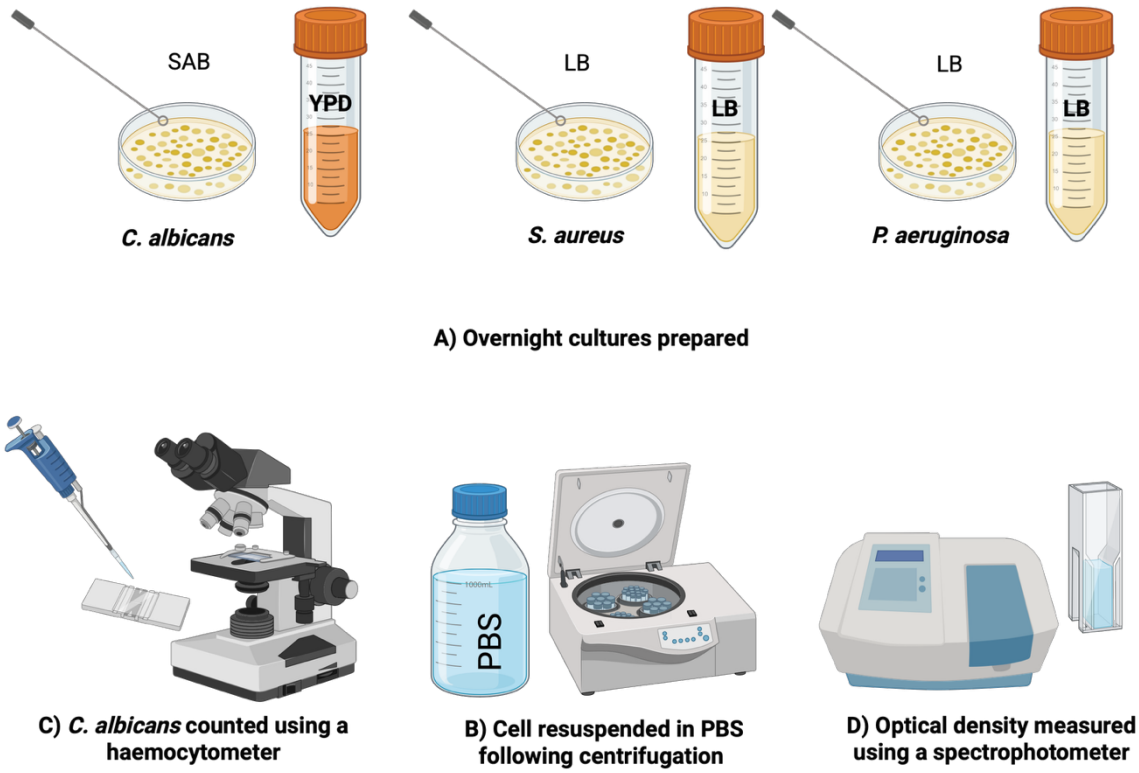

Figure 2.1: Schematic diagram summarised the microbial growth conditions and standardisation. A) Overnight cultures were prepared by inoculating microbial colonies into a specified medium for each microorganism for 16-18 h. B) Microbial cells were harvested by centrifugation and then resuspended in PBS. C) *C. albicans* were counted using a Neubauer haemocytometer (cell count × dilution factor × volume of square = CFU/mL), before being diluted to 1×10^6 CFU/mL in appropriate media. D) Bacterial cell concentrations of 1×10^8 cells/mL were obtained by measuring the OD with a spectrophotometer at 600 nm, before being diluted to 1×10^6 cells/mL in appropriate media. Diagram was created in BioRender.

2.2 Biofilm models

In the first data chapter (chapter 3) all biofilm models were grown on sterile cellulose matrix (CM) in a hydrogel (HG) system as mono and triadic species for 24 h. Notably, the triadic biofilm models were varying in their composition (e.g., *S. aureus* Newman triadic model consisting of *S. aureus* Newman, *C. albicans* SC5314 and *P. aeruginosa* PA14; *S. aureus* SH1000 triadic model consisting of *S. aureus* SH1000, *C. albicans* SC5314 and *P. aeruginosa* PA14; *S. aureus* NCTC 6571 triadic model consisting of *S. aureus* NCTC 6571, *C. albicans* SC5314 and *P. aeruginosa* PA14). This triadic model is representative of diabetic foot ulcers (DFUs)- because it explicitly includes bacterial–fungal communities that are highly prevalent and prognostically relevant in DFUs. DFUs show particularly high fungal burdens by sequencing (up to ~80% at presentation) with associations to delayed healing, so incorporating a fungal element aligns the model to DFU ecology more than to venous or pressure ulcer cohorts where fungal detection is less consistently reported (Kalan et al., 2016). Similarly, in the second data chapter (chapter 4) biofilms were grown on sterile CM in HG system as mono and triadic species for 24 h for the assessment of single and dual therapies, while the others experiment the biofilms were grown in pre-sterilised polystyrene 96-well flat-bottom microtiter plates for 24 h. In the final data chapter (chapter 5) all biofilms were grown as mono species in pre-sterilised polystyrene 96-well flat-bottom microtiter plates for 4 h (early-stage biofilms).

2.2.1 Biofilms on CM in HG model

2.2.1.1 HG preparation

The hydrogels (HGs) used in this study were composed of a mixture of several components as described by Townsend et al. (2016), Townsend et al. (2017). The primary constituents included 10% 3-sulfopropyl acrylate potassium salt, 0.95% v/v poly (ethylene glycol) deacrylate (PEG), and 0.01% v/v 1-hydroxycyclohexyl phenyl ketone. To enhance the biological relevance of the hydrogel, 50% heat-inactivated horse serum (HS) (Thermo Fisher Scientific, Loughborough, UK) was incorporated, with 2X PBS added to achieve the final volume. The HGs were prepared in 12-well flat-bottomed microtiter plates (Corning Incorporated, NY, USA). Each well received 2 mL of the hydrogel mixture. To initiate polymerisation, the plates were

exposed to ultraviolet (UV) light at 366 nm using a UV lamp (Camag, Hungerford, UK) for a duration of 1 h. This process was carried out within a class II laminar flow hood to maintain sterility. Following polymerisation, the hydrogels were stored at 4°C and remained viable for use for up to one week. This storage method ensured the stability and integrity of the HGs until they were required for experimental procedures.

2.2.1.2 Biofilm formation on CM in HG model

In the first and second data chapters (Chapter 3 and chapter 4) all mono-species and triadic biofilms were grown using a HG models on sterile CM (IPS Converters, Oldham, UK), as described by Townsend et al. (2016), Townsend et al. (2017) and is schematically represented in (Figure 2.2). All standardised isolates (final concentration of 1 $\times 10^6$ cells/mL in 10 mL sterile PBS) were allowed to attach to sterile CM (1.25 cm^2 by 1.25 cm^2) for 2 h incubation at 37°C with agitation at 180 rpm in an orbital shaker. Each matrix was washed once in PBS to remove non-adherent cells and then placed on top of the HG surface and incubated at 37°C for 24 h. Negative controls containing no inoculum were also included. All testing was carried out in triplicate, on three separate occasions.

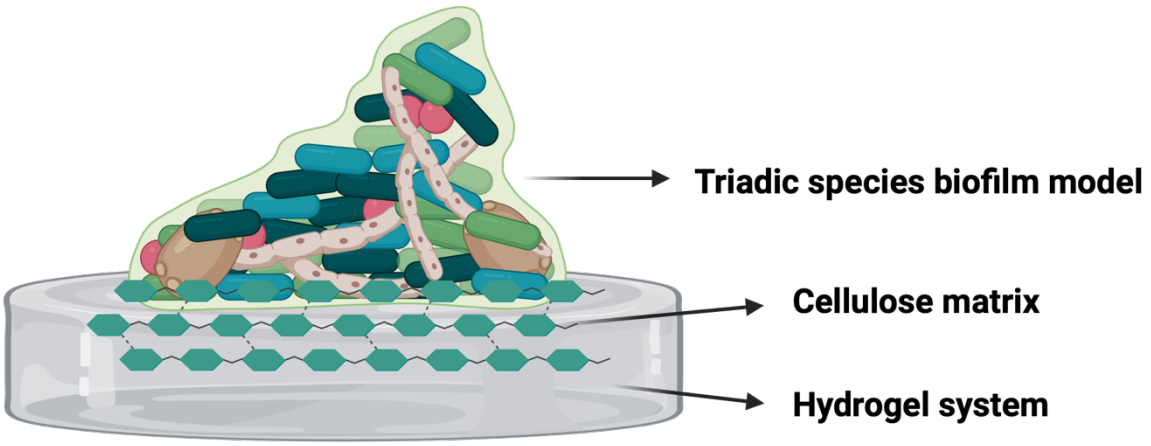

Figure 2.2: Schematic diagram shows triadic biofilm model developed on CM in HG system. All standardised isolates adhering to sterile CM during 2-h incubation at 37°C with orbital shaking 180 rpm. Non-adherent cells were removed via a single PBS wash, after which the matrices were transferred to HG surface and incubated for 24 h at 37°C. Triadic biofilm model consisting of *C. albicans* , *S. aureus* and *P. aeruginosa*. Diagram was created in BioRender.

2.2.2 Biofilm formation in microtiter well plates

In the second and third data chapters (chapter 4 and chapter 5), all microorganisms were standardised to a final working concentration of 1×10^6 cells/mL. For *C. albicans*, Roswell Park Memorial Institute (RPMI)-1640 medium (Sigma-Aldrich, Dorset, UK) was used, while LB medium was used for the bacterial strains. To assess the triadic models, experiments were conducted in a 1:1 v/v mixture of LB and RPMI media. Biofilm formation was carried out in pre-sterilised polystyrene 96-well flat-bottom microtiter plates (Corning Incorporated, NY, USA). Using a multi-channel pipette, 200 µL of the standardised microbial suspensions were dispensed into each well, following the protocol described by Ramage et al. (2001). To ensure experimental validity, negative control (wells containing only culture media) and positive control (wells containing only biofilms without treatment) were included on each plate. The inoculated plates were then incubated aerobically at 37°C for a period of 24 h to allow for biofilm formation. Data obtained is from four technical repeats from three independent experiments. The strains and biofilm models utilised in this study are detailed in (Table 2.1).

Table 2.1: Summary table of strains and biofilm models used in thesis chapters.

Strain	Biofilm model	Used in model	Chapter
C. albicans **(SC5314)**	Cellulose matrix/ Microtiter plates	Mono/ Triadic	3 & 4
S. aureus **(Newman)**	Cellulose matrix/ Microtiter plates	Mono/ Triadic	3, 4 & 5
P. aeruginosa **(PA14)**	Cellulose matrix/ Microtiter plates	Mono/ Triadic	3 & 4
S. aureus **(SH1000)**	Cellulose matrix/ Microtiter plates	Mono/ Triadic	3, 4 & 5
S. aureus **(NCTC 6571)**	Cellulose matrix	Mono/ Triadic	3
S. aureus **(S 235)**	Cellulose matrix	Mono-species	3
S. aureus **(ATCC 25923)**	Cellulose matrix	Mono-species	3
C. auris **(NCPF 8973)**	Cellulose matrix	Mono-species	3
C. auris **(NCPF 8978)**	Cellulose matrix	Mono-species	3

2.3 Treatment regimens

2.3.1 Preparation of antimicrobial agents

Three compounds effective against *C. albicans* were selected from the Tocriscreen™ 2.0 Micro library (Tocris, Bio-Techne, Abingdon, UK) as previously described by Abduljalil et al. (2022). The selected hit compounds were Polygodial (POLY), KHS101 hydrochloride (KHS) and darapladib (DARA) (chapter 4). All these compounds solubilised in 100% DMSO (w/v) according to manufacturer instructions to produce 100 mM stocks. Aliquots of each compound into sterile Eppendorf tubes were then stored at -20°C until required. The stock solution was then diluted down to double the required concentration (64 X 2 = 128 µg/mL) in the appropriate broth prior to required experiment. In addition, two traditional anti-biofilm wound therapies were chosen for anti-biofilm testing (chapter 4): Povidone iodine (PVP-I) and hydrogen peroxide (H_2O_2), both sourced from (Merck Life Sciences, Gillingham, UK). These solutions were freshly prepared in sterile double-distilled water (ddH_2O) just before use. The compounds were applied at clinically relevant concentrations, specifically 3% v/v for H_2O_2 and 10% w/v for PVP-I. For the dual-therapy investigative experiments in chapter 4, KHS and an oxidative cocktail solution of H_2O_2, nitrite (NO_2) and nitrate (NO_3), sodium nitrate ($NaNO_{3)}$ (Sigma-Aldrich, Dorset, UK) and sodium nitrite ($NaNO_{2)}$ (Thermo Fisher Scientific, Loughborough, UK) were prepared in 100 mL sterile ddH_2O at 1 Molar (1M) stock concentration in a Duran bottle (250 mL) and stored at room temperature until required. This step was carried out within a class II laminar flow hood. For H_2O_2 re-sensitisation experiments in chapter 5, Gentamicin sulfate salt (stock conc. 50 mg/mL) and Flucloxacillin sodium (stock conc. 20 mg/mL) both were dissolved in sterile ddH_2O and aliquots of each compound into sterile Eppendorf tubes were then stored at -20°C until required. Both compounds provided from (Sigma-Aldrich, Dorset, UK).

2.3.2 Cold atmospheric plasma (CAP) treatment

Following biofilm formation as previously described in section 2.2.1.2, each matrix underwent a washing step with PBS to eliminate non-adherent cells prior to CAP exposure. The CAP treatments were conducted for durations of 1, 3, and 5 minutes. The experimental setup for plasma treatment was based on the design

described by Ghimire, Szili and Short (2022), and is schematically represented in (Figure 2.3). The CAP device comprised six plasma jets arranged in a rectangular configuration. Pure argon gas (99.9999% purity) was used to generate the CAP, with an applied voltage of 8 kV peak-to-peak and a frequency of 23.5 kHz. The gas flow rate was maintained at six standard litres per minute (SLPM). During treatment, the biofilm-containing cellulose matrices (CMs) were positioned at a distance of 1 cm from the end of the quartz tube of the plasma jets. To ensure comprehensive CAP coverage, the porous cellulose matrices were inverted midway through each treatment session, allowing exposure of both sides of the material. Biofilms experiments were completed on three separate occasions with three technical replicates per experiment (n =9 in total).

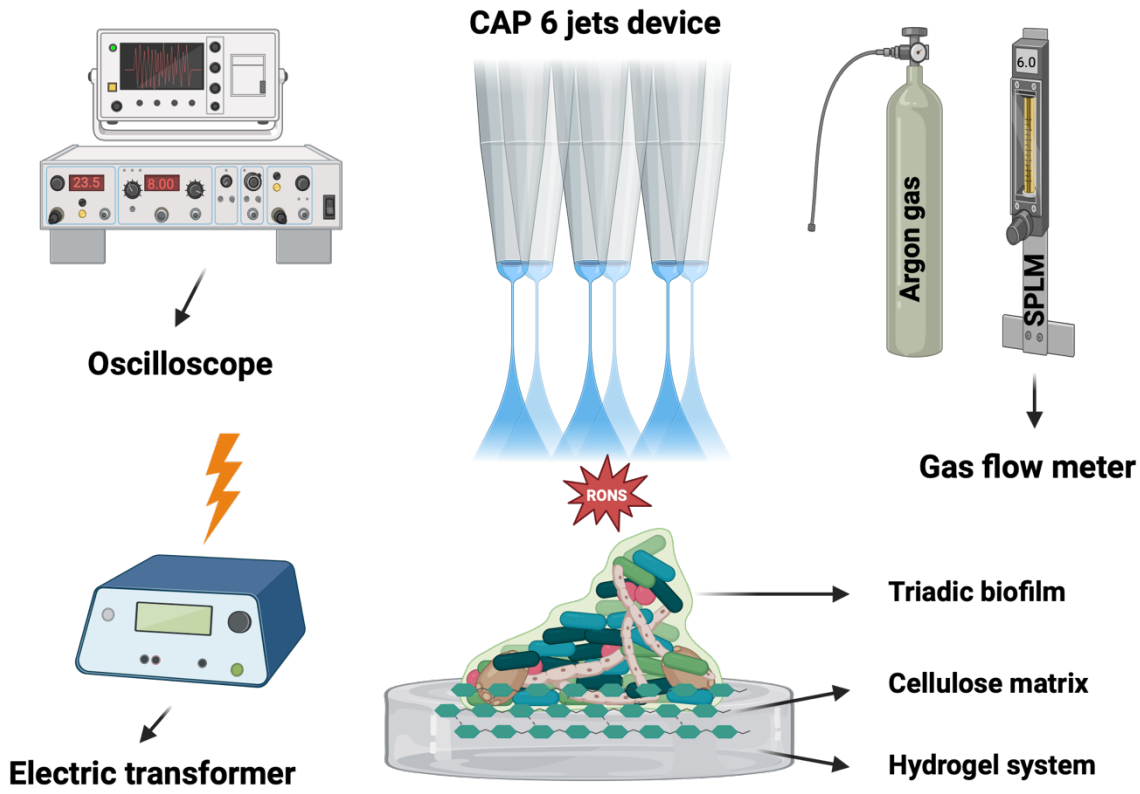

Figure 2.3: Schematic diagram shows CAP device elements. The CAP device comprised six plasma jets arranged in a rectangular configuration. Pure argon gas was used to generate the CAP, with an applied voltage of 8 kV peak-to-peak and a frequency of 23.5 kHz. The gas flow rate was maintained at 6 SLPM. Diagram was created in BioRender.

2.4 Assays and profiling

To assess the composition and viability of biofilms at a molecular level (chapter 3 and chapter 4), a viability-based quantitative polymerase chain reaction (qPCR) approach was employed. This method allows for the differentiation between viable and total cells within the biofilm community. The technique has been previously validated and applied in several studies investigating microbial populations in complex environments (Àlvarez et al., 2013, Sanchez et al., 2013, Sanchez et al., 2014, Sherry et al., 2016).

2.4.1 Propidium monoazide (PMA) treatment

Following CAP treatment of mono and triadic species biofilms, the CM was carefully removed with tweezers and placed into a bijoux containing 1 mL of sterile PBS. It was then sonicated at 35 kHz in an ultrasonic water bath (Fisherbrand, ThermoFisher Scientific Inc., Loughborough, UK) for 10 minutes to detach the biomass. The resulting 1 mL sonicate was vortexed for 30 seconds and divided between two nuclease-free 1.5 mL Eppendorf tubes. To one 500 µL aliquot, 2.5 µL of 10 mM PMA was added, a dye that penetrates only dead cells or cells with compromised membranes (Sigma-Aldrich, Irvine, Scotland) (Nocker, Cheung and Camper, 2006) (Figure 2.4). The other aliquot served as a negative control without PMA. All samples were incubated in the dark at room temperature for 10 minutes to allow PMA uptake by dead cells. They were then placed on bed of ice (to avoid excessive heating) and exposed to a 650 W halogen light from about 20 cm away for 5 minutes. Samples were stored at −20°C until DNA extraction (Sherry et al., 2016). Biofilms experiments were completed on three separate occasions with three technical replicates per experiment (n =9 in total).

2.4.2 DNA extraction

DNA extraction involved bead-beating combined with a QIAamp DNA Mini Kit (Qiagen, Crawley, UK), following the manufacturer's instructions with small modification. Samples were centrifuged at 13,000 rpm for 10 minutes, the supernatant discarded, and pellets resuspended in 180 µL of ATL buffer with 20 µL of proteinase K. They were incubated in a water bath (Grant instruments, UK) at 56°C for microbial lysis for 20 minutes. Next, 200 µL of AL buffer was added,

mixed by vortexing for 15 seconds, and incubated at 70°C for another 10 minutes. The samples were transferred to a screw cap tube (Thistle Scientific, UK) containing about 250 µL of sterile glass beads and subjected to bead beating for three cycles of 30 seconds at maximum speed using a bead beater (Fisher Bead Mill 24, UK). To precipitate nucleic acids, 200 µL of 100% ethanol was added, mixed by vortexing for 15 seconds, and centrifuged at 7000 rpm for 1 minute. The supernatant was transferred to a QIAamp spin column and centrifuged at 8000 rpm for 1 minute. After discarding the flow-through, 500 µL of buffer AW1 was added to the columns and centrifuged again at 8000 rpm for 1 minute. This step was repeated with buffer AW2 and centrifuged at 13,000 rpm for 3 minutes before transferring columns to new collection tubes. The column membranes were dried by centrifugation at 13,000 rpm for 1 minute. DNA was eluted in 100 µL of AE buffer into nuclease-free Eppendorf tubes with the lid cut off by centrifugation at 8,000 rpm for 1 minute and stored at -20°C until needed. To generate standard curves for bacterial and fungal species, pure cultures of individual bacterial and fungal species were prepared and standardised to a concentration of 1×10^8 CFU/mL in sterile PBS. These standardised suspensions were then subjected to a series of ten-fold dilutions, creating a range of concentrations from 1×10^8 to 1×10^3 CFU/mL. DNA extraction was performed on each dilution using the same methodology as described above. All biofilm experiments were completed on three separate occasions with three technical replicates per experiment (n =9 in total).

2.4.3 Live/dead qPCR

For each qPCR reaction, a master mix was prepared containing 10 µL of Fast SYBR GreenER™ (Thermo Fisher Scientific, Paisley, UK), 7 µL of UV-treated nuclease-free water, and 1 µL each of 10 µM forward and reverse primers specific to the bacterial or fungal species of interest. The primer sequences utilised in this study are detailed in (Table 2.2). To this master mix, 1 µL of extracted DNA sample was added, resulting in a total reaction volume of 20 µL. The prepared reactions were loaded into 96-well 0.1 ml reaction plate (Applied Biosystems, California, USA), which were then sealed with caps and centrifuged at 1000 rpm for 1 minute to ensure proper mixing and to eliminate air bubbles. The qPCR amplification was performed using a StepOnePlus™ real time PCR machine and StepOne software V2.3 (Life Technologies, Paisley, UK). The thermal cycling profile as follows: 50°C

for 2 minutes, 95˚C for 2 minutes, followed by 40 cycles of 95˚C for 10 seconds and 60˚C for 30 seconds (Figure 2.4). To ensure data reliability, all samples were analysed in technical duplicate. Additionally, negative control wells containing the master mix and primer sets but lacking bacterial or fungal DNA were included on each plate to rule out potential contamination. The cycle threshold (Ct) was consistently set at 0.1 for all plates to ensure standardised analysis across experiments. Colony forming equivalents per millilitre (CFE/mL) were calculated based on species-specific standard curves, as previously described by O'Donnell et al. (2016). For some experiments CFE analysis allowed for assessing % composition of the triadic model pre- and post-regrowth. Data obtained is from triplicates from three independent experiments (n =9 in total).

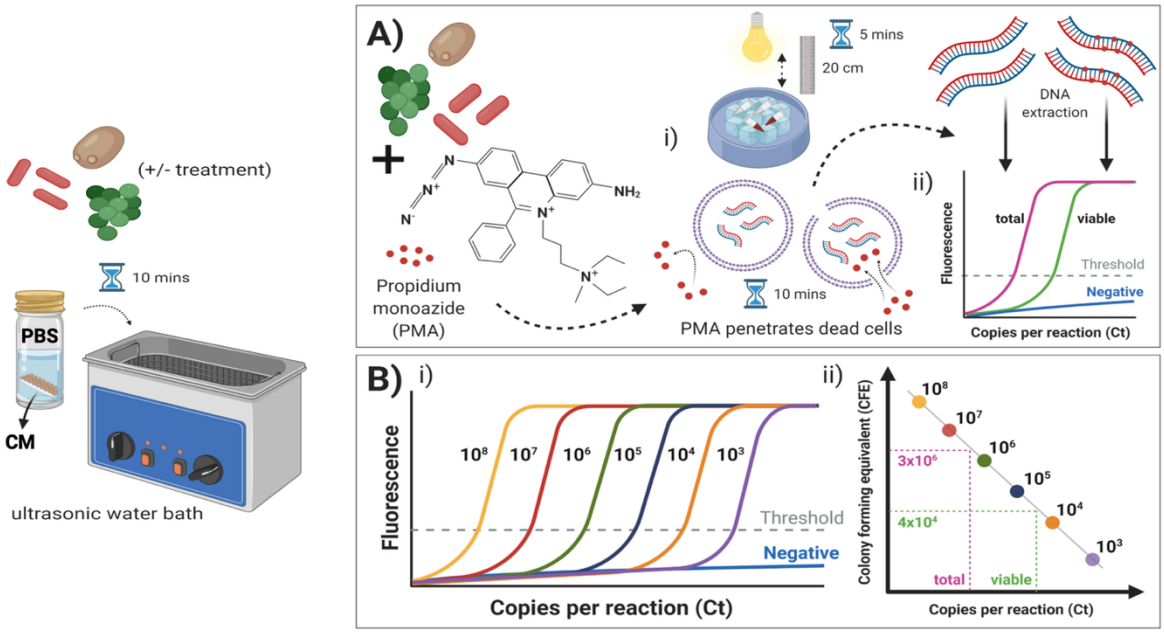

Figure 2.4: Schematic diagram illustrated PMA treatment prior Live/dead qPCR. Flowing the treatment, biofilms on CM were sonicated (35 kHz, 10 min) in PBS to dislodge cells, followed by vortexing and aliquot division. One aliquot received PMA to selectively label DNA from dead cells, while the other served as a control. Samples were incubated in the dark (10 min), exposed to halogen light (650 W, 5 min) on ice to crosslink PMA (A-i). After DNA extraction, qPCR distinguishes viable and total cells by comparing cycle threshold (Ct) values: lower Ct values correspond to untreated samples (total cells), while higher Ct values reflect PMA-treated samples (viable cells) (A-ii). To quantify colony-forming equivalents (CFE/mL) in test samples, a standard curve is generated using DNA extracted from planktonic cultures with known CFE/mL (10^8–10^3) (B-i). This curve (Ct vs. known CFE/mL) allows extrapolation of viable and total bacterial loads in unknown samples (B-ii). Diagram was created in BioRender.

Table 2.2: Primer sequences used to identify fungi and bacterial species.

Organism	Forward primer 5'-3'	Reverse primer 5'-3'
S. aureus	ATTTGGTCCCAGTGGTGTGGGTAT	GCTGTGACAATTGCCGTTTGTCGT
P. aeruginosa	GGGCGAAGAAGGAAATGGTC	CAGGTGGCGTAGGTGGAGAA
C. albicans	GAGCGTCGTTTCTCCCTCAAACCGCTGG	GGTGGACGTTACCGCCGCAAGCAATGTT
C. auris	GCATCGATGAAGAACGCAGC	TCCTCCGCTTATTGATATGC

2.4.4 Time dependant killing effect of CAP assessment

C. auris NCPF 8978 and NCPF 8973 biofilms were grown for 24 h within the CM on HG system, and treated for 1, 3 and 5 min with CAP as previously described in 2.3.2 Then samples were prepared for extraction and live/dead qPCR using colony forming equivalents/mL (CFE/mL) as above used protocols 2.4.1, 2.4.2 and 2.4.3. Total and viable counts were assessed. All biofilms experiments were completed on three separate occasions with three technical replicates per experiment (n =9 in total).

2.4.5 H_2O_2, NO_2 and NO_3 quantification assay

To evaluate the H_2O_2, NO_2 and NO_3 levels generated by CAP therapy, plasma-activated water (PAW) was produced following a protocol similar to that described by Ghimire et al. (2021). Briefly, 1.5 mL of sterile ddH_2O was dispensed into each well of a 12-well flat-bottom plate (Corning Incorporated, Corning, NY, USA) and subsequently exposed to CAP for durations of 1, 3, and 5 minutes. Following plasma activation, the concentration of H_2O_2 in the PAW was quantified using the Amplex™ Red Hydrogen Peroxide/Peroxidase Assay Kit (Thermo-Fisher, UK). The assay was performed according to the manufacturer's instructions. To ensure accuracy, a standard curve of known H_2O_2 concentrations was generated for each assay run, allowing for the precise determination of H_2O_2 levels in the plasma-activated samples. Untreated water minus CAP therapy was used for comparison. H_2O_2 levels were completed on three separate occasions with two technical replicates per experiment (n =6 in total). Notably, NO_2 and NO_3 in PAW were assayed using the Griess Reagent Kit for Nitrite Determination (G-7921, Thermo-

Fisher, UK), but no NO_2 or NO_3 signal were detected in this experiment. This likely indicates that PAW NO_2/NO_3 levels were below the kit's detection threshold (1.0 µM as stated by manufactur protocol) under the assay conditions, rather than conclusively absent.

2.4.6 Regrowth assessment

To assess the regrowth potential of the *S. aureus* Newman triadic model, 24 h biofilms were subjected to the previously described CAP treatment protocol in 2.3.2 Following treatment, the biofilms were transferred onto a fresh HG substrate for an additional 24 h incubation period. To facilitate regrowth, the CM was rehydrated with 200 µL of sterile ddH_2O and returned to the incubator at 37°C (Figure 2.5). After the regrowth phase, the biofilms were processed as above used protocols for DNA extraction, live/dead qPCR, and compositional analysis 2.4.1, 2.4.2 and 2.4.3. Regrowth experiments were completed on three separate occasions with three technical replicates per experiment (n =9 in total).

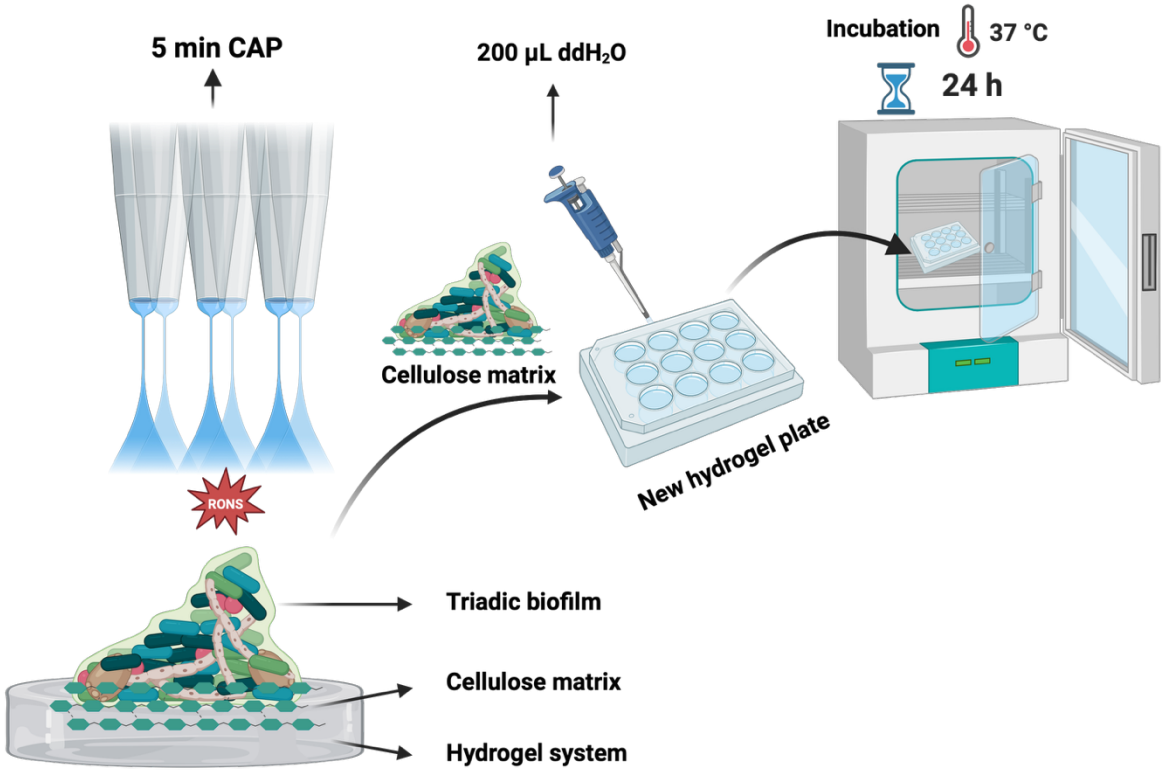

Figure 2.5: Schematic diagram illustrated the regrowth experiment. Following CAP treatment, the biofilms were transferred to new HG substrate for an additional 24 h incubation period. CMs were rehydrated with 200 µL of sterile ddH_2O and returned to the incubator at 37°C. Diagram was created in BioRender.

2.4.7 Metabolic activity assay

Following biofilm formation in pre-sterilised polystyrene 96-well flat-bottom microtiter plates as previously described in 2.2.2, the supernatant was discarded using a multi-channel pipette which was slowly inserted the tips at a 45-degree angle to avoid contact with the sides and bottom of the wells, and biofilms were washed once with 200 µL PBS to remove the loosely attached cells. Antimicrobial agents were prepared to double the required concentration (64 X 2 = 128 µg/mL) in the appropriate broth and serially diluted in fresh 96-well round-bottom microtiter plates (Corning Incorporated, NY, USA). To each well, 200 µL of the prepared antimicrobial was added (usually the first column), followed by serial doubling dilutions in the appropriate broth. Subsequently, 100 µL of the the appropriate broth was added to each well, resulting in a final volume of 200 µL. After this, the serially antimicrobial agents were fully transferred into the original 96-well flat-bottom microtiter plates using a multi-channel pipette from low concentration to the highest concentration. To ensure experimental validity, negative control (wells containing only culture media) and positive control (wells containing only biofilms without treatment) were included on each plate. The plates were incubated for 24 h at 37°C aerobically.

Following treatment, the supernatant was discarded, and neutralisation step was performed by adding 200 µL of 5% sodium thiosulfate (Fisher Chemicals, UK) for 15 minutes incubation at room temperature to deactivate the treatment effect. Sodium thiosulfate was also applied to negative and positive controls to normalise results. Following this, the neutraliser was removed, and biofilms were washed once with 200 µL PBS. After this, metabolic activity of the biofilms was assessed using AlamarBlue™ (AB) cell viability dye (Invitrogen, UK) as per manufacturer's instructions (Kirchner et al., 2012). In summary, AB was diluted 1:10 with the appropriate growth medium, and 100 µL of this solution was added to each well under dark conditions. The plates were then incubated at 37°C aerobically. A colour changes from blue to pink indicated the reduction of the fluorogenic dye resazurin to resorufin by reductase enzymes during normal cellular respiration (Figure 2.6). The colour change was monitored until the positive control exhibited a sufficient pink to serve as a 100% viability reference or for a maximum of 3 h, whichever occurred first. Afterwards, 75 µL from each well was transferred to a new 96-well flat-bottom microtiter plate for fluorescence measurement at an

excitation/emission wavelength of 544/590 nm according to the manufacturer's recommendation using a microtiter plate reader (FLUOStar Omega, BMG Labtech, Aylesbury, UK). A negative sterility control, which showed no biofilm growth, was included on the same plate to serve as a blank. This blank was used to normalise fluorescence readings by averaging its value and subtracting it from the test readings. Data obtained is from four technical repeats from three independent experiments.

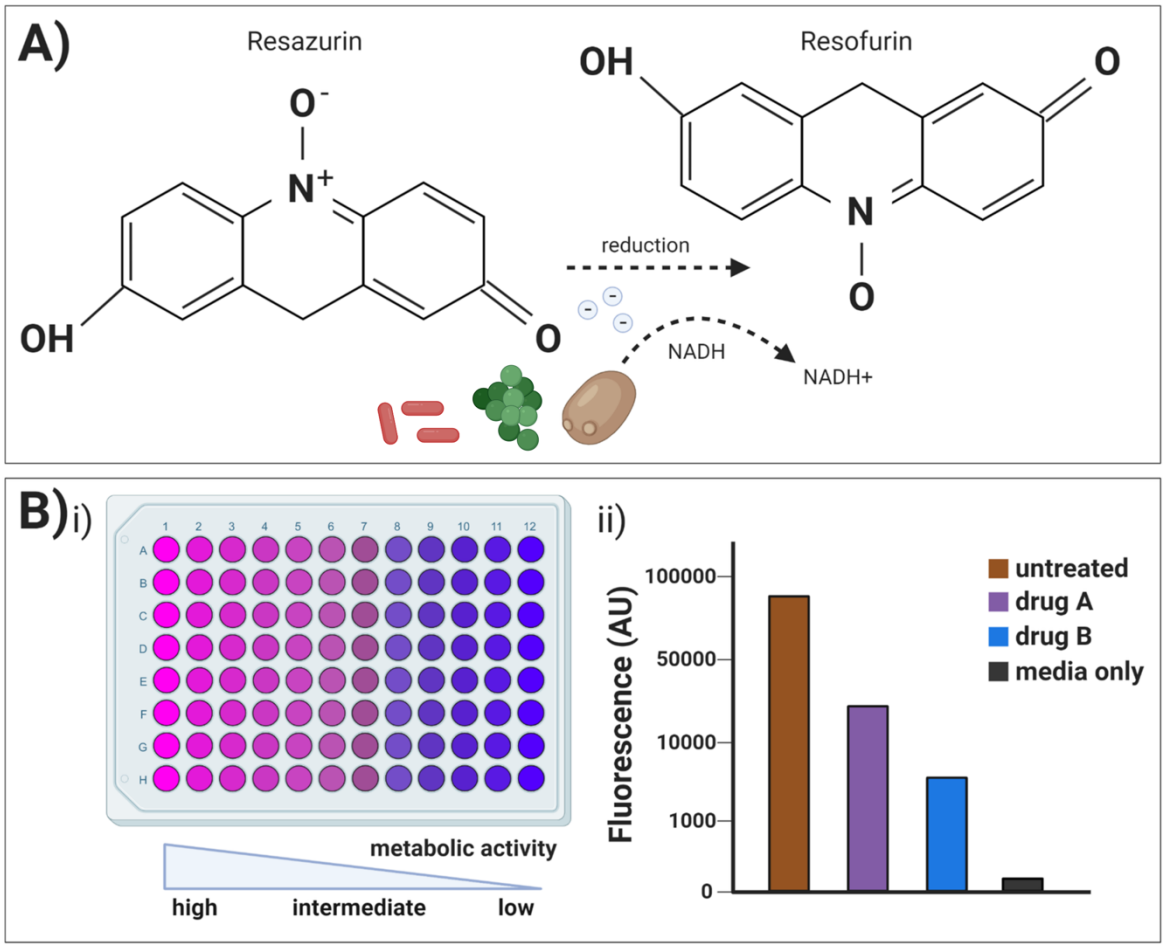

Figure 2.6: Schematic diagram illustrated AlamarBlueTM metabolic activity assay. Flowing the treatment, biofilm metabolically active cells reduce resazurin to fluorescent resofurin using NADH and other electron-donating agents (A), producing a visible colour shift from purple to pink that correlates with metabolic activity levels (B-i). This fluorescence change is quantified using a microplate reader at 544 nm excitation and 590 nm emission wavelengths, with results expressed as arbitrary units (AU) to standardise measurements across samples (B-ii). Diagram was created in BioRender.

2.4.8 Biofilm biomass assay

Following the metabolic activity measurements, biofilm biomass was assessed using crystal violet (CV) assay (Figure 2.7). The method used was based off a

modified version of a protocol first developed by Christensen et al. (1985) and subsequently modified by Allkja et al. (2020). Briefly, A stock solution of 1% w/v CV (Sigma-Aldrich, UK) was made using sterile ddH_2O and diluted to 0.05% for use. The remaining AB was removed from each well by using a multi-channel pipette which was slowly inserted the tips at a 45-degree angle to avoid biofilm disruption. Afterwards, biofilms were fixed with 200 µL of 100 % ethanol was added to each well for 15 minutes, followed by air-drying until completely dry, which took between 5 and 10 minutes. The plate was subsequently stained with 200 µL of 0.05% v/v CV per well for 15 minutes at room temperature. After staining, the plates were washed once with 200 µL of sterile ddH_2O per well using a multichannel pipette and left to air-dry for another 15 minutes. The stain was eluted with 200 µL of 100% ethanol per well for 5 minutes at room temperature. The eluted stain was mixed by pipetting up and down five times to get homogenous colour, and then 100 µL from each well was transferred to an empty 96-well flat-bottom microtiter plates using a multi-channel pipette for measurement. Biomass was quantified spectrophotometrically by reading absorbance at 570nm according to the manufacturer's recommendation (FLUOStar Omega, BMG Labtech, Aylesbury, UK). A negative sterility control, which showed no biofilm growth, was included on the same plate to serve as a blank. This blank was used to normalise absorbance readings by averaging its value and subtracting it from the test readings. Data obtained is from four technical repeats from three independent experiments.

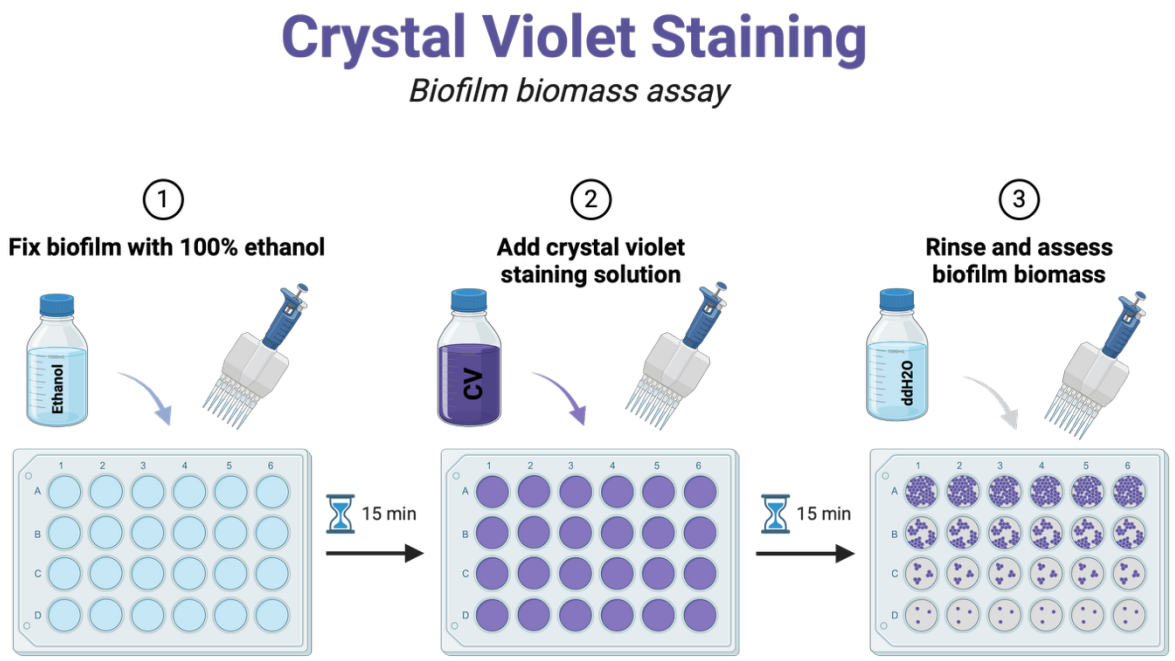

Figure 2.7: Schematic diagram described biofilm biomass assessment. Flowing the metabolic activity measurement, biofilms were fixed with 100% ethanol prior staining with crystal. Biofilm biomass was quantified spectrophotometrically by reading absorbance at 570nm. The plates that used in the schematic figure are (24 well plates) while our experiments conducted in (96 well flat bottom). Diagram was created in BioRender.

2.4.9 Molecular assessment of single and dual therapy on the HG model

Mono-species and triadic biofilm models were grown using a HG model on sterile CM for 24-h as previously described in 2.2.1 Following biofilm formation, each matrix underwent a washing step with PBS to eliminate non-adherent cells before 5 min treatment at room temperature with 500 µL of 3% H_2O_2, 10% PVP-I or 32 µg/mL of KHS 101. After 5 min treatment, 500 µL of Dey- Engley Neutralising broth (Sigma-Aldrich, London, UK) was added and incubated for 15 min at 37°C aerobically to deactivate the treatment effect. Untreated controls were neutralised though to ensure that the observed effect is solely due to applied treatments and not neutraliser. Afterwards, the neutraliser was washed by 500 µL of PBS before applied DNA extraction, and Live/dead qPCR protocols as previously described in 2.4.1, 2.4.2 and 2.4.3. For dual therapy, each matrix was treated in the same manner as above described and followed by additional 5 min CAP treatment. Following CAP therapy, Samples were prepared for DNA extraction, and Live/dead qPCR as previously described in 2.4.1, 2.4.2 and 2.4.3. All biofilms experiments were completed on three separate occasions with three technical replicates per experiment (n =9 in total).

2.4.10 Kinetic growth curve assay

Polygodial (POLY), KHS 101 hydrochloride (KHS) and darapladib (DARA) were used in this assay to assess their inhibitory effects on microbial growth. Planktonic forms of *C. albicans* SC5314, *P. aeruginosa* PA14, *S. aureus* Newman, and *S. aureus* SH1000 were involved in this experiment (chapter 4). In brief, following standardisation as previously described in 2.1, cell suspensions were prepared by adjusting yeast concentrations to 2×10^4 cells/mL in YPD broth and bacterial concentrations to 2×10^5 cells/mL in LB broth. Antimicrobial agents were prepared to double the required concentration (64 X 2 = 128 µg/mL) in the appropriate broth (YPD or LB) and serially diluted in 96-well round-bottom microtiter plates. To each well, 200 µL of the prepared antimicrobial was added (usually the first column), followed by serial doubling dilutions in the appropriate broth (YPD or LB). Subsequently, 100 µL of the standardised cell suspension was added to each well, resulting in a final volume of 200 µL. The plates were placed in a Cerillo microplate reader device (Cerillo, USA) to monitor growth, and incubated at appropriate temperature (30°C or 37°C) for 24 h aerobically with shaking at 200 rpm in an orbital shaker. Appropriate positive and negative controls were also included. OD measurements at 600 nm were taken at regular intervals every 2 h using a Cerillo microplate reader. Growth curves were generated by plotting the mean OD values against time. Data obtained is from four technical replicates of two biological repetitions.

2.4.11 Planktonic Minimum inhibitory concentration (PMIC)

The assessment of pathogen susceptibility to antimicrobials is crucial for selecting the most appropriate compounds for treating microbial infections. In the final data chapter (chapter 5), PMIC susceptibility testing was performed based on the Clinical and Laboratory Standards Institute (CLSI) documents M07-A10 standard for bacteria (CLSI, 2015) to determine the PMIC of various relevant antimicrobials against planktonic forms of *S. aureus* Newman, and *S. aureus* SH1000. The experimental procedure involved preparing cell suspensions by adjusting bacterial concentrations to 2×10^5 cells/mL in LB broth. Antimicrobial agents were prepared to double the required concentration in the LB broth and serially diluted in 96-well round-bottom microtiter plates. To each well, 200 µL of the prepared antimicrobial was added (usually the first column), followed by serial doubling

dilutions in LB. Subsequently, 100 µL of the standardised cell suspension was added to each well, resulting in a final volume of 200 µL. The plates were incubated at 37°C for 24 h aerobically. Appropriate positive and negative controls were also included. Following incubation, the $PMIC_{90}$ was determined as the lowest antimicrobial concentration that completely inhibited visible microbial growth.

2.4.12 Scanning electron microscopy (SEM)

Biofilms were grown in HG model on CM as mono-species and triadic model (*S. aureus* Newman triadic model) and treated by CAP as previously described in section 2.2.1 and 2.3.2 in the first data chapter (chapter 3). The samples were washed once with PBS before fixation. The fixation solution consisted of 2% paraformaldehyde, 2% glutaraldehyde, 0.15 M sodium cacodylate, and 0.15% w/v alcian blue, adjusted to pH 7.4. Samples were immersed in this solution for 18 hours. After fixation, the solution was replaced with 0.15 M sodium cacodylate buffer, and samples were stored at 4°C until further processing. Sample preparation for SEM followed a protocol adapted from Erlandsen et al. (2004). The fixed samples were washed three times for 5 minutes each with 0.15 M sodium cacodylate to remove residual glutaraldehyde. Subsequently, samples were treated with a 1:1 mixture of 1% osmium tetroxide and 0.15 M sodium cacodylate for 1-h in a fume hood. After osmium tetroxide treatment, samples were rinsed three times for 10 minutes each with distilled water. The samples were then treated with 0.5% uranyl acetate and incubated in darkness for 1-h. Following a quick rinse with water, the samples underwent a series of dehydration steps using increasing concentrations of ethanol. This process involved two 5-minute rinses each of 30%, 50%, 70%, and 90% ethanol, followed by four 10-minute rinses with absolute and dried absolute ethanol. To achieve complete drying, hexamethyldisilazane (HMDS) was employed. Samples were soaked in HMDS for 5 minutes, transferred to a fresh plate containing HMDS, and then placed in a desiccator overnight to allow for complete drying and evaporation of any residual HMDS. Finally, the dried specimens were mounted and sputter-coated with gold in an argon-filled chamber. SEM imaging was performed using a Jeol JSM-IT100 InTouch™ scanning electron microscope. Scanning electron microscope and representative images were taken at magnifications of ×1,500 for fungal biofilms and ×3,500 for bacterial mono-species and triadic model biofilms, respectively.

2.5 Drug interactions in checkerboard microdilution assay

2.5.1 Assessing interactions between KHS and H_2O_2

The interaction between KHS and H_2O_2 was evaluated using a checkerboard microdilution assay (chapter 4) and schematically presented in (Figure 2.8). Biofilms were grown in pre-sterilised polystyrene 96-well flat-bottom microtiter plates and incubated at 37°C for 24 h under aerobic conditions, as previously detailed in section 2.2.2. All microorganisms were adjusted to a final working concentration of 1×10^6 cells/mL. RPMI medium was employed for *C. albicans* SC5314, while LB medium was used for the bacterial strains *S. aureus* Newman, *S. aureus* SH1000, and *P. aeruginosa* PA14, respectively. For triadic models, experiments were conducted in a 1:1 v/v mixture of LB and RPMI media. Following biofilm formation, the supernatants were carefully removed using a multi-channel pipette, and biofilms were washed once with 200 µL PBS to remove loosely attached cells. Antimicrobial agents were prepared at four times the required concentration (64 X 4 = 256 µg/mL for KHS and 64 X 4 = 256 mM for H_2O_2) in the appropriate medium and serially diluted in fresh 96-well round-bottom microtiter plates. KHS (200 µL) was added to the first column, followed by serial doubling dilutions across columns 1 to 9. Subsequently, H_2O_2 (100 µL) was added to the first row, followed by serial doubling dilutions down rows A to G. The appropriate medium (100 µL) was then added to each well, resulting in a final volume of 200 µL. The serially diluted antimicrobial agents were transferred to the original 96-well flat-bottom microtiter plates containing biofilms with changing tips every time during antimicrobial agents transferring. Negative controls (wells containing only culture media) and positive controls (wells containing untreated biofilm) were included to ensure experimental validity. Plates were incubated aerobically at 37°C for 24 h.

Post-treatment, the supernatant was discarded, and a neutralisation step was performed using 200 µL of 5% sodium thiosulfate, incubated for 15 minutes at room temperature to deactivate the treatment effect. Sodium thiosulfate was also applied to control wells for result normalisation. After neutraliser removal, biofilms were washed once with 200 µL PBS, and biofilm metabolic activity was assessed using AlamarBlue™, as outlined in section 2.4.7. The efficacy of drug combination was assessed by the checkerboard microtiter assay as previously

described by Meletiadis et al. (2003). The assay was performed to evaluate the effect of combining of KHS with H_2O_2 against different mono-species and triadic biofilm models, which contained different concentrations of each drug combination. The sessile minimum inhibitory concentration (SMIC) was determined by measuring the reduction in biofilm metabolic activity using AlamarBlue™ assay. The $SMIC_{50}$ or $SMIC_{80}$ were defined as the lowest concentration of the tested compound that reduced biofilm metabolic activity by 50% or 80% compared with untreated control (Ramage et al., 2001). The data obtained from the checkerboard tests were analysed by the fractional inhibitory concentration index (FICI), which was expressed as $\sum FIC = FIC_A + FIC_B = SMIC_{AB}/SMIC_A + SMIC_{BA}/SMIC_B$, where $SMIC_A$ and $SMIC_B$ are the SMICs of drugs A and B when administered individually and $SMIC_{AB}$ and $SMIC_{BA}$ are the SMICs of drugs A and B when administered in combination, respectively. Synergy was defined as $FICI \leq 0.5$, antagonism was defined as $FICI > 4$, $0.5 < FICI \leq 1$ was considered additive, and indifferent when $1 < FICI \leq 4$ (Kemegne et al., 2021). Data were collected from three independent experiments for *C. albicans* SC5314 and two independent experiments for other microorganisms (because the first two independent experiments yielded concordant results with no differences across conditions).

2.5.2 Interaction between KHS and oxidative cocktail solution of (H_2O_2, NO_2 and NO_3)

The interaction between KHS and an oxidative cocktail solution of (H_2O_2, NO_2 and NO_3) was evaluated using a checkerboard microdilution assay (chapter 4) and schematically presented in (Figure 2.8). Biofilms were grown in pre-sterilised polystyrene 96-well flat-bottom microtiter plates and incubated at 37°C for 24-h under aerobic conditions, as previously detailed in section 2.2.2. All microorganisms were adjusted to a final working concentration of 1×10^6 cells/mL. RPMI medium was employed for *C. albicans* SC5314, while LB medium was used for the bacterial strains *S. aureus* Newman, *S. aureus* SH1000, and *P. aeruginosa* PA14. For triadic models, experiments were conducted in a 1:1 v/v mixture of LB and RPMI media. Following biofilm formation, the supernatants were carefully removed using a multi-channel pipette, and biofilms were washed once with 200 µL PBS to remove loosely attached cells. Antimicrobial agents were prepared at four times the required concentration (64 X 4 = 256 µg/mL for KHS

and 64 X 4 = 256 mM for an oxidative cocktail solution) in the appropriate medium and serially diluted in fresh 96-well round-bottom microtiter plates. KHS (200 µL) was added to the first column, followed by serial doubling dilutions across columns 1 to 9. Subsequently, an oxidative cocktail solution (100 µL) was added to the first row, followed by serial doubling dilutions down rows A to G. The appropriate medium (100 µL) was then added to each well, resulting in a final volume of 200 µL. The serially diluted antimicrobial agents were transferred to the original 96-well flat-bottom microtiter plates containing biofilms with changing tips every time during antimicrobial agents transferring. Negative controls (wells containing only culture media) and positive controls (wells containing untreated biofilm) were included to ensure experimental validity. Plates were incubated aerobically at 37°C for 24 h.

Post-treatment, the supernatant was discarded, and a neutralisation step was performed using 200 µL of 5% sodium thiosulfate, incubated for 15 minutes at room temperature to deactivate the treatment effect. Sodium thiosulfate was also applied to control wells for result normalisation. After neutraliser removal, biofilms were washed once with 200 µL PBS, and biofilm metabolic activity was assessed using AlamarBlue™, as outlined in section 2.4.7. The efficacy of drug combination was assessed by the checkerboard microtiter assay as previously described by Meletiadis et al. (2003). The assay was performed to evaluate the effect of combining of KHS with an oxidative cocktail solution of (H_2O_2, NO_2 and NO_3) against different mono-species and triadic biofilm models, which contained different concentrations of each drug combination. The SMIC was determined by measuring the reduction in biofilm metabolic activity using AlamarBlue™ assay. The $SMIC_{50}$ and $SMIC_{80}$ were defined as the lowest concentration of the tested compound that reduced biofilm metabolic activity by 50% or 80% compared with untreated control (Ramage et al., 2001). The data obtained from the checkerboard tests were analysed by the fractional inhibitory concentration index (FICI), which was expressed as $\sum FIC = FIC_A + FIC_B = SMIC_{AB}/SMIC_A + SMIC_{BA}/SMIC_B$, where $SMIC_A$ and $SMIC_B$ are the SMICs of drugs A and B when administered individually and $SMIC_{AB}$ and $SMIC_{BA}$ are the SMICs of drugs A and B when administered in combination, respectively. Synergy was defined as $FICI \leq 0.5$, antagonism was defined as $FICI > 4$, $0.5 < FICI \leq 1$ was considered additive, and indifferent when $1 < FICI \leq 4$ (Kemegne et al., 2021). Data were collected from

three independent experiments for *C. albicans* SC5314 and two independent experiments for other microorganisms (because the first two independent experiments yielded comparable results with no differences across conditions).

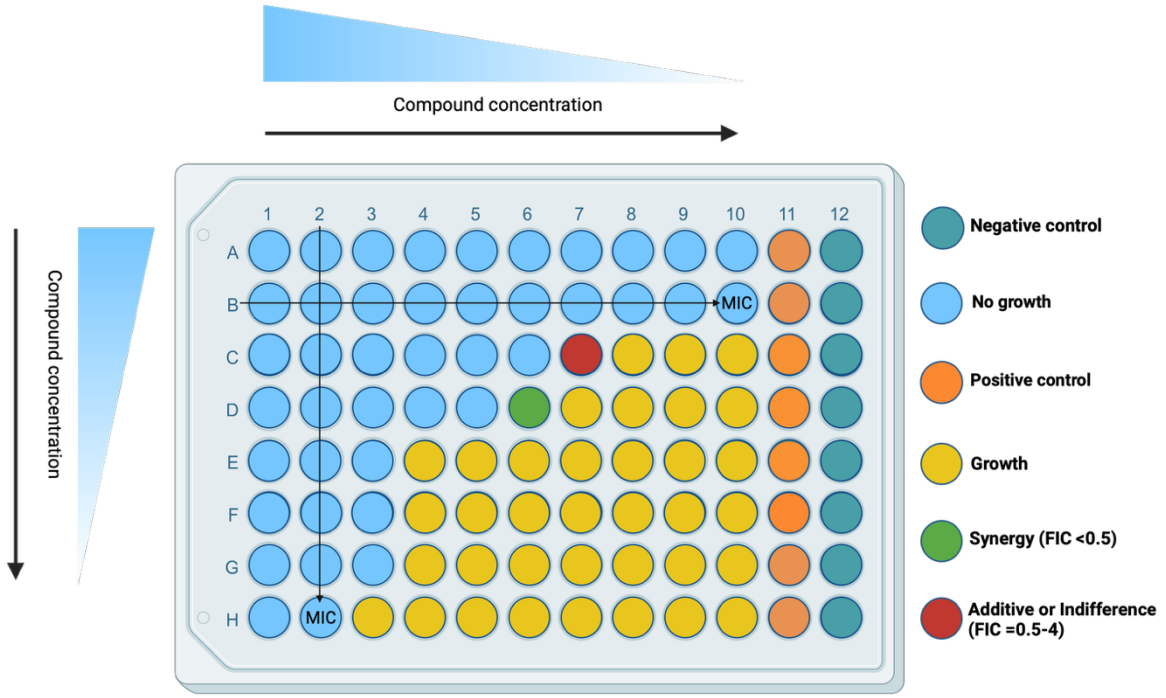

Figure 2.8: Schematic diagram illustrated drug interactions in checkerboard microdilution assay. The interaction between KHS and H_2O_2 /KHS and an oxidative cocktail solution of (H_2O_2, NO_2 and NO_3) was evaluated in this assay. Biofilms were grown in pre-sterilised polystyrene 96-well flat-bottom microtiter plates and incubated at 37°C for 24-h under aerobic conditions. RPMI medium was employed for *C. albicans* SC5314, while LB medium was used for the bacterial strains *S. aureus* Newman, *S. aureus* SH1000, and *P. aeruginosa* PA14. For triadic models, experiments were conducted in a 1:1 v/v mixture of LB and RPMI media. Following biofilm formation, the antimicrobial agents were applied using checkerboard microdilution assay. KHS (200 µL) was added to the first column, followed by serial doubling dilutions across columns 1 to 9. Subsequently, H_2O_2 or H_2O_2, NO_2 and NO_3 (100 µL) was added to the first row, followed by serial doubling dilutions down rows A to G. The appropriate medium (100 µL) was then added to each well, resulting in a final volume of 200 µL. The serially diluted antimicrobial agents were transferred to the original 96-well flat-bottom microtiter plates containing biofilms with changing tips every time during antimicrobial agents transferring. Negative controls (wells containing only culture media) and positive controls (wells containing untreated biofilm) were included to ensure experimental validity. Plates were incubated aerobically at 37°C for 24 h. Diagram was created in BioRender.

2.6 Assessment of H_2O_2 dual therapies

2.6.1 Early-stage *S. aureus* biofilm metabolic activity assessment

In final data chapter (chapter 5) we examined the synergistic potential of combining H_2O_2 with two distinct antibiotics - flucloxacillin and gentamicin - against early-stage *S. aureus* Newman and *S. aureus* SH1000 *in vitro* biofilms

model. *S. aureus* overnight broth was standardised and adjusted to a final working concentration of 1×10^6 cells/mL as previously described in section 2.1. Biofilms were grown in pre-sterilised polystyrene 96-well flat-bottom microtiter plates in LB broth and incubated at 37°C for 4 h under aerobic conditions. Following biofilm formation, the supernatants were carefully removed using a multi-channel pipette, and biofilms were washed once with 200 µL PBS to remove loosely attached cells. The biofilms were then treated with flucloxacillin, beginning at a concentration of 8 µg/mL, or gentamicin starting at 128 µg/mL. These antibiotics were serially double-diluted and combined with a constant 1 mM concentration of H_2O_2. Treatment regimens included H_2O_2 alone for 24 h, the antibiotic alone for 24 h, a simultaneous combination of the antibiotic and H_2O_2 for 24 h, pre-treatment with H_2O_2 for 10 minutes at room temperature followed by the antibiotic for 24 h, or treatment with the antibiotic for 24 h followed by a 10-minute post-treatment with H_2O_2 at room temperature. Appropriate positive and negative controls were also included (Figure 2.9). Following incubation, the supernatants were discarded, and a neutralisation step was performed using 200 µL of 5% sodium thiosulfate, incubated for 15 minutes at room temperature to deactivate the treatment effect. Sodium thiosulfate was also applied to control wells for result normalisation. After neutraliser removal, biofilms were washed once with 200 µL PBS, and biofilm metabolic activity was assessed using AlamarBlue™, as outlined in section 2.4.7. Data were collected from three independent experiments.

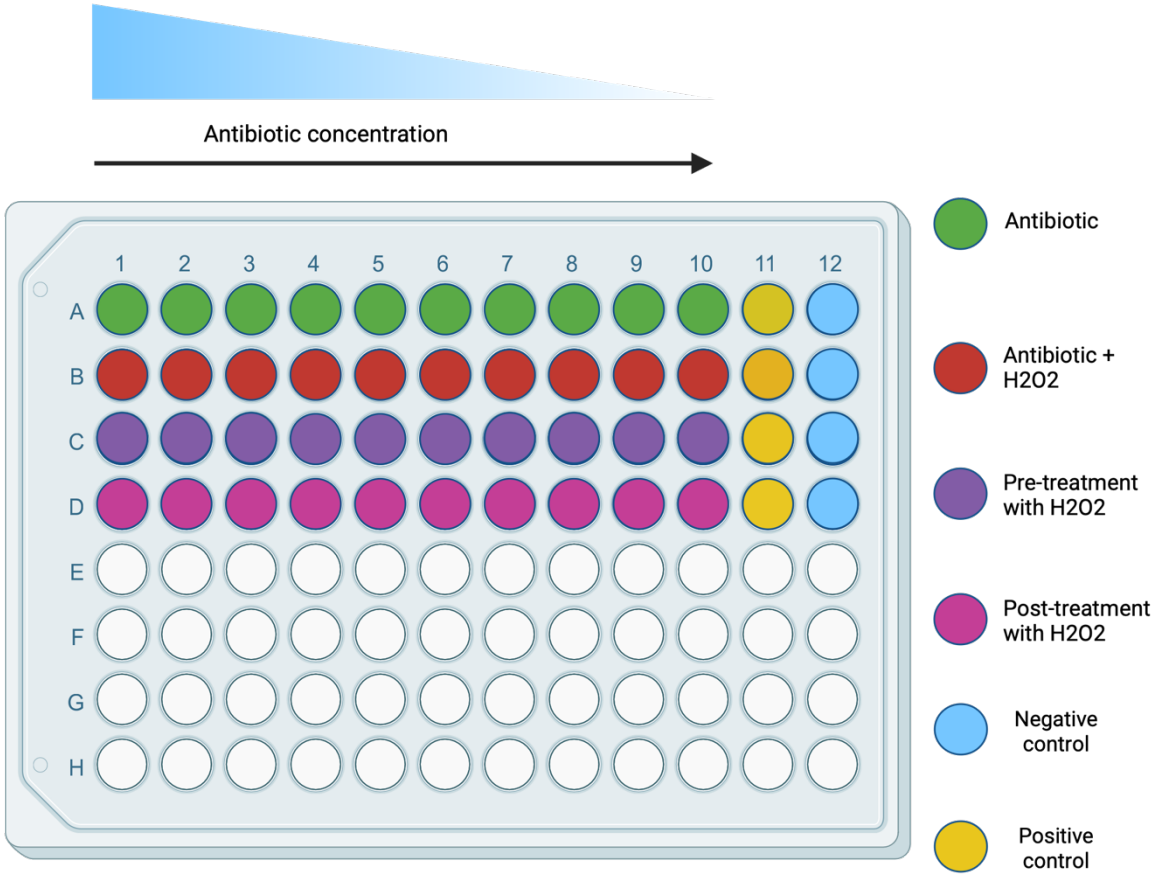

Figure 2.9: Schematic diagram illustrated combining H_2O_2 with flucloxacillin or gentamicin against early-stage S. aureus strains *in vitro* biofilms model. Biofilms were grown in pre-sterilised polystyrene 96-well flat-bottom microtiter plates in LB broth and incubated at 37°C for 4 h under aerobic conditions. Following biofilm formation, the supernatants were carefully removed using a multi-channel pipette, and biofilms were washed once with 200 µL PBS to remove loosely attached cells. The biofilms were then treated with flucloxacillin, beginning at a concentration of 8 µg/mL, or gentamicin starting at 128 µg/mL. These antibiotics were serially double-diluted and combined with a constant 1 mM concentration of H_2O_2. Treatment regimens included H_2O_2 alone for 24 h, the antibiotic alone for 24 h, a simultaneous combination of the antibiotic and H_2O_2 for 24 h, pre-treatment with H_2O_2 for 10 minutes at room temperature followed by the antibiotic for 24 h, or treatment with the antibiotic for 24 h followed by a 10-minute post-treatment with H_2O_2 at room temperature. Appropriate positive and negative controls were also included. Diagram was created in BioRender.

2.6.2 Early-stage *S. aureus* biofilm colony forming unit (CFU) assessment

In final data chapter (chapter 5) all biofilms were grown in pre-sterilised polystyrene 96-well flat-bottom microtiter plates in LB broth and incubated at 37°C for 4 h under aerobic conditions and treated with two concentrations of gentamicin (128 and 64 µg/mL) for *S. aureus* Newman, while *S. aureus* SH1000 received (8 and 2 µg/mL) doses. Flucloxacillin was applied at (0.25 and 0.0625 µg/mL) for Newman and (0.25 and 0.125 µg/mL) for SH1000. These antibiotic

regimens were applied either alone or in combination with 1 mM H_2O_2 as previously described in section 2.6.1. Following incubation, the supernatants were discarded, and a neutralisation step was performed as previously described in section 2.6.1. After neutraliser removal, biofilms were washed once with 200 µL PBS and discarded. Then 200 µL PBS were added to each well and biofilms were scraped by using the stick of wooden swab which sterile by UV prior to use. 20 µL of each scraped biofilms were transferred into fresh pre-sterilised polystyrene 96-well round-bottom microtiter plate that contained 180 µL of PBS in row A. From row A to row F 20 µL of scraped biofilms were serially diluted down from row A to F with changing tips in each dilution after mixed 5 times by multi-channel pipette. Following serially dilution step, 10 µL of each dilution were plated out in fresh LB agar in triplicate and incubated aerobically at 37°C for 24 h once dry (Figure 2.10). After which CFUs were counted using the viable plate counting technique (Allkja et al., 2021). Log_{10} CFU/mL values were calculated for each sample following overnight incubation. Data were collected from three independent experiments.

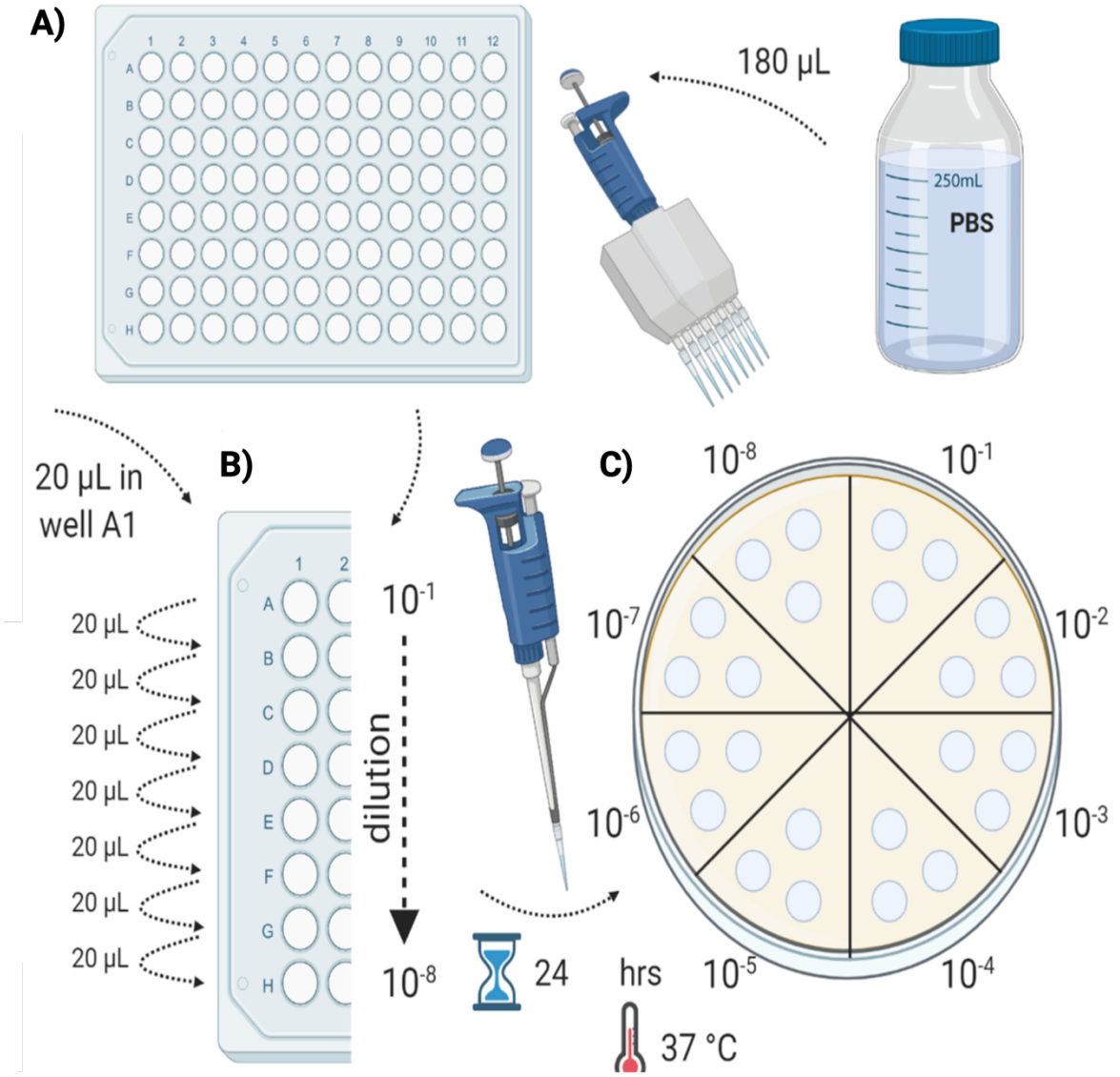

Figure 2.10: Schematic diagram described colony forming unit (CFU) assessment. First, biofilms were scraped by using the stick of wooden swab which sterile by UV prior to use. Then 20 µL of each scraped biofilms were transferred into fresh pre-sterilised polystyrene 96-well round-bottom microtiter plate that contained 180 µL of PBS in row A (A). From row A to row F 20 µL of scraped biofilms were serially diluted down from row A to F with changing tips in each dilution after mixed 5 times by multi-channel pipette (B). Following serially dilution step, 10 µL of each dilution were plated out in fresh LB agar in triplicate and incubated aerobically at 37°C for 24 h once dry (C). After which CFUs were counted using the viable plate counting technique (Allkja et al., 2021). Diagram was created in BioRender.

2.7 Statistical analysis

All statistical analyses, graphs, and distribution assessments were conducted using GraphPad Prism version 10.1.1 (GraphPad, San Diego, CA, USA). Prior to performing the analyses, data normality was evaluated using the D'Agostino-Pearson omnibus test for datasets with sample sizes of 8 or more, and the Shapiro-Wilk test for smaller datasets (sample size < 8). For comparisons between two groups involving non-normally distributed data, Mann-Whitney tests were applied to calculate p-values. In instances where data were normally distributed, unpaired t-tests were utilized for two-group comparisons. When multiple group comparisons were necessary for non-normally distributed data, Kruskal-Wallis tests followed by Dunn's post tests were employed. For normally distributed parametric data with sample sizes of 8 or more, one-way ANOVA with Tukey's post tests were used, whereas one-way ANOVA with Dunnett's post tests were applied for smaller sample sizes ($n < 8$). Differences were considered statistically significant if $p < 0.05$.

3 Chapter 3: Evaluating the potential application of cold atmospheric plasma (CAP) in treating skin and wound-relevant biofilm models

3.1 Introduction

The clinical management of wound infections, particularly diabetic foot ulcers (DFUs), presents significant challenges for healthcare professionals. These infections impose a substantial socioeconomic burden, with costs to the national health service (NHS) estimated at £8.3 billion in 2017/2018 (Guest, Fuller and Vowden, 2020), whilst global wound care and management expenditure is predicted to exceed ~$100 billion (Nussbaum et al., 2018). The inadequate treatment outcomes are predominantly attributed to microbial colonisation interfering with proper healing and tissue repair processes. Research indicates that microbial biofilms infect approximately 40% to 60% of DFUs (Jia et al., 2017, Kee, Nair and Yuen, 2019, Lin et al., 2019, Malik, Mohammad and Ahmad, 2013). These persistent wounds typically harbour diverse aerobic and anaerobic bacterial species (James et al., 2008), alongside fungal organisms (Dowd et al., 2011, Kalan and Grice, 2018, Kalan et al., 2016). Consequently, there exists a clear and pressing requirement for the development of more efficacious therapeutic approaches to combat these infections. This need is reflected in projections suggesting the global advanced wound care market will reach approximately $20 billion by 2027 (Sen, 2021).

Given the mounting concerns regarding antimicrobial resistance (AMR), alternative methodologies for infected chronic wound treatment are paramount. Cold atmospheric plasma (CAP) has emerged as a promising therapeutic option due to its antimicrobial properties, whilst simultaneously contributing to wound healing and repair processes (Braný et al., 2020). While the precise mechanism of action remains incompletely understood, CAP's antimicrobial effects are thought to stem from the generation of reactive oxygen and nitrogen species (RONS) (Leite et al., 2021, Nicol et al., 2020, Sun et al., 2012). One particular compound produced by CAP, hydrogen peroxide (H_2O_2), is widely employed as an antiseptic for topical treatment of infected chronic wounds, highlighting its relevance to wound healthcare. Several recent investigations have demonstrated promising outcomes with CAP, establishing its effectiveness against planktonic microorganisms and exploring its anti-biofilm activity (Nicol et al., 2020, Becker et al., 2019, Jungbauer et al., 2022, Theinkom et al., 2019). With regard to skin and wound applications, numerous studies have focused on individual bacterial

species, such as *Pseudomonas aeruginosa* and *Staphylococcus aureus* (Ghimire et al., 2021, Guo et al., 2021a, Huang et al., 2020, Szili et al., 2021, Xu et al., 2020), whilst CAP has also exhibited inhibitory effects against fungi including dermatophytes (Heinlin et al., 2013a) and *Candida albicans* (Leite et al., 2021, Sun et al., 2012, Rahimi-Verki et al., 2016). At the mixed-species level, evidence indicates CAP efficacy against biofilms containing *S. aureus* and *C. albicans* (Delben et al., 2016), as well as *S. aureus* with *P. aeruginosa* and *Enterococcus faecalis* (Oliveira et al., 2021). However, research into complex multi-species covering the spectrum of microbial complexity (e.g., Gram-positive, Gram-negative bacterial species, and fungi) are limited.

Wound infections frequently exhibit an interkingdom nature, making fungal consideration clinically significant; 80% of non-healing DFUs contain fungi, with *C. albicans* representing one of the most prevalent species (Kalan et al., 2016). In this context, we have previously characterised a triadic *C. albicans* inclusive model demonstrating differential responses to antibiotic therapy, where only the combination of antibacterial and antifungal agents effectively reduced consortia viability (Townsend et al., 2017). Another mycological consideration is *Candida auris*, a deadly nosocomial pathogen displaying broad antifungal resistance. This organism can exist alongside commensal bacterial and fungal microflora on the skin (Proctor et al., 2021). Since its initial identification in 2009, *C. auris* outbreaks have been reported across multiple countries globally (Proctor et al., 2021, Sathyapalan et al., 2021, Schelenz et al., 2016). The capacity of *C. auris* to readily form biofilms on biotic and abiotic surfaces presents significant challenges for hospital units attempting to fully eradicate it with antiseptic washes. Indeed, *C. auris* biofilms demonstrate considerably higher tolerance to antiseptic washes such as H_2O_2 and chlorhexidine (CHX) compared to *C. albicans*, suggesting potential for prolonged survival on abiotic surfaces (Kean et al., 2018a).

This chapter aims to evaluate the potential application of CAP in treating skin and wound-relevant biofilm models as an alternative therapy for associated infections. Our investigation builds upon existing literature reporting CAP therapy as a means to eradicate biofilms, by assessing its activity against simple mono-species models of wound-related microorganisms and a polymicrobial consortia. While *C. auris*

constituted a smaller subset of experiments in this chapter, its inclusion is motivated by its nosocomial importance, it's ability to colonize skin, mediate biofilm-related persistence on devices, environmental hardiness, and multidrug resistance within Intensive Care Unit outbreaks (Tharp et al., 2023, Chowdhary, Jain and Chauhan, 2023, Horton and Nett, 2020, Cortegiani et al., 2019). In light of its limited representation here, *C. auris* findings are framed as exploratory, to assess CAP's potential against priority fungal biofilms in hospital wound care contexts before moving into more clinically relevant wound pathogens.

3.2 Results

3.2.1 Time dependent killing effect of CAP

Previous studies have shown various treatment times for plasma-based therapies, ranging from seconds to minutes (Bolgeo et al., 2023, Kubinova et al., 2017, Isbary et al., 2012, Niemira, Boyd and Sites, 2018, Borchardt et al., 2017, Mirpour et al., 2020a). Therefore, initially, it was considered essential to determine the optimal duration for the efficacy of CAP therapy. To achieve this, two non-hyphal forming fungi, *C. auris* strains NCPF 8978 and NCPF 8973 were chosen for initial testing purposes. This was to illustrate the impact of CAP treatment durations of 1, 3, and 5 minutes. Biofilms of *C. auris* grown for 24 hours (h) were subjected to CAP treatment, and subsequently, viable colony-forming equivalent per millilitre (CFE/mL) counts were measured using live/dead quantitative polymerase chain reaction (qPCR).

(Figure 3.1) illustrates that CAP treatment exhibited a time-dependent reduction in *C. auris* NCPF 8978 viability, with the most pronounced effect observed at the 5-minute exposure. Total cell counts showed no significant changes across the 1, 3, and 5-minute time points, with untreated samples having approximately 3.16×10^6, 2.46×10^7, and 2.14×10^6 CFE/mL compared to treated samples with 1.58×10^6, 1.11×10^7, and 1.88×10^6 CFE/mL, respectively. Viable cell counts at the 1-minute mark did not differ significantly between untreated (7.83×10^5 CFE/mL) and treated (2.4-fold reduction, 3.24×10^5 CFE/mL) samples. However, significant reductions in viability were noted at both the 3-minute (6.1-fold reduction, 1.13

× 10^5 CFE/mL, ***p = 0.0008) and the 5-minute (28.9-fold reduction, 2.87 × 10^4 CFE/mL, ****p < 0.0001) treatments.

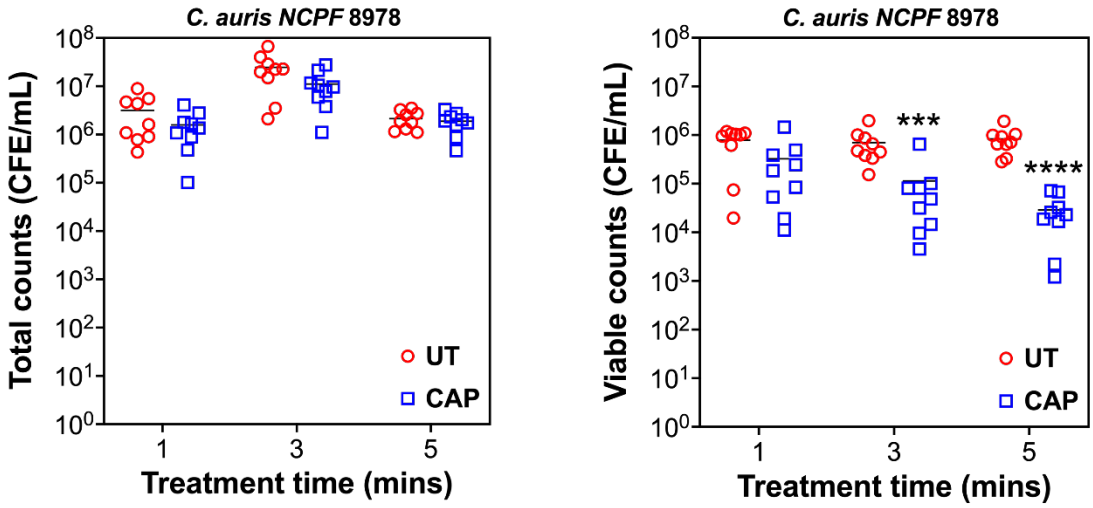

Figure 3.1: Time dependent killing effect of CAP against *C. auris* NCPF 8978. Biofilms were grown for 24 h within the cellulose matrix-hydrogel system. Following washing with PBS, biofilms were treated for 1, 3 and 5 min with CAP then total and viable counts were assessed via live/dead qPCR using colony forming equivalents/mL (CFE/mL). Biofilm experiments were completed on three separate occasions with three technical replicates per experiment (n =9 in total). Data distributions were assessed using a D'Agostino-Pearson omnibus normality test. Mann-Whitney test was used to determine the p values for two comparisons with non-parametric data. Unpaired t test was used to determine the p values for two comparisons with parametric data. Differences were considered statistically significant when p < 0.05. * Indicates statistically significant differences (*** p < 0.001, **** p < 0.0001). No significant differences were found in the total counts between all the time points and in the viable counts at 1 minute.

Similarly, (Figure 3.2) shows a comparable time-dependent effect of CAP on *C. auris* NCPF 8973, with the greatest impact also occurring at the 5-minute treatment duration. Total cell counts remained statistically unchanged at the different time points: untreated samples contained one for each timepoint and had approximately 5.95 × 10^6, 1.96 × 10^7, and 1.81 × 10^6 CFE/mL, which were grown on separate days for testing. Treated samples had approximately 2.62 × 10^6, 2.00 × 10^7, and 1.14 × 10^6 CFE/mL, respectively. At the initial minute of treatment, similar to the NCPF 8978 isolate, viable cell counts showed no significant difference between untreated (1.71 × 10^6 CFE/mL) and treated (3.01 × 10^5 CFE/mL) groups. Notably, there were significant decreases in viable cells at both the 3-minute (2.5-fold reduction, 1.57 × 10^6 CFE/mL, *p =0.0360) and the 5-minute (76.2-fold reduction, 4.70 × 10^3 CFE/mL, ***p =0.0001) treatments. These

findings underscore the efficacy of CAP in reducing *C. auris* viability in a time-dependent manner, with extended exposure times yielding greater reductions in viable cell populations across both strains tested.

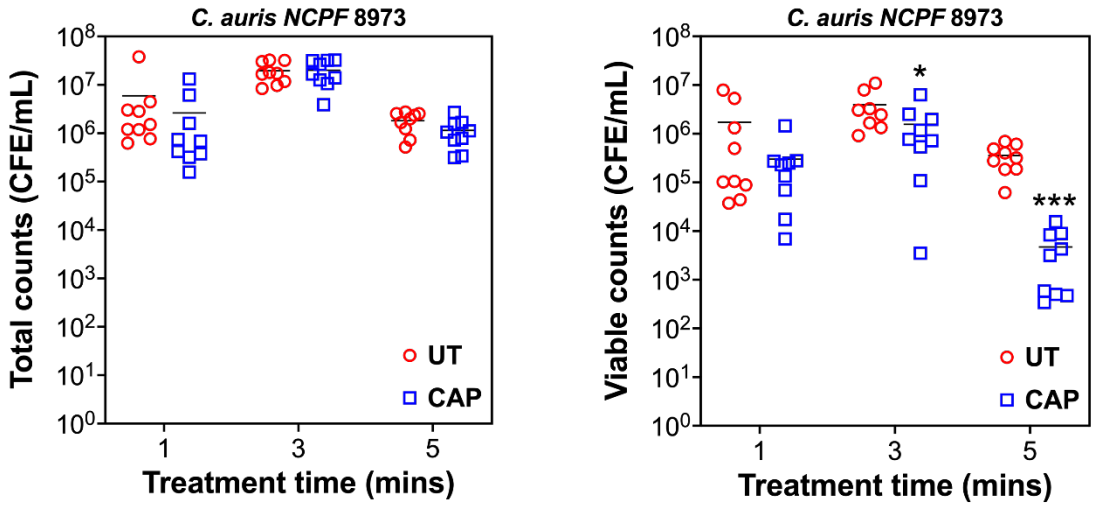

Figure 3.2: Time dependent killing effect of CAP against *C. auris* NCPF 8973. Biofilms were grown for 24 h within the cellulose matrix-hydrogel system. Following washing with PBS, biofilms were treated for 1, 3 and 5 min with CAP then total and viable counts were assessed via live/dead qPCR using colony forming equivalents/mL (CFE/mL). Biofilm experiments were completed on three separate occasions with three technical replicates per experiment (n =9 in total). Data distributions were assessed using a D'Agostino-Pearson omnibus normality test. Mann-Whitney test was used to determine the p values for two comparisons with non-parametric data. Unpaired t test was used to determine the p values for two comparisons with parametric data. Differences were considered statistically significant when $p < 0.05$. * Indicates statistically significant differences (* $p < 0.05$, *** $p < 0.001$). No significant differences were found in the total counts between all the time points and in the viable counts at 1 minute.

3.2.2 Time dependent killing effect of CAP correlates with increasing concentrations of hydrogen peroxide (H_2O_2) production

In an effort to elucidate the potential mechanism underlying the antimicrobial effects of CAP, the production of H_2O_2 was quantified following generation of CAP (Figure 3.3A). The treatment of water with CAP for durations of 1, 3, and 5 minutes revealed a dose-dependent increase in H_2O_2 concentrations within the resulting plasma-activated water (PAW). The H_2O_2 levels ranged from approximately 500 µM after 1 minute of exposure to 1500 µM following 5 minutes of treatment. While other RONS were not investigated in this study, it can be hypothesised from these observations that the observed CAP-induced microbial inactivation may be primarily attributed to the increasing levels of H_2O_2. This

proposition aligns with previous findings reported for this specific CAP device and similar systems (Ghimire et al., 2021, Ghimire, Szili and Short, 2022).

(Figure 3.3B) illustrates the relationship between the percentage viability of *C. auris* strains NCPF 8973 and NCPF 8978 and the concentration of H_2O_2 generated during CAP treatment. Biofilms were subjected to CAP treatment for durations of 1, 3, and 5 minutes as previously shown in (Figure 3.1 and Figure 3.2). The percentage viability was subsequently calculated using the live/dead qPCR results expressed as CFE/mL. The untreated biofilms of *C. auris* NCPF 8973 and NCPF 8978 exhibited initial viabilities of approximately 20% (2.00×10^6 CFE/mL) and 39% (7.71×10^5 CFE/mL), respectively. Following CAP treatment, a progressive decrease in viability was observed for both strains. After 1 minute of exposure, the viability decreased to approximately 11.5% (3.01×10^5 CFE/mL) and 20.5% (3.24×10^5 CFE/mL) for NCPF 8973 and NCPF 8978, respectively. The 3-minute treatment further reduced viability to about 7.8% (1.57×10^6 CFE/mL) for NCPF 8973 and 1% (1.13×10^5 CFE/mL) for NCPF 8978. The most pronounced effect was observed after 5 minutes of CAP treatment, with viability dropping to approximately 0.4% (4.70×10^3 CFE/mL) for NCPF 8973 and 1.5% (2.87×10^4 CFE/mL) for NCPF 8978, which correlates with the highest concentration of H_2O_2 production.

These results demonstrate a time-dependent reduction in *C. auris* biofilm viability following CAP treatment, with longer exposure times correlating with greater reductions in viable cells. The differential responses observed between the two strains suggest potential variations in susceptibility to CAP-induced stress, which may be attributed to strain-specific characteristics or biofilm architecture which will be discussed further later in this chapter.

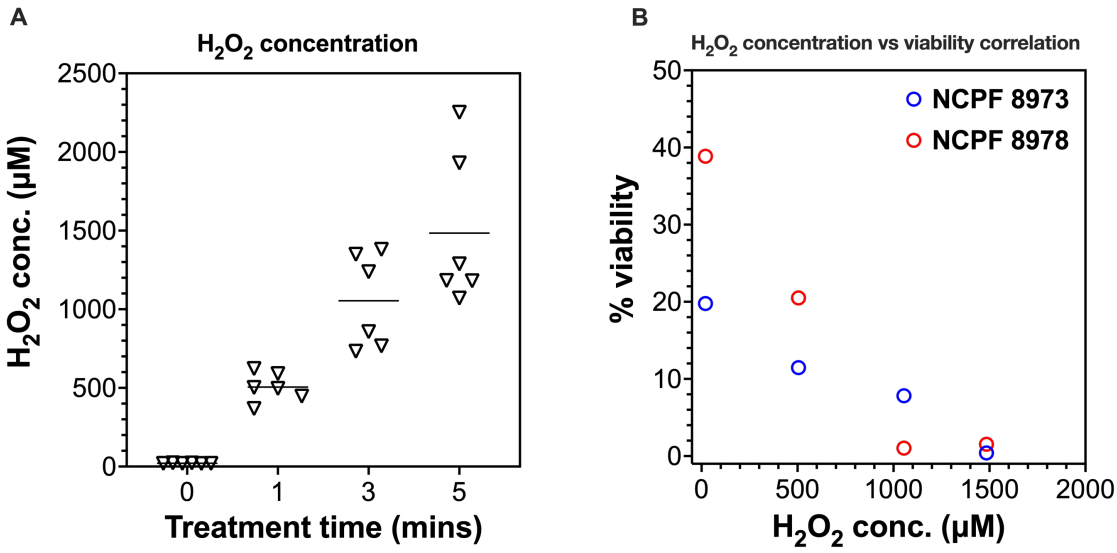

Figure 3.3 Time dependent killing effect of CAP correlates with increasing concentrations of H_2O_2. Panel (A) to generate plasma activated water (PAW), sterile ddH_2O was treated with CAP for 1, 3 and 5 min and H_2O_2 produced was quantified using the Invitrogen™ Amplex™ Red Hydrogen Peroxide/Peroxidase Assay Kit according to manufacturer's instructions. Untreated water minus CAP therapy was used for comparison (as denoted by 0 min). H_2O_2 levels were determined from 6 independently CAP-treated PAW using a standard curve of known H_2O_2 concentrations. Panel (B) *C. auris* NCPF 8973 and NCPF 8978 biofilms were grown for 24 h within the cellulose matrix-hydrogel system. Following washing with PBS, biofilms were treated for 1, 3 and 5 min with CAP then % viability was assessed via live/dead qPCR using colony forming equivalents/mL (CFE/mL). Biofilm experiments were completed on three separate occasions with three technical replicates per experiment (n =9 in total).

3.2.3 Assessment of five minutes-CAP treatment against different mono- and triadic-species biofilm models

After confirming that a 5-minute CAP treatment yielded the most significant reductions in microbial viability, the efficacy of CAP was next evaluated against ten additional biofilm models. These models included mono-species biofilms of *C. albicans* SC5314, *S. aureus* ATCC 25904 (referred to as Newman), *P. aeruginosa* PA14, *S. aureus* SH1000, *S. aureus* NCTC 6571, *S. aureus* S235 and *S. aureus* ATCC 25923. Additionally, three triadic biofilm models were tested, each containing *C. albicans* SC5314, *P. aeruginosa* PA14, and one of the following *S. aureus* strains: Newman, SH1000, or NCTC 6571. These biofilm models were selected to encompass a variety of microorganisms often identified in chronic wounds such as DFUs, whilst also covering different phenotypic and structural characteristics e.g., Gram-positive and Gram-negative bacteria, and hyphal-forming fungal species.

(Figure 3.4) demonstrates that CAP therapy effectively reduced viability across all tested biofilms, with the notable exception of *S. aureus* Newman, which displayed

a degree of tolerance to the treatment with no significant differences in viable cell counts (~1.31× 10^7 CFE/mL for untreated compared to ~6.17× 10^6 CFE/mL for treated). Significant reductions in viable cell counts were observed in mono-species biofilms of *C. albicans* (14.3-fold reduction, ***p = 0.0002) and *P. aeruginosa* (115.3-fold reduction, ****p < 0.0001).

The total cell counts remained statistically unchanged following CAP treatment for all microorganisms tested. Specifically, the total cell counts of *C. albicans* SC5314, *S. aureus* Newman, and *P. aeruginosa* PA14 showed no significant alterations after 5 minutes of CAP exposure. Untreated samples contained approximately 2.05 × 10^7, 2.59 × 10^7, and 2.64 × 10^7 CFE/mL, compared to treated samples with 9.03 × 10^6, 1.97 × 10^7, and 1.39 × 10^7 CFE/mL, respectively. This emphasises that the CAP efficacy was not a result of biofilm removal, but rather a killing effect exhibited by the therapy.

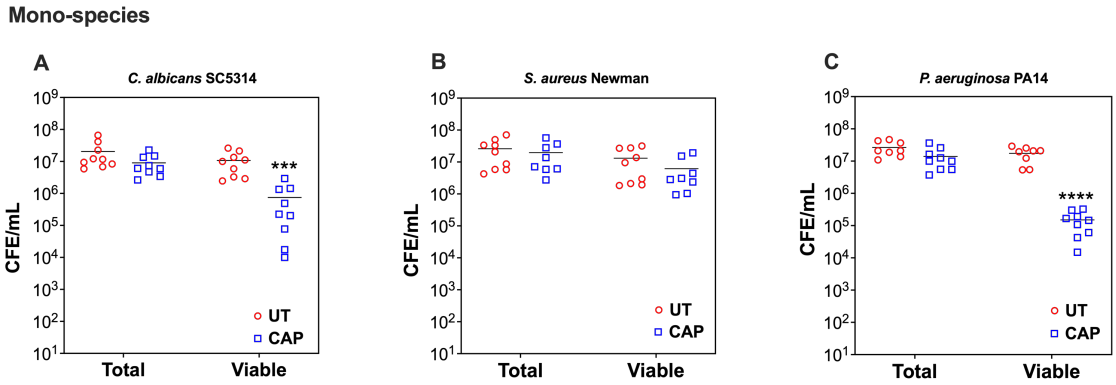

Figure 3.4: *S. aureus* Newman displays tolerance traits to CAP therapy in a mono-species biofilm model. *C. albicans* SC5314 (A), *S. aureus* Newman (B) and *P. aeruginosa* PA14 (C) biofilms were formed for 24 h within the cellulose matrix-hydrogel system then treated with CAP for 5 min. Total and viable colony forming equivalents/mL (CFE/mL) was quantified for each biofilm following treatment using live/dead qPCR. Biofilm experiments were completed on three separate occasions with three technical replicates per experiment (n=9 in total). Data distributions were assessed using a D'Agostino-Pearson omnibus normality test. Mann-Whitney test was used to determine the p values for two comparisons with non-parametric data. Unpaired t test was used to determine the p values for two comparisons with parametric data. Differences were considered statistically significant when p < 0.05. * Indicates statistically significant differences (*** p < 0.001, **** p < 0.0001). No significant differences were found in the total counts between untreated and treated biofilms across all tested strains and in the viable counts of *S. aureus* Newman.

The triadic biofilm model containing *S. aureus* Newman exhibited similar trends in viable cell count reductions following CAP treatment. Significant decreases were observed in viable cell counts for *C. albicans* (85-fold reduction, ****p < 0.001), *P. aeruginosa* (85.8-fold reduction, ***p < 0.001), and the combined

microbial population (12.2-fold reduction, **p = 0.0012) (Figure 3.5A). However, *S. aureus* Newman grown within the triadic biofilm model showed no significant change in viable counts (~1.74×10^6 CFE/mL for untreated compared to 1.18×10^6 CFE/mL for treated). In line with the mono-species biofilm results, total cell counts remained statistically unchanged following CAP treatment for all microorganisms within the triadic biofilm model. Specifically, *C. albicans* SC5314, *S. aureus* Newman , *P. aeruginosa* PA14, and the combined microbial population showed no significant alterations after 5 minutes of CAP exposure. Untreated samples contained approximately 3.40×10^6, 3.51×10^6, 2.10×10^7, and 1.40×10^7 CFE/mL, compared to treated samples with roughly 2.35×10^6, 3.54×10^6, 1.27×10^7, and 9.27×10^6 CFE/mL, respectively.

When calculating the percentage viability from the total and viable cell counts, CAP therapy reduced the percentage viability of all mono- and mixed-species biofilms compared to untreated controls, with the exception of *S. aureus* Newman, which demonstrated tolerance to CAP treatment (~43.84%, ~51.15% for untreated compared to ~29.81%, ~33.39% treated samples, respectively) (Figure 3.5B). Notably, *C. albicans* SC5314 and *P.* aeruginosa PA14 exhibited substantial decreases in percentage viability both as mono-species biofilms and within the triadic biofilm model following 5 minutes of CAP therapy. Untreated samples showed viabilities of approximately 56.2%, 48.8%, 66.7%, and 61.8%, which were reduced to roughly 6.6%, 1.1%, 1.7%, and 1.8% in treated samples, respectively.

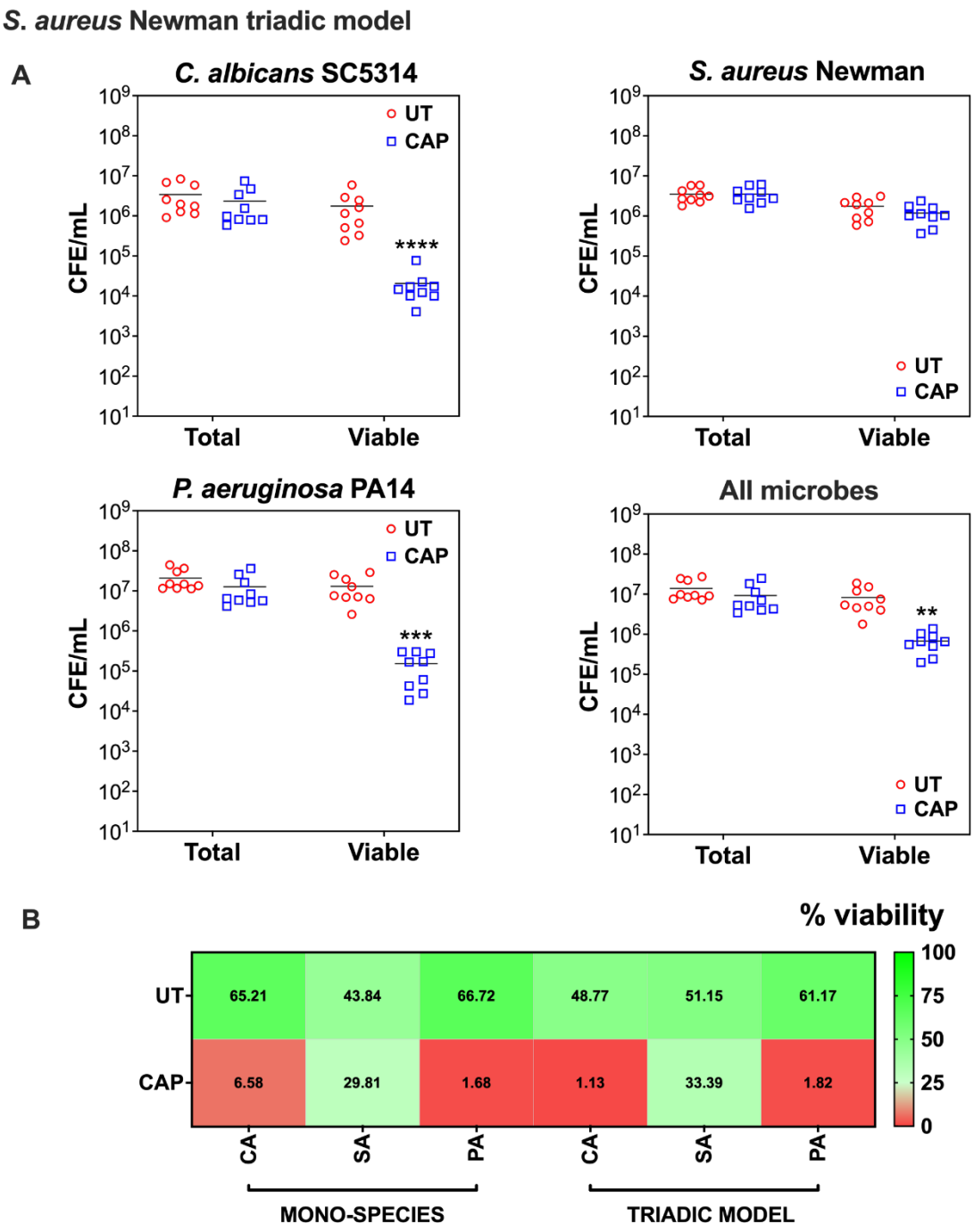

Figure 3.5: *S. aureus* Newman displays tolerance traits to CAP therapy in a triadic biofilm model. Panel (A) the triadic polymicrobial biofilm model of *C. albicans* SC5314, *S. aureus* Newman and *P. aeruginosa* PA14 biofilms were formed for 24 h within the cellulose matrix-hydrogel system then treated with CAP for 5 min. Total and viable colony forming equivalents/mL (CFE/mL) was quantified for each biofilm following treatment using live/dead qPCR. The CFE/mL counts for all combined microorganisms and for each individual microorganism are shown. Panel (B) the heatmap depicts the % viability for each microorganism when grown as mono-species biofilms, or for the triadic biofilm model. Results representative of mean values from n =9 (three technical replicates from three biological experimental repeats). Data distributions were assessed using a D'Agostino-Pearson omnibus normality test. Mann-Whitney test was used to determine the p values for two comparisons with non-parametric data. Unpaired t test was used to determine the p values for two comparisons with parametric data. Differences were considered statistically significant when $p < 0.05$. * Indicates statistically significant differences (** $p < 0.01$,*** $p < 0.001$, **** $p < 0.0001$). No significant differences were found in the total counts between untreated and treated biofilms across all tested strains and in the viable counts of *S. aureus* Newman.

These findings underscore the significant antimicrobial activity of CAP against various mono-species and polymicrobial biofilms, with differential efficacy observed across different microbial species and strains. The observed tolerance of *S. aureus* Newman to CAP warrants further investigation into the mechanisms underlying this tolerance. Thus, to evaluate whether the observed tolerance to CAP was specific to *S. aureus* Newman, four additional strains were subjected to plasma testing: NCTC 6571, SH1000, S235, and ATCC 25923. (Figure 3.6A) presents the total and viable counts for these strains alongside previously obtained results for *S. aureus* Newman. Statistical analysis revealed significant differences between treated and untreated samples for all alternative strains tested. The analysis of different *S. aureus* strains revealed varying levels of susceptibility to CAP treatment. The most pronounced reduction was observed in *S. aureus* S235, which showed a 20.8-fold reduction in viable cells (****$p < 0.0001$), with counts declining from 1.26×10^7 CFE/mL to 6.20×10^5 CFE/mL. *S. aureus* ATCC 25923 demonstrated the second-highest sensitivity, with a 15.8-fold reduction (*$p = 0.0261$) from 4.81×10^6 CFE/mL to 3.05×10^5 CFE/mL. *S. aureus* SH1000 exhibited a moderate response with a 5.4-fold reduction (****$p < 0.0001$), decreasing from 1.95×10^7 CFE/mL to 3.57×10^6 CFE/mL. The least susceptible was *S. aureus* NCTC 6571, showing a 2.8-fold reduction (**$p = 0.0059$), with viable counts decreasing from 3.85×10^6 CFE/mL to 1.36×10^6 CFE/mL.

The total cell counts of *S. aureus* ATCC 25923 and NCTC 6571, showed no significant alterations after 5 minutes of CAP exposure. Untreated samples contained approximately 1.65×10^7 and 1.83×10^7 CFE/mL, compared to treated samples with roughly 1.09×10^7 and 1.56×10^7 CFE/mL, respectively. However, significant changes were observed in the total cell counts of *S. aureus* S235 and SH1000 following 5 minutes of CAP therapy. Untreated samples contained approximately 2.61×10^7 and 4.54×10^7 CFE/mL, compared to treated samples with roughly 4.92×10^6 and 2.12×10^7 CFE/mL (****$p < 0.0001$) (*$p = 0.0106$), respectively.

As shown in (Figure 3.6B), CAP therapy reduced the percentage viability of all alternative strains compared to untreated controls, except for *S. aureus* SH1000, which exhibited a level of tolerance to CAP treatment (~38.23% for untreated compared to ~20.92% treated samples). Decreases in percentage viability were

observed for S. *aureus* NCTC 6571, ATCC 25923, and S235 following 5 minutes of CAP therapy. The viability decreased from approximately 21.90%, 22.98%, and 47.60% in untreated samples to 6.13%, 2.31%, and 12.29% in treated samples, respectively. These findings suggest that S. *aureus* susceptibility to CAP treatment varies among different strains, indicating a strain-dependent response to this antimicrobial intervention.

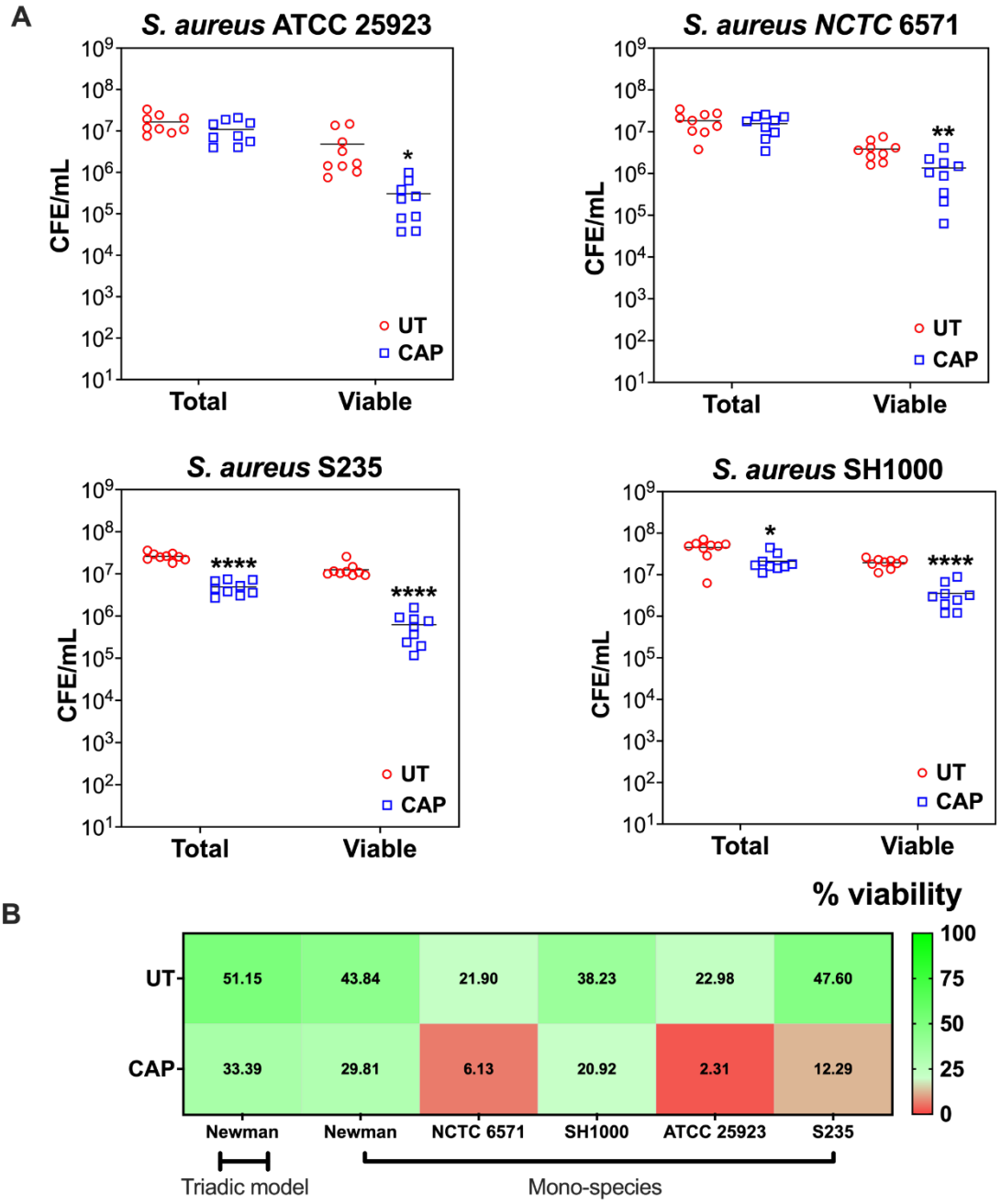

Figure 3.6: *S. aureus* strains display different tolerance traits to CAP therapy in a mono-species biofilm model. Panel (A) *S. aureus* ATCC 2593, *S. aureus* S235, *S. aureus* NCTC 6571 and *S. aureus* SH1000 biofilms were formed for 24 h within the cellulose matrix-hydrogel system then treated with CAP for 5 min. Total and viable colony forming equivalents/mL (CFE/mL) was quantified for each biofilm following treatment using live/dead qPCR. Panel (B) the heatmap depicts the % viability for each microorganism when grown as mono-species biofilms, or for the triadic biofilm model. (*S. aureus Newman* biofilm experiments results taken from Fig. 5 for comparison). Results representative of mean values from n =9 (three technical replicates from three biological experimental repeats). Data distributions were assessed using a D'Agostino-Pearson omnibus normality test. Mann-Whitney test was used to determine the p values for two comparisons with non-parametric data. Unpaired t test was used to determine the p values for two comparisons with parametric data. Differences were considered statistically significant when $p < 0.05$. * Indicates statistically significant differences (* $p < 0.05$, ** $p < 0.01$, **** $p < 0.0001$). No significant differences were found in the total counts between untreated and treated biofilms in *S. aureus* 25923 and *S. aureus* 6571.

Given that *S. aureus* SH1000 also exhibited a level of CAP tolerance similar to *S. aureus* Newman, this strain was incorporated into a triadic biofilm model. The new triadic biofilm model exhibited similar trends in viable cell count reductions following CAP treatment, to that of its counterpart. Akin to the mono-species model, significant decreases were observed in viable cell count for *S. aureus* SH1000 with a 4.9-fold reduction (***p = 0.0005) from 1.23×10^7 CFE/mL untreated to 2.49×10^6 CFE/mL treated. Interestingly, *C. albicans* numbers were much lower than the *S. aureus* Newmans triadic model. *C. albicans* SC5314 with a 42.4-fold reduction (****p < 0.0001) from 1.58×10^4 CFE/mL untreated to 3.73×10^2 CFE/mL treated, *P. aeruginosa* PA14 with a 47.6-fold reduction (****p < 0.0001) from 3.60×10^6 CFE/mL untreated to 7.57×10^4 CFE/mL treated, and the combined microbial population with a 6.2-fold reduction (***p = 0.0005) from 1.59×10^7 CFE/mL untreated to 2.57×10^6 CFE/mL treated (Figure 3.7A).

Total cell counts statistically changed following CAP treatment for all microorganisms within the triadic biofilm model. *S. aureus* SH1000, *C. albicans* SC5314, *P. aeruginosa* PA14, and the combined microbial population showed significant alterations after 5 minutes of CAP exposure. Untreated samples contained approximately 9.37×10^7, 9.03×10^4, 2.35×10^7, and 1.17×10^8 CFE/mL, compared to treated samples with 2.35×10^6, 3.54×10^6, 1.27×10^7, and 9.27×10^6 CFE/mL (***p = 0.0002) (*p = 0.0142) (***p = 0.0003)((***p = 0.0006), respectively.

Consistent with previous observations for the *S. aureus* Newman strain, CAP therapy reduced the percentage viability of *C. albicans* SC5314 and *P. aeruginosa* PA14 in mixed-species biofilms compared to untreated controls, with the exception of *S. aureus* SH1000, which demonstrated relative tolerance to CAP treatment (~16.27% for untreated compared to ~10.67% treated samples) (Figure 3.7B). Notably, *C. albicans* SC5314 and *P. aeruginosa* PA14 exhibited decreases in percentage viability following 5 minutes of CAP therapy. Untreated samples showed viabilities of approximately 24.36% and 14.57%, which were reduced to roughly 2.19% and 1.26% in treated samples, respectively.

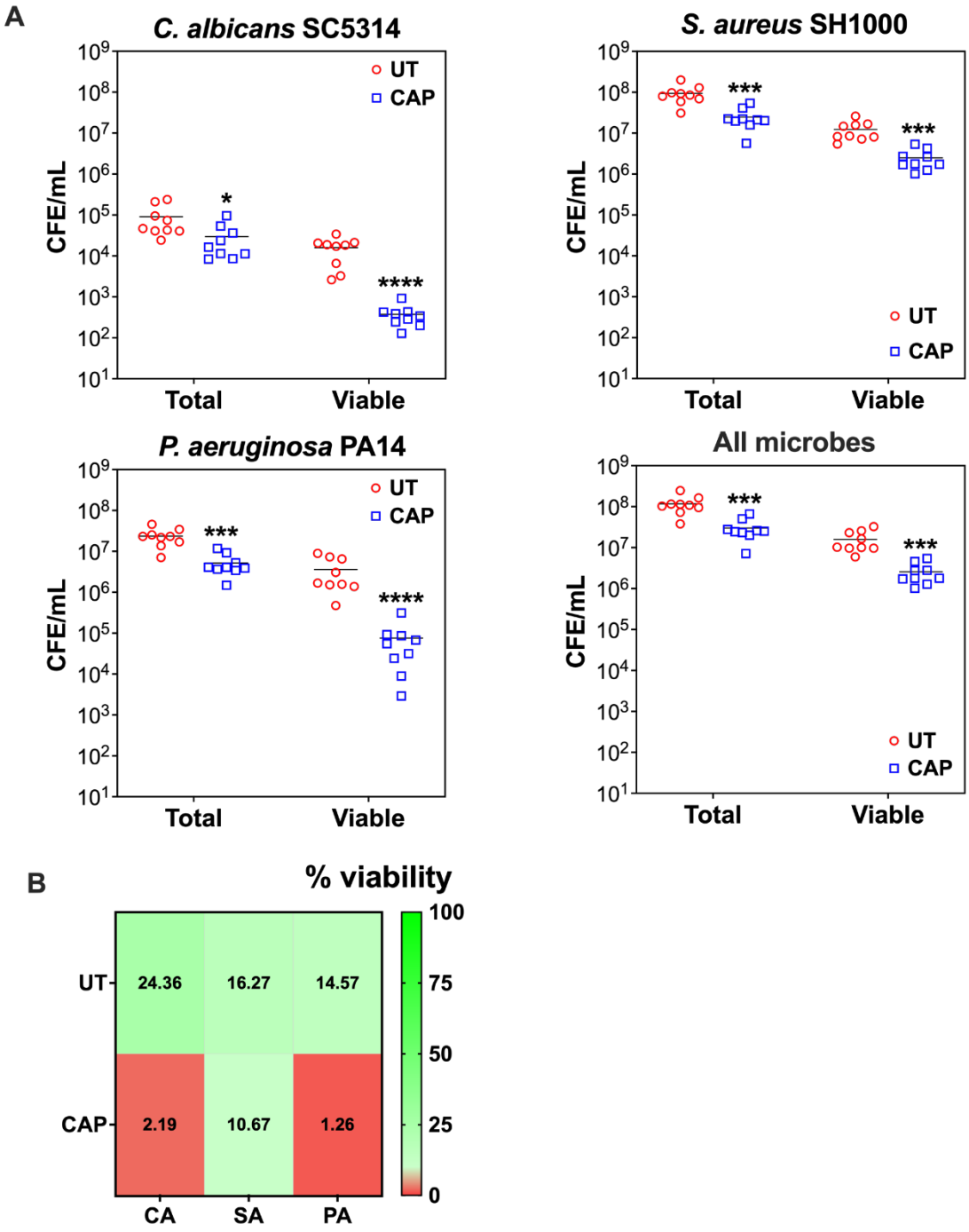

Figure 3.7: *S. aureus* SH1000 displays tolerance traits to CAP therapy in a triadic biofilm model. Panel (A) the triadic polymicrobial biofilm model of *C. albicans* SC5314, *S. aureus* SH1000 and *P. aeruginosa* PA14 biofilms were formed for 24 h within the cellulose matrix-hydrogel system then treated with CAP for 5 min. Total and viable colony forming equivalents/mL (CFE/mL) was quantified for each biofilm following treatment using live/dead qPCR. The CFE/mL counts for all combined microorganisms and for each individual microorganism are shown. Panel (B) the heatmap depicts the % viability for each microorganism when grown as the triadic biofilm model. Results representative of mean values from n =9 (three technical replicates from three biological experimental repeats). Data distributions were assessed using a D'Agostino-Pearson omnibus normality test. Mann-Whitney test was used to determine the p values for two comparisons with non-parametric data. Unpaired t test was used to determine the p values for two comparisons with parametric data. Differences were considered statistically significant when $p < 0.05$. * Indicates statistically significant differences (* $p < 0.05$, *** $p < 0.001$, **** $p < 0.0001$).

Next, one of the susceptible *S. aureus* strains (NCTC 6571; Figure 3.6) grown as mono-species biofilms were selected for further CAP testing within a third variation of the triadic model. *S. aureus* NCTC 6571 grown within the triadic biofilm model exhibited similar trends in viable cell count reductions following CAP treatment suggestive that the other microorganisms within the model did not promote additional resistance to the therapy. Significant decreases were observed in viable cell count for *S. aureus* NCTC 6571 with a 29.38-fold reduction (**p = 0.0039) from 6.60×10^5 CFE/mL untreated to 2.25×10^4 CFE/mL treated, *C. albicans* SC5314 with a 135-fold reduction (****p < 0.0001) from 1.79×10^4 CFE/mL untreated to 1.33×10^2 CFE/mL treated, *P. aeruginosa* PA14 with a 666.6-fold reduction (****p < 0.0001) from 4.61×10^6 CFE/mL untreated to 6.91×10^3 CFE/mL treated, and the combined microbial population with a 179.1-fold reduction (**p = 0.0061) from 5.28×10^6 CFE/mL untreated to 2.95×10^4 CFE/mL treated (Figure **3.8**A).

Total cell counts statistically changed following CAP treatment for all microorganisms within the triadic biofilm model with exception of *C. albicans* SC5314, which similarly to the one with *S. aureus* SH1000, colonised the model at a much lower concentration than that for the Newman triadic model. Untreated samples contained approximately 6.77×10^4 CFE/mL, compared to treated samples with roughly 3.08×10^4 CFE/mL. *S. aureus* NCTC 6571, *P. aeruginosa* PA14, and the combined microbial population showed significant alterations after 5 minutes of CAP exposure. Untreated samples contained approximately 4.93×10^6, 1.87×10^7 and 2.37×10^7 CFE/mL, compared to treated samples with roughly 1.18×10^6, 3.15×10^6 and 4.36×10^6 CFE/mL (**p = 0.0018) (***p = 0.0002) (***p = 0.0002), respectively.

CAP therapy significantly reduced the percentage viability of all microorganisms in mixed-species biofilms compared to untreated controls. *S. aureus* NCTC 6571, *C. albicans* SC5314 and *P. aeruginosa* PA14 in mixed-species biofilms exhibited substantial decreases in percentage viability following 5 minutes of CAP therapy. Untreated samples showed viabilities of approximately 12.30%, 28.45% and 20.60%, which were reduced to roughly 2.37%, 0.86% and 0.25% in treated samples, respectively (Figure **3.8**B). Taken together, these findings suggest that the effectiveness of CAP treatment is species-dependent, with some organisms

demonstrating greater resilience to this antimicrobial intervention. Furthermore, there is also evidence of strain-specific CAP tolerance exhibited by different *S. aureus* strains. This may have important implications for the development of targeted treatment strategies for polymicrobial biofilm infections, particularly if the therapy is not broad-spectrum.

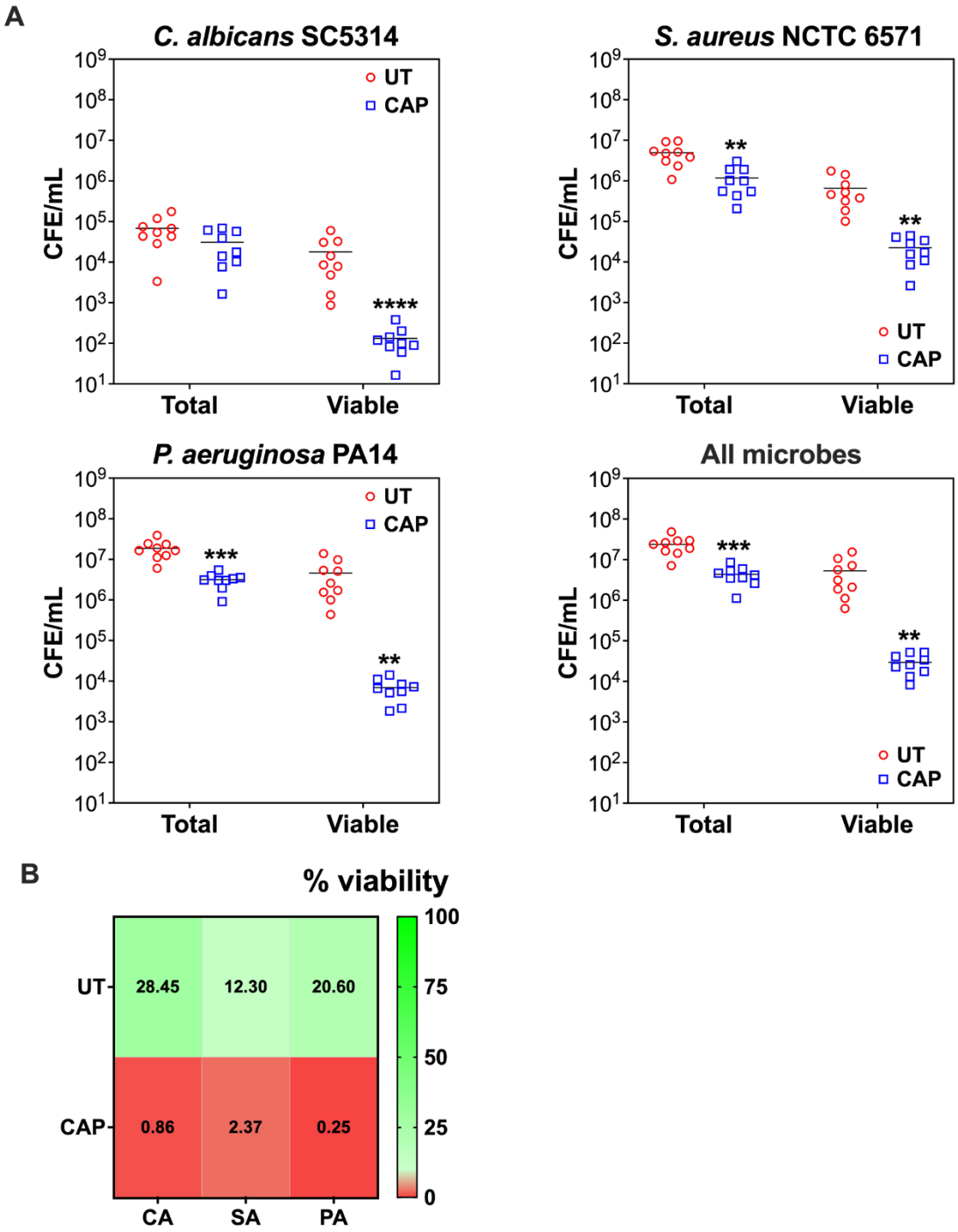

Figure 3.8: ***S. aureus* NCTC 6571 displays sensitive traits to CAP therapy in a triadic biofilm model.** Panel (A) the triadic polymicrobial biofilm model of *C. albicans* SC5314, *S. aureus* NCTC 6571 and *P. aeruginosa* PA14 biofilms were formed for 24 h within the cellulose matrix-hydrogel system then treated with CAP for 5 min. Total and viable colony forming equivalents/mL (CFE/mL) was quantified for each biofilm following treatment using live/dead qPCR. The CFE/mL counts for all combined microorganisms and for each individual microorganism are shown. Panel (B) the heatmap depicts the % viability for each microorganism when grown as the triadic biofilm model. Results representative of mean values from n =9 (three technical replicates from three biological experimental repeats). Data distributions were assessed using a D'Agostino-Pearson omnibus normality test. Mann-Whitney test was used to determine the p values for two comparisons with non-parametric data. Unpaired t test was used to determine the p values for two comparisons with parametric data. Differences were considered statistically significant when $p < 0.05$. * Indicates statistically significant differences (** $p < 0.01$, *** $p < 0.001$, **** $p < 0.0001$). No significant differences were found in the total counts between untreated and treated biofilms in *C. albicans* SC5314.

3.2.4 Compositional analysis of triadic biofilm models

The following section concerns the changes in the composition of *S. aureus* Newman triadic models following CAP treatment, compared to untreated controls. The triadic model containing *C. albicans* SC5314, *S. aureus* Newman and *P. aeruginosa* PA14 was matured for 24 h within the cellulose matrix-hydrogel system then treated with CAP for 5 min. Either, immediately after treatment, or following regrowth for 24 h. The total and viable composition of the biofilms were determined using live/dead qPCR. (Figure 3.9A) illustrates the compositional analysis of *S. aureus* Newman triadic biofilm model containing *S. aureus* Newman, *C. albicans* SC5314, and *P. aeruginosa* PA14, evaluated immediately following a 5-minute CAP treatment. The treated biofilms showed a distinct species distribution, with *S. aureus* Newman emerging as the predominant viable organism, constituting 88.5% of the viable population. *P. aeruginosa* PA14 represented the second most abundant species at 9.9%, while *C. albicans* SC5314 comprised the smallest fraction at 1.5% of viable cells. This composition contrasted significantly with the untreated biofilms, where *P. aeruginosa* PA14 was the dominant species (77.74%), followed by *S. aureus* Newman (13.24%), and *C. albicans* SC5314 (9.02%) of the viable cells. CAP treatment resulted in substantial reductions in both viable and total cell counts. The total viable population decreased from 8.26×10^6 CFE/mL to 6.78×10^5 CFE/mL following treatment. Similarly, the total cell count showed a small reduction from 1.40×10^7 CFE/mL to 9.27×10^6 CFE/mL post-treatment.

To assess the capacity of CAP therapy to inhibit microbial regrowth, the *S. aureus* Newman triadic biofilms were subjected to a 24 h regrowth period following treatment (Figure 3.9B). Analysis revealed a decrease in total viable counts of untreated biofilms from 9.41×10^6 CFE/mL to 1.16×10^6 CFE/mL. Similarly, total cell counts showed a reduction from 4.44×10^7 CFE/mL in untreated biofilms to 1.00×10^7 CFE/mL in treated biofilms. The biofilm composition underwent significant alterations during the regrowth phase. Following the 24 h regrowth period, *S. aureus* Newman established dominance in both untreated and treated biofilms, representing 64.3% and 88.6% of the viable population, respectively. *C. albicans* SC5314 emerged as the second most abundant organism, comprising 25.1% of untreated and 6.8% of treated biofilm viable cells. *P. aeruginosa* PA14

showed the lowest representation, constituting only 10.6% and 4.6% of viable cells in untreated and treated biofilms, respectively.

These findings highlight the significant impact of CAP treatment on species composition within polymicrobial biofilms and demonstrate a marked shift in population dynamics from *P. aeruginosa* PA14 to *S. aureus* Newman predominance following treatment and regrowth. This also highlights that, while still viable post-treatment with CAP, *S. aureus* Newman has the capacity to grow and exert control of the biofilm composition.

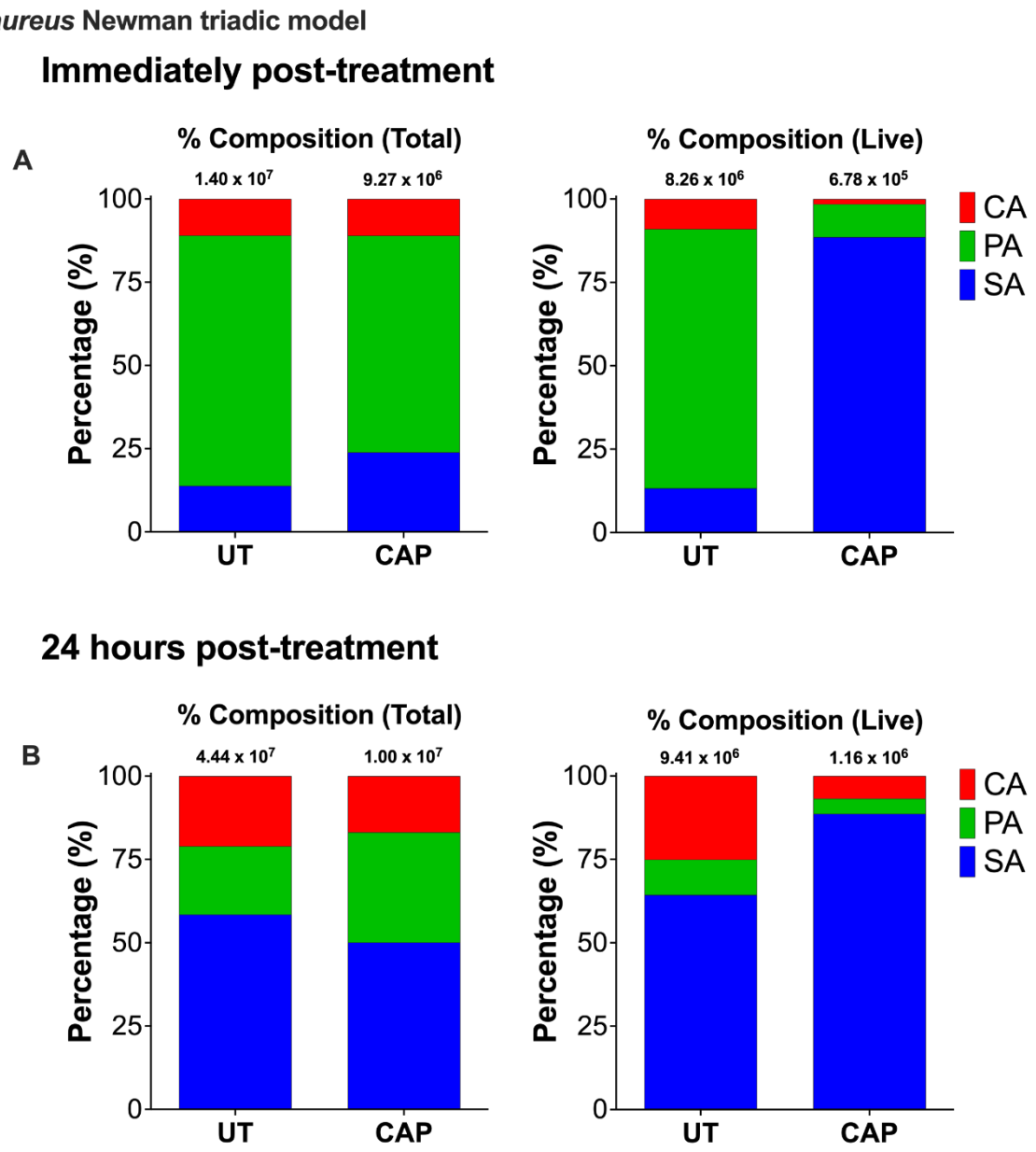

Figure 3.9: Compositional changes in *S. aureus* Newman triadic biofilm model following CAP treatment and biofilm regrowth. The triadic model containing *C. albicans* SC5314, *S. aureus* Newman and *P. aeruginosa* PA14 was matured for 24 h within the cellulose matrix-hydrogel system then treated with CAP for 5 min. Either, immediately after treatment (A), or following regrowth for 24 h (B), the total and viable composition of the biofilms were determined using live/dead qPCR. Results representative of mean values from n =9 (three technical replicates from three biological experimental repeats). CA: *C. albicans* SC5314. PA: *P. aeruginosa* PA14. SA: *S. aureus* Newman.

(Figure 3.10) demonstrates the compositional analysis of *S. aureus* SH1000 triadic biofilm model comprising *S. aureus* SH1000, *C. albicans* SC5314, and *P. aeruginosa* PA14, following exposure to a 5-minute CAP treatment. In both treated and untreated biofilms, *S. aureus* SH1000 maintained dominance as the primary viable component, representing 97.5% and 79.9% of the viable population, respectively. *P. aeruginosa* PA14 constituted the second most prevalent organism, comprising

2.5% of the treated and 20.02% of the untreated biofilm's viable cells. *C. albicans* SC5314 represented the smallest proportion, with only 0.02% viability in treated and 0.12% in untreated biofilms. The CAP treatment resulted in substantial reductions in both viable and total cell counts. The total viable population decreased from 1.60 × 10^7 CFE/mL to 2.73 × 10^6 CFE/mL following treatment. Similarly, the total cell count showed a reduction from 1.17 × 10^8 CFE/mL to 3.08 × 10^7 CFE/mL post-treatment.

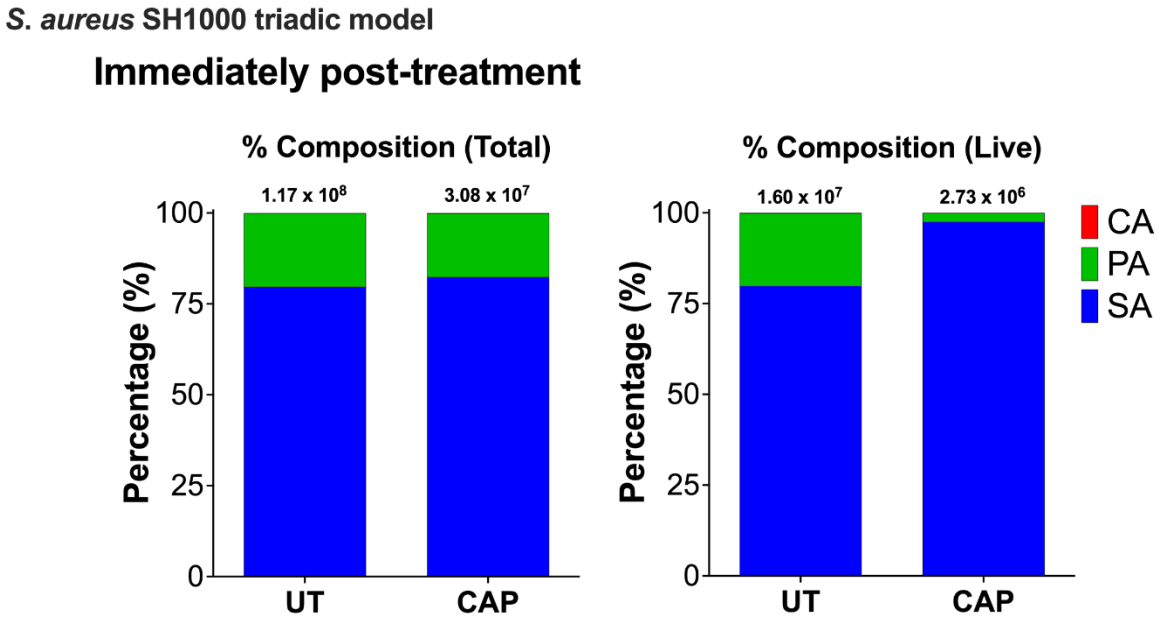

Figure 3.10: Compositional changes in *S. aureus* SH1000 triadic biofilm model following CAP treatment. The triadic model containing *C. albicans* SC5314, *S. aureus* SH1000 and *P. aeruginosa* PA14 was matured for 24 h within the cellulose matrix-hydrogel system then treated with CAP for 5 min. Immediately after treatment the total and viable composition of the biofilm was determined using live/dead qPCR. Results representative of mean values from n =9 (three technical replicates from three biological experimental repeats). CA: *C. albicans* SC5314. PA: *P. aeruginosa* PA14. SA: *S. aureus* SH1000.

(Figure 3.11) presents the compositional analysis of *S. aureus* NCTC 6571 triadic biofilm model consisting of *S. aureus* NCTC 6571, *C. albicans* SC5314, and *P. aeruginosa* PA14, evaluated immediately after exposure to a 5-minute CAP treatment. In the treated biofilms, *S. aureus* NCTC 6571 emerged as the predominant organism, representing 71.05% of the viable population, followed by *P. aeruginosa* PA14 at 28.5%, while *C. albicans* SC5314 constituted only 0.5% of viable cells. This distribution markedly differed from the untreated biofilms, where *P. aeruginosa* PA14 dominated with 84.13% of viable cells, followed by *S. aureus* NCTC 6571 at 15.6%, and *C. albicans* SC5314 comprising just 0.3% of the

population. CAP treatment resulted in substantial reductions in both viable and total cell counts. The total viable population decreased from approximately 4.36 × 10^6 CFE/mL to 2.95 × 10^4 CFE/mL following treatment. Similarly, the total cell count showed a significant reduction from 2.37 × 10^7 CFE/mL to 5.28 × 10^6 CFE/mL post-treatment.

These findings from (Figure 3.10 and Figure 3.11) demonstrate the significant impact of CAP treatment on species composition within polymicrobial biofilms and highlight the shift in population dynamics from *P. aeruginosa* PA14 dominance to *S. aureus* SH1000 and NCTC 6571 predominance following treatment, respectively. Due to the lower numbers of *C. albicans*, regrowth experiments were not conducted for these alternative triadic models with *S. aureus* SH1000 and NCTC 6571.

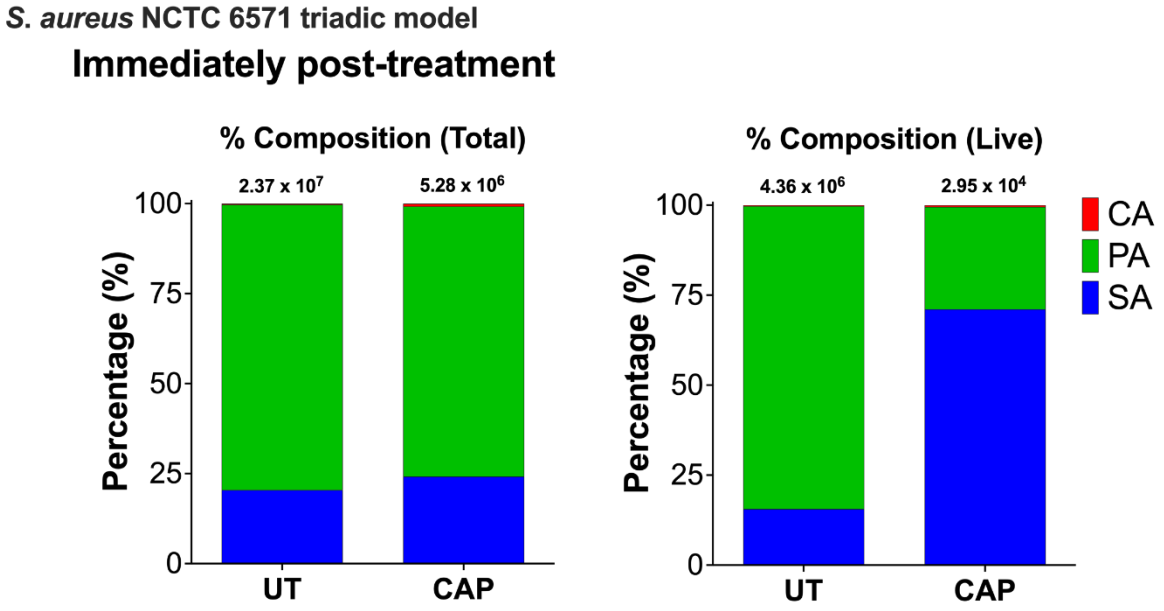

Figure 3.11: Compositional changes in *S. aureus* NCTC 6571 triadic biofilm model following CAP treatment. The triadic model containing *C. albicans* SC5314, *S. aureus* NCTC 6571 and *P. aeruginosa* PA14 was matured for 24 h within the cellulose matrix-hydrogel system then treated with CAP for 5 min. Immediately after treatment the total and viable composition of the biofilm was determined using live/dead qPCR. Results representative of mean values from n =9 (three technical replicates from three biological experimental repeats). CA: *C. albicans* SC5314. PA: *P. aeruginosa* PA14. SA: *S. aureus* NCTC 6571.

3.2.5 Scanning electron microscopy (SEM) imaging

The biofilm models ultrastructure and architectural characteristics were next examined using SEM at magnifications of ×1,500 for fungi and ×3,500 for bacterial mono-species and *S. aureus* Newman triadic biofilm model to provide detailed visualisation and further characterisation of the model phenotype post-treatment with CAP. SEM analysis revealed notable morphological alterations in biofilms exposed to CAP treatment for 5 minutes (Figure 3.12 and Figure 3.13). In the untreated *C. auris* controls, strain NCPF 8973 exhibited a single-cell phenotype with oval-shaped yeast cells, while strain NCPF 8978 displayed clustered aggregates. Following CAP treatment, both strains showed evidence of cellular damage, including deflation, wrinkling of the cell structure, and compromised cell integrity.

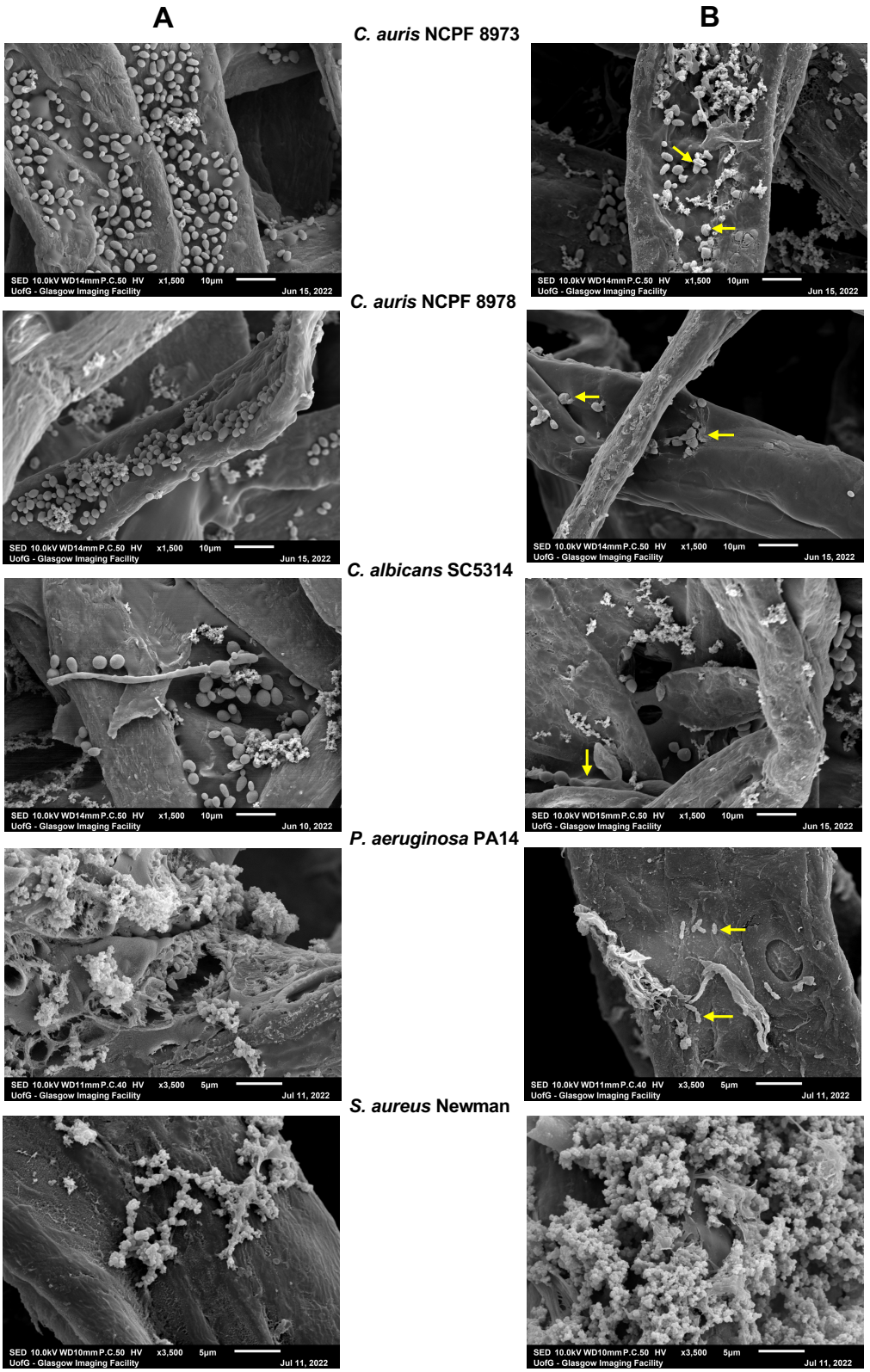

Figure 3.12: SEM images of mono-species biofilms highlights morphological changes at a cellular level following CAP therapy. Untreated or CAP-treated biofilms of *C. auris* NCPF 8973, NCPF 8978, *C. albicans* SC5314, *S. aureus* Newman and *P. aeruginosa* PA14 were visualised using SEM. All biofilms were formed for 24 h within the cellulose matrix-hydrogel system, then left untreated (A) or treated with CAP for 5 min (B), prior to processing for SEM. Yellow arrows denote changes in morphological structures, with evidence of cellular deflation and/or shrinkage. Samples were processed by Mr. Mark Butcher. Images were taken by Mrs. Margaret Mullin (University of Glasgow).

For *C. albicans* SC5314 mono-species and in *S. aureus* Newman triadic biofilms, untreated controls contained both yeast cells and hyphal forms. Post-CAP treatment, the hyphae appeared deflated, resulting in a subtle loss of their characteristic shape. *P. aeruginosa* PA14 mono-species and in *S. aureus* Newman triadic biofilm model subjected to CAP treatment demonstrated a noticeable reduction in extracellular matrix compared to their untreated counterparts. Interestingly, *S. aureus* Newman biofilms showed no apparent morphological changes following CAP exposure. Both untreated and CAP-treated *S. aureus* Newman biofilms exhibited dense extracellular matrix encapsulating clusters of cocci-shaped cells. Visual differences in *S. aureus* Newman triadic biofilm model were less apparent than in the mono-species biofilms (Figure 3.13). These observations provide insights into the differential effects of CAP treatment on various microbial species within mono- and multi-species biofilms, highlighting potential mechanisms of action and species- or strain- specific responses to this antimicrobial approach.

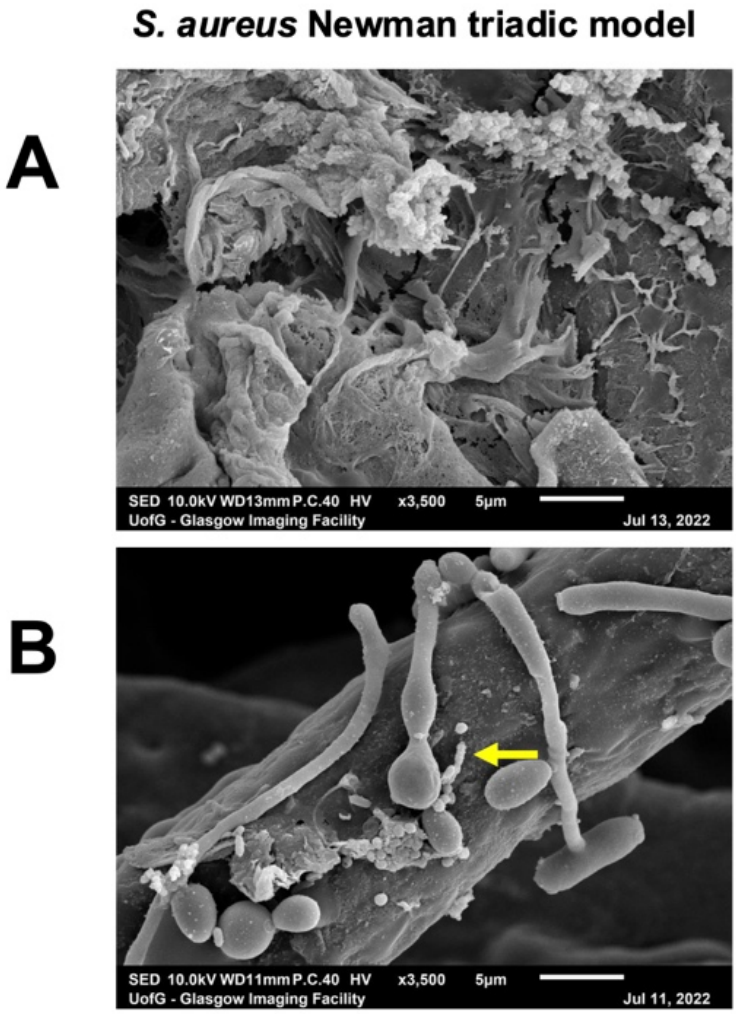

Figure 3.13: SEM images highlights morphological changes at a cellular level following CAP therapy. Untreated or CAP-treated *S. aureus* Newman triadic biofilm model of *C. albicans* SC5314, *S. aureus* Newman and *P. aeruginosa* PA14 were visualised using SEM. All biofilms were formed for 24 h within the cellulose matrix-hydrogel system, then left untreated (A) or treated with CAP for 5 min (B), prior to processing for SEM. Yellow arrows denote changes in morphological structures, with evidence of cellular deflation and/or shrinkage. Samples were processed by Mr. Mark Butcher. Images were taken by Mrs. Margaret Mullin (University of Glasgow).

3.3 Discussion

The results presented in this chapter demonstrate the significant antimicrobial potential of CAP against various mono-species and polymicrobial biofilms, with differential efficacy observed across different microbial species and strains. This section discusses the implications of these findings in the context of the broader scientific literature, considers possible mechanisms underlying the observed effects, addresses the significance of strain variation in treatment response, explores the clinical relevance of these findings, acknowledges the limitations of the current study, and proposes directions for future research.

3.3.1 Efficacy of CAP as an antimicrobial strategy against biofilms

3.3.1.1 Time-dependent antimicrobial effects of CAP

Our investigation into the time-dependent killing effect of CAP on *C. auris* biofilms revealed a progressive increase in antimicrobial efficacy with longer exposure times. The most pronounced reduction in viability was observed after 5 minutes of treatment, with significantly lesser effects at 1 and 3 minutes. This time-dependent pattern was consistent across both *C. auris* strains tested (NCPF 8978 and NCPF 8973), suggesting a robust and reproducible effect regardless of strain-specific characteristics such as aggregation tendencies. The observation that a 5-minute CAP treatment resulted in a high fold reduction in viable cells counts for *C. auris* strains (NCPF 8978 and NCPF 8973) underscores the potential of this technology as an effective antifungal strategy, particularly against emerging multidrug-resistant pathogens like *C. auris*.

Interestingly, previous studies by our research group Kean et al. (2018b) have reported that conventional antiseptics such as H_2O_2 were largely ineffective against *C. auris* biofilms, even at high concentrations and extended exposure times. The notable efficacy of CAP against *C. auris* biofilms in our study suggests that this technology may offer advantages over traditional chemical antiseptics for decontamination and potential therapeutic applications. This improved efficacy likely arose from additional antimicrobial activity mediated by other oxygen and nitrogen radicals often found produced by plasma devices (Chauvin et al., 2017, Zhai, Kong and Xia, 2022, Mai-Prochnow et al., 2021). These

observations are particularly significant considering the increasing clinical importance of *C. auris* as a nosocomial pathogen with inherent resistance to multiple antifungal drugs (Lockhart et al., 2016). Future work must expand on these findings with relation to surface sterilisation by plasma, to reduce such hospital outbreaks: indeed, several studies have shown that plasma technology can be used to in infection control measures (Mirpour et al., 2020a, Nicol et al., 2020, Tsoukou, Bourke and Boehm, 2022).

It is worth noting that similar time-dependent antimicrobial effects have been reported by Delben et al. (2016), who observed the efficacy of CAP against oral biofilms of *C. albicans* and *S. aureus* after 60 seconds of treatment time. Alkawareek et al. (2012) demonstrated a dose-dependent effect of CAP against *P. aeruginosa* biofilms, with complete eradication achieved after 10 minutes of exposure. In a prospective randomized controlled phase II trial involving 24 patients with chronic infected wounds, daily 2-minute cold atmospheric argon plasma (MicroPlaSter alpha or beta) plus standard care significantly reduced bacterial load across species while patients served as their own controls. The alpha device achieved a 40% reduction ($P < 0.016$; 70 treatments) and the beta device a 23.5% reduction ($P < 0.008$; 137 treatments), with no side-effects and good tolerability reported (Isbary et al., 2012). An *in vitro* study investigating biofilm inactivation on surfaces found that cold plasma treatment as short as 5, 10, or 15 seconds resulted in significant reductions of *Escherichia coli* O157:H7 biofilms, with greater efficacy observed at longer exposure times (Niemira, Boyd and Sites, 2018). Another experimental study on the effect of direct CAP on skin microcirculation applied plasma treatment for durations of 1.5, 3, or 4.5 minutes, demonstrating physiological effects and supporting the use of varied treatment times depending on therapeutic goals (Borchardt et al., 2017). Recent randomized, double-blind trial of 44 patients with grade 2 DFUs (22 CAP + standard care; 22 standard care), 5-minute CAP sessions three times weekly for three weeks significantly accelerated wound closure versus control, with a lower mean fraction of wound size in the CAP arm ($p = 0.02$) and a higher proportion reaching ≤0.5 of initial size at 3 weeks (77.3% vs 36.4%, $p = 0.006$). Immediate antiseptic effects were observed within sessions (pre- vs post-CAP), but between-group comparisons did not show a sustained reduction in bacterial load over weeks ($p = 0.26$),

highlighting the flexibility in plasma application protocols (Mirpour et al., 2020a). Our findings corroborate these observations whilst extending them to include emerging fungal pathogens and polymicrobial biofilm models more representative of clinical wound environments.

3.3.1.2 Antimicrobial activity against diverse microbial species

A particularly notable finding from our study is the antimicrobial activity of CAP against diverse microbial species, including Gram-positive bacteria (certain strains of *S. aureus*), Gram-negative bacteria (*P. aeruginosa*), and fungi (*C. albicans* and *C. auris*).This wide-ranging efficacy distinguishes CAP from many conventional antimicrobials, which typically target specific groups of microorganisms. The ability to simultaneously target multiple phenotypes of microorganisms is especially valuable in the context of polymicrobial infections, such as those commonly found in chronic wounds (Kalan et al., 2016). For example, studies have shown that the chronic wound microbiome can contain a wide range of different microbial species including fungi (Kalan et al., 2016, Kalan and Grice, 2018, Dowd et al., 2011, Shalaby et al., 2023, Allkja et al., 2025, Heaton et al., 2016).

The 5-minute CAP treatment demonstrated significant efficacy against *C. albicans* SC5314 (14.3-fold reduction), *P. aeruginosa* (115.3-fold reduction), and multiple *C. auris* strains. This antimicrobial activity aligns with previous reports by Braný et al. (2020), who described CAP as a powerful tool for modern medicine due to its ability to target a wide range of pathogens. Similarly, Heinlin et al. (2013b) demonstrated the efficacy of CAP against dermatophytes, whilst Sun et al. (2012) reported significant inactivation of *Candida* biofilms following CAP treatment. Murali et al. (2024) found that CAP exposure (30–90 seconds) reduced viability of *S. aureus* (80% at 60s) and *E. faecalis* (60% at 60s), while *P. aeruginosa* and *Proteus mirabilis* showed 60% reduction at 60s. Another study done by Mai-Prochnow et al. (2016) who stated that, following 10 min of CAP treatment, three Gram-negative species displayed a greater $\log_{10}$ reduction in CFU compared to the three Gram-positive strains, with *P. aeruginosa*, *P. libanensis*, and *Enterobacter cloacae* exhibiting 3.3 to 3.6 $\log_{10}$ CFU decreases, while Gram-positive species such as *Bacillus subtilis*, *S. epidermidis*, and *Kocuria carniphila* showed much lower reductions ranging from 0.6 to 2 $\log_{10}$ CFU.

The observation that CAP maintained its efficacy within a triadic biofilm models containing *C. albicans*, *P. aeruginosa*, and different *S. aureus* strains is particularly significant, as polymicrobial biofilms often exhibit enhanced resistance to antimicrobial agents compared to their mono-species counterparts (Townsend et al., 2016). This suggests that CAP may overcome some of the protective mechanisms associated with polymicrobial communities, potentially due to its multiple mechanisms of action and the ability of reactive species to penetrate the biofilm matrix (Mai-Prochnow et al., 2016, Jahid et al., 2015, Lavrikova et al., 2025). Given the polymicrobial nature of chronic wounds, CAP offers a promising therapeutic approach for cleansing wounds whilst also maintaining some tissue regenerative capacities (Stratmann et al., 2020, Mirpour et al., 2020a, van Welzen et al., 2021). This will be discussed further later in the final discussion chapter.

3.3.2 Potential mechanisms of CAP antimicrobial activity

3.3.2.1 Correlation with H_2O_2 production

Our investigation into the potential mechanisms underlying CAP's antimicrobial effects revealed a strong correlation between treatment duration and H_2O_2 production, with concentrations increasing from approximately 500 µM after 1 minute to ~1500 µM following 5 minutes of exposure. This progressive increase in H_2O_2 levels mirrored the time-dependent killing effect , suggesting a mechanistic link between reactive oxygen species (ROS) generation and antimicrobial efficacy. Moreover, it is important to note that further research is necessary to fully characterise the complete spectrum of reactive species generated by CAP and their individual contributions to the tall antimicrobial effect. Nonetheless, these results provide valuable insights into the potential mechanisms underlying CAP's efficacy against microbial biofilms.

The central role of H_2O_2 in CAP-mediated microbial inactivation aligns with findings from Ghimire et al. (2021), who reported enhanced production of H_2O_2 from an atmospheric pressure argon plasma jet with significant implications for antimicrobial activity. Similarly, Lukes et al. (2014) described the formation of various reactive species, including H_2O_2, in plasma-activated water and their subsequent bactericidal effects. The concentrations of H_2O_2 generated in our

study (500-1500 µM) are within ranges previously reported to exert antimicrobial effects, particularly against planktonic cells (Repine, Fox and Berger, 1981, Brandi et al., 1989a).

However, it is important to note that while H_2O_2 likely plays a significant role in the observed antimicrobial effects, CAP generates a complex mixture of RONS, including superoxide anions (O_2^-), hydroxyl radicals (- OH), nitric oxide (NO), peroxynitrite ($ONOO^-$), nitrite (NO_2^-), and nitrate (NO_3^-) (Zhai, Kong and Xia, 2022, Mai-Prochnow et al., 2021, Chauvin et al., 2017). Indeed a number of recent studies have investigated the importance of these alternative reactive species in driving microbial killing (Nikolaou et al., 2025, Mukherjee et al., 2024, Richards et al., 2021). These species may act synergistically to damage microbial cells through multiple pathways, potentially explaining the superior efficacy of CAP compared to H_2O_2 alone against certain resistant microorganisms such as *C. auris* (Kean et al., 2018b). For instance, Xia et al. (2023) demonstrated that PAW generated with oxygen (PAW-O_2) eradicated *E. coli* biofilms by producing a complex mixture of RONS, including O_2^-, H_2O_2, and NO derivatives. O_2^- played a pivotal role, as confirmed by electron paramagnetic resonance (EPR) and scavenger experiments: its removal reduced biofilm inactivation by 70%, highlighting its dominance in disrupting extracellular polymeric substances (EPS) and inducing oxidative stress. However, O_2^- alone was insufficient for complete biofilm removal, necessitating secondary RONS like $ONOO^-$, formed via O_2^- and NO interactions, to penetrate cells and damage DNA, proteins, and lipids. This multi-target mechanism explains why PAW outperforms H_2O_2, which primarily generates OH through Fenton reactions. Similarly, Vyas et al. (2023) showed that PAW pre-treatment enhanced antiseptic efficacy against chronic wound biofilms by leveraging RONS synergy. PAW induced intracellular RONS accumulation in *E. coli*, overwhelming antioxidant defences (e.g., superoxide dismutase) and priming cells for subsequent antiseptic action. Transcriptomic analysis revealed that PAW upregulated oxidative stress response genes (e.g., sodA, katG), while simultaneously downregulating metabolic and biofilm-associated pathways, creating a "dual strike" on viability and resilience. This combinatorial oxidative assault, unattainable with H_2O_2 alone, disrupts biofilm architecture while sensitising persister cells to conventional therapies, addressing both structural and

metabolic resistance mechanisms. Together, these studies underscore that RONS interactions-particularly between O_2^-, NO derivatives, and H_2O_2 enable CAP/PAW to circumvent microbial defences through spatially and temporally coordinated damage, offering a superior alternative to single-agent oxidative therapies.

3.3.2.2 Cellular morphological changes following CAP treatment

SEM analysis revealed significant morphological alterations in biofilms exposed to CAP treatment, providing additional insights into the mechanisms of action. The observed cellular damage included deflation, wrinkling of cell structures, and compromised cell integrity, particularly in fungal cells. These morphological changes suggest that CAP treatment affects cell membrane integrity, potentially through lipid peroxidation mediated by reactive species. Direct treatment with high concentrations of H_2O_2 such generated by CAP induces morphological changes in microbial cells, including cell deflation through membrane damage and loss of intracellular content. For instance, *E. coli* exposed to ≥10 mM H_2O_2 exhibited a marked reduction in cell volume, attributed to membrane disruption and subsequent leakage of cytoplasmic material such as lactate dehydrogenase (Brandi et al., 1989b). This deflationary effect contrasts with lower H_2O_2 concentrations (1.75 mM), which instead trigger cell filamentation without volume loss (Brandi et al., 1989b). Additionally, H_2O_2-generated reactive oxygen species (ROS) oxidize lipids and proteins in the cell envelope, further compromising structural integrity and contributing to osmotic instability (Figure 3.14) (Miller, 1969, Brandi et al., 1989b). These findings demonstrate that H_2O_2's efficacy depends on concentration-dependent mechanisms, with higher doses directly collapsing cell morphology via membrane peroxidation (Brandi et al., 1989b).

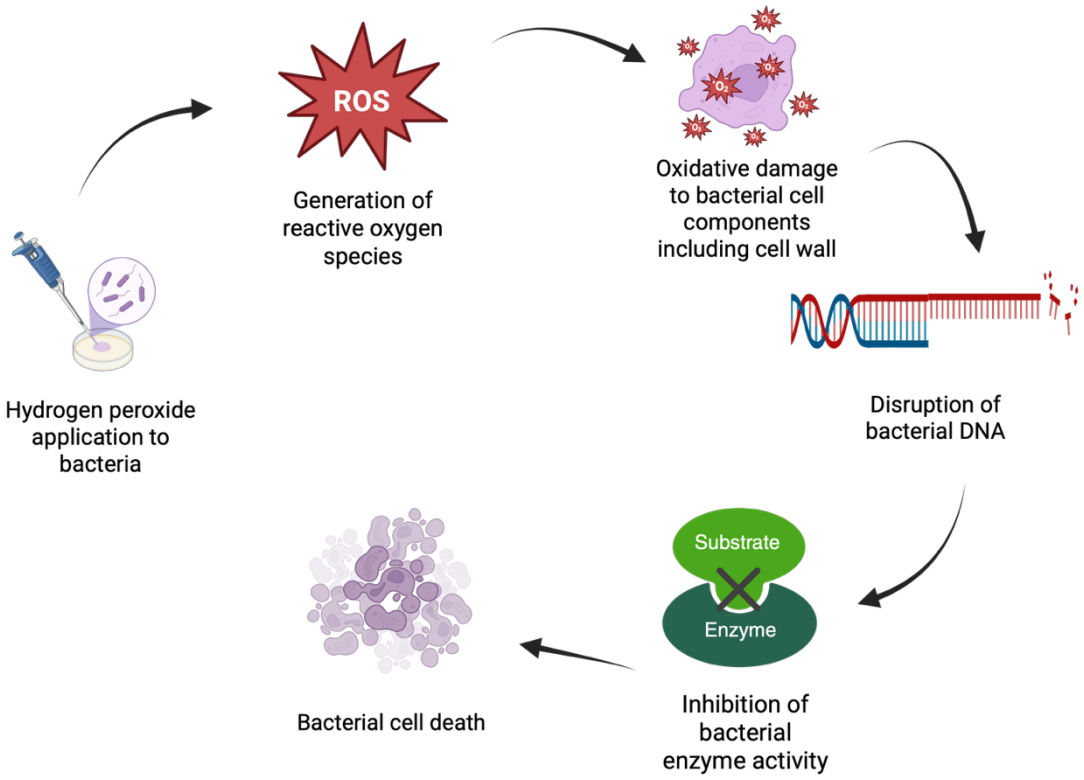

Figure 3.14: Schematic diagram illustrated H_2O2 mode of action against bacterial cell. H_2O_2 generate ROS that simultaneously attack multiple bacterial cellular targets, including cell walls, DNA, and essential enzymes. This multi-pronged oxidative assault causes structural damage, genetic disruption, and metabolic shutdown that collectively leads to bacterial cell death. Diagram was created in BioRender.

The differential morphological responses observed across microbial species may reflect varying susceptibilities to oxidative stress. For instance, *C. auris* cells exhibited more pronounced structural changes compared to *S. aureus* cells, which showed minimal morphological alterations following CAP treatment. This observation aligns with the quantitative viability data and suggests that cell envelope composition and architecture may influence susceptibility to CAP-induced damage. Similar morphological changes following CAP treatment have been reported by Rahimi-Verki et al. (2016), who observed significant alterations in *C. albicans* cell structure and suggested that these changes were associated with disruption of cell membrane integrity. Additionally, Huang et al. (2020) described differential cellular damage between *S. aureus* and *Salmonella typhimurium* following plasma treatment, attributing these differences to variations in cell wall structure and composition.

The observed reduction in extracellular matrix in *P. aeruginosa* biofilms following CAP treatment suggests that plasma may also target biofilm-specific structures beyond individual cells. This finding is in agreement with Alshraiedeh et al. (2016), who reported that CAP treatment could disrupt biofilm matrix components, potentially enhancing access of reactive species to embedded cells and increasing overall efficacy.

3.3.3 Differential susceptibility to CAP treatment

3.3.3.1 Strain-dependent tolerance in *S. aureus* strains

One of the most intriguing findings from our study was the observed tolerance of *S. aureus* Newman to CAP treatment, both in mono-species biofilms and within the triadic model. This tolerance was evident from the minimal reduction in viable cell counts following 5 minutes of CAP exposure, a stark contrast to the significant decreases observed in other species. Importantly, this tolerance appeared to be strain-dependent, as additional *S. aureus* strains (NCTC 6571, SH1000, S235, and ATCC 25923) exhibited varying levels of susceptibility to CAP treatment.

This heterogeneity in CAP susceptibility among *S. aureus* strains has significant implications for the development of CAP-based antimicrobial strategies and highlights the importance of strain selection in laboratory studies evaluating antimicrobial efficacy. This pattern suggests a spectrum of susceptibility rather than a binary response, potentially reflecting subtle genetic or phenotypic differences among strains.

The strain-dependent tolerance observed in our study aligns with reports by Klein et al. (2022), who demonstrated clonal heterogeneity in persistent *S. aureus* infections, and Giulieri et al. (2018), who identified distinctive molecular signatures associated with *S. aureus* persistence. These studies suggest that *S. aureus* populations exhibit significant genetic and phenotypic diversity, which may contribute to differential responses to antimicrobial interventions, including CAP treatment. Similar heterogeneity is well-documented in *Candida* species, where clinical isolates display marked variability in biofilm formation, antifungal tolerance, and virulence. For example, *C. albicans* bloodstream isolates exhibit

up to 4-fold differences in biofilm biomass and 8-fold variations in micafungin tolerance, linked to differential expression of biofilm-associated genes (ALS3, HWP1) and metabolic reprogramming under nutrient-limited conditions (Delaney et al., 2023). Strain-specific differences in extracellular DNA (eDNA) release further contribute to biofilm heterogeneity, with high eDNA-producing *C. albicans* strains forming denser, more antifungal-resistant biofilms compared to low eDNA producers (Rajendran et al., 2014a). Phenotypic divergence is not limited to *C. albicans*: *C. auris* aggregates (Agg) and non-aggregates (non-Agg) exhibit distinct transcriptional profiles during biofilm development, with Agg isolates upregulating cell wall integrity genes (ECM33, MP65) and elevating pro-inflammatory responses in 3D skin models (Brown et al., 2020). Even within standardised protocols, *C. albicans* biofilms demonstrate strain-dependent tolerance to endodontic irrigants like NaOCl, with regrowth observed in 40% of isolates post-treatment, underscoring the clinical implications of this variability (Alshanta et al., 2019). These findings collectively emphasise that microbial heterogeneity-whether in *Staphylococcus* or *Candida*-is a conserved adaptive strategy, necessitating personalised therapeutic approaches to address strain-specific resistance mechanisms.

3.3.3.2 Potential mechanisms of *S. aureus* tolerance to CAP

Several potential mechanisms may contribute to the observed tolerance of certain *S. aureus* strains to CAP treatment. Our study found that three *S. aureus* strains displayed a degree of tolerance to the CAP treatment with no significant differences in viable cell counts were observed compared to untreated biofilm (Baz et al., 2023). Matthes et al. (2016) conducted a study evaluating CAP against 78 genetically diverse *S. aureus* strains, focusing on its clinical and epidemiological relevance. Their findings highlighted the complexity of microbial defence mechanisms against antimicrobial therapies and confirmed strain-specific variations in *S. aureus* susceptibility to plasma treatment. Another study highlighted that *S. epidermidis* biofilms are more tolerant to H_2O_2 than planktonic cells, and this tolerance is mediated at least in part by eDNA and biofilm matrix protection (Olwal et al., 2018). One possibility is differential expression of oxidative stress response genes, as *S. aureus* possesses sophisticated systems to detoxify ROS and repair oxidative damage (Gaupp, Ledala and Somerville, 2012).

Catalase-negative *S. aureus* with katA loss-of-function and links to peroxide sensitivity. Cosgrove et al. (2007) generated katA mutants in *S. aureus* and demonstrated loss of catalase activity and marked hypersensitivity to H_2O_2; complementation restored catalase and resistance, directly linking katA sequence/function to the oxidative stress phenotype. Gaupp, Ledala and Somerville (2012) reviewed the genetic and regulatory basis of *S. aureus* oxidative stress defences and specifically discuss katA's role and catalase-negative phenotypes in the context of peroxide susceptibility, summarizing primary reports of katA lesions in clinical and laboratory isolates. Case reports describing catalase-negative *S. aureus* clinical isolates attribute the phenotype to katA defects and document increased H_2O_2 sensitivity *in vitro* (Gaupp, Ledala and Somerville, 2012). Peroxide regulator PerR mutations derepress katA and increase H_2O_2 tolerance; strain-variable katA regulation and sequence correlate with survival. Horsburgh et al. (2001) identified PerR as the peroxide stress repressor in *S. aureus*; perR mutants showed constitutive derepression of perR-regulated antioxidant genes including katA, ahpCF and dps, and exhibited increased H_2O_2 resistance, establishing the causal link between perR genotype, katA expression, and H_2O_2 tolerance. Follow-up transcriptional profiling and regulatory genetics in *S. aureus* confirmed that PerR directly controls katA and other peroxide defence loci; naturally occurring or engineered perR variants elevate katA expression and peroxide survival, while perR+ strains show strain-specific katA expression dynamics under oxidative challenge (Horsburgh et al., 2001, Gaupp, Ledala and Somerville, 2012). Strain-specific variations in these defence mechanisms could explain the heterogeneous responses observed in our study.

Another potential factor is cell wall structure and composition, which may influence the penetration of reactive species generated by CAP. Mai-Prochnow et al. (2016) Laroussi, Richardson and Dobbs (2002) and Lunov et al. (2016) proposed that the thicker peptidoglycan layer in Gram-positive bacteria, including *S. aureus*, provides enhanced protection against plasma-generated reactive species compared to Gram-negative bacteria. This structural advantage, possibly varying between strains, may contribute to the differential susceptibility observed.

Notably, because methicillin resistance can remodel the staphylococcal envelope and biofilm phenotype, results should be interpreted in the context of strain background. Methicillin-resistant S. aureus (MRSA) isolates frequently display significantly thicker cell walls than methicillin-susceptible S. aureus (MSSA) by transmission electron microscopy (TEM), a trait linked to reduced penetration and tolerance in heterogeneous vancomycin-intermediate phenotypes (Cui et al., 2021, García et al., 2017, Cazares-Dominguez et al., 2015). Envelope adaptations associated with resistance determinants (for example, mprF polymorphisms that increase lysyl-phosphatidylglycerol and accompany cell-wall thickening) also confer cross-tolerance to host defence cationic peptides, which may modulate susceptibility to oxidative and plasma-mediated stresses in MRSA compared with MSSA (Mishra et al., 2013, Mishra et al., 2011). Moreover, MRSA and MSSA can differ in biofilm formation capacity and architecture, further influencing antimicrobial responses, so conclusions from the strains tested here should not be overgeneralized across resistance backgrounds without additional, resistance-stratified panels (Hernández-Cuellar et al., 2023). For instance, García et al. (2017) used TEM in their study and revealed that MRSA strains have significantly thicker cell walls (27.3 ± 4.6 nm) compared to MSSA strains (21.0 ± 2.6 nm). Another recent study showed that the S. aureus isolated from murine kidney abscesses exhibited thicker cell walls (measured via TEM) compared to in vitro cultures (Sutton et al., 2021). While not investigated here, differences in cell-wall architecture may explain the divergent tolerance traits to CAP therapy.

The role of biofilm matrix composition in tolerance cannot be overlooked, as SEM images revealed dense extracellular matrix in *S. aureus* Newman biofilms both before and after CAP treatment. This matrix may serve as a protective barrier, scavenging reactive species before they reach the embedded cells. Different studies demonstrated that the biofilm EPS components can significantly influence susceptibility to antimicrobial agents (e.g., CAP), supporting this hypothesis (Labadie et al., 2021, Huang et al., 2023, Nadell et al., 2015). Future studies would merit further microscopic analyses of alternative *S. aureus* strains to assess if these heterogenous susceptibility profiles were due to matrix formation; indeed, previous literature has documented differential levels of biofilm biomass across *S. aureus* strains (Lamret et al., 2021a, Latorre et al., 2022, Skogman,

Vuorela and Fallarero, 2012). Furthermore, sub-lethal exposure to oxidative stress has been shown to induce adaptive responses in *S. aureus*, including the formation of small colony variants (SCVs) with enhanced resistance to oxidative damage (Painter et al., 2015). Rodríguez-Rojas et al. (2020) demonstrated that non-lethal exposure to H_2O_2 can boost bacterial survival and evolvability against oxidative stress, potentially explaining the tolerance observed in certain strains. Of course, such as phenomena may not explain the differential tolerance levels immediately after 5 minutes treatment but may explain the observations made from the regrowth experiments whereby *S. aureus* predominated the biofilm. However, this may have simply been a result of overgrowth of the tolerance organism in the triadic model, arising from reduced viability in *C. albicans* and *P. aeruginosa*. Repeat treatment interventions of the same biofilms across multiple days would help us understand the tolerance profiles of this organism. Similarly, evaluating the effects of multiple CAP treatments over time, mimicking clinical protocols (Stratmann et al., 2020, Mirpour et al., 2020a), would provide insights into optimal treatment regimens. Alternatively, combining CAP therapy with other antimicrobial techniques would be a logical advancement to this work: such experiments are reported in chapter 4.

3.3.4 Clinical relevance and potential applications

3.3.4.1 Implications for wound management and infection control

The significant efficacy of CAP against diverse microbial biofilms demonstrated in our study has important implications for wound management and infection control strategies. Chronic wounds, including DFUs, pressure ulcers, and venous leg ulcers (VLUs), are frequently colonised by polymicrobial biofilms that contribute to delayed healing and poor treatment outcomes (James et al., 2008). The ability of CAP to simultaneously target multiple microbial species, including fungi and bacteria, makes it a promising technology for treating such complex wound infections.

The World Union of Wound Healing Societies (WUWHS) estimates that biofilms are present in at least 60% of chronic wounds (Percival, McCarty and Lipsky, 2015), whilst specific to DFUs, it is estimated that between 40% and 60% are infected

with microbial biofilms (Jia et al., 2017, Kee, Nair and Yuen, 2019). The financial burden associated with wound care is substantial, with Guest, Fuller and Vowden (2020) reporting that wound care costs the NHS approximately £8.3 billion annually, whilst global costs are predicted to exceed $100 billion (Nussbaum et al., 2018). These statistics underscore the urgent need for effective biofilm management strategies. From these *in vitro* experimental results, CAP therapy may offer a suitable alternative to current antimicrobial interventions.

Recent clinical trials have reported promising results using CAP for wound treatment. Prospective randomized phase II study in 24 patients with chronic infected wounds comparing daily 2-min CAP plus standard care to the contralateral control site; CAP significantly reduced bacterial load with MicroPlaSter alpha (−40%, $P < 0.016$; 70 treatments) and MicroPlaSter beta (−23.5%, $P < 0.008$; 137 treatments) without adverse effects, demonstrating species-agnostic reduction in bioburden under daily dosing (Isbary et al., 2012). Stratmann et al. (2020) reported in a placebo-controlled, patient-blinded trial analysing 65 DFU from 45 patients (SOC + CAP-jet vs SOC + placebo) reported a significant increase in wound healing ($p = 0.03$) and faster wound area reduction from baseline ($p = 0.009$), with good tolerability; microbial load decreased in both arms, contextualizing CAP-associated healing benefits alongside standard care effects. Similarly, Mirpour et al. (2020a) reported significant improvements in wound healing rates following CAP treatment in a double-blind randomized trial in 44 grade-2 DFU patients (22 CAP + standard care vs 22 standard care) using 5-min CAP three times weekly for 3 weeks; CAP significantly accelerated closure (lower mean fraction of wound size, $p = 0.02$) and a higher proportion reached ≤0.5 of baseline area at 3 weeks (77.3% vs 36.4%, $p = 0.006$), while within-session antisepsis was evident but between-group bacterial load over weeks was not significantly different ($p = 0.26$). Another multicenter randomized open-label non-inferiority randomized clinical trial in 78 patients with chronic wounds (39 CAP-jet vs 39 best-practice dressings) over 6 weeks; CAP-jet was non-inferior and statistically superior for granulation at day 42 (mean difference 21.21 pp; non-inferiority $p < 0.0001$; superiority $p = 0.001$), reduced wound area faster ($p < 0.001$) with end-study wound area 5.32% vs 43.72% of baseline ($p < 0.0001$), achieved more complete healing (58.97% vs 5.13%) with shorter time to healing ($p < 0.0001$), faster pH neutralization ($p =$

0.0123), and quicker infection resolution (p = 0.0129), with no adverse effects / serious adverse effects. These clinical outcomes support CAP's clinical benefits on wound closure dynamics and local wound milieu (granulation, area reduction, pH, and infection control) across devices and dosing schedules, while highlighting that sustained between-arm bacterial load differences are not guaranteed and may depend on protocol frequency and endpoint selection.

3.3.4.2 CAP as an alternative to conventional antimicrobials

The increasing prevalence of antimicrobial resistance (AMR) represents a significant challenge in managing wound infections. The antimicrobial activity of CAP against biofilms, including bacteria and fungi positions this technology as a valuable possible alternative or adjunct to conventional antimicrobial agents. Unlike antibiotics, which typically target specific cellular processes, CAP generates multiple reactive species that act through diverse mechanisms, potentially reducing the likelihood of resistance development.

O'connor et al. (2014) proposed that technologies targeting multiple cellular components simultaneously, such as CAP, may be less prone to resistance development compared to conventional antibiotics. This multi-targeted approach may be particularly valuable for treating biofilms, which often exhibit enhanced tolerance to antimicrobials through various protective mechanisms, including reduced metabolic activity, EPS barriers, and persister cell formation (Høiby et al., 2010).

The observed efficacy of CAP against fungal species, including *C. albicans* and *C. auris*, is particularly noteworthy, as fungal components of polymicrobial biofilms are often overlooked in conventional wound management strategies. (Kalan et al., 2016) reported that 80% of non-healing DFUs contain fungi, with *C. albicans* being one of the most prevalent species. The ability of CAP to target both bacterial and fungal components of biofilms simultaneously may address this limitation of conventional approaches, whilst circumventing any possible complications relating to mixed species infections.

Several recent studies have started to look at combinational therapies between CAP and antibiotics, in the hope of reducing the concentrations needed to clear infections (Maybin et al., 2023, Yang et al., 2021b, Olayiwola et al., 2024, Shabani et al., 2023). For example, combining CAP with antibiotics significantly enhances the eradication of *P. aeruginosa* biofilms by disrupting bacterial defence mechanisms. CAP pre-treatment generates RONS, which induce oxidative stress, damaging cell membranes and DNA. This oxidative damage increases biofilm permeability, allowing antibiotics like ciprofloxacin and gentamicin to penetrate more effectively, reducing their required doses by up to 512-fold (Maybin et al., 2023). Another study by Guo et al. (2021b) who combined low-temperature gas plasma (LTGP) with antibiotics synergistically enhances the eradication of MRSA biofilms in both *in vitro* and *in vivo* models. *In vitro*, LTGP pre-treatment (2–6 minutes) significantly lowered the minimum bactericidal concentrations (MBCs) of antibiotics like ciprofloxacin, rifampicin, and vancomycin by up to 16-fold. For example, LTGP (6 minutes) combined with rifampicin reduced biofilm viability to near-undetectable levels. *In vivo*, LTGP combined with rifampicin effectively reduced bacterial load in murine wound infections without causing tissue damage or systemic toxicity. The synergy arises from LTGP-generated ROS, which disrupt biofilm integrity and sensitise MRSA to antibiotics (Guo et al., 2021b). These findings highlight CAP's role in sensitising biofilms to antimicrobials, offering a promising strategy to overcome antibiotic resistance through oxidative priming and targeted therapeutic synergy. To this end, such work will be discussed in the proceeding chapter which will investigate a dual-therapy system for combatting the otherwise tolerant organism in our biofilm model .

3.3.5 Limitations and Future Directions

3.3.5.1 Experimental Limitations

Whilst our study provides valuable insights into the antimicrobial efficacy of CAP against various biofilms, several limitations should be acknowledged, some of which have already been mentioned before in this discussion. The *in vitro* nature of our biofilm models, while sophisticated may not fully recapitulate the complexity of clinical wound environments, which include microbial diversity, host factors, immune components, and varying oxygen tensions (Vyas, Xia and Mai-

Prochnow, 2022, PETERSON and WESTGATE, 2022, Wu et al., 2018). Future studies incorporating more complex models, such as *ex vivo* skin explants or *in vivo* animal models, would provide additional insights into the clinical relevance of our findings. Indeed, a number of *in vivo* studies have shown that CAP offers antimicrobial efficacy in living model systems (He et al., 2020a, Blaise et al., 2024, Chatraie et al., 2018, Zhou et al., 2025).

The focus on a limited number of microbial species and strains, whilst manageable from a technical standpoint in the laboratory, restricts the breadth of our conclusions. Clinical wound infections often contain diverse microbiota, including anaerobic bacteria and additional fungal species (Choi et al., 2019, Kalan et al., 2016, Tipton et al., 2020, Wu et al., 2018), not evaluated in this study. Expanding the range of microorganisms tested would provide a more comprehensive assessment of CAP's potential against the full spectrum of wound-associated pathogens. One such study recently published from our group, utilised a 11-multi-species wound biofilm model (Brown et al., 2022), including anaerobic organisms that would provide a much more complex system for CAP testing in the future. Furthermore, while we demonstrated a correlation between H_2O_2 production and antimicrobial efficacy, we did not comprehensively characterise the full spectrum of reactive species generated by our CAP device. Future studies employing advanced spectroscopic techniques to identify and quantify additional RONS would enhance our understanding of the mechanisms underlying CAP's antimicrobial effects (Girard-Sahun et al., 2019, Gorbanev, Privat-Maldonado and Bogaerts, 2018).

The current study focused primarily on immediate microbial killing and short-term regrowth (24 h), limiting our ability to assess long-term effects and potential resistance development. Extended studies examining multiple treatment cycles and longer regrowth periods would provide insights into the durability of CAP effects and the potential for adaptive responses.

3.3.5.2 Future Research Directions

Building upon the findings and limitations of this study, several promising directions for future research have emerged. Firstly, mechanistic studies

investigating the specific molecular targets of CAP-generated reactive species in different microbial species would enhance our understanding of the differential susceptibility observed (Zhang, Zhang and Han, 2023, Rao et al., 2020). Transcriptomic and proteomic analyses of CAP-treated biofilms could reveal specific stress response pathways activated in tolerant versus susceptible strains, potentially identifying targets for combination therapies. Other groups have begun to investigate these mechanistic pathways (Maybin et al., 2023). The strain-dependent tolerance observed in *S. aureus* from this study warrants further investigation to identify genetic or phenotypic markers associated with CAP susceptibility. Comparative genomic and phenotypic analyses of strains exhibiting varying levels of tolerance might reveal specific factors contributing to resistance, enabling more targeted application of CAP therapy.

Studies examining the combined effects of CAP with conventional antimicrobials represent another promising direction as discussed before. Synergistic interactions between CAP and antibiotics have been reported (Theinkom et al., 2019), suggesting that combination approaches might enhance overall efficacy and reduce the risk of resistance development. This is an important consideration for future data chapters presented in this thesis.

3.3.6 Conclusion

Key findings from this chapter:

- CAP showed antimicrobial activity against both bacterial and fungal biofilms.

- Antimicrobial efficacy is time-dependent and correlates with increased H_2O_2 and other reactive species.

- *S. aureus* displayed a level of strain-dependent tolerance, highlighting the importance of microbial diversity in treatment outcomes.

- CAP treatment caused compositional changes in polymicrobial biofilms, reflecting complex interspecies dynamics.

- SEM revealed species-specific morphological changes, supporting oxidative damage as a main mechanism of CAP interventions.

4 Chapter 4: Cold atmospheric plasma (CAP) in dual therapy to break the tolerance of skin and wound-relevant biofilm models

4.1 Introduction

The emergence and spread of antimicrobial resistance have become one of the most pressing global public health threats, which has been largely driven by the excessive use of antimicrobials (Waddington et al., 2022, Sharma et al., 2024b). This phenomenon has significantly reduced the efficacy of conventional antimicrobial agents, necessitating the discovery and development of novel therapeutic compounds with distinct mechanisms of action (Waddington et al., 2022, Jain et al., 2024). Microbial biofilms, which are structured communities of microorganisms encased in a self-produced extracellular polymeric substance (EPS), present particular challenges due to their increased resistance to antimicrobial agents compared to their planktonic counterparts (Sharma et al., 2024b, Nwafor et al., 2024). This intrinsic resistance can be attributed to multiple factors, including limited drug penetration through the biofilm matrix, altered microenvironments within biofilms, and the presence of persister cells that exhibit physiological heterogeneity (Sharma et al., 2024b). Biofilm-associated infections are particularly problematic in healthcare settings, where they contribute significantly to chronic, recalcitrant infections that respond poorly to conventional antimicrobial therapies (Sharma et al., 2024b, Azevedo et al., 2017).

Polymicrobial biofilms, comprising multiple microbial species, introduce additional complexity to infection management due to interspecies interactions that can enhance antimicrobial resistance and pathogenicity (Pohl, 2022, Azevedo et al., 2017). These complex microbial communities often exhibit enhanced tolerance to conventional antimicrobial agents through various cooperative mechanisms, including metabolic cooperation, quorum sensing (QS), and horizontal gene transfer (Pohl, 2022). Understanding the dynamics of polymicrobial biofilms is therefore crucial for developing effective therapeutic strategies against recalcitrant infections (Pohl, 2022). Among the most clinically relevant microorganisms, *Candida albicans*, *Staphylococcus aureus*, and *Pseudomonas aeruginosa* represent significant pathogens that frequently coexist in polymicrobial infections, particularly in wounds, respiratory infections, and medical device-associated infections (Pohl, 2022, Murali et al., 2024). *C. albicans*, an opportunistic fungal pathogen, possesses numerous virulence factors, including secreted phospholipases that contribute significantly to its pathogenicity by

facilitating tissue invasion (Pohl, 2022). *S. aureus*, a Gram-positive bacteria, is a leading cause of healthcare associated infections and exhibits remarkable adaptability to antimicrobial pressure through various resistance mechanisms (Sharma et al., 2024b). *P. aeruginosa*, a Gram-negative opportunistic pathogen, is notorious for its intrinsic resistance to multiple classes of antibiotics due to its impermeable outer membrane, efflux pumps, and biofilm-forming capabilities (Sharma et al., 2024b, Murali et al., 2024).

Drug repurposing offers a promising alternative for treating biofilm-associated infections. By identifying new uses for existing drugs, this approach accelerates the development of effective therapies while bypassing the lengthy and costly process of traditional drug discovery (Oliveira, Borges and Simões, 2020). One particular drug library, the Tocriscreen™ Micro library represents a valuable resource for identifying novel compounds with therapeutic potential against various microbial targets (Abduljalil et al., 2022). These effective biologically active molecules have demonstrated biofilm inhibitory activity against several key *Candida* species, including *C. albicans*, *C. auris*, *C. glabrata*, and *C. krusei*. Polygodial (POLY), a sesquiterpene dialdehyde derived from plant sources, exhibits moderate antibacterial activity against Gram-positive bacteria including *Bacillus subtilis*, *S. aureus* and Gram-negative bacteria including *Escherichia coli* and *Salmonella choleraesuis* (Kubo et al., 2005). Darapladib (DARA) demonstrated efficacy for biofilm inhibition and treatment at concentration ranges from 8 to 32 µg/mL, and combinational testing with conventional antifungals showed synergistic effects against *Candida* strains (Abduljalil et al., 2022). KHS101 hydrochloride (KHS), a selective inducer of neuronal differentiation, represents a novel class of compounds with potential antimicrobial properties (Abduljalil et al., 2022).

Cold atmospheric plasma (CAP) has emerged as a promising antimicrobial technology that generates reactive oxygen and nitrogen species (RONS) capable of damaging microbial cells through multiple mechanisms while exhibiting minimal toxicity to host tissues (Murali et al., 2024, Marx et al., 2024). When combined with conventional antimicrobial agents, CAP has demonstrated synergistic effects against various pathogens, potentially overcoming resistance mechanisms through

complementary modes of action (Maybin et al., 2023, Prasad et al., 2023). Research has found that merging CAP and antibiotics can significantly weaken *P. aeruginosa* biofilms, making them more susceptible to treatment (Maybin et al., 2023). CAP has shown potent *in vitro* antimicrobial effects on multiple bacterial species, including *P. aeruginosa*, *Staphylococcus pseudintermedius*, *Streptococcus canis*, *Candida* species and some of *Staphylococcus* strains (Marx et al., 2024, Baz et al., 2023). The combination of novel compounds with physical treatment modalities like CAP represents an innovative approach to combating antimicrobial resistance by targeting multiple cellular pathways simultaneously (Prasad et al., 2023). This dual-therapy approach may provide enhanced efficacy against biofilm-associated infections that are typically recalcitrant to monotherapy (Prasad et al., 2023, Maybin et al., 2023). Additionally, the evaluation of potential synergism between compounds and oxidative stress inducers may reveal valuable insights into the mechanisms of antimicrobial action and resistance, potentially informing the development of more effective combination therapies (Prasad et al., 2023).

The present chapter aims to comprehensively evaluate the antimicrobial efficacy of three selected compounds from the Tocriscreen™ Micro library against multiple pathogenic skin and wound microorganisms in both planktonic and biofilm states. Additionally, this chapter explores the potential of combinational therapies, including investigating the synergistic effects of these compounds, compared with conventional antiseptics with CAP against these model systems.

4.2 Results

4.2.1 Kinetic growth curve assessment of Tocriscreen™ Micro library compounds against different microorganisms

Initial testing was conducted to assess the efficacy of novel compounds against skin and wound relevant microorganisms. Based on their previous therapeutic properties against different *Candida* strains, three hit compounds from Tocriscreen™ Micro library (Abduljalil et al., 2022) were selected for evaluation. These were tested against *C. albicans* SC5314, *P. aeruginosa* PA14, and two strains of *S. aureus* (Newman and SH1000). Firstly, to assess the dynamic antimicrobial effects over time of the Tocriscreen™ compounds, the growth kinetics of the

different microorganisms were monitored over 24 hours (h) in response to different concentrations of KHS, DARA and POLY. Growth was assessed by measuring optical density (OD) every two hours at 600 nm when microorganisms were grown under agitation in a Cerillo microplate reader device and incubated at appropriate temperature (30°C or 37°C) for 24 h aerobically with shaking at 200 rpm in an orbital shaker. Initially, for KHS, *C. albicans* demonstrated concentration-dependent growth inhibition patterns when exposed to varying levels of the compound. The untreated (UT) control culture reached a mean (OD) of 1.21 after 24 h of incubation. At the highest tested concentration (64 µg/mL), growth was substantially inhibited, with suspensions reaching a mean OD of only 0.14 after 24 h, representing an 88.4% growth inhibition compared to the UT control. Treatment with 32 µg/mL resulted in a mean OD of 0.57 (53.1% inhibition), while lower concentrations showed more modest effects: 16 µg/mL yielded a mean OD of 1.02 (15.8% inhibition), 8 µg/mL reached a mean OD of 1.13 (6.7% inhibition), and 4 µg/mL achieved a mean OD of 1.08 (10.9% inhibition) (Figure 4.1A).

In contrast, *P. aeruginosa* exhibited complete tolerance to the KHS compound, higher concentrations of KHS (64 µg/mL) reduced the initial growth rate of *P. aeruginosa*, as evidenced by delayed entry into exponential phase and slower mean OD increase during the first 6–8 h. However, after 24 h, the final mean OD of treated cultures remained comparable to UT controls (1.32 vs. 1.41 mean OD, respectively), indicating minimal impact on overall cell viability or biomass accumulation. This pattern aligns with studies demonstrating that sub-inhibitory antibiotic concentrations can transiently suppress bacterial growth kinetics without significantly altering final cell density, as metabolic activity and replication resume once stress adaption occurs (Reeks et al., 2005, Hare et al., 2024). Despite the UT control reaching a mean OD of 1.41, even the highest concentration of 64 µg/mL resulted in a mean OD of 1.32 (6.6% inhibition). This trend continued across all concentrations, with 32 µg/mL showing 9.6% inhibition (mean OD 1.28), 16 µg/mL showing 3.3% inhibition, and lower concentrations displaying negligible effects: 8 µg/mL (0.6% inhibition, mean OD 1.37) and 4 µg/mL (1.2% inhibition, mean OD 1.40) (Figure 4.1B). *S. aureus* Newman, on the other hand, demonstrated high sensitivity to the compound. From an UT control a mean

OD of 1.47, higher concentrations achieved profound growth inhibition: 64 µg/mL resulted in 96.6% inhibition (mean OD 0.05), 32 µg/mL showed 99.0% inhibition (mean OD 0.01), and 16 µg/mL completely inhibited growth. However, lower concentrations proved less effective, with 8 µg/mL and 4 µg/mL showing only 7.1% and 3.2% inhibition respectively (Figure 4.1C). Similarly, *S. aureus* SH1000 exhibited susceptibility to the compound, though with slightly different patterns to its strain counterpart. From a control mean OD of 1.58, higher concentrations demonstrated inhibition: 64 µg/mL achieved 97.1% inhibition (mean OD 0.04) and 32 µg/mL showed 98.5% inhibition (mean OD 0.02). A moderate effect was observed at 16 µg/mL (71.6% inhibition, mean OD 0.45), while lower concentrations of 8 µg/mL and 4 µg/mL showed minimal impact with 2.4% and 0.4% inhibition respectively (Figure 4.1D).These results indicate that, while KHS shows antifungal and antibacterial features against *C. albicans* and *S. aureus* strains, its limited impact on *P. aeruginosa* viability necessitates further optimisation for Gram-negative bacteria.

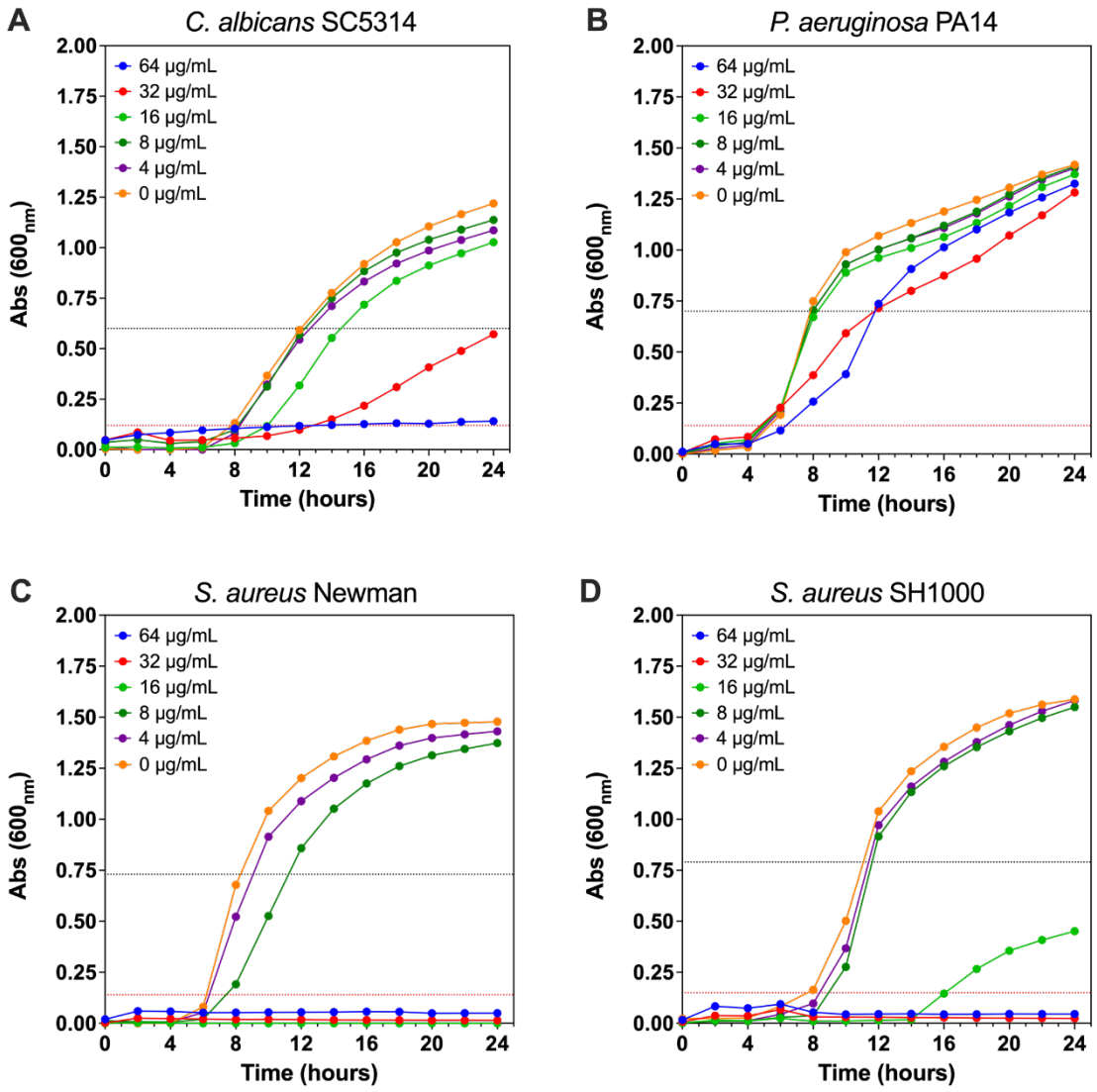

Figure 4.1: (24 h) Kinetic growth curve of different microorganisms treated with various concentration of KHS at 600 nm absorbance. (A) *C. albicans* SC5314 planktonic cells were grown in YPD broth at 30 °C in a Cerillo microplate reader device with shaking at 200 rpm. (B) *P. aeruginosa* PA14, (C) *S. aureus* Newman and (D) *S. aureus* SH1000 planktonic cells were grown in LB broth at 37 °C in a Cerillo microplate reader device with shaking at 200 rpm. The curves show the means of optical density at 600_{nm}. Each experiment was done in four technical replicates of two biological repetitions. 0 µg/mL: UT control. Dotted lines denote 50% reduction (black) and 90% reduction (red). Error bars were not included it for clarity of the data presentation.

Next, the growth kinetics of the different microorganisms were monitored over a 24-h period in response to varying concentrations of DARA, with growth assessed spectrophotometrically at 600 nm every two hours similar to before. Initially, *C. albicans* demonstrated marked sensitivity to the compound, with the UT control reaching a mean OD of 1.26. Higher concentrations showed profound inhibition: 64 µg/mL and 32 µg/mL resulted in mean ODs of 0.06 and 0.12 (94.9% and 90.3%

inhibition, respectively). Moderate to lower concentrations showed reduced effects: 16 µg/mL reached a mean OD of 0.91 (27.5% inhibition), while 8 µg/mL and 4 µg/mL achieved mean ODs of 1.16 and 1.14 (7.7% and 9.4% inhibition, respectively) (Figure 4.2A). In contrast, *P. aeruginosa* exhibited tolerance across all concentrations, similar to results for KHS. From an UT control a mean OD of 1.41, even the highest concentration of 64 µg/mL achieved minimal impact with a mean OD of 1.33 (6% inhibition). This pattern continued across decreasing concentrations: 32 µg/mL (mean OD 1.34, 5.1% inhibition), 16 µg/mL (mean OD 1.39, 1.6% inhibition), 8 µg/mL (mean OD 1.40, 0.6% inhibition), and 4 µg/mL (mean OD 1.38, 2.3% inhibition) (Figure 4.2B).

S. aureus Newman displayed moderate but consistent sensitivity to DARA at different concentrations. From an UT control mean OD of 1.57, all concentrations produced similar inhibitory effects: 64 µg/mL (mean OD 1.08, 31.4% inhibition), 32 µg/mL and 16 µg/mL (both mean OD 1.11, 29.4% and 29.3% inhibition), 8 µg/mL (mean OD 1.12, 28.6% inhibition), and 4 µg/mL (mean OD 1.07, 31.9% inhibition) (Figure 4.2C). Similarly, *S. aureus* SH1000 showed moderate sensitivity, though with a slight concentration-dependent pattern. From an UT control mean OD of 1.46, inhibition gradually decreased with concentration: 64 µg/mL (mean OD 1.03, 29.1% inhibition), 32 µg/mL (mean OD 1.10, 24.7% inhibition), 16 µg/mL (mean OD 1.16, 20.2% inhibition), 8 µg/mL (mean OD 1.18, 19.2% inhibition), and 4 µg/mL (mean OD 1.12, 22.8% inhibition) (Figure 4.2D). These results highlight DARA's potential as a narrow-spectrum antifungal agent against *C. albicans* but underscore its limited utility against Gram-negative bacteria (*P. aeruginosa*) and variable efficacy against Gram-positive bacteria (*S. aureus* Newman and SH1000), necessitating further exploration of its mechanism and synergistic combinations.

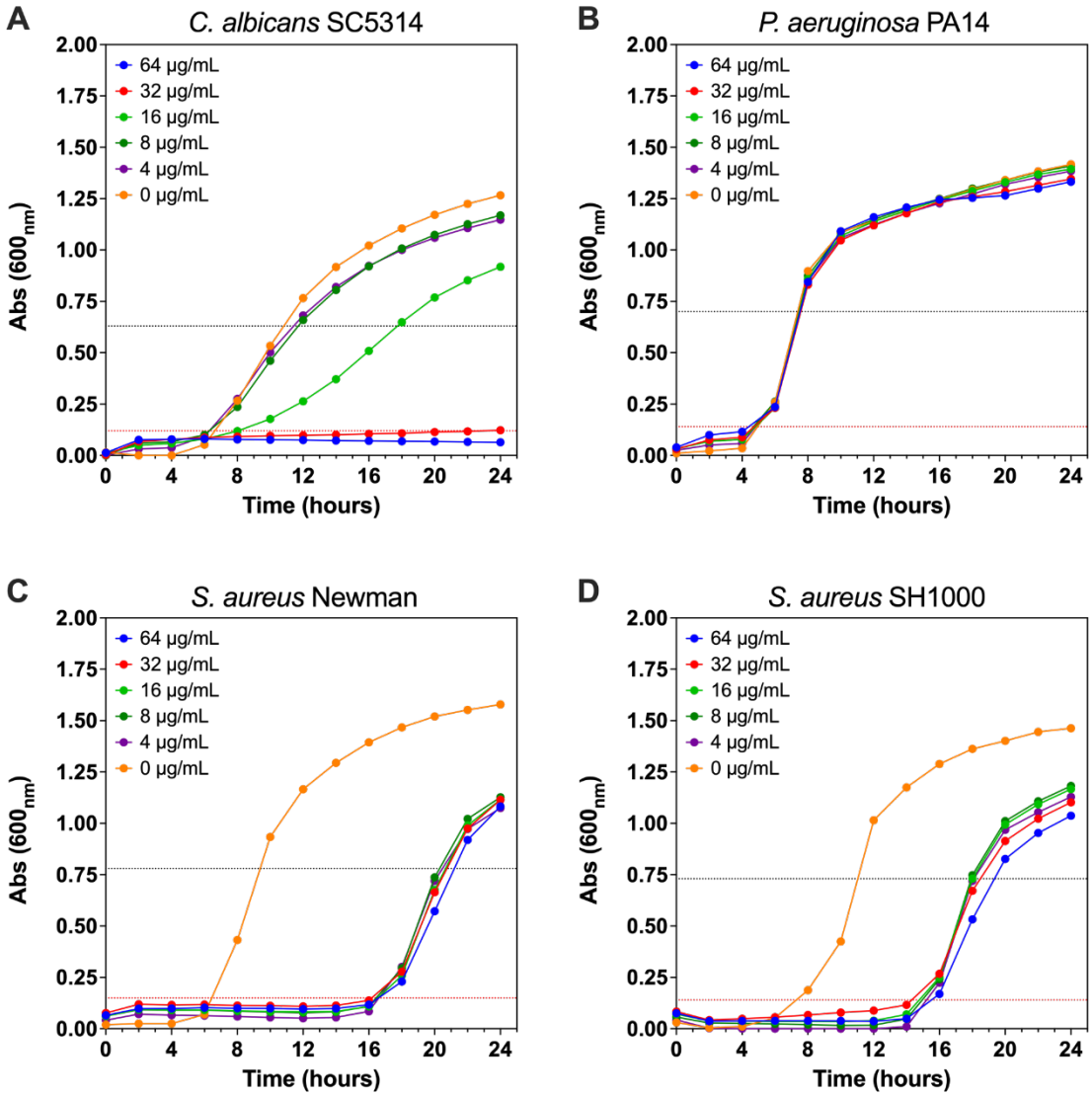

Figure 4.2: (24 h) Kinetic growth curve of different microorganisms treated with various concentration of DARA at 600 nm absorbance. (A) *C. albicans* SC5314 planktonic cells were grown in YPD broth at 30 °C in a Cerillo microplate reader device with shaking at 200 rpm. (B) *P. aeruginosa* PA14, (C) *S. aureus* Newman and (D) *S. aureus* SH1000 planktonic cells were grown in LB broth at 37 °C in a Cerillo microplate reader device with shaking at 200 rpm. The curves show the means of optical density at 600_{nm}. Each experiment was done in four technical replicates of two biological repetitions. 0 µg/mL: UT control. Dotted lines denote 50% reduction (black) and 90% reduction (red). Error bars were not included it for clarity of the data presentation.

The final Toscriscreen™ compound assessed for its antimicrobial inhibitory effects was POLY. Initially, *C. albicans* demonstrated sensitivity to the compound, with the UT control reaching an OD of 1.26. Higher concentrations showed profound inhibition: 64 µg/mL and 32 µg/mL resulted in mean ODs of 0.05 and 0.04 (95.8% and 96.8% inhibition, respectively). Moderate to lower concentrations showed diminishing effects: 16 µg/mL reached a mean OD of 0.89 (29.7% inhibition), while 8 µg/mL and 4 µg/mL achieved mean ODs of 1.14 and 1.21 (9.9% and 4.4%

inhibition, respectively) (Figure 4.3A). As with the other two compounds tested, *P. aeruginosa* exhibited complete tolerance across all concentrations. From an UT control mean OD of 1.41, the highest concentration of 64 µg/mL showed no inhibition, achieving a mean OD of 1.48. This pattern of resistance continued across decreasing concentrations: 32 µg/mL (mean OD 1.41, 0.3% inhibition), 16 µg/mL (mean OD 1.37, 3.1% inhibition), 8 µg/mL (mean OD 1.39, 1.3% inhibition), and 4 µg/mL (mean OD 1.40, 1.0% inhibition) (Figure 4.3B).

S. aureus Newman displayed moderate sensitivity to POLY, but only at higher concentrations. From an UT control mean OD of 1.49, the response was concentration-dependent: 64 µg/mL showed the strongest effect (mean OD 1.07, 27.7% inhibition), while 32 µg/mL and 16 µg/mL demonstrated modest inhibition (mean ODs 1.32 and 1.30, 11.4% and 13% inhibition). Lower concentrations had minimal impact: 8 µg/mL and 4 µg/mL (mean ODs 1.48 and 1.49, 0.5% and 0.01% inhibition) (Figure 4.3C). Similarly, *S. aureus* SH1000 showed limited sensitivity, with meaningful inhibition observed only at the highest concentration. From an UT control mean OD of 1.46, only 64 µg/mL produced notable inhibition (mean OD 1.16, 20.6% inhibition). Surprisingly, 32 µg/mL showed no inhibition (mean OD 1.49), and lower concentrations demonstrated negligible effects: 16 µg/mL (mean OD 1.44, 1.4% inhibition), while 8 µg/mL and 4 µg/mL showed no measurable inhibition (mean ODs 1.46 and 1.48) (Figure 4.3D). These results indicate that, POLY is highly effective against *C. albicans* but has weak activity against *S. aureus* (Newman and SH1000) and is ineffective against *P. aeruginosa*.

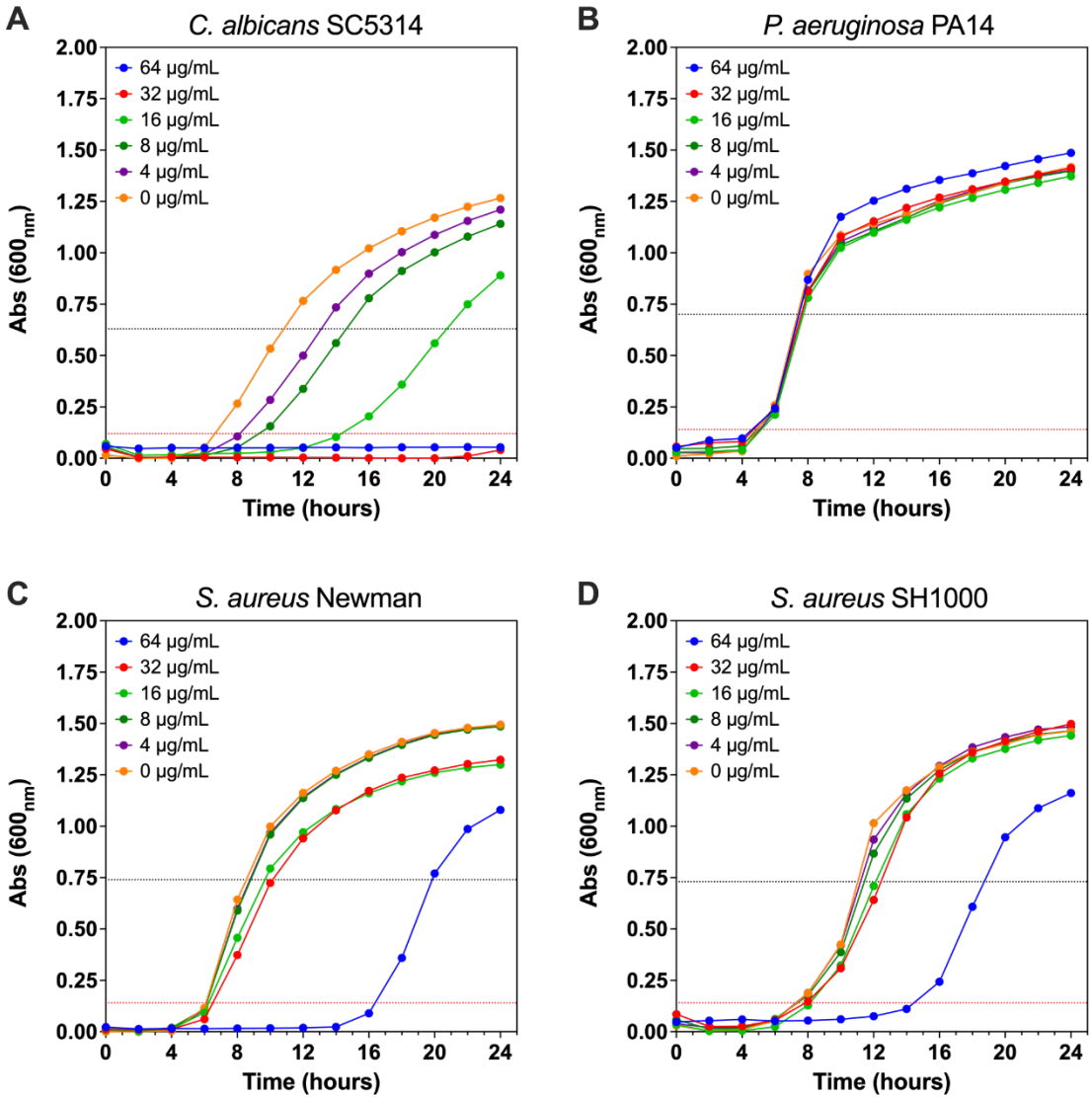

Figure 4.3: (24 h) Kinetic growth curve of different microorganisms treated with various concentration of POLY at 600 nm absorbance. (A) *C. albicans* SC5314 planktonic cells were grown in YPD broth at 30 °C in a Cerillo microplate reader device with shaking at 200 rpm. (B) *P. aeruginosa* PA14, (C) *S. aureus* Newman and (D) *S. aureus* SH1000 planktonic cells were grown in LB broth at 37 °C in a Cerillo microplate reader device with shaking at 200 rpm. The curves show the means of optical density at 600 nm. Each experiment was done in four technical replicates of two biological repetitions. 0 µg/mL: UT control. Dotted lines denote 50% reduction (black) and 90% reduction (red). Error bars were not included it for clarity of the data presentation.

4.2.2 Metabolic activity and biofilm biomass of mono- and triadic species biofilm models following treatment

Following on from planktonic testing using growth curve kinetics, the efficacy of the three candidates Tocriscreen™ Micro compounds were next assessed against biofilms of the four microorganisms grown as mono-species, or within the two triadic models (Newman and SH1000) used in the previous chapter.

4.2.2.1 *C. albicans* SC5314 biofilm

The efficacy of KHS, DARA, and POLY against *C. albicans* SC5314 biofilms was evaluated using a 24-h treatment protocol. Biofilms were initially cultivated for 24 h in RPMI broth on 96-well flat-bottom plates before compounds exposure. Biofilm metabolic activity and biomass were subsequently assessed using AlamarBlue™ and crystal violet assays, respectively as detailed in earlier methods sections 2.4.7 and 2.4.8. A total of six different concentrations of the compounds were selective, ranging from above and below the PMICs determined in the growth curve kinetic experiments.

As shown in (Figure 4.4A and Figure 4.4D), KHS demonstrated concentration-dependent effects on both biofilm metabolic activity and biomass. Higher concentrations of KHS exhibited significant reductions in biofilm metabolic activity: 64 µg/mL reduced metabolic activity to 5.52% (****p< 0.0001), 32 µg/mL to 10.10% (****p< 0.0001), and 16 µg/mL to 44.80% (****p< 0.0001) compared to UT controls. Lower concentrations showed no significant impact on biofilm metabolic activity: 8 µg/mL reduced metabolic activity to 84.69%, 4 µg/mL to 95.76% and 2 µg/mL to 96.64% compared to UT controls. Regarding biomass reduction (Figure 4.4A and Figure 4.4E), only the two highest concentrations of KHS showed significant effects: 64 µg/mL reduced biomass to 45.13% (****p< 0.0001) and 32 µg/mL to 63.24% (**p< 0.01) of UT controls. Lower concentrations did not significantly affect biofilm biomass: 16 µg/mL reduced biomass to 84.93%, 8 µg/mL to 92.07%, 4 µg/mL to 97.43% and 2 µg/mL to 96.57% compared to UT controls. These findings demonstrate that KHS exhibits potent anti-biofilm activity against *C. albicans* SC5314 at higher concentrations, affecting both cellular metabolic activity and biofilm structure.

Next, the efficacy of DARA against *C. albicans* biofilms was evaluated. As illustrated in (Figure 4.4B and Figure 4.4D), DARA demonstrated concentration-dependent inhibitory effects on both biofilm outputs. Biofilm metabolic activity was significantly reduced across most tested concentrations. The highest concentration of 64 µg/mL showed the most potent effect, reducing metabolic activity to 2.53% (****p< 0.0001), followed by progressive reductions at 32 µg/mL (19.35%, ****p< 0.0001), 16 µg/mL (52.27%, ****p< 0.0001), 8 µg/mL (77.78%, ****p< 0.0001), and 4 µg/mL (92.32%, *p< 0.05) compared to UT controls. The lowest concentration of 2 µg/mL showed no significant impact on biofilm metabolic activity. Regarding biomass reduction (Figure 4.4B and Figure 4.4E), DARA exhibited significant effects at higher concentrations: 64 µg/mL reduced biomass to 44.03% (****p< 0.0001), 32 µg/mL to 64.33% (***p< 0.001), and 16 µg/mL to 80.86% (*p< 0.05) compared to UT controls. Lower concentrations (8, 4, and 2 µg/mL) did not significantly affect biofilm biomass. These findings demonstrate that DARA exhibits potent anti-biofilm activity against *C. albicans*, with more pronounced effects on cellular metabolic activity than on biofilm biomass reduction suggestive of its ability to kill biofilms, rather than removal.

Finally, the efficacy of POLY against *C. albicans* biofilms was evaluated. As shown in (Figure 4.4C and Figure 4.4D), POLY demonstrated significant concentration-dependent effects on biofilm metabolic activity across all tested concentrations. The highest concentration of 64 µg/mL completely inhibited biofilm metabolic activity (0%, ****p< 0.0001), while 32 µg/mL reduced metabolic activity to 4.30% (****p< 0.0001). Progressive reductions in metabolic activity were observed at decreasing concentrations compared to UT controls: 16 µg/mL (24.25%, ****p< 0.0001), 8 µg/mL (30.40%, ****p< 0.0001), 4 µg/mL (56.11%, ****p< 0.0001), and 2 µg/mL (73.54%, ***p< 0.001). Regarding biofilm biomass (Figure 4.4C and Figure 4.4E), POLY exhibited significant reductions across all tested concentrations compared to UT controls. The most pronounced effects were observed at 32 µg/mL, reducing biomass to 35.46% (****p< 0.0001), followed by 64 µg/mL (43.85%, ****p< 0.0001) and 16 µg/mL (48.75%, ****p< 0.0001). Lower concentrations maintained significant but diminishing effects: 8 µg/mL (67.53%, ****p< 0.0001), 4 µg/mL (78.22%, **p< 0.01), and 2 µg/mL (82.44%, *p< 0.05). These findings demonstrate that POLY exhibits potent anti-biofilm activity against *C. albicans*,

affecting both cellular metabolic activity and biofilm structure even at lower concentrations.

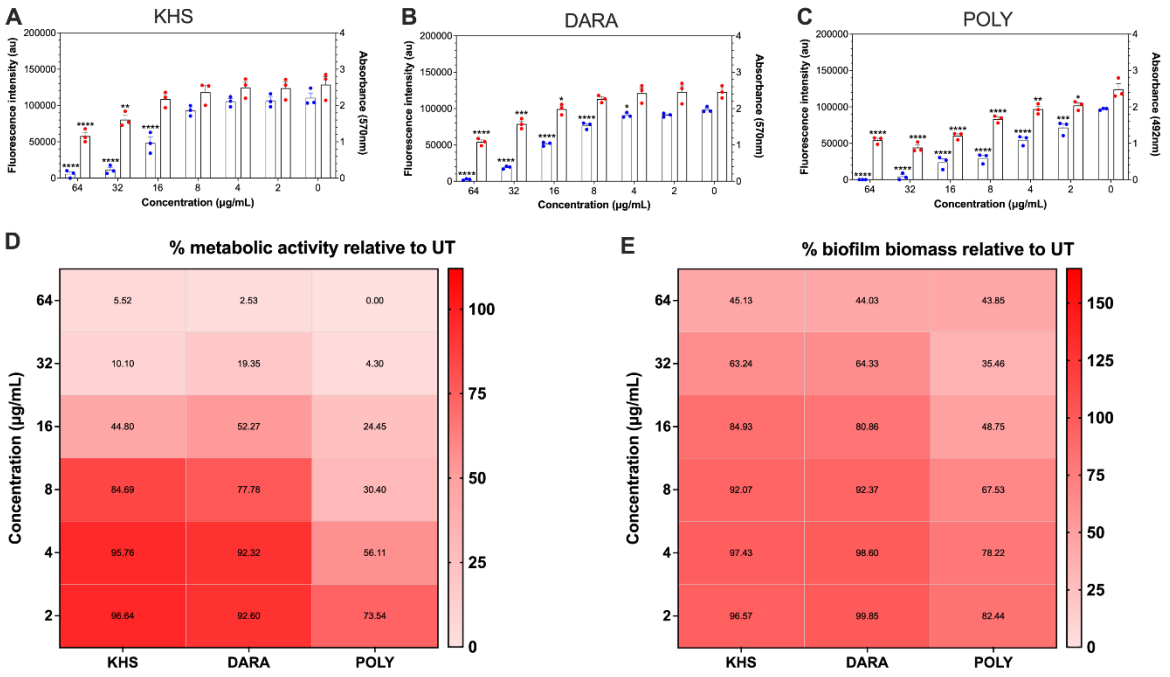

Figure 4.4: Metabolic activity and biofilm biomass of *C. albicans* SC5314 biofilms in relation to UT controls after 24 h treatment with three compounds from Tocriscreen™. *C. albicans* SC5314 biofilms were grown on 96 well flat bottom for 24 h in RPMI broth, then treated with KHS (A), DARA (B) and POLY (C) for 24 h separately. Metabolic activity and biofilm biomass were assessed by AlamarBlue™ assay (Left Y axis/ Blue dots) and crystal violet stain (Right Y axis/ Red dots) respectively. (D & E) heatmap shown percentages of metabolic activity and biofilm biomass of *C. albicans* SC5314 after treatment by KHS, DARA and POLY. AlamarBlue™ assay (fluorescence excitation wavelength, 544_{nm}; fluorescence emission wavelength, 590_{nm}), OD was measured at 570_{nm} for CV. Each bar represents the average of data obtained from four technical repeats of three independent experiments. The mean fluorescence /absorbance values are presented in a heatmap. Error bars represent the standard error of the mean. Data distributions were assessed using Shapiro-Wilk normality test and then analysed by ANOVA with Dunnett's tests to determine the P-value for multiple comparisons of normally distributed data. * Indicates statistically significant differences (*p< 0.05, **p< 0.01, ***p< 0.001, ****p< 0.0001). Data without asterisk indicates; no statistically significant differences were observed.

4.2.2.2 *P. aeruginosa* PA14 biofilm

The antimicrobial efficacy of KHS, DARA, and POLY was evaluated against *P. aeruginosa* PA14 biofilms. The biofilms were initially cultivated for 24 h in LB broth using 96-well flat-bottom plates, followed by a 24-h exposure to varying concentrations of the tested compounds.

Biofilm assessment was conducted using two complementary methods: the AlamarBlue™ assay for metabolic activity quantification and crystal violet staining

for biomass measurement as previously described in 2.4.7 and 2.4.8. As shown in (Figure 4.5), none of the tested compounds demonstrated significant reduced effects on biofilm metabolic activity across all tested concentrations (64, 32, 16, 8, 4, and 2 µg/mL) compared to UT controls. However, modest reductions in metabolic activity were observed at the highest tested concentration (64 µg/mL) for two compounds: DARA reduced metabolic activity to 68.39% (Figure 4.5B and Figure 4.5D), while POLY showed a reduction to 75.35% compared to UT biofilm (Figure 4.5C and Figure 4.5D), though these reductions were not statistically significant. Similarly, crystal violet analysis revealed no significant reductions in biofilm biomass at any concentration of the tested compounds. These findings suggest that *P. aeruginosa* PA14 biofilms exhibit substantial intrinsic tolerance to these compounds, with only minimal effects observed at high concentrations of DARA and POLY, and all drug concentrations failed to reach significant reduction in metabolic activity or biomass. These drug effects on sessile cells were comparable with observations made in (Figure 4.1, Figure 4.2 and Figure 4.3) for the planktonic cell suspensions in kinetic growth curve assay.

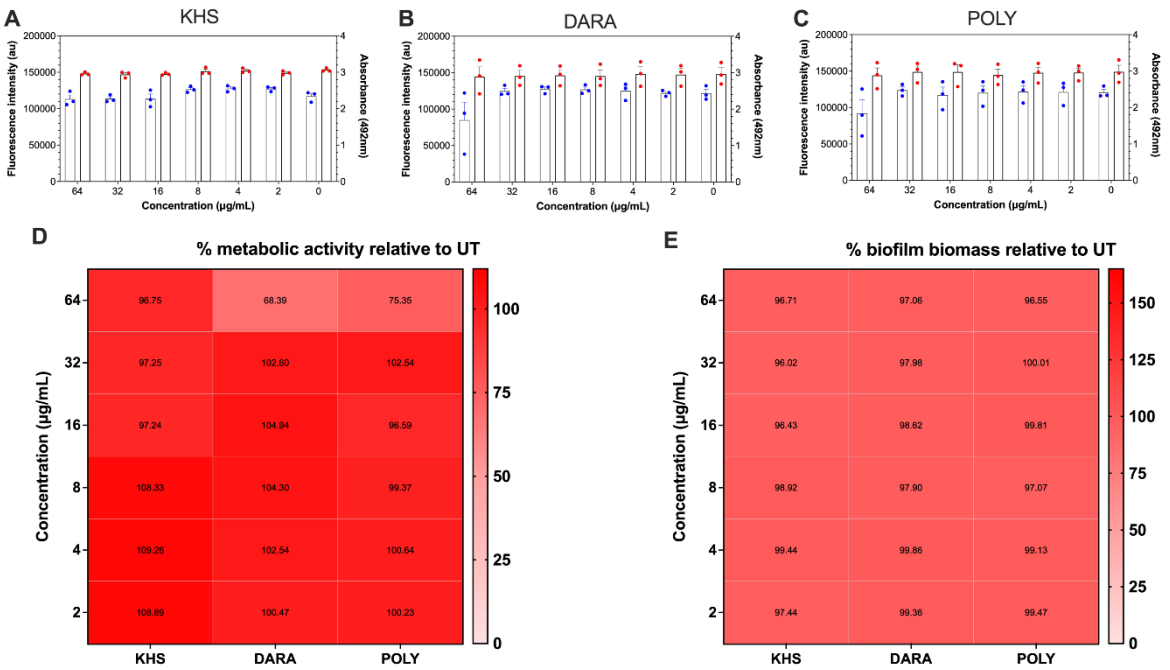

Figure 4.5: Metabolic activity and biofilm biomass of *P. aeruginosa* PA14 biofilms in relation to UT controls after 24 h treatment with three compounds from Tocriscreen™. *P. aeruginosa* PA14 biofilms were grown on 96 well flat bottom for 24 h in LB broth, then treated with KHS (A), DARA (B) and POLY (C) for 24 h separately. Metabolic activity and biofilm biomass were assessed by AlamarBlue™ assay (Left Y axis/ Blue dots) and crystal violet stain (Right Y axis/ Red dots) respectively. (D & E) heatmap shown percentages of metabolic activity and biofilm biomass of *P. aeruginosa* PA14 after treatment by KHS, DARA and POLY. AlamarBlue™ assay (fluorescence excitation wavelength, 544_{nm}; fluorescence emission wavelength, 590_{nm}), OD was measured at 570_{nm} for CV. Each bar represents the average of data obtained from four technical repeats of three independent experiments. The mean fluorescence /absorbance values are presented in a heatmap. Error bars represent the standard error of the mean. Data distributions were assessed using Shapiro-Wilk normality test and then analysed by ANOVA with Dunnett's tests to determine the P-value for multiple comparisons of normally distributed data, unless the data of KHS for crystal violet which analysed by Kruskal-Wallis with Dunn's tests for multiple comparisons of non-normally distributed data. Data without asterisk indicates; no statistically significant differences were observed.

4.2.2.3 S. aureus Newman biofilm

The effectiveness of KHS, DARA, and POLY against *S. aureus* Newman biofilms was tested using a 24-h exposure protocol. Mature biofilms were first established on 96-well plates in LB broth for 24 h, after which the compounds were applied. Following treatment, biofilm metabolic activity and total biomass were quantified using the AlamarBlue™ and crystal violet assays, respectively, as detailed in earlier methods sections 2.4.7 and 2.4.8.

As shown in (Figure 4.6A and Figure 4.6D), KHS demonstrated concentration-dependent effects on biofilm metabolic activity. The highest concentration (64 µg/mL) exhibited significant reduction in metabolic activity to 0.23% (*p< 0.05)

compared to UT controls. Intermediate concentrations showed varying effects: 32 µg/mL reduced metabolic activity to 2.85%, and 16 µg/mL to 75.74%, though these reductions were not statistically significant. Lower concentrations (8, 4, and 2 µg/mL) showed no meaningful impact on biofilm metabolic activity. Regarding biomass quantification (Figure 4.6A and Figure 4.6E), KHS at 32 µg/mL significantly reduced biofilm biomass to 37.98% (*p< 0.05) compared to UT controls. At 64 µg/mL, KHS reduced biomass to 65.98%, though this reduction was not statistically significant. Lower concentrations (16, 8, 4, and 2 µg/mL) did not significantly affect biofilm biomass. These findings demonstrate that KHS exhibits moderate anti-biofilm activity against *S. aureus* Newman, with optimal effects observed at concentrations 32 µg/mL.

Next, the efficacy of DARA against *S. aureus* Newman biofilms was evaluated through comprehensive analysis of both metabolic activity and biomass parameters. As shown in (Figure 4.6B and Figure 4.6D), DARA demonstrated significant concentration-dependent effects at higher concentrations. At 64 and 32 µg/mL, DARA dramatically reduced biofilm metabolic activity to 0.04% (****p< 0.0001) and 5.74% (****p< 0.0001) respectively, compared to UT controls. Lower concentrations (16, 8, 4, and 2 µg/mL) showed no significant impact on biofilm metabolic activity. Regarding biofilm biomass quantification (Figure 4.6B and E), DARA at 32 µg/mL significantly reduced biomass to 45.60% (**p< 0.01) compared to UT controls. At 64 µg/mL, biomass was reduced to 62.93%, this reduction did not reach statistical significance. Lower concentrations (16, 8, 4, and 2 µg/mL) showed no significant effect on biofilm biomass. These results indicate that DARA exhibits potent anti-biofilm activity against S. *aureus* Newman at higher concentrations, with more pronounced effects on cellular metabolic activity than on biofilm biomass reduction.

Finally, the efficacy of POLY against *S. aureus* Newman biofilms was evaluated. As shown in (Figure 4.6C and Figure 4.6D), POLY demonstrated limited concentration-dependent effects on biofilm characteristics. At the highest concentration tested (64 µg/mL), POLY significantly reduced biofilm metabolic activity to 94.75% (**p< 0.01) compared to UT controls. However, lower concentrations (32, 16, 8, 4, and 2 µg/mL) showed no significant impact on biofilm

metabolic activity. Regarding biofilm biomass quantification (Figure 4.6C and Figure 4.6E), POLY demonstrated no significant reduction in biofilm biomass across any of the tested concentrations (64, 32, 16, 8, 4, and 2 µg/mL) compared to UT controls. These findings suggest that POLY exhibits minimal anti-biofilm activity against *S. aureus* Newman, with only modest effects on cellular metabolic activity at the highest concentration and no appreciable impact on biofilm biomass.

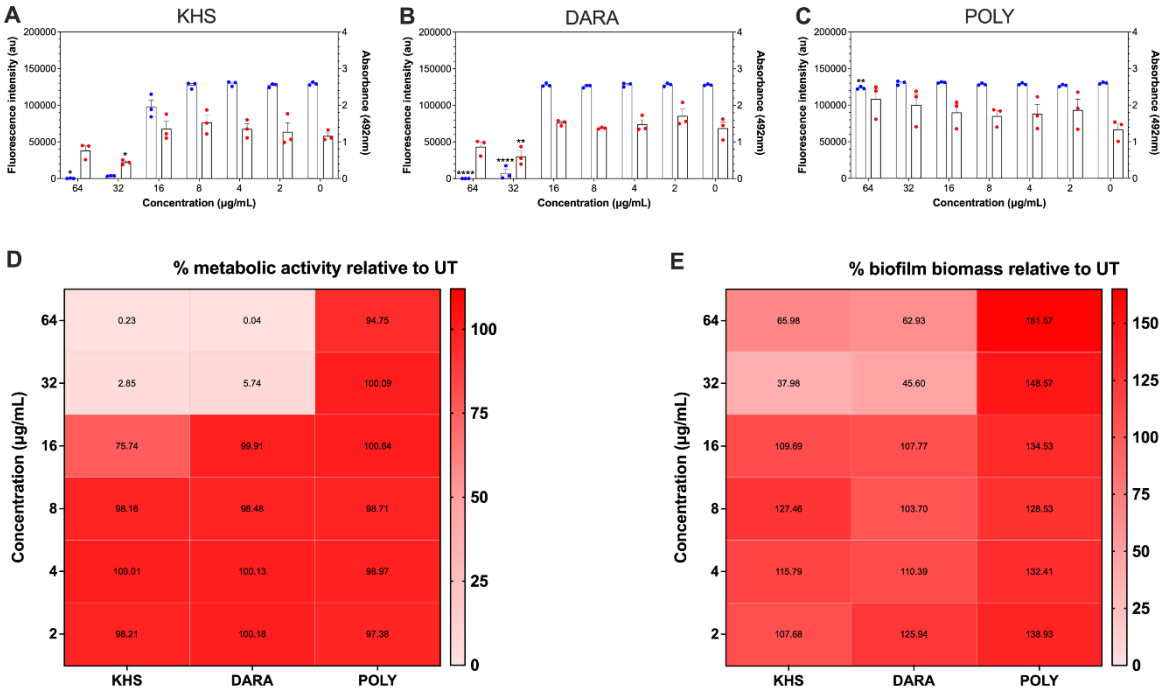

Figure 4.6: Metabolic activity and biofilm biomass of *S. aureus* Newman biofilms in relation to UT controls after 24 h treatment with three compounds from Tocriscreen™. *S. aureus* Newman biofilms were grown on 96 well flat bottom for 24 h in LB broth, then treated with KHS (A), DARA (B) and POLY (C) for 24 h separately. Metabolic activity and biofilm biomass were assessed by AlamarBlue™ assay (Left Y axls/ Blue dots) and crystal violet stain (Right Y axis/ Red dots) respectively. (D & E) heatmap shown percentages of metabolic activity and biofilm biomass of *S. aureus* Newman after treatment by KHS, DARA and POLY. AlamarBlue™ assay (fluorescence excitation wavelength, 544_{nm}; fluorescence emission wavelength, 590_{nm}), OD was measured at 570_{nm} for CV. Each bar represents the average of data obtained from four technical repeats of three independent experiments. The mean fluorescence /absorbance values are presented in a heatmap. Error bars represent the standard error of the mean. Data distributions were assessed using Shapiro-Wilk normality test and then analysed by ANOVA with Dunnett's tests to determine the P-value for multiple comparisons of normally distributed data, unless the data of KHS for AlamarBlue™ which analysed by Kruskal-Wallis with Dunn's tests for multiple comparisons of non-normally distributed data. * Indicates statistically significant differences (*p< 0.05, **p< 0.01, ****p< 0.0001). Data without asterisk indicates; no statistically significant differences were observed.

4.2.2.4 *S. aureus* SH1000 biofilm

The final microorganism used for screening of the three candidate Tocriscreen™ drugs was *S. aureus* SH1000. As shown in (Figure 4.7A and Figure 4.7D), KHS

demonstrated potent effects on biofilm metabolic activity at higher concentrations. The two highest concentrations exhibited significant reductions in metabolic activity: 64 µg/mL completely inhibited the metabolic activity (0.00%, ****p< 0.0001), while 32 µg/mL reduced metabolic activity to 0.39% (****p< 0.0001) compared to UT controls. At 16 µg/mL, KHS reduced metabolic activity to 89.12%, though this reduction was not statistically significant. Lower concentrations (8, 4 and 2 µg/mL) showed no meaningful impact on biofilm metabolic activity. Regarding biomass quantification (Figure 4.7A and Figure 4.7E), KHS demonstrated limited effects on biofilm structure. At 32 µg/mL, KHS reduced biofilm biomass to 88.66% compared to UT controls, though this reduction did not achieve statistical significance. All other tested concentrations (64, 16, 8, 4, and 2 µg/mL) showed no significant impact on biofilm biomass. These findings indicate that KHS exhibits strong anti-biofilm activity against *S. aureus* SH1000 primarily through effects on cellular metabolic activity rather than biomass reduction, with optimal effects observed at concentrations above 32 µg/mL.

Secondly, the efficacy of DARA against *S. aureus* SH1000 biofilms was evaluated. As shown in (Figure 4.7B and Figure 4.7D), DARA demonstrated moderate concentration-dependent effects on biofilm characteristics, though without reaching statistical significance. At higher concentrations, DARA showed notable reductions in biofilm metabolic activity: 64 µg/mL reduced metabolic activity to 0.12%, while 32 µg/mL decreased it to 72.64% compared to UT controls. Lower concentrations (16, 8, 4, and 2 µg/mL) showed no appreciable impact on biofilm metabolic activity. Regarding biofilm biomass quantification (Figure 4.7B and Figure 4.7E), DARA exhibited a concentration-dependent trend in biomass reduction, though these effects were not statistically significant. The three highest concentrations showed modest reductions in biofilm biomass: 64 µg/mL reduced biomass to 70.15%, 32 µg/mL to 76.09%, and 16 µg/mL to 98.09% compared to UT controls. Lower concentrations (8, 4, and 2 µg/mL) had no measurable effect on biofilm biomass. These findings suggest that while DARA demonstrates some anti-biofilm potential against *S. aureus* SH1000, its effects are modest and do not reach statistical significance at the tested concentrations.

Compound three, POLY demonstrated minimal effects on biofilm metabolic activity across tested concentrations. Treatment with 64, 32, 16, and 4 µg/mL resulted in modest reductions in metabolic activity to 97.58%, 98.92%, 99.77%, and 99.56% respectively, compared to UT controls, though none of these reductions achieved statistical significance. The remaining concentrations (8 and 2 µg/mL) showed no appreciable impact on biofilm metabolic activity. Regarding biofilm biomass quantification (Figure 4.7C and Figure 4.7E), POLY exhibited limited effects on biofilm structure. At the highest concentration of 64 µg/mL, POLY reduced biomass to 99.22% compared to UT controls, though this reduction was not statistically significant. All other tested concentrations (32, 16, 8, 4, and 2 µg/mL) showed no measurable effect on biofilm biomass. These findings suggest that POLY exhibits minimal anti-biofilm activity against *S. aureus* SH1000, with no statistically significant reductions in either metabolic activity or biomass across all tested concentrations.

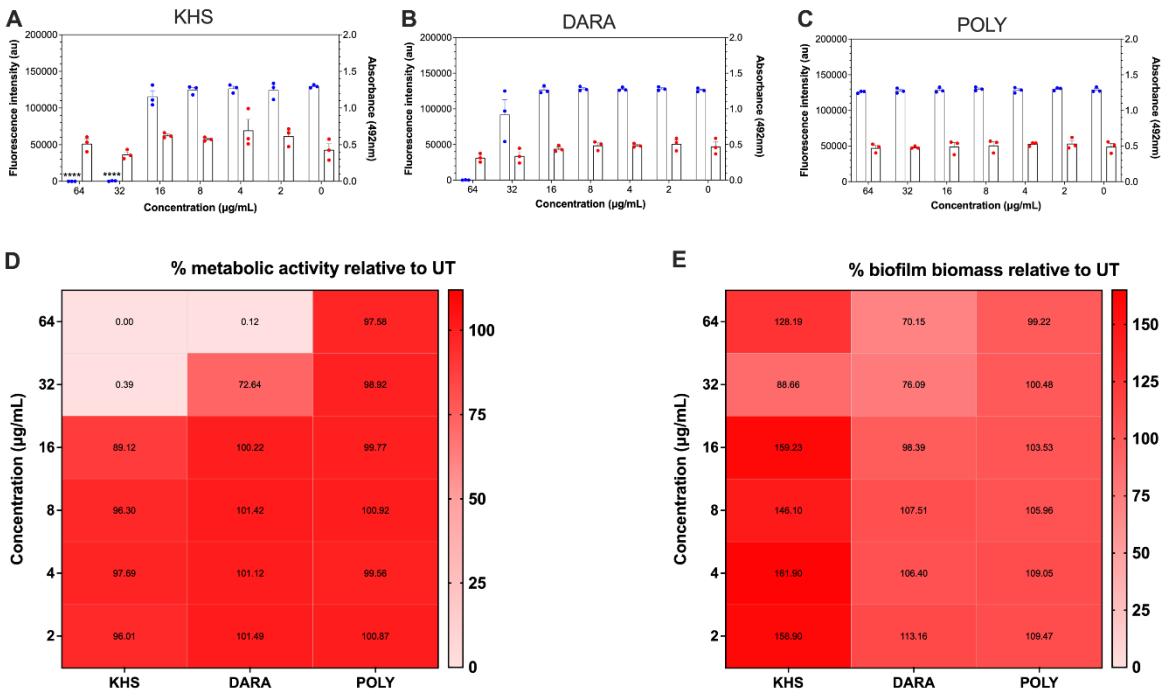

Figure 4.7: Metabolic activity and biofilm biomass of *S. aureus* SH1000 biofilms in relation to UT controls after 24 h treatment with three compounds from Tocriscreen™. *S. aureus* SH1000 biofilms were grown on 96 well flat bottom for 24 h in LB broth, then treated with KHS (A), DARA (B) and POLY (C) for 24 h separately. Metabolic activity and biofilm biomass were assessed by AlamarBlue™ assay (LEFT Y axis/ Blue dots) and crystal violet stain (Right Y axis/ Red dots) respectively. (D & E) heatmap shown percentages of metabolic activity and biofilm biomass of *S. aureus* SH1000 after treatment by KHS, DARA and POLY. AlamarBlue™ assay (fluorescence excitation wavelength, 544_{nm}; fluorescence emission wavelength, 590_{nm}), OD was measured at 570_{nm} for CV. Each bar represents the average of data obtained from four technical repeats of three independent experiments. The mean fluorescence /absorbance values are presented in a heatmap. Error bars represent the standard error of the mean. Data distributions were assessed using Shapiro-Wilk normality test and then analysed by ANOVA with Dunnett's tests to determine the P-value for multiple comparisons of normally distributed data, unless the data of DARA for AlamarBlue™ which analysed by Kruskal-Wallis with Dunn's tests for multiple comparisons of non-normally distributed data. * Indicates statistically significant differences (****p< 0.0001). Data without asterisk indicates; no statistically significant differences were observed.

In summary, among the mono-species biofilms tested, *C. albicans* was highly susceptible to all three compounds (KHS, DARA, and POLY), with POLY showing the broadest and most potent anti-biofilm activity, significantly reducing both metabolic activity and biomass even at lower concentrations. DARA and KHS also exhibited strong, concentration-dependent effects, but their impact was more pronounced at higher doses. In contrast, *P. aeruginosa* biofilms displayed substantial intrinsic tolerance, with none of the compounds achieving significant reductions in metabolic activity or biomass at any tested concentration. For *S. aureus* (Newman and SH1000) biofilms, KHS and DARA showed moderate to strong effects on metabolic activity at higher concentrations, particularly for SH1000, while POLY had minimal impact on either metabolic activity or biomass in both

strains. Overall, POLY was the most effective against *C. albicans* biofilms, while none of the compounds demonstrated notable efficacy against *P. aeruginosa* biofilms, and only KHS and DARA showed appreciable anti-biofilm activity against *S. aureus* strains at elevated concentrations.

4.2.2.5 Triadic biofilm model (Newman)

To evaluate antimicrobial efficacy in clinically relevant polymicrobial infections, a triadic biofilm model combining *C. albicans* SC5314, *S. aureus* Newman, and *P. aeruginosa* PA14 was developed. Biofilms were grown for 24 h in a 1:1 LB-RPMI medium within 96-well flat-bottom plates to mimic wound infection conditions. After maturation, KHS, DARA, and POLY were applied at concentrations spanning 2–64 µg/mL for 24 h. Post-treatment, biofilm metabolic activity (via AlamarBlue™ metabolic assay) and structural integrity (via crystal violet staining) were measured using established protocols (sections 2.4.7 and 2.4.8) to assess compound effectiveness against complex microbial communities. As shown in (Figure 4.8A and Figure 4.8D), KHS demonstrated limited effects on biofilm metabolic activity, with significant reduction observed only at the highest concentration. At 64 µg/mL, KHS significantly reduced metabolic activity to 62.17% (*$p < 0.05$) compared to UT controls. Lower concentrations showed modest, concentration-dependent reductions that did not achieve statistical significance: 32 µg/mL (85.09%), 16 µg/mL (93.80%), 8 µg/mL (94.70%), 4 µg/mL (97.92%), and 2 µg/mL (97.15%). Regarding biofilm biomass quantification (Figure 4.8A and Figure 4.8E), KHS showed minimal impact across all tested concentrations.

The second Tocriscreen™ candidate tested was DARA. As shown in (Figure 4.8B and Figure 4.8D), DARA demonstrated significant concentration-dependent effects on biofilm viability at higher concentrations. The three highest concentrations exhibited substantial reductions in metabolic activity: 64 µg/mL reduced metabolic activity to 48.50% (****$p < 0.0001$), 32 µg/mL to 48.66% (****$p < 0.0001$), and 16 µg/mL to 71.79% (***$p < 0.001$) compared to UT controls. Lower concentrations showed modest reductions in metabolic activity, though these reductions did not achieve statistical significance: 8 µg/mL (91.78%), 4 µg/mL (92.35%), and 2 µg/mL (94.40%). Regarding biofilm biomass quantification (Figure 4.8B and Figure 4.8E), DARA demonstrated a concentration-dependent trend in

biomass reduction, though these effects did not achieve statistical significance. Progressive reductions in biomass were observed at decreasing concentrations: 64 µg/mL (71.98%), 32 µg/mL (79.61%), 16 µg/mL (85.69%), 8 µg/mL (92.33%), and 4 µg/mL (96.81%). The lowest concentration (2 µg/mL) showed no appreciable effect on biofilm biomass.

Finally the efficacy of POLY against the triadic Newman polymicrobial biofilm model was evaluated through analysis of both metabolic activity and biomass parameters. As shown in (Figure 4.8C and Figure 4.8D), POLY demonstrated concentration-dependent effects on biofilm characteristics. At the highest concentration (64 µg/mL), POLY significantly reduced biofilm metabolic activity to 65.71% (**p< 0.01) compared to UT controls. Lower concentrations showed modest reductions in metabolic activity, though these reductions did not achieve statistical significance: 32 µg/mL (89.14%), 16 µg/mL (92.18%), 8 µg/mL (95.52%), 4 µg/mL (92.73%), and 2 µg/mL (94.60%). Regarding biofilm biomass quantification (Figure 4.8C and Figure 4.8E), POLY exhibited a concentration-dependent trend in biomass reduction, though these effects did not achieve statistical significance. Progressive reductions in biomass were observed with decreasing concentrations: 64 µg/mL (70.99%), 32 µg/mL (72.45%), 16 µg/mL (75.18%), 8 µg/mL (79.97%), and 4 µg/mL (90.47%). The lowest concentration (2 µg/mL) showed no appreciable effect on biofilm biomass. Taken together, results from this section highlights that Tocriscreen™ drugs may be suitable candidates against some of the mono-species biofilms, their efficacy against complex biofilms containing different microorganisms are limited.

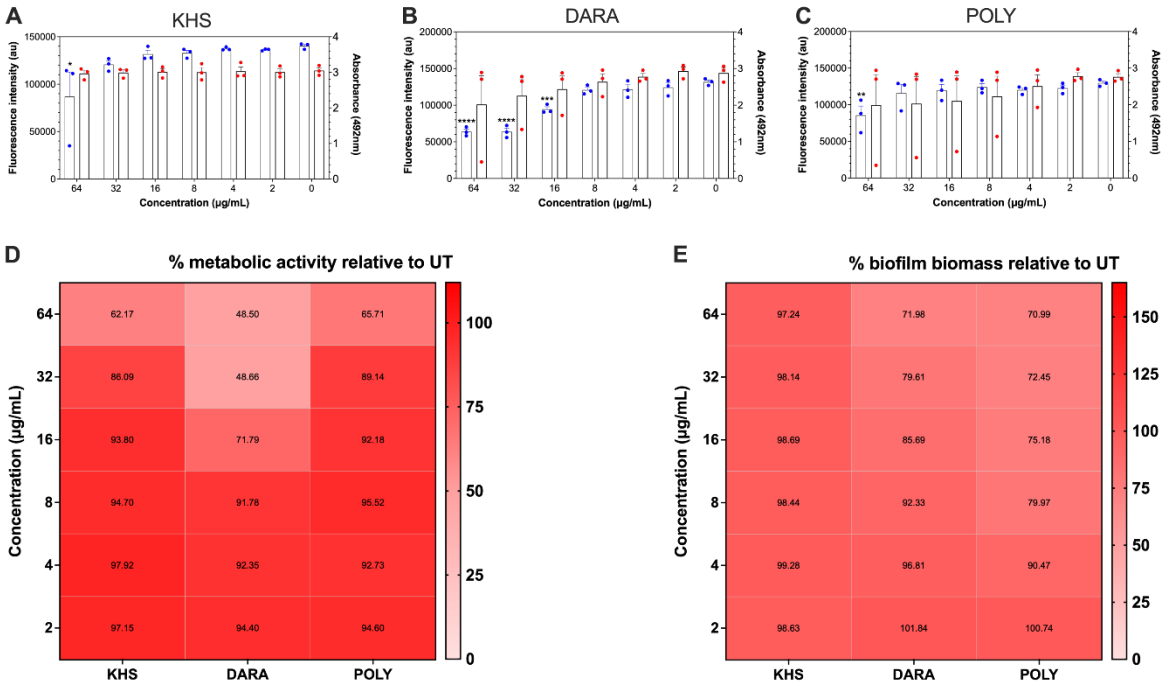

Figure 4.8: Metabolic activity and biofilm biomass of the triadic biofilms model (Newman) in relation to UT controls after 24 h treatment with three compounds from Tocriscreen™. The triadic polymicrobial biofilm model (Newman) consisting of: *C. albicans* SC5314, *S. aureus* Newman and *P. aeruginosa* PA14 biofilms were grown on 96 well flat bottom for 24 h in 1:1 v/v mixture of (LB:RPMI) broth, then treated with KHS (A), DARA (B) and POLY (C) for 24 h separately. Metabolic activity and biofilm biomass were assessed by AlamarBlue™ assay (Left Y axis/ Blue dots) and crystal violet stain (Right Y axis/ Red dots) respectively. (D & E) heatmap shown percentages of metabolic activity and biofilm biomass of triadic biofilm model (Newman) after treatment by KHS, DARA and POLY. AlamarBlue™ assay (fluorescence excitation wavelength, 544_{nm}; fluorescence emission wavelength, 590_{nm}), OD was measured at 570_{nm} for CV. Each bar represents the average of data obtained from four technical repeats of three independent experiments. The mean fluorescence /absorbance values are presented in a heatmap. Error bars represent the standard error of the mean. Data distributions were assessed using Shapiro-Wilk normality test and then analysed by ANOVA with Dunnett's tests to determine the P-value for multiple comparisons of normally distributed data, unless the data of KHS for crystal violet which analysed by Kruskal-Wallis with Dunn's tests for multiple comparisons of non-normally distributed data. * Indicates statistically significant differences (*p< 0.05, **p< 0.01, ***p< 0.001, ****p< 0.0001). Data without asterisk indicates; no statistically significant differences were observed.

4.2.2.6 Triadic biofilm model (SH1000)

The antimicrobial effectiveness of KHS, DARA and POLY was investigated using a three-species polymicrobial biofilm model consisting of *C. albicans* SC5314, *S. aureus* SH1000, and *P. aeruginosa* PA14. Biofilms were first established by co-culturing these organisms for 24 h in a mixed LB:RPMI medium on 96-well flat-bottom plates. After maturation, the biofilms were treated with a range of compound concentrations for an additional 24 h to assess their impact on biofilm metabolic activity and biomass. As shown in (Figure **4.9**A and Figure **4.9**D), KHS demonstrated significant concentration-dependent effects at higher

concentrations on biofilm metabolic activity. At 64 µg/mL, KHS significantly reduced metabolic activity to 25.71% (****p< 0.0001), while 32 µg/mL decreased metabolic activity to 75.88% (*p< 0.05) compared to UT controls. Lower concentrations showed modest reductions in metabolic activity, though these reductions did not achieve statistical significance: 16 µg/mL (86.19%), 8 µg/mL (91.10%), 4 µg/mL (93.73%), and 2 µg/mL (90.77%). Regarding biofilm biomass quantification (Figure **4.9**A and Figure **4.9**E), KHS demonstrated significant reduction only at the highest concentration, where 64 µg/mL reduced biomass to 83.24% (*p< 0.05) compared to UT controls. Lower concentrations showed modest reductions in biomass, though these reductions did not achieve statistical significance: 32 µg/mL (88.55%), 16 µg/mL (92.75%), 8 µg/mL (90.88%), 4 µg/mL (90.63%), and 2 µg/mL (89.33%).

The second compound from the Tocriscreen™ library evaluated was DARA. As shown in (Figure **4.9**B and Figure **4.9**D), DARA demonstrated significant concentration-dependent effects on biofilm metabolic activity across multiple concentrations. The four highest concentrations exhibited substantial reductions in metabolic activity: 64 µg/mL reduced viability to 50.82% (****p< 0.0001), 32 µg/mL to 64.77% (***p< 0.001), 16 µg/mL to 77.83% (*p< 0.05), and 8 µg/mL to 77.76% (*p< 0.05) compared to UT controls. Lower concentrations showed modest, non-significant reductions in metabolic activity: 4 µg/mL (91.02%) and 2 µg/mL (89.23%). Regarding biofilm biomass quantification (Figure **4.9**B and Figure **4.9**E), DARA demonstrated significant reductions at higher concentrations: 64 µg/mL reduced biomass to 69.14% (**p< 0.01) and 32 µg/mL to 70.05% (*p< 0.05) compared to UT controls. Lower concentrations showed progressive reductions in biomass, though these reductions did not achieve statistical significance: 16 µg/mL (78.23%), 8 µg/mL (85.05%), 4 µg/mL (86.49%), and 2 µg/mL (90.34%).

Finaly, the effectiveness of POLY against the three-species SH1000 polymicrobial biofilm was determined by evaluating both biofilm metabolic activity and total biomass. As shown in (Figure **4.9**C and Figure **4.9**D), POLY demonstrated concentration-dependent effects on biofilm characteristics. At the highest concentration (64 µg/mL), POLY significantly reduced biofilm metabolic activity to 54.46% (**p< 0.01) compared to UT controls. Lower concentrations showed

modest, non-significant reductions in metabolic activity: 32 µg/mL (83.29%), 16 µg/mL (83.19%), 8 µg/mL (84.31%), 4 µg/mL (90.33%), and 2 µg/mL (93.31%). Regarding biofilm biomass quantification (Figure **4.9**C and Figure **4.9**E), POLY exhibited significant reductions at two concentrations: 64 µg/mL reduced biomass to 69.62% (**p< 0.01) and 16 µg/mL to 76.08% (*p< 0.05) compared to UT controls. The remaining concentrations showed moderate reductions in biomass, though these reductions did not achieve statistical significance: 32 µg/mL (85.99%), 8 µg/mL (87.75%), 4 µg/mL (86.54%), and 2 µg/mL (90.30%). In summary, similar trends were observed in the polymicrobial community which displayed greater resilience compared to mono-species biofilms.

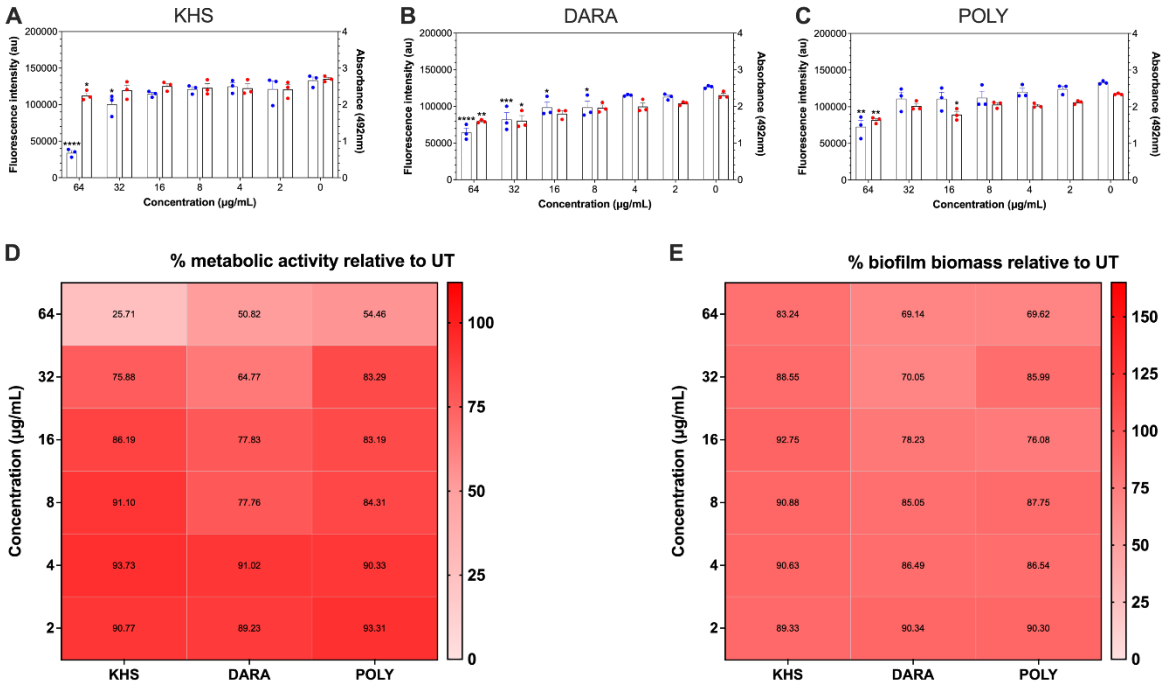

Figure 4.9: **Metabolic activity and biofilm biomass of the triadic biofilms model (SH1000) in relation to UT controls after 24 h treatment with three compounds from Tocriscreen™.** The triadic polymicrobial biofilm model (SH1000) consisting of: *C. albicans* SC5314, *S. aureus* SH1000 and *P. aeruginosa* PA14 biofilms were grown on 96 well flat bottom for 24 h in 1:1 v/v mixture of (LB:RPMI) broth, then treated with KHS (A), DARA (B) and POLY (C) for 24 h separately. Metabolic activity and biofilm biomass were assessed by AlamarBlue™ assay (Left Y axis/ Blue dots) and crystal violet stain (Right Y axis/ Red dots) respectively. (D & E) heatmap shown percentages metabolic activity and biofilm biomass of triadic biofilm model (SH1000) after treatment by KHS, DARA and POLY. AlamarBlue™ assay (fluorescence excitation wavelength, 544_{nm}; fluorescence emission wavelength, 590_{nm}), OD was measured at 570_{nm} for CV. Each bar represents the average of data obtained from four technical repeats of three independent experiments. The mean fluorescence /absorbance values are presented in a heatmap. Error bars represent the standard error of the mean. Data distributions were assessed using Shapiro-Wilk normality test and then analysed by ANOVA with Dunnett's tests to determine the P-value for multiple comparisons of normally distributed data, unless the data of DARA and POLY for crystal violet, and POLY for AlamarBlue™ which analysed by Kruskal-Wallis with Dunn's tests for multiple comparisons of non-normally distributed data. * Indicates statistically significant differences (*p< 0.05, **p< 0.01, ***p< 0.001, ****p< 0.0001). Data without asterisk indicates; no statistically significant differences were observed.

In summary, the triadic biofilm models (Newman and SH1000) demonstrated variable antimicrobial efficacy for KHS, DARA and POLY, with higher concentrations showing partial success. While DARA exhibited the most consistent concentration-dependent reductions in metabolic activity, SH1000 triadic biofilms displayed greater resilience, requiring higher doses for comparable effects. POLY showed limited activity, and KHS efficacy was strain-specific, highlighting the challenges of targeting polymicrobial communities compared to mono-species biofilms.

4.2.3 Assessment of single and dual therapy against different mono- and triadic-species biofilm models

The purpose of the proceeding sections is to assess the efficacy of one of the Tocriscreen™ compounds alongside CAP, used a treatment duration optimised in the previous chapter. Two commonly used antiseptics will be used as comparators alongside the KHS compound, which exhibited activity against the two *S. aureus* strains which displayed tolerance to CAP therapy (chapter 3). The efficacy of sequential antimicrobial dual treatments was evaluated against both mono-species and triadic-species biofilm models developed within a cellulose matrix-hydrogel system over 24-h as previously described in section 2.2.1.

Briefly, following biofilm formation, matrices underwent an initial phosphate-buffered saline (PBS) washing step to remove non-adherent microorganisms. The matrices were then subjected to one of three chemical treatments: 3% hydrogen peroxide (H_2O_2), 10% povidone-iodine (PVP-I), or 32 µg/mL KHS, with each treatment applied as a 500 µL volume for 5 minutes at room temperature. Post-chemical treatment, 500 µL of Dey-Engley neutralising broth was introduced and incubated aerobically for 15 minutes at 37°C to deactivate the antimicrobial agents. To ensure experimental validity, UT control samples also underwent neutralisation, confirming that observed effects were attributable solely to the treatments rather than the neutralising agent (data not shown). Following neutralisation, matrices were washed with 500 µL PBS prior to DNA extraction and live/dead qPCR analysis as previously described in 2.4.1, 2.4.2 and 2.4.3.

For dual therapy evaluation, matrices underwent the same initial chemical treatment protocol, followed by an additional 5-minute exposure to CAP. After the sequential treatment, samples were processed for DNA extraction and live/dead qPCR quantification following established protocols.

4.2.3.1 Assessment of single and dual therapy against *S. aureus* Newman in mono-species and triadic biofilms

The molecular analysis of *S. aureus* Newman mono-species biofilms, as illustrated in (Figure **4.10**A and Figure **4.10**C), revealed varying degrees of antimicrobial efficacy across different treatment modalities. The evaluation of total and viable cell counts demonstrated that dual therapy combinations consistently outperformed monotherapies in reducing bacterial populations. In terms of KHS alone, monotherapy resulted in a modest 0.1-$\log_{10}$ reduction on total cell counts (from 2.59×10^7 to 1.96×10^7 CFE/mL), indicating limited effectiveness, suggestive that the substrata used for biofilm formation can influence treatment efficacy (Townsend et al., 2016). However, when combined with CAP, the efficacy was significantly enhanced, achieving a notable 1.0-$\log_{10}$ reduction (**$p< 0.01$), reducing total cell counts to 2.56×10^6 CFE/mL. This highlights the superior performance of the KHS+CAP combination compared to KHS alone. For H_2O_2, monotherapy produced a moderate reduction in total cell counts, with a 0.4-$\log_{10}$ decrease (from 2.59×10^7 to 1.08×10^7 CFE/mL). In contrast, the H_2O_2+CAP combination demonstrated significantly improved activity, resulting in a 1.0-$\log_{10}$ reduction (*$p< 0.05$), lowering total cell counts to 2.59×10^6 CFE/mL. This underscores the enhanced antimicrobial effect of H_2O_2 when combined with CAP. In the case of PVP-I, monotherapy showed a more substantial reduction in total cell counts, achieving a 0.7-$\log_{10}$ decrease (from 2.59×10^7 to 5.25×10^6 CFE/mL). However, the PVP-I+CAP combination achieved a slightly better reduction with a non-significant 0.8-$\log_{10}$ decrease (to 4.55×10^6 CFE/mL), indicating that while the combination therapy was more effective than PVP-I alone, it did not reach statistical significance. In terms of CAP alone, it demonstrated minimal impact on total cell counts, achieving only a modest and non-significant 0.1-$\log_{10}$ reduction (from 2.59×10^7 to 1.97×10^7 CFE/mL).

When assessing viable cell counts, dual therapy combinations consistently exhibited superior antimicrobial activity compared to their respective monotherapies. The KHS+CAP combination demonstrated the most pronounced effect, achieving an impressive 3.8-log_{10} reduction (****p< 0.0001), reducing viable cells from 1.31 × 10^7 to 1.90 × 10^3 CFE/mL, far surpassing KHS monotherapy's modest and non-significant reduction of just 0.5-log_{10} (to 4.66 × 10^6 CFE/mL). Similarly, the H_2O_2+CAP combination exhibited significant antimicrobial efficacy with a 1.7-log_{10} reduction (**p< 0.01), reducing viable cells to 1.16 × 10^5 CFE/mL, whereas H_2O_2 alone achieved only a moderate and non-significant 1.4-log_{10} reduction (to 4.76 × 10^5 CFE/mL). For PVP-I, the combination with CAP led to a significant 2-log_{10} reduction (**p< 0.01), bringing viable counts down to 1.44 × 10^5 CFE/mL, whereas PVP-I alone also demonstrated notable efficacy with a 1.4-log_{10} reduction (to 4.69 × 10^5 CFE/mL). Interestingly, while CAP alone achieved only a modest impact on total cell counts, it showed relatively better performance in reducing viable cells, achieving a non-significant 0.3-log_{10} reduction (to 6.17 × 10^6 CFE/mL). These findings highlight that while monotherapies provide some level of antimicrobial activity, dual therapies—particularly those involving CAP—consistently demonstrate superior efficacy across all treatment strategies for both total and viable cell reductions in *S. aureus* Newman biofilms. In particular, KHS in combination with CAP was the most effective dual intervention.

The analysis of *S. aureus* Newman within triadic biofilm models revealed complex responses to various treatment modalities, as illustrated in (Figure **4.10**B and Figure **4.10**C). The quantification of total and viable CFEs/mL demonstrated varying effects among single and dual therapies when compared to untreated controls in a similar manner to mono-species biofilms. In terms of KHS, monotherapy resulted in an unexpected increase in total cell counts, showing a negative 0.4-log_{10} reduction (increase from 3.51 × 10^6 to 8.66 × 10^6 CFE/mL). Similarly, PVP-I monotherapy also led to a comparable increase in bacterial populations, with a negative 0.4-log_{10} reduction (increase to 8.35 × 10^6 CFE/mL). H_2O_2 treatment followed the same trend, producing a negative 0.1-log_{10} reduction (increase to 4.54 × 10^6 CFE/mL), while CAP alone showed a minimal increase in total cell counts with a negative 3.6 x 10^{-3}-log_{10} reduction (increase to 3.54 × 10^6 CFE/mL). In contrast, the combination therapies demonstrated more promising

results in reducing total cell counts. The KHS+CAP combination exhibited the most substantial effect, achieving a notable 0.8-log_{10} reduction (from 3.51×10^6 to 5.56×10^5 CFE/mL), outperforming all other treatments. The PVP-I+CAP combination produced a modest 0.1-log_{10} reduction (to 2.70×10^6 CFE/mL), and this reduction did not reach statistical significance. Interestingly, the H_2O_2+CAP combination showed a slight increase in total cell counts, with a negative 4.7×10^{-2}-log_{10} reduction (increase to 3.91×10^6 CFE/mL), indicating limited efficacy in this context.

When examining viable cell counts, dual therapy approaches consistently demonstrated superior antimicrobial efficacy compared to their single-agent counterparts. The KHS+CAP combination was particularly effective, achieving a significant 3.0-log_{10} reduction (****$p < 0.0001$), reducing viable cells from 1.74×10^6 in the control group to 1.58×10^3 CFE/mL post-treatment, marking the most profound reduction observed across all treatments. Similarly, the PVP-I+CAP combination exhibited significant antimicrobial activity, resulting in a 1.2-log_{10} reduction (**$p < 0.01$) and lowering viable cell counts to 1.12×10^5 CFE/mL. The combination of H_2O_2+CAP also demonstrated notable efficacy with a significant 1.4-log_{10} reduction (***$p < 0.001$), reducing viable cells to 6.82×10^4 CFE/mL. In contrast, monotherapy treatments showed more modest effects on bacterial viability and did not achieve statistical significance in most cases. CAP alone resulted in a modest 0.2-log_{10} reduction, decreasing viable cells to 1.18×10^6 CFE/mL, while KHS monotherapy led to a slight increase in bacterial counts with a negative 3×10^{-2}-log_{10} reduction, increasing to 1.87×10^6 CFE/mL. Both chemical agents performed moderately well as monotherapies but did not reach statistical significance: PVP-I resulted in a 0.6-log_{10} reduction, lowering viable cells to 4.82×10^5 CFE/mL, while H_2O_2 monotherapy achieved a similar effect with a 0.7-log_{10} reduction, reducing viable counts to 3.11×10^5 CFE/mL. These findings highlight that while monotherapies provide some level of antimicrobial activity, dual therapies—particularly those involving CAP—consistently demonstrate superior efficacy across all treatment strategies for both total and viable cell reductions in *S. aureus* Newman biofilms within triadic models.

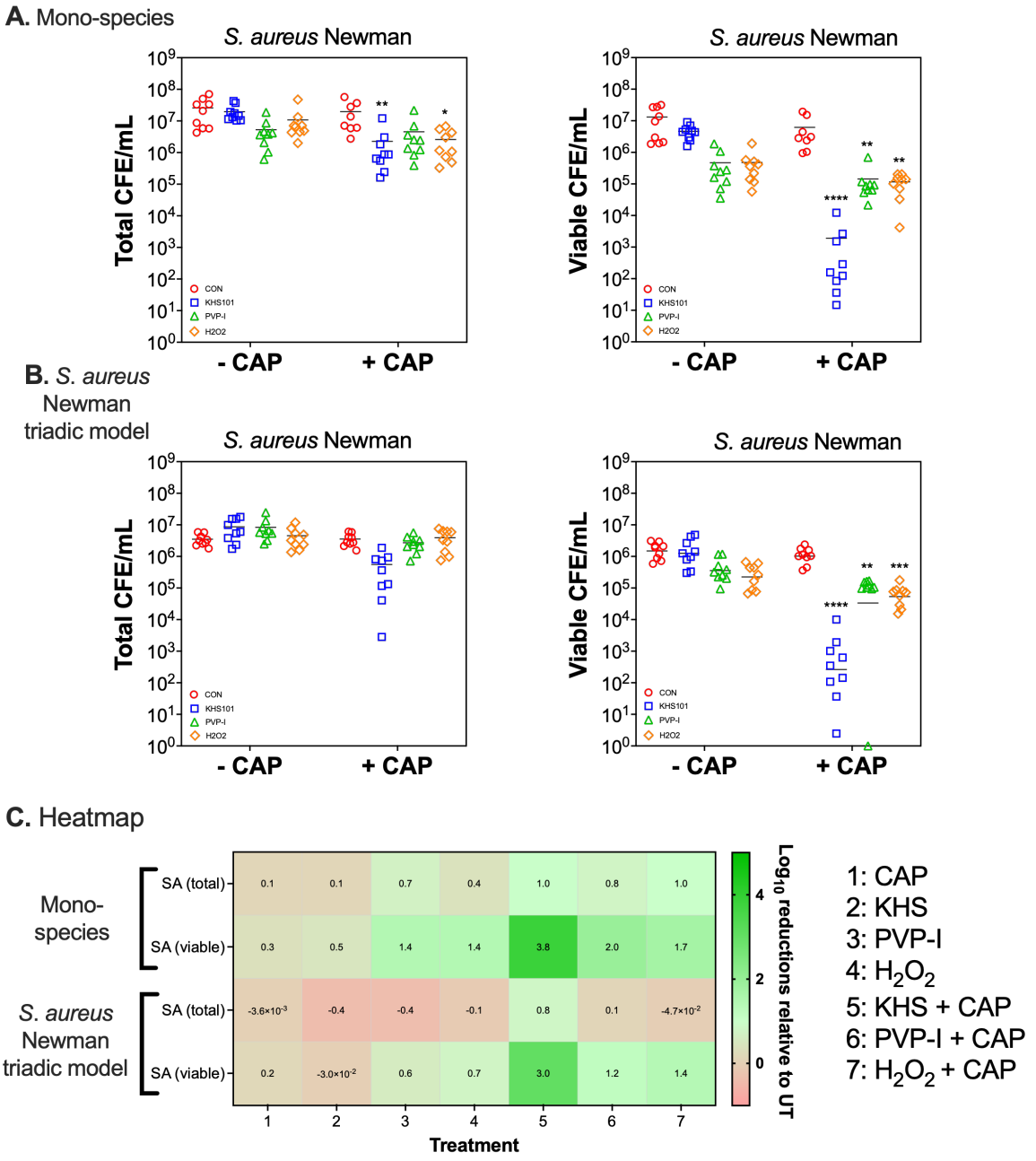

Figure 4.10**: Molecular analysis of *S. aureus* Newman mono-species and in triadic biofilm model following 5 minutes treatment by KHS, PVP-I and H_2O_2, and additional 5 min therapy within CAP (Dual therapy).** Panel (A) shows *S. aureus* Newman biofilms were formed for 24 h within the cellulose matrix-hydrogel system then treated with KHS (32 **µg/mL)**, PVP-I (10%) and H_2O_2 (3%) for 5 min alone, and additional 5 min therapy by CAP after the neutralisation by Dey-Engley broth for 15 min incubation at 37 °C. Panel (B) shows the triadic polymicrobial biofilm model of *C. albicans* SC5314, *S. aureus* Newman and *P. aeruginosa* PA14 biofilms were formed as above described and followed by similar therapy's. Panel (C) shows **log_{10}** reductions of total and viable cell count in a heatmap of *S. aureus* Newman when grown as mono-species biofilms, or in the triadic biofilm model. Total and viable colony forming equivalents/mL (CFE/mL) was quantified for each biofilm following treatment using live/dead qPCR. Results representative of mean values from n =9 (three technical replicates from three biological experimental repeats). (- CAP) means: single therapy, (+ CAP) means: dual therapy, (CON) means: control, (1): CAP, (2): KHS, (3): PVP-I, (4): H_2O_2, (5): KHS + CAP, (6): PVP-I + CAP, (7): H_2O_2 + CAP. Data distributions were assessed using D'Agostino-Pearson omnibus normality test, and then analysed by Kruskal-Wallis with Dunn's tests to determine the P-value for multiple comparisons of non-normally distributed data. * Indicates statistically significant differences (*p< 0.05, **p< 0.01, ***p< 0.001, ****p< 0.0001). Data without asterisk indicates; no statistically significant differences were observed.

4.2.3.2 Assessment of single and dual therapy against *S. aureus* SH1000 in mono-species and triadic biofilms

The analysis of *S. aureus* SH1000 mono-species and as triadic biofilms were next assessed (Figure 4.11A and Figure 4.11C). In terms of total cell populations, similar to Newman mono-species biofilms, KHS monotherapy achieved a modest 0.6-log_{10} reduction (from 4.54 x 10^7 to 1.21 x 10^7 CFE/mL). However, when combined with CAP, the efficacy was significantly enhanced, resulting in a 1.4-log_{10} reduction (****p< 0.0001) to 1.84 x10^6 CFE/mL. This demonstrates the superior performance of the KHS+CAP combination compared to KHS alone. For PVP-I, both monotherapy and combination treatments showed significant efficacy. PVP-I alone achieved a significant 1.3-log_{10} reduction (****p< 0.0001, to 7.26 x 10^6 CFE/mL), while the PVP-I+CAP combination demonstrated slightly enhanced activity with a significant 1.4-log_{10} reduction (****p< 0.0001, to 1.87 x 10^6 CFE/mL). Interestingly, H_2O_2 monotherapy and its combination with CAP showed equivalent efficacy, both achieving a 0.8-log_{10} reduction (to 7.26 x 10^6 and 6.55 x 10^6 CFE/mL, respectively), suggesting no additional benefit from the combination approach. CAP alone showed minimal impact with a 0.3-log_{10} reduction (to 2.12 x 10^7 CFE/mL).

The impact on bacterial viability revealed more pronounced differences between treatment modalities. The KHS+CAP combination demonstrated significant efficacy with a 2.9-log_{10} reduction (****p< 0.0001) from 1.95 x 10^7 to 2.62 x 10^4 CFE/mL, outperforming KHS monotherapy's modest 1.1-log_{10} reduction (to 1.41 x 10^6 CFE/mL). The H_2O_2+CAP combination exhibited the most substantial effect, achieving a significant 3.0-log_{10} reduction (****p< 0.0001, to 1.89 x 10^4 CFE/mL), surpassing H_2O_2 monotherapy's significant but lesser 2.2-log_{10} reduction (*p< 0.05, to 1.32 x 10^5 CFE/mL). Similarly, the PVP-I+CAP combination showed enhanced activity with a significant 2.9-log_{10} reduction (****p< 0.0001, to 2.32 x 10^4 CFE/mL), improving upon PVP-I monotherapy's significant 2.4-log_{10} reduction (***p< 0.001, to 7.14 x 0^4 CFE/mL). CAP monotherapy demonstrated minimal impact on bacterial viability, achieving only a 0.7-log_{10} reduction (to 3.57 x 10^6 CFE/mL). These findings highlight that while some monotherapies showed significant antimicrobial activity, combination therapies generally demonstrated superior efficacy in reducing both total and viable bacterial populations.

A comprehensive analysis of *S. aureus* SH1000 in triadic biofilm models, as illustrated in (Figure 4.11B and Figure 4.11C), revealed distinct patterns of antimicrobial efficacy between monotherapy and combination treatments. The evaluation encompassed both total and viable cell populations, demonstrating varying degrees of effectiveness across different therapeutic strategies. In terms of total cell populations, the KHS+CAP combination exhibited superior antimicrobial activity, achieving a significant 1.7-$\log_{10}$ reduction (****$p < 0.0001$) from 9.37 x 10^7 to 1.69 x 10^6 CFE/mL, markedly outperforming KHS monotherapy which yielded a non-significant 0.6-$\log_{10}$ reduction (to 2.48 x 10^7 CFE/mL). This highlights the enhanced efficacy achieved through the combination approach. Similarly, the H_2O_2+CAP combination demonstrated improved activity with a significant 1.2-$\log_{10}$ reduction (****$p < 0.0001$, to 5.54 x 10^6 CFE/mL) compared to H_2O_2 alone, which achieved a modest 0.5-$\log_{10}$ reduction (to 3.28 x 10^7 CFE/mL). The PVP-I+CAP combination also showed enhanced effectiveness with a significant 0.7-$\log_{10}$ reduction (*$p < 0.05$, to 1.84 x 10^7 CFE/mL) versus PVP-I monotherapy's minimal 0.4-$\log_{10}$ reduction (to 3.69 x 10^7 CFE/mL).

The impact on bacterial viability revealed even more pronounced differences. The KHS+CAP combination demonstrated significant efficacy with 2.8-$\log_{10}$ reduction (****$p < 0.0001$) from 1.23 x 10^7 to 2.06 x 10^4 CFE/mL, substantially surpassing KHS monotherapy's modest 0.8-$\log_{10}$ reduction (to 1.84 x 10^6 CFE/mL). The H_2O_2+CAP combination exhibited the most potent effect, achieving a significant 2.9-$\log_{10}$ reduction (****$p < 0.0001$, to 1.40 x 10^4 CFE/mL), enhancing the already substantial effect of H_2O_2 monotherapy, which demonstrated a significant 1.9-$\log_{10}$ reduction (**$p < 0.01$, to 1.44 x 10^5 CFE/mL). For PVP-I, the combination with CAP led to a significant 1.5-$\log_{10}$ reduction (**$p < 0.01$, to 4.18 x 10^5 CFE/mL), showing improved efficacy compared to PVP-I alone, which achieved a non-significant 0.7-$\log_{10}$ reduction (to 2.22 x 10^6 CFE/mL). CAP monotherapy showed modest impact on both total and viable cell counts, achieving 0.6-$\log_{10}$ and 0.7-$\log_{10}$ reductions, respectively. These findings underscore that while some monotherapies demonstrated notable antimicrobial activity, combination therapies consistently showed superior efficacy in reducing both total and viable bacterial populations in *S. aureus* SH1000 triadic biofilm models.

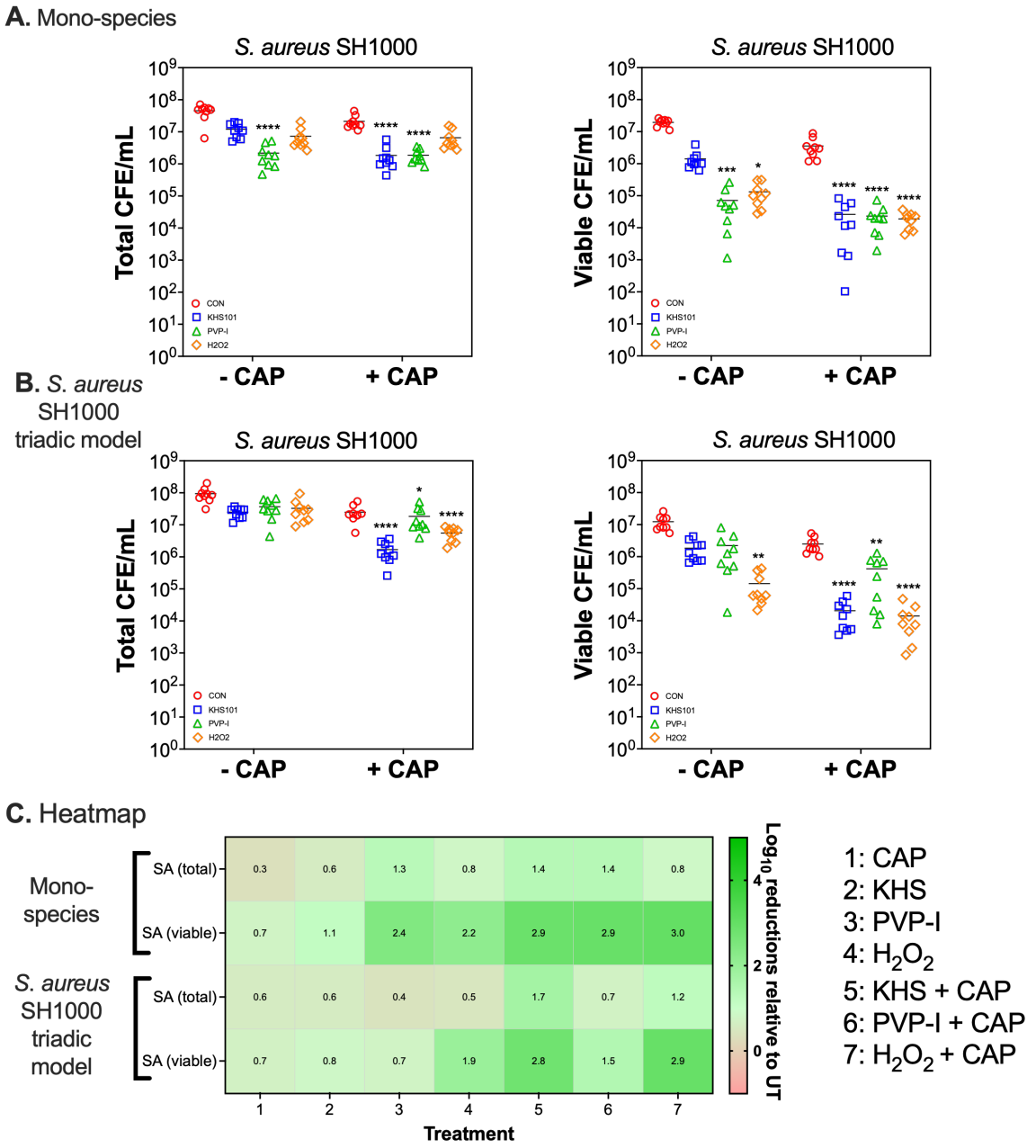

Figure 4.11: Molecular analysis of *S. aureus* SH1000 mono-species and triadic biofilm model following 5 minutes treatment by KHS, PVP-I and H_2O_2, and additional 5 min therapy within CAP (Dual therapy). Panel (A) shows *S. aureus* SH1000 biofilms were formed for 24 h within the cellulose matrix-hydrogel system then treated with KHS (32 **µg/mL)**, PVP-I (10%) and H_2O_2 (3%) for 5 min alone, and additional 5 min therapy by CAP after the neutralisation by Dey-Engley broth for 15 min incubation at 37 °C. Panel (B) shows the triadic polymicrobial biofilm model of *C. albicans* SC5314, *S. aureus* SH1000 and *P. aeruginosa* PA14 biofilms were formed as above described and followed by similar therapy's. Panel (C) shows **log_{10}** reductions of total and viable cell count in a heatmap of *S. aureus* SH1000 when grown as mono-species biofilms, or for the triadic biofilm model. Total and viable CFE/mL was quantified for each biofilm following treatment using live/dead qPCR. Results representative of mean values from n =9 (three technical replicates from three biological experimental repeats). (- CAP) means: single therapy, (+ CAP) means: dual therapy, (CON) means: control, (1): CAP, (2): KHS, (3): PVP-I, (4): H_2O_2, (5): KHS + CAP, (6): PVP-I + CAP, (7): H_2O_2 + CAP. Data distributions were assessed using D'Agostino-Pearson omnibus normality test, and then analysed by Kruskal-Wallis with Dunn's tests to determine the P-value for multiple comparisons of non-normally distributed data. * Indicates statistically significant differences (*p< 0.05, **p< 0.01, ***p< 0.001, ****p< 0.0001). Data without asterisk indicates; no statistically significant differences were observed.

4.2.3.3 Assessment of single and dual therapy against *C. albicans* SC5314 mono-species and triadic biofilms

A detailed assessment of *C. albicans* SC5314 mono-species biofilms (Figure 4.12A and Figure 4.12D) highlighted clear differences in antimicrobial effectiveness between single-agent and combination therapies. Analysis of both total and viable cell counts revealed that the degree of biofilm reduction varied depending on the treatment strategy employed. In terms of total cell populations, the KHS+CAP combination exhibited significant antimicrobial activity, achieving 3.4-$\log_{10}$ reduction (****$p < 0.0001$) from 2.05 x 10^7 to 8.92 x 10^3 CFE/mL, markedly outperforming KHS monotherapy which yielded a non-significant 2.0-$\log_{10}$ reduction (to 1.86 x 10^5 CFE/mL). This highlights the superior performance of the combination approach. Similarly, the H_2O_2+CAP combination demonstrated enhanced efficacy with a significant 2.5-$\log_{10}$ reduction (***$p < 0.001$, to 7.00 x 10^4 CFE/mL) compared to H_2O_2 alone, which achieved a non-significant 2.3-$\log_{10}$ reduction (to 9.89 x 10^4 CFE/mL). Interestingly, the PVP-I+CAP combination showed slightly lower efficacy with a 2.0-$\log_{10}$ reduction (**$p < 0.01$, to 1.89 x 10^5 CFE/mL) compared to PVP-I monotherapy, which achieved a significant 2.2-$\log_{10}$ reduction (*$p < 0.05$, to 1.28 x 10^5 CFE/mL). CAP monotherapy demonstrated minimal impact with only a 0.4-$\log_{10}$ reduction (to 9.04 x 10^6 CFE/mL), underscoring the enhanced antimicrobial efficacy achieved through combination approaches.

The differences in fungal viability between treatment groups were even more striking. The KHS+CAP combination exhibited significant efficacy with 4.4-$\log_{10}$ reduction (****$p < 0.0001$) from 1.07 x 10^7 to 4.47 x 10^2 CFE/mL, substantially surpassing KHS monotherapy's non-significant 3.8-$\log_{10}$ reduction (to 1.58 x 10^3 CFE/mL). Both H_2O_2+CAP and PVP-I+CAP combinations demonstrated remarkable activity, achieving significant 4.3-$\log_{10}$ reductions (****$p < 0.0001$ and ***$p < 0.001$, respectively) to approximately 4.87 x 10^2 CFE/mL. H_2O_2 monotherapy showed a non-significant 3.3-$\log_{10}$ reduction (to 5.32 x 10^3 CFE/mL), while PVP-I alone achieved a significant 4.3-$\log_{10}$ reduction (****$p < 0.0001$, to 4.87 x 10^2 CFE/mL), matching the efficacy of its combination treatment. CAP monotherapy showed the least impact on viable counts with a modest 1.2-$\log_{10}$ reduction (to 7.47 x 10^5 CFE/mL). These findings underscore that while some monotherapies demonstrated

significant antimicrobial activity, combination therapies consistently showed superior or equivalent efficacy in reducing both total and viable fungal populations in *C. albicans* SC5314 mono-species biofilms.

Next, *C. albicans* SC5314 in *S. aureus* Newman triadic biofilms as illustrated in (Figure 4.12B and Figure 4.12D), displayed distinct patterns of antimicrobial efficacy between monotherapy and combination treatments. The evaluation encompassed both total and viable cell populations, demonstrating varying degrees of effectiveness across different therapeutic strategies. In terms of total cell populations, the KHS+CAP combination exhibited significant antimicrobial activity, achieving 3.4-$\log_{10}$ reduction (****$p < 0.0001$) from 3.40×10^6 to 1.37×10^3 CFE/mL, markedly outperforming KHS monotherapy which yielded a non-significant 1.3-$\log_{10}$ reduction (to 1.55×10^5 CFE/mL). This highlights the superior performance of the combination approach. Similarly, the H_2O_2+CAP combination demonstrated enhanced efficacy with a significant 1.9-$\log_{10}$ reduction (***$p < 0.001$, to 4.26×10^4 CFE/mL) compared to H_2O_2 alone, which achieved a non-significant 1.4-$\log_{10}$ reduction (to 1.24×10^5 CFE/mL). The PVP-I+CAP combination also showed improved effectiveness with a significant 1.7-$\log_{10}$ reduction (**$p < 0.01$, to 7.10×10^4 CFE/mL) versus PVP-I monotherapy's modest 1.0-$\log_{10}$ reduction (to 3.13×10^5 CFE/mL). CAP monotherapy demonstrated minimal impact with only a 0.2-$\log_{10}$ reduction (to 2.35×10^6 CFE/mL), underscoring the enhanced antimicrobial efficacy achieved through combination approaches.

The impact on fungal viability revealed even more pronounced differences. The KHS+CAP combination exhibited significant efficacy with 3.9-$\log_{10}$ reduction (****$p < 0.0001$) from 1.75×10^6 to 2.21×10^2 CFE/mL, substantially surpassing KHS monotherapy's non-significant 3.0-$\log_{10}$ reduction (to 1.92×10^3 CFE/mL). The PVP-I+CAP combination demonstrated remarkable activity, achieving a significant 3.6-$\log_{10}$ reduction (****$p < 0.0001$, to 4.20×10^2 CFE/mL), showing slightly enhanced efficacy compared to PVP-I monotherapy, which achieved a significant 3.3-$\log_{10}$ reduction (**$p < 0.01$, to 9.01×10^2 CFE/mL). Similarly, the H_2O_2+CAP combination yielded a significant 3.5-$\log_{10}$ reduction (****$p < 0.0001$, to 5.15×10^2 CFE/mL), markedly outperforming H_2O_2 monotherapy's non-significant 2.1-$\log_{10}$ reduction (to 1.47×10^4 CFE/mL). CAP monotherapy showed modest impact on

viable counts with a non-significant 1.9-log_{10} reduction (to 2.06 x 10^4 CFE/mL). These findings underscore that while some monotherapies demonstrated significant antimicrobial activity, combination therapies consistently showed superior efficacy in reducing both total and viable fungal populations in *C. albicans* SC5314 in triadic biofilms (Newman model).

Similarly, *C. albicans* SC5314 in *S. aureus* SH1000 triadic biofilms, as illustrated in (Figure 4.12C and Figure 4.12D), showed distinct patterns of antimicrobial efficacy between monotherapy and combination treatments. The evaluation encompassed both total and viable cell populations, demonstrating varying degrees of effectiveness across different therapeutic strategies. In terms of total cell populations, the KHS+CAP combination demonstrated relatively improved efficacy, achieving a 1.0-log_{10} reduction (from 9.03 x 10^4 to 8.52 x 10^3 CFE/mL), contrasting with KHS monotherapy which resulted in increased fungal populations with a negative 0.3-log_{10} reduction (increase to 2.00 x 10^5 CFE/mL). This highlights the enhanced antimicrobial effect achieved through the combination approach. Similarly, the H_2O_2+CAP combination showed modest activity with a 0.2-log_{10} reduction (to 5.51 x 10^4 CFE/mL), performing better than H_2O_2 alone, which led to increased fungal burden with a negative 0.4-log_{10} reduction (increase to 2.35 x 10^5 CFE/mL). Surprisingly, both PVP-I treatments resulted in increased fungal populations, with PVP-I monotherapy showing a more pronounced increase (negative 0.8-log_{10} reduction, increase to 6.21 x 10^5 CFE/mL) compared to the PVP-I+CAP combination (negative 0.4-log_{10} reduction, increase to 2.41 x 10^5 CFE/mL). CAP monotherapy demonstrated moderate effectiveness with a 0.5-log_{10} reduction (to 2.95 x 10^4 CFE/mL), and none of these changes reached statistical significance.

The impact on fungal viability revealed more pronounced differences. The PVP-I+CAP combination exhibited superior efficacy with a significant 1.6-log_{10} reduction (***$p < 0.001$) from 1.58 x 10^4 to 4.15 x 10^2 CFE/mL, substantially outperforming PVP-I monotherapy's modest 0.6-log_{10} reduction (to 4.10 x 10^3 CFE/mL). Similarly, the H_2O_2+CAP combination demonstrated significant effectiveness with a 1.5-log_{10} reduction (**$p = 0.0071$, to 5.52 x 10^2 CFE/mL), contrasting sharply with H_2O_2 monotherapy which resulted in increased fungal

burden (negative 0.4-$\log_{10}$ reduction, increase to 3.81 x 10^4 CFE/mL). The KHS+CAP combination achieved a significant 1.4-$\log_{10}$ reduction (*p< 0.05, to 5.98 x 10^2 CFE/mL), markedly surpassing KHS alone which produced a modest 0.4-$\log_{10}$ reduction (to 6.12 x 10^3 CFE/mL). Notably, CAP monotherapy demonstrated significant efficacy with 1.6-$\log_{10}$ reduction (***p< 0.001, to 3.73 x 10^2 CFE/mL). These findings underscore that while most monotherapies showed limited or negative effects, combination therapies—particularly those involving CAP—demonstrated significantly enhanced antimicrobial efficacy against *C. albicans* in triadic biofilm configurations (SH1000 model).

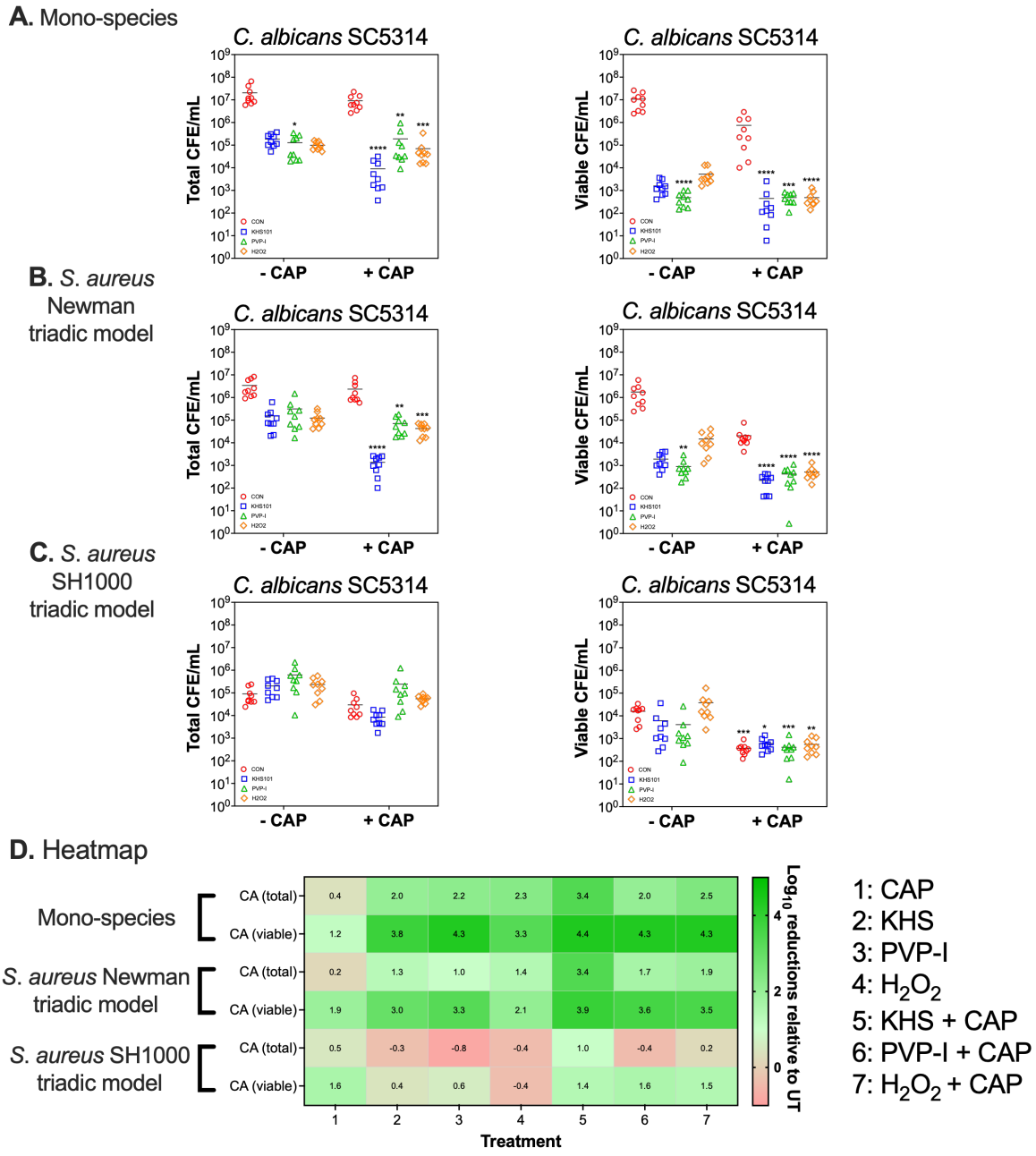

Figure 4.12: Molecular analysis of *C. albicans* SC5314 mono-species and triadic biofilm models following 5 minutes treatment by KHS, PVP-I and H_2O_2, and additional 5 min therapy within CAP (Dual therapy). Panel (A) shows *C. albicans SC5314* biofilms were formed for 24 h within the cellulose matrix-hydrogel system then treated with KHS (32 **µg/mL)**, PVP-I (10%) and H_2O_2 (3%) for 5 min alone, and additional 5 min therapy by CAP after the neutralisation by Dey-Engley broth for 15 min incubation at 37 °C. Panel (B) shows the triadic polymicrobial biofilm model of *C. albicans* SC5314, *S. aureus* Newman and *P. aeruginosa* PA14 biofilms were formed as above described and followed by similar therapy's. Panel (C) shows the triadic polymicrobial biofilm model of *C. albicans* SC5314, *S. aureus* SH1000 and *P. aeruginosa* PA14 biofilms were formed as above described and followed by similar therapies. Panel (D) shows **log_{10}** reductions of total and viable cell count in a heatmap of *C. albicans SC5314* when grown as mono-species biofilms, or for both triadic biofilm models. Total and viable CFE/mL was quantified for each biofilm following treatment using live/dead qPCR. Results representative of mean values from n =9 (three technical replicates from three biological experimental repeats). (- CAP) means: single therapy, (+ CAP) means: dual therapy, (CON) means: control, (1): CAP, (2): KHS, (3): PVP-I, (4): H_2O_2, (5): KHS + CAP, (6): PVP-I + CAP, (7): H_2O_2 + CAP. Data distributions were assessed using D'Agostino-Pearson omnibus normality test, and then analysed by Kruskal-Wallis with Dunn's tests to determine the P-value for multiple comparisons of non-normally distributed data. * Indicates statistically significant differences (*p<

0.05, **p< 0.01, ***p< 0.001, ****p< 0.0001). Data without asterisk indicates; no statistically significant differences were observed.

4.2.3.4 Assessment of single and dual therapy against *P. aeruginosa* PA14 mono-species and triadic biofilms

A comprehensive analysis of *P. aeruginosa* PA14 biofilms, as depicted in (Figure 4.13A and Figure 4.13D), revealed distinct differences in antimicrobial efficacy between monotherapy and combination treatments. The evaluation of both total and viable bacterial populations demonstrated varying levels of effectiveness across the different therapeutic strategies. In the case of KHS, monotherapy exhibited minimal impact on total cell counts, achieving only a modest 0.2-$\log_{10}$ reduction (from 2.64 x 10^7 to 1.60 x 10^7 CFE/mL). However, when combined with CAP, the efficacy was significantly enhanced, resulting in a 1.1-$\log_{10}$ reduction (****p< 0.0001), lowering the bacterial population to 2.25 x 10^6 CFE/mL. This demonstrates that the combination of KHS with CAP is substantially more effective than KHS alone. Similarly, PVP-I monotherapy also showed limited impact, with a modest 0.2-$\log_{10}$ reduction (from 2.64 x 10^7 to 1.84 x 10^7 CFE/mL). In contrast, the combination of PVP-I with CAP exhibited improved antimicrobial activity, achieving a significant 0.6-$\log_{10}$ reduction (*p< 0.05), reducing the total cell counts to 6.87 x 10^6 CFE/mL. This highlights that PVP-I's efficacy is significantly enhanced when used in conjunction with CAP. For H_2O_2, monotherapy demonstrated slightly better performance compared to KHS and PVP-I alone, achieving a 0.4-$\log_{10}$ reduction (from 2.64 x 10^7 to 1.13 x 10^7 CFE/mL). However, when combined with CAP, H_2O_2 showed significantly improved activity, resulting in a notable 0.9-$\log_{10}$ reduction (***p< 0.001), reducing the bacterial population to 3.45 x 10^6 CFE/mL. This indicates that H_2O_2's antimicrobial effect is considerably enhanced by CAP. Notably, CAP monotherapy demonstrated modest activity with a 0.3-$\log_{10}$ reduction (to 1.39 x 10^7 CFE/mL).

When evaluating viable cell counts, similar patterns were observed between monotherapy and combination treatments, with combination therapies consistently outperforming their single-agent counterparts. KHS alone resulted in a modest reduction of viable cells, achieving a non-significant 0.6-$\log_{10}$ reduction (from 1.74 x 10^7 to 3.95 x 10^6 CFE/mL). However, the combination of KHS with

CAP demonstrated a much more pronounced effect, achieving a significant 2.9-log_{10} reduction (****p< 0.0001), reducing viable counts to just 2.41 x 10^4 CFE/mL. In the case of PVP-I, monotherapy achieved a more substantial but still non-significant reduction in viable cells, with a 1.7-log_{10} reduction (to 3.10 x 10^5 CFE/mL). However, when combined with CAP, PVP-I exhibited significantly greater efficacy, resulting in a significant 2.3-log_{10} reduction (**p< 0.01), lowering viable counts to 9.49 x 10^4 CFE/mL. Similarly, H_2O_2 monotherapy was the only single-agent treatment that significantly reduced viable cell counts on its own, achieving a notable 1.9-log_{10} reduction (*p< 0.05) to 5.88 x 10^4 CFE/mL. Nevertheless, H_2O_2's efficacy was further enhanced when combined with CAP, resulting in a significant 2.5-log_{10} reduction (****p< 0.0001), reducing viable cells to just 5.88 x 10^4 CFE/mL. Interestingly, CAP monotherapy showed considerable effectiveness with a 2.1-log_{10} reduction (1.50 x 10^5 CFE/mL), and still less potent than its combination treatments. These findings highlight that while monotherapies provide some level of antimicrobial activity, combination therapies involving CAP consistently demonstrate superior efficacy across all treatment strategies for both total and viable cell reductions in *P. aeruginosa* biofilms.

Next, a detailed analysis of *P. aeruginosa* PA14 biofilms in *S. aureus* Newman triadic biofilm model, as depicted in (Figure 4.13B and Figure 4.13D), revealed distinct differences in antimicrobial efficacy between monotherapy and combination treatments. The evaluation of total bacterial populations demonstrated varying degrees of effectiveness across the different therapeutic approaches. In the case of KHS, monotherapy showed limited impact on total cell counts, achieving a modest 0.6-log_{10} reduction (from 2.10 x 10^7 to 5.45 x 10^6 CFE/mL). However, when combined with CAP, the efficacy was significantly enhanced, resulting in a 1.6-log_{10} reduction (****p< 0.0001), reducing the bacterial population to 4.74 x 10^5 CFE/mL. This highlights the superior performance of the KHS+CAP combination compared to KHS alone. For H_2O_2, monotherapy achieved a moderate reduction with a 0.5-log_{10} decrease in total cell counts (to 6.72 x 10^6 CFE/mL). In contrast, the H_2O_2+CAP combination demonstrated significantly improved efficacy, resulting in a 0.7-log_{10} reduction (**p< 0.01), lowering the bacterial population from to 4.09 x 10^6 CFE/mL. This indicates that the addition

of CAP significantly boosts the antimicrobial activity of H_2O_2. With respect to PVP-I, monotherapy had minimal effect on total cell counts, showing only a negligible reduction (2.3 x 10^{-2}-$\log_{10}$ reduction, from 2.10 x 10^7 to 1.99 x 10^7 CFE/mL). The PVP-I+CAP combination reduced total cell counts by a 0.6-$\log_{10}$ reduction (to 5.69 x 10^4 CFE/mL), this reduction did not reach statistical significance, suggesting that PVP-I benefits less from CAP compared to KHS and H_2O_2. In terms of CAP alone, it led to a decrease in total cell counts from to 1.27 × 10^7 CFE/mL (0.2-$\log_{10}$ reduction), this reduction did not achieve statistical significance.

When evaluating viable cell counts, similar trends were observed between monotherapy and combination treatments, with combination therapies consistently outperforming their single-agent counterparts. KHS alone resulted in a modest reduction in viable cells, achieving a non-significant 1.0-$\log_{10}$ reduction (from 1.30 x 10^7 to 1.23 x 10^6 CFE/mL). However, the KHS+CAP combination exhibited significantly greater efficacy, achieving a substantial 3.0-$\log_{10}$ reduction (****p< 0.0001), reducing viable counts to just 1.45 x 10^4 CFE/mL. In the case of PVP-I, monotherapy led to a moderate but non-significant reduction in viable cells, with a 1.4-$\log_{10}$ decrease (to 4.99 x 10^5 CFE/mL). When combined with CAP, PVP-I demonstrated improved efficacy with a significant 2.3-$\log_{10}$ reduction (***p< 0.001), lowering viable counts to 6.64 x 10^4 CFE/mL. Similarly, H_2O_2 monotherapy achieved a moderate reduction in viable cells with a non-significant 1.5-$\log_{10}$ decrease (to 4.58 x 10^5 CFE/mL). However, when combined with CAP, H_2O_2 exhibited significantly enhanced antimicrobial activity, resulting in a substantial 3.1-$\log_{10}$ reduction (****p< 0.0001), reducing viable counts to just 1.02 x 10^4 CFE/mL. Interestingly, CAP alone also demonstrated significant efficacy in reducing viable cell counts, achieving a notable 2.1-$\log_{10}$ reduction (*p< 0.05), lowering viable counts to 1.50 x 10^5 CFE/mL. These findings underscore that while monotherapies provide some level of antimicrobial activity, combination therapies involving CAP consistently demonstrate superior efficacy across all treatment strategies for both total and viable cell reductions in *P. aeruginosa* in the triadic biofilm (Newman model).

Similarly, the analysis of *P. aeruginosa* PA14 biofilms in *S. aureus* SH1000 triadic biofilm model, as shown in (Figure 4.13C and Figure 4.13D), revealed significant

reductions in total and viable cell counts following both monotherapy and combination treatments. The evaluation of total cell populations demonstrated varying degrees of effectiveness across the different therapeutic strategies. In terms of KHS, monotherapy resulted in a modest reduction in total cell counts, achieving a 0.5-log_{10} reduction (****p< 0.0001), from 2.35 x 10^7 to 7.73 x 10^6 CFE/mL. However, when combined with CAP, the efficacy was significantly enhanced, leading to a 1.4-log_{10} reduction (****p< 0.0001), reducing the bacterial population to 1.00 x 10^6 CFE/mL. This demonstrates the superior performance of the KHS+CAP combination compared to KHS alone. For H_2O_2, monotherapy showed moderate efficacy with a 0.4-log_{10} reduction (****p< 0.0001), decreasing total cell counts to 9.43 x 10^6 CFE/mL. In contrast, the H_2O_2+CAP combination exhibited significantly improved activity, achieving a 1.1-log_{10} reduction (****p< 0.0001), lowering the bacterial population to 1.76 x 10^6 CFE/mL. This highlights the enhanced antimicrobial effect of H_2O_2 when combined with CAP. With respect to PVP-I, monotherapy achieved a smaller reduction in total cell counts, with a 0.3-log_{10} decrease (***p< 0.001), to 1.11 x 10^7 CFE/mL. The PVP-I+CAP combination demonstrated better efficacy, resulting in a significant 0.6-log_{10} reduction (****p< 0.0001), reducing total cell counts to 6.20 x 10^6 CFE/mL. In terms of CAP alone, it exhibited moderate effectiveness with a significant 0.7-log_{10} reduction (****p< 0.0001), reducing total cell counts to 5.21 x 10^6 CFE/mL.

When assessing viable cell counts, the combination therapies consistently outperformed their monotherapy counterparts. KHS+CAP demonstrated substantial antimicrobial activity, achieving a significant 2.7-log_{10} reduction (****p< 0.0001), reducing viable cells from 3.60 x 10^6 to just 7.94 x 10^3 CFE/mL, compared to KHS monotherapy's modest and non-significant reduction of only 0.4-log_{10} (to 1.41 x 10^6 CFE/mL). Similarly, H_2O_2+CAP showed marked efficacy with a significant 2.4-log_{10} reduction (***p< 0.001), lowering viable counts to 1.49 x 10^4 CFE/mL, whereas H_2O_2 monotherapy achieved only a non-significant reduction of 0.5-log_{10} (to 1.23 x 10^6 CFE/mL). For PVP-I, the combination with CAP led to a significant reduction in viable cells by 2.5-log_{10} (***p< 0.001), bringing viable counts down from to 1.27 x 10^4 CFE/mL, whereas PVP-I alone also significantly reduced viable cells by a smaller but notable margin of 1.5-log_{10} (*p< 0.05), lowering viable counts to 1.09 x 10^5 CFE/mL. Interestingly, CAP monotherapy also

significantly reduced viable cell counts by a notable margin, achieving a significant reduction of 1.7-$\log_{10}$ (*$p < 0.05$), decreasing viable cells to 7.57 x 10^4 CFE/mL. In summary, while all treatments demonstrated some level of efficacy in reducing both total and viable cell counts, combination therapies—particularly those involving CAP—consistently outperformed their respective monotherapies across all treatment strategies for *P. aeruginosa* in the triadic biofilm (SH1000 model) in both total and viable cell reductions.

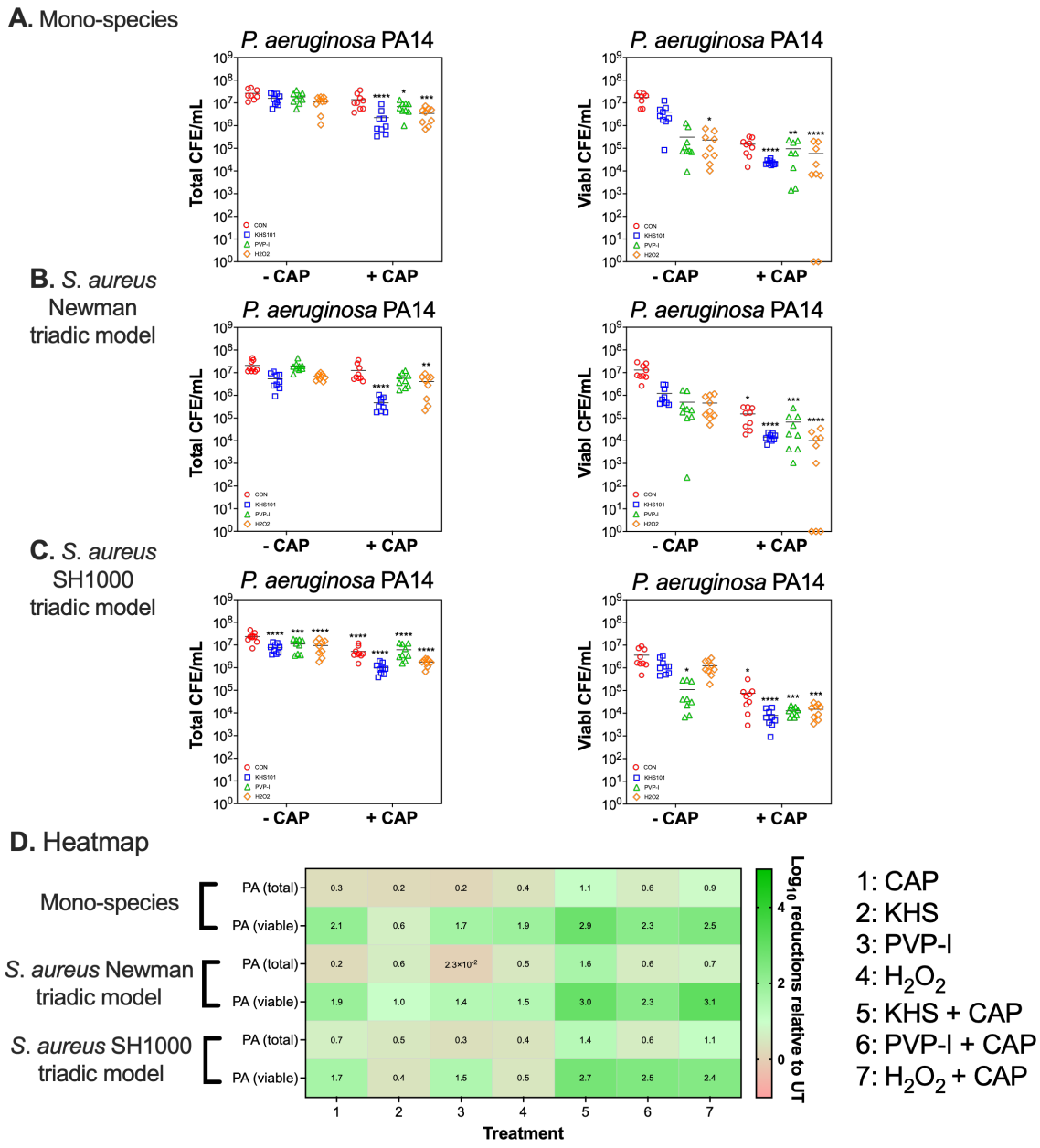

Figure 4.13: Molecular analysis of *P. aeruginosa* PA14 mono-species and triadic biofilm models following 5 minutes treatment by KHS, PVP-I and H_2O_2, and additional 5 min therapy within CAP (Dual therapy). Panel (A) shows *P. aeruginosa PA14* biofilms were formed for 24 h within the cellulose matrix-hydrogel system then treated with KHS (32 **µg/mL)**, PVP-I (10%) and H_2O_2 (3%) for 5 min alone, and additional 5 min therapy by CAP after the neutralisation by Dey-Engley broth for 15 min incubation at 37 °C. Panel (B) shows the triadic polymicrobial biofilm model of *C. albicans* SC5314, *S. aureus* Newman and *P. aeruginosa* PA14 biofilms were formed as above described and followed by similar therapy's. Panel (C) shows the triadic polymicrobial biofilm model of *C. albicans* SC5314, *S. aureus* SH1000 and *P. aeruginosa* PA14 biofilms were formed as above described and followed by similar therapies. Panel (D) shows **log_{10}** reductions of total and viable cell count in a heatmap of *P. aeruginosa PA14* when grown as mono-species biofilms, or for both triadic biofilm models. Total and viable CFE/mL was quantified for each biofilm following treatment using live/dead qPCR. Results representative of mean values from n =9 (three technical replicates from three biological experimental repeats). (- CAP) means: single therapy, (+ CAP) means: dual therapy, (CON) means: control, (1): CAP, (2): KHS, (3): PVP-I, (4): H_2O_2, (5): KHS + CAP, (6): PVP-I + CAP, (7): H_2O_2 + CAP. Data distributions were assessed using D'Agostino-Pearson omnibus normality test, and then analysed by Kruskal-Wallis with Dunn's tests to determine the P-value for multiple comparisons of non-normally distributed data, unless the data of total counts in triadic model (SH1000) which analysed by one-way ANOVA with Tukey's test to determine the P-value for multiple comparisons of normally distributed data. * Indicates statistically significant differences (*p< 0.05,

**p< 0.01, ***p< 0.001, ****p< 0.0001). Data without asterisk indicates; no statistically significant differences were observed.

4.2.4 Assessment of the interaction between KHS and H_2O_2 in checkerboard microdilution assay

Due to the increased efficacy of CAP when used in combination with KHS, the following sections aim to investigate a mode of action by which this dual therapy works. To do this, the efficacy of KHS and H_2O_2 in checkerboard microdilution assay against both mono-species and triadic-species biofilm models was evaluated using a 24-h treatment protocol as previously detailed in section 2.5.1. H_2O_2 was selected due to its presence in plasma-activated water generated following CAP therapy (chapter 3; Figure 3.3A). Concentrations selected ranged from 1 mM – 64 mM. Biofilms were initially cultivated for 24 h aerobically in appropriate broth on 96-well flat-bottom plates before compounds exposure. Biofilm metabolic activity was subsequently assessed using AlamarBlue™ assays as previously described in 2.4.7.

The checkerboard microdilution assay and AlamarBlue™ metabolic activity assessment did not reveal synergism interactions between KHS and H_2O_2 against all microorganisms (Figure 4.14). However, $SMIC_{50}$ or $SMIC_{80}$ were observed for each compound individually, $SMIC_{50}$ achieved at 64 mM of H_2O_2 alone against *C. albicans* which reduced metabolic activity by 50%, while $SMIC_{80}$ achieved at 32 of KHS which reduced the metabolic activity by 80%. $SMIC_{50}$ achieved at 64 mM of H_2O_2 alone against *P. aeruginosa* which reduced metabolic activity by 50%, while KHS did not reduce the metabolic activity by 50% or 80% across all the concentrations we have tested. Similarly, $SMIC_{50}$ and $SMIC_{80}$ achieved at 16 and 32 µg/mL, respectively of KHS alone against *S. aureus* Newman, while H_2O_2 did not reduce the metabolic activity by 50% or 80% across all the concentrations we have tested. Moreover, $SMIC_{50}$ and $SMIC_{80}$ achieved at 32 and 64 µg/mL, respectively of KHS alone against *S. aureus* SH1000, while H_2O_2 did not reduce the metabolic activity by 50% or 80% across all the concentrations we have tested. In addition, $SMIC_{50}$ achieved at 32 µg/mL of KHS alone against triadic model (SH1000) which reduced metabolic activity by 50%, while H_2O_2 did not reduce the metabolic

activity by 50% or 80% across all the concentrations we have tested. Finally, $SMIC_{50}$ or $SMIC_{80}$ did not achieved for KHS or H_2O_2 alone against triadic model (Newman).

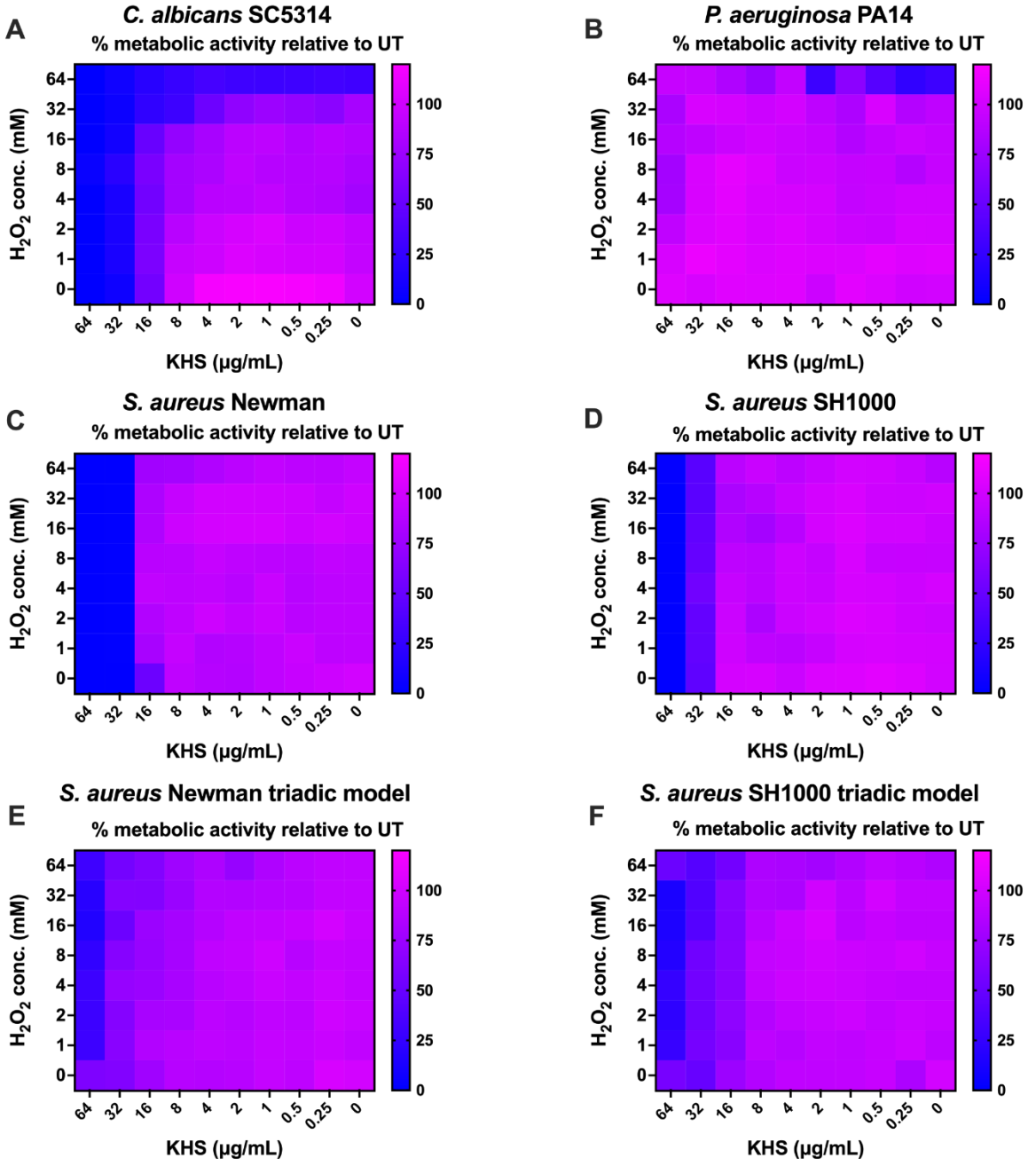

Figure 4.14: Metabolic activity percentages in a heatmap of interaction between KHS and H_2O_2 against different mono-species and triadic biofilm models in relation to UT controls after 24 h treatment by broth checkerboard microdilution assay. Biofilms were grown on 96 well flat bottom for 24 h in RPMI broth for *C. albicans* SC5314 (A) or LB broth for *p. aeruginosa* PA14 (B), *S. aureus* Newman (C) and *S. aureus* SH1000 (D), or in 1:1 v/v mixture of (LB:RPMI) broth for triadic biofilm model (Newman) (E) and triadic biofilm model (SH1000) (F) then treated with KHS and H_2O_2 for 24 h. Metabolic activity were assessed by AlamarBlue™ assay. Data obtained from three independent experiments for *C. albicans* SC5314 and two independent experiments for the other microorganisms. (µg/mL) means: microgram per millilitre. (mM) means: millimolar. (UT) means: untreated.

4.2.5 Assessment of the interaction between KHS and oxidative cocktail solution of H_2O_2, nitrite (NO_2) and nitrate (NO_3) in checkerboard microdilution assay

Given the limited synergistic effects between KHS and H_2O_2 in the previous section 4.2.4, next the efficacy of KHS and an oxidative cocktail solution of H_2O_2, NO_2 and NO_3 was tested in checkerboard microdilution assay against both mono-species and triadic-species biofilm models as previously described in 2.5.2. NO_2 and NO_3 were incorporated with H_2O_2 due to their presence as nitrogen-containing oxidative radicals reportedly produced by plasma activity (Chauvin et al., 2017, Zhai, Kong and Xia, 2022, Mai-Prochnow et al., 2021). To test this, biofilms were initially cultivated for 24-h aerobically in appropriate broth on 96-well flat-bottom plates before compounds exposure. Biofilm metabolic activity was subsequently assessed using AlamarBlue™ assays as previously described in 2.4.7.

The results of the checkerboard microdilution assay and AlamarBlue™ metabolic activity assessment (Figure 4.15E and Figure 4.15F) revealed significant synergistic interactions between KHS and an oxidative cocktail (H_2O_2, NO_2, and NO_3) against two triadic biofilm models (Newman and SH1000). The study demonstrated consistent synergy across various concentration combinations, as evidenced by the Fractional Inhibitory Concentration Index (FICI) values are outlined in (Table 4.1).

Table 4.1: FICI index values for triadic models (Newman and SH1000).

Microorganism	Assay	Drug A alone KHS	Drug B alone Cocktail	Combination (A+B)	Interpretation FICI
Triadic Newman	Checkerboard	$SMIC_{50}$ (64 µg/mL)	$SMIC_{50}$ (32 mM)	2 µg/mL + 8 mM	Synergy (FICI=0.28)
Tri Newman	Checkerboard	$SMIC_{50}$ (64 µg/mL)	$SMIC_{50}$ (32 mM)	4 µg/mL + 8 mM	Synergy (FICI=0.31)
Tri Newman	Checkerboard	$SMIC_{50}$ (64 µg/mL)	$SMIC_{50}$ (32 mM)	8 µg/mL + 8 mM	Synergy (FICI=0.37)
Tri Newman	Checkerboard	$SMIC_{50}$ (64 µg/mL)	$SMIC_{50}$ (32 mM)	8 µg/mL + 4 mM	Synergy (FICI=0.25)
Tri Newman	Checkerboard	$SMIC_{50}$ (64 µg/mL)	$SMIC_{50}$ (32 mM)	16 µg/mL + 8 mM	Synergy (FICI=0.50)
Tri Newman	Checkerboard	$SMIC_{50}$ (64 µg/mL)	$SMIC_{50}$ (32 mM)	16 µg/mL + 4 mM	Synergy (FICI=0.37)
Tri Newman	Checkerboard	$SMIC_{50}$ (64 µg/mL)	$SMIC_{50}$ (32 mM)	16 µg/mL + 2 mM	Synergy (FICI=0.31)
Triadic SH1000	Checkerboard	$SMIC_{50}$ (64 µg/mL)	$SMIC_{50}$ (32 mM)	8 µg/mL + 8 mM	Synergy (FICI=0.37)
Tri SH1000	Checkerboard	$SMIC_{50}$ (64 µg/mL)	$SMIC_{50}$ (32 mM)	8 µg/mL + 4 mM	Synergy (FICI=0.25)
Tri SH1000	Checkerboard	$SMIC_{50}$ (64 µg/mL)	$SMIC_{50}$ (32 mM)	16 µg/mL + 8 mM	Synergy (FICI=0.50)
Tri SH1000	Checkerboard	$SMIC_{50}$ (64 µg/mL)	$SMIC_{50}$ (32 mM)	16 µg/mL + 4 mM	Synergy (FICI=0.37)
Tri SH1000	Checkerboard	$SMIC_{50}$ (64 µg/mL)	$SMIC_{50}$ (32 mM)	16 µg/mL + 2 mM	Synergy (FICI=0.31)
Tri SH1000	Checkerboard	$SMIC_{50}$ (64 µg/mL)	$SMIC_{50}$ (32 mM)	16 µg/mL + 1 mM	Synergy (FICI=0.28)

The checkerboard microdilution assay revealed synergism interactions between KHS and an oxidative cocktail solution of (H_2O_2, NO_2 and NO_3) against both triadic models (Newman and SH1000).

For the triadic Newman biofilm model, the individual agents exhibited inhibitory effects at $SMIC_{50}$ = 64 µg/mL for KHS and $SMIC_{50}$ = 32 mM for the oxidative cocktail. When combined, these agents produced synergistic effects across all tested concentrations, with FICI values ranging from 0.25 to 0.50. For instance, combinations such as KHS (2 µg/mL) with the oxidative cocktail (8 mM) achieved a FICI of 0.28, while KHS (16 µg/mL) with the oxidative cocktail (2 mM) resulted in a FICI of 0.31. These values consistently fall below the threshold for synergy (FICI ≤ 0.5), indicating that the combination of KHS and the oxidative cocktail enhanced biofilm reduction significantly compared to individual treatments. For triadic Newman, KHS alone reduced metabolic activity by percentages ranging from 1.1% to 9.6%, while the oxidative cocktail alone achieved reductions between 15.8% and 36.8%. When combined, reductions in metabolic activity were markedly higher, ranging from 51% to 70.8%. For example, the combination of KHS (8 µg/mL) with the oxidative cocktail (4 mM) reduced metabolic activity by 54.4%, whereas KHS (16 µg/mL) with the oxidative cocktail (8 mM) achieved a reduction of 61.7%. These results demonstrate that the combination therapy effectively disrupted biofilm-associated cellular functions.

Similarly, for the triadic SH1000 biofilm model, individual agents exhibited inhibitory effects at $SMIC_{50}$ = 64 µg/mL for KHS and $SMIC_{50}$ = 32 mM for the oxidative cocktail. The combination therapy produced synergistic effects across all tested concentrations, with FICI values ranging from 0.25 to 0.50. For example, KHS (8 µg/mL) combined with the oxidative cocktail (4 mM) resulted in a FICI of 0.25, while (16 µg/mL) combined with the oxidative cocktail (4 mM) yielded a FICI of 0.37. These values confirm consistent synergy in biofilm reduction. The AlamarBlue™ assay results for triadic SH1000 mirrored those observed for triadic Newman, with enhanced reductions in metabolic activity when both agents were combined compared to individual treatments. For instance, KHS alone reduced metabolic activity by percentages ranging from 2.9% to 35.7%, while the oxidative cocktail alone achieved reductions between 12.4% and 32.3%. When combined, reductions ranged from 53.7% to 70.5%, demonstrating improved efficacy against biofilm-associated cells.

In summary, both checkerboard microdilution assays and AlamarBlue™ assessments consistently demonstrated synergistic interactions between KHS and the oxidative cocktail against both triadic biofilm models (Newman and SH1000). This is interesting as KHS alone, at 32 ug/mL, had limited effect on triadic biofilm models (section 4.2.2.5; Figure 4.8A and Figure 4.8D) and (section 4.2.2.6; Figure **4.9**A and Figure **4.9**D). The observed synergy suggests that these agents act through complementary mechanisms to enhance biofilm inhibition and reduce metabolic activity within biofilms more effectively than either agent alone. Such an observation may help to explain how CAP synergistically works with the Tocriscreen™ compound. These findings highlight the therapeutic potential of combining KHS with oxidative stress-inducing agents (e.g., CAP) for combating polymicrobial-biofilm-associated infections resistant to conventional monotherapies.

Taken together, these results highlight the superior efficacy of combination therapy in polymicrobial infections, where synergistic interactions disrupt complex biofilm communities. The oxidative cocktail's inclusion of H_2O_2,$NO_2$and NO_3 (plasma-derived radicals) enhanced biofilm penetration and metabolic inhibition, particularly in triadic models, which displayed tolerance to KHS alone previously in (section 4.2.2.5; Figure 4.8A and Figure 4.8D) and (section 4.2.2.6; Figure **4.9**A and Figure **4.9**D). This approach holds promise for treating recalcitrant, multi-species biofilm infections resistant to conventional therapies.

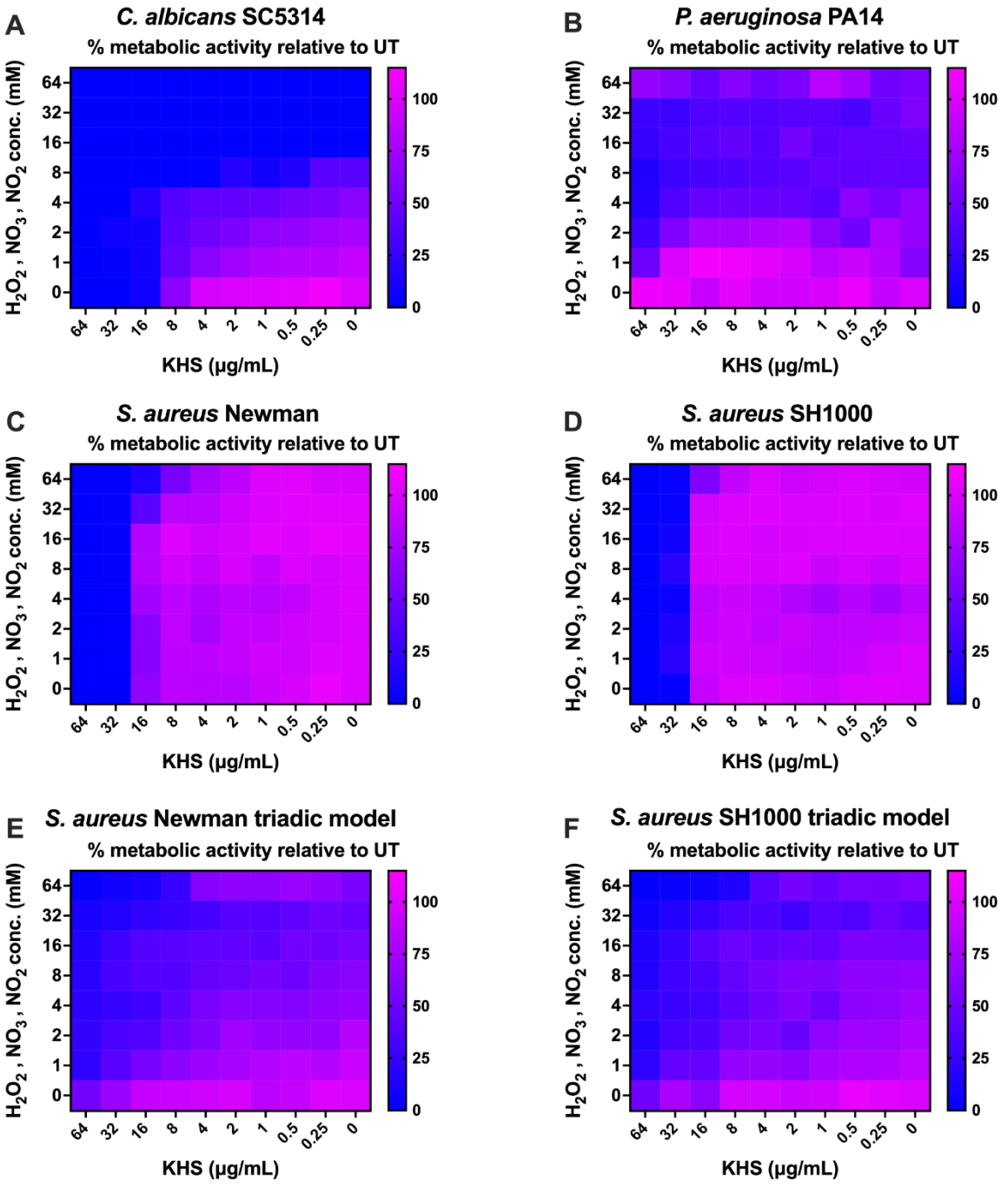

Figure 4.15: Metabolic activity percentages of interaction between KHS and the oxidative cocktail solution of H_2O_2, NO_2 and NO_3 against different mono-species and triadic biofilm models in relation to UT after 24 h treatment in broth checkerboard assay. Biofilms were grown on 96 well flat bottom for 24 h in RPMI broth for *C. albicans* SC5314 (A) or LB broth for *p. aeruginosa* PA14 (B), *S. aureus* Newman (C) and *S. aureus* SH1000 (D), or in 1:1 v/v mixture of (LB:RPMI) broth for triadic biofilm model (Newman) (E) and triadic biofilm model (SH1000) (F) then treated with KHS and the cocktail (H_2O_2, NO_2 and NO_3) for 24 h. Metabolic activity were assessed by AlamarBlue™ assay. Data obtained from three independent experiments for *C. albicans* SC5314 and two independent experiments for the other microorganisms. (µg/mL) means: microgram per millilitre. (mM) means: millimolar. (UT) means: untreated.

4.3 Discussion

4.3.1 Antimicrobial efficacy of novel compounds against simple and complex biofilms

This extensive chapter has investigated the antimicrobial potential of three compounds from the Tocriscreen™ Micro library against clinically relevant wound pathogens, both as planktonic cells and in complex biofilm formations. The findings reveal distinct antimicrobial profiles, species-specific sensitivities, and promising combinational approaches that warrant further exploration in the development of novel anti-biofilm strategies. This research demonstrates the superior efficacy of dual treatment modalities involving KHS alongside CAP for biofilm eradication, in otherwise recalcitrant communities.

4.3.1.1 Strain-specific susceptibility patterns

The antimicrobial screening of three compounds from the Tocriscreen™ Micro library revealed distinctive susceptibility patterns across the tested microbial species. *C. albicans* SC5314 demonstrated the highest sensitivity to all tested compounds, while *P. aeruginosa* PA14 exhibited complete tolerance to all three compounds. This differential susceptibility aligns with established understanding of intrinsic resistance mechanisms in *P. aeruginosa*, which possesses a formidable repertoire of defence strategies including restricted outer membrane permeability, active efflux systems, and enzymatic inactivation of antimicrobial agents (Langendonk, Neill and Fothergill, 2021, Elfadadny et al., 2024). Studies documented that the intrinsic resistance of *P. aeruginosa* stems from its highly adaptable genome and sophisticated regulatory networks that enable rapid responses to antimicrobial challenges (Elfadadny et al., 2024, Yin et al., 2024, Moradali, Ghods and Rehm, 2017).

The varying susceptibility observed between *S. aureus* strains (Newman and SH1000) merits particular attention. Both strains displayed sensitivity to DARA and KHS but exhibited strain-specific variations in planktonic minimum inhibitory concentrations (PMICs) which obtained from the kinetic growth curve experiments. This strain-dependent susceptibility could be attributed to differences in genetic backgrounds. Studies demonstrated that *S. aureus* strains

can differ substantially in their gene expression profiles and consequently in their antimicrobial resistance mechanisms (Foster, 2017, Mlynarczyk-Bonikowska et al., 2022). The observed variations between *S. aureus* Newman and SH1000 strains underscores the importance of strain selection in antimicrobial testing and highlights the challenges in developing broad-spectrum anti-staphylococcal agents. The differential tolerance of these strains to antimicrobial interventions aligns with observations made in the previous chapter that some *S. aureus* strains are less susceptible to CAP therapy. The over-arching aim of this chapter was to combine therapies to "break this tolerance" exhibited to singular modalities.

Among the tested compounds, DARA and POLY demonstrated the most potent antimicrobial activities against *C. albicans* SC53141 planktonic cells. DARA, primarily known as a phospholipase inhibitor, exhibited $PMIC_{90}$ at 32 µg/mL against *C. albicans* SC53141. DARA has shown antimicrobial activity against *C. albicans* in recent studies, particularly in the context of biofilm inhibition. Abduljalil et al. (2022) demonstrated that DARA exhibited efficacy for biofilm inhibition of *C. albicans*, with effective concentration ranges from 16 to 32 µg/mL. While this compound's activity against *C. albicans* has been documented, its application as an antimicrobial agent is still relatively novel. The antimicrobial activity against *S. aureus*, however, remains less extensively studied in the available literature. The observed anti-staphylococcal activity might be mediated through inhibition of bacterial phospholipases, which are known virulence factors in *S. aureus* pathogenesis (Nakamura et al., 2020, White et al., 2014). POLY on the other hand, exhibited remarkable antifungal efficacy with $PMIC_{90}$ at 32 µg/mL against *C. albicans* SC5314, consistent with previous findings by Kubo, Fujita and Lee (2001), who demonstrated that polygodial disrupts fungal cell membranes through interaction with membrane-associated proteins. The compound's mechanism of action involves aldehyde groups that form adducts with cellular nucleophiles, particularly amino groups, resulting in membrane perturbation and cellular damage (Kubo, Fujita and Lee, 2001).

KHS, primarily investigated for its neurogenic differentiation-inducing properties (Wurdak et al., 2010), demonstrated moderate antimicrobial activity against *C. albicans* SC5314 ($PMIC_{50}$ at 32 µg/mL). While the antimicrobial properties of KHS

against *C. albicans* have been documented in Abduljalil et al. (2022) study, its application as an antimicrobial agent is still novel, especially considering its primary development for investigations into the nervous system. The findings from Abduljalil et al. (2022) represent an interesting expansion of KHS's potential applications beyond its originally intended use, highlighting the value of drug repurposing strategies in antimicrobial research. Moreover, here KHS demonstrated moderate antimicrobial activity either against *S. aureus* strains (Newman and SH1000) ($PMIC_{90}$ at 16 and 32 µg/mL), respectively. This represents a novel finding, as the antimicrobial properties of KHS have not been previously documented in the scientific literature against bacteria. The compound's mechanism of antimicrobial action warrants further investigation but may be related to its ability to modulate cellular differentiation pathways that are conserved across eukaryotes and potentially influence microbial physiology. KHS structure-featuring a pyrimidine-2,4-diamine core, thiazole ring, and hydrophobic isobutyl group-shares key motifs with established antimicrobial agents, potentially explaining its observed activity against microbial biofilms (Abu-Hashem and Al-Hussain, 2024, Marinescu and Popa, 2022) (Figure 4.16).

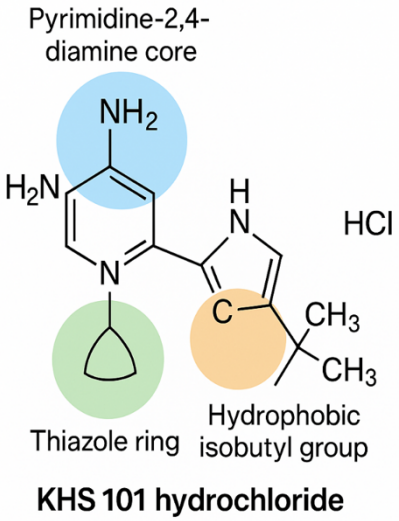

Figure 4.16: Schematic diagram illustrated the chemical structure of KHS. KHS structure-featuring a pyrimidine-2,4-diamine core, thiazole ring, and hydrophobic isobutyl group. Diagram was created in BioRender.

To illustrate this, firstly; the thiazole ring in KHS is structurally analogous to those in cephalosporins (e.g., ceftazidime) and sulfathiazole. In cephalosporins,

thiazole derivatives enhance ß-lactamase resistance and target binding (e.g., penicillin-binding proteins) (Swathykrishna et al., 2023, Nammalwar and Bunce, 2024). Sulfathiazole's thiazole moiety inhibits dihydropteroate synthase in bacterial folate synthesis (Swathykrishna et al., 2023). This suggests KHS's thiazole may similarly improve biofilm penetration or microbial interaction. Secondly, the pyrimidine-2,4-diamine core mirrors trimethoprim, a dihydrofolate reductase (DHFR) inhibitor that disrupts folate metabolism in bacteria (Nammalwar and Bunce, 2024, Ungureanu et al., 2024). While KHS targets transforming acidic coiled-coil containing protein 3 (TACC3) in eukaryotes, its pyrimidine scaffold may facilitate nucleic acid-related interactions in microbes, akin to pyrimidine-linked antibiotics like Linezolid derivatives, which exhibit antibiofilm activity against *S. aureus* and *Enterococcus* spp. (Nammalwar and Bunce, 2024). Thirdly, the isobutyl group aligns with hydrophobic moieties in fluoroquinolones (e.g., moxifloxacin), where bulky substituents (e.g., cyclopropyl) enhance membrane penetration and DNA gyrase binding (Pham, Ziora and Blaskovich, 2019). This hydrophobicity is critical for disrupting lipid-rich biofilm matrices, a feature shared with KHS's design. Finally, KHS's thiazole-pyrimidine hybrid resembles recent antimicrobial conjugates designed for dual targeting. For example, thiazole-linked pyrimidines (e.g., compound 35) show potent activity against MRSA, Linezolid-resistant *S. aureus* , Linezolid-resistant *Streptococcus pneumoniae* and vancomycin-resistant *Enterococcus* (VRE) biofilms, with minimum biofilm inhibitory concentrations (MBIC) ranging (0.5-4 µg/mL) (Nammalwar and Bunce, 2024). Thus, while KHS's primary mechanism (TACC3 inhibition) differs from classical antibiotics, its structural motifs align with antimicrobial design principles, particularly in biofilm disruption and cellular uptake. These parallels offer a plausible rationale for its observed efficacy against microbial biofilms in experimental models.

The 24-hour kinetic growth curve assessments provided valuable insights into the concentration-dependent and temporal aspects of antimicrobial activity for KHS, DARA, and POLY. Firstly, KHS demonstrated concentration-dependent inhibition of *C. albicans* SC5314, with 88.4% growth inhibition at 64 µg/mL and 53.1% at 32 µg/mL. This gradual concentration-response relationship could potentially suggest a complex mechanism of action, though further research would be needed to

elucidate the specific cellular targets or processes affected by this compound. The compound exhibited particularly potent activity against *S. aureus* strains, achieving complete inhibition of *S. aureus* Newman at 16 µg/mL and marked inhibition of *S. aureus* SH1000 at concentrations above 32 µg/mL. This selective activity against Gram-positive bacteria over *C. albicans* and *P. aeruginosa* suggests that KHS may target cellular structures or processes more prevalent in Gram-positive organisms, such as peptidoglycan synthesis or teichoic acid metabolism (Reed et al., 2015, Brown, Santa Maria Jr and Walker, 2013).

Secondly, DARA demonstrated substantial antifungal activity against *C. albicans* SC5314, with 94.9% growth inhibition at 64 µg/mL. Interestingly, the compound exhibited a more uniform inhibitory effect against *S. aureus* strains across all tested concentrations, suggesting a different mechanism of action against bacteria compared to fungi. Phospholipases are important virulence factors in both *C. albicans* and *S. aureus*, and their inhibition by DARA could explain the antimicrobial activity observed (Bandana, Jashandeep and Jagdeep, 2018). However, the concentration-independent effect against *S. aureus* contrasts with the concentration-dependent effect against *C. albicans*, suggesting that DARA may engage different cellular targets or pathways in these distinct microbial species (Zhuo and Yuan, 2020, Murakami, Sato and Taketomi, 2020).

Finally, POLY exhibited potent antifungal activity against *C. albicans* SC5314, achieving 95.8% growth inhibition at 64 µg/mL and 96.8% at 32 µg/mL. This finding aligns with previous studies by Kipanga et al. (2021), who demonstrated POLY's potent antifungal properties against various *Candida* species. The compound's activity against *S. aureus* was notably concentration-dependent and strain-specific, with greater efficacy against *S. aureus* Newman compared to SH1000. This strain-specific activity could be related to differences in membrane composition or permeability between the two *S. aureus* strains, as POLY's mechanism of action primarily involves membrane disruption (Kipanga et al., 2021, Kubo, Fujita and Lee, 2001).

Notably, the remarkable tolerance of *P. aeruginosa* PA14 to all tested compounds, even at the highest concentration of 64 µg/mL, underscores the formidable challenge this pathogen presents in antimicrobial development. This intrinsic

tolerance aligns with established understanding of *P. aeruginosa* sophisticated tolerance mechanisms, including reduced outer membrane permeability, active efflux systems, and enzymatic modification of antimicrobial agents (Grace et al., 2022, Elfadadny et al., 2024). The current findings suggest that novel approaches targeting *P. aeruginosa* specific tolerance mechanisms may be necessary for effective treatment of this recalcitrant pathogen. This could include strategies such as targeting the Type III secretion system, developing new ß-lactam/ß-lactamase inhibitor combinations, or exploring alternative therapies like bacteriophages (Kunz Coyne et al., 2022, Yin et al., 2024).

4.3.2 Anti-biofilm efficacy of novel compounds

4.3.2.1 Mono-species biofilm responses

The evaluation of compound efficacy against mono-species biofilms revealed marked differences compared to planktonic assessments, highlighting the well-documented phenomenon of biofilm-associated antimicrobial recalcitrance. This enhanced resistance in biofilms has been attributed to multiple factors, including restricted antimicrobial penetration through the EPS matrix, altered metabolic states of biofilm-embedded cells, and expression of biofilm-specific resistance mechanisms (Hall and Mah, 2017, Grooters et al., 2024).

C. albicans SC5314 biofilms demonstrated significant susceptibility to all three tested compounds (KHS, DARA, and POLY). POLY demonstrated the most potent anti-biofilm activity against *C. albicans*, reducing metabolic activity to 0% at 64 µg/mL and significantly reducing biofilm biomass across all tested concentrations. This enhanced anti-biofilm efficacy could be attributed to POLY's membrane-disrupting mechanism, which may enable better penetration through the biofilm matrix and more effective targeting of embedded cells (Kipanga et al., 2021).

P. aeruginosa PA14 biofilms exhibited remarkable tolerance to all tested compounds, mirroring the planktonic findings (in kinetic growth curve assay). This consistent tolerance across planktonic and biofilm states suggests that the intrinsic tolerance mechanisms of P. aeruginosa likely remains operative and perhaps even enhanced in biofilm communities. Studies documented that P.

aeruginosa biofilms present one of the most formidable challenges in antimicrobial therapy, often requiring combinatorial approaches for effective eradication (Elfadadny et al., 2024, Fernández-Billón et al., 2023, Yang, Xu and Liang, 2024). Beyond low permeability and Resistance–Nodulation–Division efflux pumps, P. aeruginosa commonly loses or down-regulates the outer membrane porin D (OprD) and derepresses the chromosomal AmpC ß-lactamase; jointly driving carbapenem and cephalosporin non-susceptibility, and these chromosomal changes can emerge rapidly under therapy and often co-occur with efflux upregulation in clinical isolates (Castanheira et al., 2014, Wu, Huang and Xu, 2024, Spottiswoode et al., 2023). In biofilms, the Pel and Psl exopolysaccharides and extracellular DNA limit penetration, and together with oxygen-limited metabolism that collapses the proton-motive force (PMF), depress aminoglycoside uptake and killing, so even high concentrations can fail without adjuvants that restore PMF or disrupt matrix structure (Langendonk, Neill and Fothergill, 2021). Newer agents designed to bypass these barriers, such as ceftolozane/tazobactam and cefiderocol, retain activity against many strains with AmpC overexpression and OprD loss, illustrating treatment strategies that target *P. aeruginosa* dominant resistance mechanisms (Simner et al., 2021, Murata et al., 2025). The current findings support this assertion and highlight the need for alternative strategies beyond conventional antimicrobials for P. aeruginosa biofilm control (Fernández-Billón et al., 2023, Yin et al., 2024).

S. aureus biofilms (both Newman and SH1000 strains) demonstrated variable responses to the tested compounds, with KHS and DARA showing the most promising activity. DARA reduced *S. aureus* Newman biofilm metabolic activity to 0.04% at 64 µg/mL, suggesting potential as an anti-biofilm agent. However, the more modest reductions in biofilm biomass compared to metabolic activity indicate that while DARA effectively kills biofilm cells, it may not substantially disrupt the biofilm architecture. This finding aligns with studies that highlighted this phenomenon of the antimicrobial efficacy against polymicrobial biofilms often involves cellular killing without significant structural disruption (Kean et al., 2017, Palková and Váchová, 2025).

It is particularly noteworthy that the SH1000 strain generally demonstrated greater biofilm tolerance compared to the Newman strain across all compounds. This strain-specific difference in biofilm susceptibility could be attributed to variations in biofilm architecture, matrix composition, or expression of biofilm-associated tolerance mechanisms. Studies documented that different *S. aureus* strains can produce structurally and compositionally distinct biofilms, influencing their antimicrobial susceptibility profiles (Peng et al., 2022, Lamret et al., 2021b). This strain background strongly conditions *S. aureus* biofilm formation. Restoration of rsbU (σB activation) in SH1000 enhances biofilm relative to its NCTC 8325 progenitor, demonstrating how single regulatory alleles modulate matrix production and tolerance (Horsburgh et al., 2002). In parallel, multiple studies show that natural polymorphisms in cell-wall adhesins, particularly fibronectin-binding proteins (FnBPA/FnBPB), drive marked strain-to-strain variability in biofilm architecture and antimicrobial susceptibility, including in widely used laboratory and clinical lineages (O'Neill et al., 2008, Pozzi et al., 2012, Houston et al., 2011). Given reports that Newman carries naturally occurring variants in biofilm-relevant loci, this background differences likely contribute to the comparatively lower susceptibility observed here. The current findings underscore the importance of strain selection in biofilm research and highlight the challenges in developing broadly effective anti-biofilm strategies.

4.3.2.2 Polymicrobial biofilm complexity

The investigation of compound efficacy against triadic polymicrobial biofilms (comprising *C. albicans*, *P. aeruginosa*, and either *S. aureus* Newman or SH1000) revealed complex responses that differed substantially from mono-species assessments. Similar to the previous chapter, it was deemed necessary to investigate mixed-species communities due to the polymicrobial nature of infected wounds. This altered susceptibility in polymicrobial contexts aligns with emerging understanding of interspecies interactions within mixed biofilms, where microbial cross-talk can significantly influence community behaviour and particularly, antimicrobial responses (Kean et al., 2017, Taff et al., 2013, Schilcher and Horswill, 2020, Ibberson et al., 2022)

All three tested compounds (KHS, DARA, and POLY) demonstrated reduced efficacy against polymicrobial biofilms compared to their respective mono-species counterparts, which is not an unexpected phenomenon. That being said, this observation is consistent with different studies which documented that the enhanced resistance in polymicrobial biofilms comprised of *C. albicans* and various bacterial species (Kean et al., 2017, Townsend et al., 2016, Bandara et al., 2020). The reduced efficacy could be attributed to multiple factors, including enhanced EPS production in mixed-species communities, metabolic complementation between species, and interspecies protection mechanisms. For example, studies have shown that the presence of *C. albicans* in polymicrobial biofilms can enhance the antibiotic tolerance of bacterial species (Orazi and O'Toole, 2019, Eshima et al., 2022, Stoneham et al., 2020, Ashrit et al., 2022).

DARA demonstrated the most consistent activity against polymicrobial biofilms, significantly reducing metabolic activity in both triadic models (Newman and SH1000). This antimicrobial efficacy suggests that DARA's mechanism of action, potentially involving phospholipase inhibition, may target conserved pathways across different microbial species within the biofilm community (Oh et al., 2023, Abduljalil et al., 2022). However, the more modest reductions in biofilm biomass compared to metabolic activity suggest that DARA primarily affects cellular metabolic activity rather than biofilm architecture, a limitation in the context of established biofilm infections.

The differential responses between the Newman and SH1000 triadic models highlight the impact of strain selection on polymicrobial biofilm behaviour and antimicrobial susceptibility. This strain-dependent variation in polymicrobial contexts parallels the mono-species findings but introduces additional complexity due to potential differences in interspecies interactions. Studies highlighted that the specific combinations of microbial strains in polymicrobial biofilms can significantly influence community behaviour and antimicrobial responses through strain-specific interspecies signalling mechanisms (Orazi and O'Toole, 2019, Harriott and Noverr, 2011, Karygianni et al., 2020).

4.3.3 Novel combination therapies: enhancing anti-biofilm efficacy

4.3.3.1 CAP in combinations

The evaluation of combination therapies involving CAP represents a particularly innovative aspect of this research, with significant implications for biofilm eradication strategies. While *S. aureus* demonstrated substantial tolerance to CAP treatment-evidenced by the lack of significant reduction in viable cell counts compared to UT biofilms that observed in the previous chapter, this tolerance was effectively overcome when CAP was combined with KHS. The dual therapy approach broke through the biofilm's defence mechanisms, resulting in a marked decrease in bacterial viability that was not observed with CAP alone. This finding is consistent with other studies showing that combination therapies can disrupt biofilm tolerance: for example, combining CAP with antibiotics such as rifampicin or gentamicin has been shown to significantly enhance killing of *S. aureus* biofilms by facilitating antibiotic penetration and increasing oxidative stress (Guo et al., 2021b). Similarly, synergistic effects have been reported when H_2O_2 is used alongside conventional antibiotics, with the oxidative agent destabilising the biofilm matrix and sensitising bacterial biofilm to antimicrobial action (Kwiatkowski et al., 2020, Dwyer et al., 2014). Another study found that the combination of baicalein and rifampicin exhibits synergistic effect, enhancing their bactericidal effect in completely eradicating *S. aureus* biofilms (Muniyasamy and Manjubala, 2024). These studies highlight those dual therapies, particularly those pairing CAP or oxidative agents with targeted antimicrobials, can successfully overcome the intrinsic tolerance of *S. aureus* biofilms that renders monotherapies less effective. The molecular analysis of mono-species and triadic biofilms following treatment with chemical agents alone, CAP alone, or dual therapy approaches revealed consistent and substantial enhancement of antimicrobial efficacy through combinations.

For all tested microorganisms, dual therapy approaches combining chemical agents with CAP consistently outperformed their respective monotherapies in reducing both total and viable cell counts. This synergistic effect was most pronounced for KHS+CAP combinations, which achieved $\log_{10}$ reductions in viable cell counts ranging from 2.8 to 4.4 across different microbial species and biofilm

configurations. These findings align with recent study demonstrated that CAP pre-treatment synergised with ciprofloxacin, gentamicin, and tobramycin to eradicate *P. aeruginosa* biofilms (PAO1, PA14, PA10548) by degrading EPS (512-fold lower MBECs for ciprofloxacin/gentamicin), inducing oxidative stress (via O_2^-, OH^-, NO), and damaging membranes/DNA (ATP/LDH leakage). This oxidative stress-mediated synergy overcomes biofilm tolerance, offering a targeted strategy for recalcitrant *P. aeruginosa* infections (Maybin et al., 2023).

The most striking synergistic effect was observed against *C. albicans* SC5314 mono-species biofilms, where KHS+CAP combination reduced viable cell counts by 4.4-log_{10}, compared to non-significant reductions with KHS alone (3.8-log_{10}) and modest reductions with CAP alone (1.2-log_{10}). This potent synergistic effect suggests that the combination targets complementary cellular pathways or barriers, leading to enhanced fungal cell death. Delben et al. (2016) previously demonstrated that CAP can significantly alter *C. albicans* biofilm architecture and cellular viability through oxidative damage mechanisms, which may facilitate the penetration and activity of KHS.

Against *P. aeruginosa* PA14, which demonstrated remarkable tolerance to chemical treatments alone, dual therapy approaches achieved significant reductions in viable cell counts. The H_2O_2+CAP combination reduced viable counts by 2.5-log_{10} in mono-species biofilms and up to 3.1-log_{10} in triadic models, but CAP mono-therapy was effective against *P. aeruginosa* in the previous chapter (chapter 3; Figure 3.4, Figure 3.5, Figure 3.6, Figure 3.7 and Figure **3.8**). This is highlighting the potential of this approach for recalcitrant pathogens. The enhanced efficacy against *P. aeruginosa* could be attributed to CAP-generated reactive species that may overcome the pathogen's intrinsic tolerance mechanisms (Maybin et al., 2023). Studies demonstrated that plasma-generated ROS can disrupt bacterial cell membranes and overcome efflux-mediated tolerance (Flynn et al., 2015, Maybin et al., 2023).

S. aureus biofilms (both Newman and SH1000 strains) also demonstrated enhanced susceptibility to dual therapy approaches, with KHS+CAP and H_2O_2+CAP combinations achieving the most substantial reductions in viable cell counts. The consistent efficacy of these combinations across different *S. aureus* strains

suggests a broadly applicable mechanism that may overcome strain-specific tolerance variations. Studies have documented that plasma-generated reactive species can effectively penetrate biofilm matrices and cause DNA damage in embedded cells, a mechanism that may be particularly effective against Gram-negative bacteria and some of Gram-positive bacteria with less complex cell envelopes (Mai-Prochnow et al., 2014, Mai-Prochnow et al., 2016).

In triadic polymicrobial biofilms, dual therapy approaches demonstrated remarkable efficacy despite the enhanced resistance typically associated with polymicrobial communities. This finding is particularly significant given the clinical relevance of polymicrobial infections, which often exhibit enhanced recalcitrance to conventional treatments. Different studies highlighted that polymicrobial biofilms typically require more aggressive or combinatorial treatment approaches due to interspecies protection mechanisms and enhanced EPS production (Anju et al., 2022, Orazi and O'Toole, 2019, Fanaei Pirlar et al., 2020). The current findings suggest that CAP-based dual therapies may offer a promising strategy for addressing these challenging polymicrobial scenarios.

4.3.3.2 Checkerboard microdilution assays

The checkerboard microdilution assays investigating interactions between KHS and H_2O_2, as well as between KHS and an oxidative cocktail solution of reactive species (H_2O_2, NO_2, and NO_3), provided valuable insights into potential synergistic or antagonistic interactions. The variable responses observed across different microbial species in these interaction studies suggest species-specific mechanisms of synergy or antagonism. This finding aligns with previous studies by Brochado et al. (2018), who demonstrated that antimicrobial combinations could exhibit species-specific interaction profiles based on distinct cellular targets and resistance mechanisms. While no synergism was observed with H_2O_2 alone, significant synergistic interactions were found between KHS and the oxidative cocktail solution of reactive species (H_2O_2, NO_2, and NO_3) against triadic biofilm models. This synergy suggests that combining KHS with an oxidative stress-inducing agents could be a promising strategy for combating complex, multi-species biofilms. Similar synergistic approaches have been reported in other studies, such as Li et al. (2022), who demonstrated enhanced efficacy of combined

H_2O_2 with antimicrobial photodynamic therapy against dual-species biofilm (*C. albicans* and *Streptococcus mutans*). The potential synergistic interactions observed, particularly between KHS and reactive species cocktails, provide a mechanistic basis for the enhanced efficacy of CAP-based dual therapies, as CAP generates similar reactive species during treatment.

Similar to what is reported here, future studies need to investigate mode of action of CAP by piecing together the various components that the technology produces following generation of the plasma (Chauvin et al., 2017, Zhai, Kong and Xia, 2022, Mai-Prochnow et al., 2021). This can be achieved by inactivating the radical species produced, or by simplifying the system and utilising components produced by CAP. To this end, the next chapter will build upon this idea, by utilising H_2O_2 at concentrations generated by the CAP device; while this approach has obvious limitations, as previously discussed in chapter 3 (due to the presence of other antimicrobial compounds), it allows researchers to systematically evaluate its specific contribution to the antimicrobial effects of CAP on biofilms and wound pathogens, distinguishing its activity from other CAP-generated reactive species. This targeted approach not only identifies potential synergies or limitations that could optimise CAP protocols or guide adjunct therapies but also establishes a foundational mechanistic understanding of H_2O_2's role. Such insights provide a critical framework for deciphering the multifactorial biochemical interactions underlying full CAP treatments, enabling more precise translation of laboratory findings into clinically viable strategies.

4.3.4 Limitations and future directions

4.3.4.1 Experimental limitations

While this study provides valuable insights into novel anti-biofilm approaches, several methodological limitations should be acknowledged. The evaluation of antimicrobial efficacy focused primarily on cellular metabolic activity, biomass quantification and molecular analysis, without detailed examination of biofilm architecture, matrix composition, or resistance gene expression. Advanced microscopy techniques, such as confocal laser scanning microscopy with live/dead staining, would provide more nuanced insights into the spatial aspects of

antimicrobial activity within complex biofilm structures. Similarly, transcriptomic or proteomic analyses would elucidate the molecular responses underlying observed resistance patterns.

4.3.4.2 Future research directions

This comprehensive study establishes several promising avenues for future research with both fundamental and translational significance. The unexpected antimicrobial activity of KHS warrants mechanistic investigation to identify its cellular targets and potential applications beyond the organisms tested here. Comparative genomic or transcriptomic analyses of susceptible versus tolerant strains could elucidate the molecular basis of the compound's selectivity and inform structural modifications to enhance its spectrum and potency.

The potent synergistic effects observed with CAP combinations merit further investigation, particularly regarding optimal treatment parameters, sequential effects (pre/post-treatment versus simultaneous application) will investigate in next chapter, and molecular mechanisms of synergy. Reactive species scavenging studies or genetic approaches targeting specific stress response pathways could elucidate the key mediators of CAP-enhanced antimicrobial activity.

The development of advanced delivery systems that enable controlled release or targeted application of these compounds, particularly in combination with CAP, represents an important translational direction. Biofilm-penetrating nanoparticles, plasma-activated solutions, or biofilm-responsive materials could enhance the clinical applicability of these findings for treating established biofilm infections. Incorporating KHS into a controlled-release system designed to work synergistically with CAP could address key challenges in biofilm eradication.

Finally, expanding the microbial panel to include additional clinically relevant pathogens, particularly multidrug-resistant isolates and additional strains of the species already tested, would provide a more comprehensive assessment of the therapeutic potential of these compounds and combinations.

4.3.5 Conclusion

Key findings from this chapter:

- Strain-specific antimicrobial susceptibility: *C. albicans* the highest sensitivity to tested compounds (KHS, DARA, POLY), while *P. aeruginosa* exhibited remarkable tolerance across biofilm models. However, *S. aureus*: responses varied by strain, with biofilms showing intrinsic resilience.

- Combinatorial strategies overcome biofilm tolerance: CAP monotherapy alone was insufficient against *S. aureus* biofilms. Synergistic effects observed when combining KHS with CAP or clinical antiseptics (e.g., H_2O_2, PVP-I). KHS+CAP achieved >3-$\log_{10}$ reductions in *S. aureus* viability across mono- and polymicrobial biofilms.

- KHS emerges as a lead candidate which demonstrated consistent efficacy in dual therapies, likely due to oxidative stress induction and biofilm matrix destabilisation which outperformed DARA and POLY in synergy with CAP.

- Translational potential of dual therapy: KHS+CAP combinations broke biofilm tolerance observed in prior CAP-only treatments. Such mechanisms suggest applicability for chronic wound infections and implant-associated biofilm eradication, which represents a novel therapeutic approach for recalcitrant infections.

5 Chapter 5: Enhancing antibiotic susceptibility in early-stage *Staphylococcus aureus* biofilms using hydrogen peroxide (H_2O_2)

5.1 Introduction

S. aureus represents a significant clinical challenge in healthcare environments due to its remarkable adaptability and capacity to form resilient biofilms (Craft et al., 2019, Sinha, Aggarwal and Singh, 2024, Bhattacharya et al., 2015). These structured bacterial communities embed themselves within a self-produced extracellular polymeric substance (EPS) matrix that enables adhesion to surface, evasion of immune defences, and heightened resistance to antimicrobial treatments (Zhao, Sun and Liu, 2023, Sinha, Aggarwal and Singh, 2024). The biofilm phenotype confers bacteria with dramatically increased antimicrobial tolerance—up to 1,000-fold greater than their free-floating counterparts—creating persistent infections that conventional treatments struggle to resolve (Sivori et al., 2024, Sinha, Aggarwal and Singh, 2024, Bhattacharya et al., 2015, Huang et al., 2024).

The clinical landscape has become increasingly complicated by the emergence of antibiotic-resistant *S. aureus* variants, particularly methicillin-resistant *S. aureus* (MRSA) (Asanin et al., 2019, Senobar Tahaei et al., 2021). *S. aureus*, including MRSA, is among the most prevalent bacterial species found in chronic wounds, with biofilm formation being a key virulence factor that impairs healing and promotes persistent infection (Roy et al., 2020, Simonetti et al., 2021, Banerjee, Gowda and Ananda, 2022). Biofilms formed by *S. aureus* in wounds create a protective matrix that shields bacteria from immune responses and antibiotics. This leads to delayed healing, impaired granulation tissue formation, and compromised tissue biomechanics, increasing the likelihood of wound recurrence and chronicity (Roy et al., 2020, Simonetti et al., 2021). MRSA strains are particularly problematic in wound infections due to their resistance to multiple antibiotics and their robust biofilm-forming ability. Biofilm-associated MRSA infections require prolonged treatment and often resist standard therapies, further complicating wound management (Percival, McCarty and Lipsky, 2015, Simonetti et al., 2022). The presence of biofilm-producing MRSA in wounds is directly linked to increased hospital stays, higher treatment costs, and greater risk of complications such as amputation due to persistent, non-healing wounds (Banerjee, Gowda and Ananda, 2022). The biofilm phenotype of *S. aureus* in wounds leads to the degradation of collagen and alteration of the wound matrix,

which undermines the structural integrity of healing tissue and impairs the wound's ability to repair itself (Roy et al., 2020, Simonetti et al., 2021). Biofilm formation enhances MRSA's resistance to antibiotics by impeding drug penetration, altering bacterial metabolism, and fostering the survival of highly tolerant persister cells, making infections especially difficult to eradicate (Simonetti et al., 2021, Banerjee, Gowda and Ananda, 2022). Because biofilm formation is a major driver of chronicity and antibiotic resistance in wound infections, therapies that disrupt biofilms-such as those involving H_2O_2 or combination treatments-are particularly relevant for improving wound healing outcomes (Raval et al., 2021, Shnyoor and Zgair, 2024). H_2O_2 has shown promise in reducing biofilm biomass and enhancing antibiotic efficacy, making it a valuable tool in the management of biofilm-laden wounds, including those caused by MRSA (Raval et al., 2021, Shnyoor and Zgair, 2024). Standard antibiotic monotherapies frequently fail to eliminate biofilm infections due to multiple defence mechanisms, including impaired antibiotic penetration through the biofilm matrix, altered bacterial metabolism within the biofilm environment, and the presence of cells tolerant to intervention (Parker et al., 2023, Bhattacharya et al., 2015, Wu et al., 2015, Huang et al., 2024). Consequently, researchers have begun exploring innovative combination strategies that simultaneously target both bacterial cells and the protective biofilm architecture (Shnyoor and Zgair, 2024, Wu et al., 2015, Kashi et al., 2024).

Cold atmospheric plasma (CAP) has emerged as a promising as we have seen in previous chapters, non-invasive therapy for infection control and wound healing, largely due to its ability to generate a spectrum of reactive oxygen and nitrogen species (RONS), including H_2O_2, which contribute to its strong antimicrobial and antibiofilm effects (Govaert et al., 2019, Bagheri et al., 2023, Raissi-Dehkordi et al., 2025). CAP has demonstrated efficacy against multidrug-resistant pathogens and biofilms, making it a compelling alternative or adjunct to conventional treatments in chronic and acute wound care (Raissi-Dehkordi et al., 2025, Mai-Prochnow et al., 2014, Mai-Prochnow et al., 2021, Mai-Prochnow et al., 2016). A central mechanism by which CAP exerts its effects is the production of H_2O_2 (chapter 3; Figure 3.3A) in situ at the wound site. H_2O_2 acts as a key mediator of CAP's antimicrobial action, causing oxidative damage to bacterial cells, disrupting

biofilm matrices, and modulating immune responses relevant to wound healing (Bekeschus et al., 2014). Studies have shown that the antimicrobial and wound-healing effects of CAP are, in part, replicated by direct H_2O_2 application, highlighting the importance of understanding H_2O_2's specific mode of action (Raissi-Dehkordi et al., 2025, Boekema et al., 2021). While CAP generates a complex mixture of reactive species, isolating the effects of H_2O_2 allows for a more controlled investigation of: firstly, direct antimicrobial and antibiofilm activities of H_2O_2, mirroring a major component of CAP's action (Govaert et al., 2019, Bekeschus et al., 2014, Raissi-Dehkordi et al., 2025). Secondly, synergistic effects when combined with antibiotics, which may parallel or inform combination strategies involving CAP (Baik et al., 2023, Govaert et al., 2019). Thus, by simplifying the system to study H_2O_2 alone, we can: determine the extent to which H_2O_2 accounts for CAP's observed effects on biofilms and wound pathogens. Identify potential synergies or limitations that may inform the design of more effective CAP protocols or adjunctive treatments. Establish a mechanistic baseline for interpreting the more complex, multifactorial impacts of full CAP exposure.

In this chapter, the potential synergistic interactions between H_2O_2 and two clinically relevant antibiotics: flucloxacillin and gentamicin, will be investigated. These combination therapies will be assessed against early-stage biofilms formed by two distinct *S. aureus* strains (Newman and SH1000) which displayed a level of tolerance to CAP therapy in chapter 3, by employing varied treatment protocols to determine optimal eradication strategies. These included simultaneous application of both agents, pre-treatment with H_2O_2 followed by antibiotic exposure, and antibiotic treatment with subsequent H_2O_2 application.

5.2 Results

5.2.1 H_2O_2, flucloxacillin and gentamicin activity against *S. aureus* strains

Initially, the effect of three different treatments were tested on planktonic cells of *S. aureus* Newman and SH1000 through planktonic minimum inhibitory concentration (PMIC) test as previously described in section 2.4.11. The three antimicrobials selected for testing were, H_2O_2, flucloxacillin and gentamicin.

These were chosen because their clinical relevance and distinct modes of action. H_2O_2 was included as it is a key reactive species generated by CAP and is known for its potent antibiofilm and antimicrobial properties. Flucloxacillin and gentamicin represent commonly used antibiotics with differing mechanisms, allowing for the assessment of potential synergistic effects in combination with H_2O_2. Meanwhile the two strains of *S. aureus* were included because they exhibited notable tolerance to CAP treatment in mature biofilm models, making them suitable for evaluating the efficacy of alternative or adjunctive antimicrobial strategies in a similar manner to KHS intervention in chapter 4. The results presented in (Table 5.1) demonstrated that both *S. aureus* strains exhibit susceptibility to all tested antimicrobial agents, albeit with some variation in PMIC values. For H_2O_2, the $PMIC_{90}$ for *S. aureus* Newman was determined to be 125 µM, whereas the $PMIC_{90}$ for *S. aureus* SH1000 ranged between 125-250 µM. This suggests a slightly broader range of susceptibility for SH1000 compared to Newman. Regarding gentamicin, *S. aureus* Newman displayed an $PMIC_{90}$ range of 2-4 µg/mL, while SH1000 exhibited a consistent $PMIC_{90}$ value of 2 µg/mL. These results indicate that SH1000 may be marginally more sensitive to gentamicin compared to Newman. In the case of flucloxacillin, the $PMIC_{90}$ for *S. aureus* Newman ranged from 0.125-0.25 µg/mL, whereas SH1000 demonstrated a higher $PMIC_{90}$ range of 0.25-0.50 µg/mL. This finding suggests that SH1000 requires higher concentrations of flucloxacillin for growth inhibition, indicating reduced susceptibility relative to Newman.

Table 5.1: PMIC of H_2O_2, gentamicin and flucloxacillin against *S. aureus* Newman and *S. aureus* SH1000.

Antimicrobial compound	Newman	SH1000
H_2O_2	125 μM	125-250 μM
Gentamicin	2-4 μg/mL	2 μg/mL
Flucloxacillin	0.125-0.25 μg/mL	0.25-0.50 μg/mL

Briefly, in the experimental procedure, cell suspensions were prepared by adjusting to $2x10^5$ cells/mL in a LB broth. Each drug was serially diluted in 96-well round-bottom microtiter plates. 200 μL of each drug was added to the appropriate wells of 96-well round-bottom microtiter plates and serial doubling-dilutions were performed in LB broth, followed by the addition of 100 μL of the standardised cell suspension, resulting in a final volume of 200 μL per well. The plates were then incubated at 37°C for 24 h. Following incubation, the $PMIC_{90}$ was determined by identifying the lowest drug concentration that completely inhibited visible microbial growth. Data were obtained from four technical repeats of three independent experiments. (μg/mL) : Microgram per millilitre. μM : Micromolar.

5.2.2 Metabolic activity assessment of early-stage *S. aureus* biofilms

Next, the potential synergistic effects of combining H_2O_2 with two different antibiotics: flucloxacillin and gentamicin, were investigated against sessile forms of *S. aureus*. This combination therapy was evaluated against early-stage biofilms formed by two strains of *S. aureus*: Newman and SH1000, which differs from previous chapters that focused on 24-hours mature biofilms. This shift in experimental design was motivated by observations of heightened tolerance in these strains when exposed to CAP in mature biofilm models, suggesting that earlier-stage biofilms may represent a more vulnerable therapeutic target. By focusing on nascent biofilms, this study could identify critical windows for intervention, where H_2O_2-antibiotic synergies could disrupt biofilm formation before structural complexity and antimicrobial resistance mechanisms fully developed. The experiments were conducted using an *in vitro* biofilm model similar to previous chapter to assess the efficacy of these combined treatments. In essence, our study aimed to determine whether the addition of H_2O_2 could enhance the antibacterial activity of flucloxacillin and gentamicin against nascent *S. aureus* biofilms. This work nicely follows on from chapter 4 to further investigate potential synergy between H_2O_2, a potent antimicrobial agent generated via CAP, alongside antibiotics. Additionally, by utilising two distinct *S. aureus* strains, we sought to ascertain if the synergistic effects, if any, were consistent across different bacterial strains, particularly the differences in susceptibility profiles to H_2O_2 alone (at concentrations generated via CAP).

5.2.2.1 *S. aureus* (Newman) biofilm

Biofilms were grown in pre-sterilised polystyrene 96-well flat-bottom microtiter plates in LB broth and incubated at 37°C for 4 hours under aerobic conditions before treatment regimens were conducted as previously described in section 2.6.1. Biofilm metabolic activity was assessed using the AlamarBlue™ assay as previously described in 2.4.7. The efficacy of gentamicin against *S. aureus* Newman biofilms was evaluated both alone and in combination with H_2O_2 using various treatment strategies. As illustrated in (Figure 5.1A and Figure 5.1E), gentamicin alone demonstrated concentration-dependent effects on biofilm metabolic activity. Significant reductions were observed at higher concentrations, with 128 µg/mL and 64 µg/mL decreasing metabolic activity to 45.31% (****p< 0.0001) and 80.53% (**p< 0.01), respectively, compared to untreated (UT) controls. Lower concentrations did not yield significant reductions.

When examining simultaneous treatment with gentamicin and 1 mM H_2O_2 (Figure 5.1B and Figure 5.1E), enhanced antimicrobial efficacy was observed, particularly at higher gentamicin concentrations. Metabolic activity decreased to 37.20%, 39.57%, 70.48%, and 81.49% at 128, 64, 32, and 16 µg/mL, respectively, though statistical significance was not achieved. Pre-treatment with H_2O_2 followed by gentamicin exposure (Figure 5.1C and Figure 5.1E) further improved antibacterial effects, especially at higher gentamicin concentrations. Metabolic activity reduced to 14.89%, 27.90%, and 42.92% were observed at 128, 64, and 32 µg/mL, respectively, suggesting enhanced biofilm susceptibility to gentamicin, possibly due to matrix disruption or increased permeability. However, these reductions did not reach statistical significance.

Notably, the most pronounced reductions in metabolic activity were observed with gentamicin treatment followed by H_2O_2 post-treatment (Figure 5.1D and Figure 5.1E). Significant reductions were observed across a broader range of gentamicin concentrations (128 to 4 µg/mL): 128 µg/mL reduced metabolic activity to 16.39% (****p< 0.0001), 64 µg/mL reduced metabolic activity to 35.51% (****p< 0.0001), 32 µg/mL to 55.14% (***p< 0.001), 16 µg/mL to 56.29% (***p< 0.001), 8 µg/mL to 57.93% (***p< 0.001), and 4 µg/mL to 66.29% (**p< 0.01) compared to UT,

indicating that post-treatment with H_2O_2 particularly augments gentamicin's antibacterial effects.

A heatmap summarising percentage metabolic activity across all treatment conditions (Figure 5.1E) visually confirmed the superior efficacy of pre- and post-treatment protocols combining H_2O_2 with higher gentamicin concentrations, with post-treatment consistently yielding the lowest metabolic activity percentages. Taken together, these findings collectively demonstrate that while gentamicin alone shows dose-dependent efficacy against *S. aureus* Newman biofilms, its antibacterial activity is significantly enhanced when combined with H_2O_2, particularly as a post-treatment strategy. This underscores the importance of optimising treatment timing and combination approaches for effective biofilm eradication, in otherwise tolerant bacterial species.

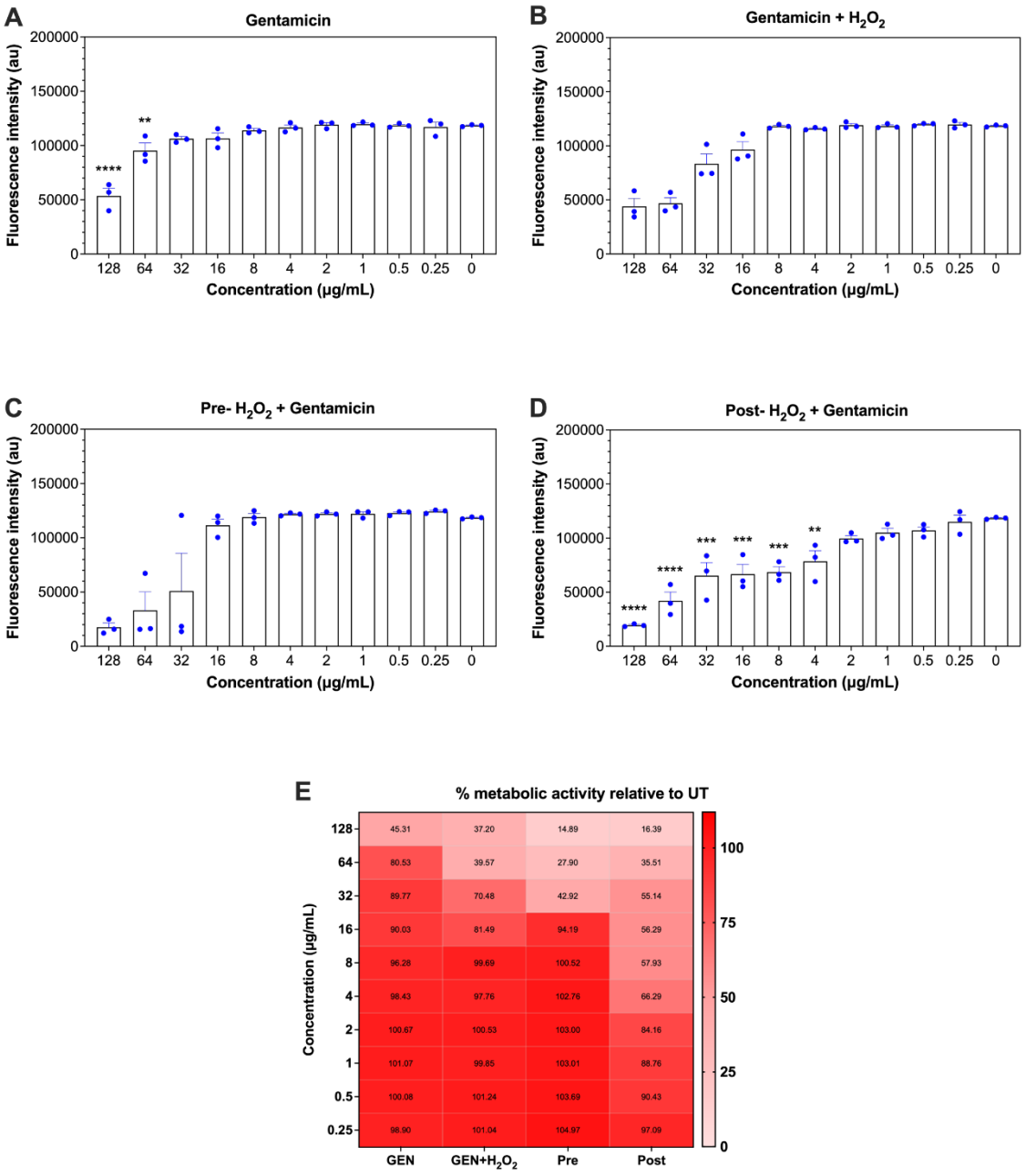

Figure 5.1: Metabolic activity and metabolic activity percentages of *S. aureus* Newman 4 h biofilms in relation to UT controls following combination treatment. *S. aureus* Newman biofilms were grown on 96 well flat bottom for 4 h in LB broth, then treated with gentamicin alone or in combination with 1 mM H_2O_2 for 24 h in panel A and B respectively, or either pre-treated with 1mM H_2O_2 for 10 mins followed by gentamicin for 24 h or treated with gentamicin for 24 h followed by 10 min post-treatment with 1 mM H_2O_2 in panel C and D respectively. Panel E heatmap shown percentages of metabolic activity across all treatment conditions. The effects of each treatment were assessed using the AlamarBlue™ metabolic activity assay. Fluorescence values were measured at (fluorescence excitation wavelength, 544_{nm}; fluorescence emission wavelength, 590_{nm}). Each bar represents the average of data obtained from three independent experiments. Error bars represent the standard error of the mean. Data distributions were assessed using Shapiro-Wilk normality test and then analysed by ANOVA with Dunnett's tests to determine the P-value for multiple comparisons of normally distributed data, unless the data of gentamicin in combination with 1 mM H_2O_2 and pre-treatment which analysed by Kruskal-Wallis with Dunn's tests for multiple comparisons of non-normally distributed data. * Indicates statistically significant differences (**p< 0.01, ***p< 0.001, ****p< 0.0001). Data without asterisks indicates; no statistically significant differences were observed.

The efficacy of flucloxacillin against *S. aureus* Newman biofilms was next evaluated using various treatment strategies, both as monotherapy and in combination with H_2O_2 as with gentamicin. As depicted in (Figure 5.2A and Figure 5.2E), flucloxacillin alone exhibited concentration-dependent antimicrobial activity against biofilm metabolic activity. At higher concentrations, significant reductions were observed, with 8, 4, and 2 µg/mL decreasing metabolic activity to 3.09%, 2.69%, and 2.99% respectively (all *p< 0.05) compared to UT controls. Additionally, lower concentrations of 1 and 0.5 µg/mL reduced metabolic activity to 10.44% and 26.02% respectively, and these reductions did not reach statistical significance. Flucloxacillin (as a ß-lactam antibiotic) demonstrated greater potency against *S. aureus* Newman biofilms compared to gentamicin (as an aminoglycoside antibiotic) due to its bactericidal mechanism targeting penicillin-binding proteins (PBPs), which disrupt cell wall synthesis in metabolically active cells-a vulnerability retained in biofilm microenvironments (Tuon et al., 2023, Fisher and Mobashery, 2021, Kapoor, Saigal and Elongavan, 2017). In contrast, gentamicin's reliance on aerobic conditions and ribosomal protein synthesis limits its efficacy against slow-growing or dormant biofilm populations, necessitating higher concentrations (Singh et al., 2022, Sharma et al., 2023, Kapoor, Saigal and Elongavan, 2017). Additionally, ß-lactams like flucloxacillin exhibit superior biofilm penetration and synergise with oxidative agents (e.g., H_2O_2) by destabilising the EPS, enhancing antimicrobial access-factors critical for eradicating biofilm-associated infections (Shnyoor and Zgair, 2024). These mechanistic and clinical advantages align with flucloxacillin's role as a first-line therapy for methicillin-sensitive *S. aureus* (MSSA) infections, while gentamicin remains limited to adjunctive use due to poor biofilm activity (Fisher and Mobashery, 2021, Menezes et al., 2019) (Senobar Tahaei et al., 2021; Parker et al., 2023).

When examining the simultaneous administration of flucloxacillin and 1 mM H_2O_2 (Figure 5.2B and Figure 5.2E), enhanced antimicrobial efficacy was observed, particularly at higher flucloxacillin concentrations. The combination therapy significantly reduced biofilm metabolic activity at 8, 4, and 2 µg/mL to 1.03%, 1.62%, and 1.71% respectively (all *p< 0.05) compared to UT controls. Furthermore, the combination therapy demonstrated dose-dependent effects at

lower concentrations, with metabolic activity decreasing to 2.43%, 4.70%, 7.64%, 19.78%, and 32.26% at 1, 0.5, 0.25, 0.125, and 0.0625 µg/mL respectively, though these reductions were not statistically significant. Notably, the sequential approach of pre-treating biofilms with 1 mM H_2O_2 followed by flucloxacillin exposure (Figure 5.2C and Figure 5.2E) yielded the most pronounced reductions in metabolic activity. This treatment strategy demonstrated improved antibacterial effects across a broader range of flucloxacillin concentrations (8 to 0.0625 µg/mL). Significant reductions were observed at 8 µg/mL (0%, **p< 0.01) and 4 µg/mL (0.25%, *p< 0.05). Moreover, metabolic activity was reduced to 0.37%, 4.63%, 1.55%, 2.45%, 4.92%, and 19.41% at 2, 1, 0.5, 0.25, 0.125, and 0.0625 µg/mL respectively, and these reductions did not achieve statistical significance.

The reverse sequential approach of flucloxacillin treatment followed by 1 mM H_2O_2 post-treatment (Figure 5.2D and Figure 5.2E) also demonstrated remarkable efficacy. This protocol produced significant reductions across a wider range of flucloxacillin concentrations (8 to 0.25 µg/mL). Metabolic activity was reduced to 1.54% at 8 µg/mL (****p< 0.0001), 2.08% at 4 µg/mL (****p< 0.0001), 1.76% at 2 µg/mL (****p< 0.0001), 4.99% at 1 µg/mL (****p< 0.0001), 24.78% at 0.5 µg/mL (***p< 0.001), and 55.84% at 0.25 µg/mL (*p< 0.05) compared to UT controls. The comprehensive heatmap visualisation (Figure 5.2E) effectively summarises percentage metabolic activity across all treatment conditions, visually confirming the superior efficacy of both simultaneous and sequential treatment protocols combining H_2O_2 with flucloxacillin. Among these, the pre-treatment approach consistently yielded the lowest metabolic activity percentages, suggesting this may be the most effective strategy for biofilm eradication.

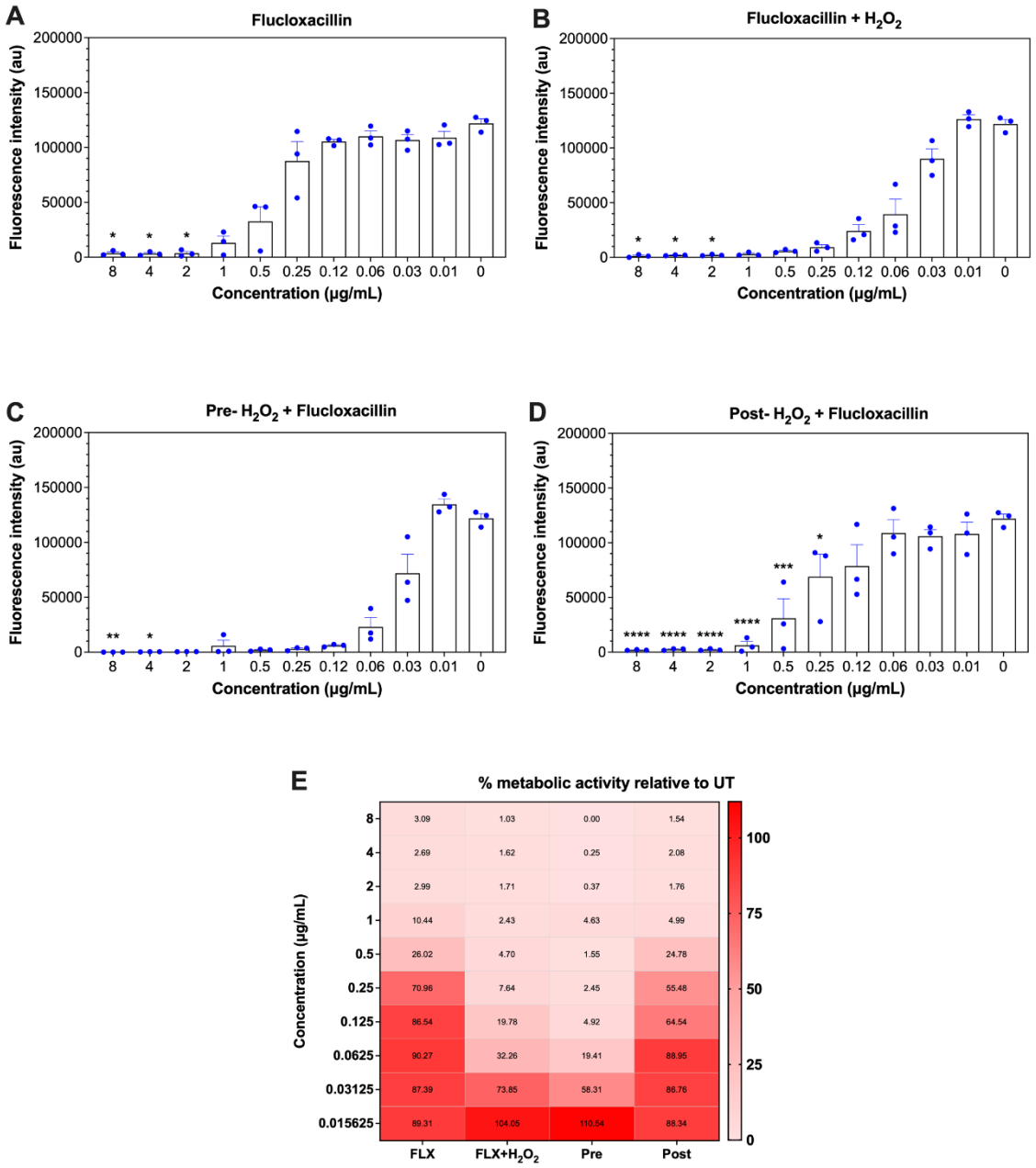

Figure 5.2: Metabolic activity and metabolic activity percentages of *S. aureus* Newman 4 h biofilms in relation to UT controls following combination treatment. *S. aureus* Newman biofilms were grown on 96 well flat bottom for 4 h in LB broth, then treated with flucloxacillin alone or in combination with 1 mM H_2O_2 for 24 h in panel A and B respectively, or either pre-treated with 1 mM H_2O_2 for 10 mins followed by flucloxacillin for 24 h or treated with flucloxacillin for 24 h followed by 10 min post-treatment with 1 mM H_2O_2 in panel C and D respectively. Panel E heatmap shown percentages of metabolic activity across all treatment conditions. The effects of each treatment were assessed using the AlamarBlue™ metabolic activity assay. Fluorescence values were measured at (fluorescence excitation wavelength, 544_{nm}; fluorescence emission wavelength, 590_{nm}). Each bar represents the average of data obtained from three independent experiments. Error bars represent the standard error of the mean. Data distributions were assessed using Shapiro-Wilk normality test and then analysed by ANOVA with Dunnett's tests to determine the P-value for multiple comparisons of normally distributed data, unless the data of flucloxacillin alone and in combination with 1 mM H_2O_2 which analysed by Kruskal-Wallis with Dunn's tests for multiple comparisons of non-normally distributed data. * Indicates statistically significant differences (*p< 0.05, **p< 0.01, ***p< 0.001. ****p< 0.0001). Data without asterisks indicates; no statistically significant differences were observed.

5.2.2.2 *S. aureus* (SH1000) biofilm

Next the *S. aureus* SH1000 biofilm was tested with the same combinational therapies. Biofilms were grown in pre-sterilised polystyrene 96-well flat-bottom microtiter plates in LB broth and incubated at 37°C for 4 hours under aerobic conditions before treatment regimens as previously described in section 2.6.1. Biofilm assessment was conducted using the AlamarBlue™ assay for metabolic activity quantification as previously described in 2.4.7.

The antimicrobial efficacy of gentamicin against *S. aureus* SH1000 biofilms was comprehensively evaluated using various treatment strategies, both as monotherapy and in combination with H_2O_2 as previously described for *S. aureus* Newman biofilms. As depicted in (Figure 5.3A and Figure 5.3E), gentamicin alone exhibited concentration-dependent antimicrobial activity against biofilm metabolic activity. At higher concentrations, significant reductions were observed, with 128 and 64 µg/mL decreasing metabolic activity to 11.43% (*p< 0.05) and 15.37% (*p< 0.05) respectively, compared to UT controls. Additionally, lower concentrations of 32, 16, 8, 4, and 2 µg/mL reduced metabolic activity to 15.61%, 20.03%, 49.64%, 62.70%, and 70.68% respectively, and these reductions did not reach statistical significance.

When examining the simultaneous administration of gentamicin and 1 mM H_2O_2 (Figure 5.3B and Figure 5.3E), enhanced antimicrobial efficacy was observed across a broader concentration range. This combination therapy significantly reduced biofilm metabolic activity at multiple concentrations: 128 µg/mL (11.81%, ****p< 0.0001), 64 µg/mL (12.64%, ****p< 0.0001), 32 µg/mL (14.15%, ****p< 0.0001), 16 µg/mL (19.39%, ****p< 0.0001), 8 µg/mL (44.30%, ****p< 0.0001), 4 µg/mL (49.62%, ***p< 0.001), 2 µg/mL (62.46%, **p< 0.01), and 1 µg/mL (71.51%, *p< 0.05) compared to UT controls. Furthermore, even lower concentrations of 0.5 and 0.25 µg/mL reduced biofilm metabolic activity to 78.46% and 85.82% respectively, though these reductions did not achieve statistical significance.

Furthermore, the sequential approach of pre-treating biofilms with 1 mM H_2O_2 followed by gentamicin exposure (Figure 5.3C and Figure 5.3E) demonstrated improved antimicrobial efficacy across a concentration range of 128 to 2 µg/mL.

A significant reduction was observed at 128 µg/mL (11.26%, *p< 0.05). Moreover, concentrations of 64, 32, 16, 8, 4, and 2 µg/mL reduced metabolic activity to 13.15%, 14.28%, 13.23%, 45.18%, 60.29%, and 68.27% respectively, and these reductions did not reach statistical significance.

Notably, the most pronounced reductions in metabolic activity were achieved with the reverse sequential approach of gentamicin treatment followed by 1 mM H_2O_2 post-treatment (Figure 5.3D and Figure 5.3E). This protocol demonstrated significant efficacy at higher gentamicin concentrations: 128 µg/mL reduced metabolic activity to 10.72% (**p < 0.01) and 64 µg/mL to 12.08% (*p < 0.05) compared to UT controls. The heatmap visualisation in (Figure 5.3E) effectively illustrates the percentages of metabolic activity across all treatment conditions, confirming that all combination approaches substantially enhanced the antimicrobial efficacy of gentamicin, with the post-treatment protocol demonstrating effectiveness at the lowest concentrations tested.

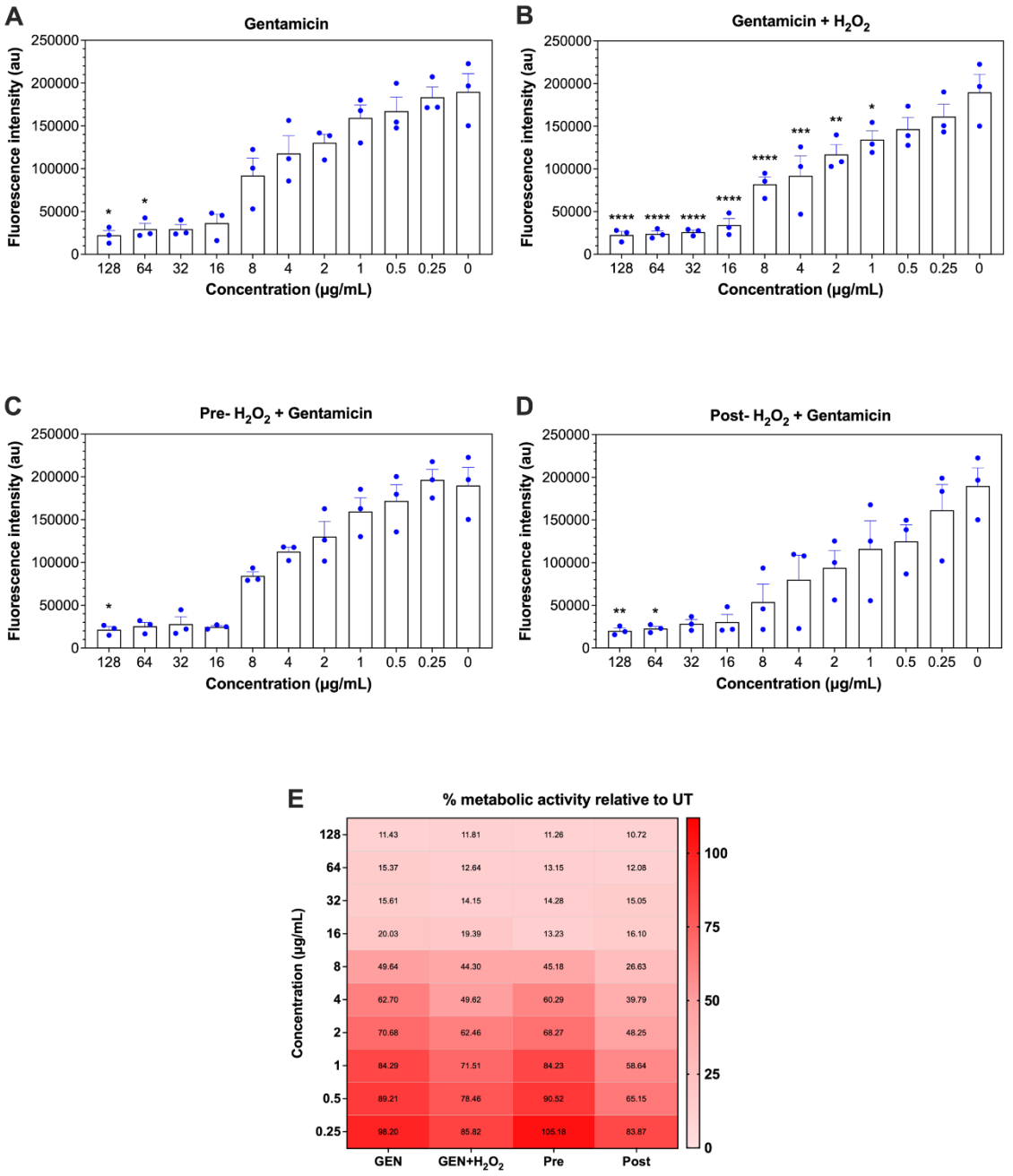

Figure 5.3: Metabolic activity and metabolic activity percentages of *S. aureus* SH1000 4 h biofilms in relation to UT controls following combination treatment. *S. aureus* SH1000 biofilms were grown on 96 well flat bottom for 4 h in LB broth, then treated with gentamicin alone or in combination with 1 mM H_2O_2 for 24 h in panel A and B respectively, or either pre-treated with H_2O_2 for 10 mins followed by gentamicin for 24 h or treated with gentamicin for 24 h followed by 10 min post-treatment with H_2O_2 in panel C and D respectively. Panel E heatmap shown percentages of metabolic activity across all treatment conditions. The effects of each treatment were assessed using the AlamarBlue™ metabolic activity assay. Fluorescence values were measured at (fluorescence excitation wavelength, 544_{nm}; fluorescence emission wavelength, 590_{nm}). Each bar represents the average of data obtained from two independent experiments. Error bars represent the standard error of the mean. Data distributions were assessed using Shapiro-Wilk normality test and then analysed by Kruskal-Wallis with Dunn's tests to determine the P-value for multiple comparisons of non-normally distributed data, unless the data of gentamicin in combination with 1 mM H_2O_2 which analysed by ANOVA with Dunnett's tests for multiple comparisons of normally distributed data. * Indicates statistically significant differences (*p< 0.05, **p< 0.01, ***p< 0.001, ****p< 0.0001). Data without asterisks indicates; no statistically significant differences were observed.

The efficacy of flucloxacillin against *S. aureus* SH1000 biofilms was comprehensively evaluated using various treatment strategies, both as monotherapy and in combination with H_2O_2. As depicted in (Figure 5.4A and Figure 5.4E), flucloxacillin alone exhibited concentration-dependent antimicrobial activity against biofilm metabolic activity. At concentrations of 4 and 1 µg/mL, significant reductions in metabolic activity to 5.42% (*p< 0.05) and 9.21% (*p< 0.05) respectively were observed compared to UT controls. Additionally, concentrations of 8, 2, 0.5, 0.25 and 0.125 µg/mL reduced metabolic activity to 7.07%, 9.40%, 15.83%, 46.67% and 67.84% respectively, and these reductions did not reach statistical significance.

When examining the simultaneous administration of flucloxacillin and 1 mM H_2O_2 (Figure 5.4B and Figure 5.4E), enhanced antimicrobial efficacy was observed across a broader concentration range. This combination therapy significantly reduced biofilm metabolic activity at multiple concentrations: 8 µg/mL (9.07%, ****p< 0.0001), 4 µg/mL (6.24%, ****p< 0.0001), 2 µg/mL (6.77%, ****p< 0.0001), 1 µg/mL (3.33%, ****p< 0.0001), 0.5 µg/mL (15.97%, ****p< 0.0001), 0.25 µg/mL (31.01%, ****p< 0.0001), 0.125 µg/mL (56.68%, ***p< 0.001), and 0.0625 µg/mL (72.38%, *p< 0.05) compared to UT controls. Furthermore, the sequential approach of pre-treating biofilms with 1 mM H_2O_2 followed by flucloxacillin exposure (Figure 5.4C and Figure 5.4E) demonstrated similar efficacy. This treatment protocol produced significant reductions across multiple concentrations: 8 µg/mL (5.78%, ****p< 0.0001), 4 µg/mL (10.34%, ****p< 0.0001), 2 µg/mL (6.16%, ****p< 0.0001), 1 µg/mL (8.02%, ****p< 0.0001), 0.5 µg/mL (11.06%, ****p< 0.0001), 0.25 µg/mL (39.02%, ****p< 0.0001), and 0.125 µg/mL (57.31%, ***p< 0.001).

Notably, the most pronounced reductions in metabolic activity were achieved with the reverse sequential approach of flucloxacillin treatment followed by 1 mM H_2O_2 post-treatment (Figure 5.4D and Figure 5.4E). This protocol demonstrated significant efficacy across the widest range of concentrations (8 to 0.03125 µg/mL): 8 µg/mL (6.40%, ****p< 0.0001), 4 µg/mL (6.45%, ****p< 0.0001), 2 µg/mL (9.07%, ****p< 0.0001), 1 µg/mL (5.82%,****p< 0.0001), 0.5 µg/mL (9.52%, ****p< 0.0001), 0.25 µg/mL (41.83%, ****p< 0.0001), 0.125 µg/mL (59.97%, ***p< 0.001),

0.0625 µg/mL (67.54%, **p< 0.01), and 0.03125 µg/mL (78.72%, *p< 0.05) compared to UT controls. The heatmap visualisation in (Figure 5.4E) effectively illustrates the percentages of metabolic activity across all treatment conditions, confirming that all combination approaches substantially enhanced the antimicrobial efficacy of flucloxacillin, with the post-treatment protocol demonstrating effectiveness at the lowest concentrations tested. Taken together the results from sections 5.2.2.1 and 5.2.2.2 show that H_2O_2 significantly enhances the efficacy of both gentamicin and flucloxacillin against early-stage *S. aureus* biofilms, with treatment timing and antibiotic class critically influencing outcomes.

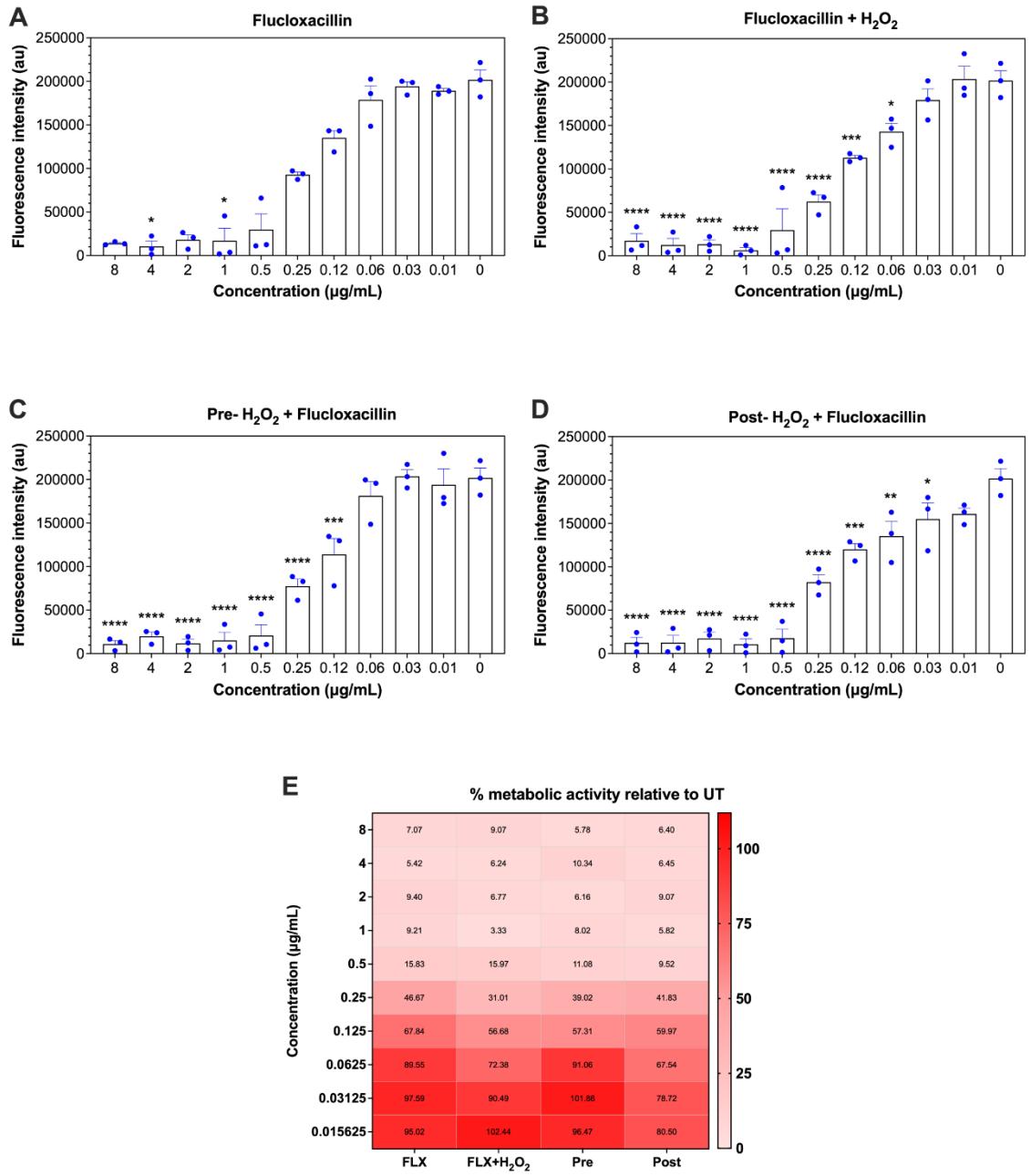

Figure 5.4: Metabolic activity and metabolic activity percentages of *S. aureus* SH1000 4 h biofilms in relation to UT controls following combination treatment. *S. aureus* SH1000 biofilms were grown on 96 well flat bottom for 4 h in LB broth, then treated with flucloxacillin alone or in combination with 1 mM H_2O_2 for 24 h in panel A and B respectively, or either pre-treated with H_2O_2 for 10 mins followed by flucloxacillin for 24 h or treated with flucloxacillin for 24 h followed by 10 min post-treatment with H_2O_2 in panel C and D respectively. Panel E heatmap shown percentages of metabolic activity across all treatment conditions. The effects of each treatment were assessed using the AlamarBlue™ metabolic activity assay. Fluorescence values were measured at (fluorescence excitation wavelength, 544_{nm}; fluorescence emission wavelength, 590_{nm}). Each bar represents the average of data obtained from three independent experiments. Error bars represent the standard error of the mean. Data distributions were assessed using Shapiro-Wilk normality test and then analysed by ANOVA with Dunnett's tests to determine the P-value for multiple comparisons of normally distributed data, unless the data of flucloxacillin alone which analysed by Kruskal-Wallis with Dunn's tests for multiple comparisons of non-normally distributed data. * Indicates statistically significant differences (*p< 0.05, **p< 0.01, ***p< 0.001. ****p< 0.0001). Data without asterisks indicates; no statistically significant differences were observed.

5.2.3 Viability of early-stage *S. aureus* biofilms

Metabolic activity assessment does not always correlate with cellular viability; cells may be metabolically dormant, yet possess the ability to regrow in the appropriate conditions when antimicrobial intervention is halted (Trinh and Lee, 2022, Zou et al., 2022). This could be concerning from a clinical standpoint, if the infectious source is not removed, or completely killed. Therefore, for the next sections, early-stage *S. aureus* biofilms were cultivated in sterilised 96-well plates for 4 hours at 37°C under aerobic conditions then treated for colony forming unit (CFU) counts as a measure of viability. Strain-specific antibiotic treatments were applied: *S. aureus* Newman received gentamicin (128 and 64 µg/mL) or flucloxacillin (0.25 and 0.0625 µg/mL), while *S. aureus* SH1000 was treated with gentamicin (8 and 2 µg/mL) or flucloxacillin (0.25 and 0.125 µg/mL). These antibiotic concentrations were selected based on their ability to reduce biofilm metabolic activity by ≤50% and were administered either alone or combined with 1 mM H_2O_2 following protocols from section 2.6.1. Log_{10} CFU/mL values were calculated for each sample following overnight incubation at 37°C aerobically.

5.2.3.1 *S. aureus* (Newman) biofilm

S. aureus Newman biofilms were cultivated in sterilised 96-well flat-bottom plates for 4 hours in LB broth and subsequently subjected to various treatment regimens. These included exposure to 1 mM H_2O_2 alone, gentamicin monotherapy at (128 and 64 µg/mL) or flucloxacillin (0.25 and 0.0625 µg/mL), or combination approaches. The combination strategies consisted of simultaneous application of gentamicin or flucloxacillin with 1 mM H_2O_2 for 24 hours; sequential treatment with H_2O_2 (10-minute pre-treatment) followed by gentamicin or flucloxacillin (24 hours); or the reverse sequence of gentamicin or flucloxacillin (24 hours) followed by H_2O_2 (10-minute post-treatment). Antimicrobial efficacy was quantified using viable plate counting method, with results presented as log_{10} CFU/mL and log_{10} reductions relative to UT control biofilms as earlier detailed in methods section 2.6.2. The results in (Figure 5.5) presents an analysis of the antimicrobial efficacy of gentamicin against *S. aureus* Newman biofilms, both alone and in combination with H_2O_2.

(Figure 5.5A) displays the bacterial viability data expressed as log_{10} CFU/mL across various treatment conditions. The UT control and H_2O_2 alone treatments show comparable bacterial counts of approximately 8-log_{10} CFU/mL, indicating that H_2O_2 alone, at concentrations produced by the CAP (chapter 3) had minimal impact on biofilm viability. In contrast, gentamicin at 128 µg/mL demonstrated substantial antimicrobial activity, reducing bacterial counts to approximately 4.8-log_{10} CFU/mL when used alone (No H_2O_2). This efficacy was significantly enhanced when combined with H_2O_2 simultaneously, achieving a reduction to approximately 3-log_{10} CFU/mL (**$p < 0.01$). The pre-treatment and post-treatment approaches yielded intermediate reductions to approximately 4.0-log_{10} CFU/mL, though these differences were not statistically significant compared to gentamicin alone. When examining the lower concentration of gentamicin (64 µg/mL), all treatment regimens demonstrated comparable efficacy. Gentamicin alone (No H_2O_2) reduced counts to approximately 5.2-log_{10} CFU/mL, whilst the simultaneous, pre-treatment, and post-treatment approaches with H_2O_2 achieved reductions to approximately 4.1-log_{10}, 4.2-log_{10}, and 4.7-log_{10} CFU/mL, respectively. Notably, no statistically significant differences were observed between these treatment strategies at the lower gentamicin concentration.

(Figure 5.5B) presents a heatmap visualising the log_{10} reductions relative to UT controls, with darker red indicating greater antimicrobial efficacy. This visualisation confirms that H_2O_2 alone had minimal effect (0.1-log_{10} reduction). For gentamicin at 128 µg/mL, the simultaneous treatment achieved the greatest log_{10} reduction (5.3-log_{10}), followed by pre-treatment (4.3-log_{10}), post-treatment (4.0-log_{10}), and gentamicin alone (3.5-log_{10}). At the lower concentration of 64 µg/mL, the pre-treatment approach demonstrated slightly superior efficacy (4.1-log_{10} reduction), followed by simultaneous treatment (4.0-log_{10}), post-treatment (3.5-log_{10}), and gentamicin alone (3.1-log_{10}). These findings collectively demonstrate that combining gentamicin with H_2O_2 enhances its antimicrobial efficacy against *S. aureus* Newman biofilms, particularly at higher antibiotic concentrations. The simultaneous application of gentamicin and H_2O_2 yielded the most substantial reduction in bacterial viability at 128 µg/mL.

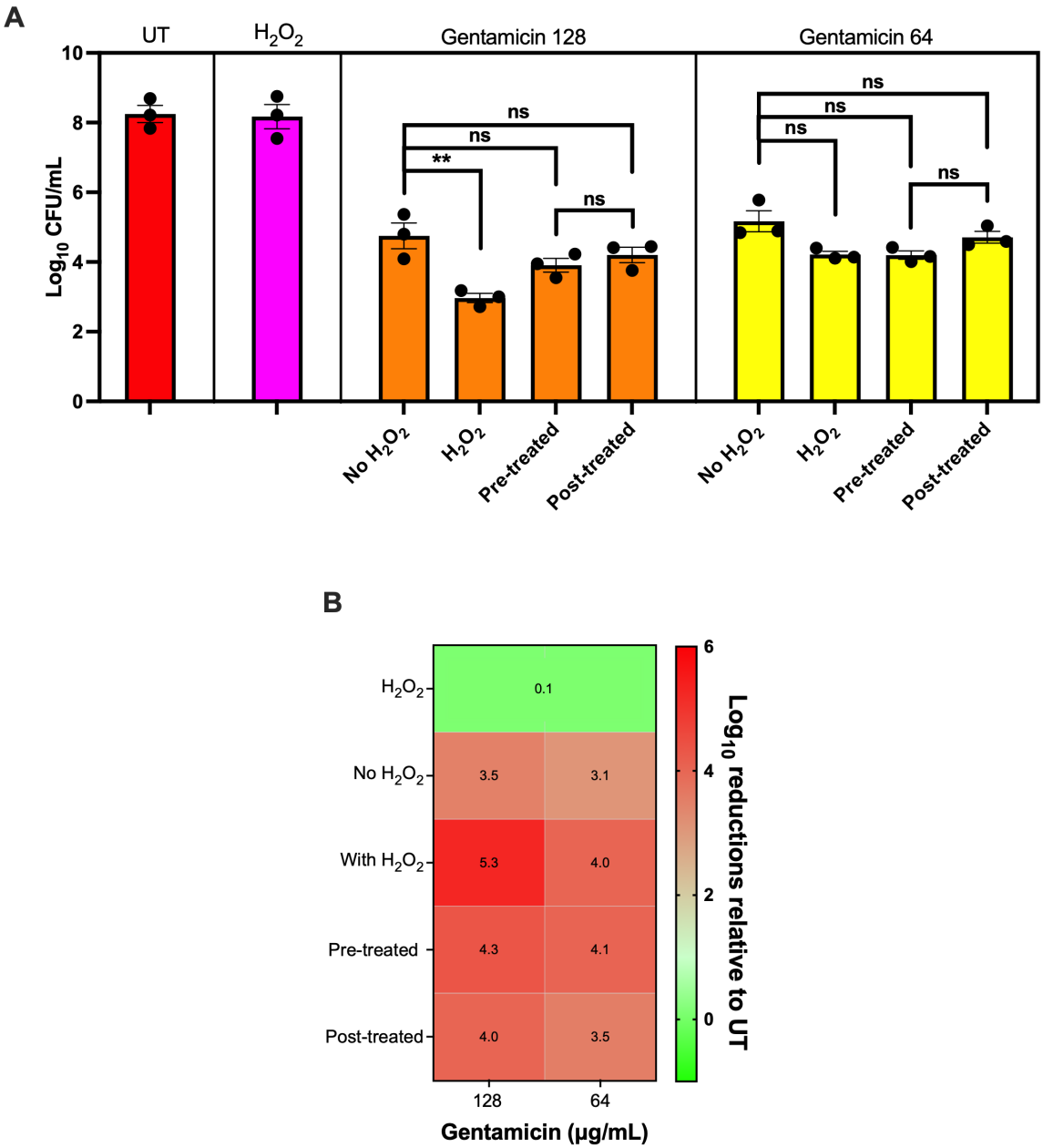

Figure 5.5: CFU and log$_{10}$ reduction in a heat map of *S. aureus* Newman 4 h biofilms in relation to UT controls following combination treatment. *S. aureus* Newman biofilms were grown on 96 well flat bottom for 4 h in LB broth, then treated with 1 mM H_2O_2 alone, or with two concentrations of gentamicin (128 and 64 µg/mL) alone or in combination with 1 mM H_2O_2 for 24 h, or either pre-treated with H_2O_2 for 10 mins followed by gentamicin for 24 h or treated with gentamicin for 24 h followed by 10 min post-treatment with H_2O_2. The effects of each treatment were assessed using the viable plate counting technique, and the results expressed as **log$_{10}$** CFU/mL (A). Panel B shows **log$_{10}$** reduction in a heat map of each treatment relative to UT biofilms. Each bar represents the average of data obtained from three independent experiments. Error bars represent the standard error of the mean. Data distributions were assessed using Shapiro-Wilk normality test and then analysed by ANOVA with Dunnett's tests to determine the P-value for multiple comparisons of normally distributed data. * Indicates statistically significant differences (**p< 0.01). Ns indicates; no statistically significant differences were observed.

The results in (Figure 5.6) presents a detailed analysis of the antimicrobial efficacy of flucloxacillin against *S. aureus* Newman biofilms, both alone and in combination

with H_2O_2. (Figure 5.6A) displays the bacterial viability data expressed as log_{10} CFU/mL across various treatment conditions. The UT control and H_2O_2 alone treatments show comparable bacterial counts of approximately 8-log_{10} CFU/mL, indicating that H_2O_2 alone had minimal impact on biofilm viability. In contrast, flucloxacillin at 0.25 µg/mL demonstrated notable antimicrobial activity, reducing bacterial counts to approximately 6.3-log_{10} CFU/mL when used alone (No H_2O_2). This efficacy was further enhanced when combined with H_2O_2, achieving a reduction to approximately 4.7-log_{10} CFU/mL. The pre-treatment approach (H_2O_2 followed by flucloxacillin) yielded the most substantial reduction to approximately 4.1-log_{10} CFU/mL, whilst the post-treatment approach (flucloxacillin followed by H_2O_2) showed slightly less efficacy with counts of approximately 5.2-log_{10} CFU/mL. However, these differences between flucloxacillin 0.25 µg/mL treatment regimens did not reach statistical significance.

When examining the lower concentration of flucloxacillin (0.0625 µg/mL), a different pattern emerged. The flucloxacillin monotherapy (No H_2O_2) showed reduced efficacy compared to the higher concentration, with bacterial counts of approximately 7.5-log_{10} CFU/mL. Notably, all combination approaches with H_2O_2 significantly enhanced the antimicrobial activity at this lower concentration, with exception of Post-treatment approach. The simultaneous treatment (With H_2O_2) reduced counts to approximately 5.5-log_{10} CFU/mL (**$p < 0.01$), whilst the pre-treatment approach achieved the greatest reduction to approximately 4.8-log_{10} CFU/mL (***$p < 0.001$). Interestingly, the post-treatment approach was less effective than the pre-treatment approach (*$p < 0.05$), with counts of approximately 6.5-log_{10} CFU/mL.

(Figure 5.6B) presents a heatmap visualising the log_{10} reductions relative to UT controls, with darker red indicating greater antimicrobial efficacy. This visualisation confirms that H_2O_2 alone had minimal effect (0.1-log_{10} reduction). For flucloxacillin at 0.25 µg/mL, the pre-treatment approach achieved the greatest log_{10} reduction (4.2-log_{10}), followed by simultaneous treatment (3.6-log_{10}), post-treatment (3.1-log_{10}), and flucloxacillin alone (2.0-log_{10}). At the lower concentration of 0.0625 µg/mL, the pre-treatment approach again demonstrated

superior efficacy (3.5-log_{10} reduction), followed by simultaneous treatment (2.7-log_{10}), post-treatment (1.7-log_{10}), and flucloxacillin alone (0.8-log_{10}).

These findings collectively demonstrate that combining flucloxacillin with H_2O_2 significantly enhances its antimicrobial efficacy against *S. aureus* Newman biofilms. Furthermore, the pre-treatment approach consistently yielded the most substantial reductions in bacterial viability, findings that corroborated with those from the Alamarblue™ assay suggesting this sequential strategy may be optimal for biofilm eradication.

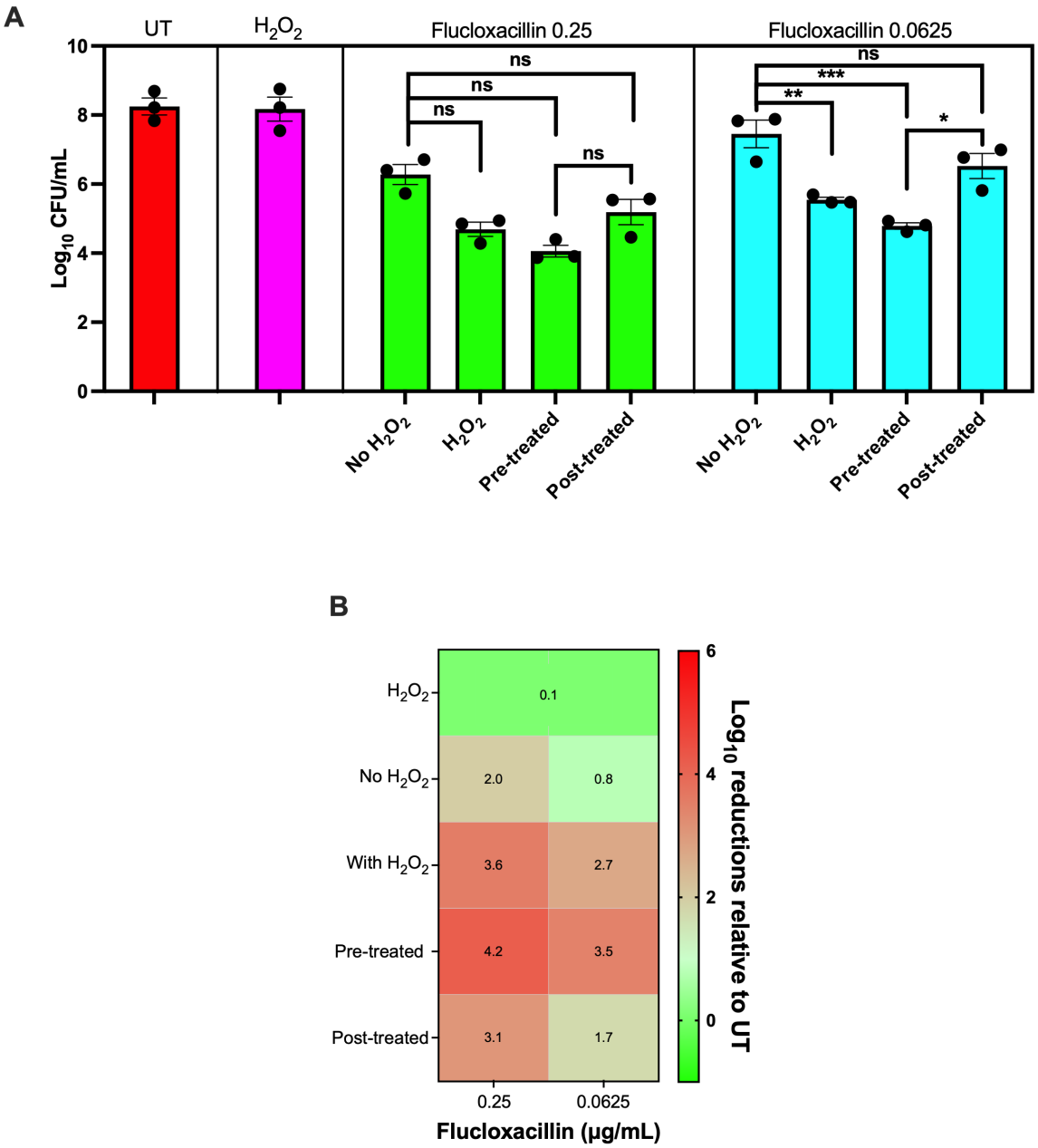

Figure 5.6: CFU and log$_{10}$ reduction in a heat map of *S. aureus* Newman 4 h biofilms in relation to UT controls following combination treatment. *S. aureus* Newman biofilms were grown on 96 well flat bottom for 4 h in LB broth, then treated with 1 mM H_2O_2 alone, or with two concentrations of flucloxacillin (0.25 and 0.0625 µg/mL) alone or in combination with 1 mM H_2O_2 for 24 h, or either pre-treated with H_2O_2 for 10 mins followed by flucloxacillin for 24 h or treated with flucloxacillin for 24 h followed by 10 min post-treatment with H_2O_2. The effects of each treatment were assessed using the viable plate counting technique, and the results expressed as **log$_{10}$** CFU/mL (A). Panel B shows **log$_{10}$** reduction in a heat map of each treatment relative to UT biofilms. Each bar represents the average of data obtained from three independent experiments. Error bars represent the standard error of the mean. Data distributions were assessed using Shapiro-Wilk normality test and then analysed by ANOVA with Dunnett's tests to determine the P-value for multiple comparisons of normally distributed data, unless the data of Flucloxacillin 0.0625 which analysed by Kruskal-Wallis with Dunn's tests for multiple comparisons of non-normally distributed data. * Indicates statistically significant differences (*p< 0.05, **p< 0.01, ***p< 0.001). Ns indicates; no statistically significant differences were observed.

5.2.3.2 *S. aureus* (SH1000) biofilm

The final set of experiments involved the other strain of *S. aureus* SH1000 biofilms. These were cultivated in the same way and subsequently subjected to various treatment regimens. These included exposure to 1 mM H_2O_2 alone, gentamicin monotherapy at (8 and 2 µg/mL) or flucloxacillin (0.25 and 0.125 µg/mL), or combination approaches. The combination strategies consisted of simultaneous application of gentamicin or flucloxacillin with 1 mM H_2O_2 for 24 hours; sequential treatment with H_2O_2 (10-minute pre-treatment) followed by gentamicin or flucloxacillin (24 hours); or the reverse sequence of gentamicin or flucloxacillin (24 hours) followed by H_2O_2 (10-minute post-treatment). Antimicrobial efficacy was quantified using viable plate counting method, with results presented as $\log_{10}$ CFU/mL and $\log_{10}$ reductions relative to UT control biofilms as earlier detailed in methods section 2.6.2.

The results in (Figure 5.7) presents a complete analysis of the antimicrobial efficacy of gentamicin against *S. aureus* SH1000 biofilms, both alone and in combination with H_2O_2. (Figure 5.7A) displays the bacterial viability data expressed as $\log_{10}$ CFU/mL across various treatment conditions. The UT control and H_2O_2 alone treatments show comparable bacterial counts of approximately 8.3-$\log_{10}$ CFU/mL, indicating that H_2O_2 alone had minimal impact on biofilm viability. In contrast, gentamicin at 8 µg/mL demonstrated modest antimicrobial activity, reducing bacterial counts to approximately 7.7-$\log_{10}$ CFU/mL when used alone (No H_2O_2). When combined with H_2O_2 simultaneously, there was a slight enhancement in efficacy, with counts reduced to approximately 7.3-$\log_{10}$ CFU/mL. The pre-treatment and post-treatment approaches yielded similar reductions to approximately 7.6-$\log_{10}$ and 7.6-$\log_{10}$ CFU/mL, respectively. Notably, none of these differences reached statistical significance.

When examining the lower concentration of gentamicin (2 µg/mL), all treatment regimens demonstrated comparable and limited efficacy. Gentamicin alone (No H_2O_2) reduced counts to approximately 7.9-$\log_{10}$ CFU/mL, whilst the simultaneous, pre-treatment, and post-treatment approaches with H_2O_2 achieved similar reductions to approximately 7.8-$\log_{10}$, 7.9-$\log_{10}$, and 7.7-$\log_{10}$ CFU/mL,

respectively. As with the higher gentamicin concentration, no statistically significant differences were observed between these treatment strategies.

(Figure 5.7B) presents a heatmap visualising the log_{10} reductions relative to UT controls, with darker red indicating greater antimicrobial efficacy. This visualisation confirms that H_2O_2 alone had a slight negative effect (-0.1-log_{10} reduction), potentially indicating a minor increase in bacterial counts. For gentamicin at 8 µg/mL, the simultaneous treatment achieved the greatest log_{10} reduction (1.0-log_{10}), followed by post-treatment (0.8-log_{10}), whilst pre-treatment and gentamicin alone both showed identical efficacy (0.6-log_{10} reduction). At the lower concentration of 2 µg/mL, the post-treatment approach demonstrated marginally superior efficacy (0.6-log_{10} reduction), followed by gentamicin alone and simultaneous treatment (both 0.4-log_{10}), and pre-treatment (0.3-log_{10}).

These findings collectively demonstrate that combining gentamicin with H_2O_2 provides only modest enhancement of antimicrobial efficacy against *S. aureus* SH1000 biofilms, with no statistically significant improvements observed. The simultaneous application of gentamicin and H_2O_2 yielded the most substantial reduction in bacterial viability at 8 µg/mL. However, the overall limited efficacy against this particular strain suggests that alternative treatment strategies may be necessary for effectively targeting *S. aureus* SH1000 biofilms.

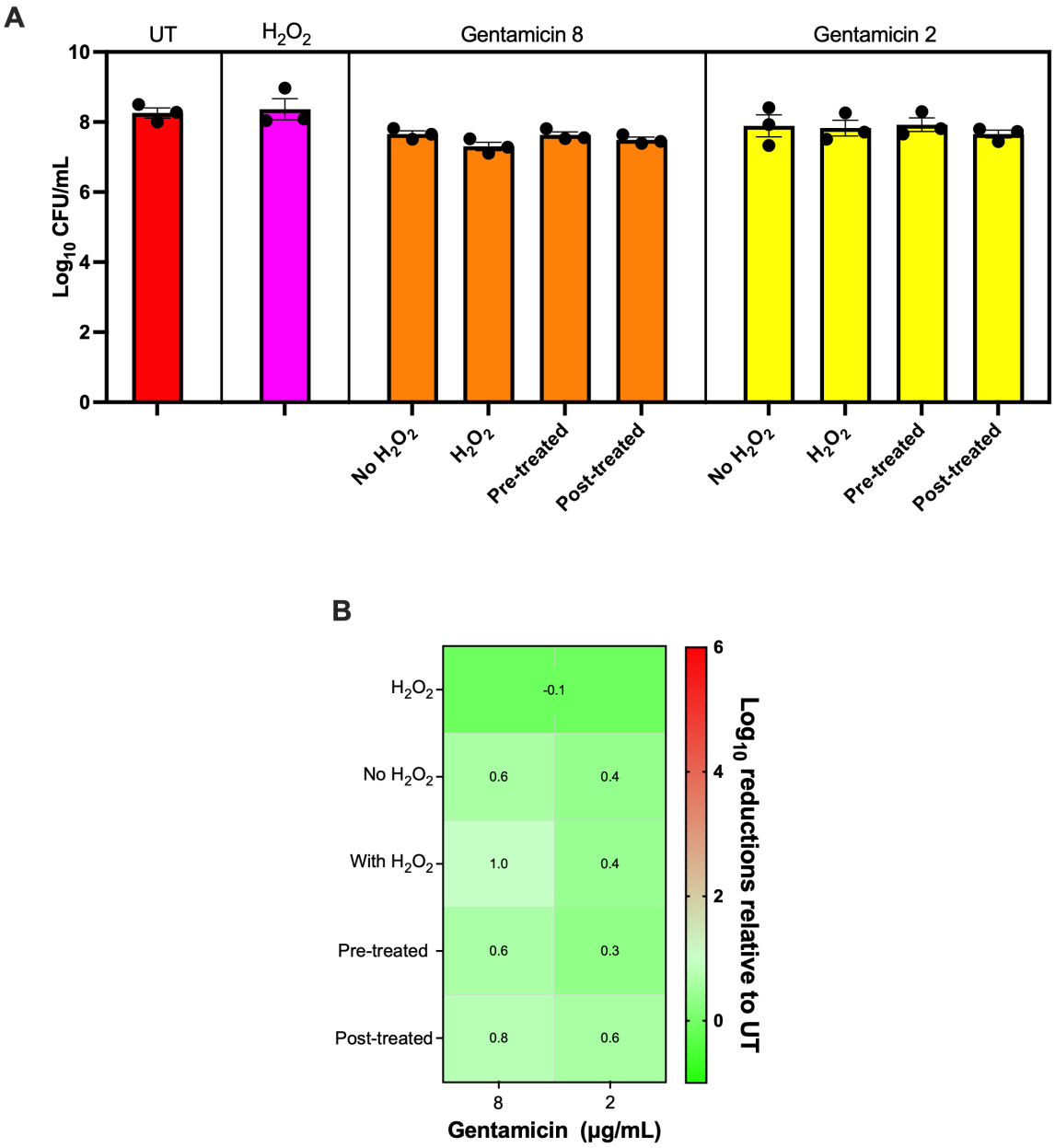

Figure 5.7: CFU and log_{10} reduction in a heat map of *S. aureus* SH1000 4 h biofilms in relation to UT controls following combination treatment. *S. aureus* SH1000 biofilms were grown on 96 well flat bottom for 4 h in LB broth, then treated with 1 mM H_2O_2 alone, or with two concentrations of gentamicin (8 and 2 µg/mL) alone or in combination with 1 mM H_2O_2 for 24 h, or either pre-treated with H_2O_2 for 10 mins followed by gentamicin for 24 h or treated with gentamicin for 24 h followed by 10 min post-treatment with H_2O_2. The effects of each treatment were assessed using the viable plate counting technique, and the results expressed as **log_{10}** CFU/mL (A). Panel B shows **log_{10}** reduction in a heat map of each treatment relative to UT biofilms. Each bar represents the average of data obtained from three independent experiments. Error bars represent the standard error of the mean. Data distributions were assessed using Shapiro-Wilk normality test and then analysed by ANOVA with Dunnett's tests to determine the P-value for multiple comparisons of normally distributed data. No statistically significant differences were observed.

(Figure 5.8) showcases a detailed evaluation of flucloxacillin's antibacterial effectiveness against *S. aureus* SH1000 biofilms, examining its performance both as monotherapy and in combination therapy with H_2O_2. (Figure 5.8A) displays the

bacterial viability data expressed as log_{10} CFU/mL across various treatment conditions. The UT control and H_2O_2 alone treatments show comparable bacterial counts of approximately 8.3-log_{10} CFU/mL, indicating that H_2O_2 alone had minimal impact on biofilm viability. In contrast, flucloxacillin at 0.25 µg/mL demonstrated substantial antimicrobial activity, reducing bacterial counts to approximately 6.1-log_{10} CFU/mL when used alone (No H_2O_2). Interestingly, when combined with H_2O_2 simultaneously, there was a slight decrease in efficacy, with counts increasing to approximately 6.5-log_{10} CFU/mL. The pre-treatment and post-treatment approaches yielded similar results to the simultaneous treatment, with counts of approximately 6.3-log_{10} and 6.2-log_{10} CFU/mL, respectively. Notably, none of these differences reached statistical significance.

When assessing the effect of flucloxacillin at the lower concentration of (0.125 µg/mL), all treatment regimens demonstrated comparable efficacy. Flucloxacillin alone (No H_2O_2) reduced counts to approximately 5.9-log_{10} CFU/mL, whilst the simultaneous, pre-treatment, and post-treatment approaches with H_2O_2 achieved similar reductions to approximately 6.1-log_{10}, 6.6-log_{10}, and 6.2-log_{10} CFU/mL, respectively. As with the higher flucloxacillin concentration, no statistically significant differences were observed between these treatment strategies.

(Figure 5.8B) displays a heatmap illustrating the log_{10} reduction values compared to UT controls, with darker red indicating greater antimicrobial efficacy. This visualisation confirms that H_2O_2 alone had a slight negative effect (-0.1-log_{10} reduction), potentially indicating a minor increase in bacterial counts. For flucloxacillin at 0.25 µg/mL, treatment with flucloxacillin alone achieved the greatest log_{10} reduction (2.2-log_{10}), followed by post-treatment (2.1-log_{10}), pre-treatment (1.9-log_{10}), and simultaneous treatment with H_2O_2 (1.7-log_{10}). At the lower concentration of 0.125 µg/mL, flucloxacillin alone and post-treatment both demonstrated superior efficacy (2.4-log_{10} and 2.1-log_{10} reductions, respectively), followed by simultaneous treatment (2.0-log_{10}) and pre-treatment (1.7-log_{10}).

Together, these results indicate that adding H_2O_2 to flucloxacillin does not improve its antimicrobial effectiveness against *S. aureus* SH1000 biofilms.–These results highlight the strain-specific nature of antimicrobial responses and

underscore the importance of tailored treatment approaches for different *S. aureus* strains in biofilm-associated infections.

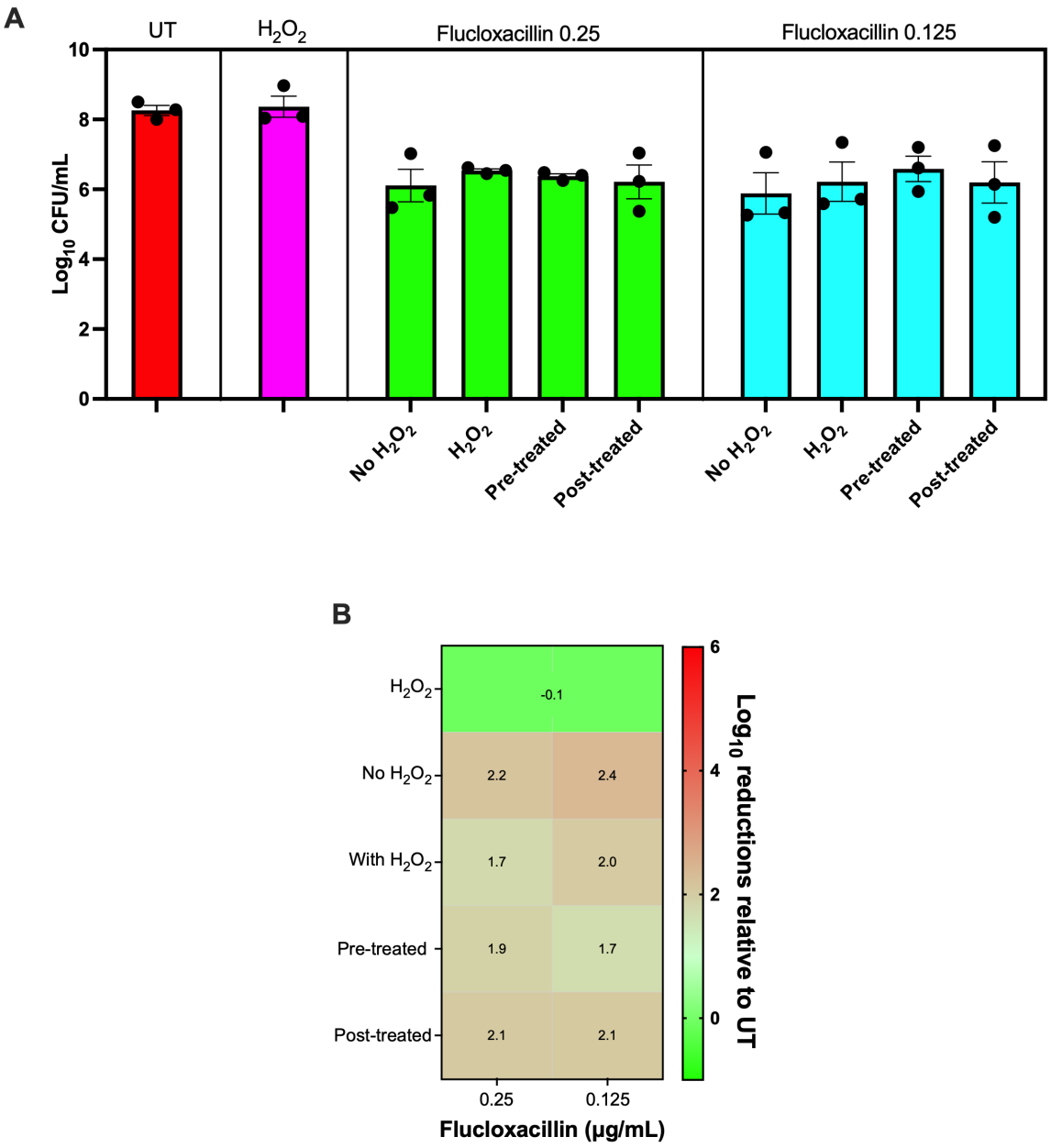

Figure 5.8: CFU and log_{10} reduction in a heat map of *S. aureus* SH1000 4 h biofilms in relation to UT controls following combination treatment. *S. aureus* SH1000 biofilms were grown on 96 well flat bottom for 4 h in LB broth, then treated with 1 mM H_2O_2 alone, or with two concentrations of flucloxacillin (0.25 and 0.125 µg/mL) alone or in combination with 1 mM H_2O_2 for 24 h, or either pre-treated with H_2O_2 for 10 mins followed by flucloxacillin for 24 h or treated with flucloxacillin for 24 h followed by 10 min post-treatment with H_2O_2. The effects of each treatment were assessed using the viable plate counting technique, and the results expressed as **log_{10}** CFU/mL. Panel B shows **log_{10}** reduction in a heat map of each treatment relative to UT biofilms. Each bar represents the average of data obtained from three independent experiments. Error bars represent the standard error of the mean. Data distributions were assessed using Shapiro-Wilk normality test and then analysed by ANOVA with Dunnett's tests to determine the P-value for multiple comparisons of normally distributed data. No statistically significant differences were observed.

5.3 Discussion

This chapter investigated the potential synergistic effects of H_2O_2 when combined with conventional antibiotics (flucloxacillin and gentamicin) against early-stage biofilms formed by two strains of *S. aureus* (Newman and SH1000). The two *S. aureus* strains, which were selected based on their demonstrated tolerance to CAP treatment in previous chapters allows us to examine the potential of combination therapy against particularly resilient biofilms, addressing a critical need in clinical settings where such resistant communities often lead to persistent infections (Craft et al., 2019, Sinha, Aggarwal and Singh, 2024, Bhattacharya et al., 2015).

Gentamicin and flucloxacillin were selected based on their distinct mechanisms of action and common use in treating *S. aureus* infections, including those associated with biofilms. Gentamicin, an aminoglycoside, inhibits protein synthesis by binding to the 30S ribosomal subunit (Figure 5.9), while flucloxacillin, a ß-lactam antibiotic, interferes with cell wall synthesis (Figure 5.10) (Kapoor, Saigal and Elongavan, 2017, Tuon et al., 2023, Fisher and Mobashery, 2021). For example, study tested gentamicin released from collagen sponges against *S. aureus* biofilms on hydroxyapatite (mimicking bone infections), and found that the high local concentrations (≥1,024 µg/mL) eradicated biofilms of gentamicin-sensitive strains and partially eradicated resistant strains after prolonged exposure (24–48 hours) (Maczynska et al., 2019). Another recent study on MRSA clinical isolates demonstrated that prolonged exposure (48–72 hours) to high gentamicin concentrations (1,024–2,048 µg/mL) significantly reduced biofilm viability-achieving a 3-$\log_{10}$ CFU decrease-even in strains harbouring the aac(6′)-aph(2″) resistance gene. However, complete eradication was not consistently achieved (Ando et al., 2024).

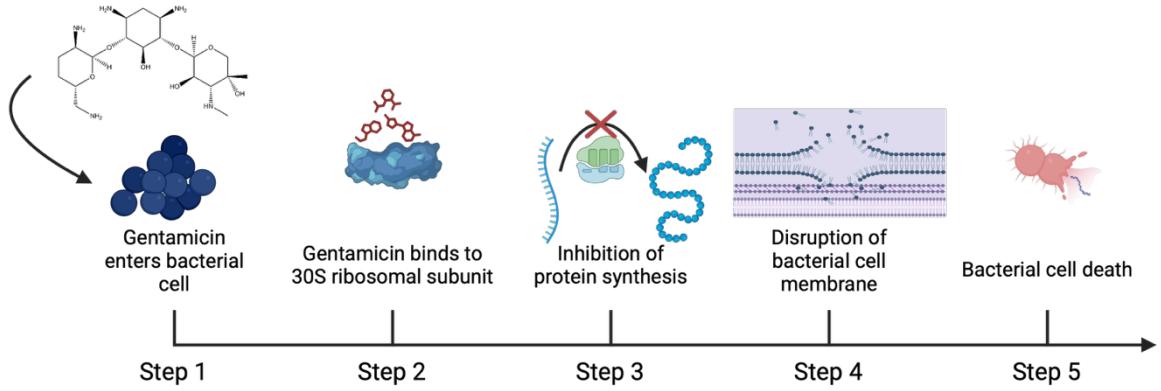

Figure 5.9: Schematic diagram described gentamicin mode of action against bacterial cell. First, gentamicin enters the bacterial cell and then binds to the 30S ribosomal subunit. This binding inhibits protein synthesis, leading to disruption of the bacterial cell membrane and ultimately resulting in bacterial cell death. Diagram was created in BioRender.

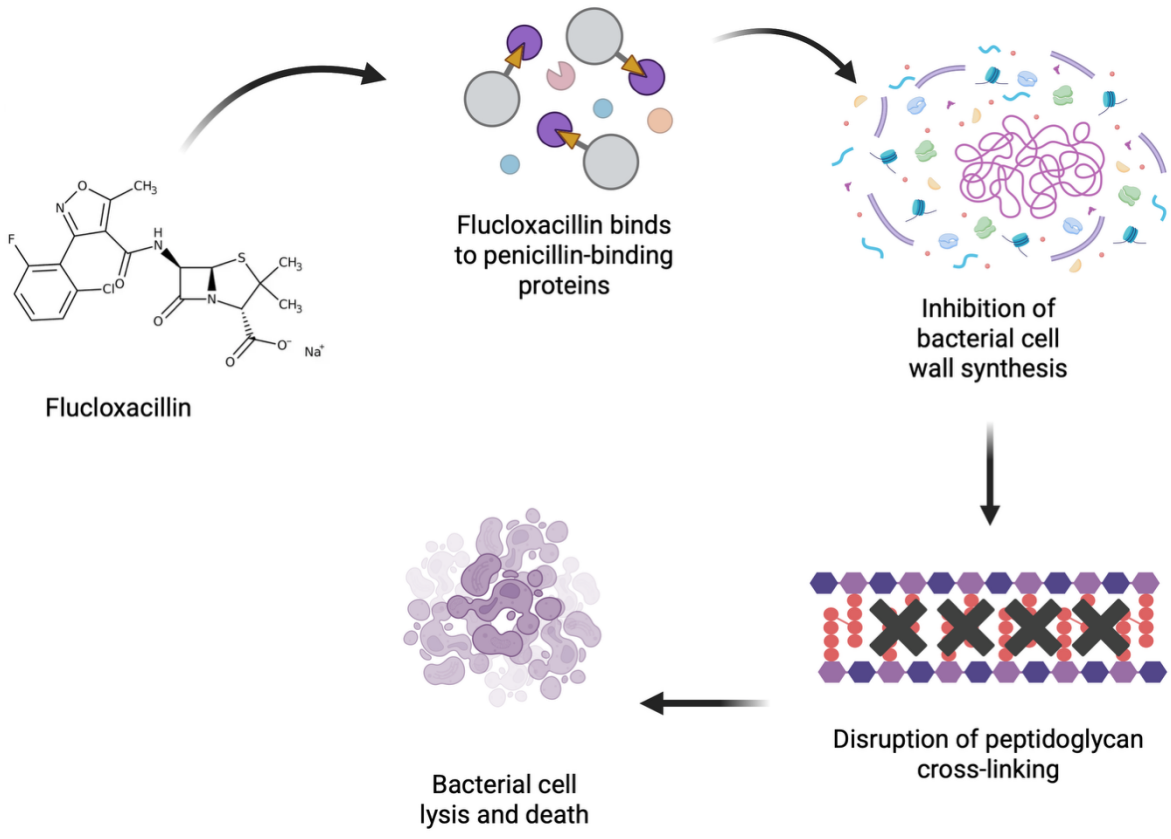

Figure 5.10: Schematic diagram described flucloxacillin mode of action against bacterial cell. Flucloxacillin binds to penicillin-binding proteins on the bacterial cell membrane, which are essential for synthesizing the cell wall. By inhibiting these proteins, flucloxacillin disrupts the cross-linking of peptidoglycan, a critical structural component of the bacterial cell wall. This inhibition weakens the cell wall, ultimately leading to cell lysis and bacterial death. Diagram was created in BioRender.

These antibiotics are frequently used in clinical settings for treating wound infections, making our findings particularly relevant to potential therapeutic applications. For instance, gentamicin has been shown to effectively target biofilms formed by *S. aureus* and other pathogens in diabetic foot ulcers (DFUs). Studies revealed significant reductions in biofilm viability when gentamicin was used, particularly in combination therapies with other agents like imipenem or calcium sulfate beads (Nazari et al., 2024, Fletcher et al., 2022). Similarly, flucloxacillin alone failed to significantly reduce *S. aureus* biofilm counts in bone, soft tissue, or implant-associated biofilms in a rat model of implant-associated osteomyelitis. However, combining flucloxacillin with rifampin achieved a highly significant reduction in bacterial viability across all tested tissues, with no reported antibiotic resistance in the combination group (Greimel et al., 2017).

The results demonstrated that biofilms exhibited enhanced susceptibility to antibiotics when H_2O_2 was present, with notable variations in effectiveness depending on the treatment protocol, antibiotic type, and bacterial strain. This chapter discussion evaluates the implications of these findings in the context of current knowledge about biofilm-related infections and antimicrobial resistance, while highlighting potential mechanisms underlying the observed synergistic effects and considering future clinical applications.

5.3.1 Synergistic effects of H_2O_2 and antibiotics against early-stage biofilms

5.3.1.1 Enhancement of gentamicin efficacy

The metabolic activity assessments revealed remarkable synergistic effects when combining H_2O_2 with gentamicin against early-stage *S. aureus* biofilms. For *S. aureus* Newman biofilms, whilst gentamicin alone demonstrated concentration-dependent reductions in metabolic activity, the addition of H_2O_2 substantially enhanced its antimicrobial efficacy. The experimental results showed that gentamicin at 128 µg/mL alone reduced metabolic activity to 45.31% (****$p < 0.0001$), while the simultaneous combination with 1 mM H_2O_2 decreased metabolic activity to 37.20%. This synergistic effect was particularly pronounced with the post-treatment protocol, where gentamicin followed by H_2O_2 post-treatment

achieved significant reductions across a broader range of gentamicin concentrations (128 to 4 µg/mL). These findings align with research by Asanin et al. (2019), who demonstrated that combining antimicrobial agents can produce enhanced effects against *S. aureus* strains with diverse genetic backgrounds. Similarly, this finding is consistent with research by Kwiatkowski et al. (2020), who reported that the combination of H_2O_2 with other antimicrobial agents produced synergistic effects against *S. aureus* biofilms.

The mechanism underlying this synergy may involve H_2O_2-mediated disruption of the biofilm matrix, subsequently facilitating enhanced antibiotic penetration. Gentamicin's polycationic structure, characterised by multiple amino and hydroxyl groups, inherently limits its diffusion through the anionic EPS of biofilms due to charge interactions with alginate and other EPS components (Heriot et al., 2019, Machado et al., 2013). Structural modifications, such as hydrophobic derivatisation (e.g., alkyl chain incorporation), could reduce polarity and improve gentamicin's penetration into lipid-rich biofilm matrices, as demonstrated by poly(lactide-co-glycolide) (PLGA) nanoparticle formulations that enhance gentamicin entrapment and release (Abdelghany et al., 2012). Additionally, H_2O_2 may sensitise bacterial cells through oxidative damage to cellular components, such as ribosomal RNA, rendering them more susceptible to gentamicin's protein synthesis inhibition. This is supported by studies showing that H_2O_2 induces oxidative stress, which disrupts biofilm architecture and downregulates biofilm-associated genes, enhancing antibiotic efficacy (Dwyer et al., 2014, Painter et al., 2015). Furthermore, oxidative stress from H_2O_2 increases extracellular DNA (eDNA) release in *S. aureus* biofilms, potentially destabilising the matrix. However, H_2O_2 alone shows limited antibiofilm activity.

5.3.1.2 Enhancement of flucloxacillin efficacy

Similarly, the combination of H_2O_2 with flucloxacillin demonstrated enhanced antimicrobial efficacy metabolically –not in cellular viability against both *S. aureus* strains, albeit with strain-specific optimal treatment strategies. For Newman biofilms, pre-treatment with H_2O_2 followed by flucloxacillin consistently yielded the most substantial reductions in metabolic activity. The experimental data showed that while flucloxacillin alone at higher concentrations (8, 4, and 2 µg/mL)

reduced metabolic activity to 3.09%, 2.69%, and 2.99% respectively (*p< 0.05), the pre-treatment approach with H_2O_2 followed by flucloxacillin exposure yielded even greater reductions, with 8 µg/mL reducing metabolic activity to 0% (**p< 0.01).

Flucloxacillin's ß-lactam structure, which includes a stabilised isoxazolyl side chain, confers resistance to ß-lactamase hydrolysis but exhibits limited penetration into hydrophilic biofilm matrices due to interactions with EPS (Kapoor, Saigal and Elongavan, 2017). Structural optimisations, such as ß-lactamase-resistant analogs or hydrophobic modifications, could enhance biofilm penetration by reducing polarity and improving diffusion through lipid-rich EPS components (Parker et al., 2023). H_2O_2 potentiates flucloxacillin by degrading biofilm EPS through oxidative cleavage of polysaccharides and eDNA, destabilising the matrix and enabling antibiotic access to PBPs (Shnyoor and Zgair, 2024, Hoogenkamp et al., 2023). Pre-treatment with H_2O_2 may disrupt bacterial membrane integrity, increasing flucloxacillin uptake and efficacy, as demonstrated by sub-MIC doses (0.0625 µg/mL) achieving greater reductions in biofilm metabolic activity (19.41%) in combination therapy (Wu et al., 2021, Parker et al., 2023). These findings align with clinical strategies advocating combination therapies for biofilm-associated *S. aureus* infections, where oxidative agents or adjuvant treatments enhance ß-lactam efficacy (Senobar Tahaei et al., 2021). Moreover, other research examining bacteriophages combined with subtherapeutic doses of antibiotics demonstrated that the cocktail synergised with flucloxacillin to eradicate biofilms, highlighting the potential of combined approaches for enhanced biofilm eradication (Save et al., 2022).

5.3.1.3 Strain-specific responses to combination therapies

A crucial finding from this investigation was the strain-specific responses to combination therapies, emphasising the importance of tailored treatment approaches for different *S. aureus* strains. The CFU assessment revealed differences between Newman and SH1000 strains in their responses to H_2O_2-antibiotic combinations. For *S. aureus* Newman, combining flucloxacillin with H_2O_2 significantly enhanced antimicrobial efficacy, with the pre-treatment approach achieving the greatest reduction (4.2-$\log_{10}$ reduction) compared to

flucloxacillin alone (2.0-log_{10} reduction). In contrast, for SH1000 biofilms, flucloxacillin monotherapy consistently yielded the most substantial reductions in bacterial viability, with flucloxacillin alone achieving a greater reduction (2.2-log_{10} reduction) than any combination with H_2O_2.

This strain-specific variability in treatment response may be attributed to differences in oxidative stress adaptation mechanisms. Similar observations were noticed in the previous chapter (chapter 3) when applied CAP against different *S. aureus* strains. Research demonstrated that *S. aureus* strains could exhibit varying degrees of susceptibility to oxidative stress due to differences in antioxidant defences and repair mechanisms (Beavers and Skaar, 2016). Additionally, *S. aureus* can adapt to oxidative stress through the production of H_2O_2-resistant small colony variants (SCVs) with enhanced catalase activity, which may contribute to varying responses to oxidative agents across different strains (Painter et al., 2015).

5.3.1.4 Pre-treatment versus post-treatment with H_2O_2

The timing of H_2O_2 application emerged as a critical factor influencing antimicrobial efficacy. For *S. aureus* Newman biofilms treated with flucloxacillin or gentamicin, the pre-treatment approach with H_2O_2 consistently yielded the greatest log reductions in bacterial viability. In contrast, the post-treatment with flucloxacillin or gentamicin strategy showed the greatest log_{10} reductions for *S. aureus* SH1000. In the experimental data, pre-treatment with H_2O_2 followed by flucloxacillin 0.25 µg/mL achieved a 4.2-log_{10} reduction, compared to 3.6-log_{10} for simultaneous treatment and 3.1-log_{10} for post-treatment for *S. aureus* Newman biofilms. In contrast, for gentamicin treatment of *S. aureus* Newman biofilms, the post-treatment protocol demonstrated superior efficacy, particularly at higher gentamicin concentrations, with simultaneous application achieving a 5.3-log_{10} reduction at 128 µg/mL compared to gentamicin alone (3.5-log_{10} reduction).

The differential efficacy of pre-treatment versus post-treatment with H_2O_2 in eradicating *S. aureus* biofilms is strongly influenced by strain-specific biofilm characteristics and adaptive stress responses (Yin et al., 2017, Painter et al., 2015). For *S. aureus* Newman biofilms pre-treatment with H_2O_2 followed by

flucloxacillin effectiveness, this is attributed to Newman's polysaccharide intercellular adhesin (PIA)-dominant biofilm matrix, which is highly susceptible to oxidative disruption by H_2O_2 (Yin et al., 2017). Pre-treatment degrades the PIA-rich EPS, enabling flucloxacillin to penetrate and target PBPs in metabolically active cells (Painter et al., 2015). Additionally, H_2O_2 downregulates biofilm-associated genes (e.g., ica operon), further sensitising cells to ß-lactams (Painter et al., 2015).

In contrast, for *S. aureus* SH1000 biofilms, post-treatment with H_2O_2 after gentamicin exposure yielded the greatest reductions in viability. SH1000 biofilms are characterised by eDNA-rich matrices, which are less vulnerable to H_2O_2 alone but become destabilised after gentamicin-induced metabolic stress (Lamret et al., 2021b, Peng et al., 2022). Gentamicin's inhibition of protein synthesis primes cells for oxidative damage, while post-treatment H_2O_2 targets residual persister cells and SCVs that evade aminoglycoside activity (Stoneham et al., 2020, Wu et al., 2021). This sequential approach mitigates SCVs survival, a common issue in gentamicin monotherapy, by leveraging H_2O_2's ability to disrupt membrane integrity and overwhelm bacterial antioxidant defences (Wu et al., 2021).

These findings suggest that the optimal timing of H_2O_2 application depends on the specific antibiotic used and potentially the mechanism of action involved. The importance of treatment timing has been observed in other antimicrobial combination studies, such as research on the antimicrobial and antibiotic-potentiating effect of calcium peroxide nanoparticles in combination with tobramycin sulfate, which demonstrated timing-dependent synergistic effects against oral bacterial biofilms (Bankar et al., 2024).

5.3.2 Limitations and future directions

5.3.2.1 Limitations of the current study:

First of all, the study utilised *in vitro* biofilm models, which may not fully replicate the complex host-microbe interactions (e.g., immune responses, nutrient gradients) observed in clinical infections. For instance, *S. aureus* biofilms in chronic wounds or implant-associated infections often coexist with host cells and

multispecies microbial communities, factors absent in monoculture polystyrene plate assays (Wang et al., 2023a, Kranjec et al., 2021). Second, early-stage biofilms (4-hour maturation) were tested in this chapter in contrast with the previous chapters (24h mature biofilms), limiting insights into therapeutic efficacy against mature or chronic biofilms. Mature biofilms exhibit greater structural complexity, metabolic heterogeneity, and persister cell enrichment, which are key drivers of treatment failure (Kranjec et al., 2021, Tuon et al., 2023). Third, the findings are limited to *S. aureus* Newman and SH1000 strains. Clinical isolates often exhibit broader genetic and phenotypic diversity, including varied biofilm matrix composition (e.g., PIA vs. eDNA dominance) and oxidative stress adaptations, which influence treatment responses (Raval et al., 2021, Banerjee, Gowda and Ananda, 2022).Finally, repeated exposure to sublethal H_2O_2-antibiotic combinations may select for resistant mutants or SCVs, as observed in studies where oxidative stress increased antibiotic tolerance in *S. aureus* (Parker et al., 2023, Kranjec et al., 2021).

5.3.2.2 Future research directions:

Translating findings to *in vivo* models (e.g., murine wound or implant infection models) and human trials is critical. For example, calcium peroxide nanoparticles (CaO_2 NP) combined with tobramycin demonstrated enhanced biofilm eradication in oral biofilms, highlighting the potential of oxygenating agents in clinical settings (Bankar et al., 2024). Explore synergies between H_2O_2 and other antibiofilm agents, such as: matrix-dispersing enzymes (Dispersin B® or DNase I), which degrade polysaccharides or eDNA, improving antibiotic penetration (Wang et al., 2023a), or nanoparticle delivery systems (PLGA-coated gentamicin or flucloxacillin) to enhance biofilm penetration and sustain drug release (Abdelghany et al., 2012). Investigate prolonged or pulsed H_2O_2-antibiotic regimens to counteract biofilm resilience. Studies show that repeated oxidative stress can exhaust bacterial antioxidant defences (e.g., bacilliredoxins BrxA and BrxB/ bacillithiol disulfide reductase YpdA pathway) which is central to *S. aureus* defence against oxidative stress, sensitising cells to antibiotics (Linzner et al., 2019, Raval et al., 2021). Monitor emergent resistance mechanisms (e.g., SCVs formation, catalase upregulation) during combination therapy. Pharmacological inhibition of redox pathways (e.g., bacillithiol metabolism) could prevent adaptive

tolerance (Linzner et al., 2019, Kranjec et al., 2021). Develop polymicrobial biofilm models to mimic clinical infections, where interspecies interactions alter antibiotic susceptibility. For example, *P. aeruginosa* co-infections can enhance *S. aureus* survival via shared matrix components (Yung, Sircombe and Pletzer, 2021, Nguyen and Oglesby-Sherrouse, 2016).

5.3.3 Conclusion

Key findings from this chapter:

- Synergistic effects.

H_2O_2 enhances antimicrobial efficacy of conventional antibiotics (e.g., flucloxacillin, gentamicin) against early-stage *S. aureus* biofilms, particularly in the Newman strain. This efficacy varies based on treatment protocol, antibiotic class, and bacterial strain.

- Proposed mechanisms.

Improved biofilm penetration by antibiotics, increased bacterial membrane permeability and metabolic reactivation of dormant cells, making them susceptible to antibiotics.

- Clinical implications.

Potential to reduce reliance on high-dose antibiotic monotherapy, mitigating antimicrobial resistance (especially MRSA). Additionally, H_2O_2-mediated re-sensitisation of biofilm-embedded bacteria offers a strategic approach to combat persistent infections.

- Broader impact.

Combination therapies could preserve existing antimicrobial arsenal effectiveness and may improve patient outcomes in biofilm-associated infections amid rising global antibiotic resistance.

6 Chapter 6: Final discussion

The experimental findings presented in this thesis demonstrate the significant antimicrobial potential of cold atmospheric plasma (CAP) and selected compounds from the Tocriscreen™ Micro library against various mono-species and polymicrobial biofilms, with differential efficacy observed across microbial species and strains. This work has revealed that CAP exhibits time-dependent killing effects against *Candida auris* biofilms, with the most pronounced reductions in viability occurring after 5 minutes of treatment. The antimicrobial activity of CAP strongly correlates with hydrogen peroxide (H_2O_2) production, suggesting a key role for these reactive oxygen species (ROS) in the observed effects. Furthermore, strain-dependent responses to CAP treatment were identified, particularly among *Staphylococcus aureus* isolates, highlighting the importance of strain selection in antimicrobial testing. Most notably, the combination of CAP with the novel agent, KHS 101 hydrochloride (KHS), consistently demonstrated superior efficacy compared to monotherapies, achieving significant reductions in both total and viable cell counts in mono-species and polymicrobial biofilms. In the final data chapter further investigation for the mode of action of CAP by utilising H_2O_2 in combination with two clinically relevant antibiotics; flucloxacillin and gentamicin in different treatment regimens. These combination therapies were assessed against early-stage biofilms formed by two distinct *S. aureus* strains—Newman and SH1000. The efficacy led to "breaking of the tolerance" exhibited by *S. aureus* Newman and SH1000 to CAP therapy. These findings have important implications for the development of novel treatment strategies for biofilm-associated infections, particularly in the context of wound care.

6.1 Complex biofilm models; advantages and limitations

The cellulose matrix-hydrogel system employed in this study for CAP therapy represents a more complex biofilm modelling compared to traditional approaches (e.g., growth on microtiter plate as used in chapter 5) (Townsend et al., 2016, Townsend et al., 2017). This system provides a three-dimensional (3D) structure that more accurately mimics the physical environment encountered in chronic wounds, allowing for more clinically relevant assessments of antimicrobial efficacy. However, It should be acknowledged that the biofilm model used in this study is nearly a decade old, and while it remains technically manageable and

reproducible, it does not fully capture the complexity of chronic wound environments now commonplace when considering the wound microbiome. More advanced models have since been developed, including *ex vivo* wounded skin systems and 3D bioengineered constructs that incorporate host tissue components, polymicrobial communities, and physiologically relevant gradients of oxygen and nutrients (PETERSON and WESTGATE, 2022, Cárdenas-Calderón et al., 2022, Martinet et al., 2025). These newer platforms can better mimic clinical conditions and will be discussed further in the next section. For example, the incorporation of cellulose fibers creates a scaffold that resembles wound tissue architecture, enabling microbial attachment and biofilm development in a manner more representative of *in vivo* conditions (Tabatabaei Hosseini et al., 2024, Khan et al., 2024, Utoiu et al., 2024). Moreover, bacterial cellulose (BC) consists of an ultrafine network of nanofibers that provides excellent tensile strength, high water absorption, and notable biocompatibility, closely mimicking the structure of the human extracellular matrix (ECM). This 3D architecture not only supports superior moisture retention and mechanical protection but also offers a physiologically relevant surface that facilitates realistic microbial attachment, growth, and biofilm development-features particularly relevant in the context of chronic wound infections (He et al., 2021). Recent studies have developed artificial wound bed models using cellulose-based materials, such as BC-tannic acid-magnesium chloride (BC-TA-Mg) composites and electro spun cellulose acetate-gelatine scaffolds (Wächter et al., 2023). This represents a significant advantage over conventional microtiter plate-based biofilm models, which lack the structural complexity of real wound environments.

The inclusion of both mono-species and triadic polymicrobial biofilms in this study addresses the complex nature of chronic wound infections, albeit still from a simplistic point of view. As demonstrated by (Kalan et al., 2016), Kalan et al. (2019), chronic wounds harbour diverse microbial communities comprising multiple bacterial and fungal species that interact in complex ways to enhance collective virulence and treatment resistance. Our triadic model incorporating *Candida albicans*, *Pseudomonas aeruginosa*, and *S. aureus* reflects this complexity, enabling the assessment of antimicrobial strategies against polymicrobial communities rather than isolated species. This polymicrobial model is mimics diabetic foot ulcers (DFUs), where inter-kingdom communities are

frequent and clinically meaningful; longitudinal sequencing of 100 non-healing DFUs showed fungal communities in up to ~80% of cases and linked mycobiome features to delayed healing and necrosis, supporting inclusion of *Candida* alongside bacterial pathogens (Kalan et al., 2016). The triad of *C. albicans*, *P. aeruginosa*, and *S. aureus* reflects dominant DFUs taxa reported across culture-based and metagenomic cohorts and enables interrogation of cross-kingdom interactions implicated in tolerance and virulence (Kalan et al., 2019, Sadeghpour Heravi et al., 2019). This approach aligns with contemporary understanding of wound infections as polymicrobial ecosystems rather than isolated pathogen colonisation (Keim et al., 2024, Kadam et al., 2019).

Recent work has further highlighted the importance of polymicrobial biofilm models in antimicrobial testing, demonstrating that interspecies interactions can significantly alter susceptibility profiles compared to mono-species testing (Richards et al., 2024). Similarly, studies have shown that the presence of fungi within bacterial biofilms can enhance overall resistance to conventional antimicrobials, necessitating the development of models that incorporate this complexity in models associated with wounds and other ecological niches (Ranjith, Nagapriya and Shivaji, 2022, Townsend et al., 2016, Kean et al., 2017). To illustrate this, a recent study within the field of oral microbiology highlighted that *C. albicans* acts as a keystone species in oral polymicrobial biofilms, increasing bacterial load by 10-fold and lactate production in 5- and 10-species consortia. These interkingdom biofilms exhibit heightened metabolic activity (2.5× higher than bacterial-only biofilms) and resistance to chlorhexidine, necessitating *C. albicans*-inclusive models for antimicrobial testing (Young et al., 2021). Another study stated that the synergy of *C. albicans* with *Streptococcus mutans* and *Actinomyces naeslundii* accelerates acid production (pH <4.5), exacerbating enamel demineralisation in early childhood caries (Arzmi et al., 2016). Our findings on the differential responses of mono-species versus triadic wound biofilms to various treatments support these observations and underscore the value of complex biofilm models in preclinical evaluation of novel antimicrobial strategies.

Despite their advantages, the biofilm models used in this study have several limitations that must be acknowledged. First, while the cellulose matrix-hydrogel

system provides structural complexity, it still lacks the dynamic immunological environment present in human wounds (Vyas, Xia and Mai-Prochnow, 2022). Studies have shown that host-derived factors such as inflammatory mediators, matrix metalloproteinases, and immune cells significantly influence biofilm formation and antimicrobial susceptibility *in vivo* (Richards et al., 2024, Fan et al., 2025, Yucel-Lindberg and Båge, 2013, Vidakovic et al., 2023). Future models could incorporate these elements through the addition of immune cells or wound exudate to better recapitulate the host-pathogen interface.

Additionally, our models do not account for the anaerobic/microaerophilic conditions often found in deeper wound tissues. Studies have demonstrated that oxygen gradients within wounds influence microbial composition and metabolic activity, with profound implications for treatment efficacy (Richards et al., 2024, Klementiev, Jin and Whiteley, 2020, Thaarup et al., 2023, Percival et al., 2018). Developing oxygen-controlled biofilm systems that simulate these gradients represents an important direction for future research.

Furthermore, while our triadic biofilm model incorporates three key pathogens, it still fails to capture the full diversity of wound microbiomes. Studies reveal that wounds host dozens of microbial species, including obligate anaerobes (*Anaerococcus*, *Finegoldia*, *Peptoniphilus*) and Gram-negative opportunists (*Proteus*, *Enterococcus*), which thrive in hypoxic niches and engage in metabolic cross-feeding with aerobic pathogens to enhance biofilm resilience (Maddocks, 2017, Bowler, Duerden and Armstrong, 2001, Choi et al., 2019). Non-albicans *Candida* species (*C. tropicalis*, *C. parapsilosis*) and filamentous fungi (*Trichophyton rubrum*, *Aspergillus*) are frequently identified in diabetic and burn wounds, where they synergise with bacteria to degrade tissue and evade immune responses (Ge and Wang, 2023, Kalan et al., 2016). For example, fungal ß-glucan matrices shield *S. aureus* from phagocytosis, while *Proteus* spp. alkalinize the wound environment, activating proteases that impede healing (Kalan et al., 2016, Bowler, Duerden and Armstrong, 2001). Excluding these species overlooks critical interactions, such as pH-mediated resistance and hyphal penetration of dressings, which are hallmarks of clinical infections (Ge and Wang, 2023, Kalan et al., 2016). Developing models that incorporate anaerobic and fungal communities, alongside aerobic bacteria; one such study recently published from our group, utilised a 11-

multi-species wound biofilm mode (Brown et al., 2022), including these organisms that would provide a much more complex system for testing in the future, and will better replicate clinical complexity and improve preclinical therapeutic testing.

6.2 Personalised biofilm models

An emerging concept in wound care is the recognition that each wound possesses a unique microbiome signature, necessitating personalised approaches to treatment. As demonstrated by Loesche et al. (2017) through metagenomic analysis of chronic wound samples, the microbial composition varies dramatically between patients and even between wounds in the same patient. This heterogeneity suggests that standardised biofilm models, while valuable for comparative studies, may not predict treatment outcomes for individual patients.

The development of patient-specific biofilm models represents a promising approach to address this challenge. Recent work by Wang et al. (2025), Sharma et al. (2024a) has explored the use of patient-derived microbiota to seed biofilm models, creating personalised *in vitro* systems that better reflect individual wound environments. Such models could potentially enable clinicians to test treatment strategies against a patient's specific microbial community before implementation, enhancing therapeutic precision. However, unculturability reflects gaps in mimicking natural microenvironments rather than biological impossibility. These microbes represent untapped phylogenetic and functional diversity with implications for ecology, medicine, and biotechnology (Lloyd et al., 2018). The inability to culture many microorganisms in laboratory settings stems from their unique physiological and ecological requirements, which standard cultivation methods fail to replicate. Some species depend on metabolites produced by neighbouring microbes, nutrient and environmental specificities, microbial competition, bacteria enter a dormant viable but non-culturable state, resisting cultivation despite metabolic activity (Stewart, 2012). This state is reversible under favourable conditions but often overlooked in standard assays. For microbiome studies, neglecting these microbes risks incomplete understanding of community dynamics, host interactions, and therapeutic targets (Kapinusova, Lopez Marin and Uhlik, 2023).

Our findings regarding strain-dependent responses to antimicrobial interventions further emphasise the importance of personalised approaches. The observation that different *S. aureus* strains exhibit varying levels of tolerance to CAP treatment, with *S. aureus* (Newman and SH1000) showing particular tolerance, highlights the potential pitfalls of generalising treatment efficacy across strains. As shown by Klein et al. (2022), even within a single species, substantial genotypic and phenotypic diversity exists that can influence treatment outcomes. This underscores the need for strain-specific testing in preclinical evaluation and the potential value of isolate characterisation in clinical settings. Future biofilm models should therefore strive to balance standardisation for comparative research with personalisation for clinical relevance. The integration of rapid microbiome characterisation technologies with tailored biofilm model development could potentially bridge this gap, allowing for more predictive preclinical testing and informed treatment selection. However, reproducibility may be reduced if using patient-species model systems as testing platforms.

6.3 Current status of CAP technology in clinical applications

CAP technology has progressed significantly from laboratory curiosity to clinical tool over the past decade (Laroussi, 2020). Our findings demonstrating the significant efficacy of CAP against diverse microbial biofilms, including multidrug-resistant pathogens like *C. auris*, highlight its potential value in wound care and general nosocomial infection control. However, several practical considerations must be addressed to facilitate widespread clinical adoption.

The optimal treatment parameters identified in our study specifically, a 5-minute exposure time align with findings from recent clinical trials. Stratmann et al. (2020) conducted a randomised clinical trial of CAP therapy for DFUs, applying a 2-minute treatment three times weekly and demonstrating significantly accelerated wound healing compared to placebo. Similarly, Mirpour et al. (2020b) implemented a protocol of 5-minute CAP treatments per week for diabetic ulcers, reporting a 77.3% reduction in wound size after 3 weeks compared to 36.4% in controls. Another clinical study on chronic wounds showed that a 2-minute CAP treatment significantly reduced bacterial load, with no adverse effects, and was

effective across different wound types and bacterial species (Isbary et al., 2012). These studies suggested that the treatment duration established in our *in vitro* work translates effectively to clinical settings without imposing impractical time burdens.

Regarding device selection, several CAP systems have received regulatory approval for wound treatment. The kINPen® MED (neoplas tools GmbH, Germany) and SteriPlas (Adtec Healthcare, UK) represent examples of commercially available plasma devices with established safety profiles (Jeyaratnam and McGovern, 2022, Breathnach et al., 2018). These systems differ in their mechanisms of plasma generation (dielectric barrier discharge versus plasma jet) (Nasiru et al., 2021), and gas compositions (argon, helium, or ambient air) (Hoffmann, Berganza and Zhang, 2013), potentially influencing their antimicrobial efficacy and tissue compatibility (Bakhtiyari-Ramezani et al., 2024). Our research utilising an argon gas plasma system provides valuable data supporting the efficacy of plasma devices. It is important to note that, while the specific device used in our study has been described in published literature (Ghimire et al., 2021, Ghimire, Szili and Short, 2022), it is not commercially available and has not yet undergone clinical testing.

6.3.1 The importance of mechanistic research and strain-dependent responses in treatment development

Our investigation into the mechanisms underlying CAP's antimicrobial effects, particularly the correlation between H_2O_2 production and microbial inactivation, exemplifies the importance of mechanistic research in advancing clinical applications. Understanding how antimicrobial technologies function at a molecular level provides numerous advantages for optimising their therapeutic use. Mechanistic insights enable rational optimisation of treatment parameters. Our finding that increasing CAP exposure time correlates with H_2O_2 production and antimicrobial efficacy provides a clear rationale for the 5-minute treatment duration identified as optimal. Similarly, the observation by Ghimire et al. (2021) that specific plasma parameters modulate reactive species generation has informed device design to maximise therapeutic species while minimising potentially harmful by-products. Without this mechanistic understanding,

optimisation would rely on empirical testing alone, dramatically increasing development time and cost.

Furthermore, mechanistic knowledge facilitates prediction of potential tolerance mechanisms. As demonstrated by Mai-Prochnow et al. (2015), understanding that reactive oxygen species (ROS) target multiple cellular components simultaneously explains the low incidence of resistance development against CAP treatment. This contrasts with conventional antibiotics, where specific molecular targets often enable rapid resistance evolution through single mutations (Igler, Rolff and Regoes, 2021). This mechanistic insight suggests that CAP-based therapies may maintain efficacy over longer periods than traditional antimicrobials, a critical consideration in an era of increasing antimicrobial resistance.

In this work, CAP exposures and exogenous H_2O_2 assays were performed as separate experiments, which do not by themselves establish causality for H_2O_2 in our system. However, our interpretation for using H_2O_2 is supported by published mechanistic studies showing that this agent is a dominant, long-lived antimicrobial in CAP-treated liquids and that catalase or H_2O_2 scavengers diminish CAP/PAW killing, particularly under mildly acidic conditions where H_2O_2–nitrite (NO_2) chemistry is most bactericidal (Ikawa, Kitano and Hamaguchi, 2010, Oehmigen et al., 2010, Oehmigen et al., 2011, Wende et al., 2015, Graves, 2014). Complementarily, the gas source can reduce reactive nitrogen species (RNS) and enrich RNS output: nitrogen (N)- or carbon dioxide (CO_2)-driven plasma jets generate RNS-dominant chemistries that retain efficacy against catalase-positive organisms, offering a practical alternative where high catalase burdens are expected (Takamatsu et al., 2014, Bruggeman et al., 2016, Lukes et al., 2014). Taken together, our data are consistent with this literature and highlight potential future avenues for tests in our models (e.g., catalase addition during CAP, selective scavengers for ROS/RNS, gas-source switching with quantitative RONS profiling) to delineate species-specific contributions to killing in wound-relevant biofilms.

The strain-dependent responses to CAP treatment observed in our study highlight how laboratory insights can directly inform clinical practice. The finding that *S. aureus* (Newman and SH1000) exhibits greater tolerance to CAP than other strains

tested suggests that strain identification might predict treatment response, potentially enabling personalised therapeutic approaches. Recent advances in rapid diagnostic technologies have made strain-level identification increasingly feasible in clinical settings. Yu et al. (2022) demonstrated that MALDI-TOF mass spectrometry can differentiate between *S. aureus* strains with different virulence and resistance profiles within hours rather than days. Combining such diagnostic capabilities with strain-specific susceptibility data could enable clinicians to select optimal treatment modalities based on the specific pathogens present in a patient's wound.

6.3.2 Safety profile and regulatory considerations

The safety of CAP for human tissues is a paramount concern for clinical translation, particularly as the technology moves from laboratory to bedside applications (Xu et al., 2021). Multiple studies have established favourable safety profiles for therapeutic plasma applications, with only minor and transient effects such as mild erythema or warming sensations, which resolve quickly without intervention (Xu et al., 2021). Mechanistic investigations have shown that therapeutic plasma doses can selectively induce oxidative stress in microbial cells while activating protective antioxidant responses in mammalian cells, creating a therapeutic window that enables antimicrobial efficacy without host toxicity (Xu et al., 2021, Wang et al., 2022). This selectivity is attributed to fundamental differences in antioxidant defence systems between prokaryotic and eukaryotic cells (Wang et al., 2022).

However, a growing body of literature-particularly from cancer biology-highlights the need for caution. CAP has been extensively studied for its anti-cancer properties, with numerous reports demonstrating that plasma-generated reactive oxygen and nitrogen species (RONS) can induce DNA damage, apoptosis, and cell death in a variety of cancer cell lines, both *in vitro* and *in vivo* (Min et al., 2022, Yan et al., 2017, Murillo et al., 2023, Sun et al., 2024, Biscop et al., 2019, Hong et al., 2017). While this is desirable in oncology, it raises concerns about potential genotoxicity in non-malignant tissues. Notably, a study from Lancaster university found that certain plasma devices, under specific conditions, induced markers of DNA damage and chromosomal instability in normal cell lines, including

micronuclei formation and increased necrosis-effects associated with carcinogenic risk (Hong et al., 2017). Other investigations have confirmed that the genotoxic and cytotoxic effects of plasma jets can vary significantly depending on cell type, exposure time, and the composition of the surrounding medium, with some normal cells showing increased sensitivity to indirect CAP treatment (Hong et al., 2017, Biscop et al., 2019).

These findings underscore the importance of rigorous, context-specific safety testing for each plasma device and clinical protocol. While current clinical and preclinical data suggest that CAP is generally safe for short-term, controlled therapeutic use, the possibility of long-term genotoxicity or cancer risk-especially with repeated or high-dose exposures-cannot be excluded without further study (Hong et al., 2017, Biscop et al., 2019, Xu et al., 2021). Future research should prioritise long-term animal studies, sensitive genotoxicity assays, and careful monitoring in clinical trials to ensure that CAP's benefits for wound care and infection control are not offset by unintended oncogenic effects or microbial adaptation (Xu et al., 2021, Wang et al., 2022). It is important to note that, prolonged CAP exposure may inadvertently drive tolerance/resistance mechanisms in microbial communities, mirroring challenges seen with antibiotic overuse. This emerging concern underscores the need for studies evaluating dose-dependent responses and evolutionary pressures on pathogens during extended treatment regimens.

Interpreting CAP safety in the clinical context requires acknowledging the host-damage liabilities of standard antiseptics: randomized and controlled studies show CAP can lower bioburden and accelerate healing without adverse effects under short exposures. Conversely, commonly used agents such as chlorhexidine, H_2O_2, iodine, and silver present concentration-dependent trade-offs that can impair host cells or underperform in mature biofilms (Chen et al., 2024, Thomas et al., 2011, Paleczny et al., 2023). Thus, CAP may reduce reliance on cytotoxic dosing of antiseptics when integrated into biofilm-based wound care pathways.

6.3.3 Ongoing clinical trials and animal models

Several clinical trials investigating CAP for wound treatment are currently in progress, expanding the evidence base for this technology. A randomised

controlled trial by Bakker et al. (2025) is evaluating the efficacy of direct CAP therapy for venous leg ulcers (VLUs). Preliminary results suggested a greater reduction in wound area after 12 weeks compared to standard care alone (referred to the conventional management of VLUs, such as wound debridement and cleaning, appropriate wound dressings and routine wound care assessments with monitoring. Beyond this, additional clinical trials have demonstrated the broader applicability of CAP for chronic wound management. For example, a randomised clinical trial involving 62 DFUs found that CAP therapy significantly accelerated wound healing compared to placebo, resulting in faster wound surface reduction and earlier transition to ambulatory care (Stratmann et al., 2020). Preliminary clinical trials have also reported that CAP can decrease bacterial load and speed up the healing of chronic wounds without harming healthy tissues (Li et al., 2023). Similarly, Mirpour et al. (2020a) reported significant improvements in wound healing rates following CAP treatment in a randomised clinical trial. In addition, a clinical investigation of chronic wounds demonstrated that a two-minute CAP application led to a marked decrease in bacterial counts without causing any side effects, and proved effective against various wound types and bacterial strains (Isbary et al., 2012).

Animal models have also provided crucial insights into the potential of CAP therapy for infected wounds. Recent murine studies demonstrate CAP's dual therapeutic action, showing both potent antimicrobial efficacy and enhanced wound healing. For example, CAP treatment significantly reduces bacterial burden in *S. aureus*-infected wounds while simultaneously promoting tissue regeneration through increased neoepidermis length and ECM formation (Blaise et al., 2024). Beyond murine models, in diabetic rat models, CAP demonstrates significant therapeutic potential by accelerating wound closure, enhancing tissue regeneration, and modulating inflammation. CAP treatment reduced wound area by improved epithelialisation and promoted collagen organisation, while lowering inflammatory cell infiltration and upregulating IL-8 mRNA (Curukoglu et al., 2023). CAP alone was as effective as CAP combined with insulin, achieving comparable wound contraction rates, suggesting its standalone sufficiency (Curukoglu et al., 2023). Exposure durations of 60s or 120s daily yielded similar improvements in contraction and epithelialisation (Tatlıcıoğlu et al., 2023). In *S. aureus*-infected diabetic rats, CAP accelerated healing with faster collagen formation and reduced

inflammation, underscoring its dual antimicrobial and regenerative actions (Dehghanpisheh et al., 2023). These studies collectively highlight CAP's ability to reduce bacterial load, enhance tissue repair, and control oxidative stress in diabetic wounds. In canine models, cold atmospheric microwave plasma (CAMP) increased keratinocyte migration and upregulated genes involved in wound healing, supporting its application in veterinary medicine (Lertpatipanpong et al., 2023, Yoo et al., 2023). Collectively, these diverse animal studies underscore CAP's broad-spectrum antimicrobial and pro-regenerative properties across species and wound types, reinforcing its promise as a multimodal therapy for complex and infected wounds.

The antimicrobial mechanism of CAP *in vivo* appears to work partly through enhancing macrophage-mediated bacterial clearance, with CAP treatment promoting the elimination of both methicillin-sensitive and methicillin-resistant *S. aureus* strains by host immune cells (Duchesne et al., 2021). Beyond infection control, CAP demonstrates direct wound healing benefits by altering keratinocyte and fibroblast migration patterns, resulting in significantly accelerated wound re-epithelialisation (days 3-9) compared to untreated controls (Schmidt et al., 2017). These animal studies collectively validate CAP's potential as a multifaceted therapeutic approach that addresses both the infectious and regenerative aspects of wound healing.

Future clinical research should focus on optimising treatment protocols, identifying patient populations most likely to benefit from CAP therapy, and evaluating long-term outcomes (Raissi-Dehkordi et al., 2025). Additionally, the development of portable or home-based plasma devices could potentially extend treatment accessibility beyond clinical settings, though such applications would require careful consideration of safety and usability factors (Kos et al., 2017).

6.3.4 Synergistic potential of combined approaches and future directions

Our findings demonstrating superior efficacy of dual therapies compared to monotherapies highlight the significant potential of combination approaches in biofilm management. The KHS+CAP combination proved particularly effective compared to modest reductions with either treatment alone. This synergistic

effect aligns with emerging literature supporting combination strategies for recalcitrant biofilm infections.

Recent work by Schramm et al. (2020) demonstrated that sequential application of CAP followed by antibiotic treatment resulted in significantly greater reductions in *Enterococcus faecalis* biofilms compared to either treatment alone. Similarly, Maybin et al. (2023) reported synergistic effects when combining CAP with conventional antimicrobial compounds against *P. aeruginosa* biofilms, achieving complete eradication at concentrations that were individually sublethal. These findings collectively suggested that CAP may disrupt biofilm architecture or cellular defences, rendering microorganisms more susceptible to secondary antimicrobial agents (Maybin et al., 2023).

The observation that CAP enhances the efficacy of KHS a compound not traditionally used as an antimicrobial is particularly noteworthy. This suggests that plasma treatment may expand the repertoire of effective antimicrobial agents by overcoming resistance mechanisms that typically limit their efficacy (Vaňková et al., 2024). As demonstrated by He et al. (2019), He et al. (2020b), CAP treatment can temporarily increase cell membrane permeability through lipid peroxidation, potentially enhancing drug uptake and accounting for the observed synergistic effects.

6.3.4.1 Potential delivery methods for combined therapies

The translation of combined CAP-antimicrobial therapies to clinical practice necessitates the development of appropriate delivery methods. Several promising approaches warrant consideration based on our findings and recent literature. Plasma-activated solutions represent one potential delivery vehicle for combined therapies. Agus et al. (2024) demonstrated that CAP treatment of saline or water generates a stable solution containing RONS that retains antimicrobial activity for several days when properly stored. Such solutions could be incorporated into wound irrigation protocols or impregnated into dressings, potentially extending the temporal effects of plasma treatment beyond direct application (Lee et al., 2023). Notably, plasma water devices are now commercially available, while extensive academic research continues to explore plasma-activated water's (PAW)

antimicrobial efficacy (Zhang et al., 2024, Xia et al., 2024, Chen, Liang and Su, 2018).

Advanced wound dressings incorporating KHS or similar compounds could be designed for sequential therapy, with compound release followed by CAP treatment during dressing changes. Gaur et al. (2023) developed a drug-loaded composite hydrogel dressing consisting of a hydrogel matrix containing gentamicin that demonstrated enhanced efficacy when combined with CAP treatment. Similar platforms could be developed incorporating repurposed compounds like KHS, potentially enabling sustained release between CAP applications. Alternatively, for systemic delivery, a review by Khalaf et al. (2024) suggested that CAP treatment may enhance the penetration of topically applied compounds through the stratum corneum, potentially improving bioavailability of topically applied agents with systemic effects. However, true systemic administration of compounds like KHS would require extensive pharmacokinetic and safety studies beyond their topical application.

The identification of KHS originally developed as a neurogenic differentiation inducer, while it is an effective antimicrobial agent highlights the value of drug repurposing approaches in addressing biofilm infections (Abduljalil et al., 2022). Our findings demonstrated significant activity against both planktonic and biofilm forms of *C. albicans* and *S. aureus* strains, suggesting broad-spectrum potential. The repurposing of existing drugs offers several advantages over de novo antimicrobial development. As noted by Miró-Canturri, Ayerbe-Algaba and Smani (2019) repurposed compounds typically have established safety profiles and manufacturing processes, potentially accelerating their path to clinical application. While drug repurposing has not yet directly led to the creation of entirely new antibiotic classes, it has facilitated the development of novel antibiotic formulations and combination therapies. For example, combining the existing cephalosporin antibiotic (ceftazidime) with avibactam, a novel ß-lactamase inhibitor. This combination restored ceftazidime's efficacy against ß-lactamase-producing Gram-negative pathogens, leading to FDA approval in 2015 (Boyd, Teng and Frei, 2021). This is particularly relevant given the current crisis in antimicrobial development, with few new classes reaching market despite increasing resistance (Murphy et al., 2022).

Understanding the mechanism of KHS antimicrobial activity remains an important research direction. While its primary pharmacological target in neural cells, Miró-Canturri, Ayerbe-Algaba and Smani (2019) stated that KHS a compound targeting the suppression of transforming acidic coiled-coil protein 3 (TACC3), is linked to various forms of human cancer. It inhibits cellular proliferation, movement, and cancer stem cell characteristics in breast cancer models, while promoting programmed cell death. It modulates biological pathways, downregulating key mitotic regulators. Similar investigations into KHS antimicrobial mechanism would inform optimisation of combination therapies and potential chemical modifications to enhance antimicrobial efficacy.

While KHS has been previously studied for its anticancer activity, no direct evidence of antimicrobial activity exists in the literature, and its safety profile for antimicrobial applications remains unexplored. Insights from oncology research—such as its dose-limiting toxicities, off-target effects on host cells, and metabolic stability challenges—could inform hypothetical antimicrobial repurposing efforts. KHS binds and inhibits heat shock protein family D member 1 (HSPD1), a mitochondrial chaperone critical for protein folding and metabolic regulation and disrupts glycolysis and oxidative phosphorylation, depleting ATP in glioblastoma (GBM) cells and Induces aggregation of metabolic enzymes (Polson et al., 2018). Another rat study highlighted that the subcutaneous KHS (6 mg/kg) crossed the blood-brain barrier and increased hippocampal neuronal differentiation without immediate adverse effects. However, long-term consequences of forced neurogenesis (e.g., circuit disruption, behavioural changes) were not evaluated (Wurdak et al., 2010). Current research on KHS is confined to oncology, with no evidence supporting antimicrobial activity. While its safety profile in cancer models is promising, repurposing for infections would require mechanistic studies, safety screens and resistance profiling to monitor for any mutations in target pathway.

6.3.4.2 Future directions in mechanistic research

While our research has provided valuable insights into the mechanisms of CAP and combination therapies, several questions remain that warrant further investigation. Future mechanistic studies should explore the molecular basis of strain-dependent responses to CAP treatment, potentially identifying genetic

markers that predict susceptibility. Transcriptomic and proteomic analyses comparing resistant and susceptible strains before and after treatment could reveal specific defence mechanisms and potential targets for intervention.

Additionally, the precise mechanisms underlying the synergistic effects observed between CAP and KHS require further elucidation, while these interactions were investigated in chapter 4. Investigating whether this synergy results from increased membrane permeability, altered metabolic states, or other factors would inform the development of optimised combination protocols. Recent advances in single-cell analysis techniques, as described by Korshoj and Kielian (2024), could provide unprecedented insights into how individual cells within biofilms respond to sequential treatments. Recent findings concluded that the synergistic antimicrobial effects of PAW and RONS involve multiple mechanisms, including membrane permeability enhancement, metabolic disruption, and biofilm matrix degradation (Nikolaou et al., 2025). The synergy between PAW/RONS and antimicrobial agents arises from combined physical disruption (membrane/EPS) and biochemical stress (metabolic inhibition). Optimising protocols requires tailoring RONS ratios, treatment sequencing, and surface-specific approaches (Mai-Prochnow et al., 2021).

The long-term effects of repeated CAP exposure on microbial communities also warrant investigation. While single treatments demonstrate significant efficacy, chronic wounds typically require repeated interventions. To illustrate this, chronic wounds typically require 4–6 treatment cycles for resolution, with 30–45% of cases needing >10 clinical visits annually due to biofilm recurrence and antimicrobial resistance (Guest, Fuller and Vowden, 2020). Infected wounds exhibit 45% healing rates within 12 months versus 59% for non-infected wounds, highlighting the impact of microbial burden on delayed recovery (Guest, Fuller and Vowden, 2020). DFUs demand a median 12.5 weeks of care, with 25% recurring within six months, often due to delayed identification and biofilm persistence (Brian et al., 2020). Biofilms drive a 3.8× higher debridement frequency compared to non-biofilm wounds, necessitating aggressive and repeated interventions (Phillips et al., 2012). Understanding whether repeated plasma exposure selects for tolerant subpopulations or alters community composition would inform clinical protocol development. Furthermore, a study found that repeated applications of CAP on *S.*

aureus biofilms demonstrated consistent antimicrobial efficacy (average 1.7-$\log_{10}$ CFU reduction per cycle) without inducing microbial resistance or habituation when administered over short intervals (Matthes, Assadian and Kramer, 2014). The results support CAP as a promising option for treating infected wounds without the risk of resistance development, even after multiple exposures.

Finally, expanding mechanistic investigations to include host responses would provide a more comprehensive understanding of CAP's therapeutic effects. Recent work by Zhai, Kong and Xia (2022), Apelqvist et al. (2023) suggested that plasma treatment not only reduces microbial burden but also modulates host inflammatory responses and promotes tissue regeneration through redox signalling. Integrating these aspects into a holistic mechanistic model would support truly translational applications of plasma technology in wound care.

6.3.5 Conclusion

The findings presented in this thesis contribute to an evolving paradigm in biofilm management that emphasises the need for alternative therapies and integrated, multi-modal approaches rather than single-agent treatments.

- CAP therapy is a potential alternative to standard wound care (as discussed in general introduction), offering a non-antibiotic approach to managing polymicrobial infections in chronic wounds.

- Dual therapy of CAP can break tolerance of otherwise recalcitrant microorganisms, This synergy may reduce antibiotic doses needed for efficacy which offering a strategic approach to mitigating antimicrobial resistance (AMR), potentially slowing resistance development.

- H_2O_2 (e.g., CAP) with antibiotics may also provide an alternative route in wound care. This approach could complement existing wound irrigation protocols or advanced dressings.

List of References

ABBAS, H. A.,ELSHERBINI, A. M. & SHALDAM, M. A. 2017. Repurposing metformin as a quorum sensing inhibitor in Pseudomonas aeruginosa. *Afr Health Sci,* 17**,** 808-819.

ABDELGHANY, S. M.,QUINN, D. J.,INGRAM, R. J.,GILMORE, B. F.,DONNELLY, R. F.,TAGGART, C. C. & SCOTT, C. J. 2012. Gentamicin-loaded nanoparticles show improved antimicrobial effects towards Pseudomonas aeruginosa infection. *Int J Nanomedicine,* 7**,** 4053-63.

ABDULJALIL, H.,BAKRI, A.,ALBASHAIREH, K.,ALSHANTA, O. A.,BROWN, J. L.,SHERRY, L.,KEAN, R.,NILE, C.,MCLEAN, W. & RAMAGE, G. 2022. Screening the Tocriscreen™ bioactive compound library in search for inhibitors of Candida biofilm formation. *Apmis,* 130**,** 568-577.

ABOELNAGA, N.,ELSAYED, S. W.,ABDELSALAM, N. A.,SALEM, S.,SAIF, N. A.,ELSAYED, M.,AYMAN, S.,NASR, M. & ELHADIDY, M. 2024. Deciphering the dynamics of methicillin-resistant Staphylococcus aureus biofilm formation: from molecular signaling to nanotherapeutic advances. *Cell Communication and Signaling,* 22**,** 188.

ABU-HASHEM, A. A. & AL-HUSSAIN, S. A. 2024. Design, Synthesis, Antimicrobial Activity, and Molecular Docking of Novel Thiazoles, Pyrazoles, 1,3-Thiazepinones, and 1,2,4-Triazolopyrimidines Derived from Quinoline-Pyrido[2,3-d] Pyrimidinones. *Pharmaceuticals (Basel),* 17.

ACHINAS, S.,CHARALAMPOGIANNIS, N. & EUVERINK, G. J. W. 2019. A brief recap of microbial adhesion and biofilms. *Applied sciences,* 9**,** 2801.

ADAM, B.,BAILLIE, G. S. & DOUGLAS, L. J. 2002. Mixed species biofilms of Candida albicans and Staphylococcus epidermidis. *Journal of medical microbiology,* 51**,** 344-349.

ADER, F.,JAWHARA, S.,NSEIR, S.,KIPNIS, E.,FAURE, K.,VUOTTO, F.,CHEMANI, C.,SENDID, B.,POULAIN, D. & GUERY, B. 2011. Short term Candida albicans colonization reduces Pseudomonas aeruginosa-related lung injury and bacterial burden in a murine model. *Critical Care,* 15**,** R150.

AGUS, R.,PIPOZ, L.,AVINO, F.,LAVRIKOVA, A.,MYERS, B. & FURNO, I. 2024. Plasma-activated water retains antimicrobial properties against Escherichia coli after 72 hours of storage. *Plasma Physics and Controlled Fusion*.

AHMADIAN, R.,BAHRAMSOLTANI, R.,MARQUES, A. M.,RAHIMI, R. & FARZAEI, M. H. 2021. Medicinal Plants as Efficacious Agents for Diabetic Foot Ulcers: A Systematic Review of Clinical Studies. *Wounds: a compendium of clinical research and practice,* 33**,** 207-218.

AHMED, N.,CANI, E.,RAYMOND, L. & ZEANA, C. P-1042. Comparison of clinical characteristics and outcomes of patients with candidemia caused by Candida auris versus other Candida species–A retrospective case-control study at a community hospital in the Bronx. Open Forum Infectious Diseases, 2025. Oxford University Press US, ofae631. 1232.

AL-KHATIB, H. D.,CORN, E. & OZIDU, V. 2024. Antibiotic Prescribing in Acute Wound Management. *BJPsych Open,* 10**,** S227-S228.

AL-BAKRI, A.,GILBERT, P. & ALLISON, D. 2004. Immigration and emigration of Burkholderia cepacia and Pseudomonas aeruginosa between and within mixed biofilm communities. *Journal of Applied Microbiology,* 96**,** 455-463.

ALAGHA, M.,ALFATIH, A.,WESTBY, D. & WALSH, S. R. 2024. Review of mixed arterial venous leg ulcers (MAVLU) disease in contemporary practice. *Vascular and Endovascular Surgery,* 58**,** 747-751.

ALASMARI, F.,WALI, A.,MUKAHAL, M.,ALSURAYHI, S.,DIRAR, Q. & TAMIM, H. P-2132. Comparison of Clinical Characteristics and Risk Factors among Adult Patients with Bloodstream Infections due to candida auris vs other candida Species: a 3-year analysis in a Large Care Tertiary Hospital, Saudi Arabia. Open Forum Infectious Diseases, 2025. Oxford University Press US, ofae631. 2287.

ALKAWAREEK, M. Y.,ALGWARI, Q. T.,LAVERTY, G.,GORMAN, S. P.,GRAHAM, W. G.,O'CONNELL, D. & GILMORE, B. F. 2012. Eradication of Pseudomonas aeruginosa biofilms by atmospheric pressure non-thermal plasma.

ALLKJA, J.,BAKRI, A.,SHORT, B.,GILMOUR, A.,BROWN, J. L.,BAL, A. M.,NEWBY, K. J. M.,JENKINS, T.,SHORT, R. D.,WILLIAMS, C. & RAMAGE, G. 2025. Investigating the Prevalence of Fungi in Diabetic Ulcers: An Under-Recognised Contributor to Polymicrobial Biofilms. *Apmis,* 133**,** e70025.

ALLKJA, J.,BJARNSHOLT, T.,COENYE, T.,COS, P.,FALLARERO, A.,HARRISON, J. J.,LOPES, S. P.,OLIVER, A.,PEREIRA, M. O. & RAMAGE, G. 2020. Minimum information guideline for spectrophotometric and fluorometric methods to assess biofilm formation in microplates. *Biofilm,* 2**,** 100010.

ALLKJA, J.,VAN CHARANTE, F.,AIZAWA, J.,REIGADA, I.,GUARCH-PEREZ, C.,VAZQUEZ-RODRIGUEZ, J. A.,COS, P.,COENYE, T.,FALLARERO, A. & ZAAT, S. A. 2021. Interlaboratory study for the evaluation of three microtiter plate-based biofilm quantification methods. *Scientific reports,* 11**,** 13779.

ALMATROUDI, A. 2025. Biofilm resilience: Molecular mechanisms driving antibiotic resistance in clinical contexts. *Biology,* 14**,** 165.

ALONSO, V. P. P.,HARADA, A. M. M. & KABUKI, D. Y. 2020. Competitive and/or Cooperative Interactions of Listeria monocytogenes With Bacillus cereus in Dual-Species Biofilm Formation. *Frontiers in Microbiology,* Volume 11 - 2020.

ALQARIHI, A.,KONTOYIANNIS, D. P. & IBRAHIM, A. S. 2023. Mucormycosis in 2023: an update on pathogenesis and management. *Front Cell Infect Microbiol,* 13**,** 1254919.

ALSHANTA, O. A.,SHABAN, S.,NILE, C. J.,MCLEAN, W. & RAMAGE, G. 2019. Candida albicans Biofilm Heterogeneity and Tolerance of Clinical Isolates: Implications for Secondary Endodontic Infections. *Antibiotics (Basel),* 8.

ALSHRAIEDEH, N. H.,HIGGINBOTHAM, S.,FLYNN, P. B.,ALKAWAREEK, M. Y.,TUNNEY, M. M.,GORMAN, S. P.,GRAHAM, W. G. & GILMORE, B. F. 2016. Eradication and phenotypic tolerance of Burkholderia cenocepacia biofilms exposed to atmospheric pressure non-thermal plasma. *International journal of antimicrobial agents,* 47**,** 446-450.

ÀLVAREZ, G.,GONZÁLEZ, M.,ISABAL, S.,BLANC, V. & LEÓN, R. 2013. Method to quantify live and dead cells in multi-species oral biofilm by real-time PCR with propidium monoazide. *Amb Express,* 3**,** 1-8.

ALVES, P. J.,BARRETO, R. T.,BARROIS, B. M.,GRYSON, L. G.,MEAUME, S. & MONSTREY, S. J. 2021. Update on the role of antiseptics in the management of chronic wounds with critical colonisation and/or biofilm. *Int Wound J,* 18**,** 342-358.

ALVES, R.,BARATA-ANTUNES, C.,CASAL, M.,BROWN, A. J. P.,VAN DIJCK, P. & PAIVA, S. 2020. Adapting to survive: How Candida overcomes host-imposed constraints during human colonization. *PLOS Pathogens,* 16**,** e1008478.

AMARI, D. T.,MARQUES, C. N. H. & DAVIES, D. G. 2013. The Putative Enoyl-Coenzyme A Hydratase DspI Is Required for Production of the Pseudomonas aeruginosa Biofilm Dispersion Autoinducer cis-2-Decenoic Acid. *Journal of Bacteriology,* 195**,** 4600-4610.

ANCIRA, J.,GABRILSKA, R.,TIPTON, C.,MILLER, C.,STICKLEY, Z.,OMEIR, K.,WAKEMAN, C.,LITTLE, T.,WOLCOTT, J. & PHILIPS, C. D. 2025. A structural equation model predicts chronic wound healing time using patient characteristics and wound microbiome composition. *Wound Repair Regen,* 33**,** e70004.

ANDERSSON, M. Å.,MADSEN, L. B.,SCHMIDTCHEN, A. & PUTHIA, M. 2021. Development of an experimental ex vivo wound model to evaluate antimicrobial efficacy of topical formulations. *International journal of molecular sciences,* 22**,** 5045.

ANDO, K.,MIYAHARA, S.,HANADA, S.,FUKUDA, K.,SAITO, M.,SAKAI, A.,MARUO, A. & ZENKE, Y. 2024. Effective biofilm eradication in MRSA isolates with aminoglycoside-modifying enzyme genes using high-concentration and prolonged gentamicin treatment. *Microbiology Spectrum,* 12**,** e00647-24.

ANJU, V.,BUSI, S.,IMCHEN, M.,KUMAVATH, R.,MOHAN, M. S.,SALIM, S. A.,SUBHASWARAJ, P. & DYAVAIAH, M. 2022. Polymicrobial infections and biofilms: clinical significance and eradication strategies. *Antibiotics,* 11**,** 1731.

APELQVIST, J.,ROBSON, A.,HELMKE, A.,ROUSSEAU, A.,BOEKEMA, B.,DEN BRABER, E.,SZILI, E.,STURMER, E.,BOCKMANN, L. & GAUR, N. 2023. Cold plasma: An emerging technology for clinical use in wound healing. *Journal of Wound Management,* 25**,** S1-S83.

ARCIOLA, C. R.,CAMPOCCIA, D. & MONTANARO, L. 2018. Implant infections: adhesion, biofilm formation and immune evasion. *Nature Reviews Microbiology,* 16**,** 397-409.

ARCIOLA, C. R.,CAMPOCCIA, D.,RAVAIOLI, S. & MONTANARO, L. 2015. Polysaccharide intercellular adhesin in biofilm: structural and regulatory aspects. *Frontiers in Cellular and Infection Microbiology,* Volume 5 - 2015.

ARZMI, M. H.,ALNUAIMI, A. D.,DASHPER, S.,CIRILLO, N.,REYNOLDS, E. C. & MCCULLOUGH, M. 2016. Polymicrobial biofilm formation by Candida albicans, Actinomyces naeslundii, and Streptococcus mutans is Candida albicans strain and medium dependent. *Med Mycol,* 54**,** 856-64.

ARZMI, M. H.,DASHPER, S.,CATMULL, D.,CIRILLO, N.,REYNOLDS, E. C. & MCCULLOUGH, M. 2015. Coaggregation of Candida albicans, Actinomyces naeslundii and Streptococcus mutans is Candida albicans strain dependent. *FEMS Yeast Research,* 15.

ASANIN, J.,MISIC, D.,AKSENTIJEVIC, K.,TAMBUR, Z.,RAKONJAC, B.,KOVACEVIC, I.,SPERGSER, J. & LONCARIC, I. 2019. Genetic profiling and comparison of human and animal methicillin-resistant Staphylococcus aureus (MRSA) isolates from Serbia. *Antibiotics,* 8**,** 26.

ASHFIELD, T.,HUGHES, S.,BALTAS, I.,AMOS, J.,COORAY, M. & MOORE, L. S. P. 2023. P08 Overview of general antimicrobial prescribing guidance across NHS trusts in the United Kingdom: analysis of the Induction™ MicroGuide platform with a focus on hospital-acquired pneumonia (HAP) disease definitions. *JAC-Antimicrobial Resistance,* 5.

ASHRIT, P.,SADANANDAN, B.,SHETTY, K. & VANIYAMPARAMBATH, V. 2022. Polymicrobial Biofilm Dynamics of Multidrug-Resistant Candida albicans and Ampicillin-Resistant Escherichia coli and Antimicrobial Inhibition by Aqueous Garlic Extract. *Antibiotics,* 11**,** 573.

ASSEFA, M. & AMARE, A. 2022. Biofilm-Associated Multi-Drug Resistance in Hospital-Acquired Infections: A Review. *Infect Drug Resist,* 15**,** 5061-5068.

ATTINGER, C. & WOLCOTT, R. 2012. Clinically Addressing Biofilm in Chronic Wounds. *Adv Wound Care (New Rochelle),* 1**,** 127-132.

AYRAPETYAN, M.,WILLIAMS, T. & OLIVER, J. D. 2018. Relationship between the viable but nonculturable state and antibiotic persister cells. *Journal of bacteriology,* 200**,** 10.1128/jb. 00249-18.

AZEVEDO, A. S.,ALMEIDA, C.,MELO, L. F. & AZEVEDO, N. F. 2017. Impact of polymicrobial biofilms in catheter-associated urinary tract infections. *Critical reviews in microbiology,* 43**,** 423-439.

AZEVEDO, M.-M.,LISBOA, C.,COBRADO, L.,PINA-VAZ, C. & RODRIGUES, A. 2020. Hard-to-heal wounds, biofilm and wound healing: An intricate interrelationship. *British Journal of Nursing,* 29**,** S6-S13.

BAGHERI, M.,VON KOHOUT, M.,ZORIC, A.,FUCHS, P. C.,SCHIEFER, J. L. & OPLÄNDER, C. 2023. Can Cold Atmospheric Plasma Be Used for Infection Control in Burns? A Preclinical Evaluation. *Biomedicines,* 11**,** 1239.

BAHAMONDEZ-CANAS, T. F.,HEERSEMA, L. A. & SMYTH, H. D. C. 2019. Current Status of In Vitro Models and Assays for Susceptibility Testing for Wound Biofilm Infections. *Biomedicines,* 7.

BAIK, K. Y.,JO, H.,KI, S. H.,KWON, G.-C. & CHO, G. 2023. Synergistic Effect of Hydrogen Peroxide and Cold Atmospheric Pressure Plasma-Jet for Microbial Disinfection. *Applied Sciences,* 13**,** 3324.

BAKHTIYARI-RAMEZANI, M.,NOHEKHAN, M.,AKBARI, M. E.,ABBASVANDI, F.,BAYAT, M.,AKBARI, A. & NASIRI, M. 2024. Comparative assessment of direct and indirect cold atmospheric plasma effects, based on helium and argon, on human glioblastoma: an in vitro and in vivo study. *Sci Rep,* 14**,** 3578.

BAKKER, O.,SMITS, P.,VAN WEERSCH, C.,QUAADEN, M.,BRULS, E.,VAN LOON, A. & VAN DER KLEIJ, J. 2025. Improved Wound Healing by Direct Cold Atmospheric Plasma Once or Twice a Week: A Randomized Controlled Trial on Chronic Venous Leg Ulcers. *Adv Wound Care (New Rochelle),* 14**,** 1-13.

BANDANA, K.,JASHANDEEP, K. & JAGDEEP, K. 2018. Phospholipases in bacterial virulence and pathogenesis. *Adv Biotechnol Microbiol,* 10**,** 106-113.

BANDARA, H. M. H. N.,WOOD, D. L. A.,VANWONTERGHEM, I.,HUGENHOLTZ, P.,CHEUNG, B. P. K. & SAMARANAYAKE, L. P. 2020. Fluconazole resistance in Candida albicans is induced by Pseudomonas aeruginosa quorum sensing. *Scientific Reports,* 10**,** 7769.

BANERJEE, B.,GOWDA, P. & ANANDA, K. T. 2022. Biofilm Formation and antibiotic resistance of S. aureus strains isolated from chronic traumatic wounds. *Journal of Pure and Applied Microbiology,* 16**,** 424-429.

BANGASH, F.,MUDDASSIR, M. & BARLOW, G. 2023. Surgical site application of antibiotics: A potential game changer for fracture-related infection care and antibiotic stewardship. *J Orthop,* 46**,** 139-142.

BANKAR, N.,LATTA, L.,LORETZ, B.,REDA, B.,DUDEK, J.,HÄHL, H.,HANNIG, M. & LEHR, C.-M. 2024. Antimicrobial and antibiotic-potentiating effect of calcium peroxide nanoparticles on oral bacterial biofilms. *npj Biofilms and Microbiomes,* 10**,** 106.

BARRIENTOS, S.,STOJADINOVIC, O.,GOLINKO, M. S.,BREM, H. & TOMIC-CANIC, M. 2008. Growth factors and cytokines in wound healing. *Wound repair and regeneration,* 16**,** 585-601.

BARWELL, N. D.,DEVERS, M. C.,KENNON, B.,HOPKINSON, H. E.,MCDOUGALL, C.,YOUNG, M. J.,ROBERTSON, H. M.,STANG, D.,DANCER, S. J. & SEATON, A. 2017. Diabetic foot infection: Antibiotic therapy and good practice recommendations. *International journal of clinical practice,* 71**,** e13006.

BAXTER, K. J.,SARGISON, F. A.,FITZGERALD, J. R.,MCCONNELL, G. & HOSKISSON, P. A. 2024. Time-lapse mesoscopy of Candida albicans and Staphylococcus aureus dual-species biofilms reveals a structural role for the hyphae of C. albicans in biofilm formation. *Microbiology,* 170**,** 001426.

BAZ, A.,BAKRI, A.,BUTCHER, M.,SHORT, B.,GHIMIRE, B.,GAUR, N.,JENKINS, T.,SHORT, R. D.,RIGGIO, M.,WILLIAMS, C.,RAMAGE, G. & BROWN, J. L. 2023. Staphylococcus aureus strains exhibit heterogenous tolerance to direct cold atmospheric plasma therapy. *Biofilm,* 5**,** 100123.

BEAUDOIN, T.,YAU, Y. C. W.,STAPLETON, P. J.,GONG, Y.,WANG, P. W.,GUTTMAN, D. S. & WATERS, V. 2017. Staphylococcus aureus interaction with Pseudomonas aeruginosa biofilm enhances tobramycin resistance. *npj Biofilms and Microbiomes,* 3**,** 25.

BEAVERS, W. N. & SKAAR, E. P. 2016. Neutrophil-generated oxidative stress and protein damage in Staphylococcus aureus. *FEMS Pathogens and Disease*, 74**,** ftw060.

BECKER, S.,ZIMMERMANN, J. L.,BAUMEISTER, P.,BRUNNER, T. F.,SHIMIZU, T.,LI, Y.-F.,MORFILL, G. E.,HARRÉUS, U. & WELZ, C. 2019. Effects of cold atmospheric plasma (CAP) on bacteria and mucosa of the upper aerodigestive tract. *Auris Nasus Larynx,* 46**,** 294-301.

BEKESCHUS, S.,KOLATA, J.,WINTERBOURN, C.,KRAMER, A.,TURNER, R.,WELTMANN, K. D.,BRÖKER, B. & MASUR, K. 2014. Hydrogen peroxide: A central player in physical plasma-induced oxidative stress in human blood cells. *Free Radic Res,* 48**,** 542-9.

BESSA, L. J.,FAZII, P.,DI GIULIO, M. & CELLINI, L. 2015. Bacterial isolates from infected wounds and their antibiotic susceptibility pattern: some remarks about wound infection. *International wound journal,* 12**,** 47-52.

BESSE, A.,GROLEAU, M.-C.,TROTTIER, M.,VINCENT, A. T. & DÉZIEL, E. 2022. Pseudomonas aeruginosa strains from both clinical and environmental origins readily adopt a stable small-colony-variant phenotype resulting from single mutations in c-di-GMP pathways. *Journal of bacteriology,* 204**,** e00185-22.

BEYENE, R. T.,DERRYBERRY, S. L. & BARBUL, A. 2020. The effect of comorbidities on wound healing. *Surgical Clinics,* 100**,** 695-705.

BHATTACHARYA, M. & HORSWILL, A. R. 2024. The role of human extracellular matrix proteins in defining Staphylococcus aureus biofilm infections. *FEMS Microbiol Rev,* 48.

BHATTACHARYA, M.,WOZNIAK, D. J.,STOODLEY, P. & HALL-STOODLEY, L. 2015. Prevention and treatment of Staphylococcus aureus biofilms. *Expert Rev Anti Infect Ther,* 13**,** 1499-516.

BHATTARAI, B. & CHRISTOPHER, G. F. 2025. Mechanical properties of Staphylococcus aureus and Pseudomonas aeruginosa dual-species biofilms grown in chronic wound-based models. *Soft Matter*.

BISCOP, E.,LIN, A.,BOXEM, W. V.,LOENHOUT, J. V.,BACKER, J.,DEBEN, C.,DEWILDE, S.,SMITS, E. & BOGAERTS, A. A. 2019. Influence of Cell Type and Culture Medium on Determining Cancer Selectivity of Cold Atmospheric Plasma Treatment. *Cancers (Basel),* 11.

BISWAS, L. & GÖTZ, F. 2022. Molecular Mechanisms of Staphylococcus and Pseudomonas Interactions in Cystic Fibrosis. *Frontiers in Cellular and Infection Microbiology,* Volume 11 - 2021.

BISWAS, T.,AHMED, M. & MONDAL, S. 2024. Mixed species biofilm: structure, challenge and its intricate involvement in hospital associated infections. *Microbial Pathogenesis***,** 106866.

BLAISE, O.,DUCHESNE, C.,CAPUZZO, E.,NAHORI, M. A.,FERNANDES, J.,CONNOR, M. G.,HAMON, M. A.,PIZARRO-CERDA, J.,LATAILLADE, J. J.,MCGUCKIN, C.,ROUSSEAU, A.,BANZET, S.,DUSSURGET, O. & FRESCALINE, N. 2024. Infected wound repair correlates with collagen I induction and NOX2 activation by cold atmospheric plasma. *NPJ Regen Med,* 9**,** 28.

BOEKEMA, B.,STOOP, M.,VLIG, M.,VAN LIEMPT, J.,SOBOTA, A.,ULRICH, M. & MIDDELKOOP, E. 2021. Antibacterial and safety tests of a flexible cold atmospheric plasma device for the stimulation of wound healing. *Appl Microbiol Biotechnol,* 105**,** 2057-2070.

BOLGEO, T.,MACONI, A.,GARDALINI, M.,GATTI, D.,DI MATTEO, R.,LAPIDARI, M.,LONGHITANO, Y.,SAVIOLI, G.,PICCIONI, A. & ZANZA, C. 2023. The Role of Cold Atmospheric Plasma in Wound Healing Processes in Critically Ill Patients. *J Pers Med,* 13.

BORCHARDT, T.,ERNST, J.,HELMKE, A.,TANYELI, M.,SCHILLING, A. F.,FELMERER, G. & VIÖL, W. 2017. Effect of direct cold atmospheric plasma (diCAP) on microcirculation of intact skin in a controlled mechanical environment. *Microcirculation,* 24.

BORMAN, A. M.,SZEKELY, A. & JOHNSON, E. M. 2016. Comparative pathogenicity of United Kingdom isolates of the emerging pathogen Candida auris and other key pathogenic Candida species. *MSphere,* 1**,** 10.1128/msphere. 00189-16.

BOSANQUET, D. C.,RANGARAJ, A.,RICHARDS, A. J.,RIDDELL, A.,SARAVOLAC, V. M. & HARDING, K. G. 2013. Topical steroids for chronic wounds displaying abnormal inflammation. *Ann R Coll Surg Engl,* 95**,** 291-6.

BOWLER, P.,DUERDEN, B. & ARMSTRONG, D. G. 2001. Wound microbiology and associated approaches to wound management. *Clinical microbiology reviews,* 14**,** 244-269.

BOYD, N. K.,TENG, C. & FREI, C. R. 2021. Brief Overview of Approaches and Challenges in New Antibiotic Development: A Focus On Drug Repurposing. *Frontiers in Cellular and Infection Microbiology,* Volume 11 - 2021.

BRACKMAN, G. & COENYE, T. 2015. In vitro and in vivo biofilm wound models and their application. *Advances in Microbiology, Infectious Diseases and Public Health: Volume 1***,** 15-32.

BRANDI, G.,CATTABENI, F.,ALBANO, A. & CANTONI, O. 1989a. Role of hydroxyl radicals in escherzchza colz killing induced by hydrogen peroxide. *Free radical research communications,* 6**,** 47-55.

BRANDI, G.,FIORANI, M.,PIEROTTI, C.,ALBANO, A.,CATTABENI, F. & CANTONI, O. 1989b. Morphological changes in Escherichia coli cells exposed to low or high concentrations of hydrogen peroxide. *Microbiol Immunol,* 33**,** 991-1000.

BRANÝ, D.,DVORSKÁ, D.,HALAŠOVÁ, E. & ŠKOVIEROVÁ, H. 2020. Cold atmospheric plasma: A powerful tool for modern medicine. *International journal of molecular sciences,* 21**,** 2932.

BREATHNACH, R.,MCDONNELL, K. A.,CHEBBI, A.,CALLANAN, J. J. & DOWLING, D. P. 2018. Evaluation of the effectiveness of kINPen Med plasma jet and bioactive agent therapy in a rat model of wound healing. *Biointerphases,* 13**,** 051002.

BRIAN, J. P.,SICCO, A. B.,GARY, M. R.,DAVID, R. L.,LAWRENCE, A. L. & DAVID, G. A. 2020. Recurrence rates suggest delayed identification of plantar ulceration for patients in diabetic foot remission. *BMJ Open Diabetes Research & Care,* 8**,** e001697.

BROCHADO, A. R.,TELZEROW, A.,BOBONIS, J.,BANZHAF, M.,MATEUS, A.,SELKRIG, J.,HUTH, E.,BASSLER, S.,ZAMARREÑO BEAS, J. & ZIETEK, M. 2018. Species-specific activity of antibacterial drug combinations. *Nature,* 559**,** 259-263.

BROWN, J. L.,DELANEY, C.,SHORT, B.,BUTCHER, M. C.,MCKLOUD, E.,WILLIAMS, C.,KEAN, R. & RAMAGE, G. 2020. Candida auris Phenotypic Heterogeneity

Determines Pathogenicity In Vitro. *mSphere*, 5, 10.1128/msphere.00371-20.

BROWN, J. L.,TOWNSEND, E.,SHORT, R. D.,WILLIAMS, C.,WOODALL, C.,NILE, C. J. & RAMAGE, G. 2022. Assessing the inflammatory response to in vitro polymicrobial wound biofilms in a skin epidermis model. *npj Biofilms and Microbiomes,* 8, 19.

BROWN, N. M.,GOODMAN, A. L.,HORNER, C.,JENKINS, A. & BROWN, E. M. 2021. Treatment of methicillin-resistant Staphylococcus aureus (MRSA): updated guidelines from the UK. *JAC Antimicrob Resist,* 3, dlaa114.

BROWN, S.,SANTA MARIA JR, J. P. & WALKER, S. 2013. Wall teichoic acids of gram-positive bacteria. *Annual review of microbiology,* 67, 313-336.

BRUGGEMAN, P. J.,KUSHNER, M. J.,LOCKE, B. R.,GARDENIERS, J. G.,GRAHAM, W.,GRAVES, D. B.,HOFMAN-CARIS, R.,MARIC, D.,REID, J. P. & CERIANI, E. 2016. Plasma–liquid interactions: a review and roadmap. *Plasma sources science and technology,* 25, 053002.

BURNET, M.,METCALF, D. G.,MILO, S.,GAMERITH, C.,HEINZLE, A.,SIGL, E.,EITEL, K.,HAALBOOM, M. & BOWLER, P. G. 2022. A host-directed approach to the detection of infection in hard-to-heal wounds. *Diagnostics,* 12, 2408.

CABALLERO-SÁNCHEZ, N.,ALONSO-ALONSO, S. & NAGY, L. 2024. Regenerative inflammation: When immune cells help to re-build tissues. *The FEBS journal,* 291, 1597-1614.

CAI, Y. M. & WEBB, J. S. 2020. Optimization of nitric oxide donors for investigating biofilm dispersal response in Pseudomonas aeruginosa clinical isolates. *Appl Microbiol Biotechnol,* 104, 8859-8869.

CALDWELL, M. D. 2020. Bacteria and antibiotics in wound healing. *Surgical Clinics,* 100, 757-776.

CALEY, M. P.,MARTINS, V. L. & O'TOOLE, E. A. 2015. Metalloproteinases and wound healing. *Advances in wound care,* 4, 225-234.

CAMPOCCIA, D.,MONTANARO, L. & ARCIOLA, C. R. 2021. Extracellular DNA (eDNA). A major ubiquitous element of the bacterial biofilm architecture. *International journal of molecular sciences,* 22, 9100.

CAO, L.,MI, J.,HE, Y.,XUAN, G.,WANG, J.,LI, M. & TONG, Y. 2025. Quorum sensing inhibits phage infection by regulating biofilm formation of P. aeruginosa PAO1. *J Virol,* 99, e0187224.

CÁRDENAS-CALDERÓN, C.,VELOSO-GIMÉNEZ, V.,GONZÁLEZ, T.,WOZNIAK, A.,GARCÍA, P.,MARTÍN, S. S.,VARAS, J. F.,CARRASCO-WONG, I.,VERA, M. & EGAÑA, J. T. 2022. Development of an implantable three-dimensional model of a functional pathogenic multispecies biofilm to study infected wounds. *Scientific Reports,* 12**,** 21846.

CASTANHEIRA, M.,MILLS, J. C.,FARRELL, D. J. & JONES, R. N. 2014. Mutation-driven β-lactam resistance mechanisms among contemporary ceftazidime-nonsusceptible Pseudomonas aeruginosa isolates from U.S. hospitals. *Antimicrob Agents Chemother,* 58**,** 6844-50.

CASTONGUAY, M.-H.,VAN DER SCHAAF, S.,KOESTER, W.,KROONEMAN, J.,VAN DER MEER, W.,HARMSEN, H. & LANDINI, P. 2006. Biofilm formation by Escherichia coli is stimulated by synergistic interactions and co-adhesion mechanisms with adherence-proficient bacteria. *Research in Microbiology,* 157**,** 471-478.

CAZARES-DOMINGUEZ, V.,CRUZ-CORDOVA, A.,OCHOA, S. A.,ESCALONA, G.,ARELLANO-GALINDO, J.,RODRIGUEZ-LEVIZ, A.,HERNANDEZ-CASTRO, R.,LOPEZ-VILLEGAS, E. O. & XICOHTENCATL-CORTES, J. 2015. Vancomycin tolerant, methicillin-resistant Staphylococcus aureus reveals the effects of vancomycin on cell wall thickening. *PLoS One,* 10**,** e0118791.

CHAHAL, R.,NANDA, A.,AKKOL, E. K.,SOBARZO-SÁNCHEZ, E.,ARYA, A.,KAUSHIK, D.,DUTT, R.,BHARDWAJ, R.,RAHMAN, M. H. & MITTAL, V. 2021. Ageratum conyzoides L. and Its Secondary Metabolites in the Management of Different Fungal Pathogens. *Molecules,* 26.

CHAPLIN, S. 2020. NICE on antimicrobial prescribing for leg ulcer infection. *Prescriber,* 31**,** 27-30.

CHAPMAN, A. L. N.,PATEL, S.,HORNER, C.,GREEN, H.,GULERI, A.,HEDDERWICK, S.,SNAPE, S.,STATHAM, J.,WILSON, E.,GILCHRIST, M. & SEATON, R. A. 2019. Updated good practice recommendations for outpatient parenteral antimicrobial therapy (OPAT) in adults and children in the UK. *JAC Antimicrob Resist,* 1**,** dlz026.

CHATRAIE, M.,TORKAMAN, G.,KHANI, M.,SALEHI, H. & SHOKRI, B. 2018. In vivo study of non-invasive effects of non-thermal plasma in pressure ulcer treatment. *Scientific Reports,* 8**,** 5621.

CHAUVIN, J.,JUDÉE, F.,YOUSFI, M.,VICENDO, P. & MERBAHI, N. 2017. Analysis of reactive oxygen and nitrogen species generated in three liquid media by low temperature helium plasma jet. *Scientific Reports,* 7**,** 4562.

CHEN, R.,SAINT BEZARD, J.,SWANN, M. J.,WATSON, F. & PERCIVAL, S. L. 2024. An In Vitro Artificial Wound Slough–Biofilm Model Developed for Evaluating a Novel Antibiofilm Technology. *Microorganisms,* 12**,** 2223.

CHEN, T. P.,LIANG, J. & SU, T. L. 2018. Plasma-activated water: antibacterial activity and artifacts? *Environ Sci Pollut Res Int,* 25**,** 26699-26706.

CHEN, X.,LORENZEN, J.,XU, Y.,JONIKAITE, M.,THAARUP, I. C.,BJARNSHOLT, T.,KIRKETERP-MØLLER, K. & THOMSEN, T. R. 2021. A novel chronic wound biofilm model sustaining coexistence of Pseudomonas aeruginosa and Staphylococcus aureus suitable for testing of antibiofilm effect of antimicrobial solutions and wound dressings. *Wound Repair and Regeneration,* 29**,** 820-829.

CHEN, X. & STEWART, P. S. 2002. Role of electrostatic interactions in cohesion of bacterial biofilms. *Applied microbiology and biotechnology,* 59**,** 718-720.

CHEW, S. C.,KUNDUKAD, B.,SEVIOUR, T.,MAAREL, J. R. C. V. D.,YANG, L.,RICE, S. A.,DOYLE, P. & KJELLEBERG, S. 2014. Dynamic Remodeling of Microbial Biofilms by Functionally Distinct Exopolysaccharides. *mBio,* 5**,** e01536-14.

CHOI, Y.,BANERJEE, A.,MCNISH, S.,COUCH, K. S.,TORRALBA, M. G.,LUCAS, S.,TOVCHIGRECHKO, A.,MADUPU, R.,YOOSEPH, S.,NELSON, K. E.,SHANMUGAM, V. K. & CHAN, A. P. 2019. Co-occurrence of Anaerobes in Human Chronic Wounds. *Microbial Ecology,* 77**,** 808-820.

CHONG, P. P.,CHIN, V. K.,WONG, W. F.,MADHAVAN, P.,YONG, V. C. & LOOI, C. Y. 2018. Transcriptomic and Genomic Approaches for Unravelling Candida albicans Biofilm Formation and Drug Resistance-An Update. *Genes (Basel),* 9.

CHOUDHURY, M. & DOWNIE, F. 2022. A biofilm based wound care pathway in the community setting: a review. *Wounds UK,* 18.

CHOWDHARY, A.,JAIN, K. & CHAUHAN, N. 2023. Candida auris Genetics and Emergence. *Annual Review of Microbiology,* 77**,** 583-602.

CHRISTENSEN, G. D.,SIMPSON, W. A.,YOUNGER, J.,BADDOUR, L.,BARRETT, F.,MELTON, D. & BEACHEY, E. 1985. Adherence of coagulase-negative staphylococci to plastic tissue culture plates: a quantitative model for the

adherence of staphylococci to medical devices. *Journal of clinical microbiology,* 22**,** 996-1006.

CIAROLLA, A. A.,LAPIN, N.,WILLIAMS, D.,CHOPRA, R. & GREENBERG, D. E. 2022. Physical Approaches to Prevent and Treat Bacterial Biofilm. *Antibiotics (Basel),* 12.

CLSI 2015. *Methods for Dilution Antimicrobial Susceptibility Tests for Bacteria That Grow Aerobically; Approved Standard—Tenth Edition*. CLSI document M07-A10. Wayne, PA: Clinical and Laboratory Standard Institute; 2015.

COLUCCIO, A.,LOPEZ PALOMERA, F. & SPERO, M. A. 2024. Anaerobic bacteria in chronic wounds: Roles in disease, infection and treatment failure. *Wound Repair Regen,* 32**,** 840-857.

CONTI, A.,BRILLI, M.,NORGINI, E.,FALINI, S.,DE FINA, L.,SPARGI, G. & GASPERINI, S. 2023. Blue light photobiomodulation: a therapy to reactivate the healing process of stagnant wounds of different aetiologies. *Wound International*, 14**,** 41-45.

CORTEGIANI, A.,MISSERI, G.,GIARRATANO, A.,BASSETTI, M. & EYRE, D. 2019. The global challenge of Candida auris in the intensive care unit. *Crit Care,* 23**,** 150.

CORTES-PENFIELD, N. W.,ARMSTRONG, D. G.,BRENNAN, M. B.,FAYFMAN, M.,RYDER, J. H.,TAN, T. W. & SCHECHTER, M. C. 2023. Evaluation and Management of Diabetes-related Foot Infections. *Clin Infect Dis,* 77**,** e1-e13.

COSGROVE, K.,COUTTS, G.,JONSSON, I. M.,TARKOWSKI, A.,KOKAI-KUN, J. F.,MOND, J. J. & FOSTER, S. J. 2007. Catalase (KatA) and alkyl hydroperoxide reductase (AhpC) have compensatory roles in peroxide stress resistance and are required for survival, persistence, and nasal colonization in Staphylococcus aureus. *J Bacteriol,* 189**,** 1025-35.

COUTO, N.,NEWTON, J. R.,RUSSO, C.,KARUNAKARAN, E.,ACHOUR, B.,AL-MAJDOUB, Z. M.,SIDAWAY, J.,ROSTAMI-HODJEGAN, A.,CLENCH, M. R. & BARBER, J. 2021. Label-free quantitative proteomics and substrate-based mass spectrometry imaging of xenobiotic metabolizing enzymes in ex vivo human skin and a human living skin equivalent model. *Drug Metabolism and Disposition,* 49**,** 39-52.

COX, C. A.,MANAVATHU, E. K.,WAKADE, S.,MYNTTI, M. & VAZQUEZ, J. A. 2024. Efficacy of biofilm disrupters against Candida auris and other Candida species in monomicrobial and polymicrobial biofilms. *Mycoses,* 67**,** e13684.

CRAFT, K. M.,NGUYEN, J. M.,BERG, L. J. & TOWNSEND, S. D. 2019. Methicillin-resistant Staphylococcus aureus (MRSA): antibiotic-resistance and the biofilm phenotype. *MedChemComm,* 10**,** 1231-1241.

CUI, J.,ZHANG, H.,MO, Z.,YU, M. & LIANG, Z. 2021. Cell wall thickness and the molecular mechanism of heterogeneous vancomycin-intermediate Staphylococcus aureus. *Lett Appl Microbiol,* 72**,** 604-609.

CURUKOGLU, A.,GUNGOR, G. C. A.,AKAN, G.,KUKNER, A.,OGUTCU, G.,KALAYCI, M.,TEMIZEL, M. & OZGENCIL, F. E. 2023. The effect of cold atmospheric plasma (NO) alone and in combination with NPH insulin on the full-thickness excisional wound healing in a diabetic rat model. *Vet Med (Praha),* 68**,** 152-163.

DARVISHI, S.,TAVAKOLI, S.,KHARAZIHA, M.,GIRAULT, H. H.,KAMINSKI, C. F. & MELA, I. 2022. Advances in the sensing and treatment of wound biofilms. *Angewandte Chemie International Edition,* 61**,** e202112218.

DAVENPORT, E. K.,CALL, D. R. & BEYENAL, H. 2014. Differential protection from tobramycin by extracellular polymeric substances from Acinetobacter baumannii and Staphylococcus aureus biofilms. *Antimicrob Agents Chemother,* 58**,** 4755-61.

DAVIES, D. G. & MARQUES, C. N. 2009. A fatty acid messenger is responsible for inducing dispersion in microbial biofilms. *Journal of bacteriology,* 191**,** 1393-1403.

DAVIS, S. & HORZEMPA, J. 2024. The Pseudomonas aeruginosa 1244 pilin glycan increases susceptibility to human beta defensin 2 but enhances twitching motility. *Proceedings of the West Virginia Academy of Science*.

DE GAETANO, S.,MIDIRI, A.,MANCUSO, G.,AVOLA, M. G. & BIONDO, C. 2024. Candida auris Outbreaks: Current Status and Future Perspectives. *Microorganisms,* 12.

DE SOIR, S.,PARÉE, H.,KAMARUDIN, N. H. N.,WAGEMANS, J.,LAVIGNE, R.,BRAEM, A.,MERABISHVILI, M.,DE VOS, D.,PIRNAY, J. P. & VAN BAMBEKE, F. 2024. Exploiting phage-antibiotic synergies to disrupt Pseudomonas aeruginosa PAO1 biofilms in the context of orthopedic infections. *Microbiol Spectr,* 12**,** e0321923.

DE SOUSA, T.,HÉBRAUD, M.,ALVES, O.,COSTA, E.,MALTEZ, L.,PEREIRA, J. E.,MARTINS, Â.,IGREJAS, G. & POETA, P. 2023. Study of Antimicrobial Resistance, Biofilm Formation, and Motility of Pseudomonas aeruginosa Derived from Urine Samples. *Microorganisms,* 11.

DE VOR, L.,ROOIJAKKERS, S. H. M. & VAN STRIJP, J. A. G. 2020. Staphylococci evade the innate immune response by disarming neutrophils and forming biofilms. *FEBS Letters,* 594**,** 2556-2569.

DEHGHANPISHEH, P.,JAHANDIDEH, A.,ASGHARI, A.,MORTAZAVI, P. & GHORANNEVIS, M. 2023. Effects of cold atmospheric plasma on infectious diabetic wound healing in rat models.

DELANEY, C.,SHORT, B.,RAJENDRAN, R.,KEAN, R.,BURGESS, K.,WILLIAMS, C.,MUNRO, C. A. & RAMAGE, G. 2023. An integrated transcriptomic and metabolomic approach to investigate the heterogeneous Candida albicans biofilm phenotype. *Biofilm,* 5**,** 100112.

DELBEN, J. A.,ZAGO, C. E.,TYHOVYCH, N.,DUARTE, S. & VERGANI, C. E. 2016. Effect of atmospheric-pressure cold plasma on pathogenic oral biofilms and in vitro reconstituted oral epithelium. *PloS one,* 11**,** e0155427.

DEMIDOVA-RICE, T. N.,HAMBLIN, M. R. & HERMAN, I. M. 2012. Acute and impaired wound healing: pathophysiology and current methods for drug delivery, part 1: normal and chronic wounds: biology, causes, and approaches to care. *Advances in skin & wound care,* 25**,** 304-314.

DEO, R.,USHA, L.,MIHIR, O.,KUMAR, N. V. & AND SHARMA, S. R. 2024. Exopolysaccharides in microbial interactions: signalling, quorum sensing, and community dynamics. *Natural Product Research***,** 1-16.

DEVEAU, A.,BONITO, G.,UEHLING, J.,PAOLETTI, M.,BECKER, M.,BINDSCHEDLER, S.,HACQUARD, S.,HERVÉ, V.,LABBÉ, J. & LASTOVETSKY, O. A. 2018a. Bacterial–fungal interactions: ecology, mechanisms and challenges. *FEMS microbiology reviews,* 42**,** 335-352.

DEVEAU, A.,BONITO, G.,UEHLING, J.,PAOLETTI, M.,BECKER, M.,BINDSCHEDLER, S.,HACQUARD, S.,HERVÉ, V.,LABBÉ, J.,LASTOVETSKY, O. A.,MIESZKIN, S.,MILLET, L. J.,VAJNA, B.,JUNIER, P.,BONFANTE, P.,KROM, B. P.,OLSSON, S.,VAN ELSAS, J. D. & WICK, L. Y. 2018b. Bacterial–fungal interactions: ecology, mechanisms and challenges. *FEMS Microbiology Reviews,* 42**,** 335-352.

DHEKANE, R.,MHADE, S. & KAUSHIK, K. S. 2022. Adding a new dimension: Multi-level structure and organization of mixed-species Pseudomonas aeruginosa and Staphylococcus aureus biofilms in a 4-D wound microenvironment. *Biofilm,* 4**,** 100087.

DIBAN, F.,DI LODOVICO, S.,DI FERMO, P.,D'ERCOLE, S.,D'ARCANGELO, S.,DI GIULIO, M. & CELLINI, L. 2023. Biofilms in Chronic Wound Infections: Innovative Antimicrobial Approaches Using the In Vitro Lubbock Chronic Wound Biofilm Model. *Int J Mol Sci,* 24.

DISSEMOND, J.,EBERLEIN, T.,BÜLTEMANN, A.,RIEPE, G.,STOFFELS, I.,STEPHEN-HAYNES, J.,ROES, C. & ABEL, M. 2018. A purpose-designed monofilament-fibre pad for debridement of hard-to-reach wounds: experience in clinical practice. *J Wound Care,* 27**,** 421-425.

DOWD, S.,DELTON HANSON, J.,REES, E.,WOLCOTT, R.,ZISCHAU, A.,SUN, Y.,WHITE, J.,SMITH, D.,KENNEDY, J. & JONES, C. 2011. Survey of fungi and yeast in polymicrobial infections in chronic wounds. *Journal of wound care,* 20**,** 40-47.

DOWD, S. E.,SUN, Y.,SECOR, P. R.,RHOADS, D. D.,WOLCOTT, B. M.,JAMES, G. A. & WOLCOTT, R. D. 2008a. Survey of bacterial diversity in chronic wounds using Pyrosequencing, DGGE, and full ribosome shotgun sequencing. *BMC Microbiology,* 8**,** 43.

DOWD, S. E.,WOLCOTT, R. D.,SUN, Y.,MCKEEHAN, T.,SMITH, E. & RHOADS, D. 2008b. Polymicrobial nature of chronic diabetic foot ulcer biofilm infections determined using bacterial tag encoded FLX amplicon pyrosequencing (bTEFAP). *PloS one,* 3**,** e3326.

DUCHESNE, C.,FRESCALINE, N.,BLAISE, O.,LATAILLADE, J.-J.,BANZET, S.,DUSSURGET, O. & ROUSSEAU, A. 2021. Cold Atmospheric Plasma Promotes Killing of Staphylococcus aureus by Macrophages. *mSphere,* 6**,** 10.1128/msphere.00217-21.

DÜHRING, S. & SCHUSTER, S. 2024. Studying mixed-species biofilms of Candida albicans and Staphylococcus aureus using evolutionary game theory. *PLOS ONE,* 19**,** e0297307.

DURAND, B. A.,POUGET, C.,MAGNAN, C.,MOLLE, V.,LAVIGNE, J.-P. & DUNYACH-REMY, C. 2022. Bacterial interactions in the context of chronic wound biofilm: a review. *Microorganisms,* 10**,** 1500.

DUTHIE, E. & LORENZ, L. L. 1952. Staphylococcal coagulase: mode of action and antigenicity. *Microbiology,* 6**,** 95-107.

DWYER, D. J.,BELENKY, P. A.,YANG, J. H.,MACDONALD, I. C.,MARTELL, J. D.,TAKAHASHI, N.,CHAN, C. T. Y.,LOBRITZ, M. A.,BRAFF, D.,SCHWARZ, E. G.,YE, J. D.,PATI, M.,VERCRUYSSE, M.,RALIFO, P. S.,ALLISON, K. R.,KHALIL, A. S.,TING, A. Y.,WALKER, G. C. & COLLINS, J. J. 2014. Antibiotics induce redox-related physiological alterations as part of their lethality. *Proceedings of the National Academy of Sciences,* 111**,** E2100-E2109.

EDSBERG, L. E.,BLACK, J. M.,GOLDBERG, M.,MCNICHOL, L.,MOORE, L. & SIEGGREEN, M. 2016. Revised National Pressure Ulcer Advisory Panel Pressure Injury Staging System: Revised Pressure Injury Staging System. *J Wound Ostomy Continence Nurs,* 43**,** 585-597.

EDWARD, E. A.,EL SHEHAWY, M. R.,ABOUELFETOUH, A. & ABOULMAGD, E. 2023. Prevalence of different virulence factors and their association with antimicrobial resistance among Pseudomonas aeruginosa clinical isolates from Egypt. *BMC Microbiol,* 23**,** 161.

EDWARDS-JONES, V. 2018. Biofilm-based wound care: how to cleanse, debride and manage chronic wounds. *Wounds UK,* 14**,** 10-16.

EDWARDS-JONES, V. 2020. Antimicrobial stewardship in wound care. *British Journal of Nursing,* 29**,** S10-S16.

EGOROVA, D. A.,SOLOVYEV, A. I.,POLYAKOV, N. B.,DANILOVA, K. V.,SCHERBAKOVA, A. A.,KRAVTSOV, I. N.,DMITRIEVA, M. A.,RYKOVA, V. S.,TUTYKHINA, I. L.,ROMANOVA, Y. M. & GINTSBURG, A. L. 2022. Biofilm matrix proteome of clinical strain of P. aeruginosa isolated from bronchoalveolar lavage of patient in intensive care unit. *Microb Pathog,* 170**,** 105714.

EICHELBERGER, K. R. & CASSAT, J. E. 2021. Metabolic adaptations during Staphylococcus aureus and Candida albicans co-infection. *Frontiers in immunology,* 12**,** 797550.

EICHELBERGER, K. R.,PAUL, S.,PETERS, B. M. & CASSAT, J. E. 2023. Candida-bacterial cross-kingdom interactions. *Trends in microbiology,* 31**,** 1287-1299.

EISELT, V. A.,BERESWILL, S. & HEIMESAAT, M. M. 2024. Phage therapy in prosthetic joint infections caused by Staphylococcus aureus - A literature review. *Eur J Microbiol Immunol (Bp),* 14**,** 75-85.

EIX, E. F. & NETT, J. E. 2022. Modeling Candida auris skin colonization: Mice, swine, and humans. *PLoS Pathog,* 18**,** e1010730.

EL HUSSEINI, N.,CARTER, J. A. & LEE, V. T. 2024. Urinary tract infections and catheter-associated urinary tract infections caused by Pseudomonas aeruginosa. *Microbiol Mol Biol Rev,* 88**,** e0006622.

ELFADADNY, A.,RAGAB, R. F.,ALHARBI, M.,BADSHAH, F.,IBÁÑEZ-ARANCIBIA, E.,FARAG, A.,HENDAWY, A. O.,DE LOS RÍOS-ESCALANTE, P. R.,ABOUBAKR, M. & ZAKAI, S. A. 2024. Antimicrobial resistance of Pseudomonas aeruginosa: navigating clinical impacts, current resistance trends, and innovations in breaking therapies. *Frontiers in Microbiology,* 15**,** 1374466.

ERIKSSON, E.,LIU, P. Y.,SCHULTZ, G. S.,MARTINS-GREEN, M. M.,TANAKA, R.,WEIR, D.,GOULD, L. J.,ARMSTRONG, D. G.,GIBBONS, G. W. & WOLCOTT, R. 2022. Chronic wounds: Treatment consensus. *Wound repair and regeneration,* 30**,** 156-171.

ERLANDSEN, S. L.,KRISTICH, C. J.,DUNNY, G. M. & WELLS, C. L. 2004. High-resolution visualization of the microbial glycocalyx with low-voltage scanning electron microscopy: dependence on cationic dyes. *Journal of Histochemistry & Cytochemistry,* 52**,** 1427-1435.

ESHIMA, S.,KURAKADO, S.,MATSUMOTO, Y.,KUDO, T. & SUGITA, T. 2022. Candida albicans Promotes the Antimicrobial Tolerance of Escherichia coli in a Cross-Kingdom Dual-Species Biofilm. *Microorganisms,* 10.

FAN, F.,LIU, Y.,LIU, Y.,LV, R.,SUN, W.,DING, W.,CAI, Y.,LI, W.,LIU, X. & QU, W. 2022. Candida albicans biofilms: antifungal resistance, immune evasion, and emerging therapeutic strategies. *International Journal of Antimicrobial Agents,* 60**,** 106673.

FAN, Y.,SEKAR, A.,MCCANNE, M.,YUH, J.,KANNAMBADI, D. D.,LEKKALA, S.,MURATOGLU, O. K. & ORAL, E. 2025. Immune response against antibiotic-resistant and antibiotic-sensitive staphylococcus aureus in a rat model of implant infection. *Scientific Reports,* 15**,** 13264.

FANAEI PIRLAR, R.,EMANEINI, M.,BEIGVERDI, R.,BANAR, M.,B. VAN LEEUWEN, W. & JABALAMELI, F. 2020. Combinatorial effects of antibiotics and enzymes against dual-species Staphylococcus aureus and Pseudomonas aeruginosa biofilms in the wound-like medium. *PLOS ONE,* 15**,** e0235093.

FEHRMANN, C.,JURK, K.,BERTLING, A.,SEIDEL, G.,FEGELER, W.,KEHREL, B. E.,PETERS, G.,BECKER, K. & HEILMANN, C. 2013. Role for the fibrinogen-

binding proteins Coagulase and Efb in the Staphylococcus aureus–Candida interaction. *International Journal of Medical Microbiology,* 303**,** 230-238.

FERNÁNDEZ-BILLÓN, M.,LLAMBÍAS-CABOT, A. E.,JORDANA-LLUCH, E.,OLIVER, A. & MACIÀ, M. D. 2023. Mechanisms of antibiotic resistance in Pseudomonas aeruginosa biofilms. *Biofilm,* 5**,** 100129.

FISHER, J. F. & MOBASHERY, S. 2021. ß-Lactams against the Fortress of the Gram-Positive Staphylococcus aureus Bacterium. *Chemical Reviews,* 121**,** 3412-3463.

FLEMING, D.,NIESE, B.,REDMAN, W.,VANDERPOOL, E.,GORDON, V. & RUMBAUGH, K. P. 2022. Contribution of Pseudomonas aeruginosa Exopolysaccharides Pel and Psl to Wound Infections. *Front Cell Infect Microbiol,* 12**,** 835754.

FLEMMING, H.-C.,WINGENDER, J.,SZEWZYK, U.,STEINBERG, P.,RICE, S. A. & KJELLEBERG, S. 2016. Biofilms: an emergent form of bacterial life. *Nature Reviews Microbiology,* 14**,** 563-575.

FLEMMING, H.-C. & WUERTZ, S. 2019. Bacteria and archaea on Earth and their abundance in biofilms. *Nature Reviews Microbiology,* 17**,** 247-260.

FLETCHER, J.,PORTER, R.,BOULTON, Z.,BROWN, L.,KNIGHT, B.,ROMANCZUK, L.,AIKEN, S.,DELURY, C. & MICHELL, S. 2022. In vitro efficacy of antibiotic loaded calcium sulfate beads (Stimulan Rapid Cure) against polymicrobial communities and individual bacterial strains derived from diabetic foot infections. *Journal of Medical Microbiology,* 71**,** 001517.

FLYNN, P. B.,HIGGINBOTHAM, S.,NID'A, H. A.,GORMAN, S. P.,GRAHAM, W. G. & GILMORE, B. F. 2015. Bactericidal efficacy of atmospheric pressure non-thermal plasma (APNTP) against the ESKAPE pathogens. *International journal of antimicrobial agents,* 46**,** 101-107.

FONZI, W. A. & IRWIN, M. Y. 1993. Isogenic strain construction and gene mapping in Candida albicans. *Genetics,* 134**,** 717-28.

FORGÁCS, L.,BORMAN, A. M.,PRÉPOST, E.,TÓTH, Z.,KARDOS, G.,KOVÁCS, R.,SZEKELY, A.,NAGY, F.,KOVACS, I. & MAJOROS, L. 2020. Comparison of in vivo pathogenicity of four Candida auris clades in a neutropenic bloodstream infection murine model. *Emerg Microbes Infect,* 9**,** 1160-1169.

FOSTER, T. J. 2017. Antibiotic resistance in Staphylococcus aureus. Current status and future prospects. *FEMS Microbiology Reviews,* 41**,** 430-449.

FRANCOLINI, I.,VUOTTO, C.,PIOZZI, A. & DONELLI, G. 2017. Antifouling and antimicrobial biomaterials: an overview. *APMIS,* 125**,** 392-417.

FRYKBERG, R. G. & BANKS, J. 2015. Challenges in the treatment of chronic wounds. *Advances in wound care,* 4**,** 560-582.

FUGÈRE, A.,LALONDE SÉGUIN, D.,MITCHELL, G.,DÉZIEL, E.,DEKIMPE, V.,CANTIN, A. M.,FROST, E. & MALOUIN, F. 2014. Interspecific small molecule interactions between clinical isolates of Pseudomonas aeruginosa and Staphylococcus aureus from adult cystic fibrosis patients. *PLoS One,* 9**,** e86705.

GAÁLOVÁ-RADOCHOVÁ, B.,KENDRA, S.,JORDAO, L.,KURSAWE, L.,KIKHNEY, J.,MOTER, A. & BUJDÁKOVÁ, H. 2023. Effect of quorum sensing molecule farnesol on mixed biofilms of Candida albicans and Staphylococcus aureus. *Antibiotics,* 12**,** 441.

GABRILSKA, R. A. & RUMBAUGH, K. P. 2015. Biofilm models of polymicrobial infection. *Future microbiology,* 10**,** 1997-2015.

GAO, Y.,CAO, Q.,XIAO, Y.,WU, Y.,DING, L.,HUANG, H.,LI, Y.,YANG, J. & MENG, L. 2024. The progress and future of the treatment of Candida albicans infections based on nanotechnology. *J Nanobiotechnology,* 22**,** 568.

GARCÍA, A. B.,VIÑUELA-PRIETO, J. M.,LÓPEZ-GONZÁLEZ, L. & CANDEL, F. J. 2017. Correlation between resistance mechanisms in Staphylococcus aureus and cell wall and septum thickening. *Infection and drug resistance***,** 353-356.

GAUPP, R.,LEDALA, N. & SOMERVILLE, G. A. 2012. Staphylococcal response to oxidative stress. *Frontiers in cellular and infection microbiology,* 2**,** 33.

GAUR, N.,PATENALL, B. L.,GHIMIRE, B.,THET, N. T.,GARDINER, J. E.,LE DOARE, K. E.,RAMAGE, G.,SHORT, B.,HEYLEN, R. A. & WILLIAMS, C. 2023. Cold atmospheric plasma-activated composite hydrogel for an enhanced and on-demand delivery of antimicrobials. *ACS Applied Materials & Interfaces,* 15**,** 19989-19996.

GE, Y. & WANG, Q. 2023. Current research on fungi in chronic wounds. *Frontiers in molecular biosciences,* 9**,** 1057766.

GEBREMARIAM, T.,LIN, L.,LIU, M.,KONTOYIANNIS, D. P.,FRENCH, S.,EDWARDS, J. E., JR.,FILLER, S. G. & IBRAHIM, A. S. 2016. Bicarbonate correction of ketoacidosis alters host-pathogen interactions and alleviates mucormycosis. *J Clin Invest,* 126**,** 2280-94.

GHIMIRE, B.,SZILI, E. J.,PATENALL, B. L.,LAMICHHANE, P.,GAUR, N.,ROBSON, A. J.,TRIVEDI, D.,THET, N. T.,JENKINS, A. T. A. & CHOI, E. H. 2021. Enhancement of hydrogen peroxide production from an atmospheric

pressure argon plasma jet and implications to the antibacterial activity of plasma activated water. *Plasma Sources Science and Technology,* 30**,** 035009.

GHIMIRE, B.,SZILI, E. J. & SHORT, R. D. 2022. A conical assembly of six plasma jets for biomedical applications. *Applied Physics Letters,* 121**,** 084102.

GIAOURIS, E.,HEIR, E.,DESVAUX, M.,HÉBRAUD, M.,MØRETRØ, T.,LANGSRUD, S.,DOULGERAKI, A.,NYCHAS, G.-J.,KAČÁNIOVÁ, M.,CZACZYK, K.,ÖLMEZ, H. & SIMÕES, M. 2015. Intra- and inter-species interactions within biofilms of important foodborne bacterial pathogens. *Frontiers in Microbiology,* Volume 6 - 2015.

GIRARD-SAHUN, F.,BADETS, V.,LEFRANÇOIS, P.,SOJIC, N.,CLEMENT, F. & ARBAULT, S. 2019. Reactive Oxygen Species Generated by Cold Atmospheric Plasmas in Aqueous Solution: Successful Electrochemical Monitoring in Situ under a High Voltage System. *Anal Chem,* 91**,** 8002-8007.

GIULIERI, S. G.,BAINES, S. L.,GUERILLOT, R.,SEEMANN, T.,GONÇALVES DA SILVA, A.,SCHULTZ, M.,MASSEY, R. C.,HOLMES, N. E.,STINEAR, T. P. & HOWDEN, B. P. 2018. Genomic exploration of sequential clinical isolates reveals a distinctive molecular signature of persistent Staphylococcus aureus bacteraemia. *Genome medicine,* 10**,** 1-17.

GORBANEV, Y.,PRIVAT-MALDONADO, A. & BOGAERTS, A. 2018. Analysis of Short-Lived Reactive Species in Plasma–Air–Water Systems: The Dos and the Do Nots. *Analytical Chemistry,* 90**,** 13151-13158.

GÓRSKI, A.,BOLLYKY, P. L.,PRZYBYLSKI, M.,BORYSOWSKI, J.,MIĘDZYBRODZKI, R.,JOŃCZYK-MATYSIAK, E. & WEBER-DĄBROWSKA, B. 2019. Perspectives of Phage Therapy in Non-bacterial Infections. *Frontiers in Microbiology,* Volume 9 - 2018.

GOVAERT, M.,SMET, C.,VERHEYEN, D.,WALSH, J. L. & VAN IMPE, J. F. 2019. Combined effect of cold atmospheric plasma and hydrogen peroxide treatment on mature Listeria monocytogenes and Salmonella Typhimurium biofilms. *Frontiers in microbiology,* 10**,** 2674.

GRACE, A.,SAHU, R.,OWEN, D. R. & DENNIS, V. A. 2022. Pseudomonas aeruginosa reference strains PAO1 and PA14: A genomic, phenotypic, and therapeutic review. *Frontiers in Microbiology,* 13**,** 1023523.

GRAINHA, T.,JORGE, P.,ALVES, D.,LOPES, S. P. & PEREIRA, M. O. 2020. Unraveling Pseudomonas aeruginosa and Candida albicans Communication in

Coinfection Scenarios: Insights Through Network Analysis. *Frontiers in Cellular and Infection Microbiology,* Volume 10 - 2020.

GRAVES, D. B. 2014. Reactive species from cold atmospheric plasma: Implications for cancer therapy. *Plasma Processes and Polymers,* 11**,** 1120-1127.

GREIMEL, F.,SCHEUERER, C.,GESSNER, A.,SIMON, M.,KALTEIS, T.,GRIFKA, J.,BENDITZ, A.,SPRINGORUM, H. R. & SCHAUMBURGER, J. 2017. Efficacy of antibiotic treatment of implant-associated Staphylococcus aureus infections with moxifloxacin, flucloxacillin, rifampin, and combination therapy: an animal study. *Drug Des Devel Ther,* 11**,** 1729-1736.

GRINHOLC, M.,WEGRZYN, G. & KURLENDA, J. 2007. Evaluation of biofilm production and prevalence of the icaD gene in methicillin-resistant and methicillin-susceptible Staphylococcus aureus strains isolated from patients with nosocomial infections and carriers. *FEMS Immunol Med Microbiol,* 50**,** 375-9.

GROOTERS, K. E.,KU, J. C.,RICHTER, D. M.,KRINOCK, M. J.,MINOR, A.,LI, P.,KIM, A.,SAWYER, R. & LI, Y. 2024. Strategies for combating antibiotic resistance in bacterial biofilms. *Frontiers in cellular and infection microbiology,* 14**,** 1352273.

GUEST, J. F.,AYOUB, N.,MCILWRAITH, T.,UCHEGBU, I.,GERRISH, A.,WEIDLICH, D.,VOWDEN, K. & VOWDEN, P. 2015. Health economic burden that wounds impose on the National Health Service in the UK. *BMJ open,* 5**,** e009283.

GUEST, J. F.,FULLER, G. W. & VOWDEN, P. 2020. Cohort study evaluating the burden of wounds to the UK's National Health Service in 2017/2018: update from 2012/2013. *BMJ open,* 10**,** e045253.

GÜLMEZ, D.,BROWN, J. L.,BUTCHER, M. C.,DELANEY, C.,KEAN, R.,RAMAGE, G. & SHORT, B. 2022. Investigating dual-species Candida auris and staphylococcal biofilm antiseptic challenge. *Antibiotics,* 11**,** 931.

GUO, L.,YANG, L.,QI, Y.,NIYAZI, G.,HUANG, L.,GOU, L.,WANG, Z.,ZHANG, L.,LIU, D. & WANG, X. 2021a. Cold atmospheric-pressure plasma caused protein damage in methicillin-resistant Staphylococcus aureus cells in biofilms. *Microorganisms,* 9**,** 1072.

GUO, L.,YANG, L.,QI, Y.,NIYAZI, G.,ZHENG, J.,XU, R.,CHEN, X.,ZHANG, J.,XI, W.,LIU, D.,WANG, X.,CHEN, H. & KONG, M. G. 2021b. Low-Temperature Gas Plasma Combined with Antibiotics for the Reduction of Methicillin-

Resistant Staphylococcus aureus Biofilm Both In Vitro and In Vivo. *Life*, 11, 828.

GUO, S. A. & DIPIETRO, L. A. 2010. Factors affecting wound healing. *Journal of dental research*, 89, 219-229.

HAJDAMOWICZ, N. H.,HULL, R. C.,FOSTER, S. J. & CONDLIFFE, A. M. 2019. The impact of hypoxia on the host-pathogen interaction between neutrophils and Staphylococcus aureus. *International journal of molecular sciences*, 20, 5561.

HAKANSSON, A.,ORIHUELA, C. & BOGAERT, D. 2018. Bacterial-host interactions: physiology and pathophysiology of respiratory infection. *Physiological reviews*, 98, 781-811.

HALL, C. W. & MAH, T.-F. 2017. Molecular mechanisms of biofilm-based antibiotic resistance and tolerance in pathogenic bacteria. *FEMS microbiology reviews*, 41, 276-301.

HAN, A.,ZENILMAN, J. M.,MELENDEZ, J. H.,SHIRTLIFF, M. E.,AGOSTINHO, A.,JAMES, G.,STEWART, P. S.,MONGODIN, E. F.,RAO, D.,RICKARD, A. H. & LAZARUS, G. S. 2011. The importance of a multifaceted approach to characterizing the microbial flora of chronic wounds. *Wound Repair Regen*, 19, 532-41.

HAQ, K.,FIGGITT, M. & LEE, D. 2024. Phage Therapy Against Antibiotic-Resistant and Multidrug-Resistant Infections Involving Nonhealing Wounds and Prosthetic Joint Infections Associated With Biofilms: A Mini-Review. *Can J Infect Dis Med Microbiol*, 2024, 6252415.

HARE, P. J.,GONZALEZ, J. R.,QUELLE, R. M.,WU, Y. I. & MOK, W. W. K. 2024. Metabolic and transcriptional activities underlie stationary-phase Pseudomonas aeruginosa sensitivity to Levofloxacin. *Microbiol Spectr*, 12, e0356723.

HARIDAS, D. & ATREYA, C. D. 2022. The microbicidal potential of visible blue light in clinical medicine and public health. *Frontiers in Medicine*, Volume 9 - 2022.

HARMS, A.,MAISONNEUVE, E. & GERDES, K. 2016. Mechanisms of bacterial persistence during stress and antibiotic exposure. *Science*, 354, aaf4268.

HARRIOTT, M. M. & NOVERR, M. C. 2009. Candida albicans and Staphylococcus aureus form polymicrobial biofilms: effects on antimicrobial resistance. *Antimicrobial agents and chemotherapy*, 53, 3914-3922.

HARRIOTT, M. M. & NOVERR, M. C. 2011. Importance of Candida–bacterial polymicrobial biofilms in disease. *Trends in microbiology,* 19**,** 557-563.

HE, R.,LI, Q.,SHEN, W.,WANG, T.,LU, H.,LU, J.,LU, F.,LUO, M.,ZHANG, J.,GAO, H.,WANG, D.,XING, W.,JIA, W. & LIU, F. 2020a. The efficacy and safety of cold atmospheric plasma as a novel therapy for diabetic wound in vitro and in vivo. *Int Wound J,* 17**,** 851-863.

HE, W.,ZHANG, Z.,CHEN, J.,ZHENG, Y.,XIE, Y.,LIU, W.,WU, J. & MOSSELHY, D. A. 2021. Evaluation of the anti-biofilm activities of bacterial cellulose-tannic acid-magnesium chloride composites using an in vitro multispecies biofilm model. *Regenerative biomaterials,* 8**,** rbab054.

HE, X. S. & SHI, W. Y. 2009. Oral microbiology: past, present and future. *Int J Oral Sci,* 1**,** 47-58.

HE, Y.-W.,DENG, Y.,MIAO, Y.,CHATTERJEE, S.,TRAN, T. M.,TIAN, J. & LINDOW, S. 2023. DSF-family quorum sensing signal-mediated intraspecies, interspecies, and inter-kingdom communication. *Trends in Microbiology,* 31**,** 36-50.

HE, Z.,LIU, K.,SCALLY, L.,MANALOTO, E.,GUNES, S.,NG, S. W.,MAHER, M.,TIWARI, B.,BYRNE, H. J. & BOURKE, P. 2019. Low dose cold atmospheric plasma induces membrane oxidation, stimulates endocytosis and enhances uptake of nanomaterials in glioblastoma multiforme cells. *BioRxiv***,** 805192.

HE, Z.,LIU, K.,SCALLY, L.,MANALOTO, E.,GUNES, S.,NG, S. W.,MAHER, M.,TIWARI, B.,BYRNE, H. J.,BOURKE, P.,TIAN, F.,CULLEN, P. J. & CURTIN, J. F. 2020b. Cold Atmospheric Plasma Stimulates Clathrin-Dependent Endocytosis to Repair Oxidised Membrane and Enhance Uptake of Nanomaterial in Glioblastoma Multiforme Cells. *Scientific Reports,* 10**,** 6985.

HEALY, B. & FREEDMAN, A. 2006. Infections. *Bmj,* 332**,** 838-41.

HEATON, S. M.,WEINTROB, A. C.,DOWNING, K.,KEENAN, B.,AGGARWAL, D.,SHAIKH, F.,TRIBBLE, D. R. & WELLS, J. 2016. Histopathological techniques for the diagnosis of combat-related invasive fungal wound infections. *BMC Clin Pathol,* 16**,** 11.

HEIDARI, R.,FARAJZADEH SHEIKH, A.,HASHEMZADEH, M.,FARSHADZADEH, Z.,SALMANZADEH, S. & SAKI, M. 2022. Antibiotic resistance, biofilm production ability and genetic diversity of carbapenem-resistant Pseudomonas aeruginosa strains isolated from nosocomial infections in southwestern Iran. *Mol Biol Rep,* 49**,** 3811-3822.

HEINLIN, J.,MAISCH, T.,ZIMMERMANN, J. L.,SHIMIZU, T.,HOLZMANN, T.,SIMON, M.,HEIDER, J.,LANDTHALER, M.,MORFILL, G. & KARRER, S. 2013a. Contact-free inactivation of Trichophyton rubrum and Microsporum canis by cold atmospheric plasma treatment. *Future Microbiology,* 8**,** 1097-1106.

HEINLIN, J.,TIM, M.,L., Z. J.,TETSUJI, S.,THOMAS, H.,MICHAELA, S.,JUDITH, H.,MICHAEL, L.,GREGOR, M. & AND KARRER, S. 2013b. Contact-Free Inactivation of Trichophyton Rubrum and Microsporum Canis by Cold Atmospheric Plasma Treatment. *Future Microbiology,* 8**,** 1097-1106.

HERIOT, M.,NOTTELET, B.,GARRIC, X.,D'ESTE, M.,RICHARDS, G. R.,MORIARTY, F. T.,EGLIN, D. & GUILLAUME, O. 2019. Interaction of gentamicin sulfate with alginate and consequences on the physico-chemical properties of alginate-containing biofilms. *Int J Biol Macromol,* 121**,** 390-397.

HERNANDEZ-CUELLAR, E.,GUERRERO-BARRERA, A. L.,AVELAR-GONZALEZ, F. J.,DÍAZ, J. M.,SANTIAGO, A. S. D.,CHÁVEZ-REYES, J. & POBLANO-SÁNCHEZ, E. 2022. Characterization of Candida albicans and Staphylococcus aureus polymicrobial biofilm on different surfaces. *Revista Iberoamericana de Micología,* 39**,** 36-43.

HERNÁNDEZ-CUELLAR, E.,TSUCHIYA, K.,VALLE-RÍOS, R. & MEDINA-CONTRERAS, O. 2023. Differences in biofilm formation by methicillin-resistant and methicillin-susceptible Staphylococcus aureus strains. *Diseases,* 11**,** 160.

HESS, C. T. 2020. Venous Ulcer Assessment and Management: Using the Updated CEAP Classification System. *Advances in Skin & Wound Care,* 33**,** 614-615.

HOFFMAN, L. R.,DÉZIEL, E.,D'ARGENIO, D. A.,LÉPINE, F.,EMERSON, J.,MCNAMARA, S.,GIBSON, R. L.,RAMSEY, B. W. & MILLER, S. I. 2006. Selection for Staphylococcus aureus small-colony variants due to growth in the presence of Pseudomonas aeruginosa. *Proceedings of the National Academy of Sciences,* 103**,** 19890-19895.

HOFFMANN, C.,BERGANZA, C. & ZHANG, J. 2013. Cold Atmospheric Plasma: methods of production and application in dentistry and oncology. *Med Gas Res,* 3**,** 21.

HØIBY, N.,BJARNSHOLT, T.,GIVSKOV, M.,MOLIN, S. & CIOFU, O. 2010. Antibiotic resistance of bacterial biofilms. *International journal of antimicrobial agents,* 35**,** 322-332.

HOLLAND, D. B.,BOJAR, R. A.,JEREMY, A. H.,INGHAM, E. & HOLLAND, K. T. 2008. Microbial colonization of an in vitro model of a tissue engineered human skin equivalent–a novel approach. *FEMS microbiology letters,* 279**,** 110-115.

HONG, S.-H.,SZILI, E. J.,FENECH, M.,GAUR, N. & SHORT, R. D. 2017. Genotoxicity and cytotoxicity of the plasma jet-treated medium on lymphoblastoid WIL2-NS cell line using the cytokinesis block micronucleus cytome assay. *Scientific Reports,* 7**,** 3854.

HOOGENKAMP, M. A.,MAZUREL, D.,DEUTEKOM-MULDER, E. & DE SOET, J. J. 2023. The consistent application of hydrogen peroxide controls biofilm growth and removes Vermamoeba vermiformis from multi-kingdom in-vitro dental unit water biofilms. *Biofilm,* 5**,** 100132.

HORSBURGH, M. J.,AISH, J. L.,WHITE, I. J.,SHAW, L.,LITHGOW, J. K. & FOSTER, S. J. 2002. sigmaB modulates virulence determinant expression and stress resistance: characterization of a functional rsbU strain derived from Staphylococcus aureus 8325-4. *J Bacteriol,* 184**,** 5457-67.

HORSBURGH, M. J.,CLEMENTS, M. O.,CROSSLEY, H.,INGHAM, E. & FOSTER, S. J. 2001. PerR controls oxidative stress resistance and iron storage proteins and is required for virulence in Staphylococcus aureus. *Infect Immun,* 69**,** 3744-54.

HORTON, M. V. & NETT, J. E. 2020. Candida auris infection and biofilm formation: going beyond the surface. *Curr Clin Microbiol Rep,* 7**,** 51-56.

HOTTERBEEKX, A.,KUMAR-SINGH, S.,GOOSSENS, H. & MALHOTRA-KUMAR, S. 2017. In vivo and In vitro Interactions between Pseudomonas aeruginosa and Staphylococcus spp. *Frontiers in Cellular and Infection Microbiology,* Volume 7 - 2017.

HOU, J.,WANG, L.,ALM, M.,THOMSEN, P.,MONSEN, T.,RAMSTEDT, M. & BURMØLLE, M. 2022. Enhanced Antibiotic Tolerance of an In Vitro Multispecies Uropathogen Biofilm Model, Useful for Studies of Catheter-Associated Urinary Tract Infections. *Microorganisms,* 10.

HOUSTON, P.,ROWE, S. E.,POZZI, C.,WATERS, E. M. & O'GARA, J. P. 2011. Essential role for the major autolysin in the fibronectin-binding protein-mediated Staphylococcus aureus biofilm phenotype. *Infection and immunity,* 79**,** 1153-1165.

HU, Y.,WEBB, J. S. & AN, S. Q. 2023. Host cell-based screening assays for identification of molecules targeting Pseudomonas aeruginosa cyclic di-GMP signaling and biofilm formation. *Front Microbiol,* 14**,** 1279922.

HUANG, D.,WANG, Y.,XIAO, J.,WANG, Y.,ZHU, X.,XU, B. & WANG, M. 2023. Scavenging of reactive oxygen species effectively reduces Pseudomonas aeruginosa biofilms through disrupting policing. *Environ Res,* 220**,** 115182.

HUANG, M.,ZHUANG, H.,ZHAO, J.,WANG, J.,YAN, W. & ZHANG, J. 2020. Differences in cellular damage induced by dielectric barrier discharge plasma between Salmonella Typhimurium and Staphylococcus aureus. *Bioelectrochemistry,* 132**,** 107445.

HUANG, M.-B.,BRENA, D.,WU, J. Y.,SHELTON, M. & BOND, V. C. 2024. SMR peptide antagonizes Staphylococcus aureus biofilm formation. *Microbiology Spectrum,* 12**,** e02583-23.

HURLOW, J. & BOWLER, P. G. 2022a. Acute and chronic wound infections: microbiological, immunological, clinical and therapeutic distinctions. *Journal of wound care,* 31**,** 436-445.

HURLOW, J. & BOWLER, P. G. 2022b. Acute and chronic wound infections: microbiological, immunological, clinical and therapeutic distinctions. *J Wound Care,* 31**,** 436-445.

HURLOW, J.,COUCH, K.,LAFORET, K.,BOLTON, L.,METCALF, D. & BOWLER, P. 2015. Clinical biofilms: a challenging frontier in wound care. *Advances in wound care,* 4**,** 295-301.

HUSSAIN, M. A.,RATHNAYAKE, I. & HUYGENS, F. 2016. The importance of anaerobic bacteria in non-healing wounds. *Wound Practice & Research: Journal of the Australian Wound Management Association,* 24**,** 218-223.

IBBERSON, C. B.,BARRAZA, J. P.,HOLMES, A. L.,CAO, P. & WHITELEY, M. 2022. Precise spatial structure impacts antimicrobial susceptibility of S. aureus in polymicrobial wound infections. *Proceedings of the National Academy of Sciences,* 119**,** e2212340119.

IBRAHIM, A. S.,SPELLBERG, B.,WALSH, T. J. & KONTOYIANNIS, D. P. 2012. Pathogenesis of mucormycosis. *Clin Infect Dis,* 54 Suppl 1**,** S16-22.

IGLER, C.,ROLFF, J. & REGOES, R. 2021. Multi-step vs. single-step resistance evolution under different drugs, pharmacokinetics, and treatment regimens. *Elife,* 10.

IKAWA, S.,KITANO, K. & HAMAGUCHI, S. 2010. Effects of pH on bacterial inactivation in aqueous solutions due to low-temperature atmospheric pressure plasma application. *Plasma Processes and Polymers,* 7**,** 33-42.

ISBARY, G.,HEINLIN, J.,SHIMIZU, T.,ZIMMERMANN, J. L.,MORFILL, G.,SCHMIDT, H. U.,MONETTI, R.,STEFFES, B.,BUNK, W.,LI, Y.,KLAEMPFL, T.,KARRER, S.,LANDTHALER, M. & STOLZ, W. 2012. Successful and safe use of 2 min cold atmospheric argon plasma in chronic wounds: results of a randomized controlled trial. *Br J Dermatol,* 167**,** 404-10.

JABBAR AL-SABTI, K. H. & HUSSAIN SHABAA, R. A. 2024. Relationship of biofilm strength levels in Candida albicans isolates with the type of clinical specimens. *Magazine of Al-Kufa University for Biology,* 16.

JAGMANN, N.,BRACHVOGEL, H. P. & PHILIPP, B. 2010. Parasitic growth of Pseudomonas aeruginosa in co-culture with the chitinolytic bacterium Aeromonas hydrophila. *Environmental microbiology,* 12**,** 1787-1802.

JAGMANN, N.,VON REKOWSKI, K. S. & PHILIPP, B. 2012. Interactions of bacteria with different mechanisms for chitin degradation result in the formation of a mixed-species biofilm. *FEMS microbiology letters,* 326**,** 69-75.

JAHID, I. K.,HAN, N.,ZHANG, C.-Y. & HA, S.-D. 2015. Mixed culture biofilms of Salmonella Typhimurium and cultivable indigenous microorganisms on lettuce show enhanced resistance of their sessile cells to cold oxygen plasma. *Food Microbiology,* 46**,** 383-394.

JAIN, A.,MAHAJAN, M.,UPAGANLAWAR, A. & UPASANI, C. 2024. Impact of Antimicrobial Resistance in Health and Economic Outcomes: A Review. *Adv. Pharmacol. Clin. Trials,* 9**,** 000234.

JAKOBSEN, T. H.,RUMBAUGH, K.,COENYE, T. & BJARNSHOLT, T. 2025. Microbial biofilms and chronic wounds: Facts and speculation. *Journal of Wound Management,* 26**,** 54-56.

JAMES, G. A.,SWOGGER, E.,WOLCOTT, R.,PULCINI, E. D.,SECOR, P.,SESTRICH, J.,COSTERTON, J. W. & STEWART, P. S. 2008. Biofilms in chronic wounds. *Wound Repair and regeneration,* 16**,** 37-44.

JENSEN, L. K.,JOHANSEN, A. S. & JENSEN, H. E. 2017. Porcine models of biofilm infections with focus on pathomorphology. *Frontiers in Microbiology,* 8**,** 1961.

JEYARATNAM, J. & MCGOVERN, M. 2022. SteriPlas® and PlasmaTact®. *In:* METELMANN, H.-R., VON WOEDTKE, T., WELTMANN, K.-D. & EMMERT, S.

(eds.) *Textbook of Good Clinical Practice in Cold Plasma Therapy*. Cham: Springer International Publishing.

JIA, L.,PARKER, C. N.,PARKER, T. J.,KINNEAR, E. M.,DERHY, P. H.,ALVARADO, A. M.,HUYGENS, F.,LAZZARINI, P. A. & DIABETIC FOOT WORKING GROUP, Q. S. D. C. N. 2017. Incidence and risk factors for developing infection in patients presenting with uninfected diabetic foot ulcers. *PloS one,* 12**,** e0177916.

JIANG, Y.,ZHANG, Q.,WANG, H.,VÄLIMÄKI, M.,ZHOU, Q.,DAI, W. & GUO, J. 2024. Effectiveness of silver and iodine dressings on wound healing: a systematic review and meta-analysis. *BMJ Open,* 14**,** e077902.

JING, G.,HU, C.,FANG, K.,LI, Y. & WANG, L. 2024. How Nanoparticles Help in Combating Chronic Wound Biofilms Infection? *Int J Nanomedicine,* 19**,** 11883-11921.

JNEID, J.,LAVIGNE, J.,LA SCOLA, B. & CASSIR, N. 2017. The diabetic foot microbiota: a review. *Human Microbiome Journal,* 5**,** 1-6.

JO, J.,PRICE-WHELAN, A. & DIETRICH, L. E. P. 2022. Gradients and consequences of heterogeneity in biofilms. *Nature Reviews Microbiology,* 20**,** 593-607.

JOHNSON, D. I. 2018. Bacterial Virulence Factors. *In:* JOHNSON, D. I. (ed.) *Bacterial Pathogens and Their Virulence Factors*. Cham: Springer International Publishing.

JOHNSON, T. R.,GÓMEZ, B. I.,MCINTYRE, M. K.,DUBICK, M. A.,CHRISTY, R. J.,NICHOLSON, S. E. & BURMEISTER, D. M. 2018. The cutaneous microbiome and wounds: new molecular targets to promote wound healing. *International journal of molecular sciences,* 19**,** 2699.

JONES, C. J. & WOZNIAK, D. J. 2017. Psl produced by mucoid Pseudomonas aeruginosa contributes to the establishment of biofilms and immune evasion. *MBio,* 8**,** 10.1128/mbio. 00864-17.

JUNGBAUER, G.,FAVARO, L.,MÜLLER, S.,SCULEAN, A. & EICK, S. 2022. The in-vitro activity of a cold atmospheric plasma device utilizing ambient air against bacteria and biofilms associated with periodontal or peri-implant Diseases. *Antibiotics,* 11**,** 752.

JUNTKE, J.,MURGIA, X.,GÜNDAY TÜRELI, N.,TÜRELI, A. E.,THORN, C. R.,SCHNEIDER, M.,SCHNEIDER-DAUM, N.,DE SOUZA CARVALHO-WODARZ, C. & LEHR, C. M. 2021. Testing of aerosolized ciprofloxacin nanocarriers on cystic fibrosis airway cells infected with P. aeruginosa biofilms. *Drug Deliv Transl Res,* 11**,** 1752-1765.

KADAM, S.,MADHUSOODHANAN, V.,DHEKANE, R.,BHIDE, D.,UGALE, R.,TIKHOLE, U. & KAUSHIK, K. S. 2021. Milieu matters: An in vitro wound milieu to recapitulate key features of, and probe new insights into, mixed-species bacterial biofilms. *Biofilm,* 3**,** 100047.

KADAM, S.,NADKARNI, S.,LELE, J.,SAKHALKAR, S.,MOKASHI, P. & KAUSHIK, K. S. 2019. Bioengineered platforms for chronic wound infection studies: how can we make them more human-relevant? *Frontiers in bioengineering and biotechnology,* 7**,** 418.

KADHIM, A. F. 2024. Strategies and Emerging Mechanisms in Managing Pseudomonas aeruginosa Biofilm-Associated Antibiotic Resistance in Renal Catheters. *Al-Esraa University College Journal for Medical Sciences*.

KAHL, B. C.,BECKER, K. & LÖFFLER, B. 2016. Clinical Significance and Pathogenesis of Staphylococcal Small Colony Variants in Persistent Infections. *Clinical Microbiology Reviews,* 29**,** 401-427.

KAHL, L. J.,STREMMEL, N.,ESPARZA-MORA, M. A.,WHEATLEY, R. M.,MACLEAN, R. C. & RALSER, M. 2023. Interkingdom interactions between Pseudomonas aeruginosa and Candida albicans affect clinical outcomes and antimicrobial responses. *Current Opinion in Microbiology,* 75**,** 102368.

KALAN, L. & GRICE, E. A. 2018. Fungi in the wound microbiome. *Advances in wound care,* 7**,** 247-255.

KALAN, L.,LOESCHE, M.,HODKINSON, B. P.,HEILMANN, K.,RUTHEL, G.,GARDNER, S. E. & GRICE, E. A. 2016. Redefining the chronic-wound microbiome: fungal communities are prevalent, dynamic, and associated with delayed healing. *MBio,* 7**,** 10.1128/mbio. 01058-16.

KALAN, L. R.,MEISEL, J. S.,LOESCHE, M. A.,HORWINSKI, J.,SOAITA, I.,CHEN, X.,UBEROI, A.,GARDNER, S. E. & GRICE, E. A. 2019. Strain- and Species-Level Variation in the Microbiome of Diabetic Wounds Is Associated with Clinical Outcomes and Therapeutic Efficacy. *Cell Host Microbe,* 25**,** 641-655.e5.

KALLSTROM, G. 2014. Are quantitative bacterial wound cultures useful? *J Clin Microbiol,* 52**,** 2753-6.

KAMBLE, E. & PARDESI, K. 2021. Antibiotic Tolerance in Biofilm and Stationary-Phase Planktonic Cells of Staphylococcus aureus. *Microbial Drug Resistance,* 27**,** 3-12.

KANDÁROVÁ, H.,LIEBSCH, M.,GERNER, I.,SCHMIDT, E.,GENSCHOW, E.,TRAUE, D. & SPIELMANN, H. 2005. The EpiDerm test protocol for the upcoming ECVAM validation study on in vitro skin irritation tests—An assessment of the performance of the optimised test. *Alternatives to Laboratory Animals,* 33**,** 351-367.

KANDHWAL, M.,BEHL, T.,SINGH, S.,SHARMA, N.,ARORA, S.,BHATIA, S.,AL-HARRASI, A.,SACHDEVA, M. & BUNGAU, S. 2022. Role of matrix metalloproteinase in wound healing. *American journal of translational research,* 14**,** 4391.

KAPINUSOVA, G.,LOPEZ MARIN, M. A. & UHLIK, O. 2023. Reaching unreachables: Obstacles and successes of microbial cultivation and their reasons. *Frontiers in Microbiology,* Volume 14 - 2023.

KAPOOR, G.,SAIGAL, S. & ELONGAVAN, A. 2017. Action and resistance mechanisms of antibiotics: A guide for clinicians. *Journal of Anaesthesiology Clinical Pharmacology,* 33**,** 300-305.

KAR, A.,MUKHERJEE, S. K.,BARIK, S. & HOSSAIN, S. T. 2024. Antimicrobial Activity of Trigonelline Hydrochloride Against Pseudomonas aeruginosa and Its Quorum-Sensing Regulated Molecular Mechanisms on Biofilm Formation and Virulence. *ACS Infect Dis,* 10**,** 746-762.

KARNA, S. L.,D'ARPA, P.,CHEN, T.,QIAN, L. W.,FOURCAUDOT, A. B.,YAMANE, K.,CHEN, P.,ABERCROMBIE, J. J.,YOU, T. & LEUNG, K. P. 2016. RNA-Seq Transcriptomic Responses of Full-Thickness Dermal Excision Wounds to Pseudomonas aeruginosa Acute and Biofilm Infection. *PLoS One,* 11**,** e0165312.

KARYGIANNI, L.,REN, Z.,KOO, H. & THURNHEER, T. 2020. Biofilm matrixome: extracellular components in structured microbial communities. *Trends in microbiology,* 28**,** 668-681.

KASETTY, S.,MOULD, D. L.,HOGAN, D. A. & NADELL, C. D. 2021. Both Pseudomonas aeruginosa and Candida albicans Accumulate Greater Biomass in Dual-Species Biofilms under Flow. *mSphere,* 6**,** e0041621.

KASHI, M.,NOEI, M.,CHEGINI, Z. & SHARIATI, A. 2024. Natural compounds in the fight against Staphylococcus aureus biofilms: a review of antibiofilm strategies. *Front Pharmacol,* 15**,** 1491363.

KEAN, R.,DELANEY, C.,RAJENDRAN, R.,SHERRY, L.,METCALFE, R.,THOMAS, R.,MCLEAN, W.,WILLIAMS, C. & RAMAGE, G. 2018a. Gaining insights from

Candida biofilm heterogeneity: one size does not fit all. *Journal of Fungi*, 4, 12.

KEAN, R.,MCKLOUD, E.,TOWNSEND, E. M.,SHERRY, L.,DELANEY, C.,JONES, B. L.,WILLIAMS, C. & RAMAGE, G. 2018b. The comparative efficacy of antiseptics against Candida auris biofilms. *International Journal of Antimicrobial Agents,* 52**,** 673-677.

KEAN, R.,RAJENDRAN, R.,HAGGARTY, J.,TOWNSEND, E. M.,SHORT, B.,BURGESS, K. E.,LANG, S.,MILLINGTON, O.,MACKAY, W. G.,WILLIAMS, C. & RAMAGE, G. 2017. Candida albicans Mycofilms Support Staphylococcus aureus Colonization and Enhances Miconazole Resistance in Dual-Species Interactions. *Frontiers in Microbiology,* 8.

KEAN, R. & RAMAGE, G. 2019. Combined Antifungal Resistance and Biofilm Tolerance: the Global Threat of Candida auris. *mSphere,* 4.

KEE, K. K.,NAIR, H. K. & YUEN, N. P. 2019. Risk factor analysis on the healing time and infection rate of diabetic foot ulcers in a referral wound care clinic. *Journal of wound care,* 28**,** S4-S13.

KEIM, K.,BHATTACHARYA, M.,CROSBY, H. A.,JENUL, C.,MILLS, K.,SCHURR, M. & HORSWILL, A. 2024. Polymicrobial interactions between Staphylococcus aureus and Pseudomonas aeruginosa promote biofilm formation and persistence in chronic wound infections. *bioRxiv*.

KEMEGNE, G. A.,KAMDEM, S. L. S.,NYEGUE, M. A.,MENUT, C. & ETOA, F.-X. 2021. Comparing checkerboard, isobologram and CCD methods for drug combination: a case study of ciprofloxacin and plant extracts on Escherichia coli and Shigella. *Journal of Medicinal Plants Research,* 5**,** 479-489.

KHALAF, A. T.,ABDALLA, A. N.,REN, K. & LIU, X. 2024. Cold atmospheric plasma (CAP): a revolutionary approach in dermatology and skincare. *Eur J Med Res,* 29**,** 487.

KHALID, A.,COOKSON, A. R.,WHITWORTH, D. E.,BEETON, M. L.,ROBINS, L. I. & MADDOCKS, S. E. 2023. A Synthetic Polymicrobial Community Biofilm Model Demonstrates Spatial Partitioning, Tolerance to Antimicrobial Treatment, Reduced Metabolism, and Small Colony Variants Typical of Chronic Wound Biofilms. *Pathogens,* 12.

KHAN, F.,INDIKA, B. N.,NGUYEN, P. D. T.,NAZIA, T.,AHMAD, K. M. S. & AND KIM, Y.-M. 2021. Mixed biofilms of pathogenic Candida-bacteria: regulation

mechanisms and treatment strategies. *Critical Reviews in Microbiology,* 47**,** 699-727.

KHAN, R.,ASLAM KHAN, M. U.,STOJANOVIĆ, G. M.,JAVED, A.,HAIDER, S. & ABD RAZAK, S. I. 2024. Fabrication of Bilayer Nanofibrous-Hydrogel Scaffold from Bacterial Cellulose, PVA, and Gelatin as Advanced Dressing for Wound Healing and Soft Tissue Engineering. *ACS Omega,* 9**,** 6527-6536.

KIM, J. H.,RUEGGER, P. R.,LEBIG, E. G.,VANSCHALKWYK, S.,JESKE, D. R.,HSIAO, A.,BORNEMAN, J. & MARTINS-GREEN, M. 2020. High Levels of Oxidative Stress Create a Microenvironment That Significantly Decreases the Diversity of the Microbiota in Diabetic Chronic Wounds and Promotes Biofilm Formation. *Front Cell Infect Microbiol,* 10**,** 259.

KIM, J. H.,SPERO, M.,LEBIG, E. G.,LONERGAN, Z. R.,TRINDADE, I. B.,NEWMAN, D. K. & MARTINS-GREEN, M. 2024. Targeting Anaerobic Respiration in Pseudomonas aeruginosa with Chlorate Improves Healing of Chronic Wounds. *Adv Wound Care (New Rochelle),* 13**,** 53-69.

KIPANGA, P. N.,DEMUYSER, L.,VRIJDAG, J.,ESKES, E.,D'HOOGE, P.,MATASYOH, J.,CALLEWAERT, G.,WINDERICKX, J.,VAN DIJCK, P. & LUYTEN, W. 2021. Investigating the antifungal mechanism of action of polygodial by phenotypic screening in Saccharomyces cerevisiae. *International journal of molecular sciences,* 22**,** 5756.

KIRCHNER, S.,FOTHERGILL, J. L.,WRIGHT, E. A.,JAMES, C. E.,MOWAT, E. & WINSTANLEY, C. 2012. *Use of Artificial Sputum Medium to Test Antibiotic Efficacy Against Pseudomonas aeruginosa in Conditions More Relevant to the Cystic Fibrosis Lung;* 64. 1940-087X; 2012.

KITADOKORO, J.,HIROKAWA, T.,KAMO, M.,FURUBAYASHI, N.,OKUNO, Y.,HIKIMA, T.,YAMAMOTO, M.,INAKA, K.,MAENAKA, K.,KAMITANI, S. & KITADOKORO, K. 2025. Structural analysis shows the mode of inhibition for Staphylococcus aureus lipase by antipsychotic penfluridol. *Scientific Reports,* 15**,** 11876.

KLEIN, S.,MORATH, B.,WEITZ, D.,SCHWEIZER, P. A.,SÄHR, A.,HEEG, K.,BOUTIN, S. & NURJADI, D. 2022. Comparative genomic reveals clonal heterogeneity in persistent Staphylococcus aureus infection. *Frontiers in Cellular and Infection Microbiology,* 12**,** 817841.

KLEMENTIEV, A. D.,JIN, Z. & WHITELEY, M. 2020. Micron Scale Spatial Measurement of the O(2) Gradient Surrounding a Bacterial Biofilm in Real Time. *mBio,* 11.

KONG, E. F.,TSUI, C.,KUCHARÍKOVÁ, S.,ANDES, D.,DIJCK, P. V. & JABRA-RIZK, M. A. 2016. Commensal Protection of Staphylococcus aureus against Antimicrobials by Candida albicans Biofilm Matrix. *mBio,* 7**,** e01365-16.

KONG, E. F.,TSUI, C.,KUCHARÍKOVÁ, S.,DIJCK, P. V. & JABRA-RIZK, M. A. 2017. Modulation of Staphylococcus aureus Response to Antimicrobials by the Candida albicans Quorum Sensing Molecule Farnesol. *Antimicrobial Agents and Chemotherapy,* 61**,** 10.1128/aac.01573-17.

KORSHOJ, L. E. & KIELIAN, T. 2024. Bacterial single-cell RNA sequencing captures biofilm transcriptional heterogeneity and differential responses to immune pressure. *Nat Commun,* 15**,** 10184.

KOS, S.,BLAGUS, T.,CEMAZAR, M.,FILIPIC, G.,SERSA, G. & CVELBAR, U. 2017. Safety aspects of atmospheric pressure helium plasma jet operation on skin: In vivo study on mouse skin. *PloS one,* 12**,** e0174966.

KRANJEC, C.,MORALES ANGELES, D.,TORRISSEN MÅRLI, M.,FERNÁNDEZ, L.,GARCÍA, P.,KJOS, M. & DIEP, D. B. 2021. Staphylococcal biofilms: Challenges and novel therapeutic perspectives. *Antibiotics,* 10**,** 131.

KUBINOVA, S.,ZAVISKOVA, K.,UHERKOVA, L.,ZABLOTSKII, V.,CHURPITA, O.,LUNOV, O. & DEJNEKA, A. 2017. Non-thermal air plasma promotes the healing of acute skin wounds in rats. *Scientific Reports,* 7**,** 45183.

KUBO, I.,FUJITA, K. I. & LEE, S. H. 2001. Antifungal mechanism of polygodial. *Journal of Agricultural and Food Chemistry,* 49**,** 1607-1611.

KUBO, I.,FUJITA, K. I.,LEE, S. H. & HA, T. J. 2005. Antibacterial activity of polygodial. *Phytotherapy Research: An International Journal Devoted to Pharmacological and Toxicological Evaluation of Natural Product Derivatives,* 19**,** 1013-1017.

KULAYTA, K.,ZERDO, Z.,SEID, M.,DUBALE, A.,MANILAL, A.,KEBEDE, T.,ALAHMADI, R. M.,RAMAN, G. & AKBAR, I. 2024. Biofilm formation and antibiogram profile of bacteria from infected wounds in a general hospital in southern Ethiopia. *Scientific Reports,* 14**,** 26359.

KUMAR, M. M.,POOVAZHAGI, V.,ANBALAGAN, S. & DEVASENA, N. 2014. Rhino-orbito-cerebral mucormycosis in a child with diabetic ketoacidosis. *Indian J Crit Care Med,* 18**,** 334-5.

KUNZ COYNE, A. J.,EL GHALI, A.,HOLGER, D.,REBOLD, N. & RYBAK, M. J. 2022. Therapeutic strategies for emerging multidrug-resistant Pseudomonas aeruginosa. *Infectious diseases and therapy,* 11**,** 661-682.

KWIATKOWSKI, P.,GRYGORCEWICZ, B.,PRUSS, A.,WOJCIUK, B.,GIEDRYS-KALEMBA, S.,DOŁĘGOWSKA, B.,ZIELIŃSKA-BLIŹNIEWSKA, H.,OLSZEWSKI, J.,SIENKIEWICZ, M. & KOCHAN, E. 2020. Synergistic effect of fennel essential oil and hydrogen peroxide on bacterial biofilm. *Advances in Dermatology and Allergology/Postępy Dermatologii i Alergologii,* 37**,** 690-698.

LABADIE, M.,MARCHAL, F.,MERBAHI, N.,GIRBAL-NEUHAUSER, E.,FONTAGNÉ-FAUCHER, C. & MARCATO-ROMAIN, C.-E. 2021. Response of controlled cell load biofilms to cold atmospheric plasma jet: evidence of extracellular matrix contribution. *Life,* 11**,** 694.

LABADIE, M.,MARCHAL, F.,MERBAHI, N.,GIRBAL-NEUHAUSER, E.,FONTAGNÉ-FAUCHER, C. & MARCATO-ROMAIN, C. E. 2024. Cell density and extracellular matrix composition mitigate bacterial biofilm sensitivity to UV-C LED irradiation. *Appl Microbiol Biotechnol,* 108**,** 286.

LAM, T.,BERAJA, G. E. & LEV-TOV, H. 2025. Efficacy of Larval Therapy for Wounds: A Systematic Review and Meta-Analysis. *J Clin Med,* 14.

LAMRET, F.,COLIN, M.,MONGARET, C.,GANGLOFF, S. C. & REFFUVEILLE, F. 2020. Antibiotic tolerance of Staphylococcus aureus biofilm in periprosthetic joint infections and antibiofilm strategies. *Antibiotics,* 9**,** 547.

LAMRET, F.,VARIN-SIMON, J.,VELARD, F.,TERRYN, C.,MONGARET, C.,COLIN, M.,GANGLOFF, S. C. & REFFUVEILLE, F. 2021a. Staphylococcus aureus Strain-Dependent Biofilm Formation in Bone-Like Environment. *Front Microbiol,* 12**,** 714994.

LAMRET, F.,VARIN-SIMON, J.,VELARD, F.,TERRYN, C.,MONGARET, C.,COLIN, M.,GANGLOFF, S. C. & REFFUVEILLE, F. 2021b. Staphylococcus aureus strain-dependent biofilm formation in bone-like environment. *Frontiers in Microbiology,* 12**,** 714994.

LANDÉN, N. X.,LI, D. & STÅHLE, M. 2016. Transition from inflammation to proliferation: a critical step during wound healing. *Cellular and Molecular Life Sciences,* 73**,** 3861-3885.

LANGENDONK, R. F.,NEILL, D. R. & FOTHERGILL, J. L. 2021. The building blocks of antimicrobial resistance in Pseudomonas aeruginosa: implications for current resistance-breaking therapies. *Frontiers in Cellular and Infection Microbiology,* 11**,** 665759.

LARKIN, E. L.,DHARMAIAH, S. & GHANNOUM, M. A. 2018. Biofilms and beyond: expanding echinocandin utility. *J Antimicrob Chemother,* 73**,** i73-i81.

LAROUSSI, M. 2020. Cold plasma in medicine and healthcare: The new frontier in low temperature plasma applications. *Frontiers in Physics,* 8**,** 74.

LAROUSSI, M.,RICHARDSON, J. P. & DOBBS, F. C. 2002. Effects of nonequilibrium atmospheric pressure plasmas on the heterotrophic pathways of bacteria and on their cell morphology. *Applied Physics Letters,* 81**,** 772-774.

LATORRE, M. C.,ALONSO, B.,CRUCES, R.,SANZ, A.,MUÑOZ, P. & GUEMBE, M. 2022. The classification of Staphylococcus aureus strains by biofilm production differs depending on the method used. *Enfermedades Infecciosas y Microbiologia Clinica,* 40**,** 134-137.

LAVRIKOVA, A.,JANDA, M.,BUJDÁKOVÁ, H. & HENSEL, K. 2025. Eradication of single- and mixed-species biofilms of P. aeruginosa and S. aureus by pulsed streamer corona discharge cold atmospheric plasma. *Science of The Total Environment,* 959**,** 178184.

LEAPER, D.,ASSADIAN, O. & EDMISTON, C. E. 2015. Approach to chronic wound infections. *British Journal of Dermatology,* 173**,** 351-358.

LEAPER, D.,ROCHON, M.,PINKNEY, T. & EDMISTON, C. E. 2019. Guidelines for the prevention of surgical site infection: an update from NICE. *Infect Prev Pract,* 1**,** 100026.

LEBEAUX, D.,CHAUHAN, A.,RENDUELES, O. & BELOIN, C. 2013. From in vitro to in vivo models of bacterial biofilm-related infections. *Pathogens,* 2**,** 288-356.

LEE, C.-H.,HSIEH, M.-J.,CHANG, S.-H.,LIN, Y.-H.,LIU, S.-J.,LIN, T.-Y.,HUNG, K.-C.,PANG, J.-H. S. & JUANG, J.-H. 2014a. Enhancement of Diabetic Wound Repair Using Biodegradable Nanofibrous Metformin-Eluting Membranes: in Vitro and in Vivo. *ACS Applied Materials & Interfaces,* 6**,** 3979-3986.

LEE, H. R.,KANG, S. U.,KIM, H. J.,JI, E. J.,YUN, J. H.,KIM, S.,JANG, J. Y.,SHIN, Y. S. & KIM, C. H. 2023. Liquid plasma as a treatment for cutaneous wound healing through regulation of redox metabolism. *Cell Death Dis,* 14**,** 119.

LEE, K. W. K.,PERIASAMY, S.,MUKHERJEE, M.,XIE, C.,KJELLEBERG, S. & RICE, S. A. 2014b. Biofilm development and enhanced stress resistance of a model, mixed-species community biofilm. *The ISME journal,* 8**,** 894-907.

LEE, V. E. & O'NEILL, A. J. 2019. Potential for repurposing the personal care product preservatives bronopol and bronidox as broad-spectrum antibiofilm

agents for topical application. *Journal of Antimicrobial Chemotherapy,* 74**,** 907-911.

LEITE, L. D. P.,OLIVEIRA, M. A. C. D.,VEGIAN, M. R. D. C.,SAMPAIO, A. D. G.,NISHIME, T. M. C.,KOSTOV, K. G. & KOGA-ITO, C. Y. 2021. Effect of cold atmospheric plasma jet associated to polyene antifungals on Candida albicans biofilms. *Molecules,* 26**,** 5815.

LEREBOUR, G.,CUPFERMAN, S. & BELLON-FONTAINE, M. 2004. Adhesion of Staphylococcus aureus and Staphylococcus epidermidis to the Episkin® reconstructed epidermis model and to an inert 304 stainless steel substrate. *Journal of applied microbiology,* 97**,** 7-16.

LERTPATIPANPONG, P.,SILLAPACHAIYAPORN, C.,OH, G.,KANG, Y. H.,HWANG, C. Y. & BAEK, S. J. 2023. Effect of cold atmospheric microwave plasma (CAMP) on wound healing in canine keratinocytes. *Front Cell Dev Biol,* 11**,** 1105692.

LI, Y.,DU, J.,HUANG, S.,WANG, S.,WANG, Y.,CAI, Z.,LEI, L. & HUANG, X. 2022. Hydrogen peroxide potentiates antimicrobial photodynamic therapy in eliminating Candida albicans and Streptococcus mutans dual-species biofilm from denture base. *Photodiagnosis and photodynamic therapy,* 37**,** 102691.

LI, Z.,ZHOU, Q.,YANG, J.,QIU, X.,FU, S. & CHEN, Q. 2023. Effect of cold atmospheric plasma therapy on wound healing in patients with diabetic foot ulcers: protocol for a systematic review and meta-analysis. *BMJ Open,* 13**,** e066628.

LIN, C.-W.,ARMSTRONG, D. G.,LIN, C.-H.,LIU, P.-H.,HUNG, S.-Y.,LEE, S.-R.,HUANG, C.-H. & HUANG, Y.-Y. 2019. Nationwide trends in the epidemiology of diabetic foot complications and lower-extremity amputation over an 8-year period. *BMJ Open Diabetes Research and Care,* 7**,** e000795.

LIN, Y. J.,ALSAD, L.,VOGEL, F.,KOPPAR, S.,NEVAREZ, L.,AUGUSTE, F.,SEYMOUR, J.,SYED, A.,CHRISTOPH, K. & LOOMIS, J. S. 2013. Interactions between Candida albicans and Staphylococcus aureus within mixed species biofilms. *Bios,* 84**,** 30-39.

LINDSAY, A. K. & HOGAN, D. A. 2014. Candida albicans: Molecular interactions with Pseudomonas aeruginosa and Staphylococcus aureus. *Fungal Biology Reviews,* 28**,** 85-96.

LINZ, M. S.,MATTAPPALLIL, A.,FINKEL, D. & PARKER, D. 2023. Clinical impact of Staphylococcus aureus skin and soft tissue infections. *Antibiotics,* 12**,** 557.

LINZNER, N.,LOI, V. V.,FRITSCH, V. N.,TUNG, Q. N.,STENZEL, S.,WIRTZ, M.,HELL, R.,HAMILTON, C. J.,TEDIN, K. & FULDE, M. 2019. Staphylococcus aureus uses the bacilliredoxin (BrxAB)/bacillithiol disulfide reductase (YpdA) redox pathway to defend against oxidative stress under infections. *Frontiers in microbiology,* 10**,** 1355.

LIPSKY, B. A.,DRYDEN, M.,GOTTRUP, F.,NATHWANI, D.,SEATON, R. A. & STRYJA, J. 2016. Antimicrobial stewardship in wound care: a Position Paper from the British Society for Antimicrobial Chemotherapy and European Wound Management Association. *Journal of Antimicrobial Chemotherapy,* 71**,** 3026-3035.

LIU, C.,PONSERO, A. J.,ARMSTRONG, D. G.,LIPSKY, B. A. & HURWITZ, B. L. 2020. The dynamic wound microbiome. *BMC medicine,* 18**,** 1-12.

LIU, J.,YAO, X.,XU, Z.,WU, Y.,PEI, F.,ZHANG, L.,LI, M.,SHI, M.,DU, X. & ZHAO, H. 2024a. Modified tibial cortex transverse transport for diabetic foot ulcers with Wagner grade ≥ II: a study of 98 patients. *Frontiers in Endocrinology,* Volume 15 - 2024.

LIU, Y.,LONG, S.,WANG, H. & WANG, Y. 2024b. Biofilm therapy for chronic wounds. *Int Wound J,* 21**,** e14667.

LLOYD, K. G.,STEEN, A. D.,LADAU, J.,YIN, J. & CROSBY, L. 2018. Phylogenetically Novel Uncultured Microbial Cells Dominate Earth Microbiomes. *mSystems,* 3**,** 10.1128/msystems.00055-18.

LOCKHART, S. R.,ETIENNE, K. A.,VALLABHANENI, S.,FAROOQI, J.,CHOWDHARY, A.,GOVENDER, N. P.,COLOMBO, A. L.,CALVO, B.,CUOMO, C. A.,DESJARDINS, C. A.,BERKOW, E. L.,CASTANHEIRA, M.,MAGOBO, R. E.,JABEEN, K.,ASGHAR, R. J.,MEIS, J. F.,JACKSON, B.,CHILLER, T. & LITVINTSEVA, A. P. 2016. Simultaneous Emergence of Multidrug-Resistant Candida auris on 3 Continents Confirmed by Whole-Genome Sequencing and Epidemiological Analyses. *Clinical Infectious Diseases,* 64**,** 134-140.

LOESCHE, M.,GARDNER, S. E.,KALAN, L.,HORWINSKI, J.,ZHENG, Q.,HODKINSON, B. P.,TYLDSLEY, A. S.,FRANCISCUS, C. L.,HILLIS, S. L.,MEHTA, S.,MARGOLIS, D. J. & GRICE, E. A. 2017. Temporal Stability in Chronic Wound Microbiota Is Associated With Poor Healing. *J Invest Dermatol,* 137**,** 237-244.

LU, Z. & IMLAY, J. A. 2021. When anaerobes encounter oxygen: mechanisms of oxygen toxicity, tolerance and defence. *Nature reviews microbiology,* 19**,** 774-785.

LUKES, P.,DOLEZALOVA, E.,SISROVA, I. & CLUPEK, M. 2014. Aqueous-phase chemistry and bactericidal effects from an air discharge plasma in contact with water: evidence for the formation of peroxynitrite through a pseudo-second-order post-discharge reaction of H2O2 and HNO2. *Plasma Sources Science and Technology,* 23**,** 015019.

LUNOV, O.,ZABLOTSKII, V.,CHURPITA, O.,JÄGER, A.,POLÍVKA, L.,SYKOVÁ, E.,DEJNEKA, A. & KUBINOVÁ, Š. 2016. The interplay between biological and physical scenarios of bacterial death induced by non-thermal plasma. *Biomaterials,* 82**,** 71-83.

LUO, A.,WANG, F.,SUN, D.,LIU, X. & XIN, B. 2022. Formation, Development, and Cross-Species Interactions in Biofilms. *Frontiers in Microbiology,* Volume 12 - 2021.

MA'AITAH, S. 2024. Pseudomonas aeruginosa biofilm formation: Antibiofilm Strategies and conventional methods of evaluation. *Journal of Basic and Applied Research in Biomedicine*.

MACHADO, I.,GRAÇA, J.,LOPES, H.,LOPES, S. & PEREIRA, M. O. 2013. Antimicrobial Pressure of Ciprofloxacin and Gentamicin on Biofilm Development by an Endoscope-Isolated Pseudomonas aeruginosa. *ISRN Biotechnol,* 2013**,** 178646.

MACZYNSKA, B.,SECEWICZ, A.,SMUTNICKA, D.,SZYMCZYK, P.,DUDEK-WICHER, R.,JUNKA, A. & BARTOSZEWICZ, M. 2019. In vitro efficacy of gentamicin released from collagen sponge in eradication of bacterial biofilm preformed on hydroxyapatite surface. *PLOS ONE,* 14**,** e0217769.

MADDOCKS, S. 2017. Microbial communities within the chronic wound. *Microbiology Today,* 2017**,** 70-73.

MAGALHÃES, A. P.,FRANÇA, A.,PEREIRA, M. O. & CERCA, N. 2022. Unveiling Co-Infection in Cystic Fibrosis Airways: Transcriptomic Analysis of Pseudomonas aeruginosa and Staphylococcus aureus Dual-Species Biofilms. *Front Genet,* 13**,** 883199.

MAI-PROCHNOW, A.,BRADBURY, M.,OSTRIKOV, K. & MURPHY, A. B. 2015. Pseudomonas aeruginosa biofilm response and resistance to cold

atmospheric pressure plasma is linked to the redox-active molecule phenazine. *PloS one,* 10**,** e0130373.

MAI-PROCHNOW, A.,CLAUSON, M.,HONG, J. & MURPHY, A. B. 2016. Gram positive and Gram negative bacteria differ in their sensitivity to cold plasma. *Scientific Reports,* 6**,** 38610.

MAI-PROCHNOW, A.,MURPHY, A. B.,MCLEAN, K. M.,KONG, M. G. & OSTRIKOV, K. K. 2014. Atmospheric pressure plasmas: infection control and bacterial responses. *International journal of antimicrobial agents,* 43**,** 508-517.

MAI-PROCHNOW, A.,ZHOU, R.,ZHANG, T.,OSTRIKOV, K. K.,MUGUNTHAN, S.,RICE, S. A. & CULLEN, P. J. 2021. Interactions of plasma-activated water with biofilms: inactivation, dispersal effects and mechanisms of action. *NPJ Biofilms Microbiomes,* 7**,** 11.

MALIC, S.,HILL, K. E.,PLAYLE, R.,THOMAS, D. W. & WILLIAMS, D. W. 2011. In vitro interaction of chronic wound bacteria in biofilms. *journal of wound care,* 20**,** 569-577.

MALIK, A.,MOHAMMAD, Z. & AHMAD, J. 2013. The diabetic foot infections: biofilms and antimicrobial resistance. *Diabetes & Metabolic Syndrome: Clinical Research & Reviews,* 7**,** 101-107.

MALIK, A.,SHALLAL, A.,ALANGADEN, G. & SULEYMAN, G. 2024. Risk Factors and Outcomes of Candida auris in Southeast Michigan. *Antimicrobial Stewardship & Healthcare Epidemiology,* 4**,** s92-s93.

MALONE, M.,BJARNSHOLT, T.,MCBAIN, A. J.,JAMES, G. A.,STOODLEY, P.,LEAPER, D.,TACHI, M.,SCHULTZ, G.,SWANSON, T. & WOLCOTT, R. D. 2017. The prevalence of biofilms in chronic wounds: a systematic review and meta-analysis of published data. *Journal of wound care,* 26**,** 20-25.

MANANDHAR, S.,SINGH, A.,VARMA, A.,PANDEY, S. & SHRIVASTAVA, N. 2018. Biofilm Producing Clinical Staphylococcus aureus Isolates Augmented Prevalence of Antibiotic Resistant Cases in Tertiary Care Hospitals of Nepal. *Front Microbiol,* 9**,** 2749.

MANCUSO, G.,MIDIRI, A.,GERACE, E. & BIONDO, C. 2022. Role of the innate immune system in host defence against fungal infections. *Eur Rev Med Pharmacol Sci,* 26**,** 1138-1147.

MARIN, L. M.,XIAO, Y.,CURY, J. A. & SIQUEIRA, W. L. 2022. Modulation of Streptococcus mutans adherence to hydroxyapatite by engineered salivary peptides. *Microorganisms,* 10**,** 223.

MARINESCU, M. & POPA, C.-V. 2022. Pyridine Compounds with Antimicrobial and Antiviral Activities. *International Journal of Molecular Sciences,* 23**,** 5659.

MARTIN, P. & NUNAN, R. 2015. Cellular and molecular mechanisms of repair in acute and chronic wound healing. *British Journal of Dermatology,* 173**,** 370-378.

MARTINET, M. G.,THOMAS, M.,BOJUNGA, J.,PLETZ, M. W.,VEHRESCHILD, M. J. G. T. & WÜRSTLE, S. 2025. The landscape of biofilm models for phage therapy: mimicking biofilms in diabetic foot ulcers using 3D models. *Frontiers in Microbiology,* Volume 16 - 2025.

MARX, A. H.,OLTMANNS, H.,MEISSNE, J.,VERSPOHL, J.,FUCHSLUGER, T. & BUSSE, C. 2024. Argon cold atmospheric plasma eradicates pathogens in vitro that are commonly associated with canine bacterial keratitis. *Frontiers in veterinary science,* 10**,** 1320145.

MASET, R. G.,HAPESHI, A.,LAPAGE, J.,HARRINGTON, N.,LITTLER, J.,PERRIER, S. & HARRISON, F. 2023. Combining SNAPs with antibiotics shows enhanced synergistic efficacy against S. aureus and P. aeruginosa biofilms. *NPJ Biofilms Microbiomes,* 9**,** 36.

MASHBURN, L. M.,JETT, A. M.,AKINS, D. R. & WHITELEY, M. 2005. Staphylococcus aureus serves as an iron source for Pseudomonas aeruginosa during in vivo coculture. *Journal of bacteriology,* 187**,** 554-566.

MATTHES, R.,ASSADIAN, O. & KRAMER, A. 2014. Repeated applications of cold atmospheric pressure plasma does not induce resistance in Staphylococcus aureus embedded in biofilms. *GMS Hyg Infect Control,* 9**,** Doc17.

MATTHES, R.,LÜHRMAN, A.,HOLTFRETER, S.,KOLATA, J.,RADKE, D.,HÜBNER, N.-O.,ASSADIAN, O. & KRAMER, A. 2016. Antibacterial Activity of Cold Atmospheric Pressure Argon Plasma against 78 Genetically Different (mecA, luk-P, agr or Capsular Polysaccharide Type) Staphylococcus aureus Strains. *Skin Pharmacology and Physiology,* 29**,** 83-91.

MAYBIN, J.-A.,THOMPSON, T. P.,FLYNN, P. B.,SKVORTSOV, T.,HICKOK, N. J.,FREEMAN, T. A. & GILMORE, B. F. 2023. Cold atmospheric pressure plasma-antibiotic synergy in Pseudomonas aeruginosa biofilms is mediated via oxidative stress response. *Biofilm,* 5**,** 100122.

MCCAFFERTY, C. E.,AGHAJANI, M. J.,ABI-HANNA, D.,GOSBELL, I. B. & JENSEN, S. O. 2018. An update on gastrointestinal endoscopy-associated infections and their contributing factors. *Ann Clin Microbiol Antimicrob,* 17**,** 36.

MCLEAN, R. J.,LAM, J. S. & GRAHAM, L. L. 2012. Training the Biofilm Generation--a tribute to J. W. Costerton. *J Bacteriol,* 194**,** 6706-11.

MEAR, J. B.,GOSSET, P.,KIPNIS, E.,FAURE, E.,DESSEIN, R.,JAWHARA, S.,FRADIN, C.,FAURE, K.,POULAIN, D. & SENDID, B. 2014. Candida albicans airway exposure primes the lung innate immune response against Pseudomonas aeruginosa infection through innate lymphoid cell recruitment and interleukin-22-associated mucosal response. *Infection and immunity,* 82**,** 306-315.

MELETIADIS, J.,MOUTON, J. W.,MEIS, J. F. & VERWEIJ, P. E. 2003. In vitro drug interaction modeling of combinations of azoles with terbinafine against clinical Scedosporium prolificans isolates. *Antimicrobial Agents and Chemotherapy,* 47**,** 106-117.

MENEZES, M. N. D.,APARECIDA, D. M. B.,MASQUIO, F. F. A.,ALEXANDER, Z.,CAROLINA, K. A. & AND SALGADO, H. R. N. 2019. Flucloxacillin: A Review of Characteristics, Properties and Analytical Methods. *Critical Reviews in Analytical Chemistry,* 49**,** 67-77.

MENGESHA, R. E.,KASA, B. G.,SARAVANAN, M.,BERHE, D. F. & WASIHUN, A. G. 2014. Aerobic bacteria in post surgical wound infections and pattern of their antimicrobial susceptibility in Ayder Teaching and Referral Hospital, Mekelle, Ethiopia. *BMC Res Notes,* 7**,** 575.

MICHAELIS, C. & GROHMANN, E. 2023. Horizontal gene transfer of antibiotic resistance genes in biofilms. *Antibiotics,* 12**,** 328.

MILLER, T. E. 1969. Killing and lysis of gram-negative bacteria through the synergistic effect of hydrogen peroxide, ascorbic acid, and lysozyme. *J Bacteriol,* 98**,** 949-55.

MIN, T.,XIE, X.,REN, K.,SUN, T.,WANG, H.,DANG, C. & ZHANG, H. 2022. Therapeutic Effects of Cold Atmospheric Plasma on Solid Tumor. *Front Med (Lausanne),* 9**,** 884887.

MIRÓ-CANTURRI, A.,AYERBE-ALGABA, R. & SMANI, Y. 2019. Drug repurposing for the treatment of bacterial and fungal infections. *Frontiers in microbiology,* 10**,** 41.

MIRPOUR, M. & ZAHMATKESH, H. 2024. Ketoprofen attenuates Las/Rhl quorum-sensing (QS) systems of Pseudomonas aeruginosa: molecular and docking studies. *Mol Biol Rep,* 51**,** 133.

MIRPOUR, S.,FATHOLLAH, S.,MANSOURI, P.,LARIJANI, B.,GHORANNEVISS, M.,MOHAJERI TEHRANI, M. & AMINI, M. R. 2020a. Cold atmospheric plasma as an effective method to treat diabetic foot ulcers: A randomized clinical trial. *Scientific reports,* 10**,** 10440.

MIRPOUR, S.,FATHOLLAH, S.,MANSOURI, P.,LARIJANI, B.,GHORANNEVISS, M.,MOHAJERI TEHRANI, M. & AMINI, M. R. 2020b. Cold atmospheric plasma as an effective method to treat diabetic foot ulcers: A randomized clinical trial. *Sci Rep,* 10**,** 10440.

MISHRA, N. N.,MCKINNELL, J.,YEAMAN, M. R.,RUBIO, A.,NAST, C. C.,CHEN, L.,KREISWIRTH, B. N. & BAYER, A. S. 2011. In vitro cross-resistance to daptomycin and host defense cationic antimicrobial peptides in clinical methicillin-resistant Staphylococcus aureus isolates. *Antimicrobial agents and chemotherapy,* 55**,** 4012-4018.

MISHRA, N. N.,YANG, S.-J.,CHEN, L.,MULLER, C.,SALEH-MGHIR, A.,KUHN, S.,PESCHEL, A.,YEAMAN, M. R.,NAST, C. C. & KREISWIRTH, B. N. 2013. Emergence of daptomycin resistance in daptomycin-naive rabbits with methicillin-resistant Staphylococcus aureus prosthetic joint infection is associated with resistance to host defense cationic peptides and mprF polymorphisms. *PLoS One,* 8**,** e71151.

MISIC, A. M.,GARDNER, S. E. & GRICE, E. A. 2014. The wound microbiome: modern approaches to examining the role of microorganisms in impaired chronic wound healing. *Advances in wound care,* 3**,** 502-510.

MITCHELL, G.,SÉGUIN, D. L.,ASSELIN, A.-E.,DÉZIEL, E.,CANTIN, A. M.,FROST, E. H.,MICHAUD, S. & MALOUIN, F. 2010. Staphylococcus aureus sigma B-dependent emergence of small-colony variants and biofilm production following exposure to Pseudomonas aeruginosa 4-hydroxy-2-heptylquinoline-N- oxide. *BMC Microbiology,* 10**,** 33.

MLYNARCZYK-BONIKOWSKA, B.,KOWALEWSKI, C.,KROLAK-ULINSKA, A. & MARUSZA, W. 2022. Molecular Mechanisms of Drug Resistance in Staphylococcus aureus. *Int J Mol Sci,* 23.

MOHAMMED, A.,SEID, M. E.,GEBRECHERKOS, T.,TIRUNEH, M. & MOGES, F. 2017. Bacterial isolates and their antimicrobial susceptibility patterns of wound infections among inpatients and outpatients attending the University of Gondar Referral Hospital, Northwest Ethiopia. *International journal of microbiology,* 2017**,** 8953829.

MOHANRAJ, H.,VINODHINI, V. M. & VAJRAVELU, L. K. 2024. Evaluation of Epidemiological Pattern of Candida Species Associated with Candidemia from A Tertiary Care Facility in South India. *Journal of Pure and Applied Microbiology*.

MORADALI, M. F.,GHODS, S. & REHM, B. H. A. 2017. Pseudomonas aeruginosa Lifestyle: A Paradigm for Adaptation, Survival, and Persistence. *Frontiers in Cellular and Infection Microbiology,* Volume 7 - 2017.

MOREE, W. J.,PHELAN, V. V.,WU, C.-H.,BANDEIRA, N.,CORNETT, D. S.,DUGGAN, B. M. & DORRESTEIN, P. C. 2012. Interkingdom metabolic transformations captured by microbial imaging mass spectrometry. *Proceedings of the National Academy of Sciences,* 109**,** 13811-13816.

MORELLI, K. A.,KERKAERT, J. D. & CRAMER, R. A. 2021. Aspergillus fumigatus biofilms: Toward understanding how growth as a multicellular network increases antifungal resistance and disease progression. *PLOS Pathogens,* 17**,** e1009794.

MORGUETTE, A. E. B.,BARTOLOMEU-GONÇALVES, G.,ANDRIANI, G. M.,BERTONCINI, G. E. S.,CASTRO, I. M.,SPOLADORI, L. F. A.,BERTÃO, A. M. S.,TAVARES, E. R.,YAMAUCHI, L. M. & YAMADA-OGATTA, S. F. 2023. The Antibacterial and Wound Healing Properties of Natural Products: A Review on Plant Species with Therapeutic Potential against Staphylococcus aureus Wound Infections. *Plants (Basel),* 12.

MORSLI, M.,SALIPANTE, F.,MAGNAN, C.,DUNYACH-REMY, C.,SOTTO, A. & LAVIGNE, J. P. 2024. Direct metagenomics investigation of non-surgical hard-to-heal wounds: a review. *Ann Clin Microbiol Antimicrob,* 23**,** 39.

MORTON, L. M. & PHILLIPS, T. J. 2016. Wound healing and treating wounds: Differential diagnosis and evaluation of chronic wounds. *Journal of the American Academy of Dermatology,* 74**,** 589-605.

MOSER, C.,PEDERSEN, H. T.,LERCHE, C. J.,KOLPEN, M.,LINE, L.,THOMSEN, K.,HØIBY, N. & JENSEN, P. Ø. 2017. Biofilms and host response – helpful or harmful. *APMIS,* 125**,** 320-338.

MOWAT, E.,RAJENDRAN, R.,WILLIAMS, C.,MCCULLOCH, E.,JONES, B.,LANG, S. & RAMAGE, G. 2010. Pseudomonas aeruginosa and their small diffusible extracellular molecules inhibit Aspergillus fumigatus biofilm formation. *FEMS microbiology letters,* 313**,** 96-102.

MUKHERJEE, D.,ROY CHOWDHURY, A.,GHOSH, P.,VISHWA, N.,RAO, L. & CHAKRAVORTTY, D. 2024. Reactive nitrogen species (RNS) and its reaction intermediates with reactive oxygen species (ROS) in pH-neutral high-strength plasma-activated water determines the antimicrobial activity against ESKAPE Pathogens. *bioRxiv*, 2024.10. 06.616848.

MULCAHY, H.,CHARRON-MAZENOD, L. & LEWENZA, S. 2008. Extracellular DNA chelates cations and induces antibiotic resistance in Pseudomonas aeruginosa biofilms. *PLoS pathogens,* 4, e1000213.

MUNIYASAMY, R. & MANJUBALA, I. 2024. Synergistic combination of baicalein and rifampicin against Staphylococcus aureus biofilms. *Front Microbiol,* 15, 1458267.

MURAKAMI, M.,SATO, H. & TAKETOMI, Y. 2020. Updating phospholipase A2 biology. *Biomolecules,* 10, 1457.

MURALI, R.,SINGH, P.,RAGUNATHAN, D.,DAMARLA, R.,KICHENARADJOU, D.,SURRIYANARAYANAN, K. M.,JAYARAM, S. K.,CHANDRAMOORTHY, H. C.,KUMAR, A. & KRISHNAN, M. E. G. 2024. Antimicrobial Activity of Cold Atmospheric Plasma on Bacterial Strains Derived from Patients with Diabetic Foot Ulcers. *Journal of Microbiology and Biotechnology,* 34, 2353.

MURATA, M.,KOSAI, K.,MITSUMOTO-KASEIDA, F.,KAKU, N.,HASEGAWA, H.,IZUMIKAWA, K.,MUKAE, H. & YANAGIHARA, K. 2025. Antimicrobial susceptibility and resistance mechanisms to antipseudomonal β-lactams in Pseudomonas aeruginosa isolates from blood. *Microbiology Spectrum,* 13, e02790-24.

MURILLO, D.,HUERGO, C.,GALLEGO, B.,RODRÍGUEZ, R. & TORNÍN, J. 2023. Exploring the Use of Cold Atmospheric Plasma to Overcome Drug Resistance in Cancer. *Biomedicines,* 11.

MURPHY, R. A.,COATES, M.,THRANE, S.,SABNIS, A.,HARRISON, J.,SCHELENZ, S.,EDWARDS, A. M.,VORUP-JENSEN, T. & DAVIES, J. C. 2022. Synergistic Activity of Repurposed Peptide Drug Glatiramer Acetate with Tobramycin against Cystic Fibrosis Pseudomonas aeruginosa. *Microbiology Spectrum,* 10, e00813-22.

NADELL, C. D.,DRESCHER, K.,WINGREEN, N. S. & BASSLER, B. L. 2015. Extracellular matrix structure governs invasion resistance in bacterial biofilms. *The ISME Journal,* 9, 1700-1709.

NAIR, H. K.,AHMAD, N. W.,ISMAIL, A.,ALABED, A. A. A.,ZHEMING, B. O.,KAUR, G.,HASSAN, H. & SUPAAT, N. I. 2021. Maggot debridement therapy to treat hard-to-heal diabetic foot ulcers: a single-centre study. *Journal of Wound Care,* 30**,** S30-S36.

NAIR, N.,BISWAS, R.,GÖTZ, F. & BISWAS, L. 2014. Impact of Staphylococcus aureus on pathogenesis in polymicrobial infections. *Infection and immunity,* 82**,** 2162-2169.

NAKAMURA, Y.,KANEMARU, K.,SHOJI, M.,TOTOKI, K.,NAKAMURA, K.,NAKAMINAMI, H.,NAKASE, K.,NOGUCHI, N. & FUKAMI, K. 2020. Phosphatidylinositol-specific phospholipase C enhances epidermal penetration by Staphylococcus aureus. *Scientific reports,* 10**,** 17845.

NAMMALWAR, B. & BUNCE, R. A. 2024. Recent Advances in Pyrimidine-Based Drugs. *Pharmaceuticals (Basel),* 17.

NASIRU, M. M.,FRIMPONG, E. B.,MUHAMMAD, U.,QIAN, J.,MUSTAPHA, A. T.,YAN, W.,ZHUANG, H. & ZHANG, J. 2021. Dielectric barrier discharge cold atmospheric plasma: Influence of processing parameters on microbial inactivation in meat and meat products. *Compr Rev Food Sci Food Saf,* 20**,** 2626-2659.

NAZARI, M.,TAHERI, M.,NOURI, F.,BAHMANZADEH, M. & ALIKHANI, M. Y. 2024. The antimicrobial and antibiofilm effects of gentamicin, imipenem, and fucoidan combinations against dual-species biofilms of Staphylococcus aureus and Acinetobacter baumannii isolated from diabetic foot ulcers. *Annals of Clinical Microbiology and Antimicrobials,* 23**,** 101.

NEOPANE, P.,NEPAL, H. P.,SHRESTHA, R.,UEHARA, O. & ABIKO, Y. 2018. In vitro biofilm formation by Staphylococcus aureus isolated from wounds of hospital-admitted patients and their association with antimicrobial resistance. *International journal of general medicine***,** 25-32.

NETT, J. E. 2018. Special Issue: Candida and Candidiasis. *J Fungi (Basel),* 4.

NGUYEN, A. T. & OGLESBY-SHERROUSE, A. G. 2016. Interactions between Pseudomonas aeruginosa and Staphylococcus aureus during co-cultivations and polymicrobial infections. *Applied Microbiology and Biotechnology,* 100**,** 6141-6148.

NICOL, M. J.,BRUBAKER, T. R.,HONISH, B. J.,SIMMONS, A. N.,KAZEMI, A.,GEISSEL, M. A.,WHALEN, C. T.,SIEDLECKI, C. A.,BILÉN, S. G. & KNECHT, S. D. 2020. Antibacterial effects of low-temperature plasma generated by

atmospheric-pressure plasma jet are mediated by reactive oxygen species. *Scientific reports,* 10**,** 3066.

NIEMIRA, B. A.,BOYD, G. & SITES, J. 2018. Cold Plasma Inactivation of Escherichia coli O157:H7 Biofilms. *Frontiers in Sustainable Food Systems,* Volume 2 - 2018.

NIKOLAOU, A.,SALVADOR, M.,WRIGHT, I.,WANTOCK, T.,SANDISON, G.,HARLE, T.,CARTA, D. & GUTIERREZ-MERINO, J. 2025. The ratio of reactive oxygen and nitrogen species determines the type of cell death that bacteria undergo. *Microbiological Research,* 292**,** 127986.

NOCKER, A.,CHEUNG, C.-Y. & CAMPER, A. K. 2006. Comparison of propidium monoazide with ethidium monoazide for differentiation of live vs. dead bacteria by selective removal of DNA from dead cells. *Journal of microbiological methods,* 67**,** 310-320.

NUSSBAUM, S. R.,CARTER, M. J.,FIFE, C. E.,DAVANZO, J.,HAUGHT, R.,NUSGART, M. & CARTWRIGHT, D. 2018. An economic evaluation of the impact, cost, and medicare policy implications of chronic nonhealing wounds. *Value in health,* 21**,** 27-32.

NWAFOR, I. R.,ALHASSAN, Y.,UDOH, J. I.,ODANIBEH, D.,OYANIYI, J.,EFOLI-BAM, V. K.,AZUBUIKE, E. O.,OJOBOR, J.-F. C. & NWOKAFOR, C. V. 2024. Plant-derived Bioactive Compounds and Their Mechanistic Roles in Combating Microbial Biofilms. *Microbiology Research Journal International* 34**,** 74-85.

O'CONNOR, N.,CAHILL, O.,DANIELS, S.,GALVIN, S. & HUMPHREYS, H. 2014. Cold atmospheric pressure plasma and decontamination. Can it contribute to preventing hospital-acquired infections? *Journal of hospital infection,* 88**,** 59-65.

O'DONNELL, L. E.,SMITH, K.,WILLIAMS, C.,NILE, C. J.,LAPPIN, D. F.,BRADSHAW, D.,LAMBERT, M.,ROBERTSON, D. P.,BAGG, J. & HANNAH, V. 2016. Dentures are a reservoir for respiratory pathogens. *Journal of Prosthodontics,* 25**,** 99-104.

O'NEILL, A. 2010. Staphylococcus aureus SH1000 and 8325-4: comparative genome sequences of key laboratory strains in staphylococcal research. *Letters in applied microbiology,* 51**,** 358-361.

O'NEILL, E.,POZZI, C.,HOUSTON, P.,HUMPHREYS, H.,ROBINSON, D. A.,LOUGHMAN, A.,FOSTER, T. J. & O'GARA, J. P. 2008. A novel Staphylococcus aureus

biofilm phenotype mediated by the fibronectin-binding proteins, FnBPA and FnBPB. *Journal of bacteriology,* 190**,** 3835-3850.

O'TOOLE, G. A. 2016. Classic Spotlight: Before They Were Biofilms. *J Bacteriol,* 198**,** 5.

OEHMIGEN, K.,HÄHNEL, M.,BRANDENBURG, R.,WILKE, C.,WELTMANN, K. D. & VON WOEDTKE, T. 2010. The role of acidification for antimicrobial activity of atmospheric pressure plasma in liquids. *Plasma processes and polymers,* 7**,** 250-257.

OEHMIGEN, K.,WINTER, J.,HÄHNEL, M.,WILKE, C.,BRANDENBURG, R.,WELTMANN, K. D. & VON WOEDTKE, T. 2011. Estimation of possible mechanisms of Escherichia coli inactivation by plasma treated sodium chloride solution. *Plasma Processes and Polymers,* 8**,** 904-913.

OH, M.,JANG, S. Y.,LEE, J.-Y.,KIM, J. W.,JUNG, Y.,KIM, J.,SEO, J.,HAN, T.-S.,JANG, E. & SON, H. Y. 2023. The lipoprotein-associated phospholipase A2 inhibitor Darapladib sensitises cancer cells to ferroptosis by remodelling lipid metabolism. *Nature communications,* 14**,** 5728.

OLAYIWOLA, B.,O'NEILL, F.,FREWEN, C.,KAVANAGH, D. F.,O'HARA, R. & O'NEILL, L. 2024. Cold Plasma Deposition of Tobramycin as an Approach to Localized Antibiotic Delivery to Combat Biofilm Formation. *Pathogens,* 13.

OLIVEIRA, I. M.,BORGES, A. & SIMÕES, M. 2020. Chapter 14 - The potential of drug repurposing to face bacterial and fungal biofilm infections. *In:* SIMOES, M., BORGES, A. & CHAVES SIMOES, L. (eds.) *Recent Trends in Biofilm Science and Technology*. Academic Press.

OLIVEIRA, M. A. C. D.,LIMA, G. D. M. G.,NISHIME, T. M. C.,GONTIJO, A. V. L.,MENEZES, B. R. C. D.,CALIARI, M. V.,KOSTOV, K. G. & KOGA-ITO, C. Y. 2021. Inhibitory effect of cold atmospheric plasma on chronic wound-related multispecies biofilms. *Applied Sciences,* 11**,** 5441.

OLIVEIRA, W. F.,SILVA, P. M. S.,SILVA, R. C. S.,SILVA, G. M. M.,MACHADO, G.,COELHO, L. C. B. B. & CORREIA, M. T. S. 2018. Staphylococcus aureus and Staphylococcus epidermidis infections on implants. *Journal of Hospital Infection,* 98**,** 111-117.

OLWAL, C. O.,ANG'IENDA, P. O.,ONYANGO, D. M. & OCHIEL, D. O. 2018. Susceptibility patterns and the role of extracellular DNA in Staphylococcus epidermidis biofilm resistance to physico-chemical stress exposure. *BMC Microbiol,* 18**,** 40.

OMAR, A.,WRIGHT, J. B.,SCHULTZ, G.,BURRELL, R. & NADWORNY, P. 2017. Microbial biofilms and chronic wounds. *Microorganisms,* 5**,** 9.

ORAZI, G. & O'TOOLE, G. A. 2017. Pseudomonas aeruginosa Alters Staphylococcus aureus Sensitivity to Vancomycin in a Biofilm Model of Cystic Fibrosis Infection. *mBio,* 8**,** 10.1128/mbio.00873-17.

ORAZI, G. & O'TOOLE, G. A. 2019. "It takes a village": mechanisms underlying antimicrobial recalcitrance of polymicrobial biofilms. *Journal of Bacteriology,* 202**,** 10.1128/jb. 00530-19.

ORAZI, G.,RUOFF, K. L. & O'TOOLE, G. A. 2019. Pseudomonas aeruginosa Increases the Sensitivity of Biofilm-Grown Staphylococcus aureus to Membrane-Targeting Antiseptics and Antibiotics. *mBio,* 10.

ÖZTÜRK, A. M.,TAŞBAKAN, M.,METIN, D. Y.,YENER, C.,UYSAL, S.,YILDIRIM ŞIMŞIR, I.,ERTAM, İ.,PULLUKÇU, H.,ARDA, B. & ÇETINKALP, Ş. 2019. A neglected causative agent in diabetic foot infection: a retrospective evaluation of 13 patients with fungal etiology. *Turk J Med Sci,* 49**,** 81-86.

PAES LEME, R. C. & DA SILVA, R. B. 2021. Antimicrobial Activity of Non-steroidal Anti-inflammatory Drugs on Biofilm: Current Evidence and Potential for Drug Repurposing. *Frontiers in Microbiology,* Volume 12 - 2021.

PAINTER, K. L.,STRANGE, E.,PARKHILL, J.,BAMFORD, K. B.,ARMSTRONG-JAMES, D. & EDWARDS, A. M. 2015. Staphylococcus aureus adapts to oxidative stress by producing H2O2-resistant small-colony variants via the SOS response. *Infection and immunity,* 83**,** 1830-1844.

PALECZNY, J.,BROŻYNA, M.,DUDEK, B.,WOYTOŃ, A.,CHODACZEK, G.,SZAJNIK, M. & JUNKA, A. 2023. Culture shock: an investigation into the tolerance of pathogenic biofilms to antiseptics in environments resembling the chronic wound milieu. *International Journal of Molecular Sciences,* 24**,** 17242.

PALKOVÁ, Z. & VÁCHOVÁ, L. 2025. Cell differentiation, aging, and death in spatially organized yeast communities: mechanisms and consequences. *Cell Death & Differentiation*.

PAMMI, M.,LIANG, R.,HICKS, J.,MISTRETTA, T.-A. & VERSALOVIC, J. 2013. Biofilm extracellular DNA enhances mixed species biofilms of Staphylococcus epidermidis and Candida albicans. *BMC Microbiology,* 13**,** 257.

PARAMBATH, S.,DAO, A.,KIM, H. Y.,ZAWAHIR, S.,IZQUIERDO, A. A.,TACCONELLI, E.,GOVENDER, N.,OLADELE, R.,COLOMBO, A.,SORRELL, T.,RAMON-PARDO, P.,FUSIRE, T.,GIGANTE, V.,SATI, H.,MORRISSEY, C. O.,ALFFENAAR, J. W. &

BEARDSLEY, J. 2024. Candida albicans-A systematic review to inform the World Health Organization Fungal Priority Pathogens List. *Med Mycol,* 62.

PARKER, D. M.,KOCH, J. A.,GISH, C. G.,BROTHERS, K. M.,LI, W.,GILBERTIE, J.,ROWE, S. E.,CONLON, B. P.,BYRAPOGU, V. K. & URISH, K. L. 2023. Hydrogen peroxide, povidone-iodine and chlorhexidine fail to eradicate Staphylococcus aureus biofilm from infected implant materials. *Life,* 13**,** 1230.

PARNELL, L. K. & VOLK, S. W. 2019. The evolution of animal models in wound healing research: 1993–2017. *Advances in wound care,* 8**,** 692-702.

PASTAR, I.,NUSBAUM, A. G.,GIL, J.,PATEL, S. B.,CHEN, J.,VALDES, J.,STOJADINOVIC, O.,PLANO, L. R.,TOMIC-CANIC, M. & DAVIS, S. C. 2013. Interactions of methicillin resistant Staphylococcus aureus USA300 and Pseudomonas aeruginosa in polymicrobial wound infection. *PloS one,* 8**,** e56846.

PENG, Q.,TANG, X.,DONG, W.,SUN, N. & YUAN, W. 2022. A review of biofilm formation of Staphylococcus aureus and its regulation mechanism. *Antibiotics,* 12**,** 12.

PERCIVAL, S. L.,MALONE, M.,MAYER, D.,SALISBURY, A. M. & SCHULTZ, G. 2018. Role of anaerobes in polymicrobial communities and biofilms complicating diabetic foot ulcers. *International wound journal,* 15**,** 776-782.

PERCIVAL, S. L.,MCCARTY, S. M. & LIPSKY, B. 2015. Biofilms and wounds: an overview of the evidence. *Advances in wound care,* 4**,** 373-381.

PERCIVAL, S. L.,THOMAS, J. G. & WILLIAMS, D. W. 2010. Biofilms and bacterial imbalances in chronic wounds: anti-Koch. *Int Wound J,* 7**,** 169-75.

PEREIRA, R.,DOS SANTOS FONTENELLE, R. O.,DE BRITO, E. H. S. & DE MORAIS, S. M. 2021. Biofilm of Candida albicans: formation, regulation and resistance. *Journal of Applied Microbiology,* 131**,** 11-22.

PEREIRA, S. G.,MOURA, J.,CARVALHO, E. & EMPADINHAS, N. 2017. Microbiota of Chronic Diabetic Wounds: Ecology, Impact, and Potential for Innovative Treatment Strategies. *Frontiers in Microbiology,* Volume 8 - 2017.

PETERS, B. M. & NOVERR, M. C. 2013. Candida albicans-Staphylococcus aureus polymicrobial peritonitis modulates host innate immunity. *Infection and immunity,* 81**,** 2178-2189.

PETERS, B. M.,OVCHINNIKOVA, E. S.,KROM, B. P.,SCHLECHT, L. M.,ZHOU, H.,HOYER, L. L.,BUSSCHER, H. J.,VAN DER MEI, H. C.,JABRA-RIZK, M. A. &

SHIRTLIFF, M. E. 2012. Staphylococcus aureus adherence to Candida albicans hyphae is mediated by the hyphal adhesin Als3p. *Microbiology,* 158**,** 2975-2986.

PETERS, B. M.,WARD, R. M.,RANE, H. S.,LEE, S. A. & NOVERR, M. C. 2013. Efficacy of ethanol against Candida albicans and Staphylococcus aureus polymicrobial biofilms. *Antimicrobial agents and chemotherapy,* 57**,** 74-82.

PETERSON, M. & WESTGATE, S. 2022. Insights into ex vivo skin models for microbiological and healing properties of wound dressings. *Wounds UK,* 18.

PHAM, T. D. M.,ZIORA, Z. M. & BLASKOVICH, M. A. T. 2019. Quinolone antibiotics. *Medchemcomm,* 10**,** 1719-1739.

PHAN, S.,FENG, C. H.,HUANG, R.,LEE, Z. X.,MOUA, Y.,PHUNG, O. J. & LENHARD, J. R. 2023. Relative abundance and detection of Pseudomonas aeruginosa from chronic wound infections globally. *Microorganisms,* 11**,** 1210.

PHILLIPS, P.,WOLCOTT, R.,FLETCHER, J. & SCHULTZ, G. 2012. Biofilms Made Easy. Wounds International 2010; 1 (3). *Available at: bit. ly/1CJUTUX (accessed February 2016)*.

PIER, G. B.,COLEMAN, F.,GROUT, M.,FRANKLIN, M. & OHMAN, D. E. 2001. Role of alginate O acetylation in resistance of mucoid Pseudomonas aeruginosa to opsonic phagocytosis. *Infect Immun,* 69**,** 1895-901.

PINTO, A. M.,CERQUEIRA, M. A.,BAÑOBRE-LÓPES, M.,PASTRANA, L. M. & SILLANKORVA, S. 2020a. Bacteriophages for Chronic Wound Treatment: from Traditional to Novel Delivery Systems. *Viruses,* 12.

PINTO, R. M.,SOARES, F. A.,REIS, S.,NUNES, C. & VAN DIJCK, P. 2020b. Innovative strategies toward the disassembly of the EPS matrix in bacterial biofilms. *Frontiers in Microbiology,* 11**,** 952.

PLATTFAUT, I.,DEMIR, E.,FUCHS, P. C.,SCHIEFER, J. L.,STÜRMER, E. K.,BRÜNING, A. K. E. & OPLÄNDER, C. 2021. Characterization of Blue Light Treatment for Infected Wounds: Antibacterial Efficacy of 420, 455, and 480 nm Light-Emitting Diode Arrays Against Common Skin Pathogens Versus Blue Light-Induced Skin Cell Toxicity. *Photobiomodulation, Photomedicine, and Laser Surgery,* 39**,** 339-348.

POHL, C. H. 2022. Recent advances and opportunities in the study of Candida albicans polymicrobial biofilms. *Frontiers in Cellular and Infection Microbiology,* 12**,** 836379.

POLSON, E. S.,KUCHLER, V. B.,ABBOSH, C.,ROSS, E. M.,MATHEW, R. K.,BEARD, H. A.,DA SILVA, B.,HOLDING, A. N.,BALLEREAU, S.,CHUNTHARPURSAT-BON, E.,WILLIAMS, J.,GRIFFITHS, H. B. S.,SHAO, H.,PATEL, A.,DAVIES, A. J.,DROOP, A.,CHUMAS, P.,SHORT, S. C.,LORGER, M.,GESTWICKI, J. E.,ROBERTS, L. D.,BON, R. S.,ALLISON, S. J.,ZHU, S.,MARKOWETZ, F. & WURDAK, H. 2018. KHS101 disrupts energy metabolism in human glioblastoma cells and reduces tumor growth in mice. *Science Translational Medicine,* 10**,** eaar2718.

PONDE, N. O.,LORTAL, L.,RAMAGE, G.,NAGLIK, J. R. & RICHARDSON, J. P. 2021. Candida albicans biofilms and polymicrobial interactions. *Critical reviews in microbiology,* 47**,** 91-111.

POUGET, C.,DUNYACH-REMY, C.,BERNARDI, T.,PROVOT, C.,TASSE, J.,SOTTO, A. & LAVIGNE, J.-P. 2022a. A relevant wound-like in vitro media to study bacterial cooperation and biofilm in chronic wounds. *Frontiers in Microbiology,* 13**,** 705479.

POUGET, C.,DUNYACH-REMY, C.,MAGNAN, C.,PANTEL, A.,SOTTO, A. & LAVIGNE, J. P. 2022b. Polymicrobial Biofilm Organization of Staphylococcus aureus and Pseudomonas aeruginosa in a Chronic Wound Environment. *Int J Mol Sci,* 23.

POZZI, C.,WATERS, E. M.,RUDKIN, J. K.,SCHAEFFER, C. R.,LOHAN, A. J.,TONG, P.,LOFTUS, B. J.,PIER, G. B.,FEY, P. D.,MASSEY, R. C. & O'GARA, J. P. 2012. Methicillin resistance alters the biofilm phenotype and attenuates virulence in Staphylococcus aureus device-associated infections. *PLoS Pathog,* 8**,** e1002626.

PRASAD, K.,SASI, S.,WEERASINGHE, J.,LEVCHENKO, I. & BAZAKA, K. 2023. Enhanced Antimicrobial Activity through Synergistic Effects of Cold Atmospheric Plasma and Plant Secondary Metabolites: Opportunities and Challenges. *Molecules,* 28.

PROCTOR, D. M.,DANGANA, T.,SEXTON, D. J.,FUKUDA, C.,YELIN, R. D.,STANLEY, M.,BELL, P. B.,BASKARAN, S.,DEMING, C. & CHEN, Q. 2021. Integrated genomic, epidemiologic investigation of Candida auris skin colonization in a skilled nursing facility. *Nature medicine,* 27**,** 1401-1409.

PUGAZHENDHI, A. S.,WEI, F.,HUGHES, M. & COATHUP, M. 2022. Bacterial Adhesion, Virulence, and Biofilm Formation. *In:* COATHUP, M. (ed.) *Musculoskeletal Infection*. Cham: Springer International Publishing.

RAGUPATHI, H.,PUSHPARAJ, M. M.,GOPI, S. M.,GOVINDARAJAN, D. K. & KANDASWAMY, K. 2024. Biofilm matrix: a multifaceted layer of biomolecules and a defensive barrier against antimicrobials. *Archives of Microbiology,* 206**,** 432.

RAHIM, K.,QASIM, M.,RAHMAN, H.,KHAN, T. A.,AHMAD, I.,KHAN, N.,ULLAH, A.,BASIT, A. & SALEHA, S. 2016. Antimicrobial resistance among aerobic biofilm producing bacteria isolated from chronic wounds in the tertiary care hospitals of Peshawar, Pakistan. *J Wound Care,* 25**,** 480-6.

RAHIM, K.,SALEHA, S.,ZHU, X.,HUO, L.,BASIT, A. & FRANCO, O. L. 2017. Bacterial contribution in chronicity of wounds. *Microbial ecology,* 73**,** 710-721.

RAHIMI-VERKI, N.,SHAPOORZADEH, A.,RAZZAGHI-ABYANEH, M.,ATYABI, S.-M.,SHAMS-GHAHFAROKHI, M.,JAHANSHIRI, Z. & GHOLAMI-SHABANI, M. 2016. Cold atmospheric plasma inhibits the growth of Candida albicans by affecting ergosterol biosynthesis and suppresses the fungal virulence factors in vitro. *Photodiagnosis and photodynamic therapy,* 13**,** 66-72.

RAHME, L. G.,STEVENS, E. J.,WOLFORT, S. F.,SHAO, J.,TOMPKINS, R. G. & AUSUBEL, F. M. 1995. Common virulence factors for bacterial pathogenicity in plants and animals. *Science,* 268**,** 1899-1902.

RAISSI-DEHKORDI, N.,RAISSI-DEHKORDI, N.,EBRAHIMIBAGHA, H.,TAYEBI, T.,MOEINABADI-BIDGOLI, K.,HASSANI, M. & NIKNEJAD, H. 2025. Advancing chronic and acute wound healing with cold atmospheric plasma: cellular and molecular mechanisms, benefits, risks, and future directions. *Frontiers in Medicine,* 12**,** 1527736.

RAJABI, H.,SALIMIZAND, H.,KHODABANDEHLOO, M.,FAYYAZI, A. & RAMAZANZADEH, R. 2022. Prevalence of algD, pslD, pelF, Ppgl, and PAPI-1 Genes Involved in Biofilm Formation in Clinical Pseudomonas aeruginosa Strains. *Biomed Res Int,* 2022**,** 1716087.

RAJENDRAN, R.,SHERRY, L.,LAPPIN, D. F.,NILE, C. J.,SMITH, K.,WILLIAMS, C.,MUNRO, C. A. & RAMAGE, G. 2014a. Extracellular DNA release confers heterogeneity in Candida albicans biofilm formation. *BMC Microbiol,* 14**,** 303.

RAJENDRAN, R.,SHERRY, L.,LAPPIN, D. F.,NILE, C. J.,SMITH, K.,WILLIAMS, C.,MUNRO, C. A. & RAMAGE, G. 2014b. Extracellular DNA release confers heterogeneity in Candida albicans biofilm formation. *BMC Microbiology,* 14**,** 303.

RAMAGE, G.,O'DONNELL, L. E.,KEAN, R.,TOWNSEND, E. & RAJENDRAN, R. 2017. Clinical implications of interkingdom fungal and bacterial biofilms. *Microbial Biofilms*. CRC Press.

RAMAGE, G.,RAJENDRAN, R.,SHERRY, L. & WILLIAMS, C. 2012. Fungal biofilm resistance. *International journal of microbiology,* 2012**,** 528521.

RAMAGE, G.,VANDE WALLE, K.,WICKES, B. L. & LÓPEZ-RIBOT, J. L. 2001. Standardized method for in vitro antifungal susceptibility testing of Candida albicans biofilms. *Antimicrobial agents and chemotherapy,* 45**,** 2475-2479.

RANJITH, K.,NAGAPRIYA, B. & SHIVAJI, S. 2022. Polymicrobial biofilms of ocular bacteria and fungi on ex vivo human corneas. *Scientific Reports,* 12**,** 11606.

RAO, Y.,SHANG, W.,YANG, Y.,ZHOU, R. & RAO, X. 2020. Fighting Mixed-Species Microbial Biofilms With Cold Atmospheric Plasma. *Frontiers in Microbiology,* Volume 11 - 2020.

RATHER, M. A.,GUPTA, K. & MANDAL, M. 2021. Microbial biofilm: formation, architecture, antibiotic resistance, and control strategies. *Brazilian Journal of Microbiology,* 52**,** 1701-1718.

RATHNA, R. P. & KULANDHAIVEL, M. 2024. Advancements in wound healing: integrating biomolecules, drug delivery carriers, and targeted therapeutics for enhanced tissue repair. *Archives of Microbiology,* 206**,** 199.

RAVAL, Y. S.,FLURIN, L.,MOHAMED, A.,GREENWOOD-QUAINTANCE, K. E.,BEYENAL, H. & PATEL, R. 2021. In Vitro Antibacterial Activity of Hydrogen Peroxide and Hypochlorous Acid, Including That Generated by Electrochemical Scaffolds. *Antimicrobial Agents and Chemotherapy,* 65**,** 10.1128/aac.01966-20.

RAZIYEVA, K.,KIM, Y.,ZHARKINBEKOV, Z.,KASSYMBEK, K.,JIMI, S. & SAPAROV, A. 2021. Immunology of acute and chronic wound healing. *Biomolecules,* 11**,** 700.

REDDERSEN, K.,TITTELBACH, J. & WIEGAND, C. 2022. 3D biofilm models containing multiple species for antimicrobial testing of wound dressings. *Microorganisms,* 10**,** 2027.

REECE, E.,BETTIO, P. H. D. A. & RENWICK, J. 2021. Polymicrobial interactions in the cystic fibrosis airway microbiome impact the antimicrobial susceptibility of Pseudomonas aeruginosa. *Antibiotics,* 10**,** 827.

REED, P.,ATILANO, M. L.,ALVES, R.,HOICZYK, E.,SHER, X.,REICHMANN, N. T.,PEREIRA, P. M.,ROEMER, T.,FILIPE, S. R. & PEREIRA-LEAL, J. B. 2015.

Staphylococcus aureus survives with a minimal peptidoglycan synthesis machine but sacrifices virulence and antibiotic resistance. *Plos pathogens,* 11**,** e1004891.

REEKS, B. Y.,CHAMPLIN, F. R.,PAULSEN, D. B.,SCRUGGS, D. W. & LAWRENCE, M. L. 2005. Effects of sub-minimum inhibitory concentration antibiotic levels and temperature on growth kinetics and outer membrane protein expression in Mannheimia haemolytica and Haemophilus somnus. *Canadian journal of veterinary research,* 69**,** 1.

RENDUELES, O. & GHIGO, J.-M. 2015. Mechanisms of Competition in Biofilm Communities. *Microbiology Spectrum,* 3**,** 10.1128/microbiolspec.mb-0009-2014.

RENDUELES, O.,TRAVIER, L.,LATOUR-LAMBERT, P.,FONTAINE, T.,MAGNUS, J.,DENAMUR, E. & GHIGO, J.-M. 2011. Screening of Escherichia coli Species Biodiversity Reveals New Biofilm-Associated Antiadhesion Polysaccharides. *mBio,* 2**,** e00043-11.

REPINE, J.,FOX, R. B. & BERGER, E. 1981. Hydrogen peroxide kills Staphylococcus aureus by reacting with staphylococcal iron to form hydroxyl radical. *Journal of Biological Chemistry,* 256**,** 7094-7096.

RICHARDS, B.,ROBERTSON, S.,MARTINEZ POMARES, L. & CÁMARA, M. 2024. Development of a Polymicrobial Colony Biofilm Model to Test Antimicrobials in Cystic Fibrosis. *J Vis Exp*.

RICHARDS, T.,HARRHY, J. H.,LEWIS, R. J.,HOWE, A. G. R.,SULDECKI, G. M.,FOLLI, A.,MORGAN, D. J.,DAVIES, T. E.,LOVERIDGE, E. J.,CROLE, D. A.,EDWARDS, J. K.,GASKIN, P.,KIELY, C. J.,HE, Q.,MURPHY, D. M.,MAILLARD, J.-Y.,FREAKLEY, S. J. & HUTCHINGS, G. J. 2021. A residue-free approach to water disinfection using catalytic in situ generation of reactive oxygen species. *Nature Catalysis,* 4**,** 575-585.

RODRIGUES, M. E.,GOMES, F. & RODRIGUES, C. F. 2019. Candida spp./bacteria mixed biofilms. *Journal of Fungi,* 6**,** 5.

RODRIGUES, M. L. & NOSANCHUK, J. D. 2023. Recognition of fungal priority pathogens: What next? *PLoS Negl Trop Dis,* 17**,** e0011136.

RODRÍGUEZ-ROJAS, A.,KIM, J. J.,JOHNSTON, P. R.,MAKAROVA, O.,ERAVCI, M.,WEISE, C.,HENGGE, R. & ROLFF, J. 2020. Non-lethal exposure to H2O2 boosts bacterial survival and evolvability against oxidative stress. *PLoS genetics,* 16**,** e1008649.

ROES, C.,CALLADINE, L. & MORRIS, C. 2019. Biofilm management using monofilament fibre debridement technology: outcomes and clinician and patient satisfaction. *J Wound Care,* 28**,** 608-622.

ROGUET, R.,COHEN, C.,DOSSOU, K. & ROUGIER, A. 1994. Episkin, a reconstituted human epidermis for assessing in vitro the irritancy of topically applied compounds. *Toxicology in vitro,* 8**,** 283-291.

ROQUE-BORDA, C. A.,PRIMO, L. M. D. G.,MEDINA-ALARCÓN, K. P.,CAMPOS, I. C.,NASCIMENTO, C. D. F.,SARAIVA, M. M.,BERCHIERI JUNIOR, A.,FUSCO-ALMEIDA, A. M.,MENDES-GIANNINI, M. J. S. & PERDIGÃO, J. 2025. Antimicrobial Peptides: A Promising Alternative to Conventional Antimicrobials for Combating Polymicrobial Biofilms. *Advanced Science*, 12**,** 2410893.

ROY, S.,SANTRA, S.,DAS, A.,DIXITH, S.,SINHA, M.,GHATAK, S.,GHOSH, N.,BANERJEE, P.,KHANNA, S.,MATHEW-STEINER, S.,GHATAK, P. D.,BLACKSTONE, B. N.,POWELL, H. M.,BERGDALL, V. K.,WOZNIAK, D. J. & SEN, C. K. 2020. Staphylococcus aureus Biofilm Infection Compromises Wound Healing by Causing Deficiencies in Granulation Tissue Collagen. *Ann Surg,* 271**,** 1174-1185.

SABINO, F. & AUF DEM KELLER, U. 2015. Matrix metalloproteinases in impaired wound healing. *Metalloproteinases In Medicine***,** 1-8.

SADEGHPOUR HERAVI, F.,ZAKRZEWSKI, M.,VICKERY, K.,G. ARMSTRONG, D. & HU, H. 2019. Bacterial diversity of diabetic foot ulcers: current status and future prospectives. *Journal of clinical medicine,* 8**,** 1935.

SADIQ, F. A.,HANSEN, M. F.,BURMØLLE, M.,HEYNDRICKX, M.,FLINT, S.,LU, W.,CHEN, W. & ZHANG, H. 2022. Trans-kingdom interactions in mixed biofilm communities. *FEMS microbiology reviews,* 46**,** fuac024.

SADOWSKA, B.,WALENCKA, E.,WIECKOWSKA-SZAKIEL, M. & RÓŻALSKA, B. 2010. Bacteria competing with the adhesion and biofilm formation by Staphylococcus aureus. *Folia microbiologica,* 55**,** 497-501.

SAHOO, K. & MESHRAM, S. 2024. Biofilm Formation in Chronic Infections: A Comprehensive Review of Pathogenesis, Clinical Implications, and Novel Therapeutic Approaches. *Cureus,* 16**,** e70629.

SALEM, H. S. & MONT, M. A. 2021. A Novel Biofilm-Disrupting Wound Care Technology for the Prevention of Surgical Site Infections Following Total Joint Arthroplasty: A Conceptual Review. *Surg Technol Int,* 38**,** 361-370.

SANCHEZ, M.,MARIN, M.,FIGUERO, E.,LLAMA-PALACIOS, A.,HERRERA, D. & SANZ, M. 2013. Analysis of viable vs. dead A ggregatibacter actinomycetemcomitans and P orphyromonas gingivalis using selective quantitative real-time PCR with propidium monoazide. *Journal of Periodontal Research,* 48**,** 213-220.

SANCHEZ, M.,MARIN, M.,FIGUERO, E.,LLAMA-PALACIOS, A.,LEON, R.,BLANC, V.,HERRERA, D. & SANZ, M. 2014. Quantitative real-time PCR combined with propidium monoazide for the selective quantification of viable periodontal pathogens in an in vitro subgingival biofilm model. *Journal of Periodontal Research,* 49**,** 20-28.

SÁNCHEZ-PEÑA, A.,WINANS, J. B.,NADELL, C. D. & LIMOLI, D. H. 2024. Pseudomonas aeruginosa surface motility and invasion into competing communities enhances interspecies antagonism. *bioRxiv*.

SĂNDULESCU, O. & SĂNDULESCU, M. 2023. Oral biofilms - pivotal role in understanding microbes and their relevance to the human host. *Germs,* 13**,** 7-9.

SANYAOLU, A.,OKORIE, C.,MARINKOVIC, A.,ABBASI, A. F.,PRAKASH, S.,MANGAT, J.,HOSEIN, Z.,HAIDER, N. & CHAN, J. 2022. Candida auris: An Overview of the Emerging Drug-Resistant Fungal Infection. *Infect Chemother,* 54**,** 236-246.

SAPAAR, B.,NUR, A.,HIROTA, K.,YUMOTO, H.,MURAKAMI, K.,AMOH, T.,MATSUO, T.,ICHIKAWA, T. & MIYAKE, Y. 2014. Effects of extracellular DNA from Candida albicans and pneumonia-related pathogens on Candida biofilm formation and hyphal transformation. *Journal of applied microbiology,* 116**,** 1531-1542.

SATHYAPALAN, D. T.,ANTONY, R.,NAMPOOTHIRI, V.,KUMAR, A.,SHASHINDRAN, N.,JAMES, J.,THOMAS, J.,PRASANNA, P.,SUDHIR, A. S. & PHILIP, J. M. 2021. Evaluating the measures taken to contain a Candida auris outbreak in a tertiary care hospital in South India: an outbreak investigational study. *BMC Infectious Diseases,* 21**,** 425.

SAUER, K.,STOODLEY, P.,GOERES, D. M.,HALL-STOODLEY, L.,BURMØLLE, M.,STEWART, P. S. & BJARNSHOLT, T. 2022. The biofilm life cycle: expanding the conceptual model of biofilm formation. *Nature Reviews Microbiology,* 20**,** 608-620.

SAVE, J.,QUE, Y. A.,ENTENZA, J. M.,KOLENDA, C.,LAURENT, F. & RESCH, G. 2022. Bacteriophages combined with subtherapeutic doses of flucloxacillin act synergistically against Staphylococcus aureus experimental infective endocarditis. *Journal of the American Heart Association,* 11**,** e023080.

SCALES, B. S. & HUFFNAGLE, G. B. 2013. The microbiome in wound repair and tissue fibrosis. *J Pathol,* 229**,** 323-31.

SCHELENZ, S.,HAGEN, F.,RHODES, J. L.,ABDOLRASOULI, A.,CHOWDHARY, A.,HALL, A.,RYAN, L.,SHACKLETON, J.,TRIMLETT, R. & MEIS, J. F. 2016. First hospital outbreak of the globally emerging Candida auris in a European hospital. *Antimicrobial Resistance & Infection Control,* 5**,** 1-7.

SCHILCHER, K. & HORSWILL, A. R. 2020. Staphylococcal biofilm development: structure, regulation, and treatment strategies. *Microbiology and Molecular Biology Reviews,* 84**,** 10.1128/mmbr. 00026-19.

SCHLECHT, L. M.,PETERS, B. M.,KROM, B. P.,FREIBERG, J. A.,HÄNSCH, G. M.,FILLER, S. G.,JABRA-RIZK, M. A. & SHIRTLIFF, M. E. 2015. Systemic Staphylococcus aureus infection mediated by Candida albicans hyphal invasion of mucosal tissue. *Microbiology,* 161**,** 168-181.

SCHMIDT, A.,BEKESCHUS, S.,WENDE, K.,VOLLMAR, B. & VON WOEDTKE, T. 2017. A cold plasma jet accelerates wound healing in a murine model of full-thickness skin wounds. *Exp Dermatol,* 26**,** 156-162.

SCHMIDT, B. M.,KAYE, K. S.,ARMSTRONG, D. G. & POP-BUSUI, R. 2023. Empirical Antibiotic Therapy in Diabetic Foot Ulcer Infection Increases Hospitalization. *Open Forum Infectious Diseases,* 10.

SCHRAMM, S.,HILLER, K. A.,CANTZLER, S.,WEILEMANN, H.,CANTZLER, M.,ZIMMERMANN, J. L.,CIEPLIK, F. & MAISCH, T. 2020. The Latest Time Point of Retreatment (LTPR) as a Novel Method to Determine Antibacterial Effects for Binary Use of Cold Atmospheric Plasma and Conventional Agents. *Front Microbiol,* 11**,** 576500.

SCHULTZ, G. S.,WOO, K.,WEIR, D. & YANG, Q. 2018. Effectiveness of a monofilament wound debridement pad at removing biofilm and slough: ex vivo and clinical performance. *Journal of wound care,* 27**,** 80-90.

SEDIGHI, O.,BEDNARKE, B.,SHERRIFF, H. & DOIRON, A. L. 2024. Nanoparticle-Based Strategies for Managing Biofilm Infections in Wounds: A Comprehensive Review. *ACS Omega,* 9**,** 27853-27871.

SEN, C. K. 2019. Human wounds and its burden: an updated compendium of estimates. Mary Ann Liebert, Inc., Publishers 140 Huguenot Street, 3rd Floor New ….

SEN, C. K. 2021. Human wound and its burden: updated 2020 compendium of estimates. *Advances in wound care,* 10**,** 281-292.

SENNEVILLE, E.,ALBALAWI, Z.,VAN ASTEN, S. A.,ABBAS, Z. G.,ALLISON, G.,ARAGON-SANCHEZ, J.,EMBIL, J. M.,LAVERY, L. A.,ALHASAN, M. & OZ, O. 2024. IWGDF/IDSA Guidelines on the Diagnosis and Treatment of Diabetes-related Foot Infections (IWGDF/IDSA 2023)(may, 10.1093/cid/ciad527, 2024). *CLINICAL INFECTIOUS DISEASES,* 79**,** 286-286.

SENOBAR TAHAEI, S. A.,STÁJER, A.,BARRAK, I.,OSTORHÁZI, E.,SZABÓ, D. & GAJDÁCS, M. 2021. Correlation Between Biofilm-Formation and the Antibiotic Resistant Phenotype in Staphylococcus aureus Isolates: A Laboratory-Based Study in Hungary and a Review of the Literature. *Infect Drug Resist,* 14**,** 1155-1168.

SERRA, R.,GRANDE, R.,BUTRICO, L.,ROSSI, A.,SETTIMIO, U. F.,CAROLEO, B.,AMATO, B.,GALLELLI, L. & DE FRANCISCIS, S. 2015a. Chronic wound infections: the role of Pseudomonas aeruginosa and Staphylococcus aureus. *Expert review of anti-infective therapy,* 13**,** 605-613.

SERRA, R.,GRANDE, R.,BUTRICO, L.,ROSSI, A.,SETTIMIO, U. F.,CAROLEO, B.,AMATO, B.,GALLELLI, L. & DE FRANCISCIS, S. 2015b. Chronic wound infections: the role of Pseudomonas aeruginosa and Staphylococcus aureus. *Expert Rev Anti Infect Ther,* 13**,** 605-13.

SHABANI, H.,DEZHPOUR, A.,JAFARI, S.,MOGHADDAM, M. J. M. & NILKAR, M. 2023. Antimicrobial activity of cold atmospheric-pressure argon plasma combined with chicory (Cichorium intybus L.) extract against P. aeruginosa and E. coli biofilms. *Scientific Reports,* 13**,** 9441.

SHAH, P.,INTURI, R.,ANNE, D.,JADHAV, D.,VISWAMBHARAN, V.,KHADILKAR, R.,DNYANMOTE, A. & SHAHI, S. 2022. Wagner's Classification as a Tool for Treating Diabetic Foot Ulcers: Our Observations at a Suburban Teaching Hospital. *Cureus,* 14**,** e21501.

SHALABY, R. S.,GAAFAR, M. M.,EL BASSHAR, M. A.,SOLIMAN, M. S.,YOUSRY, M. M. & ELMAHDY, Y. A. 2023. Clinical Study of Coexistence of Fungal Infections in Diabetic Foot Ulcers by 18s rRNA Gene Polymerase Chain Reaction. *Open Access Macedonian Journal of Medical Sciences,* 11**,** 36-40.

SHARMA, A. D.,JARMAN, E. H.,KUPPALLI, K.,MURPHY, M. J.,LONGAKER, M. T.,GURTNER, G. & FOX, P. M. 2024a. Successful topical treatment of human biofilms using multiple antibiotic elution from a collagen-rich hydrogel. *Scientific Reports,* 14**,** 5621.

SHARMA, D. K. & RAJPUROHIT, Y. S. 2024. Multitasking functions of bacterial extracellular DNA in biofilms. *Journal of Bacteriology,* 206**,** e00006-24.

SHARMA, H.,SHARMA, S.,KRISHNAN, A.,YUAN, D.,VANGAVETI, V. N.,MALABU, U. H. & HALEAGRAHARA, N. 2022. The efficacy of inflammatory markers in diagnosing infected diabetic foot ulcers and diabetic foot osteomyelitis: Systematic review and meta-analysis. *PLoS One,* 17**,** e0267412.

SHARMA, R.,GUPTA, N.,KUMAR, V.,PAL, S.,KAUNDAL, V. & SHARMA, V. 2017. Silver colloid dressings score over conventional dressings in diabetic foot ulcer: a randomized clinical trial. *International Surgery Journal,* 4**,** 2627-2631.

SHARMA, S.,CHAUHAN, A.,RANJAN, A.,MATHKOR, D. M.,HAQUE, S.,RAMNIWAS, S.,TULI, H. S.,JINDAL, T. & YADAV, V. 2024b. Emerging challenges in antimicrobial resistance: implications for pathogenic microorganisms, novel antibiotics, and their impact on sustainability. *Frontiers in microbiology,* 15**,** 1403168.

SHARMA, S.,MOHLER, J.,MAHAJAN, S. D.,SCHWARTZ, S. A.,BRUGGEMANN, L. & AALINKEEL, R. 2023. Microbial biofilm: a review on formation, infection, antibiotic resistance, control measures, and innovative treatment. *Microorganisms,* 11**,** 1614.

SHASTRY, R. P. & REKHA, P. D. 2021. Bacterial cross talk with gut microbiome and its implications: a short review. *Folia Microbiologica,* 66**,** 15-24.

SHAW, T. J. & MARTIN, P. 2009. Wound repair at a glance. *Journal of cell science,* 122**,** 3209-3213.

SHEPHERD, J.,DOUGLAS, I.,RIMMER, S.,SWANSON, L. & MACNEIL, S. 2009. Development of three-dimensional tissue-engineered models of bacterial infected human skin wounds. *Tissue Engineering Part C: Methods,* 15**,** 475-484.

SHERRY, L.,LAPPIN, G.,O'DONNELL, L. E.,MILLHOUSE, E.,MILLINGTON, O. R.,BRADSHAW, D. J.,AXE, A. S.,WILLIAMS, C.,NILE, C. J. & RAMAGE, G. 2016. Viable compositional analysis of an eleven species oral polymicrobial biofilm. *Frontiers in Microbiology,* 7**,** 912.

SHNYOOR, H. A. S. & ZGAIR, A. 2024. Exploring the Effects of Hydrogen Peroxide on Biofilm Development and Antibiotic Susceptibility. *World Journal of Experimental Biosciences (ISSN: 2313-3937)*, 26-31.

SHORT, B.,BAKRI, A.,BAZ, A.,WILLIAMS, C.,BROWN, J. & RAMAGE, G. 2023. There is more to wounds than bacteria: fungal biofilms in chronic wounds. *Current Clinical Microbiology Reports,* 10, 9-16.

SHREE, P.,SINGH, C. K.,SODHI, K. K.,SURYA, J. N. & SINGH, D. K. 2023. Biofilms: Understanding the structure and contribution towards bacterial resistance in antibiotics. *Medicine in Microecology,* 16, 100084.

SIBLEY, C. D.,DUAN, K.,FISCHER, C.,PARKINS, M. D.,STOREY, D. G.,RABIN, H. R. & SURETTE, M. G. 2008a. Discerning the complexity of community interactions using a Drosophila model of polymicrobial infections. *PLoS pathogens,* 4, e1000184.

SIBLEY, C. D.,PARKINS, M. D.,RABIN, H. R.,DUAN, K.,NORGAARD, J. C. & SURETTE, M. G. 2008b. A polymicrobial perspective of pulmonary infections exposes an enigmatic pathogen in cystic fibrosis patients. *Proceedings of the National Academy of Sciences,* 105, 15070-15075.

SIMNER, P. J.,BEISKEN, S.,BERGMAN, Y.,POSCH, A. E.,COSGROVE, S. E. & TAMMA, P. D. 2021. Cefiderocol Activity Against Clinical Pseudomonas aeruginosa Isolates Exhibiting Ceftolozane-Tazobactam Resistance. *Open Forum Infect Dis,* 8, ofab311.

SIMONETTI, O.,MARASCA, S.,CANDELORA, M.,RIZZETTO, G.,RADI, G.,MOLINELLI, E.,BRESCINI, L.,CIRIONI, O. & OFFIDANI, A. 2022. Methicillin-resistant Staphylococcus aureus as a cause of chronic wound infections: Alternative strategies for management. *AIMS Microbiol,* 8, 125-137.

SIMONETTI, O.,RIZZETTO, G.,RADI, G.,MOLINELLI, E.,CIRIONI, O.,GIACOMETTI, A. & OFFIDANI, A. 2021. New Perspectives on Old and New Therapies of Staphylococcal Skin Infections: The Role of Biofilm Targeting in Wound Healing. *Antibiotics (Basel),* 10.

SINGH, A.,AMOD, A.,PANDEY, P.,BOSE, P.,PINGALI, M. S.,SHIVALKAR, S.,VARADWAJ, P. K.,SAHOO, A. K. & SAMANTA, S. K. 2022. Bacterial biofilm infections, their resistance to antibiotics therapy and current treatment strategies. *Biomedical Materials,* 17, 022003.

SINGH, D. P.,MALIK, D. S. & LAL, V. 2024. Understanding the Distribution of Candida auris and Its Antifungal Susceptibility in Diverse Samples. *International Journal of Innovative Research in Medical Science*.

SINHA, S.,AGGARWAL, S. & SINGH, D. V. 2024. Efflux pumps: gatekeepers of antibiotic resistance in Staphylococcus aureus biofilms. *Microb Cell,* 11**,** 368-377.

SIVORI, F.,CAVALLO, I.,TRUGLIO, M.,PELAGALLI, L.,MARIANI, V.,FABRIZIO, G.,ABRIL, E.,SANTINO, I.,FRADIANI, P. A. & SOLMONE, M. 2024. Biofilm-mediated antibiotic tolerance in Staphylococcus aureus from spinal cord stimulation device-related infections. *Microbiology Spectrum,* 12**,** e01683-24.

SKARIYACHAN, S.,SRIDHAR, V. S.,PACKIRISAMY, S.,KUMARGOWDA, S. T. & CHALLAPILLI, S. B. 2018. Recent perspectives on the molecular basis of biofilm formation by Pseudomonas aeruginosa and approaches for treatment and biofilm dispersal. *Folia Microbiol (Praha),* 63**,** 413-432.

SKOGMAN, M. E.,VUORELA, P. M. & FALLARERO, A. 2012. Combining biofilm matrix measurements with biomass and viability assays in susceptibility assessments of antimicrobials against Staphylococcus aureus biofilms. *The Journal of Antibiotics,* 65**,** 453-459.

SLOAN, T. J.,TURTON, J. C.,TYSON, J.,MUSGROVE, A.,FLEMING, V. M.,LISTER, M. M.,LOOSE, M. W.,SOCKETT, R. E.,DIGGLE, M. & GAME, F. L. 2019. Examining diabetic heel ulcers through an ecological lens: microbial community dynamics associated with healing and infection. *Journal of medical microbiology,* 68**,** 230-240.

SMITH, K.,RAJENDRAN, R.,KERR, S.,LAPPIN, D. F.,MACKAY, W. G.,WILLIAMS, C. & RAMAGE, G. 2015. Aspergillus fumigatus enhances elastase production in Pseudomonas aeruginosa co-cultures. *Medical mycology,* 53**,** 645-655.

SOKOU, R.,PALIOURA, A. E.,KOPANOU TALIAKA, P.,KONSTANTINIDI, A.,TSANTES, A. G.,PIOVANI, D.,TSANTE, K. A.,GOUNARI, E. A.,ILIODROMITI, Z.,BOUTSIKOU, T.,TSANTES, A. E.,BONOVAS, S. & IACOVIDOU, N. 2024. Candida auris Infection, a Rapidly Emerging Threat in the Neonatal Intensive Care Units: A Systematic Review. *J Clin Med,* 13.

SOLTANI BORCHALOEE, A.,MOOSAKAZEMI MOHAMMADI, L. S.,KHOSH RAVESH, R.,ALLAMEH, S. F.,TABATABAIE POYA, F. S. & FATEHI MARJ, A. 2024. Prevalence of biofilm and efflux pump genes expression by PCR and

antibiotic resistance pattern in Pseudomonas aeruginosa. *Archives of Razi Institute,* 79**,** 1281-1286.

SØNDERHOLM, M.,BJARNSHOLT, T.,ALHEDE, M.,KOLPEN, M.,JENSEN, P. Ø.,KÜHL, M. & KRAGH, K. N. 2017. The consequences of being in an infectious biofilm: microenvironmental conditions governing antibiotic tolerance. *International journal of molecular sciences,* 18**,** 2688.

SOUTHWICK, K.,ADAMS, E. H.,GREENKO, J.,OSTROWSKY, B.,FERNANDEZ, R.,PATEL, R.,QUINN, M.,VALLABHANENI, S.,DENIS, R. J. & ERAZO, R. 2039. New York State 2016–2018: progression from Candida auris colonization to bloodstream infection. Open Forum Infectious Diseases, 2018. Oxford University Press US, S594-S595.

SPOTTISWOODE, N.,HAO, S.,SANCHEZ-GUERRERO, E.,DETWEILER, A. M.,MEKONEN, H.,NEFF, N.,MACMILLAN, H.,SCHWARTZ, B. S.,ENGEL, J.,DERISI, J. L.,MILLER, S. A. & LANGELIER, C. R. 2023. In host evolution of beta lactam resistance during active treatment for Pseudomonas aeruginosa bacteremia. *Front Cell Infect Microbiol,* 13**,** 1241608.

STACY, A.,EVERETT, J.,JORTH, P.,TRIVEDI, U.,RUMBAUGH, K. P. & WHITELEY, M. 2014. Bacterial fight-and-flight responses enhance virulence in a polymicrobial infection. *Proceedings of the National Academy of Sciences,* 111**,** 7819-7824.

STEWART, E. J. 2012. Growing Unculturable Bacteria. *Journal of Bacteriology,* 194**,** 4151-4160.

STONEHAM, S. M.,CANTILLON, D. M.,WADDELL, S. J. & LLEWELYN, M. J. 2020. Spontaneously Occurring Small-Colony Variants of Staphylococcus aureus Show Enhanced Clearance by THP-1 Macrophages. *Frontiers in Microbiology,* Volume 11 - 2020.

STRATMANN, B.,COSTEA, T.-C.,NOLTE, C.,HILLER, J.,SCHMIDT, J.,REINDEL, J.,MASUR, K.,MOTZ, W.,TIMM, J. & KERNER, W. 2020. Effect of cold atmospheric plasma therapy vs standard therapy placebo on wound healing in patients with diabetic foot ulcers: a randomized clinical trial. *JAMA network open,* 3**,** e2010411-e2010411.

STROHAL, R.,DIETRICH, S.,MITTLBÖCK, M. & HÄMMERLE, G. 2022. Chronic wounds treated with cold atmospheric plasmajet versus best practice wound dressings: a multicenter, randomized, non-inferiority trial. *Scientific Reports,* 12**,** 3645.

SUBRAMANIAN, A. 2024. Emerging roles of bacteriophage-based therapeutics in combating antibiotic resistance. *Frontiers in Microbiology,* Volume 15 - 2024.

SUD, I. & FEINGOLD, D. S. 1982. Action of antifungal imidazoles on Staphylococcus aureus. *Antimicrobial Agents and Chemotherapy,* 22**,** 470-474.

SUN, Y.,YU, S.,SUN, P.,WU, H.,ZHU, W.,LIU, W.,ZHANG, J.,FANG, J. & LI, R. 2012. Inactivation of Candida biofilms by non-thermal plasma and its enhancement for fungistatic effect of antifungal drugs. *PloS one,* 7**,** e40629.

SUN, Z.,DING, C.,WANG, Y.,LU, T. & SONG, W. 2024. Plasma-Activated Medium Inhibited the Proliferation and Migration of Non-Small Cell Lung Cancer A549 Cells in 3D Culture. *Int J Mol Sci,* 25.

SUTCLIFFE, J. E.,THRASIVOULOU, C.,SERENA, T. E.,MADDEN, L.,RICHARDS, T.,PHILLIPS, A. R. & BECKER, D. L. 2017. Changes in the extracellular matrix surrounding human chronic wounds revealed by 2-photon imaging. *International wound journal,* 14**,** 1225-1236.

SUTTON, J. A. F.,CARNELL, O. T.,LAFAGE, L.,GRAY, J.,BIBOY, J.,GIBSON, J. F.,POLLITT, E. J. G.,TAZOLL, S. C.,TURNBULL, W.,HAJDAMOWICZ, N. H.,SALAMAGA, B.,PIDWILL, G. R.,CONDLIFFE, A. M.,RENSHAW, S. A.,VOLLMER, W. & FOSTER, S. J. 2021. Staphylococcus aureus cell wall structure and dynamics during host-pathogen interaction. *PLOS Pathogens,* 17**,** e1009468.

SWANSON, T.,OUSEY, K.,HAESLER, E.,BJARNSHOLT, T.,CARVILLE, K.,IDENSOHN, P.,KALAN, L.,KEAST, D. H.,LARSEN, D.,PERCIVAL, S.,SCHULTZ, G.,SUSSMAN, G.,WATERS, N. & WEIR, D. 2022. IWII Wound Infection in Clinical Practice consensus document: 2022 update. *Journal of Wound Care,* 31**,** S10-S21.

SWATHYKRISHNA, C. S.,AMRITHANJALI, G.,SHAJI, G. & KUMAR R., A. 2023. Antimicrobial Activity and Synthesis of Thiazole Derivatives: A Recent Update. *Journal of Chemical Reviews,* 5**,** 221-240.

SZILI, E. J.,GHIMIRE, B.,PATENALL, B. L.,ROHAIM, M.,MISTRY, D.,FELLOWS, A.,MUNIR, M.,JENKINS, A. T. A. & SHORT, R. D. 2021. On-demand cold plasma activation of acetyl donors for bacteria and virus decontamination. *Applied Physics Letters,* 119.

TABATABAEI HOSSEINI, B. S.,MEADOWS, K.,GABRIEL, V.,HU, J. & KIM, K. 2024. Biofabrication of Cellulose-based Hydrogels for Advanced Wound Healing: A Special Emphasis on 3D Bioprinting. *Macromol Biosci,* 24**,** e2300376.

TAFF, H. T.,MITCHELL, K. F.,EDWARD, J. A. & ANDES, D. R. 2013. Mechanisms of Candida biofilm drug resistance. *Future Microbiol,* 8**,** 1325-37.

TAIT, K. & SUTHERLAND, I. 2002. Antagonistic interactions amongst bacteriocin-producing enteric bacteria in dual species biofilms. *Journal of applied microbiology,* 93**,** 345-352.

TAJANE, S. B.,PAWAR, S. & PATIL, S. 2024. Emerging Healthcare Threat Candida auris: A Prevalence Study From a Rural Tertiary Referral Centre in Western India. *Cureus,* 16**,** e72676.

TAJDARI, H. 2024. Ibuprofen and Antibiotic Co-Delivery via Nanoparticles: A Novel Approach to Treating Pseudomonas aeruginosa Infections in Cystic Fibrosis - A Protocol Study. *Undergraduate Research in Natural and Clinical Science and Technology (URNCST) Journal*.

TAKAMATSU, T.,UEHARA, K.,SASAKI, Y.,MIYAHARA, H.,MATSUMURA, Y.,IWASAWA, A.,ITO, N.,AZUMA, T.,KOHNO, M. & OKINO, A. 2014. Investigation of reactive species using various gas plasmas. *Rsc Advances,* 4**,** 39901-39905.

TATLICIOĞLU, G.,ÇÜRÜKOĞLU, A.,AKAN, G.,YEŞILOVALI, G.,ÖĞÜTÇÜ, G.,AKTAŞ, R.,KÜKNER, A.,TEMIZEL, M.,SARITAŞ, Z. K. & ÖZGENCIL, F. E. 2023. Effect of cold atmospheric plasma/NO gas application with different exposure times on healing in wounds with tissue loss in diabetic rats. *Pol J Vet Sci,* 26**,** 441-447.

TCHUEDJI, Y. L. G. N.,II, Y. B.,LYONGA, E.,SADO, S.,NKOUÉ, A.,MESEMBE, M. T.,SAKE, C.,NGOME, R.,KAMGUIA, M. S. D.,KAMGA, H. G. & ETOA, F. X. 2024. Contribution of biofilm and Cell Surface Hydrophobicity in the resistance of Pseudomonas aeruginosa from some Healthcare settings of Yaounde. *International Journal of Medical Science and Clinical Research Studies*.

THAARUP, I. C.,LICHTENBERG, M.,NØRGAARD, K. T. H.,XU, Y.,LORENZEN, J.,THOMSEN, T. R. & BJARNSHOLT, T. 2023. A collagen-based layered chronic wound biofilm model for testing antimicrobial wound products. *Wound Repair Regen,* 31**,** 500-515.

THARP, B.,ZHENG, R.,BRYAK, G.,LITVINTSEVA, A. P.,HAYDEN, M. K.,CHOWDHARY, A. & THANGAMANI, S. 2023. Role of Microbiota in the Skin Colonization of Candida auris. *mSphere,* 8**,** e00623-22.

THEINKOM, F.,SINGER, L.,CIEPLIK, F.,CANTZLER, S.,WEILEMANN, H.,CANTZLER, M.,HILLER, K.-A.,MAISCH, T. & ZIMMERMANN, J. L. 2019. Antibacterial efficacy of cold atmospheric plasma against Enterococcus faecalis planktonic cultures and biofilms in vitro. *PLoS One,* 14**,** e0223925.

THOMAS, J. G.,MOTLAGH, H.,POVEY, S. B. & PERCIVAL, S. L. 2011. 2 - The role of micro-organisms and biofilms in dysfunctional wound healing. *In:* FARRAR, D. (ed.) *Advanced Wound Repair Therapies*. Woodhead Publishing.

THOMAS, S.,EL-ZAYAT, A. S.,GURNEY, J.,RATTRAY, J. B. & BROWN, S. P. 2023. The las and rhl Quorum Sensing Systems in Pseudomonas aeruginosa Form a Multi-Signal Reciprocal Network Which Can Tune Reactivity to Variations in Physical and Social Environments. *bioRxiv*.

TIPTON, C. D.,WOLCOTT, R. D.,SANFORD, N. E.,MILLER, C.,PATHAK, G.,SILZER, T. K.,SUN, J.,FLEMING, D.,RUMBAUGH, K. P.,LITTLE, T. D.,PHILLIPS, N. & PHILLIPS, C. D. 2020. Patient genetics is linked to chronic wound microbiome composition and healing. *PLOS Pathogens,* 16**,** e1008511.

TOM, I. M.,IBRAHIM, M. M.,UMORU, A. M.,UMAR, J. B.,BUKAR, M. A.,HARUNA, A. B. & ALIYU, A. 2019. Infection of wounds by potential bacterial pathogens and their resistogram. *Open Access Library Journal,* 6**,** 1-13.

TOMBULTURK, F. K.,SOYDAS, T. & KANIGUR-SULTUYBEK, G. 2024. Topical metformin accelerates wound healing by promoting collagen synthesis and inhibiting apoptosis in a diabetic wound model. *Int Wound J,* 21**,** e14345.

TOMIC-CANIC, M.,BURGESS, J. L.,O'NEILL, K. E.,STRBO, N. & PASTAR, I. 2020. Skin microbiota and its interplay with wound healing. *American journal of clinical dermatology,* 21**,** 36-43.

TOWNSEND, E. M.,SHERRY, L.,KEAN, R.,HANSOM, D.,MACKAY, W. G.,WILLIAMS, C.,BUTCHER, J. & RAMAGE, G. 2017. Implications of antimicrobial combinations in complex wound biofilms containing fungi. *Antimicrobial agents and chemotherapy,* 61**,** 10.1128/aac. 00672-17.

TOWNSEND, E. M.,SHERRY, L.,RAJENDRAN, R.,HANSOM, D.,BUTCHER, J.,MACKAY, W. G.,WILLIAMS, C. & RAMAGE, G. 2016. Development and characterisation of a novel three-dimensional inter-kingdom wound biofilm model. *Biofouling,* 32**,** 1259-1270.

TRAN, H. Q.,SHAHRIAR, S. M. S.,YAN, Z. & XIE, J. 2023. Recent Advances in Functional Wound Dressings. *Adv Wound Care (New Rochelle),* 12**,** 399-427.

TRINH, K. T. L. & LEE, N. Y. 2022. Recent Methods for the Viability Assessment of Bacterial Pathogens: Advances, Challenges, and Future Perspectives. *Pathogens,* 11.

TRUONG, Y. L.,GERGES, B. Z.,ROSENBLATT, J. & RAAD, I. I. 2124. Novel Polygalacturonic and Caprylic Acid (PG+ CAP) Antimicrobial Wound Ointment Effectiveness in Eradicating C. auris Biofilms In Vitro. Open Forum Infectious Diseases, 2023. Oxford University Press US, ofad500. 1747.

TSOUKOU, E.,BOURKE, P. & BOEHM, D. 2022. Efficacy of plasma activated saline in a co-culture infection control model. *Scientific Reports,* 12**,** 20230.

TUCHSCHERR, L.,LÖFFLER, B. & PROCTOR, R. A. 2020. Persistence of Staphylococcus aureus: Multiple Metabolic Pathways Impact the Expression of Virulence Factors in Small-Colony Variants (SCVs). *Frontiers in Microbiology,* Volume 11 - 2020.

TUON, F. F.,SUSS, P. H.,TELLES, J. P.,DANTAS, L. R.,BORGES, N. H. & RIBEIRO, V. S. T. 2023. Antimicrobial treatment of Staphylococcus aureus biofilms. *Antibiotics,* 12**,** 87.

UBEROI, A.,MCCREADY-VANGI, A. & GRICE, E. A. 2024. The wound microbiota: microbial mechanisms of impaired wound healing and infection. *Nature Reviews Microbiology,* 22**,** 507-521.

UNGUREANU, D.,TIPERCIUC, B.,NASTASĂ, C.,IONUȚ, I.,MARC, G.,ONIGA, I. & ONIGA, O. 2024. An Overview of the Structure-Activity Relationship in Novel Antimicrobial Thiazoles Clubbed with Various Heterocycles (2017-2023). *Pharmaceutics,* 16.

UTOIU, E.,MANOIU, V. S.,OPRITA, E. I. & CRACIUNESCU, O. 2024. Bacterial Cellulose: A Sustainable Source for Hydrogels and 3D-Printed Scaffolds for Tissue Engineering. *Gels,* 10.

VALLE, J.,DA RE, S.,HENRY, N.,FONTAINE, T.,BALESTRINO, D.,LATOUR-LAMBERT, P. & GHIGO, J.-M. 2006. Broad-spectrum biofilm inhibition by a secreted bacterial polysaccharide. *Proceedings of the National Academy of Sciences,* 103**,** 12558-12563.

VAN WELZEN, A.,HOCH, M.,WAHL, P.,WEBER, F.,RODE, S.,TIETZE, J. K.,BOECKMANN, L.,EMMERT, S. & THIEM, A. 2021. The Response and Tolerability of a Novel Cold Atmospheric Plasma Wound Dressing for the

Healing of Split Skin Graft Donor Sites: A Controlled Pilot Study. *Skin Pharmacology and Physiology*, 34**,** 328-336.

VAŇKOVÁ, E.,JULÁK, J.,MACHKOVÁ, A.,OBROVÁ, K.,KLANČNIK, A.,SMOLE MOŽINA, S. & SCHOLTZ, V. 2024. Overcoming antibiotic resistance: non-thermal plasma and antibiotics combination inhibits important pathogens. *Pathog Dis,* 82.

VERBANIC, S.,SHEN, Y.,LEE, J.,DEACON, J. M. & CHEN, I. A. 2020. Microbial predictors of healing and short-term effect of debridement on the microbiome of chronic wounds. *npj Biofilms and Microbiomes,* 6**,** 21.

VERMA, N.,BAJIYA, M.,DOLHEY, R.,SURABHI,YADAV, A. S.,CHAUDHARY, C.,MEENA, D.,ARYA, H.,BHATT, T. K.,YADAV, J. K.,SHUKLA, J. N.,SWAROOP, S. & PANDEY, J. 2025. Mechanistic Insights into the Antibiofilm Activity of Simvastatin and Lovastatin against Bacillus subtilis. *Molecular Pharmaceutics*.

VERSEY, Z.,DA CRUZ NIZER, W. S.,RUSSELL, E.,ZIGIC, S.,DEZEEUW, K. G.,MAREK, J. E.,OVERHAGE, J. & CASSOL, E. 2021. Biofilm-innate immune interface: contribution to chronic wound formation. *Frontiers in immunology,* 12**,** 648554.

VESTWEBER, P. K.,WÄCHTER, J.,PLANZ, V.,JUNG, N. & WINDBERGS, M. 2024. The interplay of Pseudomonas aeruginosa and Staphylococcus aureus in dual-species biofilms impacts development, antibiotic resistance and virulence of biofilms in in vitro wound infection models. *Plos one,* 19**,** e0304491.

VIDAKOVIC, L.,MIKHALEVA, S.,JECKEL, H.,NISNEVICH, V.,STRENGER, K.,NEUHAUS, K.,RAVEENDRAN, K.,BEN-MOSHE, N. B.,AZNAOUROVA, M.,NOSHO, K.,DRESCHER, A.,SCHMECK, B.,SCHULTE, L. N.,PERSAT, A.,AVRAHAM, R. & DRESCHER, K. 2023. Biofilm formation on human immune cells is a multicellular predation strategy of Vibrio cholerae. *Cell,* 186**,** 2690-2704.e20.

VIEHMAN, J. A.,CLANCY, C. J.,LIU, G.,CHENG, S.,OLEKSIUK, L.-M.,SHIELDS, R. K. & NGUYEN, M.-H. 383. An Increased Rate of Candida parapsilosis Infective Endocarditis Is Associated with Injection Drug Use. Open Forum Infectious Diseases, 2018. S148.

VILLA, F.,MARCHANDIN, H.,LAVIGNE, J.-P.,SCHULDINER, S.,CELLIER, N.,SOTTO, A. & LOUBET, P. 2024. Anaerobes in diabetic foot infections: pathophysiology,

epidemiology, virulence, and management. *Clinical Microbiology Reviews,* 37**,** e00143-23.

VYAS, H. K. N.,XIA, B.,ALAM, D.,GRACIE, N. P.,ROTHWELL, J. G.,RICE, S. A.,CARTER, D.,CULLEN, P. J. & MAI-PROCHNOW, A. 2023. Plasma activated water as a pre-treatment strategy in the context of biofilm-infected chronic wounds. *Biofilm,* 6**,** 100154.

VYAS, H. K. N.,XIA, B. & MAI-PROCHNOW, A. 2022. Clinically relevant in vitro biofilm models: A need to mimic and recapitulate the host environment. *Biofilm,* 4**,** 100069.

WÄCHTER, J.,VESTWEBER, P. K.,PLANZ, V. & WINDBERGS, M. 2023. Unravelling host-pathogen interactions by biofilm infected human wound models. *Biofilm,* 6**,** 100164.

WADDINGTON, C.,CAREY, M. E.,BOINETT, C. J.,HIGGINSON, E.,VEERARAGHAVAN, B. & BAKER, S. 2022. Exploiting genomics to mitigate the public health impact of antimicrobial resistance. *Genome medicine,* 14**,** 15.

WANG, C. C.,YANG, P. W.,YANG, S. F.,HSIEH, K. P.,TSENG, S. P. & LIN, Y. C. 2016. Topical simvastatin promotes healing of Staphylococcus aureus-contaminated cutaneous wounds. *Int Wound J,* 13**,** 1150-1157.

WANG, P.,LI, H.,ZHANG, X.,WANG, X.,SUN, W.,ZHANG, X.,CHI, B.,GO, Y.,CHAN, X. H. F.,WU, J. & HUANG, Q. 2025. Microecology in vitro model replicates the human skin microbiome interactions. *Nature Communications,* 16**,** 3085.

WANG, S.,ZHAO, Y.,BRESLAWEC, A. P.,LIANG, T.,DENG, Z.,KUPERMAN, L. L. & YU, Q. 2023a. Strategy to combat biofilms: a focus on biofilm dispersal enzymes. *npj Biofilms and Microbiomes,* 9**,** 63.

WANG, S.-H.,SHYU, V. B.-H.,CHIU, W.-K.,HUANG, R.-W.,LAI, B.-R. & TSAI, C.-H. 2023b. An overview of clinical examinations in the evaluation and assessment of arterial and venous insufficiency wounds. *Diagnostics,* 13**,** 2494.

WANG, Y.,BIAN, Z. & WANG, Y. 2022. Biofilm formation and inhibition mediated by bacterial quorum sensing. *Applied Microbiology and Biotechnology,* 106**,** 6365-6381.

WANG, Y.,MANG, X.,LI, X.,CAI, Z. & TAN, F. 2022. Cold atmospheric plasma induces apoptosis in human colon and lung cancer cells through modulating

mitochondrial pathway. *Frontiers in Cell and Developmental Biology,* Volume 10 - 2022.

WATNICK, P. & KOLTER, R. 2000. Biofilm, city of microbes. *J Bacteriol,* 182**,** 2675-9.

WEIDT, S.,HAGGARTY, J.,KEAN, R.,COJOCARIU, C. I.,SILCOCK, P. J.,RAJENDRAN, R.,RAMAGE, G. & BURGESS, K. E. V. 2016. A novel targeted/untargeted GC-Orbitrap metabolomics methodology applied to Candida albicans and Staphylococcus aureus biofilms. *Metabolomics,* 12**,** 189.

WENDE, K.,WILLIAMS, P.,DALLUGE, J.,VAN GAENS, W.,ABOUBAKR, H.,BISCHOF, J.,VON WOEDTKE, T.,GOYAL, S. M.,WELTMANN, K.-D. & BOGAERTS, A. 2015. Identification of the biologically active liquid chemistry induced by a nonthermal atmospheric pressure plasma jet. *Biointerphases,* 10.

WESTGEEST, A. C.,BUIS, D. T. P.,SIGALOFF, K. C. E.,RUFFIN, F.,VISSER, L. G.,YU, Y.,SCHIPPERS, E. F.,LAMBREGTS, M. M. C.,TONG, S. Y. C.,DE BOER, M. G. J. & FOWLER, V. G. 2023. Global Differences in the Management of Staphylococcus aureus Bacteremia: No International Standard of Care. *Clin Infect Dis,* 77**,** 1092-1101.

WHITE, M. J.,BOYD, J. M.,HORSWILL, A. R. & NAUSEEF, W. M. 2014. Phosphatidylinositol-specific phospholipase C contributes to survival of Staphylococcus aureus USA300 in human blood and neutrophils. *Infection and immunity,* 82**,** 1559-1571.

WILCOX, M.,WALKER, C.,WINSTANLEY, T. & LIMB, D. 1996. True identity of control Staphylococcus aureus strains and their performance in the tube coagulase test. *Journal of medical microbiology,* 44**,** 496-499.

WILGUS, T. A.,ROY, S. & MCDANIEL, J. C. 2013. Neutrophils and wound repair: positive actions and negative reactions. *Advances in wound care,* 2**,** 379-388.

WILKINSON, H. N. & HARDMAN, M. J. 2020. Wound healing: cellular mechanisms and pathological outcomes. *Open biology,* 10**,** 200223.

WILKINSON, H. N.,MCBAIN, A. J.,STEPHENSON, C. & HARDMAN, M. J. 2016. Comparing the Effectiveness of Polymer Debriding Devices Using a Porcine Wound Biofilm Model. *Adv Wound Care (New Rochelle),* 5**,** 475-485.

WISPLINGHOFF, H.,BISCHOFF, T.,TALLENT, S. M.,SEIFERT, H.,WENZEL, R. P. & EDMOND, M. B. 2004. Nosocomial bloodstream infections in US hospitals:

analysis of 24,179 cases from a prospective nationwide surveillance study. *Clinical infectious diseases,* 39**,** 309-317.

WOLCOTT, R.,COSTERTON, J.,RAOULT, D. & CUTLER, S. 2013. The polymicrobial nature of biofilm infection. *Clinical Microbiology and Infection,* 19**,** 107-112.

WOLCOTT, R. D. 2017. Biofilms cause chronic infections. MA Healthcare London.

WOLCOTT, R. D.,HANSON, J. D.,REES, E. J.,KOENIG, L. D.,PHILLIPS, C. D.,WOLCOTT, R. A.,COX, S. B. & WHITE, J. S. 2016. Analysis of the chronic wound microbiota of 2,963 patients by 16S rDNA pyrosequencing. *Wound repair and regeneration,* 24**,** 163-174.

WOLCOTT, R. D.,RUMBAUGH, K. P.,JAMES, G.,SCHULTZ, G.,PHILLIPS, P.,YANG, Q.,WATTERS, C.,STEWART, P. S. & DOWD, S. E. 2010. Biofilm maturity studies indicate sharp debridement opens a time- dependent therapeutic window. *J Wound Care,* 19**,** 320-8.

WOLLENBERG, M. S.,CLAESEN, J.,ESCAPA, I. F.,ALDRIDGE, K. L.,FISCHBACH, M. A. & LEMON, K. P. 2014. Propionibacterium Produced Coproporphyrin III Induces Staphylococcus aureus Aggregation and Biofilm Formation. *mBio,* 5**,** e01286-14.

WONG, G. C. L.,ANTANI, J. D.,LELE, P. P.,CHEN, J.,NAN, B.,KÜHN, M. J.,PERSAT, A.,BRU, J.-L.,HØYLAND-KROGHSBO, N. M.,SIRYAPORN, A.,CONRAD, J. C.,CARRARA, F.,YAWATA, Y.,STOCKER, R.,V BRUN, Y.,WHITFIELD, G. B.,LEE, C. K.,DE ANDA, J.,SCHMIDT, W. C.,GOLESTANIAN, R.,O'TOOLE, G. A.,FLOYD, K. A.,YILDIZ, F. H.,YANG, S.,JIN, F.,TOYOFUKU, M.,EBERL, L.,NOMURA, N.,ZACHAROFF, L. A.,EL-NAGGAR, M. Y.,YALCIN, S. E.,MALVANKAR, N. S.,ROJAS-ANDRADE, M. D.,HOCHBAUM, A. I.,YAN, J.,STONE, H. A.,WINGREEN, N. S.,BASSLER, B. L.,WU, Y.,XU, H.,DRESCHER, K. & DUNKEL, J. 2021. Roadmap on emerging concepts in the physical biology of bacterial biofilms: from surface sensing to community formation. *Physical Biology,* 18**,** 051501.

WU, H.,MOSER, C.,WANG, H.-Z.,HØIBY, N. & SONG, Z.-J. 2015. Strategies for combating bacterial biofilm infections. *International Journal of Oral Science,* 7**,** 1-7.

WU, M.,LI, Y.,GUO, D.,KUI, G.,LI, B.,DENG, Y. & LI, F. 2018. Microbial Diversity of Chronic Wound and Successful Management of Traditional Chinese Medicine. *Evid Based Complement Alternat Med,* 2018**,** 9463295.

WU, S.,LIU, Y.,LEI, L. & ZHANG, H. 2021. Antisense yycG modulates the susceptibility of Staphylococcus aureus to hydrogen peroxide via the sarA. *BMC microbiology,* 21**,** 1-12.

WU, W.,HUANG, J. & XU, Z. 2024. Antibiotic influx and efflux in Pseudomonas aeruginosa: Regulation and therapeutic implications. *Microb Biotechnol,* 17**,** e14487.

WU, Y.-K.,CHENG, N.-C. & CHENG, C.-M. 2019. Biofilms in chronic wounds: pathogenesis and diagnosis. *Trends in biotechnology,* 37**,** 505-517.

WURDAK, H.,ZHU, S.,MIN, K. H.,AIMONE, L.,LAIRSON, L. L.,WATSON, J.,CHOPIUK, G.,DEMAS, J.,CHARETTE, B. & HALDER, R. 2010. A small molecule accelerates neuronal differentiation in the adult rat. *Proceedings of the National Academy of Sciences,* 107**,** 16542-16547.

XAVIER, J. B. 2016. Sociomicrobiology and Pathogenic Bacteria. *Microbiology Spectrum,* 4**,** 10.1128/microbiolspec.vmbf-0019-2015.

XIA, B.,VYAS, H. K. N.,RICE, S. A.,NEWSOME, T. P.,CULLEN, P. J. & MAI-PROCHNOW, A. 2024. Antimicrobial mechanism of in-situ plasma activated water treatment of pathogenic Escherichia coli and Staphylococcus aureus biofilms. *bioRxiv***,** 2024.07.07.602420.

XIA, B.,VYAS, H. K. N.,ZHOU, R.,ZHANG, T.,HONG, J.,ROTHWELL, J. G.,RICE, S. A.,CARTER, D.,OSTRIKOV, K.,CULLEN, P. J. & MAI-PROCHNOW, A. 2023. The importance of superoxide anion for Escherichia coli biofilm removal using plasma-activated water. *Journal of Environmental Chemical Engineering,* 11**,** 109977.

XU, Y.,PENG, S.,LI, B.,WANG, S.,ZHANG, H.,LI, Q.,LIU, Z.,GUO, B.,LIU, D. & XU, D. 2021. Systematic Safety Evaluation of Cold Plasma-Activated Liquid in Rabbits. *Frontiers in Physics,* Volume 9 - 2021.

XU, Z.,ZHOU, X.,YANG, W.,ZHANG, Y.,YE, Z.,HU, S.,YE, C.,LI, Y.,LAN, Y. & SHEN, J. 2020. In vitro antimicrobial effects and mechanism of air plasma-activated water on Staphylococcus aureus biofilm. *Plasma Processes and Polymers,* 17**,** 1900270.

YADAV, S.,PAWAR, S. & PATIL, S. 2025. Inhibition of Pseudomonas aeruginosa Biofilm Formation Using Silver Nanoparticles. *Cureus,* 17**,** e77848.

YAN, D.,CUI, H.,ZHU, W.,NOURMOHAMMADI, N.,MILBERG, J.,ZHANG, L. G.,SHERMAN, J. H. & KEIDAR, M. 2017. The Specific Vulnerabilities of

Cancer Cells to the Cold Atmospheric Plasma-Stimulated Solutions. *Scientific Reports,* 7**,** 4479.

YANG, F.,BAI, X.,DAI, X. & LI, Y. 2021a. The biological processes during wound healing. *Regenerative medicine,* 16**,** 373-390.

YANG, J.,XU, J. F. & LIANG, S. 2024. Antibiotic resistance in Pseudomonas aeruginosa: mechanisms and emerging treatment. *Crit Rev Microbiol***,** 1-19.

YANG, L.,LIU, Y.,MARKUSSEN, T.,HØIBY, N.,TOLKER-NIELSEN, T. & MOLIN, S. 2011. Pattern differentiation in co-culture biofilms formed by Staphylococcus aureus and Pseudomonas aeruginosa. *FEMS immunology & medical microbiology,* 62**,** 339-347.

YANG, L.,NIYAZI, G.,QI, Y.,YAO, Z.,HUANG, L.,WANG, Z.,GUO, L. & LIU, D. 2021b. Plasma-Activated Saline Promotes Antibiotic Treatment of Systemic Methicillin-Resistant Staphylococcus aureus Infection. *Antibiotics (Basel),* 10.

YAO, S.,HAO, L.,ZHOU, R.,JIN, Y.,HUANG, J. & WU, C. 2022. Multispecies biofilms in fermentation: Biofilm formation, microbial interactions, and communication. *Comprehensive reviews in food science and food safety,* 21**,** 3346-3375.

YI, Q.,HUANG, Z. & TANG, B. 2025. Impact of Silver Dressings on Wound Healing Rate in Patients with Lower Extremity Ulcers: A Systematic Review and Meta-Analysis of Randomized Controlled Trials. *Med Princ Pract,* 34**,** 13-24.

YIN, C.,ALAM, M. Z.,FALLON, J. T. & HUANG, W. 2024. Advances in development of novel therapeutic strategies against multi-drug resistant Pseudomonas aeruginosa. *Antibiotics,* 13**,** 119.

YIN, S.,JIANG, B.,HUANG, G.,GONG, Y.,YOU, B.,YANG, Z.,CHEN, Y.,CHEN, J.,YUAN, Z.,LI, M.,HU, F.,ZHAO, Y. & PENG, Y. 2017. Burn Serum Increases Staphylococcus aureus Biofilm Formation via Oxidative Stress. *Frontiers in Microbiology,* Volume 8 - 2017.

YOO, J.,KANG, Y.-H.,BAEK, S. J. & HWANG, C.-Y. 2023. Application of cold atmospheric microwave plasma as an adjunct therapy for wound healing in dogs and cats. *J Vet Sci,* 24.

YOUNG, T.,ALSHANTA, O.-A.,KEAN, R.,BRADSHAW, D.,PRATTEN, J.,WILLIAMS, C.,WOODALL, C.,RAMAGE, G. & BROWN, J. L. 2021. Candida albicans as an Essential “Keystone” Component within Polymicrobial Oral Biofilm Models? *Microorganisms,* 9**,** 59.

YU, J.,TIEN, N.,LIU, Y.-C.,CHO, D.-Y.,CHEN, J.-W.,TSAI, Y.-T.,HUANG, Y.-C.,CHAO, H.-J. & CHEN, C.-J. 2022. Rapid Identification of Methicillin-Resistant Staphylococcus aureus Using MALDI-TOF MS and Machine Learning from over 20,000 Clinical Isolates. *Microbiology Spectrum,* 10**,** e00483-22.

YUCEL-LINDBERG, T. & BÅGE, T. 2013. Inflammatory mediators in the pathogenesis of periodontitis. *Expert reviews in molecular medicine,* 15**,** e7.

YUNG, D. B. Y.,SIRCOMBE, K. J. & PLETZER, D. 2021. Friends or enemies? The complicated relationship between Pseudomonas aeruginosa and Staphylococcus aureus. *Mol Microbiol,* 116**,** 1-15.

ZHAI, S.-Y.,KONG, M. G. & XIA, Y.-M. 2022. Cold atmospheric plasma ameliorates skin diseases involving reactive oxygen/nitrogen species-mediated functions. *Frontiers in Immunology,* 13**,** 868386.

ZHANG, D.,LEONG, A. S. W. & MCMULLIN, G. 2023. Blue light therapy in the management of chronic wounds: a narrative review of its physiological basis and clinical evidence. *Wounds: a compendium of clinical research and practice,* 35**,** 91-98.

ZHANG, H.,WEI, J.,XV, H.,KHAN, I.,SUN, Q.,ZHAO, X.,GAO, J.,LIU, S. & WEI, S. 2024. Bactericidal efficacy of plasma-activated water against Vibrio parahaemolyticus on Litopenaeus vannamei. *Frontiers in Nutrition,* Volume 11 - 2024.

ZHANG, H.,ZHANG, C. & HAN, Q. 2023. Mechanisms of bacterial inhibition and tolerance around cold atmospheric plasma. *Appl Microbiol Biotechnol,* 107**,** 5301-5316.

ZHANG, M.,JIN, J.,LIU, Y.,BEN, C.,LI, H.,CHENG, D.,SUN, Y.,GUANG-YI, W. & ZHU, S. 2023. Analysis of povidone iodine, chlorhexidine acetate and polyhexamethylene biguanide as wound disinfectants: in vitro cytotoxicity and antibacterial activity. *BMJ Nutr Prev Health,* 6**,** 21-27.

ZHANG, X.,LI, Z.,PANG, S.,JIANG, B.,YANG, Y.,DUAN, Q. & ZHU, G. 2021. The impact of cell structure, metabolism and group behavior for the survival of bacteria under stress conditions. *Archives of Microbiology,* 203**,** 431-441.

ZHAO, A.,SUN, J. & LIU, Y. 2023. Understanding bacterial biofilms: From definition to treatment strategies. *Frontiers in cellular and infection microbiology,* 13**,** 1137947.

ZHAO, G.,USUI, M. L.,LIPPMAN, S. I.,JAMES, G. A.,STEWART, P. S.,FLECKMAN, P. & OLERUD, J. E. 2013. Biofilms and inflammation in chronic wounds. *Advances in wound care,* 2**,** 389-399.

ZHENG, Y.,HE, L.,ASIAMAH, T. K. & OTTO, M. 2018. Colonization of medical devices by staphylococci. *Environmental Microbiology,* 20**,** 3141-3153.

ZHOU, J.,SUN, Z.,WANG, X.,WANG, S.,JIANG, W.,TANG, D.,XIA, T. & XIAO, F. 2025. Low-temperature cold plasma promotes wound healing by inhibiting skin inflammation and improving skin microbiome. *Frontiers in Bioengineering and Biotechnology,* Volume 13 - 2025.

ZHU, S.,YU, Y.,REN, Y.,XU, L.,WANG, H.,LING, X.,JIN, L.,HU, Y.,ZHANG, H. & MIAO, C. 2021. The emerging roles of neutrophil extracellular traps in wound healing. *Cell death & disease,* 12**,** 984.

ZHUO, S. & YUAN, C. 2020. Active site competition is the mechanism for the inhibition of lipoprotein-associated phospholipase A2 by detergent micelles or lipoproteins and for the efficacy reduction of darapladib. *Scientific Reports,* 10**,** 17232.

ŽIEMYTĖ, M.,CARDA-DIÉGUEZ, M.,RODRÍGUEZ-DÍAZ, J. C.,VENTERO, M. P.,MIRA, A. & FERRER, M. D. 2021. Real-time monitoring of Pseudomonas aeruginosa biofilm growth dynamics and persister cells' eradication. *Emerg Microbes Infect,* 10**,** 2062-2075.

ZOBELL, C. E. 1943. The Effect of Solid Surfaces upon Bacterial Activity. *J Bacteriol,* 46**,** 39-56.

ZOU, J.,PENG, B.,QU, J. & ZHENG, J. 2022. Are Bacterial Persisters Dormant Cells Only? *Frontiers in Microbiology,* Volume 12 - 2021.